The mineralogy, geochemistry, and petrogenesis of the grønnedal-íka alkaline igneous complex, south-west Greenland

Christopher M. Bedford

THE MINERALOGY, GEOCHEMISTRY, AND PETROGENESIS OF THE GRØNNEDAL-ÍKA ALKALINE IGNEOUS COMPLEX, SOUTH-WEST GREENLAND

by

Christopher M. Bedford, BA(Oxon), F.G.S.

A thesis submitted for the degree of Doctor of Philosophy
at the Department of Geological Sciences, University of Durham.

November 1989

ABSTRACT

At 1299±17 Ma (Blaxland *et al.*, 1978), the Grønnedal-Íka is the oldest of the Gardar centres, situated in the extreme north-west of the province. Rare-earth element (REE) trends suggest that the nepheline-syenites which make up the bulk of the complex were derived from a parental magma formed by a few percent of partial melting of a garnet-lherzolite mantle source during an episode of rifting in the Early Gardar.

In contrast to other undersaturated Gardar centres, the syenites of Grønnedal-Íka show some striking mineralogical differences. The scarcity of amphibole and lack of olivine indicate a magma with a relatively high oxygen fugacity. Opaque oxide compositions and pyroxene trends provide further support for this idea. Additionally, the occurrence of zircon in all units of the complex is unusual, and is probably related to post-magmatic alteration processes.

Fractionation of apatite and zircon appears to have been responsible for the observed variations in REE content, although later alteration and variations in the composition of the intercumulus liquid have given rise to a considerable scatter in major and trace element abundances. Normative compositions show the evidence for the development of a 'sandwich' horizon in both the Lower and Upper Series.

At a later stage, a plug of xenolithic syenite was intruded, which was followed by a the emplacement of a body of xenolithic carbonatite, containing fragments of the earlier syenites. This unit is predominantly søvitic, but with increasing fractionation, more iron-rich (ferrcarbonatite) compositions were developed. Compared to many carbonatites, the rock at Grønnedal is rather poor in 'exotic' minerals. Trace element abundances, however, show extreme enrichment in Sr, Th, REE's, and Y, and depletion in Zr, Ti, and K compared to the syenites. These variations are comparable to the observed concentrations in the Igaliko carbonatite dykes (Pearce, 1988). Hf, Ta, and REE distributions between the carbonatite and syenitic rocks suggest that the carbonatite was derived by liquid immiscibility from a CO_2-saturated phonolitic magma, with the conjugate silicate phase possibly intruded as the Xenolithic Porphyritc Syenite.

Patchy metasomatic alteration has affected all units, and has given rise to the Coarse-Grained Brown Syenite, which occurs in both the Lower and Upper Series. More intense alteration has affected the syenites, giving carbonate-rich 'carbosyenites', and xenoliths of country rock within the syenites and carbonatite; the surrounding country-rock is not as severely affected as might have been expected. The presence of zircon, alkali mafics, sodalite veins, and recrystallisation of feldspar in the altered rocks is attributed to the effects of peralkaline, Cl- and CO_2-rich late-stage fluids derived from both the syenites and carbonatite.

CONTENTS

CHAPTER 4: MINERALOGY

CHAPTER 5: GEOCHEMISTRY

CHAPTER 6: CARBONATITES

CHAPTER 7: METASOMATISM AND ALTERATION ASSOCIATED WITH THE COMPLEX

COPYRIGHT

ACKNOWLEDGEMENTS

There are numerous individuals and organisations who have assisted me in the course of this thesis, but several are particularly worthy of mention. Firstly, I would like to thank the Natural Environment Research Council for financing the project with grant GT4/86/GS/127, and for assistance with travelling expenses and course fees.

At Durham, I am very grateful to Dr. C.H. Emeleus for his support and assistance, particularly in the field and during the final stages of the project. For instruction in the use of electron microprobe facilities, Drs. A. Peckett (Durham), J. Craven, P. Hill (Edinburgh), D. Plant, and T. Hopkins (Manchester) have put their time and facilities at my disposal, for which I am very grateful. For whole-rock analyses, I am indebted to Dr. P. Leat for assistance and instruction in the use of the neutron activation facilities at Durham, and to Mr. Ron Hardy for great perseverance with the XRF. Ron Lambert and George Randall are thanked for the preparation of countless thin-sections of a high quality, and Paul Laverick for the use of the geochemistry laboratory. Dave Asbery and Dave Schofield provided constant assistance with numerous sundry favours. My postgraduate colleagues, Simon Day and Dr. Nick Pearce, provided many varied and stimulating discussions on the subject of igneous petrology (among other things). The computer programs used during the course of this work were written by Nick Pearce, without which this thesis would have taken considerably longer to complete.

Assistance with the fieldwork was provided by the Grønlands Geologiske Undersøgelse, who are thanked for the hire of equipment, and Laurits Møller & Sønner for their excellent ration boxes. At Grønnedal, I am extremely grateful to the Admiral of the Base for putting the facilities of the officers mess at our disposal, Leif and Anne-Marie Vangaard for their hospitality, and all members of the Base who assisted with the setting up and movement of the field camps.

Finally, my deepest thanks go to Teresa Knight for giving me the first opportunity to sample the geology of the Gardar, and for continuing moral support throughout the course of this work.

FRONTISPIECE: Looking NNW from the head of Urdal, with the Xenolithsø just visible on the right of the field of view. The foreground and cliffs to the left of centre in the middle distance consist of Upper Series Syenite, to the right of which the carbonatite forms a more gentle escarpment. The hill to the right of centre consists mainly of Xenolithic Porphyritic Syenite, while in the far distance, the Ketilidian granite complex of the Pyramidefjeld massif (1130m) can be seen.

CHAPTER 1: INTRODUCTION

1.1: Geographical setting and terrain

Lying in the north-west of the province (fig. 1.1.1), Grønnedal-Íka is one of the smaller Gardar complexes, its present elongate outline measuring 8km NNW-SSE, and 3km NE-SW. In contrast with the majority of Gardar centres, it forms relatively gentle topography, the syenites and carbonatites weathering easily to form rounded, scree covered hills rising to a maximum height of 585m. An important effect of this is that while the exposure is not as good as in other complexes, what is present is usually accessible.

A glacially carved 'bowl' forms the central area, floored by thick, well-vegetated moraines, giving rise to the 'Green-Valley' (Grønne Dal) from which the complex takes part of its name. Exposure here is minimal, but improves dramatically on the surrounding higher, rockier ground, especially in the NW of the complex. Lakes to the east and south of the Grønne Dal drain into Arsûk fjord by rivers and streams which carve deep ravines in the moraine, down to the bedrock, and offer some of the most continuous exposures in the complex. In the south-east, the steep-sided SW-NE trending Íka fjord cuts across the extreme south-east corner of the complex, giving rise to the least accessible part of the area.

There are no Inuit villages present, the only settlement being the Danish Naval base of Grønnedal where the Bryggerens Elv, draining the Grønne Dal, enters Arsûk fjord, from which a rough track runs in an easterly direction to a hut, Jernhat, at 400m altitude in the centre of the carbonatite area.

Grønnedal experiences the usual vagaries of Greenland weather, though its exposed location relatively near to the open sea results in the area being especially prone to poor weather, and particularly sea-fog or low cloud, often resulting in a late start to the days work.

Fig. 1.1.1

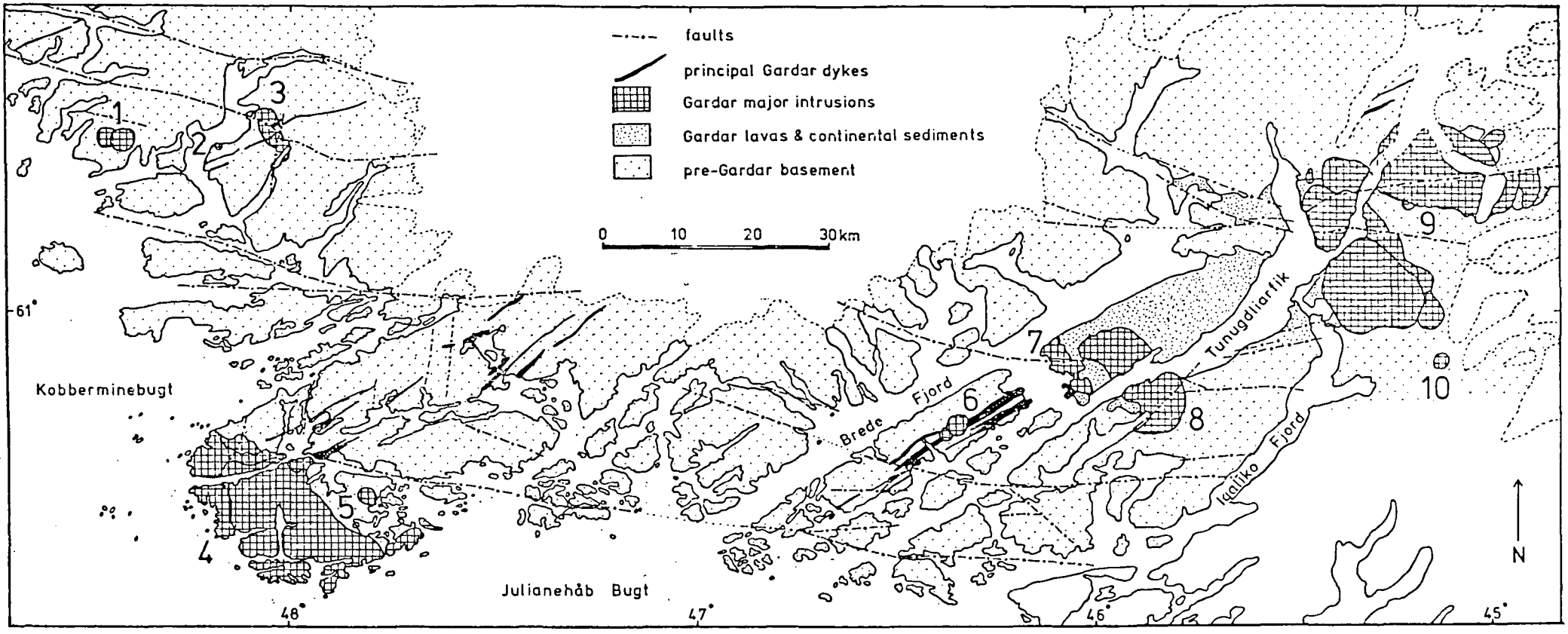

General geological map of the Gardar Province showing major faults, positions of main dyke swarms and major intrusive complexes: 1 Kûngnât, 2 Ivigtut, 3 Grønnedal-Íka, 4 Nunarssuit, 5 Puklen, 6 Central Tugtutôq, 7 Dyrnaes-Narssaq, 8 Ilímaussaq, 9 Igaliko, 10 Klokken.

Stable scree areas are generally well-vegetated with mosses, arctic flowers, and dwarf birch, areas of the latter proving particularly difficult to cross. Arctic foxes were common around the camps and near to the base, scavenging in the refuse tips, while several muskox were observed on the day that they were introduced into the 'commune' (bounded by Arsûk fjord, Qôrnoq, and the ice-cap) as a scientific experiment, though nothing more was seen of them after this. The reader is referred to other workers for descriptions of the ubiquitous mosquitoes, which give way to black-flies at the beginning of August in this, one of the worst affected areas in the whole of south-west Greenland (Emeleus *et al.*, pers. comm.).

1.2: General geology and relationships to Gardar igneous activity

A brief outline of the basic geology of the complex will be given here, and an attempt to relate this to events occurring in the Gardar on a larger scale. A summary of Gardar geology is given by Emeleus and Upton (1976) and an up to date synthesis by Upton and Emeleus (1987).

Lying in the border zone between the Ketilidian mobile belt to the south and the Archaean block to the north (fig. 1.1.1), the country-rocks around the complex consist of banded quartzo-feldspathic gneisses with occasional amphibolites. The latter were intruded during the Ketilidian and Archaean, while the gneisses are regarded as reworked Archaean rocks (Henriksen 1969).

Intra-plate alkaline magmatism in south-west Greenland between 1320 and 1120 Ma (the Gardar) can be related to repetitive rifting within the Proterozoic supercontinent which was composed of present-day North America, Greenland, and Europe (Piper 1982). Three main cycles of igneous activity have been proposed (Early, Mid, and Late-Gardar), each commencing with uprising of olivine-basalt or hawaiite magmas during crustal extension, and terminating with emplacement of the central complexes towards the end of the extensional phase. Exceptions to this, however, include the South Qôroq and Igdlerfigssalik centres, which were

emplaced at the start of the Late-Gardar cycle. Lying to the north of the province and consisting mainly of just-peralkaline to subalkaline nepheline-normative syenites (foyaites), Grønnedal-Íka is consistent with the observation that oversaturated centres predominate in the south while undersaturated centres tend to occur in the north.

The Grønnedal-Íka complex has been dated at 1299±17Ma (Blaxland *et al.* 1978), making it the oldest of the central complexes, emplaced at the end of the Early-Gardar cycle. In the well-exposed north-west region of the complex, two syenite units were distinguished by Emeleus (1964), who used these to show that movement along a major EW-trending pre-Ketilidian line, the Laksenæs fault (Henriksen 1960) continued into the Gardar. The Lower Series syenites ('syenite' used here when 'nepheline-syenite' is implied, unless otherwise stated), form a crescentic outcrop in the north-west of the area, separated from the Upper Series syenites forming the bulk of the complex, by a gneiss 'raft'. Both series are well laminated, as defined by tabular orthoclase crystals, the lamination dipping towards the centre of the complex. A marginal suite of syenites is developed in the north-west, concentric to the Lower Series, and possibly cogenetic with them, while a pyroxene-rich facies of the Upper Series contains possible mafic layering. Microsyenite dykes and sheets cut these syenites, possibly representing quench facies of these rocks.

Forceful emplacement of a magma rich in phenocrysts (?xenocrysts) and xenoliths of the earlier crystallised syenites then took place, forming a central stock-like intrusion several hundred metres across. This was followed in turn by a carbonatitic magma, similarly rich in xenoliths and cutting earlier units to form a central plug, and completes the plutonic igneous activity of the area. This occurrence of carbonatite is the most significant in the Gardar, and is apparently unrelated to any ultramafic lamprophyres, as has been proposed for some of the minor occurrences elsewhere in the Gardar (eg. Qagssiarssuk, Stewart 1980), but which do

not outcrop at Grønnedal. However, Pearce (1988), working on dykes from the Igaliko complex, has suggested that CO_2-saturated phonolitic magma may have been a source for the carbonatite dykes there.

Following emplacement of the Early-Gardar complexes, basic dykes of Mid-Gardar age were intruded across the whole region, the latest of which were doleritic in composition (so-called 'brown dykes'). Three generations of these (BD0,1,2) cut across the syenites at Grønnedal, while a fourth (BD3) is recognised elsewhere. Observed displacements along these dykes has enabled the post-intrusive offset along the faults to be determined, movement along which throughout the Gardar period has led to considerable distortion of the outline of the complex (Emeleus 1964). Finally, a sub-parallel swarm of alkaline dykes of phonolitic, trachytic, and lamprophyric compositions (distinct from the microsyenite dykes and sheets which are related to the formation of the complex), trending roughly ENE-WSW, represents a resurgence of alkaline activity in the area, possibly of Late-Gardar age. These do not form part of the work in this thesis, but have been extensively studied by Gill (1972a,b).

1.3: Previous research

Although the earliest record of nepheline-syenite in the area was made by Taylor in 1855, it was not until the early 20th century that the first attempt at systematic mapping was undertaken by N.V. Ussing and O.B. Bøggild. Other early observations of significance were made by Holst (1886), with the discovery of 'limestone' with iron-ore near Íka, and by Callisen (1943), who made the first petrographic distinctions between the syenites and investigated their igneous relationships.

The first detailed mapping of the area was carried out by Emeleus over three field seasons between 1956 and 1960. He distinguished the Lower and Upper Series syenites, separated by a gneiss 'raft', the late-stage forceful emplacement

of xenolithic syenite and carbonate plugs, and a marginal suite of rocks in the north-west of the complex. The recognition of the extent of the faulting in the area was also of significant importance, allowing a restoration of the complex to be made, and the unfaulted margins and contact relationships to be postulated.

The first detailed geochemical study of the complex was made by Gill (1972a) who explained the chemical variations across the units described by Emeleus in terms of the nature and proportion of the phases fractionating. He also examined the chemical relationships between the units, and distinguished three primary magma types, as well as investigating in detail the later alkaline dykes in the area.

Most recently, a survey of the economic potential of Grønnedal-Íka in terms of niobium and phosphorous was made by Morteani *et al.* (1986), and compared with that of the Motzfeldt centre, Igaliko. This investigation, which included a few microprobe and bulk-rock analyses, concluded that no workable quantities of niobium were present, though some units, particularly the carbonatite, contained significant amounts of phosphorous.

1.4: Aims

This work follows a similar pattern to that of Stephenson (1973), Chambers (1976), and Jones (1980) on the South and North Qôroq, and Motzfeldt centres respectively. It supplements the bulk-rock geochemical work of Gill (1972a) on Grønnedal-Íka, who ignored the carbonatites and concentrated instead on the syenites and alkaline dykes. The latter are not considered, while the carbonatites and syenites are the subject of this thesis.

Detailed and systematic microprobe investigations of the mineralogy of all of the rock units was made to observe the evolution of the physical and chemical characteristics of the Grønnedal-Íka magma types, and to make comparisons with

other Gardar central complexes. Unusual compositions have been investigated, together with the rare-earth element (REE) abundancies of certain phases (apatite, zircon), to amplify the work of Morteani *et al.* (*op. cit.*).

Bulk-rock major and trace-element geochemistry was undertaken for comparison with Gill's work and to investigate genetic relationships between the syenites. Using this and REE data from neutron-activation analysis, the aim was to derive a petrogenetic model for the complex, and to constrain the nature of the source or sources.

The carbonatites are examined in some detail, and compared with the Igaliko carbonatite dykes (Pearce 1988). Using REE data, any relationships to other units exposed in the complex are investigated in an attempt to determine their origin and subsequent evolution.

Finally, the metasomatic alteration of the country-rock and of the syenites themselves is investigated to determine the nature of the metasomatising fluids, whether from the syenites, the carbonatites, or from both. This will be compared with similar alteration in the North Qôroq centre which has lead to the growth of late-stage alkali feldspars (Rae and Chambers 1988), and with other parts of the world where metasomatic alteration associated with alkaline complexes has occurred.

1.5: Fieldwork and sampling

Fieldwork and sampling were carried out over six weeks in July and August 1987 from two camps within the complex. Most of the time was spent in the Grønne Dal, 1.5km up the road from the base to the hut, from where the central and southern part of the complex was studied. A second camp was set up at the outlet of the Kontaktelv for one week in order to examine and sample the well exposed rocks in the north-west of the area. The small size of the complex and

the relatively straightforward terrain meant that moving and setting-up camps could be done easily, with help from the base.

Using the geological map of Emeleus (map 1, back of thesis), observations were made of the contacts between units and the margins of the complex, together with a comparison of the various lithologies. It was intended to supplement the samples collected by Emeleus in the 1950's and by Gill and Stephenson in 1973, by making systematic transects across the units with a view to collecting for XRF and microprobe analysis. Samples of 1.5 to 2kg were taken due to the generally coarse grain-size of the rock, and located using aerial photographs or the geological map, whichever was thought to be the most accurate. However, the generally poor exposure meant that good coverage was not easy to obtain, as part of the transect would inevitably cross poorly-exposed or badly-weathered ground. Good, continuous, though not always accessible exposure could be found in the ravines which cut through the moraine in the central part of the area (eg. Bryggerens Elv, Radioelv), while in the well-exposed north-west part of the complex, several detailed transects were obtained through the marginal syenites, and into the Lower Series.

It is likely that by more concentrated sampling in one region of the complex (such as in the well-exposed north-west), and by collecting fresh samples as far as possible, a bias may be introduced. Despite the difficulties, though, much care and effort was taken in an attempt to build up a representative collection of samples from each of the units over as large an area as possible.

CHAPTER 2: FIELD RELATIONSHIPS

2.1: Introduction

As field and petrographic descriptions are given by Emeleus (1964), this chapter introduces new field observations made during the 1987 field season. On fresh, unweathered surfaces, the different units are usually easy to distinguish using Emeleus' descriptions, though variations in the modal proportions of nepheline, feldspar, biotite and pyroxene (the principle phases) and grain size, sometimes cause confusion. This is particularly the case in 'disturbed' areas, such as adjacent to the gneiss raft in the Bryggerens Elv, and in the Radioelv between the Upper and Lower Series, where intermingling of magma-types appears to have occurred in a zone *c.*300m wide (cf. section 2.4).

As described in chapter 1, exposure is not always good, and even where present, the rock is often so badly weathered that it is impossible to obtain a fresh surface for examination. A certain type of alteration has also resulted in the weathering-out and staining of the material between the feldspars, giving a false impression of the proportion of mafic minerals present, as on the north-west shore of the Langesø, in the Upper Series.

Bearing these problems in mind, there was found to be little disagreement between the observations made in 1987 and the geological map of Emeleus (map 1), though some areas of discrepancy were found. The eastern boundary of the gneiss outcrop in the Kontaktelv was observed to be further to the west than indicated by the map, so that syenite of the Lower Series was found where tributary joins from the south-east. In addition, to the north-west of the Langesø, the pyroxene-rich syenites did not appear to outcrop on the lake shore, but were found higher up the hillside. Finally, the exposures in the tributaries of the Bryggerens Elv have been recorded as belonging to the Upper Series Syenite as opposed to the Coarse-Grained Syenite, due to a greater resemblance of the rock to the former

than the latter. These alterations are shown on map 3, the sample locality map for the 1987 field-season.

2.2: The country-rock

The syenites were emplaced in well-foliated quartz+feldspar±biotite gneisses, which are occasionally altered and recrystallised, especially where they occur as xenoliths within the syenites (chapter 7). In the north-west, an arcuate outcrop of quartzo-feldspathic gneiss *c.*500 × 1500m in size separates the Upper and Lower Series Syenite, possibly having spalled-off the roof of the intrusion (Emeleus 1964), while near the north-west margin, gneiss occurs interleaved with sheets of granular syenite. As mentioned in section 2.12, these syenites have a rather gneissose appearance themselves, making this a confusing area to examine and sample.

Foliated augen gneiss occurs adjacent to the syenite on the south-east side of Íka (samples G113 and G114, map 3), while on the shores of the fjord, highly contorted schistose rocks were found (G105 and G106). These very strongly metasomatised rocks have distinct blue tinge due to impregnation by sodic amphibole (chapter 7, plate 7.3), and may correlate with the Sermilik Group of metasediments on Arsuk Ø, 12km to the WSW (Wegmann 1938).

2.3: Lower Series Syenite

This is the best exposed of the syenite units, and forms a crescent-shaped outcrop in the north-west of the complex, while to the west it outcrops on the north-east flanks of Rypefjeld and in the Radioelv gorge.

The rock is generally coarse-grained with variable amounts of alkali feldspar (*c.*10mm × 7mm × 1-2mm), nepheline, alkali pyroxene, and biotite (all generally equant, 2-4mm in diameter; plate 2.1), the tabular feldspars defining a distinct lamination which dips towards the centre of the intrusion and steepens towards the margins. On a large scale, this lamination manifests itself as a series of terraces,

the dip-slopes of which are directed towards the centre of the intrusion, parallel to the orientation of the feldspars. These features were also observed on aerial photographs of the area, where they appear as a series of distinct pale-coloured ridges parallel to the trend of the Lower Series outcrop.

Two distinct facies of this unit were identified in the field, with a gradation of rock-types between the two end-members. The first of these, forming the bulk of the Lower Series, is grey in colour, and appeared to be relatively unaltered, though often crumbling to a gravel with only very light hammering. The second facies occurs as rusty-weathering outcrops and appears to be the same rock-type as mapped by Emeleus as Coarse-Grained Brown Syenite and is thus described in section 2.7.

The proportion of mafic and felsic minerals varies considerably, in extreme cases resulting in a rock composed almost entirely of alkali-feldspar (pulaskite), equivalent to the type IV syenite distinguished by Gill on a geochemical basis (1972a). This pulaskitic facies is variably developed, though with a slight tendency to be more extensive towards the top of the unit.

Other features observed in 1987 were rare xenoliths of a biotite-rich Lower Series-type syenite, and fine grained, mafic-looking clots a few centimetres in size, around which the feldspars are flow-banded, occurring on the north-west side of the Cirkus.

2.4: Upper Series Syenite

This unit is the most extensive in the complex, forming an elliptical outcrop measuring 3.3km × 4.8 km on the reconstructed map (map 2). It is generally distinguished from the Lower Series Syenites by the coarser grain-size of the feldspars (17mm × 12mm × 3mm), though the distinction is sometimes unclear. For example, in the Radioelv at the junction of the Upper and Lower Series Syenite, variations in the degree of lamination and proportions of mafics results in a banded,

almost gneissose appearance over a zone several hundred metres across. A large body of gneiss was observed in the lower parts of the stream and 500m to the north-east in the Bryggerens Elv, and it is possible that the disruption has resulted from fragments of country-rock which have sunk through the magma. As mentioned in the introduction, this unit also outcrops in the central part of the complex, in the Bryggerens Elv gorge, and is clearly different from the much coarser 'Coarse-Grained Syenite' described in section 2.8. The syenites are laminated, though not quite as finely as in the Lower Series, probably due to the coarser grain-size of the feldspars. Poorly laminated areas are quite common, especially on the shores of Nedre Radiosø, and on the peninsula on the north-west shore of the Langesø, possibly caused by a reduction in the strength of magmatic convection currents which might otherwise tend to orientate the feldspars.

The mineralogy is broadly similar to that of the Lower Series, though there is a greater tendency for large variations in modal mineralogy in the Upper Series. A facies very rich in nepheline (up to *c.*70%) was observed, which is not simply an artefact due to alteration rendering the nephelines more clearly visible. This facies occurs as dykes and veins which penetrate blocks of gneiss within the Upper Series in the Bryggerens Elv (sample G238), and on the north-west flanks of the 410m peak to the west of Jernhat (sample G72). Accumulations of mafic minerals also occur quite commonly, in the form of smeared-out patches and streaks on a scale of millimetres to tens of centimetres. These *'schlieren'* occur throughout the Upper Series, but are particularly well-exposed on the south-east shore of Íka fjord, where the feldspar lamination appears to wrap around the edge of the schlieren (plate 2.2). Stephenson (1973) suggests that such mafic accumulations may be the result of slumping of crystal-rich 'slurry' in the South Qôroq centre, although it cannot be ruled-out that they may have formed as a result of concentrations of expelled interstitial liquids as a result of compaction, and distorted during continued compaction.

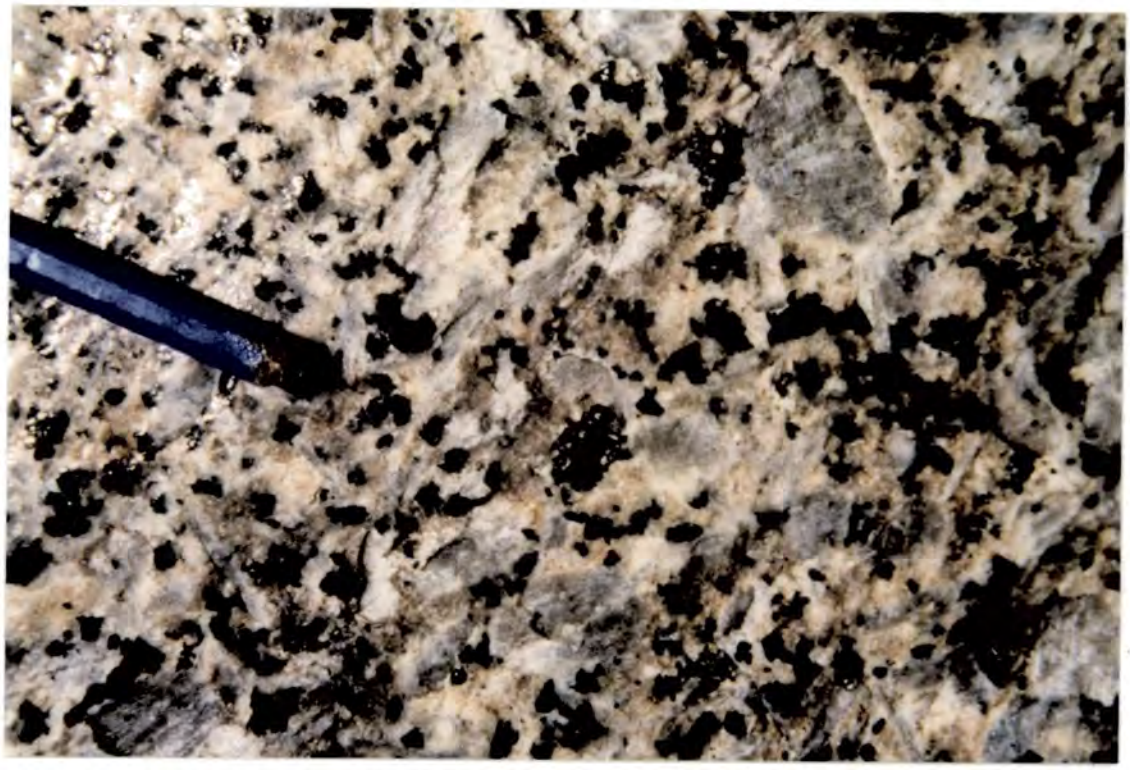

Plate 2.1. Lower Series Syenite exposed in slabs of the Kontaktelv gorge, clearly showing the mineralogy. The dominant phase is alkali feldspar (grey, tabular), though the lamination is not particularly obvious in this view. Pink nepheline is also clearly visible, together with poikilitic plates of biotite enclosing smaller grains of nepheline. The smaller, more euhedral dark grains are aegirine-augite.

Plate 2.2. Mafic schlieren of in Upper Series Syenite on the south-east shore of Íka fjord. The highly contorted nature of the schlieren and the 'swirled' feldspars are suggestive of deposition by slumping of mafic accumulations as has been proposed for similar textures in the South Qôroq Centre by Stephenson (1973). Hammer head is 12cm long.

2.5: Mafic Upper Series Syenite

This unit, up to *c.*400m in width, forms an intermittent horizon within the Upper Series Syenite, which is rather indistinct near the Radio lakes in the south, but more continuous in the north and north-west.

Mineralogically and texturally, the rock is similar to the Upper Series Syenite, but with a greater proportion of pyroxene at the expense of alkali feldspar and nepheline, so that in places it approaches the composition of malignite (50% pyroxene, 25% alkali feldspar, 25% nepheline). The proportion of pyroxene is very variable, though, so that this unit grades into Upper Series Syenite above and below. Nepheline is sometimes very scarce or even absent.

Layering has been described from a locality within this unit, 200m south-east of Toffelsø (Emeleus 1964, and plate 2.3, this volume), where centimetre-thick layers of pyroxene are developed parallel to the lamination, continuous for several metres, and grading laterally into more diffuse areas of mafic schlieren. This was the only example of mafic layering seen in either the mafic or non-mafic Upper Series Syenite, where the pyroxene-rich layers are parallel to the feldspar lamination, though irregular areas of schlieren are very common.

2.6: Granular Syenites

These rocks form a distinctive marginal facies, occurring as a series of narrow (<100m wide), steeply dipping, cross-cutting, sheet-like bodies concentric to the outer margins of the Lower Series Syenite and Coarse-Grained Brown Syenite in the north-west of the complex. Two types of Granular Syenite were distinguished, and designated 'GS-A' and 'GS-B'.

2.6.1 GS-A

This unit, equivalent to Gill's 'GS-2' (Gill 1972a), is a fine to medium grained rock, characterised by an abundance of sharp, prismatic pyroxenes, sub-millimetre

Plate 2.3. 'Mafic layering' in the Mafic Upper Series Syenite, 250m south-east of the Tøffelsø in the north-west of the complex (see also Emeleus, fig. 4). The pyroxene-rich layers are parallel to the lamination, which dips towards the centre of the intrusion at around 50°, and are laterally continuous for several metres. Hammer head is 12cm long.

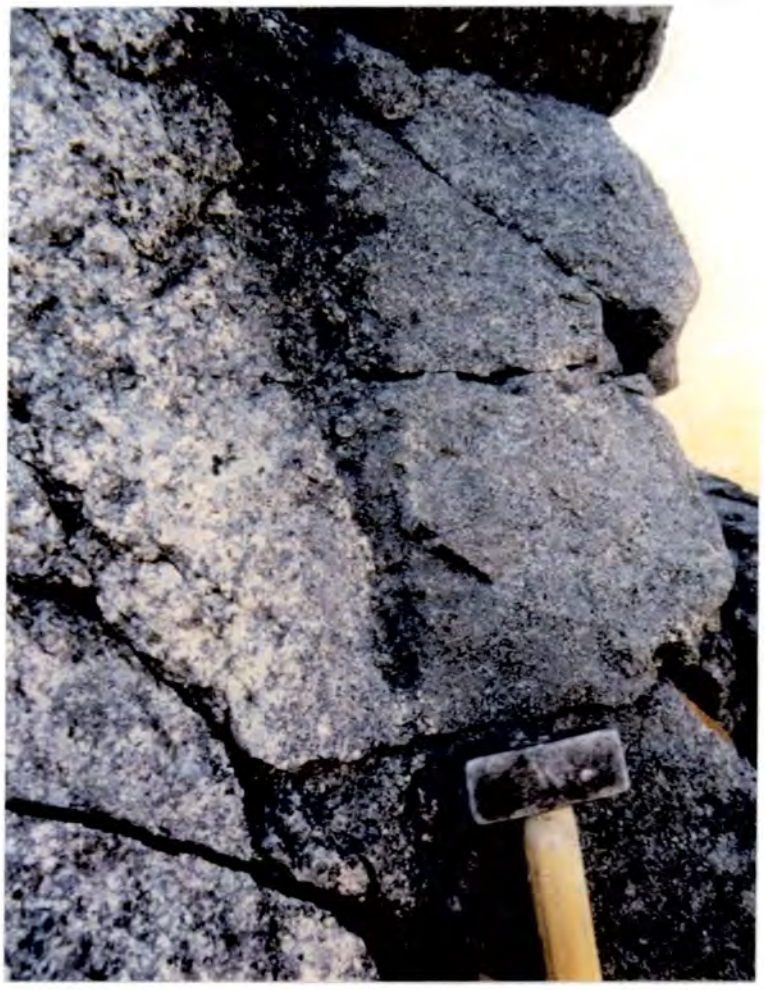

Plate 2.4. Contact of GS-A (to the right) against GS-B (to the left). The grain-size of the former decreases towards the latter, suggestive of a chilled contact and later emplacement. The steep, outward-dipping contact and overall shape of the outcrop of GS-A is suggestive of a ring-dyke (Emeleus 1964).

to a few millimetres in size, and randomly orientated tabular feldspars up to 10mm × 7mm × 2mm. It appears to form a ring-dyke, cutting across the country rock gneisses and GS-B on the north-west side of the complex, and is seen in steeply outward-dipping contact with the latter at one locality (plate 2.4). The contact is quite sharp, the change from GS-A to GS-B taking place over a few millimetres, with the ring-dyke chilled to a sub-millimetre grain-size over a distance of several centimetres.

2.6.2 GS-B

More abundant than GS-A, this unit occurs as sheets cutting country-rock gneiss, the Coarse-Grained Brown Syenite, and the lowest parts of the Lower Series Syenite. It is equivalent to Gill's GS-1 syenite, and Emeleus' biotite-rich syenite. As this name would imply, it contains plates of biotite up to 12mm in size, with equant as opposed to tabular feldspars, which are only weakly flow-orientated. The rock has a medium grain-size, with most crystals a few millimetres in diameter, while modal proportions of the mafic minerals are somewhat variable, leading to a heterogeneity on a centimetre to metre scale. Small-scale mafic layering was even observed at one locality, with a sharp, crenulate-based mafic layer grading upwards into less-mafic syenite over several millimetres (plate 2.5).

Slight grain-size reduction towards the country-rock occurs, indicative of chilling adjacent to the margins, but as with all other units of this complex, sharp contacts were not observed (cf. section 2.12).

2.7: Coarse-Grained Brown Syenite

This is marked on the geological map (map 1) as a fairly continuous unit lying on the north-west (outside) of the Lower Series Syenite, and is thought to be a continuation of this unit (Emeleus, pers. comm.). In the field, however, though very common in this area, it passes repeatedly into Lower Series Syenite both across and parallel to the strike of the lamination over a few tens of metres (plate

Plate 2.5. Small-scale mafic-layering in GS-B. In contrast to the layering in the Mafic Upper Series Syenite (plate 2.3), this shows an irregular (though still sharp) base, and grades upwards into more homogenous rock. Hammer head is 5cm in diameter.

Plate 2.6. Looking down strike of the lamination in the Lower Series Syenite, towards Eqaluit (middle distance) and Arsûk fjord (far distance). Brown-weathering syenite reminiscent of the Coarse-Grained Brown Syenite passes repeatedly into unaltered grey syenite and back again.

2.6). Additionally, it is patchily developed in the Upper Series Syenite, and is thus regarded as an alteration facies of the laminated syenites which is far more widespread than map 1 would suggest.

Texturally, it is distinct from the Lower or Upper Series Syenites in being both coarser (tabular feldspars often exceeding 20mm across), and very poorly laminated. The feldspars are characteristically bleached on weathered surfaces, while the rock as a whole is rust-brown in colour, possibly due to leaching of iron from the feldspars, and redeposition on the surface as oxides. A green, interstitial micaceous mineral is common, probably from alteration of original mafics, and resinous-brown octahedra of zircon, which were found up to 10mm across from a pegmatitic patch in the Coarse-Grained Brown Syenite, *c.*1.5km due north of the Base (sample G258).

2.8: Coarse-Grained Syenite

This distinctive, minor syenite body outcrops at the head of Urdal where it is disrupted by shearing and faulting (section 2.13). As the name suggests, it is extremely coarse grained, with euhedral nephelines up to 20mm across, tabular alkali feldpars up to 50mm in diameter, and altered interstitial mafics (plate 2.7). The rock is very poorly laminated, and appears to grade into the Upper Series with decreasing grain-size. These exposures bear little resemblance to the rocks in Bryggerens Elv, identified as Coarse-Grained Syenite by Emeleus, which are correlated with the Upper Series Syenite on the basis of field evidence in this work.

2.9: Xenolithic Porphyritic Syenite

This, the youngest of the intrusive syenites at Grønnedal-Íka, forms an extensive outcrop to the west of the Langesø around the 530m peak, together with minor outcrops some tens to hundreds of metres across to the south and west. It

forms characteristic angular weathering outcrops, with the rock itself breaking to give very sharp fragments.

The xenoliths, which range from millimetre-sized groups of crystals to metre sized blocks, are sharply-bounded and very angular, as if formed by explosive fracturing of the country-rock. The distribution of compositions present as xenoliths appears to reflect the local rock-types which occur around each outcrop, eg. Upper Series Syenite is abundant in the main outcrop, and Coarse-Grained Syenite in the minor intrusions at the head of Urdal. Occasional fragments of gneiss and a fine-grained basic material (?basement amphibolite) occur, though the commonest rock of all is a fairly coarse granular syenite, which does not resemble any of the rocks exposed, but is presumably present at depth.

The host-rock itself consists of fine-grained (millimetre to sub-millimetre) pyroxene, nepheline, and alkali feldspar, with phenocrysts (?xenocrysts) of these phases, a few millimetres in size. The feldspars are often flow-orientated around the xenoliths, and become increasingly abundant towards the top of the unit (sample G134), possibly grading into Upper Series Syenite which is present on the summit of the 530m peak (sample G135).

The distribution of both phenocrysts and xenoliths is rather uneven, with areas very poor in both occurring in the north-west part of the outcrop, which is here very feldspathic. Contacts with the country-rock (usually Upper Series Syenite) are very difficult to trace even in very well-exposed areas, due to the strongly brecciated, highly irregular nature of the margins. It is seen chilled against Upper Series Syenite just south of the 530m peak.

Carbonated Xenolithic Porphyritic Syenite

To the east of the Cirkus, between the 510m and 530m peaks, a dyke-like body of highly xenolithic, porphyritic, amygdaloidal rock occurs. Well-rounded xenoliths of Xenolithic Porphyritic Syenite, amphibolite, and syenite, a few centimetres

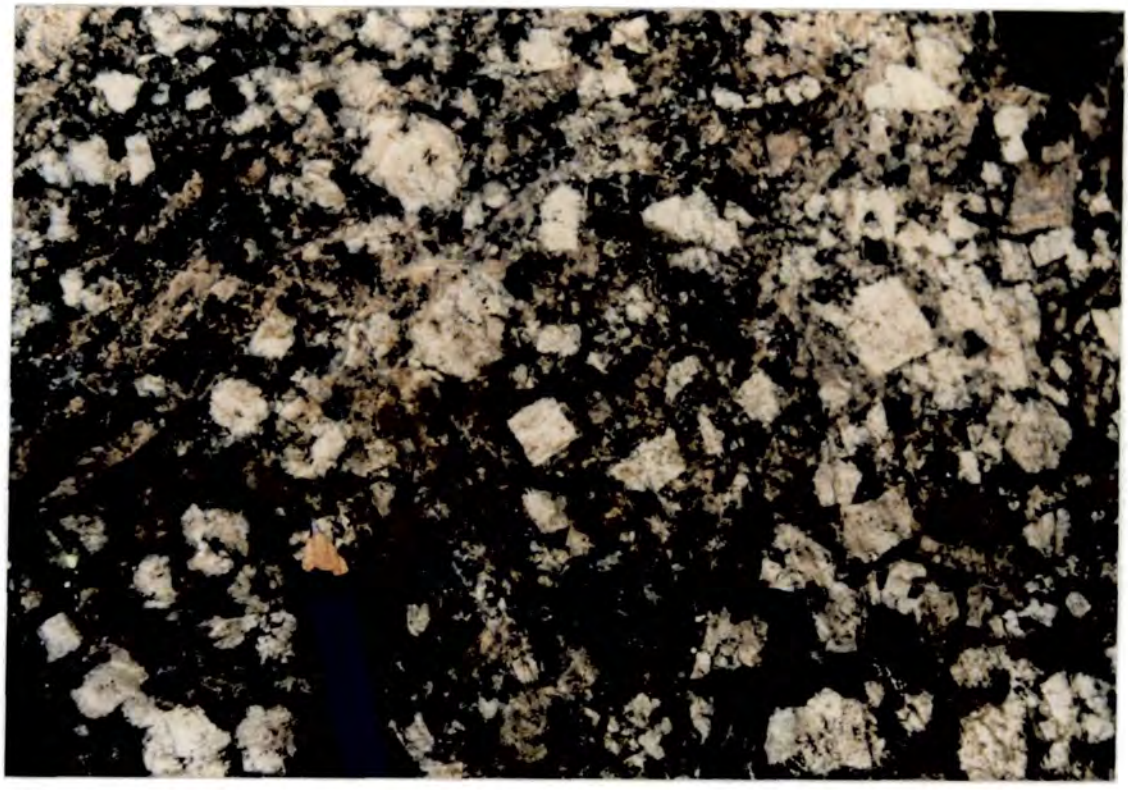

Plate 2.7. Coarse-Grained Syenite, showing prominent euhedral nephelines up to 2cm in diameter. Dark green interstitial pyroxenes can also be seen, and tabular alkali feldspar above and to the left of the pencil point.

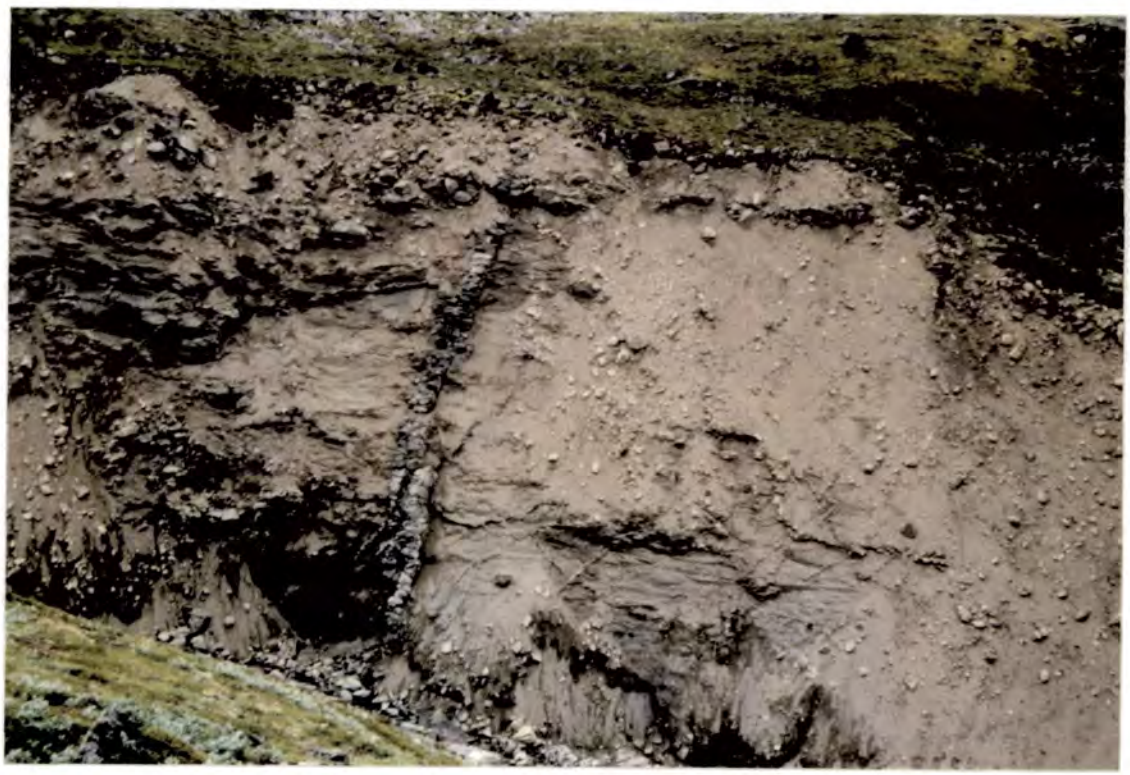

Plate 2.8. Variation in degree of weathering of microsyenite dykes and Lower Series Syenite in the Kontaktelv gorge. The dykes are more resistant, while the syenite weathers easily to a gravel, with narrow, more resistant veins as a result of impregnation by deposited material. The weathered face is around 60m high.

to tens of centimetres in size occur in a dark microcrystalline, carbonate-rich matrix, with phenocrysts of nepheline and alkali feldspar, a few millimetres in size. Two samples of this peculiar, carbonated variety of xenolithic and porphyritic syenite were collected (G58, G136).

2.10: Porphyritic Microsyenites

This section describes those fine-grained syenites with varying proportions of tabular feldspar and occasionally nepheline phenocrysts, which occur as dykes and possibly sheets cutting across earlier units of the complex. They are evenly distributed throughout the Upper and Lower Series Syenite, and are far more numerous than Emeleus' 1964 geological map (map 1) suggests. The group does not include the later alkaline dykes, which represent a (?Late Gardar) resurgence of alkaline activity in the area (Gill 1972b) and are aphyric, nor the marginal microsyenites, which are described in section 2.12. In general, the Porphyritic Microsyenites are less susceptible to weathering than the laminated syenites (plate 2.8), possibly due to tighter packing of the grains than the more open framework of the coarser units.

Set in a sub millimetre-sized groundmass, the tabular feldspar phenocrysts are frequently flow orientated. Where the rock occurs as dykes (tens of centimetres to 1m across), it tends to be poorer in phenocrysts, but where present, these are are aligned parallel to the trend of the dyke, the alignment increasing towards the margins due to greater liquid shear stress. Dyke margins tend to be knife-sharp, and pick-out indentations around feldspars in the Upper Series Syenite, which has split in a direction roughly perpendicular to the lamination in the rock (plate 2.9). Dyke orientations are very variable, and no consistent pattern emerges, though they are straight-sided and occasionally anastamosing, as in the Upper Series Syenite to the north-east of the Base.

Cutting the Upper and Lower Series Syenites and the gneiss raft in the north-west of the area are a series of microsyenites which tend to be richer in phenocrysts

(mainly feldspar) than the dykes, forming up to 70% of the rock. Flow orientation is common, but the margins to these exposures are rarely seen, so it is difficult to determine the form of the intrusions, whether dykes or sills.

2.11: Pegmatites

These occur either as patches within the syenites, or as veins and dykes which cross-cut earlier textures and structures. The former are present as irregular patches of a coarser grained facies of the surrounding rock, some tens of centimetres to 1m across. Sometimes diffuse, though usually sharply bounded, they may be the result of local concentrations of volatiles, and are particularly common in the Granular Syenites around the north-west margin of the complex (plate 2.10). Pegmatites also occur as dykes up to 1m across within the syenites, though also within the country-rock to the north of the complex. These consist mainly of nepheline, feldspar, and pale-green, coarse acicular pyroxenes, up to several centimetres in length (sample G183).

2.12: Marginal syenites and contacts with the country-rock

Though the actual contact of the syenites with the country-rock is very rarely exposed, it can usually be located to within a few metres, and is sometimes indicated by a change in slope, as on the northern side of the Kontaktelv, where the more resistant gneiss forms crags, while the more easily eroded syenite has weathered to form a more gentle slope below. Chilled marginal rocks are likewise rare, possibly due to intrusion into relatively hot country-rock, which could result in a very narrow zone of chilled rock which may be only rarely exposed. At one locality in the north-west of the area, Lower Series Syenite remains coarse right up to an area of gneiss in the Kontaktelv (plate 2.11). The orientation of the feldspar tablets suggests flow of magma adjacent to the gneiss, strong liquid shearing resulting in the alignment of crystals parallel to the margin, with no apparent chilling. Complex relationships exist between the GS-B variety of the Granular

Plate 2.11. Contact of Lower Series Syenite with metabasic gneiss in the lower part of the Kontaktelv in the north-west of the complex. The syenite shows no chilling against the gneiss, and the feldspars are flow-orientated parallel to the contact, suggesting that emplacement occurred as a crystal-charged magma into pre-heated country-rock.

Plate 2.12. Dyke of amphibole-rich marginal microsyenite intruding Upper Series Syenite. The amphiboles (dark spots *c*.5mm in diameter) are concentrated towards the dyke margin, possibly as a result of higher volatile concentrations adjacent to the country-rock.

Syenite and the country-rock in the north-west of the area. Here the syenite is streaky and rather gneissose itself, and though actual contacts are observed, chilling is again absent. However, in the Upper Series Syenite in the north of the area, chilling adjacent to the contact is observed at one locality (samples G37 and G38, map 3). Sample G37, 15cm from the contact itself, is a fine-grained (sub-millimetre), pale-coloured granular rock, with biotite plates around 1-2mm across. Sample G38, 50cm from the contact, is coarser, with millimetre-sized tabular feldspars defining a lamination which dips steeply northwards at around 80°, roughly parallel to the outward-dipping margin. Here, therefore, the 'chilled margin' is less than a metre in width, but in the south-west of the complex, 500m north-west of Nedre Radiosø, an area of very fine-grained microsyenite is seen a few metres from the country-rock gneiss (sample G64). Though the contact itself is not observed, the lateral extent and proximity to the country-rock of this unit suggests that this microsyenite represents part of a chilled margin.

The final type of marginal facies rock occurs sporadically, and is restricted to within a few metres of the margins of the intrusion, eg. just south of Tolvsøer (sample G44), further to the south in the screes above Íkasletten, and in the Radioelv. It is characterised by dark, equant amphibole crystals, 5-10mm across, giving the rock a spotted appearance. Generally very fresh, it occurs as patches and dykes some tens of centimetres in width, with the amphibole concentrated towards the margins (plate 2.12).

2.13: Faulting

Partly as a result of its location at the intersection of two major strike-slip faults, and partly because of its age (the oldest Gardar intrusion; section 1.2), the Grønnedal-Íka complex has suffered a considerable amount of deformation and faulting. Stephenson (1976b) has described how the elliptical shape of the complex and the faulting are the result of ductile deformation within a sinistral shear zone, which changed to brittle deformation (faulting) as the rocks cooled following

Plate 2.13. Looking north along the Urdal gorge, weathered-out along the main north-south trending dextral fault. The rocks forming the walls of the ravine are intensely altered and shattered, and impossible to sample. The waterfall in the foreground is around 20m high.

emplacement. The combination of this shearing, giving rise to the original NW-SE–trending elliptical outline, followed by later faulting, are the main factors responsible for the present outline of the complex.

On a small scale, well-defined shear-zones a few centimetres thick, and less well-defined zones several metres thick result in deformation of the constituent minerals in the Coarse-Grained Syenite at the head of Urdal. These outcrops occur near the intersection of the main north-south and ESE-WNW–trending faults, and may be the result of minor conjugate shears, giving rise to a sub-mylonitic fabric in the rock.

The two main WNW-ESE (sinistral) and N-S (dextral) faults weather-out as small valleys or even ravines (eg. the Urdal gorge, plate 2.13). They give rise to a zone of intense crushing and brecciation several metres to tens of metres across, associated with much carbonation and carbonate veining of the rock, possibly as a result of remobilisation of the carbonatite. In the upper part of the Bryggerens Elv, thickening of the outcrop of a large dolerite dyke occurs due to multiple faulting, and has also resulted in much alteration and brecciation, making the rocks difficult to distinguish in this region. Wedges of gneiss, dolerite, Xenolithic Porphyritic Syenite, Upper Series Syenite, and carbonatite, each some tens of metres across, all occur in this complex area. Horizontal slickensiding in the Hyttelv, on surfaces mineralised with blue amphibole and green pyroxene, shows that the last phase of movement, here at least, was a strike-slip motion.

CHAPTER 3: PETROGRAPHY OF THE SYENITES

3.1: General

This chapter describes the petrography of the syenite units, whose field appearance and relationships to each other were described in the previous chapter. As already mentioned (section 2.1), the metasomatised rocks and carbonatites form distinctive groups, and are described in separate chapters.

Some generalisations can be made concerning the textures and mineralogy of the rocks, which are characteristic of an alkaline, undersaturated bulk-rock chemistry, and in order of decreasing abundance usually consist of alkali feldspar+nepheline±aegirine-augite±biotite±apatite±opaques. All of these phases are usually present, though sometimes either biotite or aegirine-augite are absent, and very occasionally, both of these are missing. The alkali feldspar is almost always perthitic, often quite coarsely exsolved, with microcline sometimes acting as the host instead of orthoclase, and the nepheline is invariably partly or completely altered to the fine-grained micaceous mineral, gieseckite (plate 3.1).

As in the field, the degree of alteration seen in thin-section varies considerably, giving rise to a distinctive facies, the Coarse-Grained Brown Syenite (section 2.7) or in extreme cases, metasomatic alteration (chapter 7). Cancrinite is a common poikilitic mineral, usually associated with nepheline. It occurs as a low-relief, colourless mineral in plane-polarised light, but is prominent in crossed polars, with up to 2nd-order interference colours, and forms large (up to 2cm) poikilitic crystals partially or entirely enclosing the nephelines (plate 3.3). It results from late-crystallisation of CO_2-rich fluids, and increases in abundance with overall degree of alteration of the rock.

3.2: Lower Series Syenite

The dominant mineral is alkali feldspar, which occurs as simple-twinned, thin, tabular, euhedral to subhedral crystals, and forms up to *c.*60% of the rock by

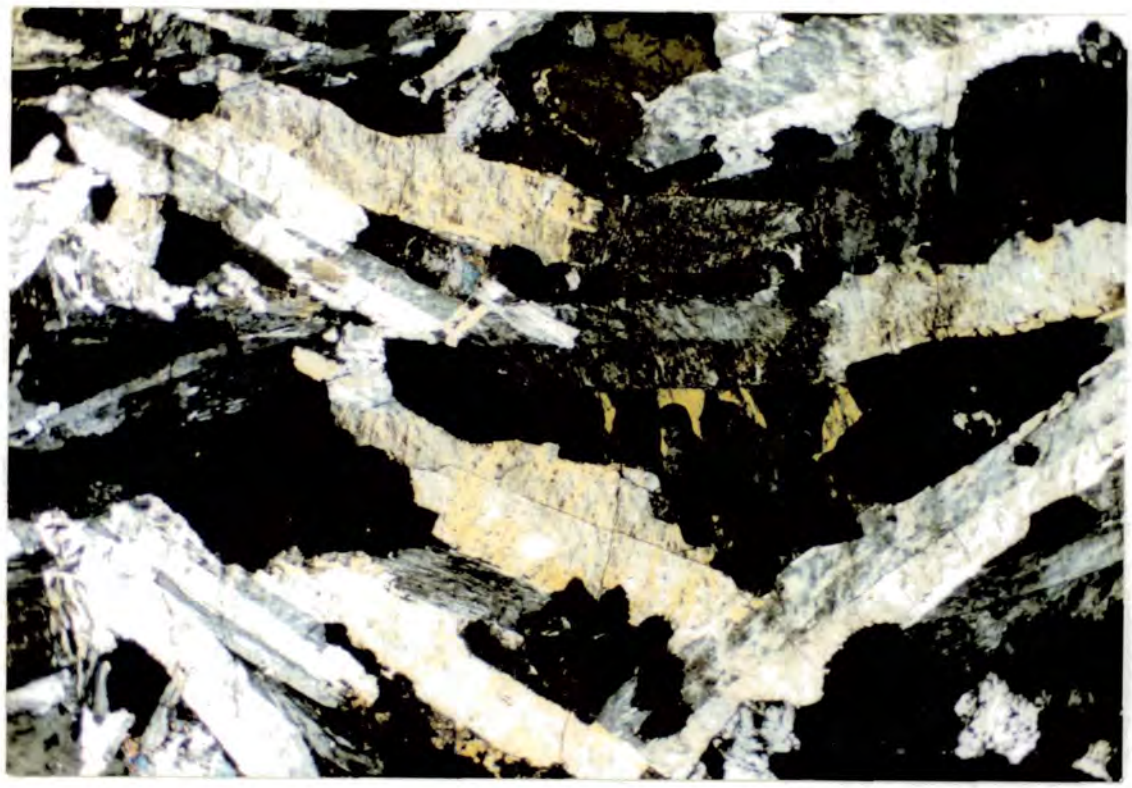

Plate 3.1. G232. ×11. XPL. Typical laminated syenite from the Upper Series. Tabular, perthitic alkali feldspars define the lamination, with aegirine-augite (just above and to the left of centre), and nepheline (mainly altered to brown gieseckite). Interstitial cancrinite (with yellow interference colours) can be seen in the centre of the field of view.

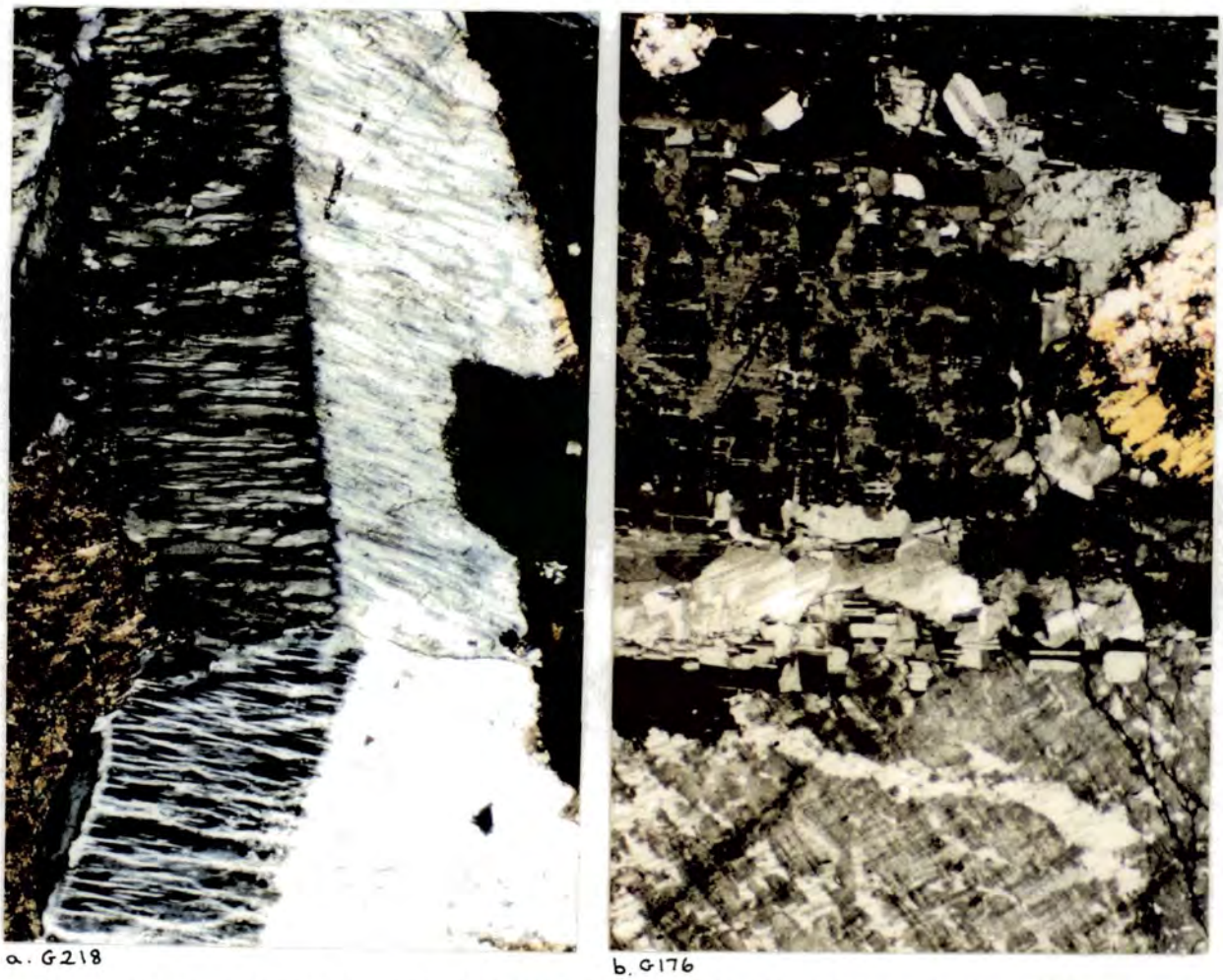

Plate 3.2a,b. G218, G176. ×35. XPL. Plate 3.2a shows braid-perthite exsolution in feldspar showing Carlsbad twinning, the most common form of twinning and exsolution in the alkali feldspars. 'Patch-perthite' illustrated in plate 3.2b, showing exsolution of microcline and plagioclase-rich phases.

volume, the more feldspathic samples tending to occur at the top of the unit. The feldspars almost always show perthitic exsolution, which takes at least two different forms (plate 3.2). The commonest of these shows a pattern of braided lamellae, each one up to *c.*100μm across, and symmetrical about the twin-plane (cf. 'braid-perthite', Parsons 1978; plate 3.2a). Much coarser exsolution has resulted in patches of microcline and exsolved material (usually plagioclase) up to 0.5mm across ('patch perthite', plate 3.2b), though a gradation between the two textures seems to occur, and the precise orientation of the feldspar crystal probably affects the appearance of the perthite as seen in thin-section. Occasional crystals of antiperthite and individual grains of microcline also occur.

Nepheline is always present, although frequently altered to gieseckite, which pseudomorphs the original outline of the crystal. The euhedral shape of the nephelines, with a square or rectangular cross-section, is suggestive of a cumulus origin. Optically continuous overgrowth is occasionally indicated by an internal rim of inclusions, marking the earlier euhedral crystal outline, and forming a more subhedral shape to the crystal. The nephelines occasionally shows signs of recrystallisation (sample G176; plate 3.11), in which the millimetre-sized grains have a granoblastic texture in places. The same sample shows evidence of feldspar recrystallisation along discrete zones 1-2mm across, with polygonal grains 50-100μm in size, some of which show plagioclase twinning. These may be the result of relatively late-stage ductile fracturing of the rock, followed by fluid-enhanced recrystallisation localised along these fractures.

Aegirine-augite is the commonest mafic phase in the Lower Series Syenite, occurring as subhedral or poikilitic/interstitial grains up to 5mm across. It shows the typical pleochroism of alkali-pyroxenes (α emerald-green; β pale-green; γ yellow-brown), and is frequently zoned from paler green cores to darker rims. The lowest rocks of the unit show the most euhedral pyroxenes, which become more interstitial at higher levels in the series, and are generally absent from the highest parts of

the Lower Series Syenite. These highly feldspathic samples show the most strongly developed lamination of any part of the complex (eg. samples G222, 27136). The other common mafic phase is biotite, occurring as poikilitic or interstitial grains up to several millimetres across. It is intensely pleochroic (α pale-brown, rusty-brown/orange, green-brown; β, γ very dark blue-green), and occasionally zoned from paler rims to slightly deeper coloured cores. The cleavages and edges of the biotites are very often highlighted by minute opaque grains, which sometimes occur so densely that the whole grain appears opaque. Larger (up to 0.5mm) discrete opaque grains occur scattered throughout most samples of the Lower Series Syenite. The remaining primary mineral phase is apatite, which is extremely common as fine, elongated prismatic crystals with a hexagonal cross-section, 100-200μm across, and up to *c.*3mm in length, forming up to around 5% of the area viewed in thin-section.

The remaining phases are generally regarded as being of secondary origin, ie. they did not form part of the original mineral assemblage, but may have been introduced from outside the system, or formed by low-temperature reaction of late-stage fluids with primary phases. Sodalite is sometimes present, especially in the more altered parts of the Lower Series Syenite, where it occurs as irregular isotropic grains associated with cancrinite (plate 3.3), whose association with nepheline has already been mentioned. Zircon is surprisingly common as small, brown, high-relief, high birefringence grains up to *c.*0.5mm in size, increasing in abundance with increasing degree of alteration (eg. samples G13, G193).

Carbonate, usually occurring as interstitial grains in the more altered rocks, also occurs in relatively fresh samples (eg. G156), apparently crystallising as a late-stage phase. The presence of carbonate in the Lower Series Syenite and many of the other syenite units, has interesting implications for the petrogenesis of the carbonatite plug at Grønnedal-Íka (chapter 6, and plate 3.4).

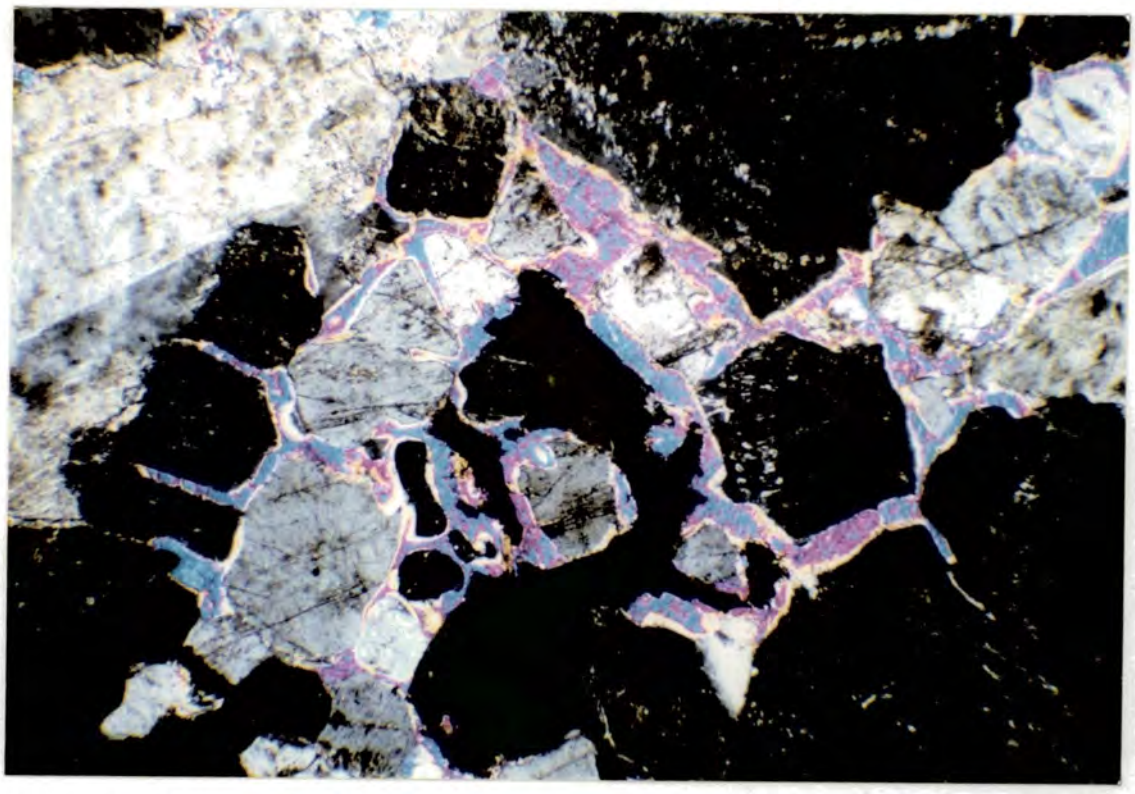

Plate 3.3. G219. ×35. XPL. Poikilitic cancrinite in typical Lower Series Syenite, enclosing mainly nepheline, but also some prominent green aegirine-augite. The occurrence and texture of the cancrinite in these rocks suggests the presence of late-stage, CO_2-rich magmatic fluids.

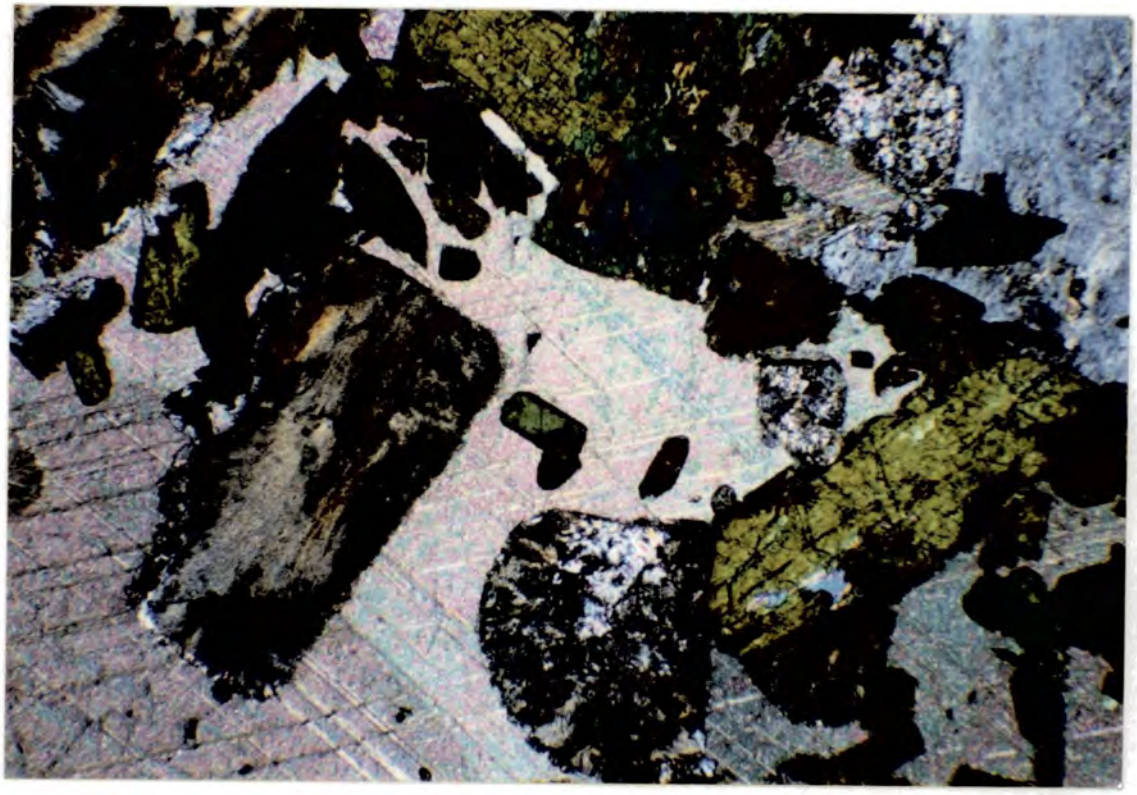

Plate 3.4. G156. ×35. XPL. Poikilitic calcite in Upper Series Syenite. In contrast to many of the syenites which contain calcite, this sample is extraordinarily fresh.

3.3: Upper Series Syenite

Generally, the only appreciable difference between this unit and the Lower Series Syenite is one of texture, the Upper Series being coarser and less well-laminated. The mineralogy is almost identical, even down to the presence of zircon in the more altered samples (eg. sample G17), the presence of interstitial carbonate, and the absence of aegirine-augite in some (eg. sample G16). Adcumulus growth is apparent in the nepheline in G135, an internal rim of pyroxene grains marking the original grain-boundary of the nepheline, overgrown with more material in optical continuity (plate 3.5).

The nepheline-rich facies (sample G24) described in section 2.4 shows much interstitial carbonate in thin-section, together with biotite, aegirine-augite, zircon, sodalite, and cancrinite, while the nepheline is entirely altered to a white micaceous mineral.

Sample G118, from the border-zone between the Upper and Lower Series Syenite exposed in the Radioelv, consists mainly of altered, ragged looking alkali feldspar, and resorbed-looking pyroxene apparently in a state of disequilibrium, with a small amount of cancrinite and micaceous alteration.

3.4: Mafic Upper Series Syenite

Texturally, these rocks are similar to the Upper Series Syenites, but are richer in aegirine-augite (up to *c.*50%) with optically continuous, euhedral to subhedral pyroxenes up to 4mm × 2.5mm. The smaller grains tend to be better formed, while the larger ones develop a poikilitic texture (plate 3.6). Many are continuously zoned from paler cores to darker rims, while some show a sharper colour-change, more indicative of a discrete phase of crystal growth (eg. sample G187). Apatite is particularly common in the Mafic Upper Series Syenite, occurring as individual hexagonal prisms up to 0.5mm across, or clustered together in bundles (G187). Somewhat unusually, in view of its general absence in other units, amphibole

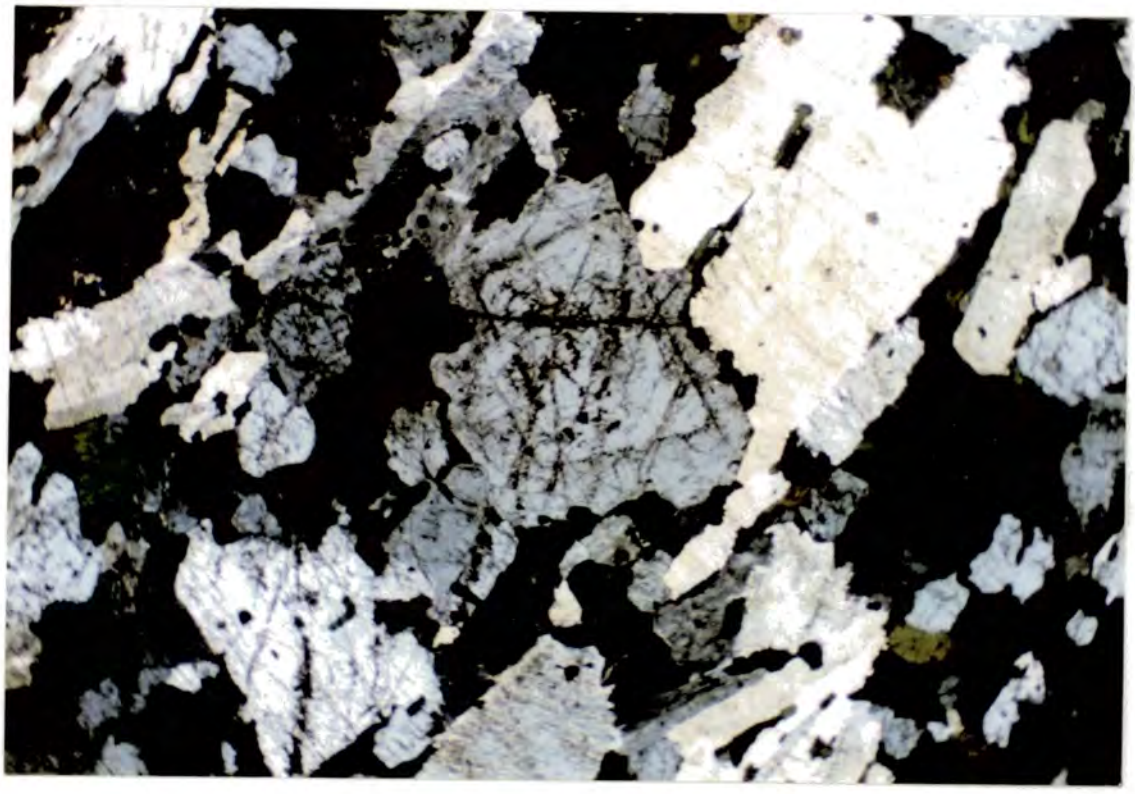

Plate 3.5. G135. ×35. XPL. Overgrowth of nepheline on an earlier crystallised, euhedral nepheline core. The original crystal outline is marked by a rim of inclusions and small pyroxene grains, with the later material crystallising in optical continuity.

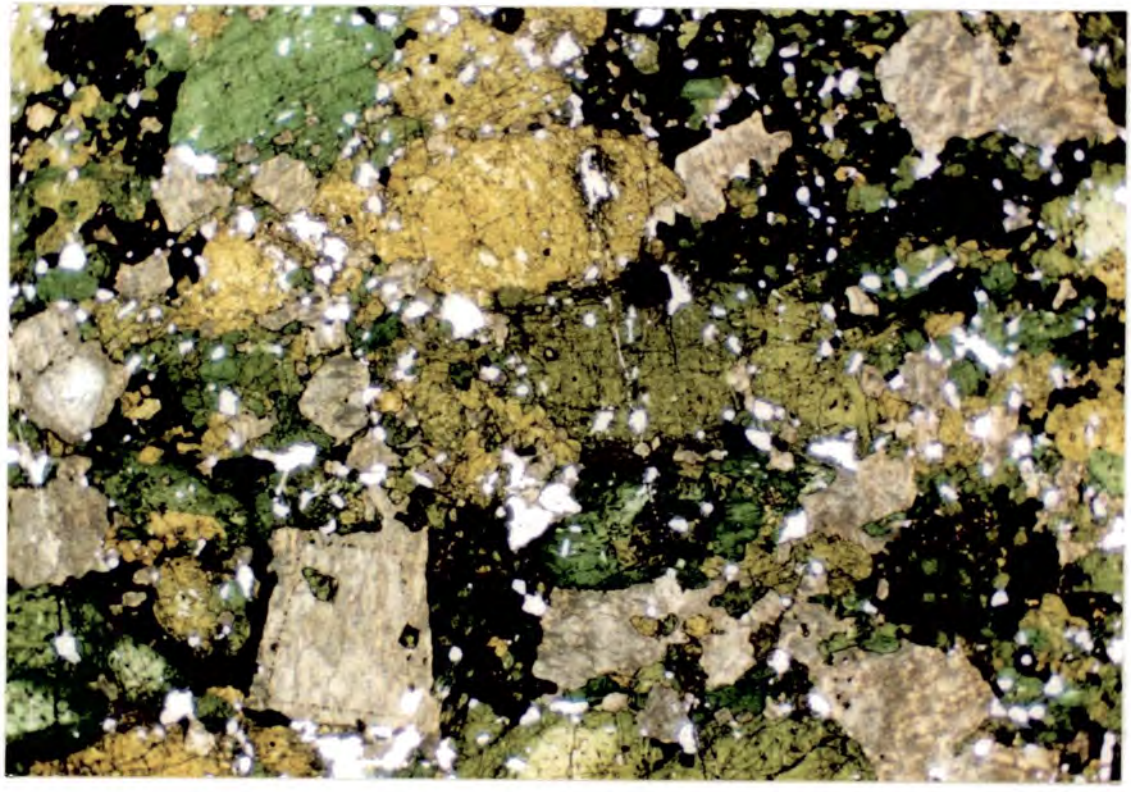

Plate 3.6. G190. ×11. PPL. Mafic Upper Series Syenite, from the Emeleus' layered locality (map 1). Coarse yellow-green aegirine-augites are seen poikilitically enclosing numerous small, euhedral apatites, with poikilitic biotites (dark areas) enclosing apatite and small pyroxenes. Some zoning can be seen in grains to the lower left of the field of view. The remaining minerals are nepheline (mostly altered to gieseckite), with some overgrowth apparent in the large grain to the lower left of centre. There is a slight suggestion of pyroxene orientation, defining a weak lamination running horizontally across the field of view.

occurs in one section of sample 27193. It occurs as strongly pleochroic (α grey-green; β very dark-green; γ olive-brown), poikilitic crystals, several millimetres across, apparently partly replacing the pyroxene that it encloses.

Nepheline and alkali feldspar are present in lesser amounts than in the Upper Series Syenite, their place taken by the additional pyroxene. Biotite is also common, strongly coloured, and often very rich in opaque inclusions, while the relative lack of cancrinite may reflect the smaller amount of nepheline. Zircon and interstitial carbonate are once again present in minor amounts.

3.5: Granular Syenite

3.5.1 GS-A

In thin-section, this unit is characterised by an abundance of very fresh, sharp, clean-looking prisms and radiating sprays of alkali-pyroxene, typically 2mm × 0.5mm in size. They are intensely zoned, usually from a pale grass-green core through a darker emerald-green, and back to a much paler green colour at the crystal margin; some show a discrete rim of darker-green pyroxene on a paler-coloured, often euhedral core (plate 3.7). Pleochroism is strong (α blue or emerald-green; β pale-green; γ pale yellow-brown).

Alkali-feldspars occur as untwinned, euhedral laths up to 3mm × 1mm, with perthitic exsolution occurring as fine lamellae parallel to the length of the crystal. The feldspars are unlaminated, and often occur as stellate or fan-shaped sprays. Nepheline is commonly altered to gieseckite, and in contrast to the other syenite units is rarely euhedral, occurring as an interstitial phase to the alkali feldspar, poikilitically enclosing the pyroxene instead. Interstitial biotites up to *c.*1mm across are common, strongly zoned from orange-brown cores to deeper red-brown rims, and intensely pleochroic to very dark brown. Occasionally, rather altered-looking amphiboles occur, (α blue-green; ?β green-brown; ?γ very dark-brown). Apatite was not observed in any of the samples.

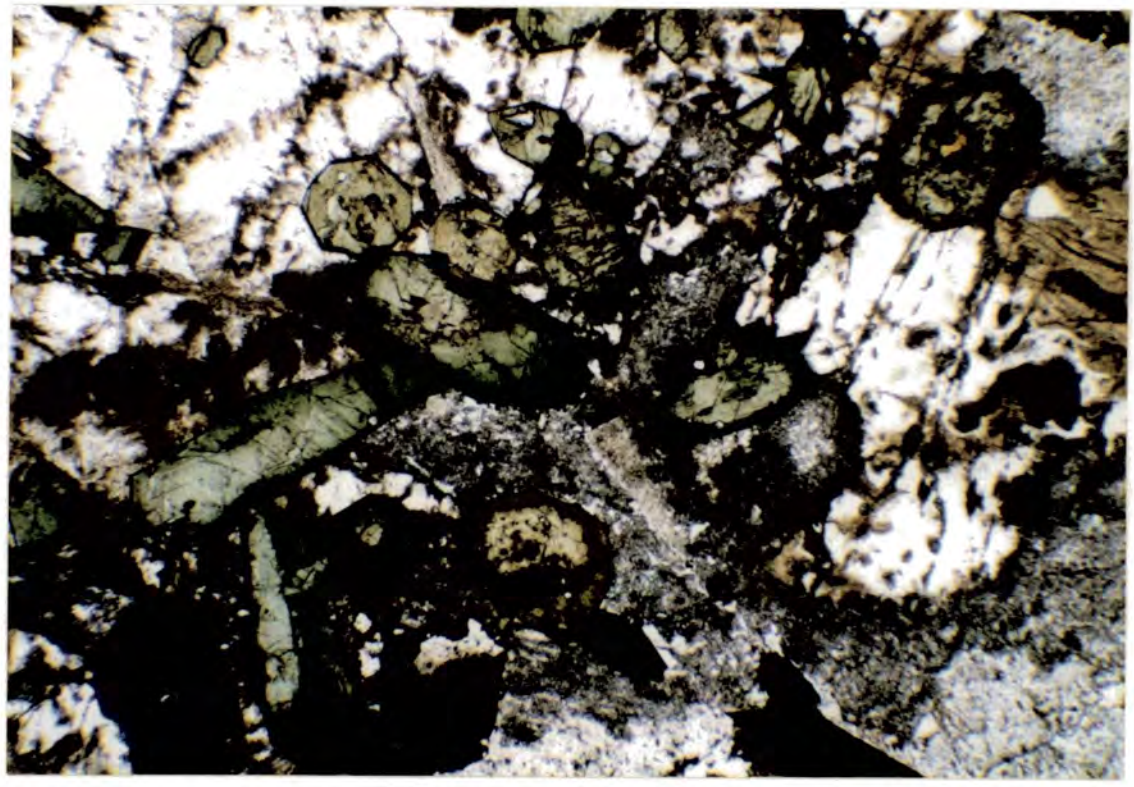

Plate 3.7. G172. ×35. PPL. Granular Syenite (GS-A) with prominent zoned prismatic pyroxenes seen in longitudinal and cross section. These are enclosed by nepheline (white, altered to brown gieseckite along cracks), and rather turbid alkali feldspar.

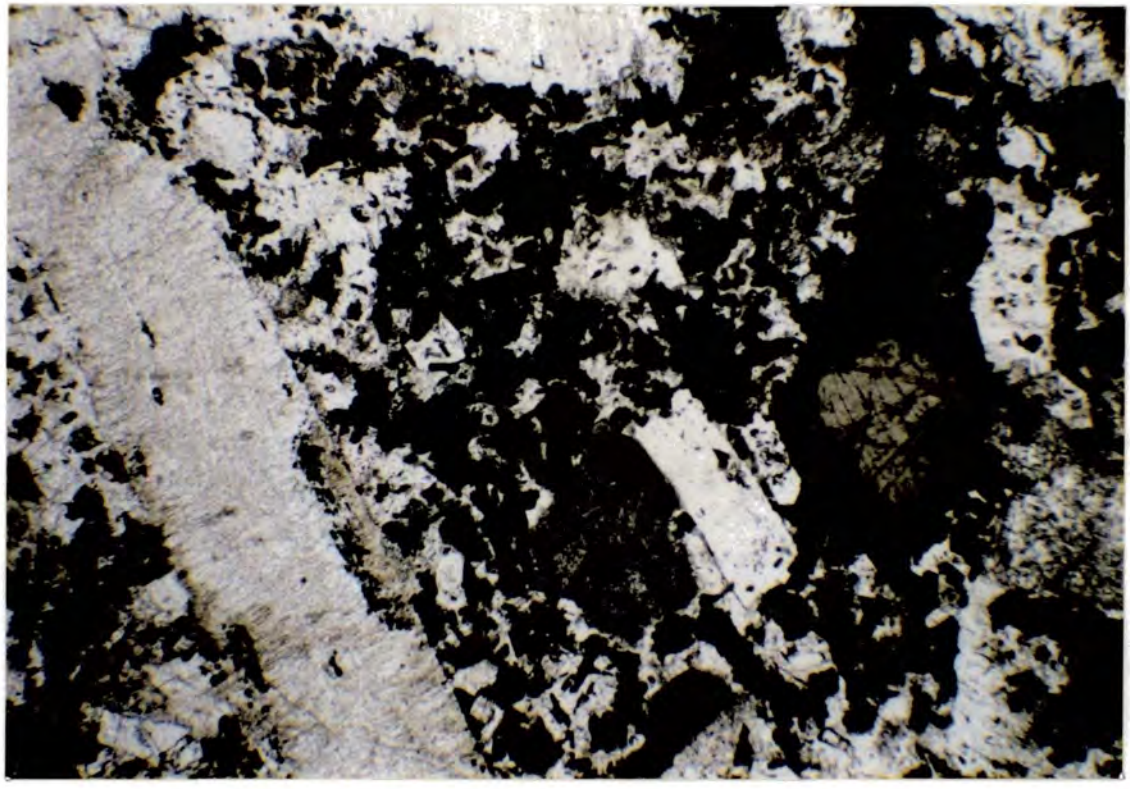

Plate 3.8. G41. ×35. PPL. Xenolithic Porphyritic Syenite showing coarse, tabular perthitic alkali feldspar phenocrysts and a prominent pyroxene phenocryst with an overgrowth of sodic pyroxene on a more diopsidic core. The groundmass is seen to consist of prismatic aegirine-augite and feldspar, with some altered nephelines.

Late-stage alteration of the nepheline has already been mentioned, but in addition, areas of fine-grained cancrinite occur, as well as occasional sodalite.

3.5.2 GS-B

This unit is characterised in thin-section by the presence of unlaminated, granular (as oppposed to tabular) alkali feldspar, and poikilitic biotites up to 13mm × 8mm. The feldspars are coarsely exsolved, forming braid- and patch-perthites, with microcline occasionally acting as the host phase. Nepheline occurs as millimetre-sized, equant, euhedral crystals, often enclosed by biotite, and frequently with an internal rim of pyroxene grains, marking the edge of the crystal between phases of growth. The pyroxenes are subhedral to euhedral aegirine-augites, up to 3mm × 2mm in size, with no noticeable zonation apparent in thin-section, and partly or wholly enclose smaller grains of nepheline and apatite (a very common phase in this unit, contrasting with its absence in GS-A). Opaques are common, especially along the cleavage planes of biotite, and include a Cu-Fe sulphide in sample G168.

The presence of large, poikilitic amphiboles up to *c.*10mm across (α green-blue; ?β very dark-green; ?γ pale-brown) in samples G84 and G246 is of particular interest. It encloses small grains of pyroxene and nepheline in G84, partly replacing the pyroxene, and as described in section 3.1, does not occur in syenites forming the bulk of the complex, in contrast to the majority of undersaturated Gardar complexes. Poikilitic cancrinite and sodalite comprise the late-stage/alteration products in this unit.

3.6: Coarse-Grained Brown Syenite

This unit typically has very coarse alkali feldspar laths (up to 3mm × 13mm) which are generally poorly or moderately well-laminated. In thin-section, the rock is characteristically altered, the nepheline always pseudomorphed by gieseckite and usually associated with some cancrinite, while the pyroxenes are altered to

a pale-green chloritic material. A colourless mica with moderate birefringence (mid 2nd-order) sometimes replaces the nepheline, forming radiating, fan-shaped sprays. The alkali feldspars, however, are generally unaltered, and coarse poikilitic biotites up to 12mm across, plechroic from green to yellow-brown, are frequently present. Small opaque or very deep-red grains occur in areas of chloritic alteration, presumably oxides of iron as a by-product of pyroxene breakdown.

Two minerals which are characteristic of the altered rocks at Grønnedal-Íka in general are zircon and carbonate. In the Coarse-Grained Brown Syenite, both are common and form subhedral grains or interstitial areas up to 2mm across. Finally, as in the majority of the syenites, interstitial sodalite and fine prismatic crystals of apatite occur.

3.7: Coarse-Grained Syenite

Most samples of this unit are strongly altered, with pyroxenes replaced by pale-green chloritic material, nepheline altered to gieseckite, and interstitial zircon and carbonate, as in the Coarse-Grained Brown Syenite. Sample G275 is somewhat fresher, though, and shows very coarse, twinned, elongated perthitic alkali-feldspar some 2-3cm long, and millimetre- to centimetre-sized nephelines, rimmed by cancrinite. The unaffected pyroxenes are comparable in size to those in the other syenite units (*c.*2-3mm across). They are subhedral, slightly zoned from pale cores to darker rims, and show some adcumulus growth. Poikilitic biotite and prismatic apatite are also present.

3.8: Xenolithic Porphyritic Syenite

This late-stage syenite plug generally shows a bimodal distribution of grain-sizes, with centimetre-sized, ragged-rimmed phenocrysts of alkali feldspar, and somewhat smaller phenocrysts of aegirine-augite, nepheline, and biotite, in a matrix of the same minerals with grains less than *c.*0.5mm across.

Alkali-feldspar, the most abundant phenocryst phase, occurs as tabular, perthitic crystals up to 15mm long, and often zoned (sample G145) or internally rimmed with very fine pyroxene grains (sample G41). The tabular crystals usually show little preferred orientation, though G145 shows a fairly well-developed lamination. There is also a suggestion of strain in the feldspars, many of them showing shadowy extinction, possibly as a result of emplacement of the magma as a partly consolidated 'mush', as this feature does not appear to bear any relationship to the faulting which cuts this unit. Aegirine-augite is abundant both in the matrix of the rock and as phenocrysts. The latter are frequently zoned from pale cores to darker rims, but a characteristic of the pyroxenes from this unit is an overgrowth of green aegirine-augite a few tens to several hundreds of microns thick, on a core of pink-purple augite. These overgrown pyroxenes, up to 1mm × 1.5mm in size, are generally euhedral, and the change from core to rim is very distinct. Pyroxenes in the groundmass are usually granular, euhedral prisms less than 0.5mm in length. Nepheline is not as common as in the laminated syenites, but when present, occurs as euhedral grains up to 4mm across, usually entirely altered to gieseckite. Biotite is occasionally present as poikilitic areas several millimetres across, or as small flakes in the groundmass, pleochroic from pale-brown to very dark-green, often intergrown with pyroxene, and with opaques along the cleavage planes. Apatite is a particularly abundant groundmass phase in the Xenolithic Porphyritic Syenite, occurring as bunches and bundles, with quite coarse individual crystals, up to *c.*0.7mm across (eg. sample G78). The ubiquitous zircon is also present as small, sub millimetre-sized grains, along with interstitial carbonate and poikilitic cancrinite, again in the more altered samples (plate 3.8).

The xenoliths in this unit consist mainly of a severely altered rock rich in coarse, perthitic alkali feldspar, with occasional gieseckite-pseudomorphed nepheline, and less abundant chloritic material, presumably after pyroxene. They are not sharply bounded when viewed in thin-section, the fine groundmass of the Xenolithic Porphyritic Syenite penetrating and separating the individual crystals

of the xenolith. By this process of disaggregation, the components of the xenolith could be entirely separated from each other, and it is thus quite likely that many of the alkali feldspar and nepheline 'phenocrysts' present in the host rock are in fact xenocrysts.

Carbonated Xenolithic Porphyritic Syenite

This very peculiar, highly altered rock, of which two samples were collected (G58 and G136), consists of a fine-grained carbonate-rich matrix with biotite, altered prismatic pyroxenes, and a dusting of opaques, within which relict phenocrysts of euhedral nepheline, alkali feldspar, and biotite occur. Coarse sparry calcite and sodalite fill vuggy areas in the rock, 0.5mm to 1mm across.

3.9: Porphyritic Microsyenites

This unit consists of varying quantities of alkali feldspar, aegirine-augite, nepheline, biotite, and opaques, occurring as phenocrysts set in a fine groundmass of the same minerals. One sample (G178) shows evidence of slight recrystallisation, with some of the groundmass feldspars having a polygonal outline, each grain 100μm to 200μm across. The proportion of phenocrysts making up the rock varies from about 70% (eg. G40, G184) down to samples with occasional coarser grains, forming around 20% of the rock. Cancrinite and gieseckite are absent from samples with few phenocrysts, but occur where these are more abundant.

More than one phase of nepheline crystallisation is apparent, as indicated by an internal rim of small pyroxene grains, and multiple phases show up as alternating inclusion-rich and inclusion-poor zones (plate 3.9a). Using the highest power objective available (×100), these inclusions are seen to be acicular or prismatic euhedral grains up to 20μm × 4μm in size, with a very pale-green colour, probably pyroxene (plate 3.9b). The more elongated grains appear to be aligned parallel

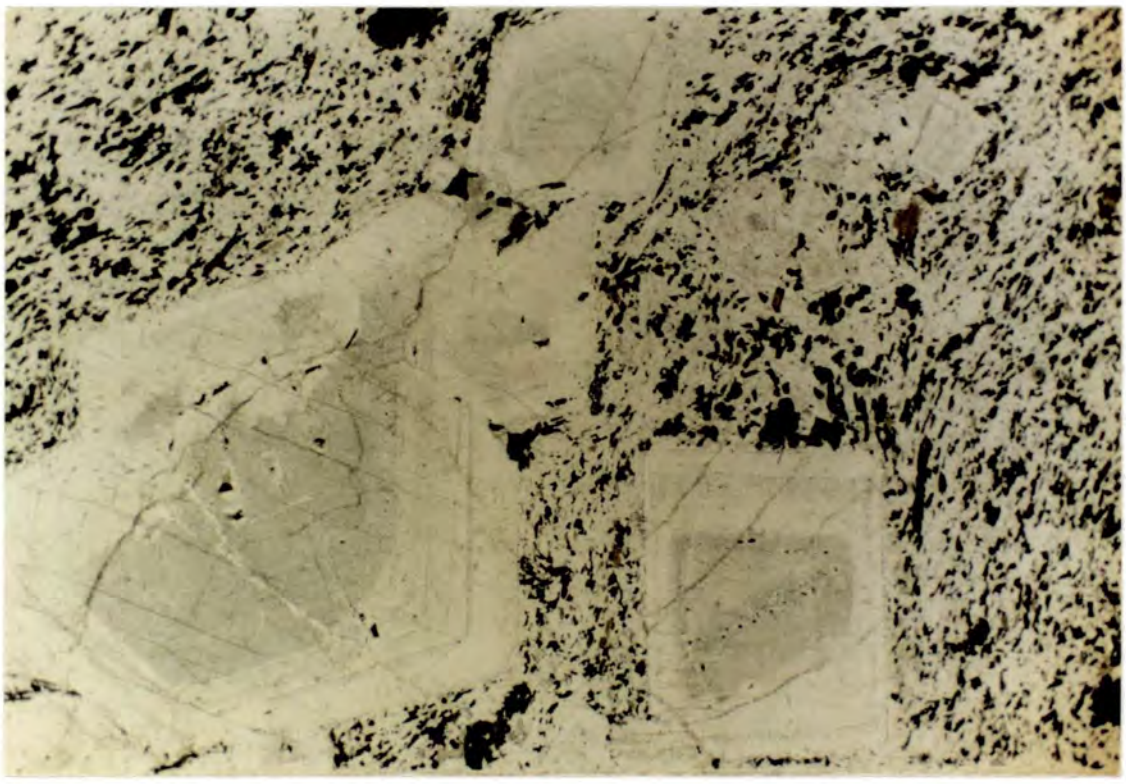

Plate 3.9a. G178. ×11. PPL. Nepheline phenocrysts in Porphyritic Microsyenite, each grain showing concentric inclusion-rich and inclusion-poor zones, possibly related to episodic phases of crystal growth. Groundmass of alkali feldspar, pyroxene, biotite, and opaques.

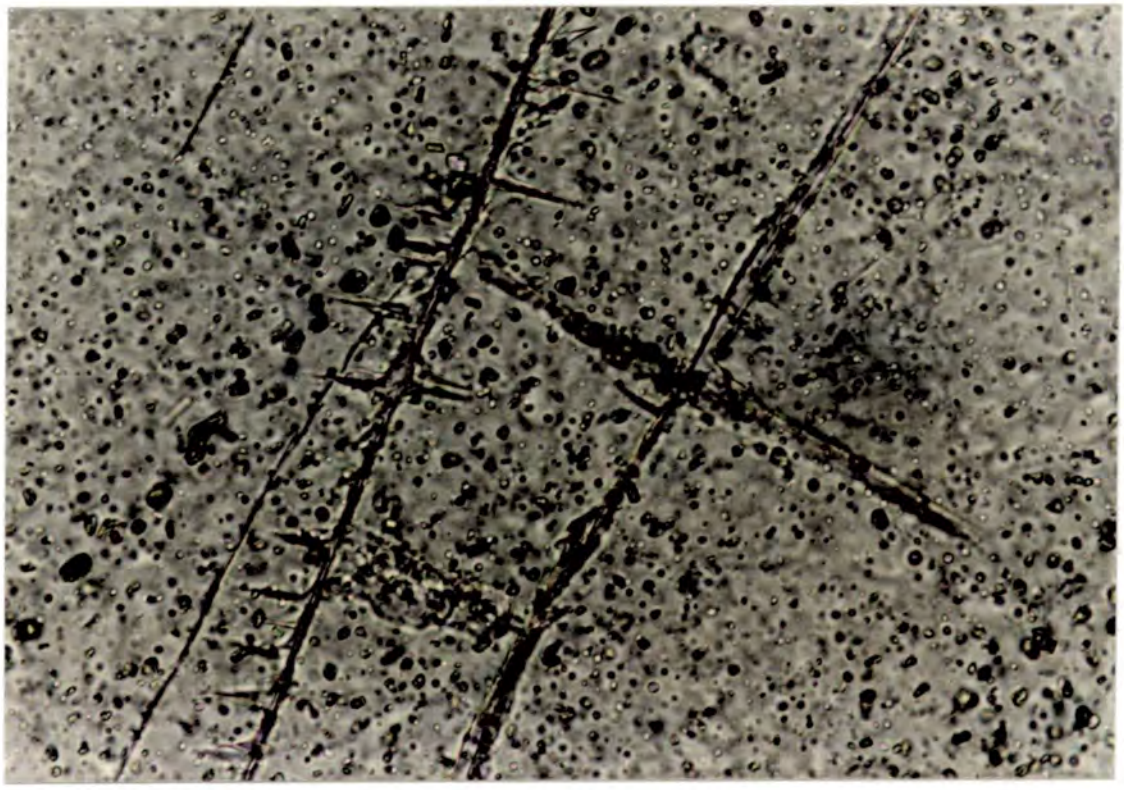

Plate 3.9b. G178. ×100. PPL. Detail of inclusions in plate 3.9a, showing them to be very pale yellow-green, prismatic grains, probably of sodium-rich pyroxene.

to the nepheline cleavage. Episodic growth is not confined to nepheline, also occurring in the alkali feldspars, which often show a discrete phase of overgrowth as well as more gradual zonation.

Pyroxenes are again the commonest of the mafic phases, frequently showing gradational, or even multiple zoning (sample G224), and sometimes occurring as glomerocrysts with biotite. Amphibole is present in G186 and G224 as small grains *c.*1mm across (α pale-brown; β green-brown; γ dark blue-green), poikilitically enclosing pyroxene grains. Opaque oxides are occasionally present as small phenocrysts, often rimmed by, or associated with biotite, presumably as a result of reactions with late-stage, potassic, hydrothermal fluids.

Flow-banding is a common feature of the Porphyritic Microsyenites, and is most strongly developed in samples with fewer phenocrysts. They typically show strong alignment of elongate alkali feldspar, pyroxene, and biotite grains, wrapping around euhedral phenocrysts of nepheline, feldspar, and pyroxene, which are usually flow-orientated themselves.

3.10: Pegmatites

What were described as pegmatites in the field, due to the presence of large pyroxenes and the vein-like occurrence of the rock, consist of a groundmass of randomly orientated laths of alkali feldspar, *c.*100-200μm in length, and ragged-looking, partially resorbed aegirine-augites which are slightly pleochroic from pale-green to very pale-green, sometimes with darker green cores (eg. sample G183). Large sprays of cancrinite occur over areas of several millimetres, suggesting that the fluid from which this rock crystallised was rich in CO_2, though no interstitial carbonate was seen in the samples examined.

3.11: Marginal Microsyenites

Many of the textures and mineralogies observed in these rocks are similar to those of the Porphyritic Microsyenites, ie. phenocrysts of alkali feldspar,

nepheline, aegirine-augite, and biotite, with a fine-grained, felted groundmass of the same minerals. Apatite is present in the marginal rocks, however, which does not occur in the Porphyritic Microsyenites. Sample G37, 15cm from the contact, shows prominent opaque grains with reaction rims of orange-brown to dark-brown pleochroic biotite, but few other phenocrysts. The groundmass is quite rich in felsic grains, with alkali feldspar and ?nepheline *c.*100μm in size, while the distribution of pyroxene grains is uneven, being concentrated into millimetre-sized 'schlieren'.

At 50cm from the contact (sample G38), the proportion of phenocrysts is an order of magnitude greater (*c.*80% of the rock by volume), consisting mainly of alkali feldspar and nepheline, with some biotite. Interstitial cancrinite is present here, as well as apatite, although pyroxene is not abundant as a phenocryst.

The occurrence of amphibole in one of the marginal syenites has already been mentioned (section 2.12). In thin-section, this rock (sample G44) shows strongly pleochroic, coarse poikilitic amphiboles up to 1cm across (α deep blue-green; ?β very dark-green; ?γ pale-brown) enclosing beautifully flow-orientated, elongate alkali feldspar, generally around 0.5mm long. These wrap around the nepheline grains (*c.*0.5mm across), while being enclosed by the amphibole, which therefore appears to be a late-stage mineral which grew after the flow-orientation was established (plate 3.10).

A highly unusual assemblage occurs in 27131, a marginal syenite from the southern tributary of the Radioelv, which contains quartz, riebeckitic amphibole, and possible aenigmatite. The quartz occurs as interstitial areas between slightly recrystallised plagioclase and alkali feldspars, while the riebeckite occurs as ragged, flaky grains, and the ?aenigmatite as deep-red, rather blocky crystals 100-500μm in size. Nepheline is not surprisingly absent, possibly as a result of wall-rock interaction and contamination resulting in a higher silica/alkali ratio, and may

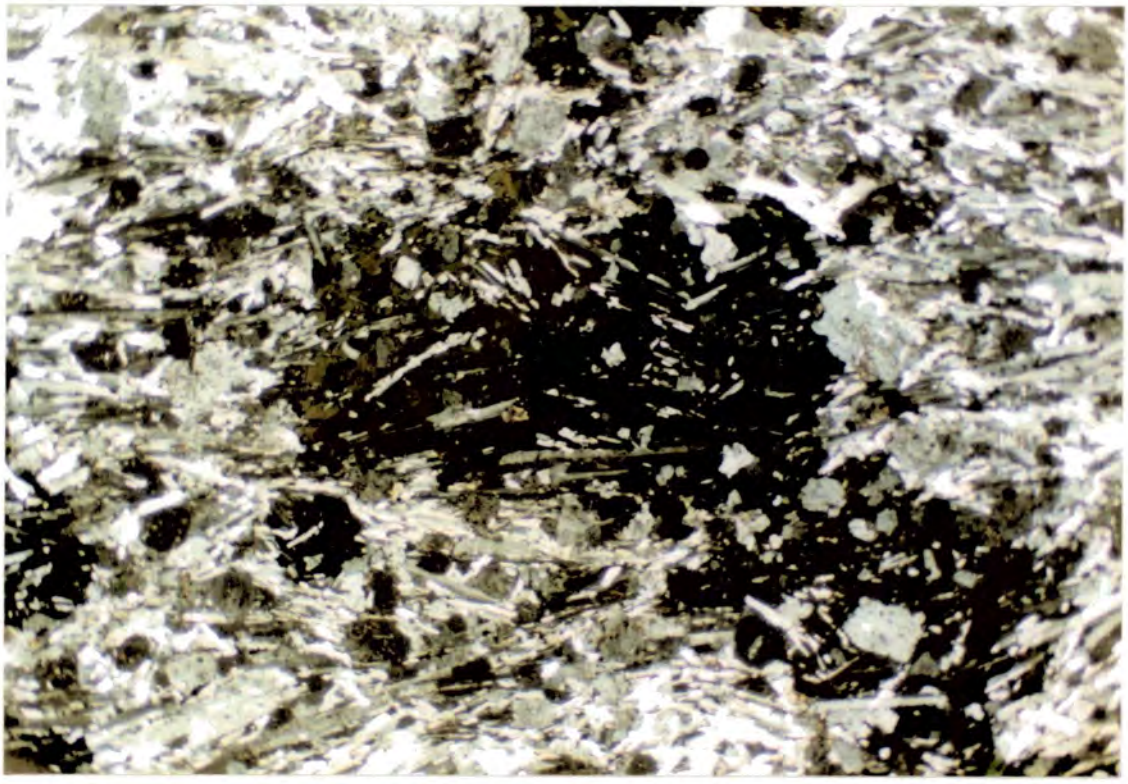

Plate 3.10. G44. ×11. PPL. Marginal microsyenite with poikilitic amphiboles enclosing flow-orientated alkali feldspar laths. The feldspars wrap around the nephelines, but are enclosed by the amphiboles, which thus appear to have grown after the flow-orientation was established.

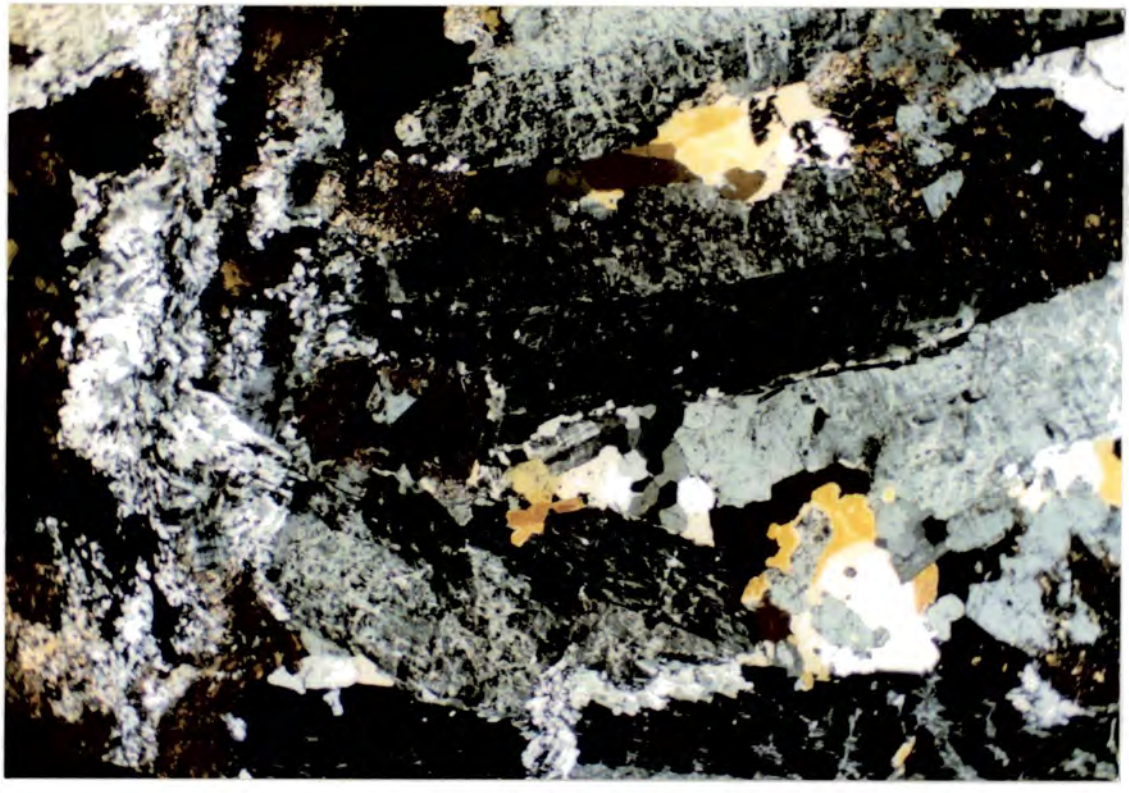

Plate 3.11. G176. ×11. XPL. Recrystallisation textures in Lower Series Syenite. Granoblastic nepheline grains occur on the right-hand side of the field of view, while to the left, a linear zone of recrystallised feldspars can be seen running vertically.

also have given rise to a sufficient increase in water content for the amphibole to be stabilised.

3.12: Conclusions from petrography

A detailed discussion of the complex, incorporating all mineralogical and geochemical data will be left until chapter 8, although some general comments and conclusions from the petrographic observations will be made here.

3.12.1 Magma chemistry and crystallisation

The syenites are undersaturated, with nepheline (invariably), alkali feldspar (usually), and aegirine-augite (occasionally) forming subhedral to euhedral crystals, and suggestive of a cumulus origin. Nepheline in particular is almost always euhedral (plate 3.1) and often enclosed by later crystallising alkali feldspar in the lower parts of the laminated syenites, while towards the tops of these units, nepheline is often absent and alkali feldspar forms the dominant cumulus phase. The pyroxenes are frequently subhedral to euhedral at the base of the laminated syenites, becoming more interstitial with increasing height, and entirely absent from the tops of these units.

3.12.2 Presence of volatiles

The late-stage build-up of volatiles is indicated by the presence of certain phases. Perthitic exsolution in alkali feldspar is thought to be facilitated by the action of fluids (Parsons 1978, plate 3.2), while interstitial sodalite in some samples indicates the presence of chlorine. Poikilitic cancrinite, generally in association with nepheline, shows a build-up of CO_2 in the magma, possibly resulting in the interstitial carbonate in a few samples.

3.12.3 Alteration

Late-stage alteration has affected all of the syenites to varying degrees, from the partial replacement of nepheline by gieseckite to complete alteration and chloritisation of pyroxene grains in the Coarse-Grained Brown Syenite. Accompanying

these changes are feldspar textures which are reminiscent of those seen in fenitised rocks (Le Bas, pers. comm.), and also in the altered syenites and gneisses of this complex (chapter 7) where the most extreme effects of metasomatism are seen. These textures are also present in the GS-A Granular Syenites, and these rocks, as well as the Coarse-Grained Brown Syenites, have undoubtedly suffered at least some late metasomatic alteration.

3.12.4 Absence of certain phases

The syenites at Grønnedal-Íka are notable for the lack of certain phases which are common or even abundant in many other Gardar central complexes. The scarcity of amphibole in the great majority of syenites suggests a low water activity (a_{H_2O}) in all but some samples from the marginal dykes (sample G44) and sheets (G80, G246). The complete absence of olivine is also interesting, and probably relates to the oxygen fugacity (f_{O_2}) of the magma (cf. section 4.11). Finally, the absence of phases such as aenigmatite (apart from a possible occurrence in sample 27131, a Marginal Syenite), eudialyte, rinkite, etc., which frequently occur in generally small amounts in other Gardar complexes again probably relates to the physical conditions of the magma, particularly the f_{O_2}.

3.12.5 Zircon

This mineral, which is common at Grønnedal-Íka, occurs only rarely as a groundmass phase elsewhere in the Gardar (eg. Stephenson 1973, Powell 1976, Chambers 1976), though Jones (1980) found it occurring in unit SM3 of the Motzfeldt centre, north of the Flink's Dal fault, and Emeleus (pers. comm.) reports its presence in other parts of the Igaliko Complex. Chambers (1976) does not mention it in connection with the alteration of the North Qôroq centre, though it increases in abundance with increasing alteration of the syenites at Grønnedal, and is a common groundmass phase in the Coarse-Grained Brown Syenite (cf. chapter 7).

3.12.6 Recrystallisation

A few samples show the partial development of granoblastic texture (plate 3.11), although recrystallisation does not appear to be a general feature of the complex. Poikilitic textures have been taken to indicate recrystallisation by Chambers (1976), though the presence of such grains (such as the amphiboles in G44, G80, and G246) does not appear to coincide with the extensive development of a granoblastic groundmass.

Given the sporadic occurrence of recrystallisation throughout the area, it may have been caused by the later doleritic and alkaline dykes which post-date all units of the complex.

3.12.7 Interstitial carbonate

The presence of areas of poikilitic carbonate in most altered syenites may be due to a late build-up of CO_2 in the magma (cf. section 3.12.2). However, one sample of Lower Series Syenite which shows interstitial carbonate is remarkably fresh (G156, plate 3.4), and this may be important in helping to determine the origin of the carbonatite (chapter 6).

CHAPTER 4: MINERALOGY

4.1: Introduction

This chapter describes and discusses electron microprobe analyses of the mineral phases from the eleven units which comprise the syenitic component of the complex. The mineralogy of the carbonatites and metasomatised rocks will be considered in chapters six and seven respectively.

The analysed samples were selected to give a wide geographical coverage and chemical variation (based on petrographic observations) within each unit. The results are displayed using different symbols for the different units, with the original classification of Emeleus (1964), which was confirmed both in the field and from thin-section evidence, being used throughout.

Analyses were carried out using energy-dispersive microprobes at the Universities of Durham and Manchester, and the wavelength dispersive microprobe at Edinburgh University. Full operating conditions and mineral analyses are presented in Appendix II.

4.2: Pyroxenes

4.2.1 General

Pyroxene is the commonest mafic mineral in the Grønnedal-Íka syenites, occurring in all of the units distinguished in the field, and absent from only a few very felsic samples. They are all monoclinic (clinopyroxenes), and invariably show the pleochroic scheme typical of aegirine-augite (α bright green, β yellow-green, γ yellow-brown). Zoning is a common feature, with paler cores grading continuously into darker rims, though discontinuously zoned pyroxenes occur in some samples of the Xenolithic Porphyritic Syenite (section 4.2.5). Both cores and rims of three or four pyroxene grains per section were analysed, resulting in six to eight analyses per sample, though in some cases of extreme zonation (such as in GS-A, section 4.2.5), more analyses were required to cover the range of compositions.

Fig. 4.2.1A. Classification of alkali pyroxenes after Deer *et al.* (1982) and Jones (1980) in terms of variations of end-member proportions in the system Diopside-Hedenbergite-Acmite.

Fig. 4.2.1B. Pyroxenes from Grønnedal-Íka syenites in the system Mg-(Fe^{2+}+Mn)-Na. A trend away from Mg resulting from the substitution CaMg $\rightleftharpoons$ Ca(Fe^{2+}+Mn) and increasing Na as a result of Ca(Fe^{2+}+Mn,Mg) $\rightleftharpoons$ $NaFe^{3+}$ can be seen. This diagram is not strictly the same as fig. 4.2.1A as it does not allow for Na-rich end-members other than acmite, but enables direct comparisons with results of other workers to be made, and is used throughout this section.

Fig. 4.2.1A

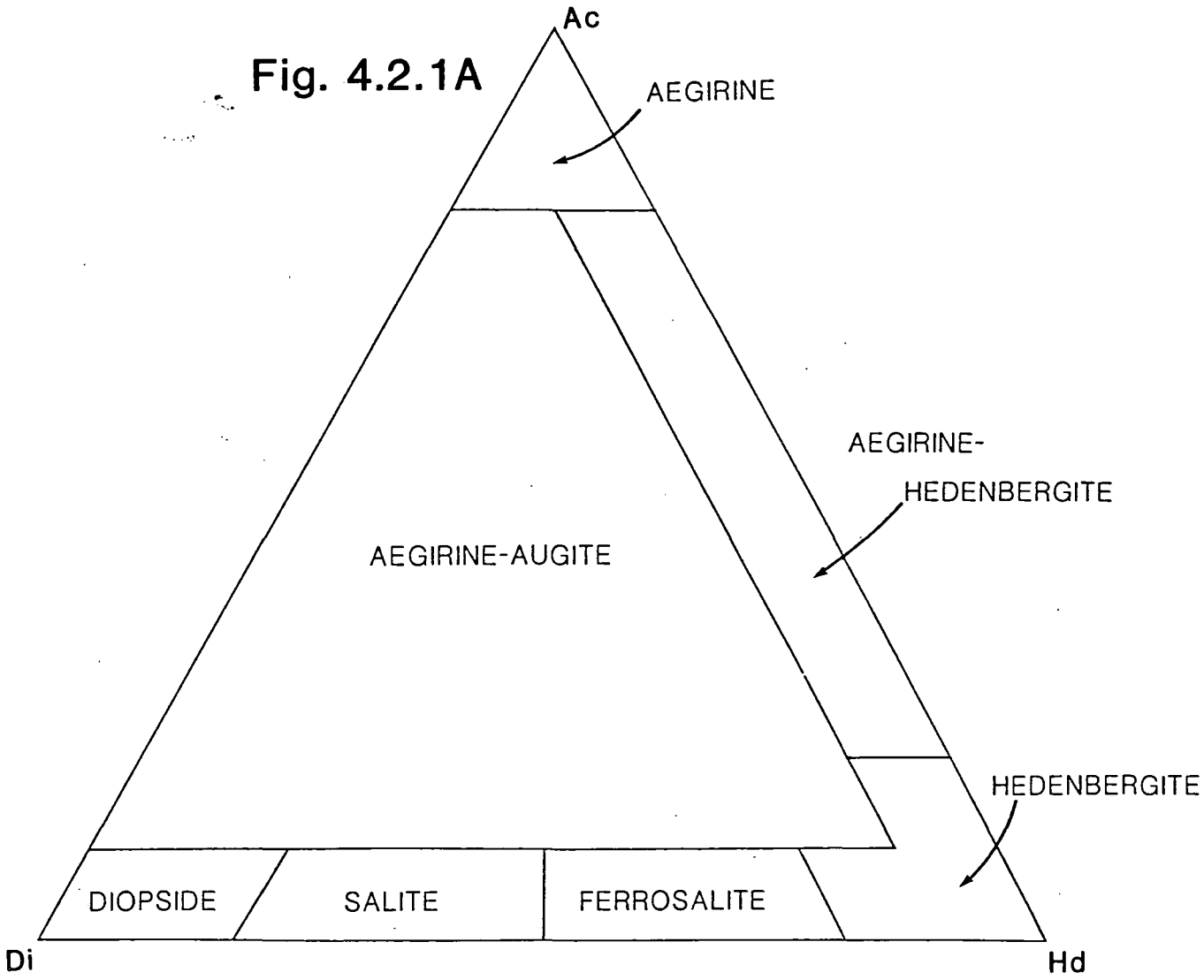

Fig. 4.2.1B

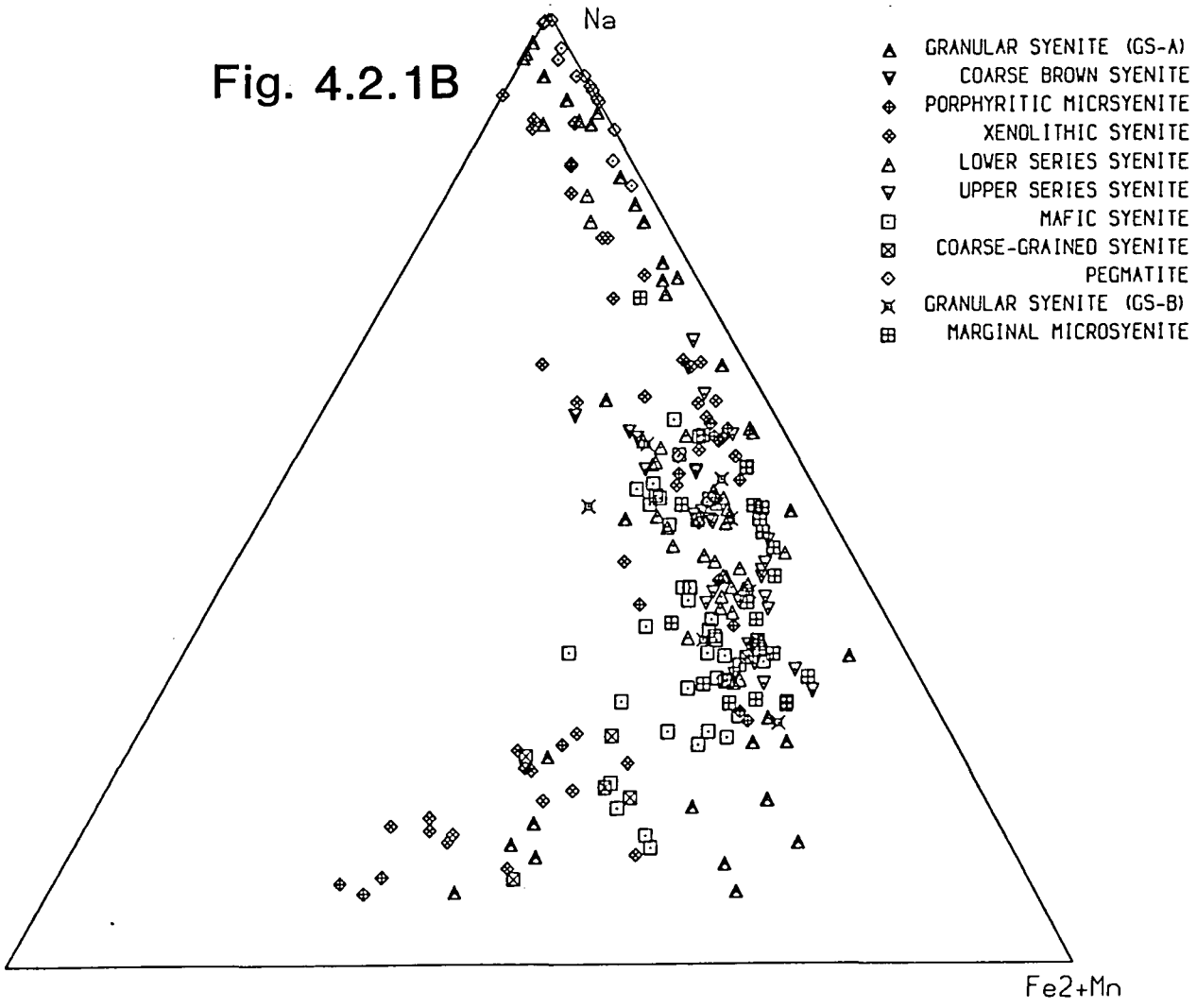

Because of their abundance and the large amount of relevant literature available, the pyroxenes received the most detailed examination of any mineral group.

4.2.2 Recalculation, projection, and nomenclature

Microprobe analyses are given with all iron reported as Fe^{2+}. The amount of Fe^{3+} is not simply equal to (Na+K), as alkaline end-members other than acmite ($NaFe^{3+}Si_2O_6$) will almost certainly be present (eg. jadeite, $NaAlSi_2O_6$). In this study, Fe^{3+} is determined by assuming stoichiometry of the pyroxene, and recalculating the analysis by assuming the deficiency in oxygen atoms is due solely to Fe^{3+}. This method assumes four cations to six oxygens, and that other multivalent cations (such as Ti^{2+}, Ti^{3+}, Mn^{4+}) and unanalysed elements are present in insignificant quantities. Pyroxene formulae were recalculated by this method using the program `IRON3.STOIC` written by Dr. N.J.G. Pearce (Pearce 1988).

Alkali pyroxenes may be illustrated in the projection *diopside-hedenbergite-acmite* (fig. 4.2.1A), commonly evolving towards more Na-rich compositions by the substitution $Ca(Fe^{2+},Mg)\rightleftharpoons NaFe^{3+}$ (fig. 4.2.3). This diagram also shows the classification according to Deer *et al.* (1982) and Jones (1980). It is tempting to make direct comparisons with fig. 4.2.1B, which shows all syenitic pyroxenes plotted as Mg–(Fe^{2+}+Mn)–Na, the projection most commonly used for alkali pyroxenes (eg. Stephenson 1973, Chambers 1976, Larsen 1976, Jones 1980, Pearce 1988). However, the presence of Na in end members other than acmite (such as jadeite) means that the two diagrams are not strictly interchangeable. Calculation of pyroxene end-member proportions referred to in later parts of this section have been carried out using the program `PYROXENE.F4B` written by Dr. A. Peckett of Durham University (Appendix II, and Jones and Peckett 1980).

4.2.3 Site Occupancy

A review of site occupancy in monoclinic pyroxenes is given by Deer *et al.* (1982), but a summary will be given here as it is relevant to later discussions. The general formula for pyroxenes is $X^{(vi-viii)}Y^{(vi)}Z^{(iv)}{}_2O_6$, with X, Y, and Z representing different cation sites as follows:

Z (T site): The tetrahedral site, occupied by Si and Al, and under certain conditions by Fe^{3+} in the ferri-Tschermak's component $CaFe^{3+}_yFe^{3+}_zSiO_6$ (Huckenholz *et al.*, 1969).

Y (M1 site): The octahedral site, essentially occupied by Mg, Fe^{2+}, and Fe^{3+} in the alkali pyroxenes, but also by Al, Ti, and Zr.

Z (M2 site): A disordered six to eight-fold co-ordinated site, occupied by Ca and Na in alkali pyroxenes, together with Mn, Fe^{2+}, and small amounts of K. The latter reaches a maximum of 0.492 wt.% K_2O in the marginal microsyenite G38.

4.2.4 Pyroxene variations in different rock-units

Fig. 4.2.2 shows the range of pyroxene compositions within each unit described in chapter 3, plotted in terms of Mg–Fe^{2+}+Mn–Na, with units showing similar trends discussed together below. It should be borne in mind that the wide range of compositions in some units partly results from strong zonation within individual pyroxenes (eg. GS-A), and the trends thus represent a composite of the pyroxene analyses (cf. fig. 4.2.4).

Lower and Upper Series Syenite, Marginal Microsyenite

These three groups have a fairly restricted range from $Mg_{12}(Fe^{2+},Mn)_{60}Na_{28}$ to $Mg_5(Fe^{2+},Mn)_{30}Na_{65}$, indicating that the dominant substitution taking place is $Ca_x(Fe^{2+},Mn)_y \rightleftharpoons Na_xFe^{3+}_y$. Two analyses from the Lower Series Syenite

Fig. 4.2.2(two pages). Variations in the system Mg-(Fe^{2+}+Mn)-Na for each syenite unit described in chapter 3. Symbols are the same as those used in fig. 4.2.1B.

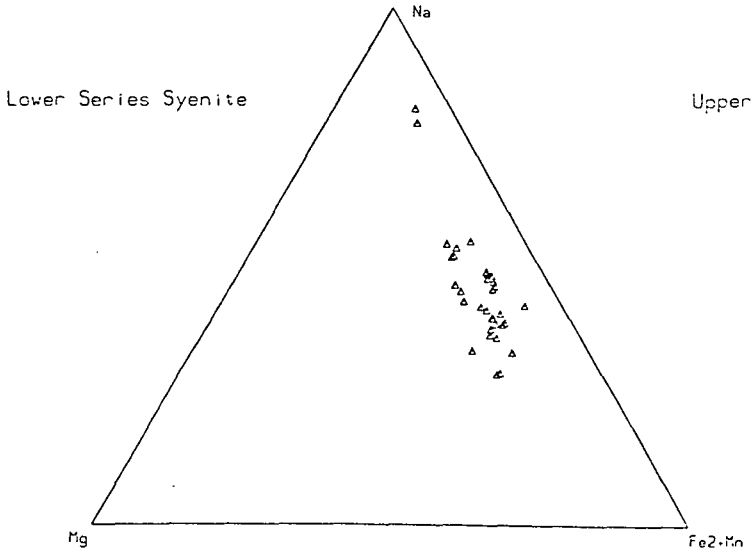
Lower Series Syenite
Na
Mg
Fe2+Mn

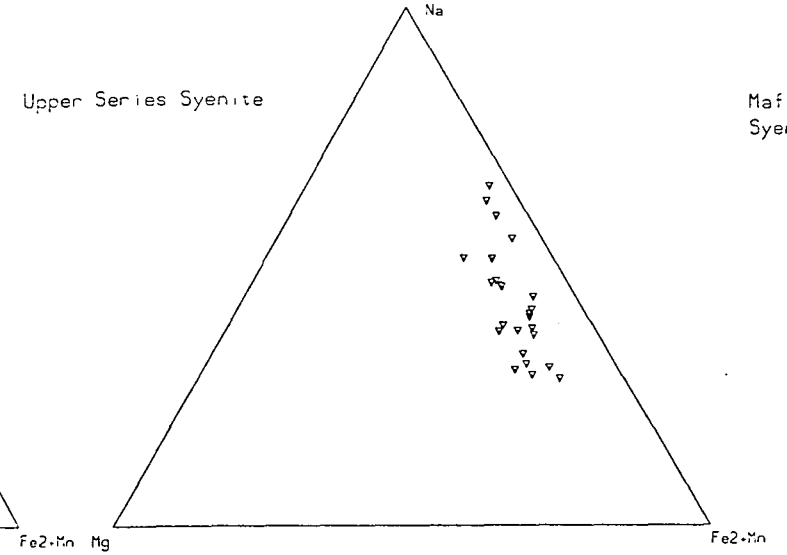
Upper Series Syenite
Na
Mg
Fe2+Mn

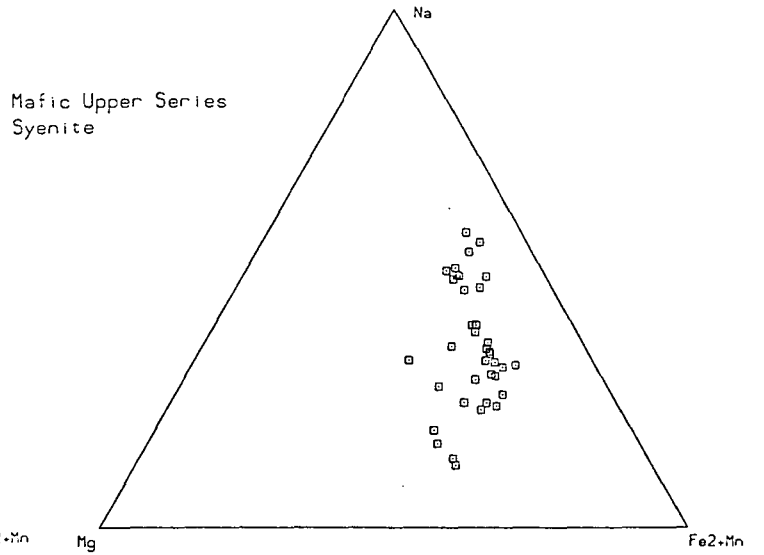
Mafic Upper Series Syenite
Na
Mg
Fe2+Mn

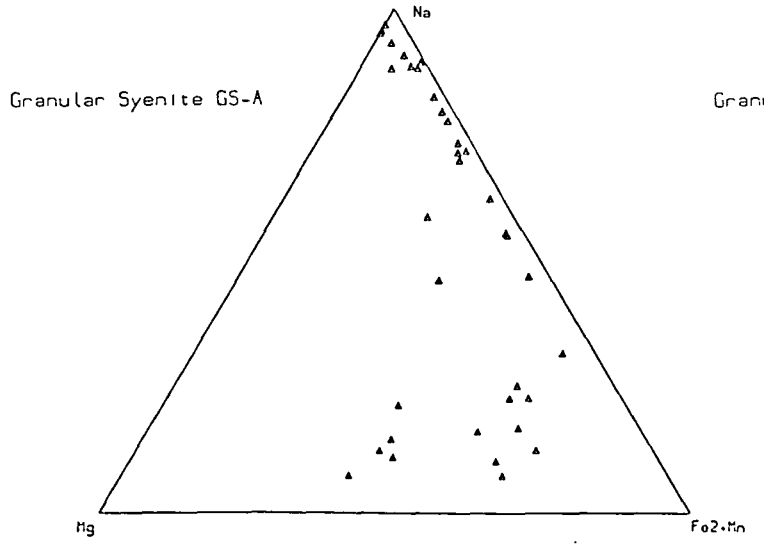
Granular Syenite GS-A
Na
Mg
Fe2+Mn

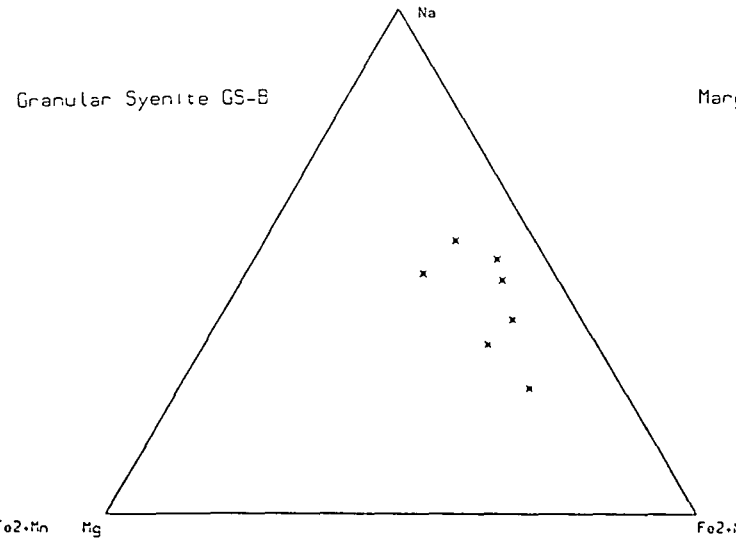
Granular Syenite GS-B
Na
Mg
Fe2+Mn

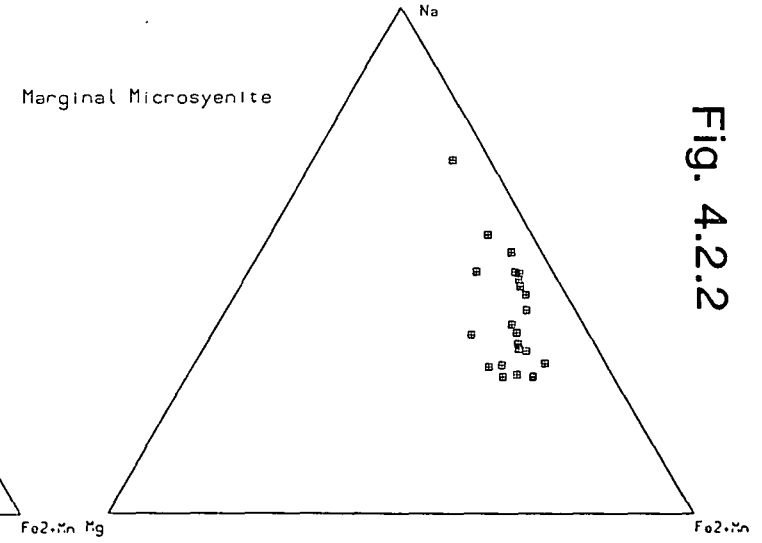
Marginal Microsyenite
Na
Mg
Fe2+Mn

Fig. 4.2.2

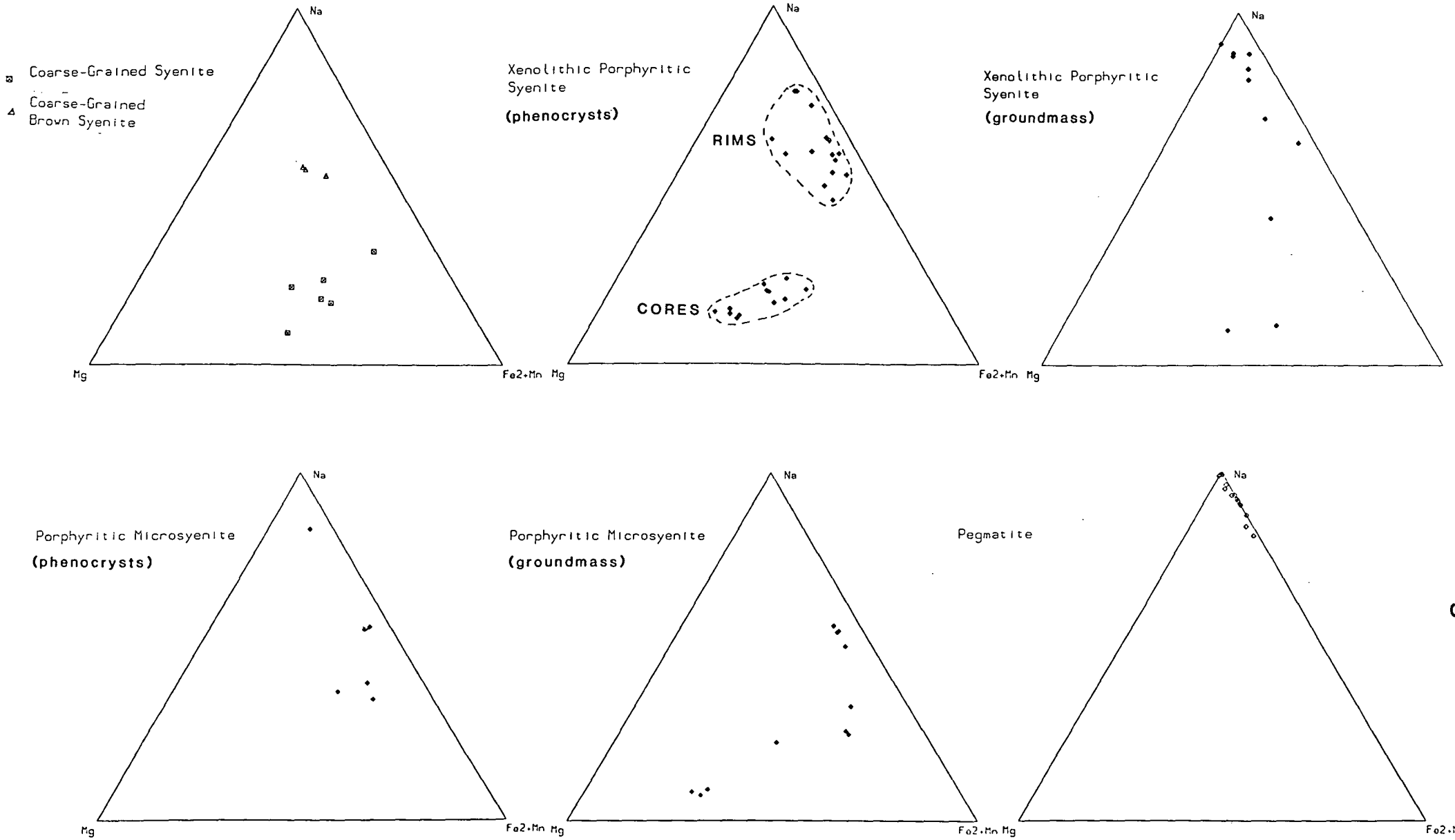
Coarse-Grained Syenite
Coarse-Grained Brown Syenite
Na
Mg
Fe2+Mn
Xenolithic Porphyritic Syenite
(phenocrysts)
RIMS
CORES
Xenolithic Porphyritic Syenite
(groundmass)
Porphyritic Microsyenite
(phenocrysts)
Porphyritic Microsyenite
(groundmass)
Pegmatite

Fig. 4.2.2 (cont.)

(138055.15 and 138055.17) have compositions up to Na_{82}, the high alkali content resulting from late-stage crystallisation from residual intercrystalline liquid (section 4.2.5). The marginal microsyenite pyroxenes show considerable compositional overlap with those from both the Lower and Upper Series Syenite, and have a similar compositional range. This is consistent with the field evidence which suggests that these microsyenites represent a chilled marginal of the Lower and Upper Series, and would also imply that little *in situ* fractionation of the pyroxenes took place, the compositional range having been established prior to emplacement. Late-stage pyroxenes with a wide variety of compositions do, however, appear to have crystallised from pockets of trapped residual liquids (cf. section 4.2.5, sample 138044).

Mafic Upper Series Syenite

This pyroxene-rich unit within the Upper Series shows a slightly wider range of compositions than the group just described, and is also generally less strongly fractionated, being poorer in Na and richer in Mg, ranging down to Mg_{35} $(Fe^{2+},Mn)_{53}Na_{12}$.

GS-A

Pyroxenes from this unit show the widest range of compositions found at Grønnedal-Íka, from the least fractionated ($Mg>Fe^{2+}+Mn$) to the most fractionated (up to Na_{95}), becoming strongly depleted in Mg with increasing Na substitution. The wide variation and large number of analyses is due to the examination of two very strongly zoned pyroxenes in G169 (section 4.2.5).

GS-B

This unit occurs as sheets within the country-rock and other marginal syenites around the north-west margin of the complex, and is possibly coeval with the emplacement of the Lower and Upper Series Syenites. Pyroxene compositions have a fairly restricted range, as in the Lower and Upper Series, though are slightly more magnesian than the latter group.

Coarse-grained and Coarse-Grained Brown Syenite

Only three pyroxene analyses were possible from the Coarse-Grained Brown Syenite due to the strong alteration of this unit. They are fairly evolved, and form a close group approximating to $Mg_{15}(Fe^{2+},Mn)_{30}Na_{55}$. Similarly, few analyses were possible for the Coarse-Grained Syenite due to alteration. All six were recorded from G275, and indicate fairly primitive compositions.

Xenolithic Porphyritic Syenite

Pyroxenes from this unit show a wide variety of compositions and relatively early enrichment of Na. Phenocryst and groundmass compositions are shown separately, the former showing a distinct bimodal distribution, with cores representing the least evolved, and rims the most evolved compositions (cf. section 4.2.5). Groundmass pyroxenes show a range of compositions, but tend to be strongly enriched in Na, as would occur if they crystallised from a more evolved magma than the phenocrysts.

Porphyritic Microsyenite

The Porphyritic Microsyenites have the most primitive pyroxene composition determined ($Mg_{65}(Fe^{2+}Mn)_{26}Na_9$), but otherwise show many similarities to the trend from the Xenolithic Porphyritic Syenite, and for this reason, the two groups are shown together in fig. 4.2.3A. Again, phenocryst and groundmass compositions are illustrated separately, though unlike the the Xenolithic Porphyritic Syenite, the groundmass pyroxenes show less evolved compositions than the phenocrysts. Stephenson (1976) has suggested that alkali feldspar compositions lying on the K-rich side of the 5kb eutectic in the $Ab - Or - An$ system is a result of early crystallisation of Na-rich phases, such as nepheline, which tend to deplete the magma in Na. This may also account for the later groundmass pyroxenes being relatively depleted in Na, nepheline occurring as large phenocrysts in these rocks.

Pegmatites

All compositions in this unit were recorded from two samples (G183, 138055), and show a limited range of compositions, with low Mg and extreme enrichment in Na (up to Na_{99} in G183.01).

Trends for pyroxenes from these different groups are shown in fig. 4.2.3A, and other alkali-pyroxene trends in fig. 4.2.3B for comparison. A common feature is the initial trend away from Mg towards (Fe^{2+}+Mn) at low, relatively constant values of Na, as a result of the substitution CaMg⇌Ca(Fe^{2+}+Mn). With increasing fractionation, the substitution Ca(Mg,Fe^{2+}+Mn)⇌$NaFe^{3+}$ takes over, and the trends turn towards the Na apex of the triangle, beginning at different stages of pyroxene evolution in different suites.

Many workers have appealed to the f_{O_2} as the controlling factor in the timing of acmite enrichment (eg. Aoki 1964, Yagi 1966, Larsen 1976, Jones 1980, Stephenson and Upton 1982). They suggest that the point at which the f_{O_2} rises above the quartz-fayalite-magnetite (QFM) buffer determines when enrichment in $NaFe^{3+}$ becomes dominant, and that this will commence earlier in magmas with a higher f_{O_2}. However, Mitchell and Platt (1978) point out that f_{O_2} will fall with decreasing temperature, and Nash and Wilkinson (1970) suggest that Na enrichment in pyroxenes from the Shonkin Sag laccolith occurs because the f_{O_2} and temperature of the magma fall at a rate less than that required to maintain a constant Fe^{3+} /Fe^{2+} ratio, so that $a_{Fe^{3+}}$ and therefore a_{acmite} increase. Work by Carmichael and Nicholls (1967) shows that $a_{Fe^{3+}}$ is also controlled by the alkali content of the magma, Fe^{3+}/Fe^{2+}+Fe^{3+} increasing with increasing alkalis (the 'alkali-ferric iron effect'). Another suggestion, by Brouce and Rançon (1984), is that liquid structure is also important, as it controls the partitioning of elements between the magma and crystallising phases.

Many factors may obviously be involved in controlling the evolution of the alkali-pyroxenes, though it is possible that the f_{O_2} controls the timing of acmite

Fig. 4.2.3A. Summary of trends illustrated in fig. 4.2.2, showing grouping of units with similar trends as described in section 4.2.4.

PEG = Pegmatite

LUMS = Lower and Upper Series Syenite, marginal microsyenite

MUS = Mafic Upper Series Syenite

GS-A = Granular Syenite GS-A

GS-B = Granular Syenite GS-B

CGS = Coarse-Grained Syenite

XPS+PMS = Xenolithic Porphyritic Syenite and Porphyritic Microsyenite

Analyses from the Coarse-Grained Brown Syenite have been omitted as only three results were obtained.

Fig. 4.2.3B. Alkali pyroxene tends from various other rock-suites in the system Mg-(Fe^{2+}+Mn)-Na for comparison.

1. Auvergne, France (Varet 1969)
2. Itapirapuã, Brazil (Gomes *et al.* 1970)
3. Uganda (Tyler and King 1967)
4. South Qôroq (Stephenson 1972)
5. Motzfeldt (Jones 1980)
6. Igdlerfigssalik (Powell 1976)
7. Ilímaussaq (Larsen 1976)

Fig. 4.2.3A

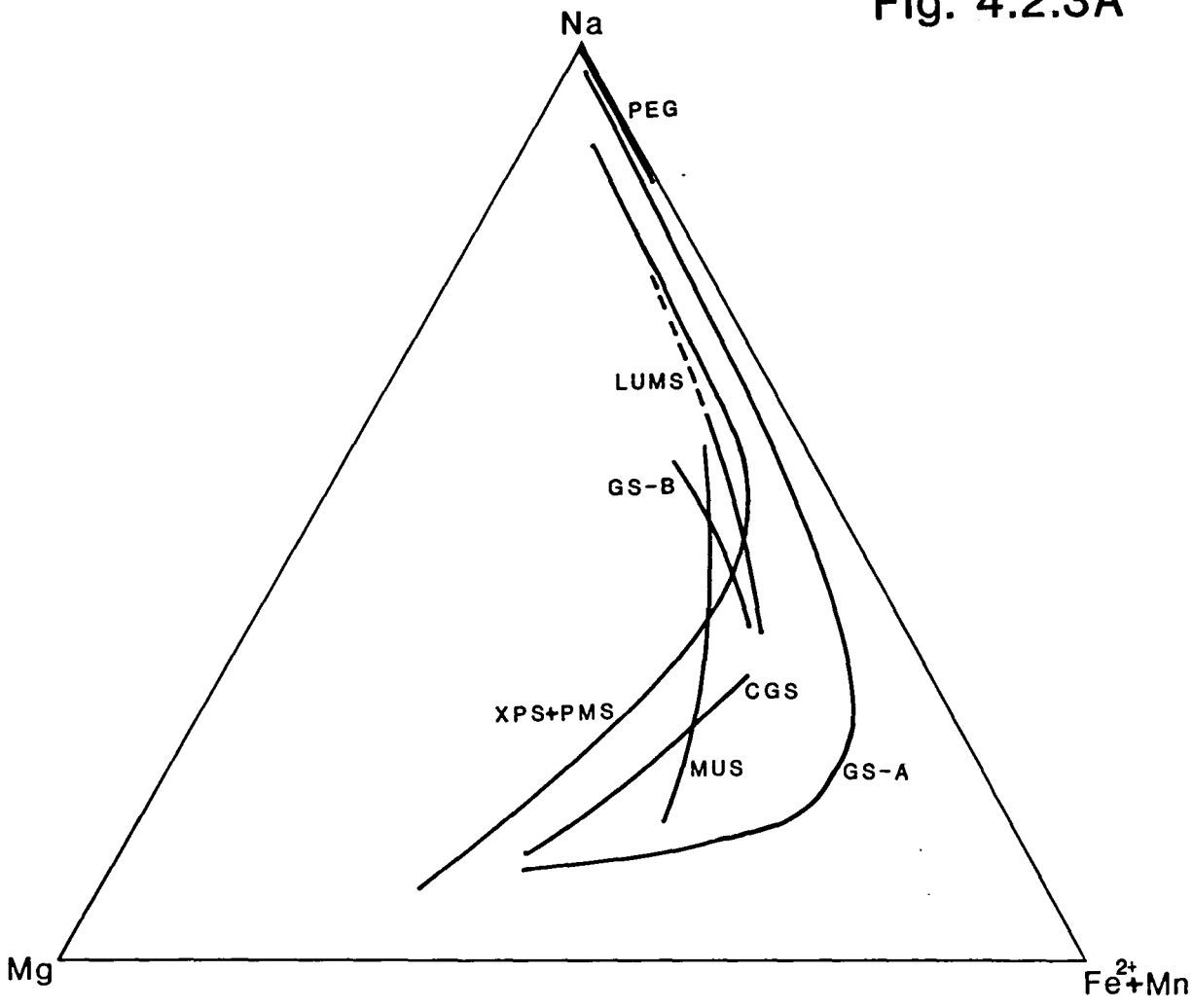

Fig. 4.2.3B

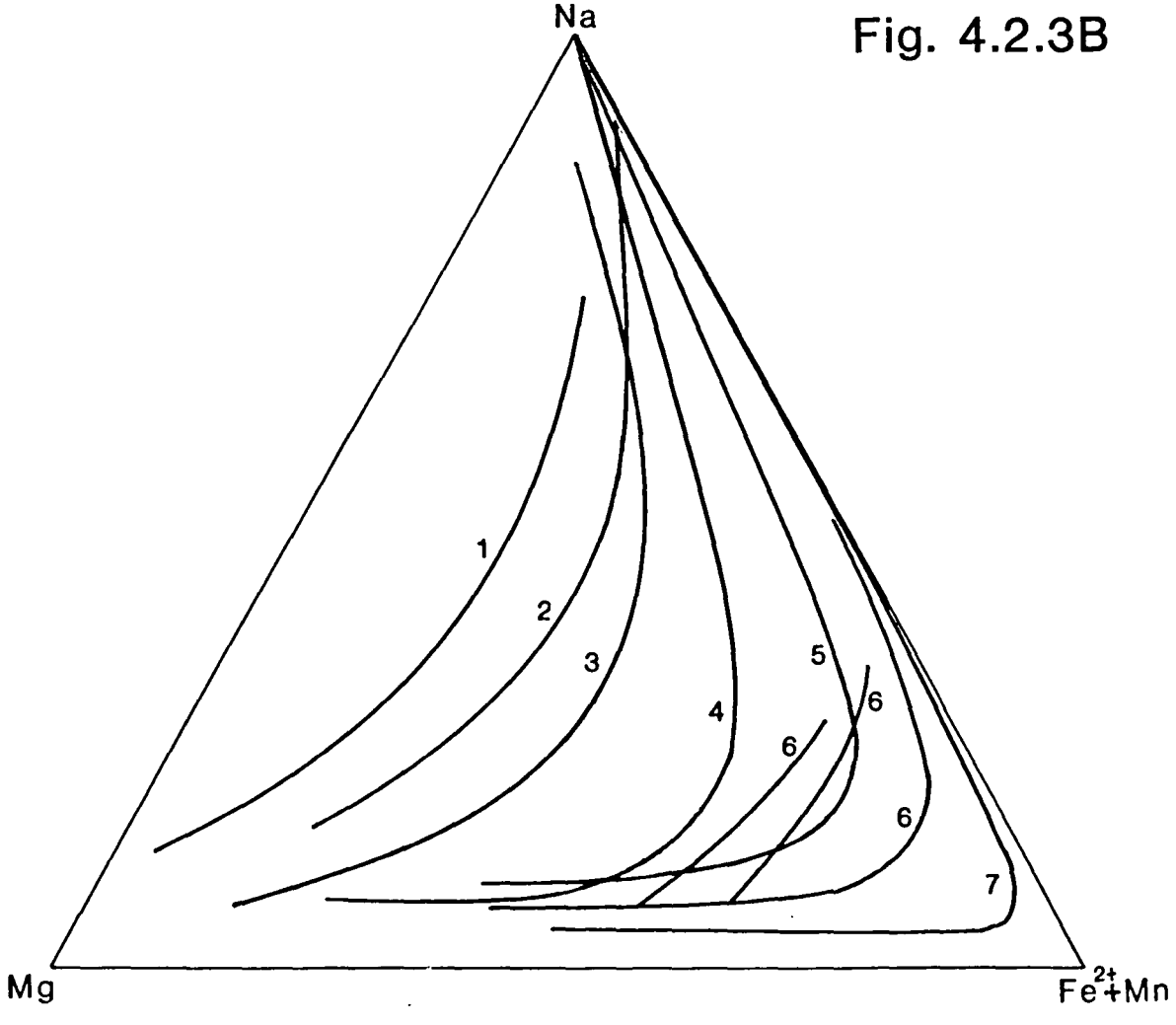

enrichment, while the peralkalinity determines how far towards Na this proceeds. The strong compositional zoning of many grains suggests that the final liquids from which the outer parts of the crystal grew were significantly different from the magma from which these pyroxenes originally crystallised.

4.2.5 Zonation and textural controls on composition

Continuous pyroxene zonation is a common feature of most samples observed. Compositional variations between core and rim confirm that the slightly darker rims are richer in Na than the rather paler cores.

The most spectacular continuous zonation occurs in GS-A (cf. section 3.5.1, plates 3.7, 4.1, and 4.2), the compositional variations across which are shown in fig. 4.2.4A. Fig. 4.2.4B shows the variation of Zr across each pyroxene, expressed in terms of atoms per six oxygens. This element shows a sympathetic variation with Na enrichment, with a sharp increase towards the rim, reaching some of the highest Zr contents analysed (2.35% ZrO_2, equivalent to 0.044 atoms per six oxygens), though still well below the 6.96% reported by Jones (1980) in one sample from unit SM3 of the Motzfeldt centre.

Fig. 4.2.5A shows the variation in three continuously zoned pyroxenes from the Xenolithic Porphyritic Syenite, while fig. 4.2.5B shows the compositional differences between cores and rims of discontinuously zoned (ie. rimmed) pyroxenes from several samples. Plate 3.8 shows the optical appearance of such a grain: pink-grey cores overgrown by emerald-green rims, which petrographic observation alone would suggest were more sodic. This is confirmed by microprobe analysis, and a strong bimodal distribution is evident. The pink-grey colour of the cores in plane-polarised light is reminiscent of titanian augites (Deer *et al.*, 1982), but they are not unusually rich in Ti, and none of the other elements analysed would seem to be responsible for the colour.

Fig. 4.2.4. Compositional variations across two zoned pyroxenes from sample G169 from the Granular Syenite GS-A. The numbers refer to analysis points as presented in appendix I and illustrated in plates 4.1 and 4.2, which show the position of the analyses.

Extreme enrichment in Na towards the rims is evident from fig. 4.2.4A, while a sympathetic trend in Zr is shown in fig. 4.2.4B.

Fig. 4.2.5. Variations across zoned pyroxenes from the Xenolithic Porphyritic Syenite

Fig. 4.2.5A shows variations across three continuously zoned grains, while fig.4.2.5B shows the strong bimodal distribution of core and rim compositions across discontinuously zoned (ie. rimmed) pyroxenes.

Fig 4.2.6. Variations of pyroxene composition with height in the Lower Series Syenite in the north-western part of the complex. The map (fig 4.2.6A) shows the location of the three samples from the Lower Series (stippled), while fig. 4.2.6B shows the differences in composition and range of compositions of pyroxenes from different levels in the series.

Fig. 4.2.4A

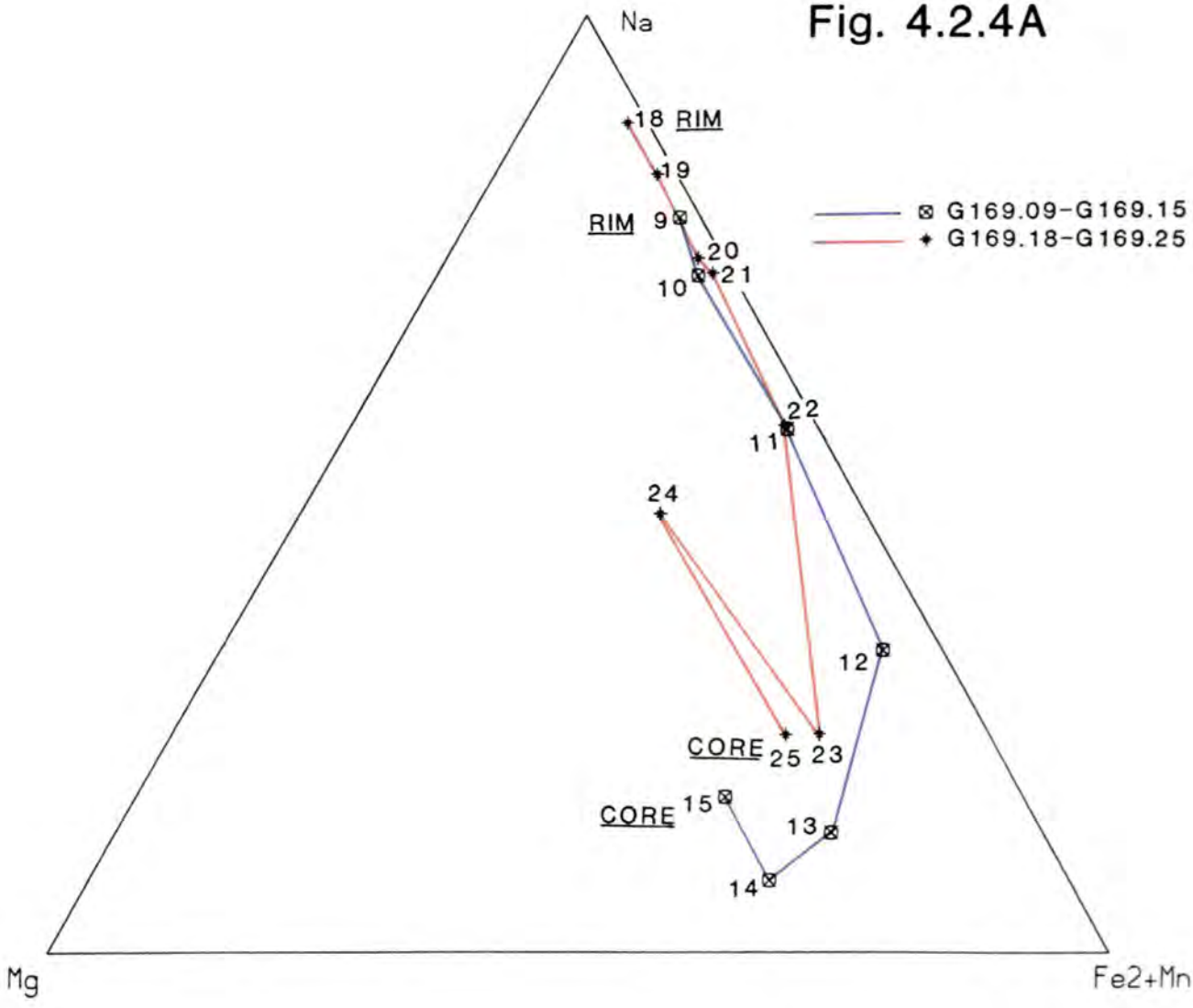

Fig. 4.2.4B

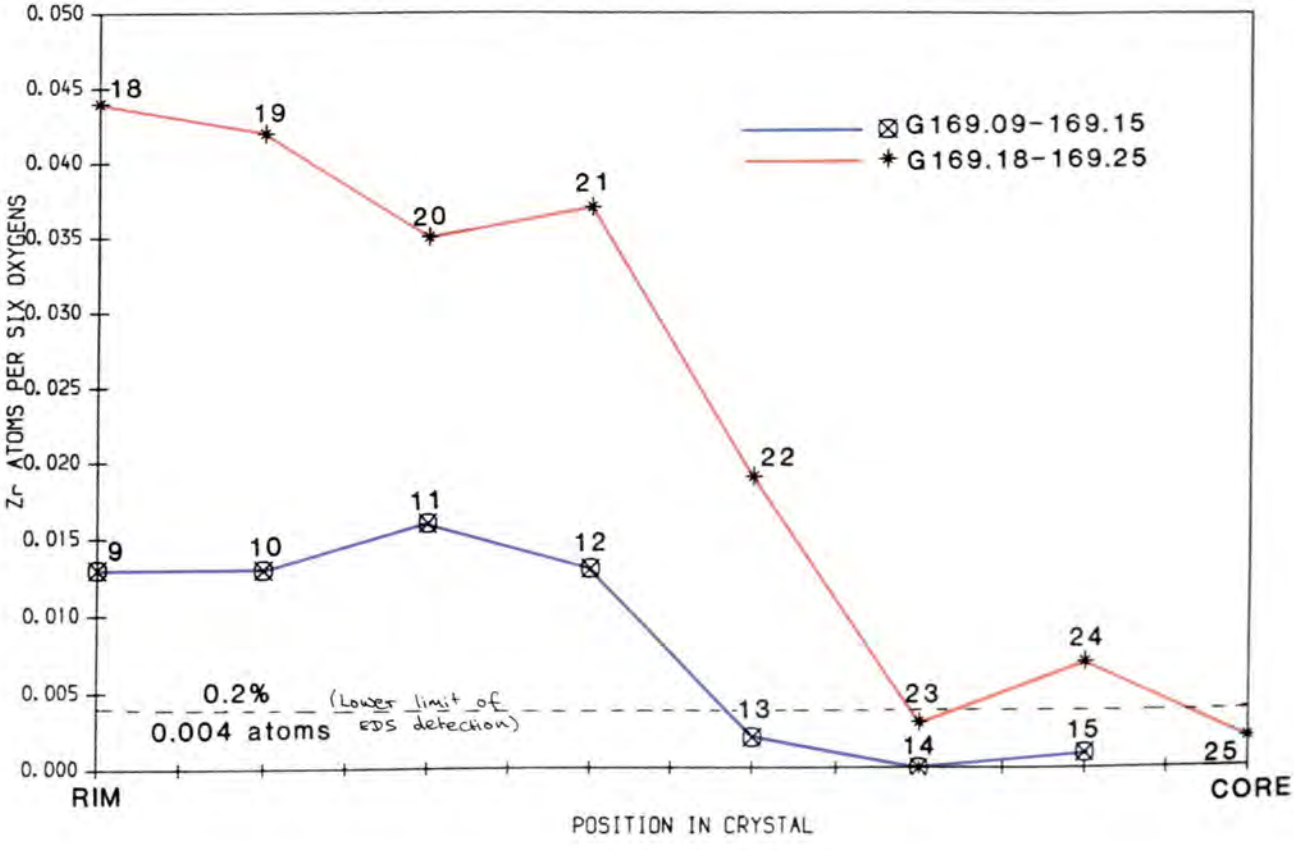

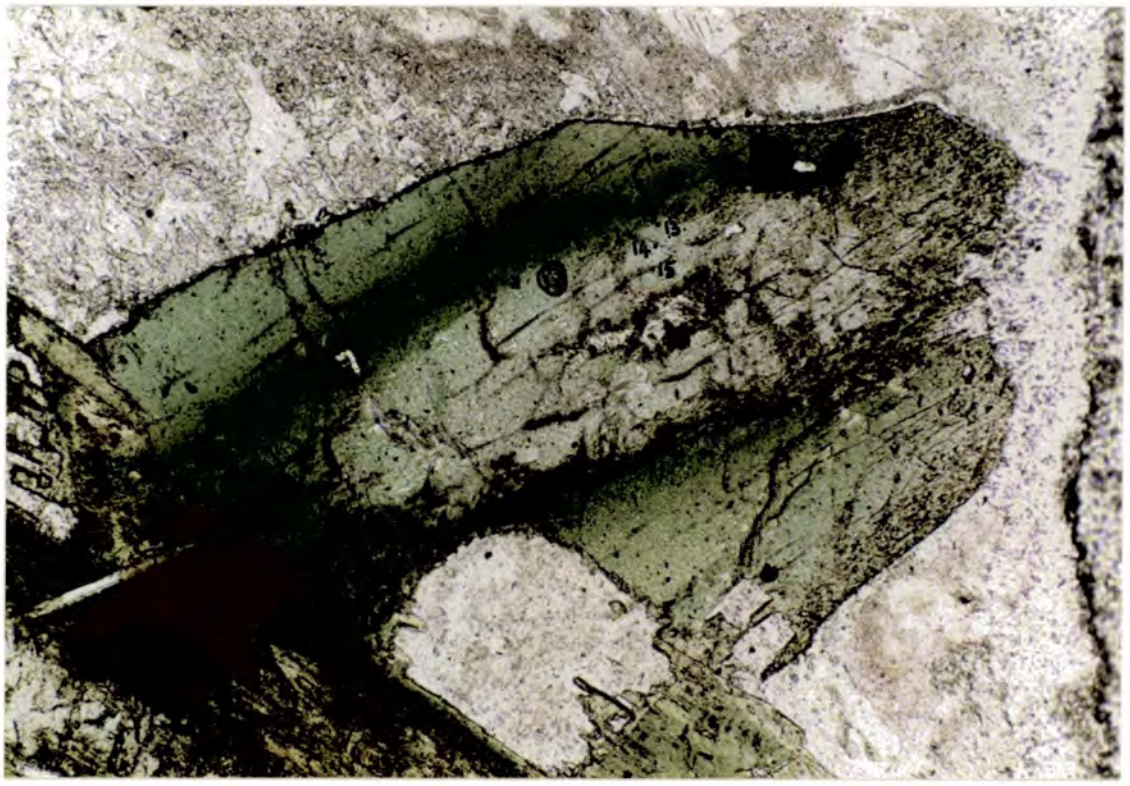

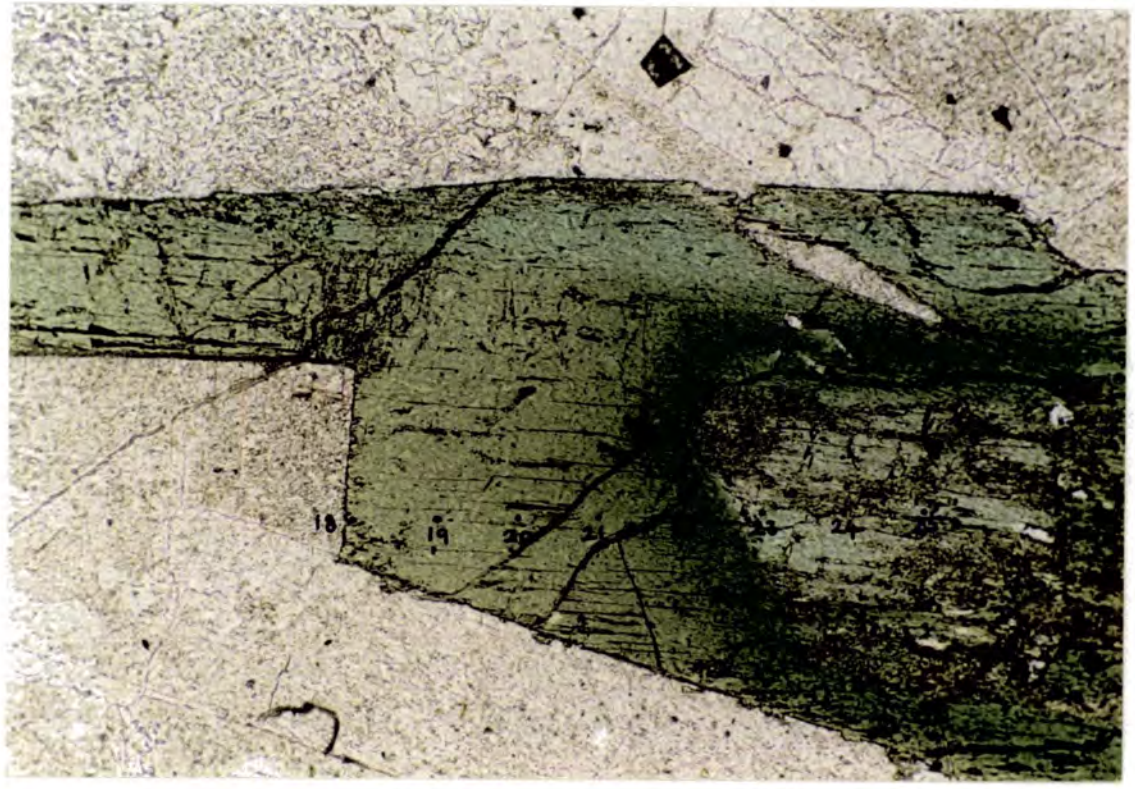

Plates 4.1, 4.2. G169. ×100. PPL. Positions of analyses referred to in fig. 4.4.2 and Appendix II for two exceptionally zoned pyroxene grains in GS-A.

Fig. 4.2.5A

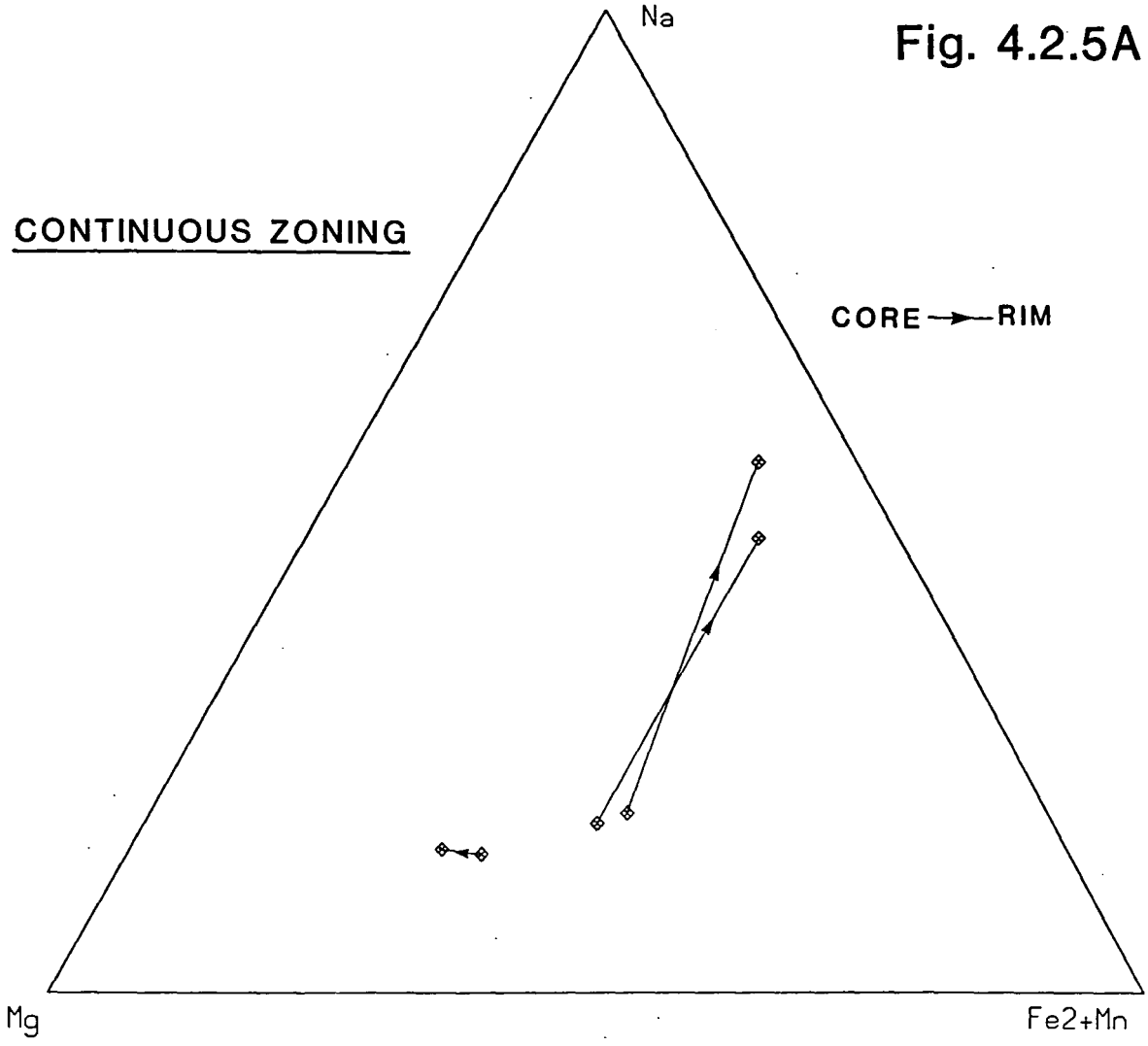

Fig. 4.2.5B

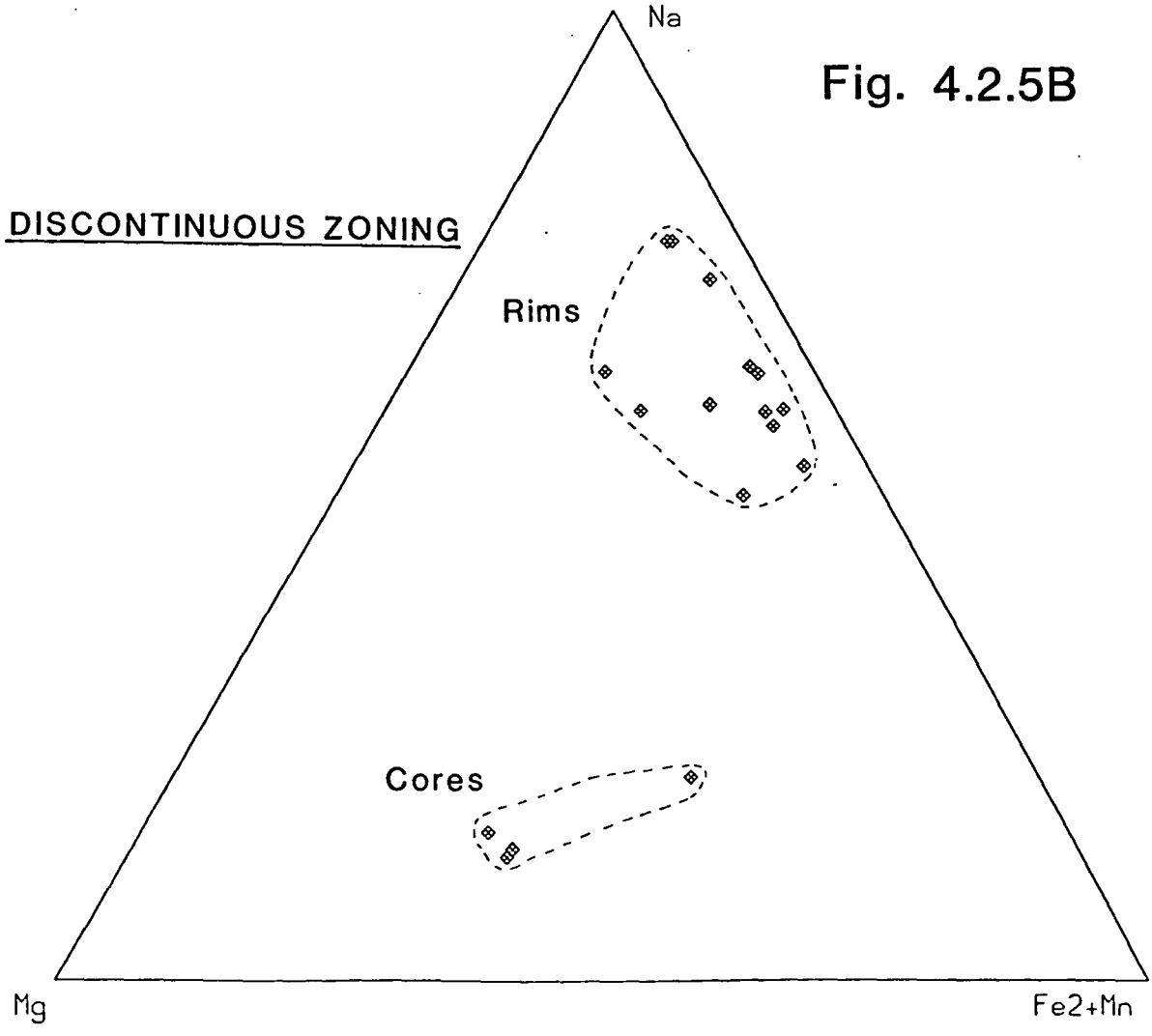

Fig. 4.2.6A

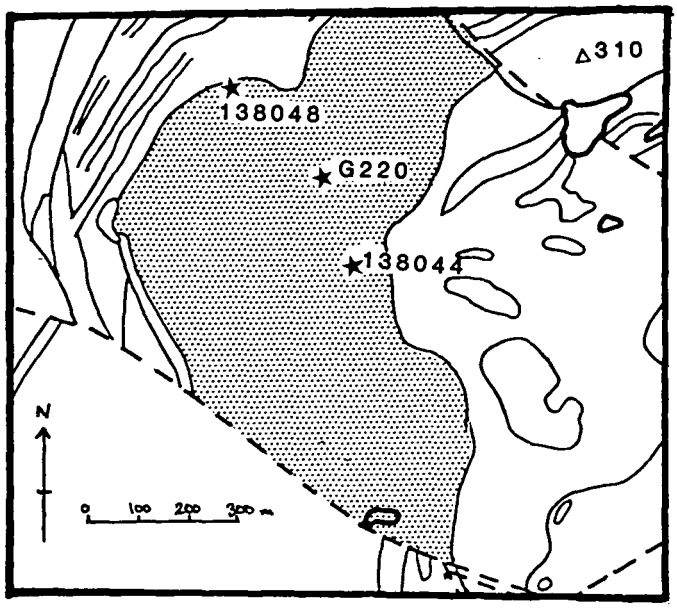

Fig.4.2.6B

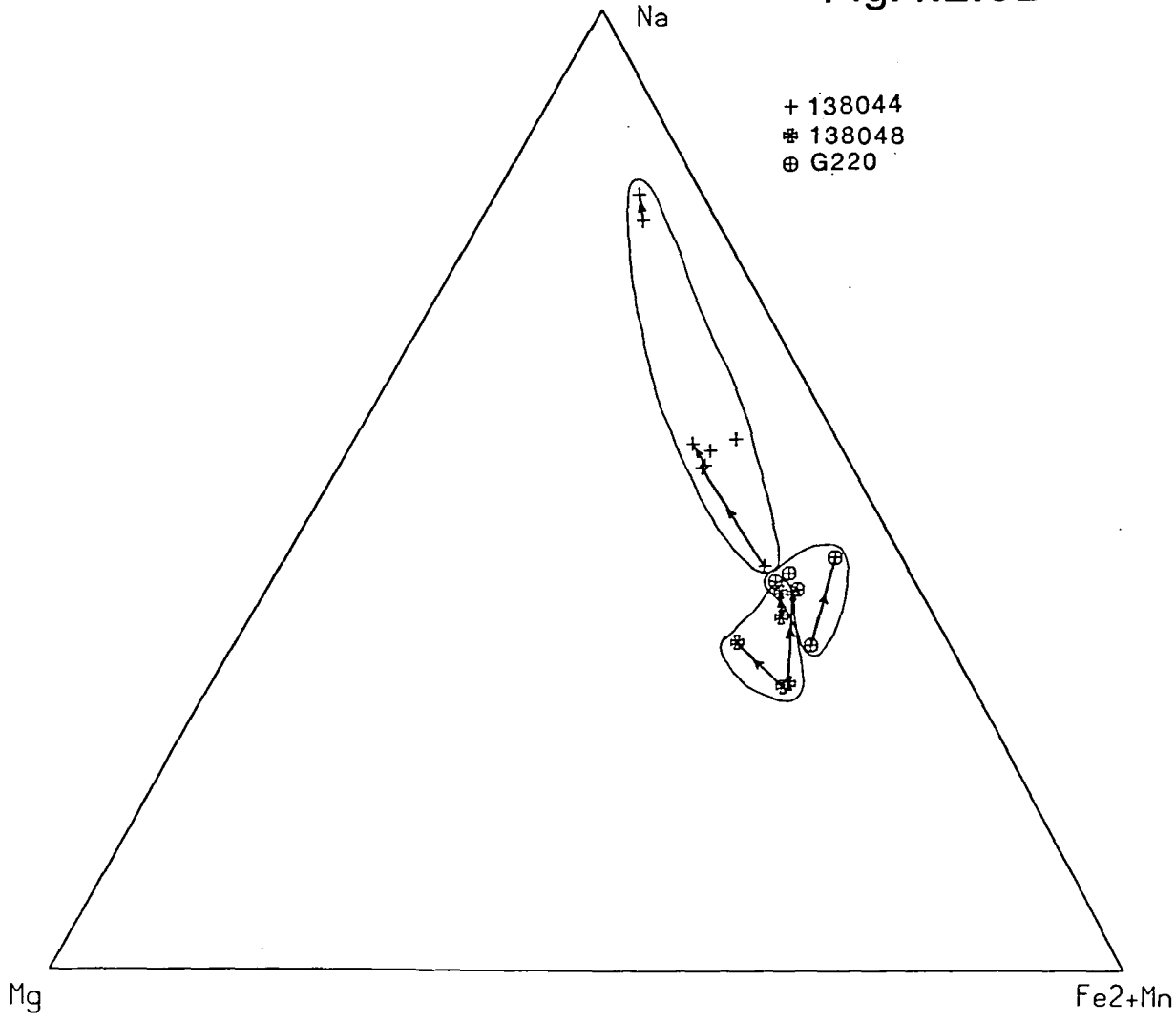

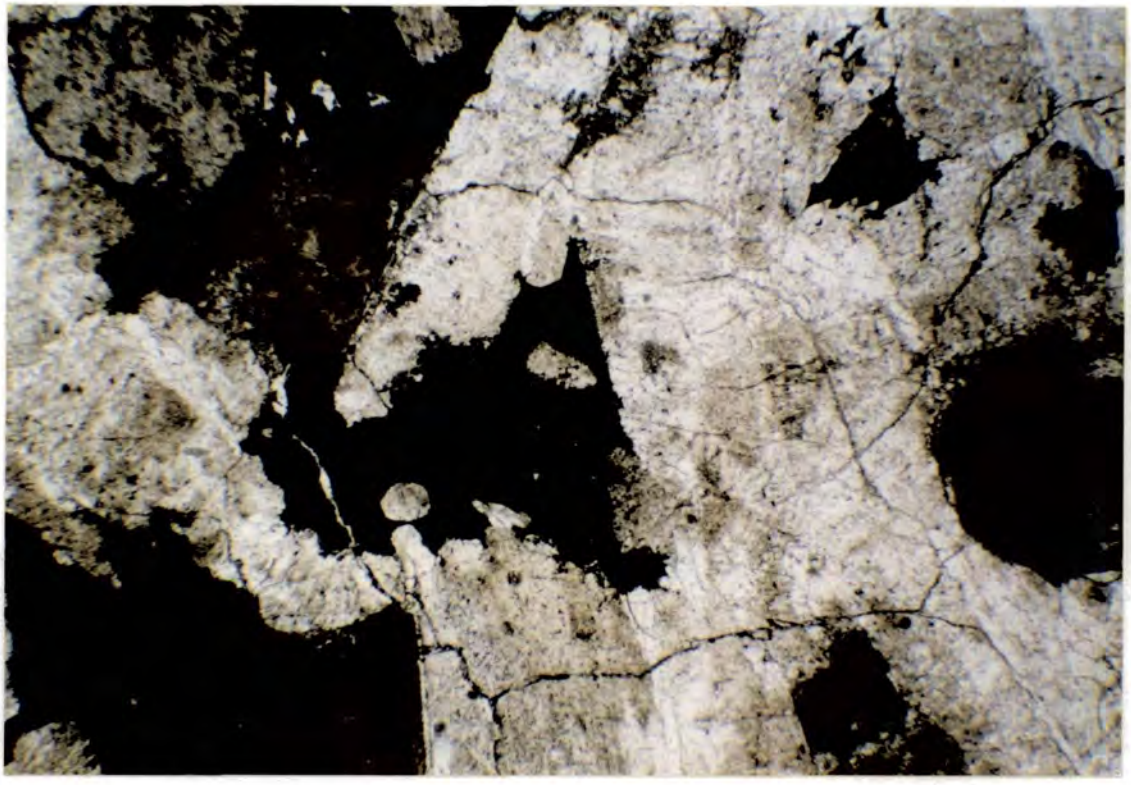

Plate 4.3. 138048. ×35. PPL. Pyroxene from near the top of the Lower Series Syenite (fig. 4.2.6A), with a distinctly interstitial relationship to the surrounding alkali feldspar. These pyroxenes have a relatively wide range of compositions compared to those from the base of this unit (138048.15 and 138048.17 from this grain.

Plate 4.4. 138044. ×35. PPL. Pyroxene from near the base of the Lower Series Syenite (fig. 4.2.6A), showing a distinctly euhedral outline, with a more restricted range of compositions than those from the top of the unit, suggesting very little crystallisation from interstitial liquids has occurred.

Fig. 4.2.6 shows the variation of pyroxene compositions in samples collected from different levels in the Lower Series Syenite. Not only is there an increase in Na-enrichment (ie. fractionation) with increasing height, but the *range* of compositions is greatest for pyroxenes from the highest levels in the series (sample 138044). This sample contains the most interstitial-looking pyroxenes (plate 4.3) compared to 138048 from the base of the Lower Series Syenite (plate 4.4), where they are distinctly euhedral, with relatively little overgrowth.

Thus not only does pyroxene fractionation increase with structural level within the Lower Series Syenite, but those from near the top of the unit have crystallised from interstitial liquids which have evolved independently to produce a wide range of chemical compositions, despite being only a few millimetres apart.

4.2.7 Major element variation

Variations in major and minor elements are illustrated in fig. 4.2.7, which shows the number of cations per six oxygens plotted against fractionation index (FI). The FI, equivalent to the number of Na atoms minus the number of Mg atoms per six oxygens, enables the entire range of pyroxene compositions to be shown (Stephenson 1973). Elements considered in this section are Si, Fe^{3+}, Fe^{2+}, Mg, Ca, and Na. End member proportions quoted in this and the following section have been calculated using `PYROXENE.F4B`. See fig. 4.2.7 for a discussion of major element trends.

4.2.8 Minor element variation

The sympathetic trend of Ti and Al has been noted by many workers (eg. Larsen 1976), and occurs at Grønnedal-Íka, where relatively high values at a low FI (0.28 Al and 0.055 Ti atoms per six oxygens) decrease further to a minimum at FI=0.2, before gradually increasing again to around 0.3 Al and 0.07 Ti atoms 6(O). Al occurs as Ca-Ts ($CaAl_2SiO_6$) in less evolved pyroxenes, but more jadeite (Jd) is present with increasing FI. The presence of Na-rich end-members other than

Fig 4.2.7 (three pages). Major and minor element variation with fractionation index (FI=Na-Mg, after Stephenson 1973). Trends for South Qôroq (Stephenson 1973), Ilímaussaq (Larsen 1976), and Motzfeldt (Jones 1980) are shown where relevant.

Si shows a considerable range of values, but generally increase with FI, from *c.*1.8 to 2.06 (both samples from the Xenolithic Porphyritic Syenite), though is generally between 1.96 and 1.98, the deficiency in the Z-site made up by Al.

Fe^{3+} and Na show a sympathetic increase from around 0.1 to just over 1.0 for Na. Ca and Mg, on the other hand, show a decrease with FI, while Fe^{2+} and Mn increase to a maximum at FI=0 before decreasing again. All of these features can be explained in terms of the substitution $Ca(Mg,Fe^{2+}+Mn) \rightleftharpoons NaFe^{3+}$, the inflection in the trend of Ca representing the point at which this exchange begins to occur (the point at which the trends in fig. 4.2.3B turn towards Na). In the case of Grønnedal-Íka, there is no sharp inflection compared to, say, Ilímaussaq, as evident from the tightness of the respective curves.

– – – – – SOUTH QÔROQ

..... ILÍMAUSSAQ

–·–·–·– MOTZFELDT

Fig. 4.2.7

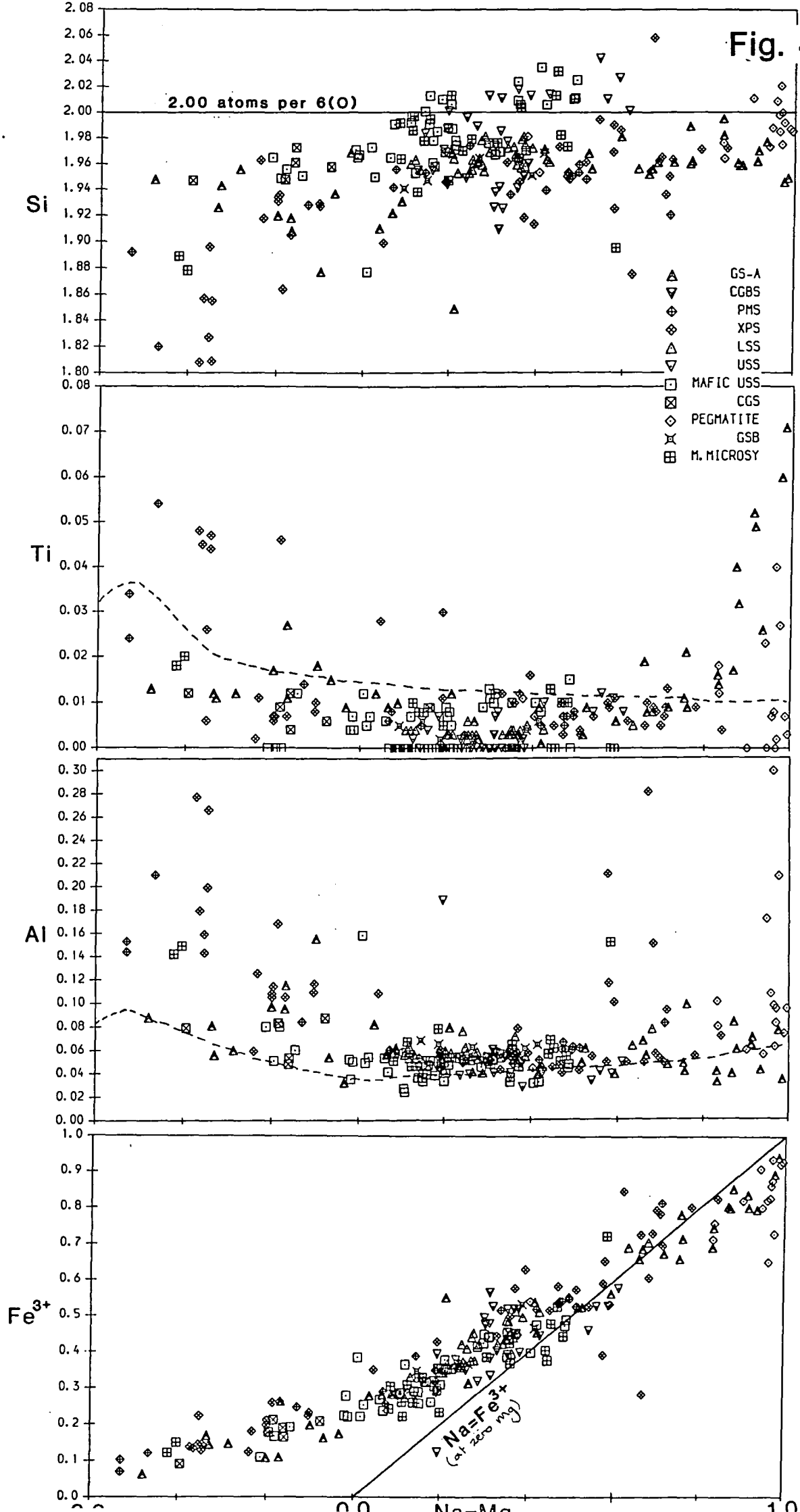
Si
2.00 atoms per 6(O)
Ti
Al
Fe3+
Na=Fe3+
(at zero mg)
Na-Mg
GS-A
CGBS
PMS
XPS
LSS
USS
MAFIC USS
CGS
PEGMATITE
GSB
M. MICROSY

Fig. 4.2.7 (cont.)

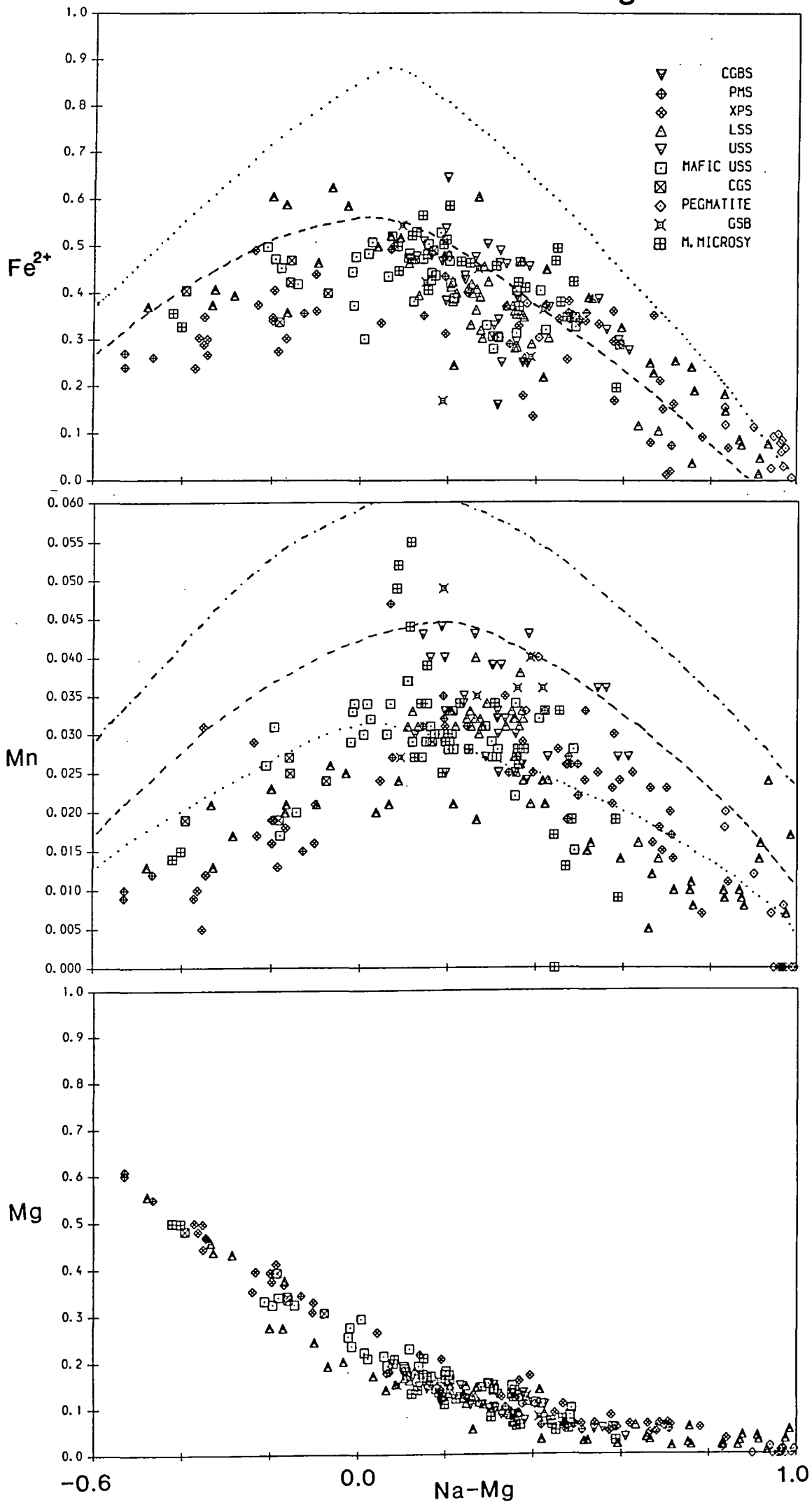
CGBS
PMS
XPS
LSS
USS
MAFIC USS
CGS
PEGMATITE
GSB
M. MICROSY
Fe2+
Mn
Mg
Na-Mg
-0.6
0.0
1.0

Fig. 4.2.7 (cont.)

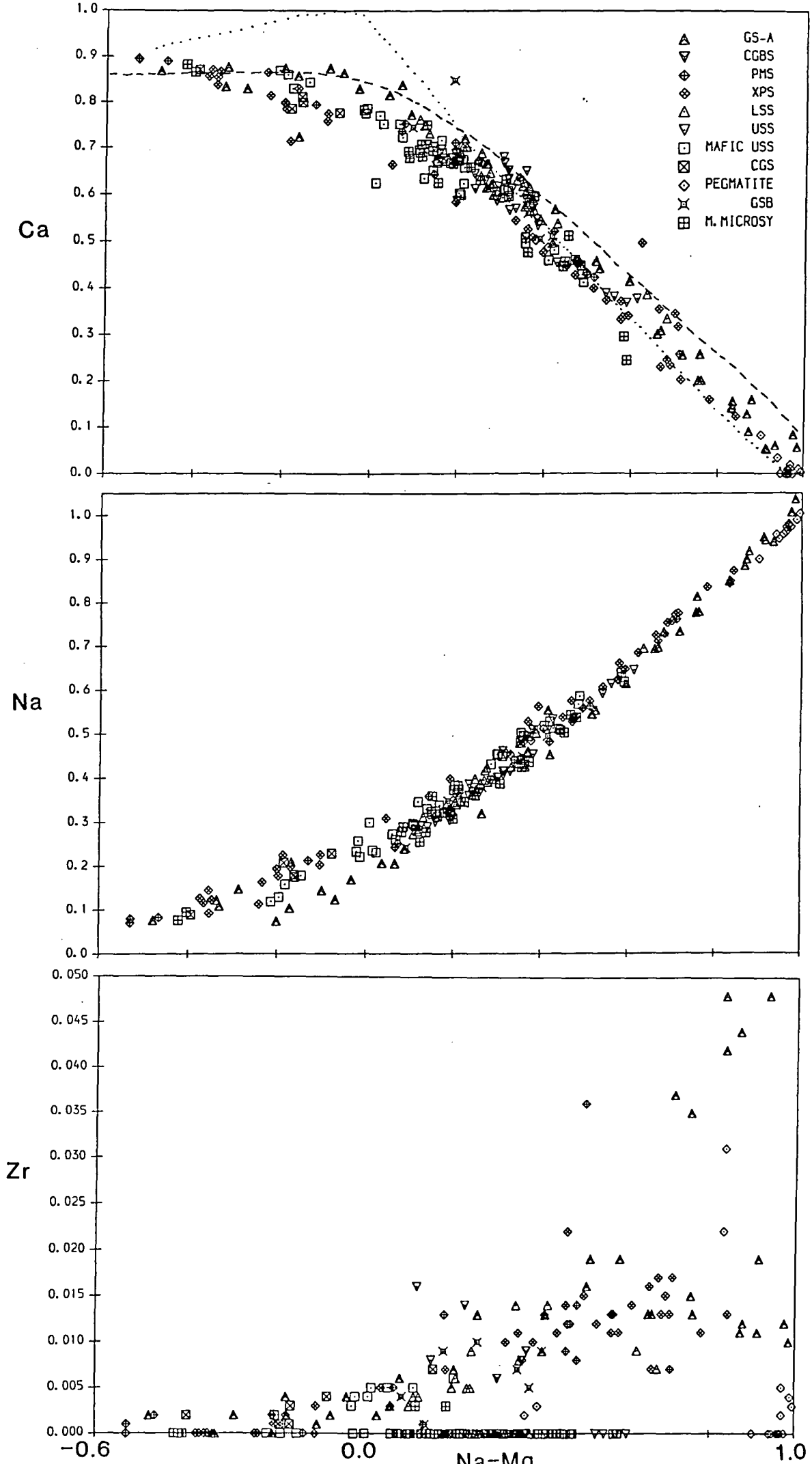
Ca
Na
Zr
GS-A
CGBS
PMS
XPS
LSS
USS
MAFIC USS
CGS
PEGMATITE
GSB
M. MICROSY
1.0
0.9
0.8
0.7
0.6
0.5
0.4
0.3
0.2
0.1
0.0
0.050
0.045
0.040
0.035
0.030
0.025
0.020
0.015
0.010
0.005
0.000
−0.6
0.0
1.0
Na−Mg

acmite is indicated by compositions lying to the right of the line representing $Na=Fe^{3+}$ in fig. 4.2.7. The pyroxenes from the pegmatites show the greatest enrichment of Al with fractionation, with up to 29.6% Jd in 138055.02. Ti occurs with Al in end-members such as $NaAlTiSiO_6$ (NATAL) at high values of FI (up to 5.48% in the pegmatites) and $NaTi_{0.5}(Fe^{2+},Mg)_{0.5}Si_2O_6$ (NAT). The latter occurs in the marginal syenite GS-A (up to 8.89%) which also contain the highest levels of Ti, but low Al contents.

Mn behaves in a similar manner to Fe^{2+} , reaching a maximum at FI=0.2, after which it decreases again. It occurs principally as $CaMnSi_2O_6$ (johansennite), and like Fe^{2+} its behaviour results in increasing fractionation towards (Fe^{2+}+Mn) in fig. 4.2.3 before increasing acmite substitution takes over.

Zr contents generally increase with increasing FI, reaching a maximum of 2.58% (0.048 atoms per six oxygens) in G169.06 and G169.07. However, fig. 4.2.7 gives a misleading impression, as many of the highest levels of Zr were recorded from only two pyroxenes in G169 (section 4.2.5). Zr is reported in pyroxenes from other Gardar centres (eg. Ilímaussaq, Larsen 1976; Motzfeldt, Jones 1980), and present in end-members such as $NaZrAlSiO_6$ (NAZAL) and $Na(Fe^{2+},Mg)_{0.5}Zr_{0.5}Si_2O_6$ (FM-NAZ) as proposed by Jones and Peckett (1980). Examination of Al and Zr trends in fig. 4.2.7 shows that the highest levels of Zr (in GS-A) are not accompanied by high Al values in the same rock-type, and one would predict that FM-NAZ would be the more abundant of the two mentioned. This is confirmed by the use of `PYROXENE.F4B`, which shows that up to 9.62% FM-NAZ is present in G169.01 (GS-A) and 6.21% in pegmatitic pyroxenes, with no NAZAL being recorded in either of these highly fractionated rocks.

The very high contents of Zr (nearly 7% ZrO_2) recorded by Pearce (1988) and Jones (1980) do not occur in the Grønnedal pyroxenes, and apart from the examples mentioned, do not generally exceed about 1% ZrO_2. This is despite similar bulk-rock Zr concentrations, and can be explained by the presence of zircon

in a large number of samples examined, which would act as a sink for Zr. The high values recorded from GS-A are from strongly zoned grains whose textures suggest crystallisation from trapped interstitial liquids.

Experimental work by Watson (1979) showed that the solubility of Zr in felsic melts is largely dependant on the peralkalinity, becoming increasingly soluble in more peralkaline liquids. Jones (1980) found that the Zr-rich pyroxenes tend to have high Fe^{2+}/Fe^{3+} ratios, clearly the opposite of the case at Grønnedal where the Fe^{3+}-rich, acmitic pyroxenes are the most zirconian. Though the bulk-rock peralkalinity of the Grønnedal-Íka syenites rarely exceeds about 1.1 (section 5.2), trapped residual liquids could become strongly peralkaline through continued crystallisation of aluminous phases such as alkali feldspar. Thus in GS-A, residual liquids could become strongly enriched in Zr through increasing peralkalinity, which as suggested by Carmichael and Nicholls (1967) would also increase the $Fe^{3+}/Fe^{2+}+Fe^{3+}$ ratio ('alkali-ferric iron effect'), resulting in the eventual crystallisation of acmitic pyroxenes with high Zr contents. The textural and compositional relationships illustrated in plates 4.1 and 4.2, and fig. 4.2.4 would appear to confirm these ideas.

4.3: Amphiboles

4.3.1 General

As has been emphasised on several previous occasions, amphiboles are a very scarce phase in the syenites of Grønnedal-Íka. This is in marked contrast to other Gardar centres where this mineral is very abundant, and indeed "probably the most abundant mafic mineral in the Motzfeldt centre" (Jones 1980). In contrast, amphiboles are a major constituent of the metasomatised rocks, which are discussed in chapter 7.

Amphiboles from four units were analysed (GS-A, GS-B, the Porphyritic Microsyenites, and the marginal microsyenite) from a total of six samples, and it

is perhaps significant that these are either marginal or a late-stage, cross cutting facies. Ernst (1962) suggests that alkali amphiboles are unstable at high values of f_{O_2}, though the late-stage/marginal nature of these units suggests that it was only in these rocks that the volatile pressures were high enough to enable amphibole crystallisation to take place. It is also notable that unlike the amphiboles of many other Gardar centres, those at Grønnedal do not appear to be rimming pyroxenes, but seem to have crystallised independently (eg. the poikilitic amphiboles in the marginal syenite G44, plate 3.10).

4.3.2 Recalculation and classification

The amphiboles are a highly complex group of minerals, due to the wide variety of cation sites available. Like the pyroxenes, Fe from microprobe analysis is expressed as FeO, but unlike the pyroxenes, they contain a variable number of cations (between 15 and 16 per 23 oxygens) and stoichiometry cannot be assumed for recalculation purposes. One method, suggested by Leake (1978) and used by Pearce (1988) recalculates to 23(O) and adjusts the number of tetrahedral (8 cations) and octahedral (5 cations) sites to 5+8=13 by varying the Fe^{2+}/Fe^{3+} ratio. This method has been carried out here using the program `IRON3.AMP` (Pearce 1988).

The amphiboles are classified according to Leake (1978), based on the general amphibole formula $A_{0-1}B_2C_5T_8O_{23}(OH,F,Cl)_2$ in which cations are assigned to sites in the following order:

T (tetrahedral site): Si, Al, Fe^{3+}, Ti to total 8.00.

C (octahedral site): Excess Al, Fe^{3+}, Ti, then Zr, Mg, Fe^{2+}, Mn to total 5.00.

B (6 to 8-fold site): Excess Mg, Fe^{2+}, Mn, then Ca, Ba, Na to total 2.00.

A (8 to 10-fold site): Excess Na, then K. Should total between 0.00 and 1.00.

The Leake method is preferred to the Phillips (1966) classification scheme, as it uses a larger number of parameters and thus gives a more precise classification.

For example, Phillips' scheme takes no account of Fe^{3+}, and thus arfvedsonite, an important alkali end-member amphibole, is represented by eckermannite in this classification.

Having assigned the cations, the amphiboles can then be classified using the Leake (1978) method, which divides them into four groups based on the B-site occupancy:

$(Ca+Na)_B$ <1.34. Iron-magnesium amphiboles.

$(Ca+Na)_B \geq 1.34$ and Na_B <0.67. Calcic amphiboles.

$(Ca+Na)_B \geq 1.34$ and $0.67 \leq Na_B$ <1.34. Sodic-calcic amphiboles.

$Na_B \geq 1.34$. Alkali amphiboles.

These groups are then subdivided on the basis of $Mg/Mg+Fe^{2+}$ plotted against Si or $Fe^{3+}/Fe^{3+}+Al_C$. Site assignments and classifications have been carried out using the program `AMPH.CLAS` (Pearce 1988).

Using this scheme, the majority (90%) of amphiboles are katophorites or with increasing alkalis, arfvedsonites (α blue-green, β green-brown, γ very dark brown). The latter are restricted to GS-A, while the katophorites are present as poikilitic crystals in the marginal syenite G44 and the Porphyritic Microsyenite dyke G186 (α deep blue-green, β pale brown, γ very dark-green). The remainder are calcic amphiboles with a variety of compositions (fig. 4.3.1), though all have a partially filled A-site, with $(Na+K)_A \geq 0.5$ and low Ti (less than 0.5 atoms per 23(O)). Subcalcic ferro-edenitic and hastingsitic hornblendes (low $Mg/Mg+Fe^{2+}$) occur in GS-B (α green-blue, β pale brown, γ very dark-green), while a ferroan pargasite and magnesian hastingsites (α pale yellow, β red-brown, γ green-brown) occur in a Porphyritic Microsyenite dyke cutting the GS-B in the north-west of the complex.

Fig. 4.3.1. Classification of the Grønnedal-Íka amphiboles according to Leake (1978), showing only the nomenclature relevant to those amphiboles which were present. There are no members of the iron-magnesium group, the majority being alkali or sodic-calcic amphiboles. The full classification scheme is shown in Leake (1978).

Fig. 4.3.2A. Al_T and Na vs. Ca_B.
Al_T increases while Na decreases with increasing Ca_B, suggesting the substitution which occurs in amphiboles from other Gardar centres, ie.

$$Ca_B + Al_T \rightleftharpoons Na_B + Si_T$$

is occurring at Grønnedal.

SQ=comparitive trend from South Qôroq (Stephenson 1973).

Fig 4.3.2B. Variation of Al_T with total Al follows a gradient of nearly 1, though slightly greater at higher values of Al (less fractionated samples), suggesting the presence of some Al_C.

Fig. 4.3.1

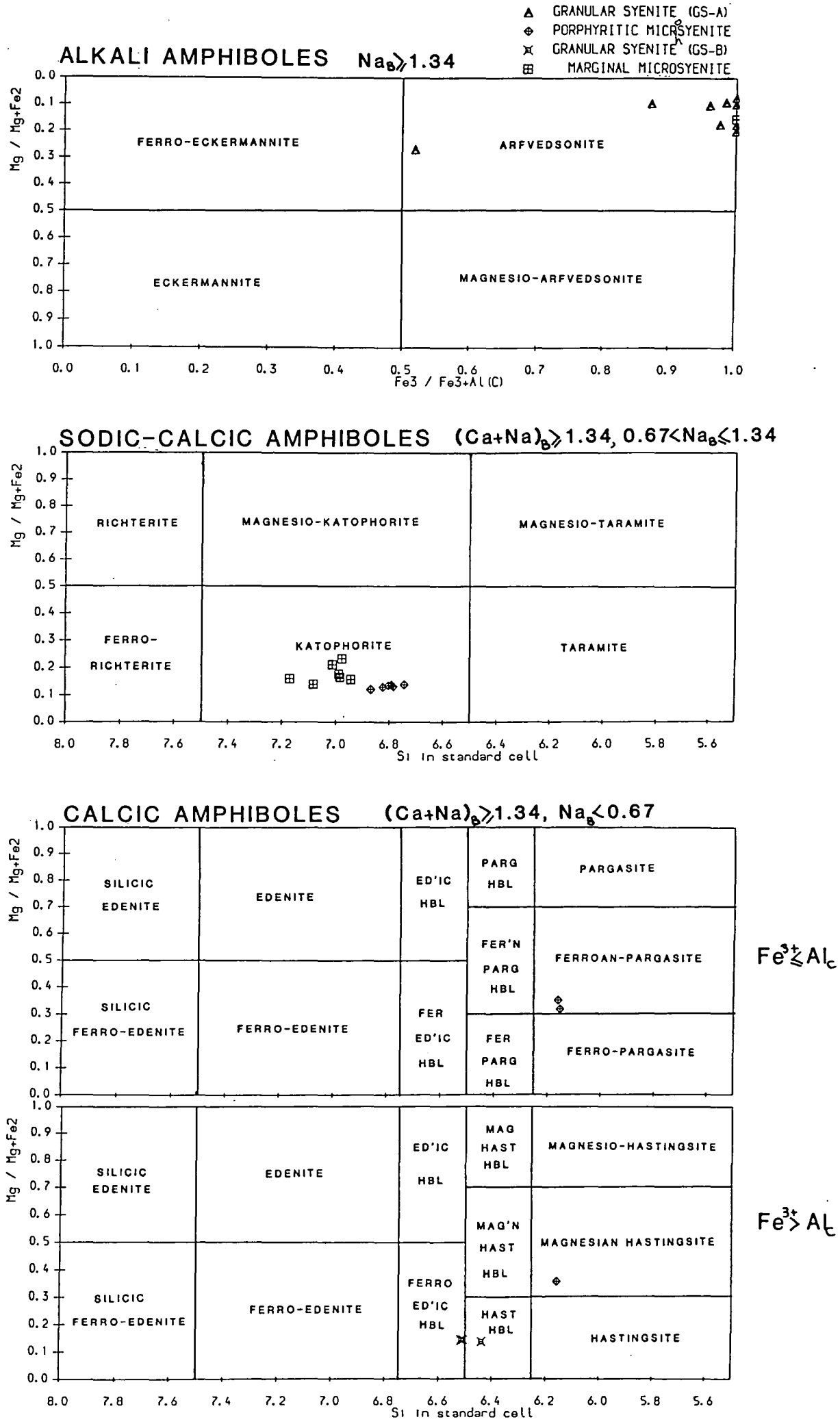
GRANULAR SYENITE (GS-A)
PORPHYRITIC MICROSYENITE
GRANULAR SYENITE (GS-B)
MARGINAL MICROSYENITE
ALKALI AMPHIBOLES $Na_B \geqslant 1.34$
FERRO-ECKERMANNITE
ARFVEDSONITE
ECKERMANNITE
MAGNESIO-ARFVEDSONITE
Mg / Mg+Fe2
Fe3 / Fe3+Al (C)
SODIC-CALCIC AMPHIBOLES $(Ca+Na)_B \geqslant 1.34$, $0.67 < Na_B \leqslant 1.34$
RICHTERITE
MAGNESIO-KATOPHORITE
MAGNESIO-TARAMITE
FERRO-RICHTERITE
KATOPHORITE
TARAMITE
Si in standard cell
CALCIC AMPHIBOLES $(Ca+Na)_B \geqslant 1.34$, $Na_B < 0.67$
SILICIC EDENITE
EDENITE
ED'IC HBL
PARG HBL
PARGASITE
FER'N PARG HBL
FERROAN-PARGASITE
$Fe^{3+} \leqslant Al_C$
SILICIC FERRO-EDENITE
FERRO-EDENITE
FER ED'IC HBL
FER PARG HBL
FERRO-PARGASITE
MAG HAST HBL
MAGNESIO-HASTINGSITE
MAG'N HAST HBL
MAGNESIAN HASTINGSITE
$Fe^{3+} > Al_C$
FERRO ED'IC HBL
HAST HBL
HASTINGSITE

4.3.3 Chemical variation

The dominant substitution affecting Gardar amphiboles is:

$$Na_B + Si_T \rightleftharpoons Ca_B + Al_T$$

(cf. Chambers 1976, Larsen 1976, Jones 1980, Pearce 1988), and results in a trend from hastingsite through katophorite to arfvedsonite with increasing alkalis. Though it is difficult to draw too many conclusions from analyses from such a narrow range of samples, and there is a natural tendency for compositions from the same sample to cluster together, a similar substitution seems to be affecting the amphiboles from Grønnedal-Íka (fig. 4.3.2). This diagram also shows that most of the Al is present in the T-site, with $Al_T \approx Al_{total}$ for most compositions, the greatest amount of Al_C occurring in the Porphyritic Microsyenite (sample G253), reaching a maximum of 0.225 atoms in G253.07.

Fig. 4.3.3. shows two triangular plots, Mg–(Fe^{2+}+Fe^{3+}+Mn)–(Na+K) and Mg–Ca–Na, both of which have been used by various workers to compare amphibole and pyroxene trends. Fig. 4.3.3A shows increasing Na enrichment at nearly constant Mg/Ca, while fig. 4.3.3B compares amphibole trends from both undersaturated (S.Qôroq and Ilímaussaq) and oversaturated complexes (Nunarssuit). Not surprisingly, the Grønnedal-Íka amphiboles follow the undersaturated trend towards increasing alkalis following the initial depletion in Mg and enrichment in (Fe+Mn). As with the pyroxenes, the most evolved compositions (arfvedsonites) occur in GS-A.

The variation of major and minor elements with fractionation is shown in fig. 4.3.4, where the fractionation index (FI) is represented by Na_B-Al_T (Chambers 1976), enabling the entire range of compositions to be shown.

Si, which only ever occupies the T-site, never falls below 6.0 and shows a gradual increase to just under 8.0 with increasing FI. The deficit in the T-site is made up mainly by Al, and the remainder by a small amount of Fe^{3+}, there being

Fig. 4.3.3A. Variation of amphiboles in terms of Mg-Ca-Na. A continuous trend at almost constant Mg/Ca towards alkali enrichment occurs.

Fig. 4.3.3B. Variation in terms of Mg-(ΣFe+Mn)-Σalkalis. Compositions follow the 'undersaturated' trend, intermediate between those of South Qôroq and Ilímaussaq.

SQ=South Qôroq (Stephenson 1973)

IL=Ilímaussaq (Larsen 1976)

NU=Nunarssuit (Anderson 1974)

Fig. 4.3.4 (two pages). Chemical variation in amphiboles as a function of Na_B-Al_T (Chambers 1976) as the fractionation index (FI).

Some elements show a wide scatter of variation, with apparently little dependance on the FI. However, a few trends can be made out.

Si and Ca show a sympathetic variation as a result of the substitution $Ca_B+Al_T \rightleftharpoons Si_T+Na_B$.

Fe^{2+} maintains a fairly constant value of 3.0-3.5 atoms per 23(O) throughout the range of fractionation.

$Na_A+K \sim 1.0$, despite minor fluctuations with FI, though some anomalously Na-rich compositions occur in GS-A, with Na_A+K up to *c.*1.5.

Zr shows a slight decrease with FI, in contrast to the trends from the Igaliko dykes (Pearce 1989). Three samples show anomalously high values, though there is insufficient data to draw too many conclusions.

Fig. 4.3.2A

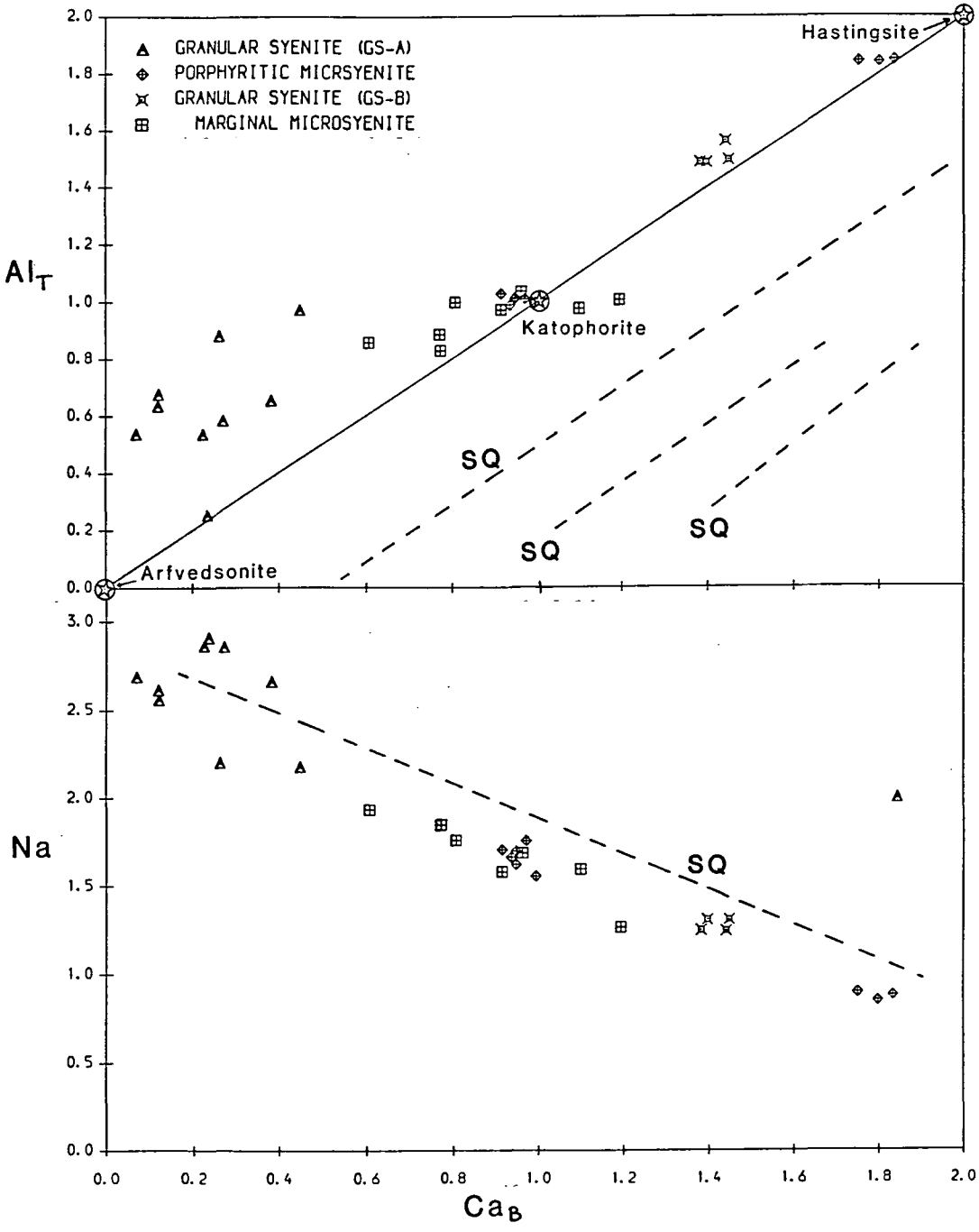

Fig. 4.3.2B

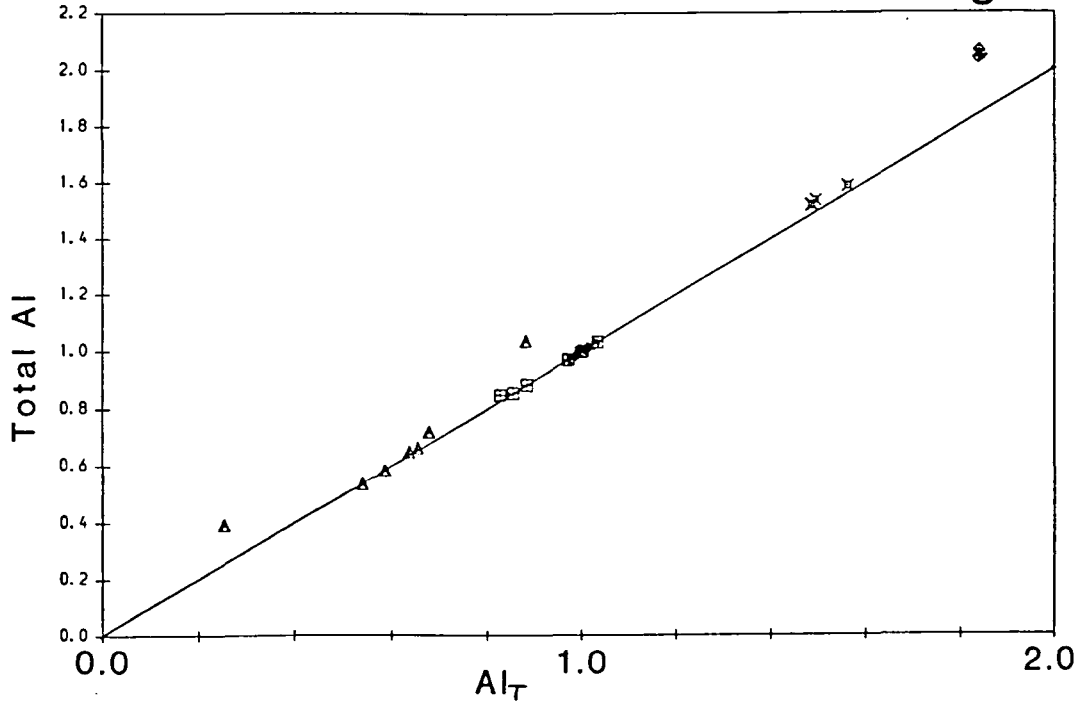

Fig. 4.3.3A

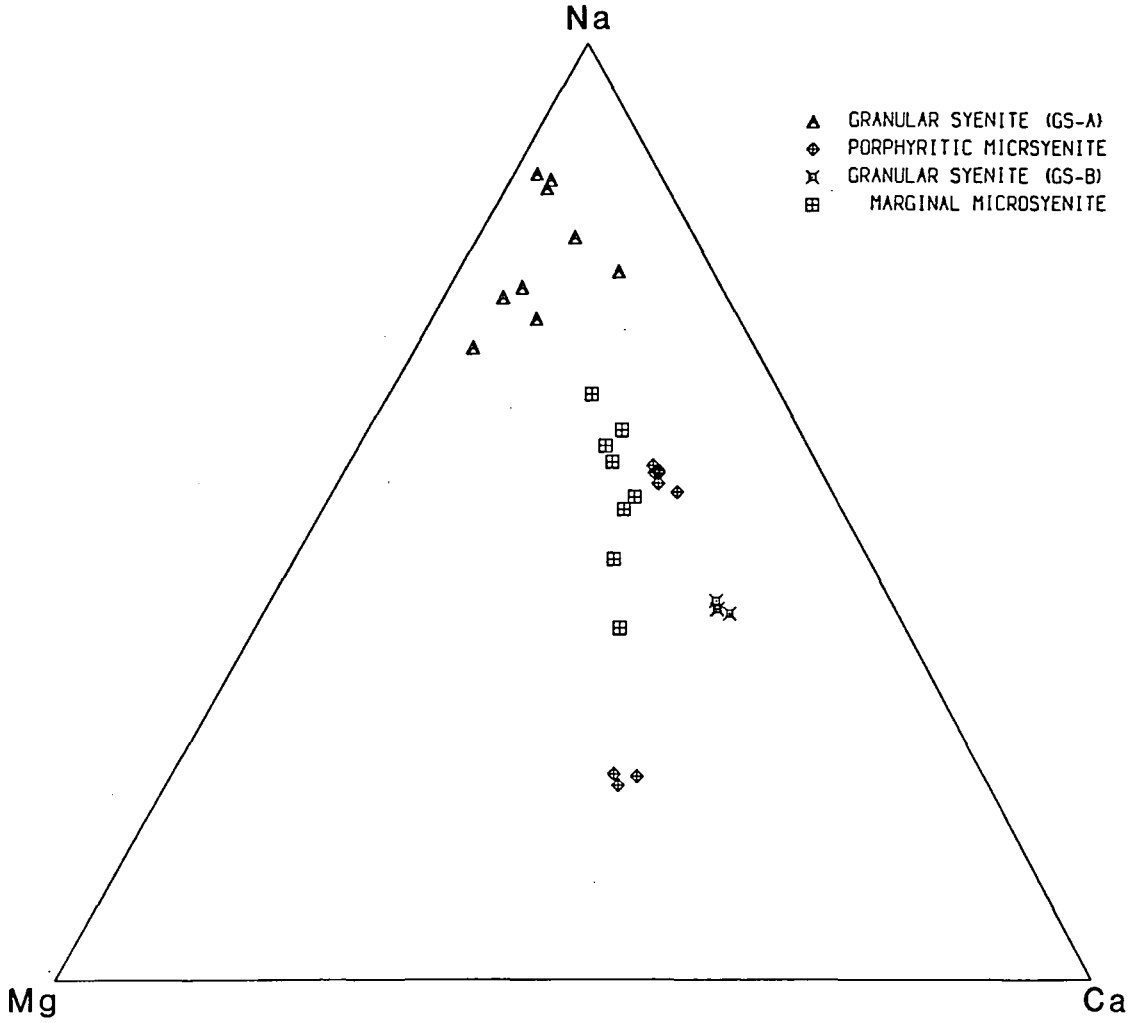

Fig. 4.3.3B

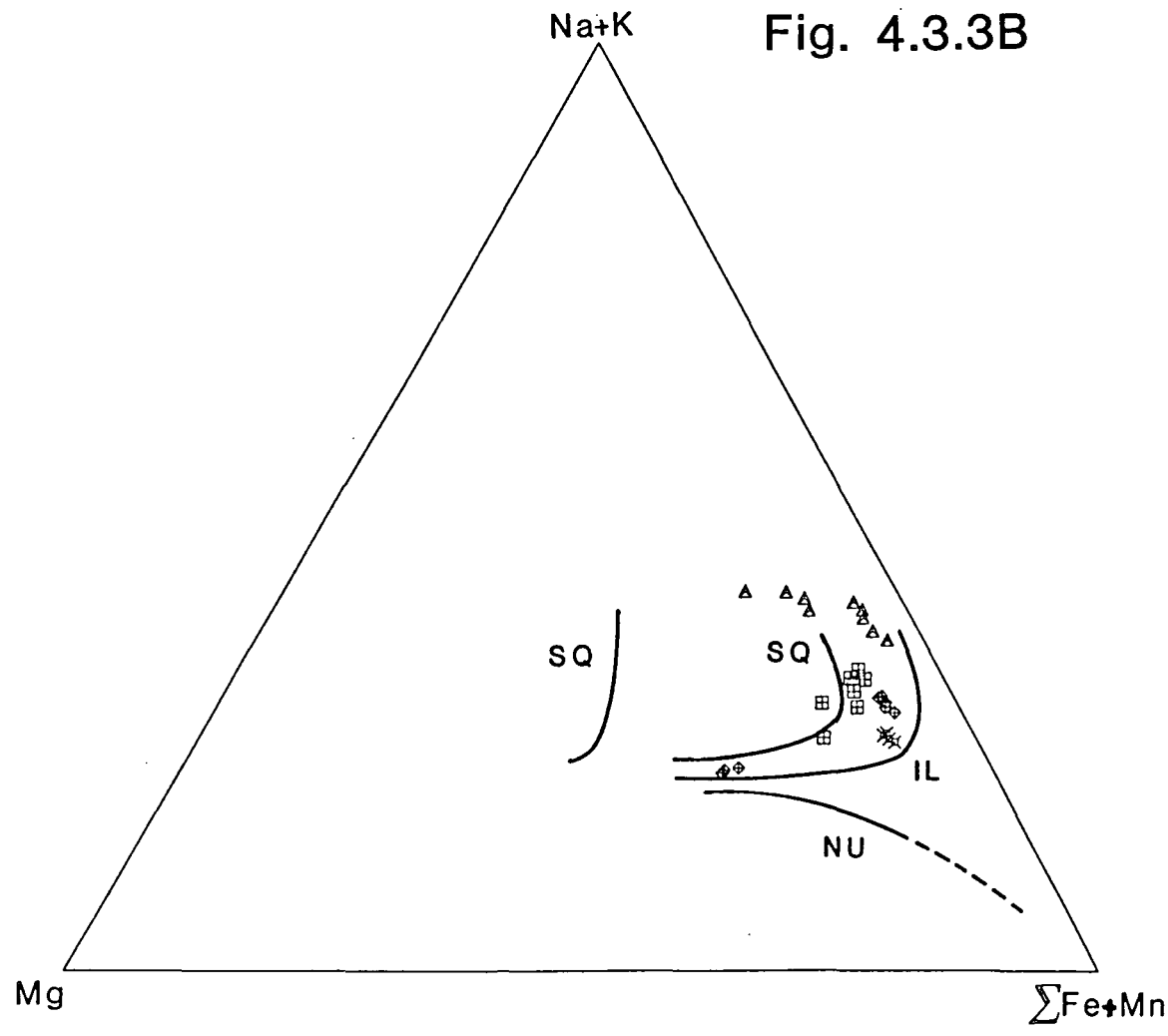

Fig. 4.3.4

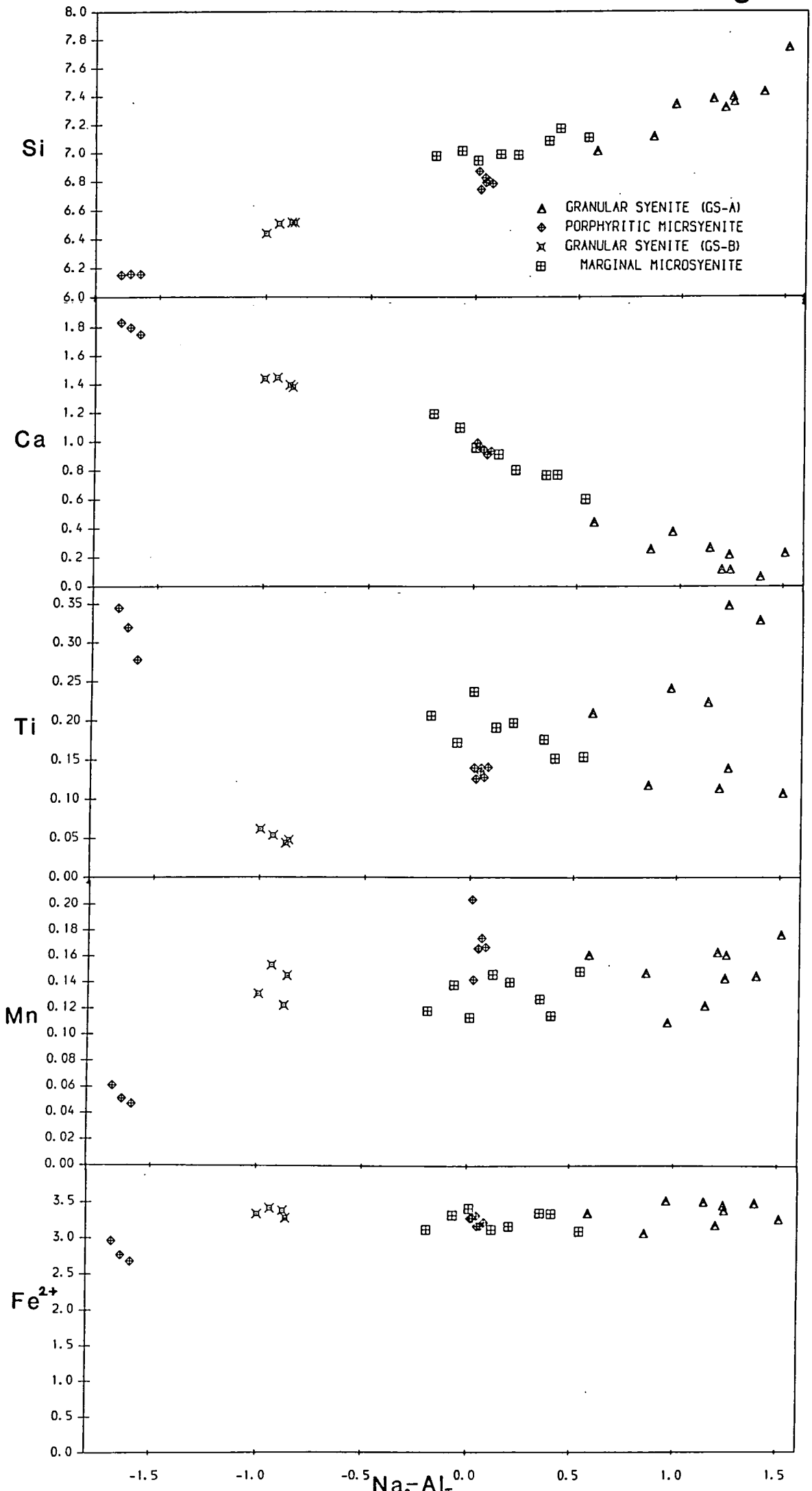
Si
Ca
Ti
Mn
Fe2+
GRANULAR SYENITE (GS-A)
PORPHYRITIC MICRSYENITE
GRANULAR SYENITE (GS-B)
MARGINAL MICROSYENITE
Na-Al

Fig. 4.3.4 (cont.)

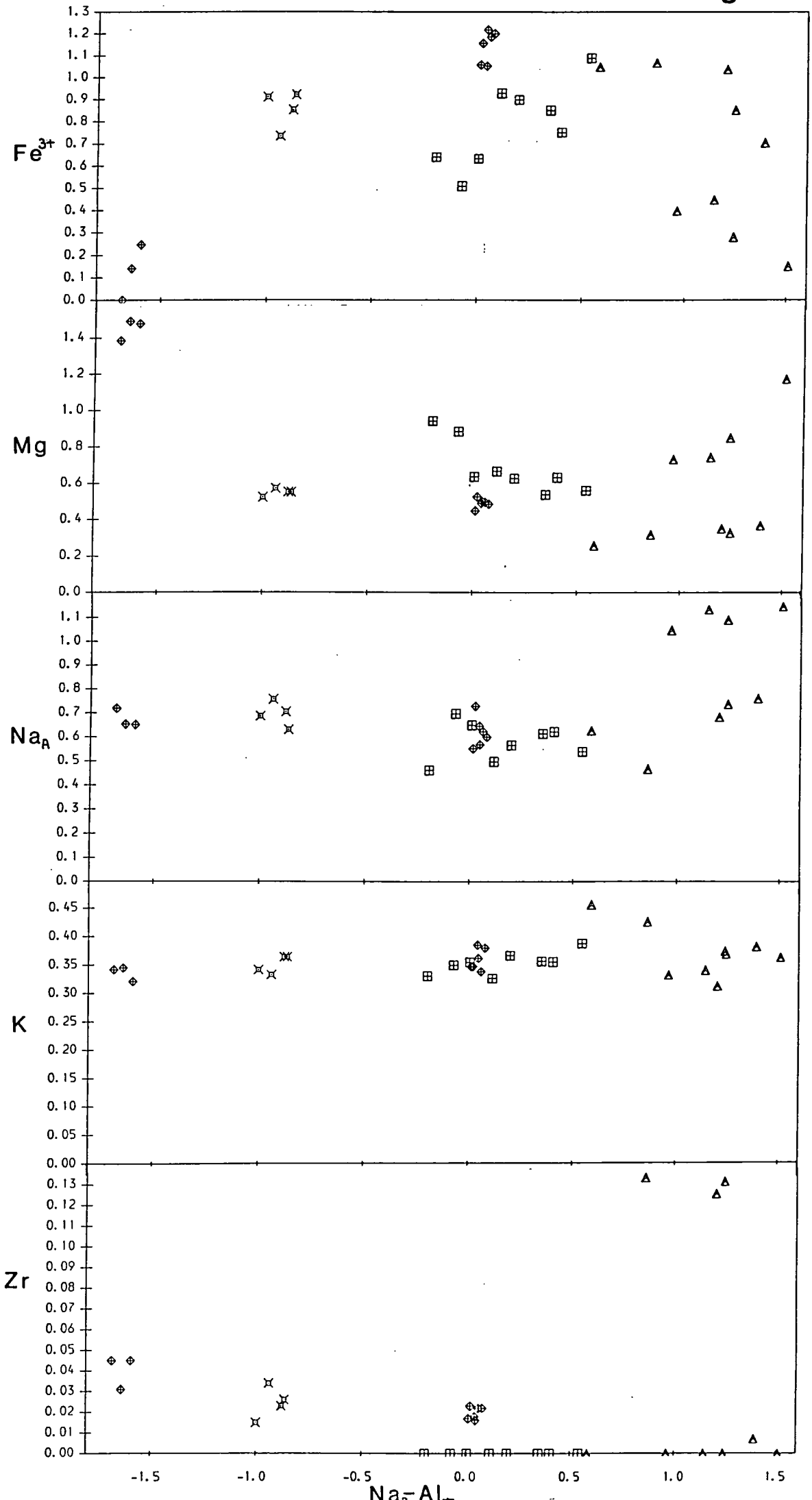
Fe3+
Mg
NaA
K
Zr
1.3
1.2
1.1
1.0
0.9
0.8
0.7
0.6
0.5
0.4
0.3
0.2
0.1
0.0
1.4
0.45
0.40
0.35
0.30
0.25
0.20
0.15
0.10
0.05
0.00
0.13
0.12
0.11
0.09
0.08
0.07
0.06
0.04
0.03
0.02
0.01
-1.5
-1.0
-0.5
0.0
0.5
1.0
1.5
Na=Al

no tetrahedral Ti in the Grønnedal-Íka amphiboles. Ca, which always occupies the B-site, shows an antithetic relationship with Si, conforming to the exchange $Na_B + Si_T \rightleftharpoons Ca_B + Al_T$.

Ti always occupies the C-site in the Grønnedal amphiboles and never exceeds 0.35 atoms per 23(O), comparable to amounts reported from Ilímaussaq (Larsen 1976) and Motzfeldt (Jones 1980), but much less than the one atom per formula unit which occurs in amphiboles from the lamprophyres of the Igaliko dyke swarm (Pearce 1988). In these examples, Ti shows a decrease with FI, which Helz (1973) suggests is due to falling temperature of crystallisation, though no obvious trend is apparent in the Grønnedal-Íka amphiboles.

Mn and Mg show a wide scatter of values, though Fe^{2+}, which shows a sympathetic trend with Mn in the pyroxenes, is fairly constant at around 2.5-3.5 atoms per 23(O), and occupies the C-site alone. Fe^{3+} also shows a wide range of values, even in the same sample. This may be attributed to the alkali-ferric iron effect (Carmichael and Nicholls 1967), described in section 4.2.4, in which the ratio $Fe^{3+}/Fe^{2+}+Fe^{3+}$, and hence $a_{Fe^{3+}}$, is controlled by the amount of alkalis. Textural evidence suggsts that the amphiboles crystallised late in the cooling history of the host-rock, from isolated pockets of intercrystalline liquid, which could evolve to produce a wide range of alkalinities and a variety of a_{Fe3+} values. Fe^{3+} occurs mainly in the C-site, but the katophorites from G186 (the Porphyritic Microsyenites) contain between 0.135 and 0.246 atoms per 23(O) in the tetrahedral site. No deficiency in Al_T is apparent in these samples (fig. 4.3.1, the calcic amphiboles), while Si_T is slightly depleted, so that the presence of Fe^{3+}_T relates to a deficit of Si in the tetrahedral site.

Na_A and K maintain fairly constant values at around 0.65 and 0.35 atoms per 23 oxygens respectively, and completely fill the A-site. However, four analyses from GS-A (sample 138007) show rather anomalously high Na_A values up to 1.15, with only a slight decrease in the amount of K.

Fig. 4.3.5. Variation of Zr with Ca_B, Na_B, and Al_T. These are the only site occupancies to show any sort of correlation with Zr, and suggest that this element is controlled by more complex exchanges than:

$$Zr_C^{4+} + Al_T^{3+} \rightleftharpoons Fe_C^{3+} + Si_T^{4+} \text{ or}$$

$$Fe_C^{3+} + Si_T^{4+} \rightleftharpoons Zr_C^{4+} + Fe_T^{3+}$$

as proposed by Pearce (1989).

Fig. 4.3.5

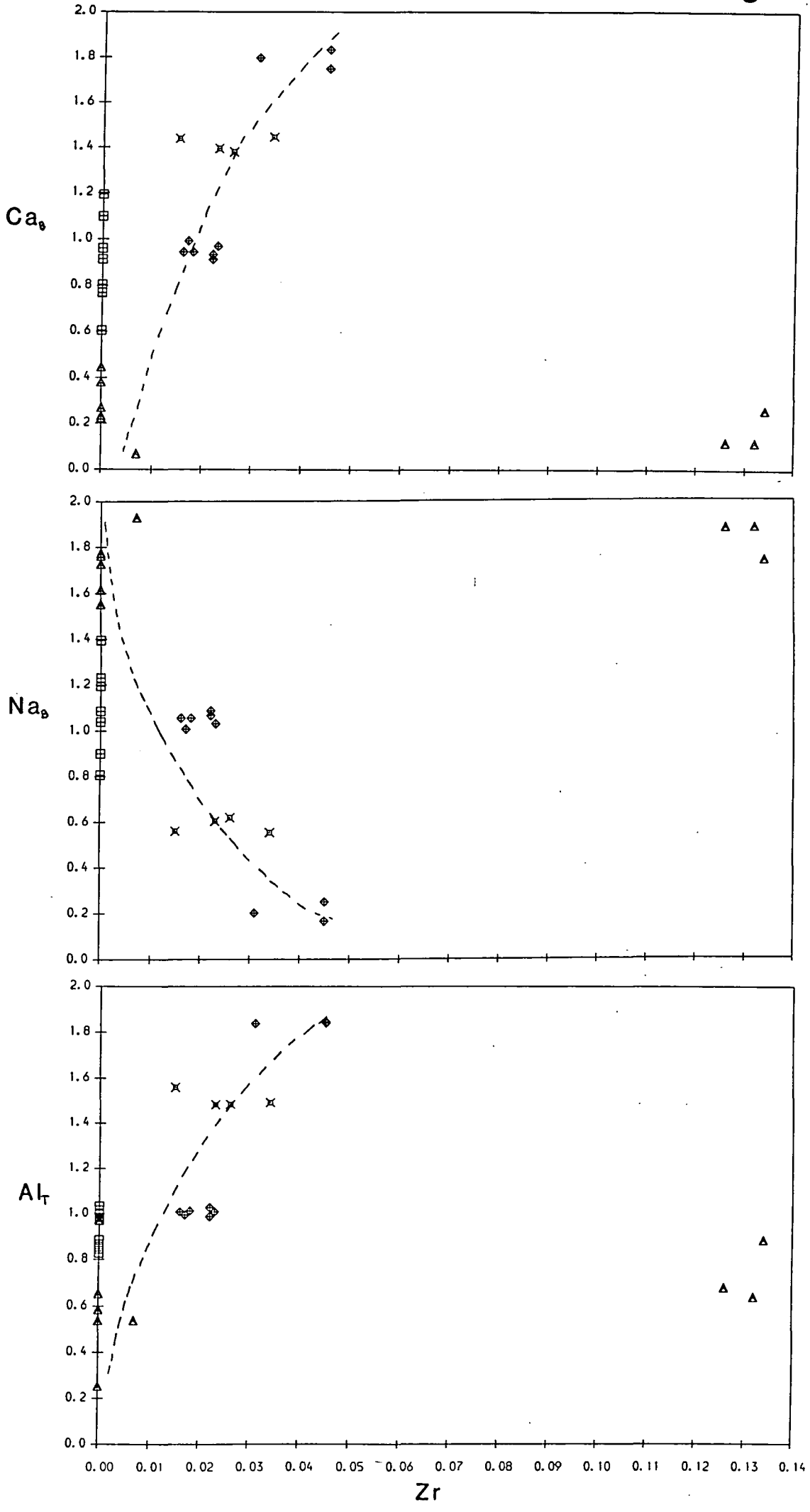
Ca_B
Na_B
Al_T
Zr
0.0
0.2
0.4
0.6
0.8
1.0
1.2
1.4
1.6
1.8
2.0
0.00
0.01
0.02
0.03
0.04
0.05
0.06
0.07
0.08
0.09
0.10
0.11
0.12
0.13
0.14

Unlike at Motzfeldt (Jones 1980) and in the Igaliko dykes (Pearce 1989) where Zr shows a systematic increase with FI, the amphiboles at Grønnedal-Íka contain a wide variety of Zr levels. Three samples (from GS-A) have relatively large amounts of Zr compared to other analyses, with up to 0.14 atoms of Zr per 23(O) (1.77%, G169.34). This is more than twice the amount occurring in the Ilímaussaq and Motzfeldt amphiboles (0.75% and 0.78% respectively), but less than half the 4.13% (0.33 atoms per 23(O)) found by Pearce (1989) in a benmoreite dyke from the Igaliko swarm. The Zr-rich Grønnedal amphiboles are all from G169, in which many of the pyroxenes are highly enriched in Zr (section 4.2.5). In addition, no such relationship between the amount of Zr in pyroxenes and co-existing amphiboles was found, in contrast to Ilímaussaq, where pyroxenes contain twice the amount as the amphiboles in rocks of the same composition.

Pearce (1989) suggests exchanges such as:

$$Zr_C^{4+} + Al_T^{3+} \rightleftharpoons Fe_C^{3+} + Si_T^{4+} \text{ or}$$

$$Fe_C^{3+} + Si_T^{4+} \rightleftharpoons Zr_C^{4+} + Fe_T^{3+}$$

to account for the presence of Zr, present in the zirconian arfvedsonite end-member $Na_3Fe_4^{2+}ZrSi_7AlO_{22}(OH)_2$. Excluding the three anomalously high values, Zr shows a slight decrease with increasing FI (and hence a decrease with Na_B and an increase with Al_T and Ca_B), but no simple exchange relationship appears to be controlling the substitution of Zr in the Grønnedal-Íka amphiboles (fig. 4.3.5).

4.4: Biotites

4.4.1 General

Biotite is a common late-stage mineral in all syenite units, occurring as large millimetre-sized interstitial or poikilitic plates, and occasionally as rims on oxide grains in the microsyenites.

It is intensely pleochroic in a variety of colours (α orange-brown; β, γ very dark green-brown or green-blue). The orange colour of biotites is thought to be

due to Ti, and green, which is very common in the Grønnedal biotites, to Fe^{3+} (Deer *et al.* 1966)

Almost invariably, the biotites contain minute grains of opaque oxides along the cleavages. This could be the result of crystallisation or sub-solidus re-equilibration as a result of the reaction *biotite* $\rightleftharpoons$ *magnetite* + *sanidine* + *gas* (Powell 1978), and may result in errors in some of the microprobe analyses.

4.4.2 Chemical variation

The general formula of biotites is $X_2Y_{4-6}Z_8O_{22}(OH,F)_4$, with the various cation sites occupied as follows:

Z (tetrahedral site): Si, Al, Fe^{3+}, possibly Ti.

Y (octahedral site): Fe^{2+}, Fe^{3+}, Mg, Ti, Mn, and excess Al.

X (12-fold co-ordinated site): K, Na, Ba.

Again, Fe is reported as FeO when analysed by the microprobe, though due to the lack of stoichiometry and incomplete analysis of the biotites (H_2O was not determined), no attempt has been made to distinguish between Fe^{2+} and Fe^{3+}. Most analyses have Si+Al>8.0, so that some Al must be present in octahedral co-ordination. However, a few have a deficit in the Z (tetrahedral) site which is probably made up by Fe^{3+}, though Ti may occupy the Z-site at high temperatures and under more alkaline conditions.

Fig. 4.4.1A shows the compositional range of the Grønnedal-Íka biotites in terms of the four end-members phlogopite, siderophyllite, annite, and eastonite (Deer *et al.* 1966), most of which are annite-rich. With increasing fractionation, Si increases and Al_Z decreases, while Fe/Fe+Mg increases, so that there is a trend roughly away from the eastonite corner towards annite. The Y-site is usually filled by six cations in the tri-octahedral micas (which include the biotites), though as observed by Jones (1980) and Chambers (1976), a slight deficit and tendency towards the di-octahedral micas occurs in a few analyses (fig. 4.4.1B).

Fig. 4.4.1A. Biotite classification in terms of eastonite-phlogopite-annite-siderophyllite as defined by Al_Z vs. Fe/Fe+Mg. Fractionation will drive compositions towards annite, as suggested by the trends of the marginal microsyenite and Mafic Upper Series Syenite.

Fig. 4.4.1B. Plot of the sum of the Y-site cations (Fe, Mg, Ti, Mn, and excess Al) against Fe/Fe+Mg. Y-site occupancy increases from being intermediate between tri- and di-octahedral micas to true tri-octahedral compositions (Y=6) with increasing fractionation.

Fig. 4.4.2A. Like Al_Z, Al/Al+Si decreases with Fe/Fe+Mg. Trends for Motzfeldt (Jones 1980) and Klokken (Parsons 1979) shown for comparison.

Fig. 4.4.2B. Mn shows a rapid increase with increasing Fe/Fe+Mg, though there is a fairly broad scatter of data.

Fig. 4.4.3A. Al in tetrahedral co-ordination (Al_Z) vs. MnO (wt.%). Compositional fields from North Qôroq (Chambers 1976) and Motzfeldt (Jones 1980) shown for comparison. Highest MnO contents generally occur for compositions with highest Al_Z (ie. least evolved).

Fig. 4.4.3B. TiO_2 (wt.%) vs. Al_Z. A broad scatter of data is apparent, but shows a gradual increase with increasing Al_Z (decreasing fractionation).

Fig. 4.4.3C. Mg-ΣFe-Ti. Gradually decreasing Ti with increasing Fe/Fe+Mg occurs, comparable to the syenite-syenodiorite trend from Klokken (Parsons 1979).

Fig. 4.4.1A

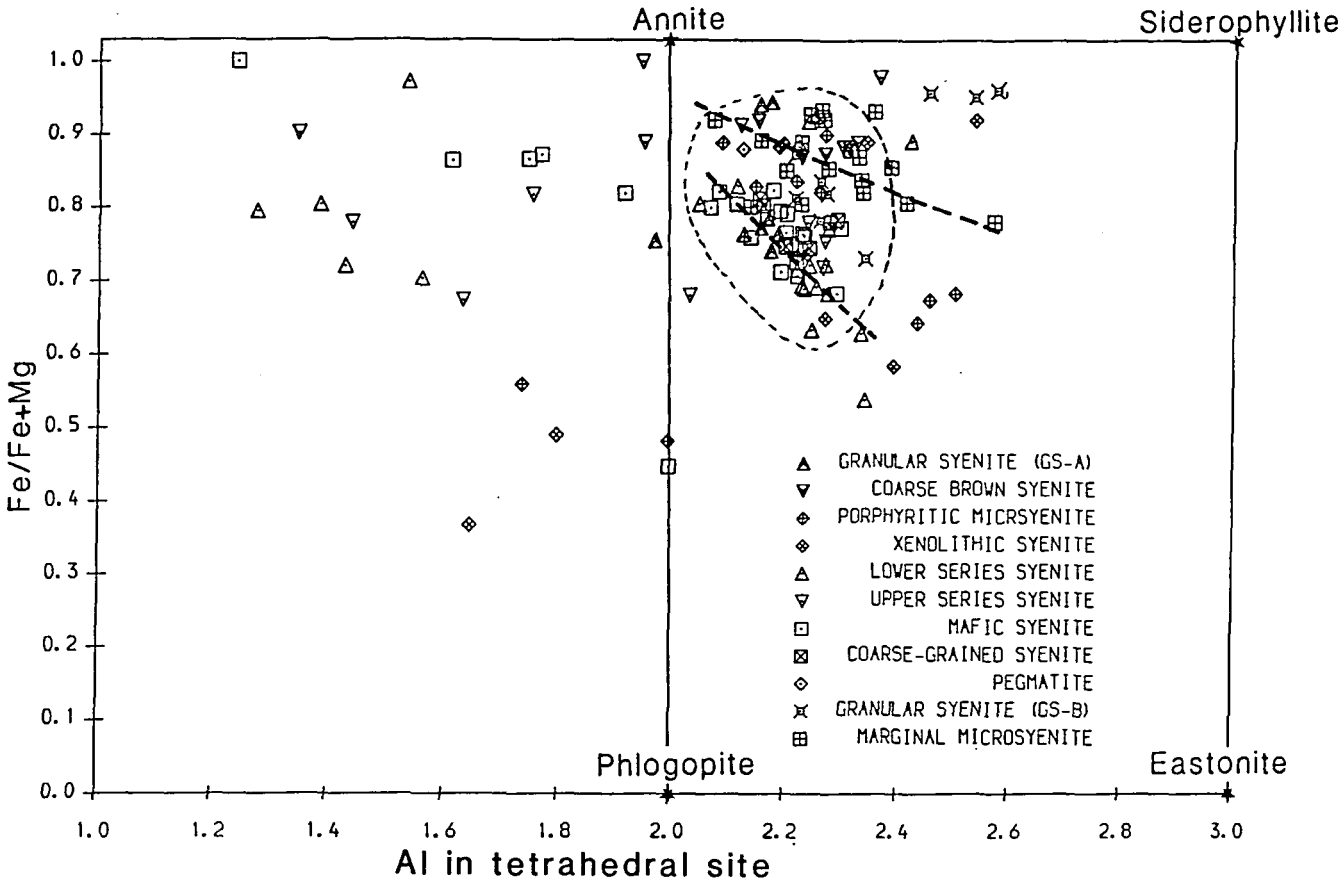

Fig. 4.4.1B

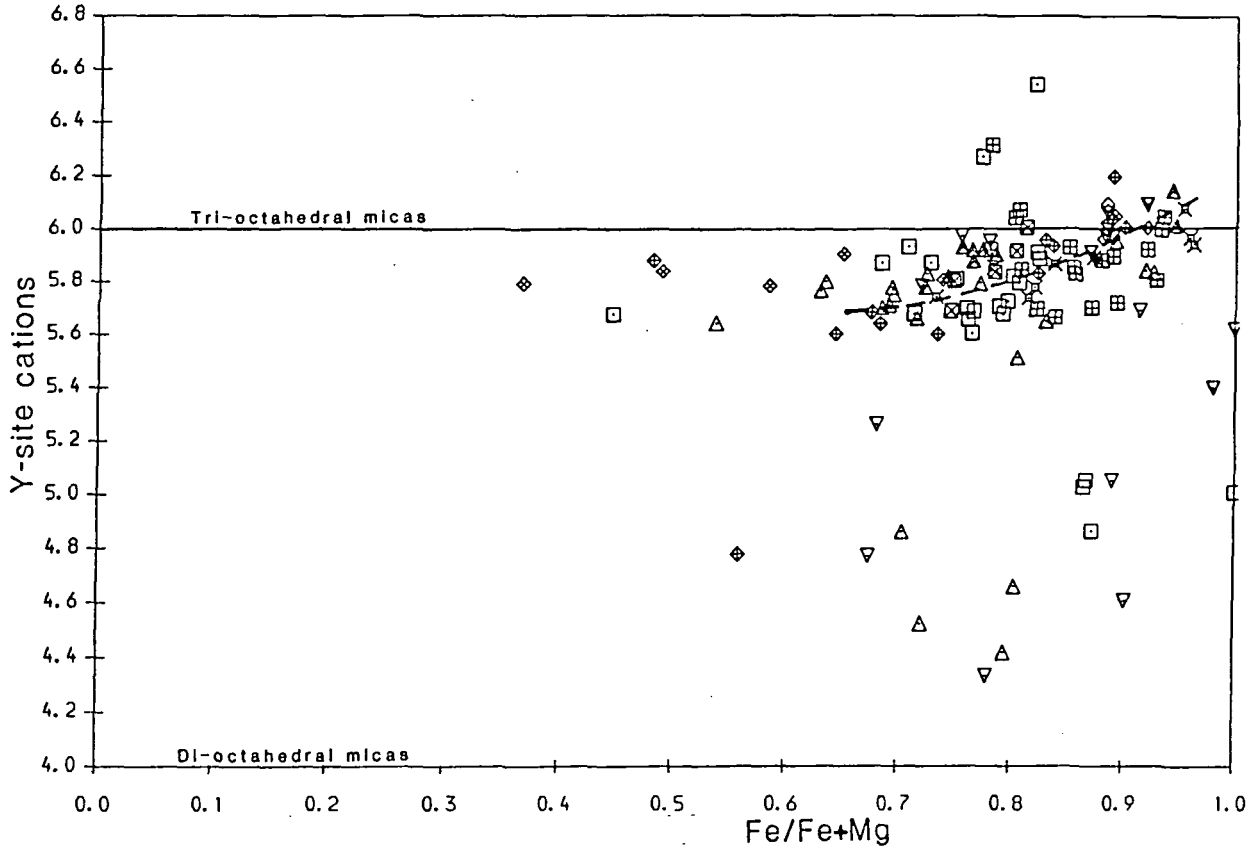

Fig. 4.4.2A

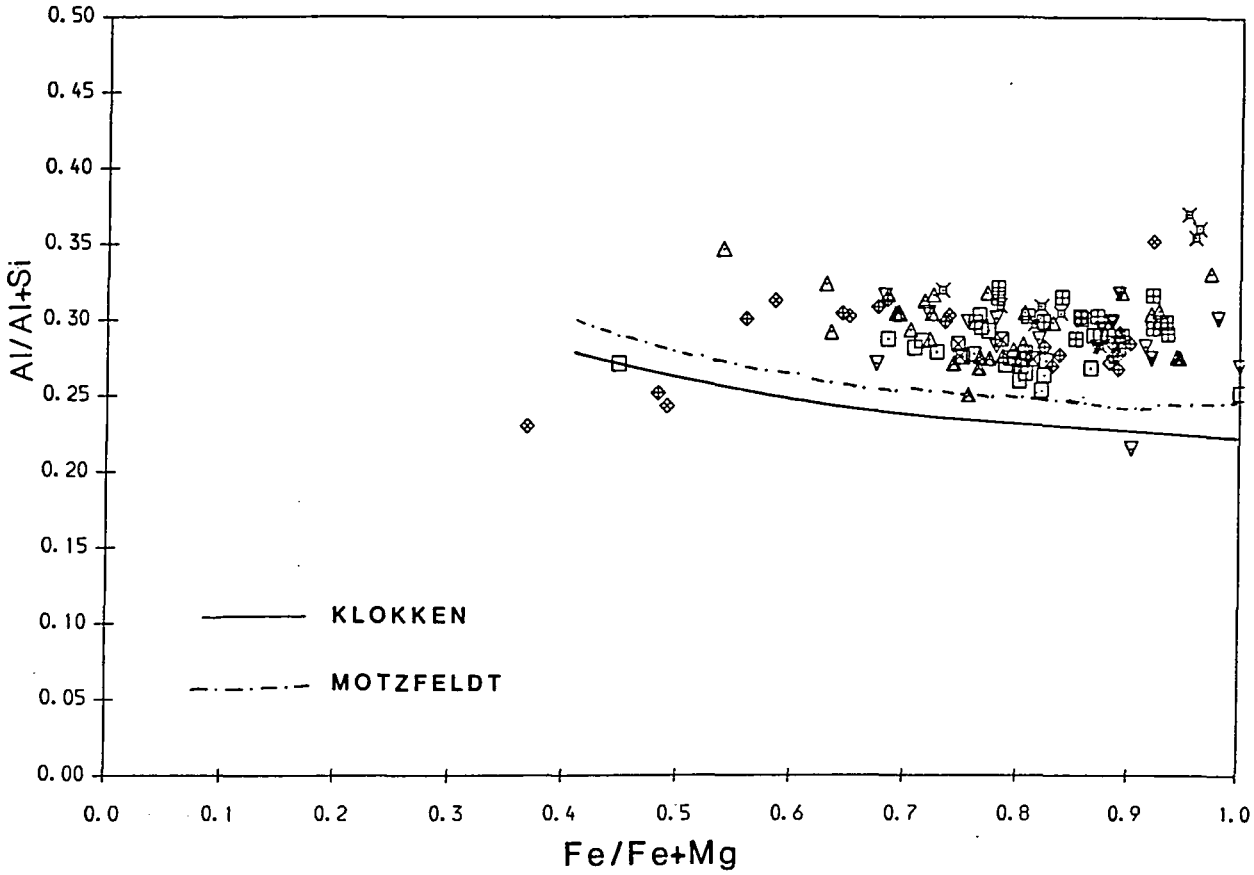

Fig. 4.4.2B

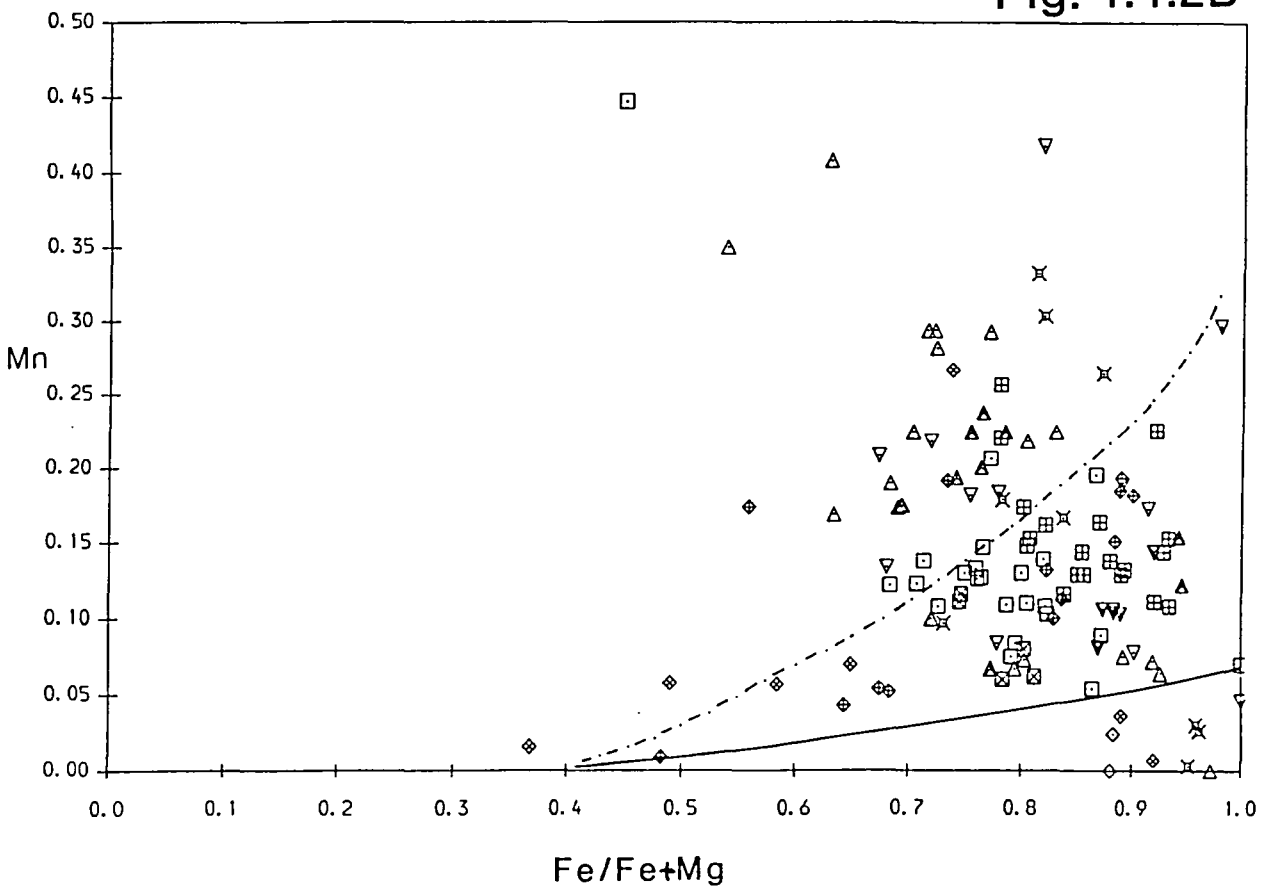

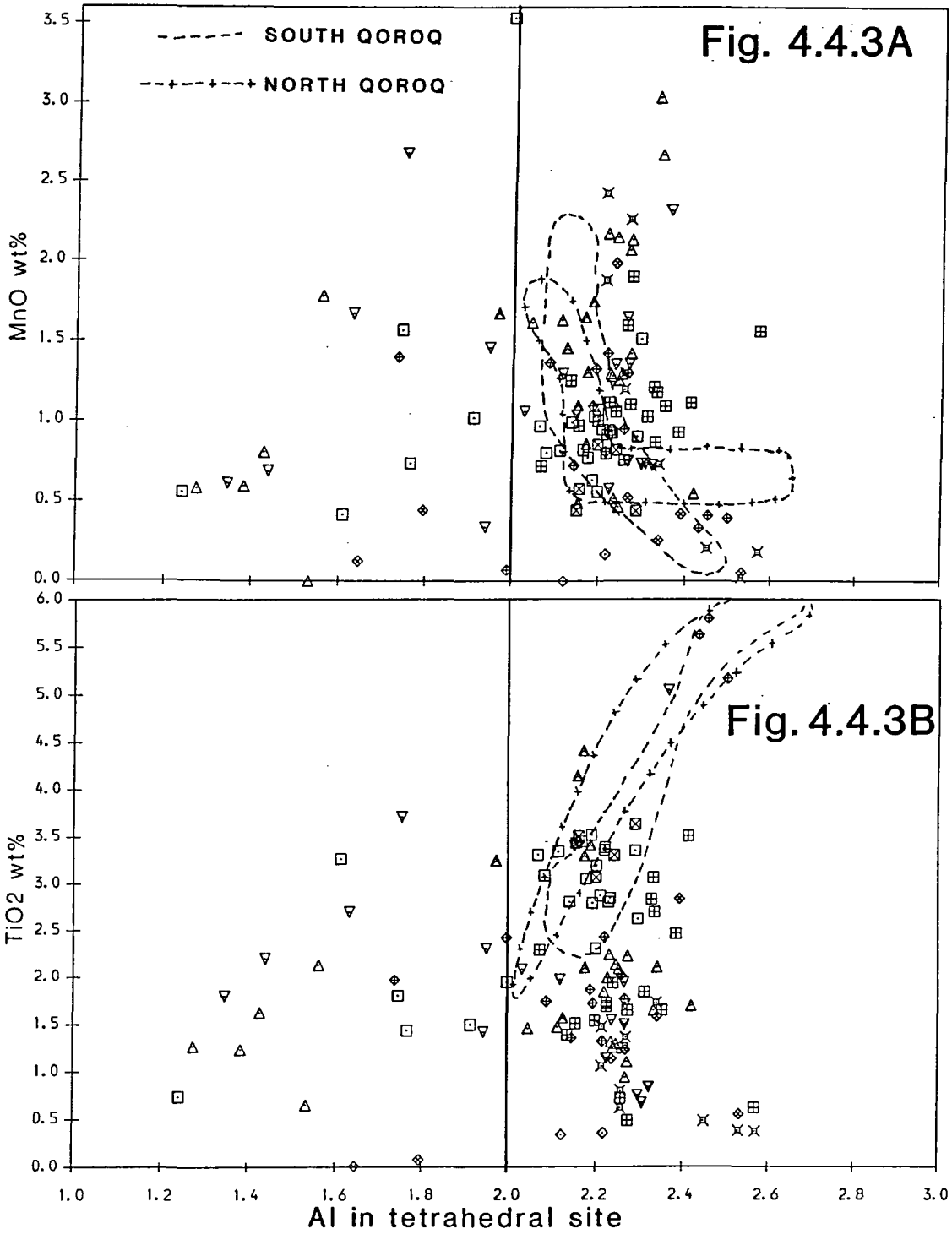

Fig. 4.4.3A

Fig. 4.4.3B

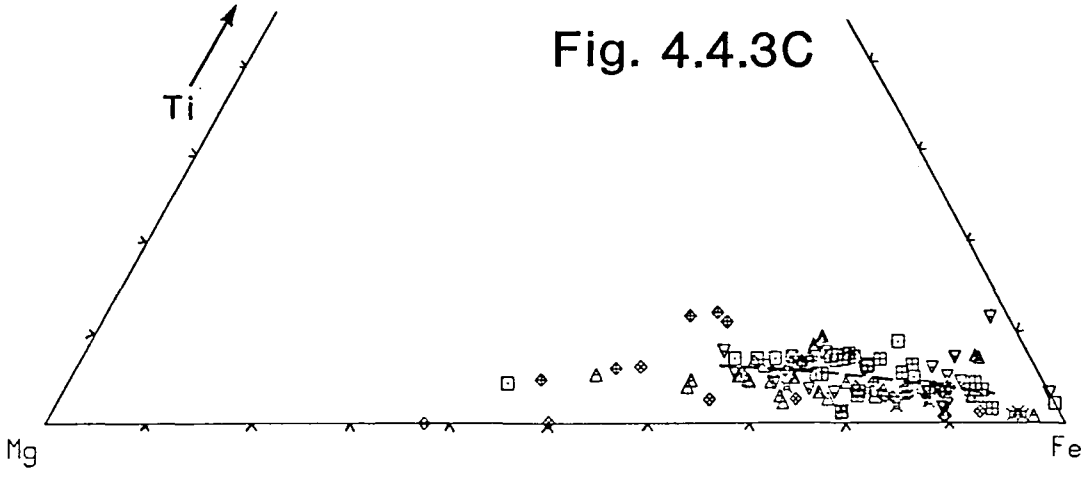

Fig. 4.4.3C

Element variations are shown in fig. 4.4.2 using the same parameters as Jones (1980) and Pearce (1988) for ease of comparison with other Gardar trends. Ba was not detected in any sample, while Zr and Cl occur in only trace amounts.

Al/Al+Si, as well as Al_Z, decreases with increasing fractionation (increasing Fe/Fe+Mg), though not as sharply as in the Klokken and Motzfeldt biotites (Parsons 1979, and Jones 1980 respectively), while Mn shows a large variation at fairly high, rather restricted values of Fe/Fe+Mg. This is in contrast to the trends from Motzfeldt and Klokken, which show a steady increase in Mn with Fe/Fe+Mg. Fig. 4.4.3A shows the lowest values of MnO (weight %) at the lowest levels of Al_Z, and an increase with decreasing fractionation is also suggested. A maximum of 3.53% MnO, corresponding to about 9 mol.% manganophyllite, occurs in G248.08 (Mafic Upper Series Syenite). This compares with 1 mol.% manganophyllite in the Klokken biotites (Parsons 1979), and 45% from the Shonkin Sag laccolith (Nash and Wilkinson 1970).

Ti shows an increase with decreasing fractionation in the North Qôroq centre (Chambers 1976) and Motzfeldt (Jones 1980), and while such a trend is suggested in the Grønnedal-Íka biotites (fig.4.3.3B), like Mn they tend to show a wide variety of values (up to 5.8 wt.% TiO_2 in the Porphyritic Microsyenites) over a fairly narrow range of Al_Z (*c*.2.1-2.3 atoms). Fig. 4.4.3C is a triangular plot of Mg–(ΣFe)–Ti, which shows the decrease of Ti with increasing fractionation (increasing Fe/Mg) more clearly, and is comparable to the syenite-syenodiorite trend of biotites from Klokken (Parsons 1979).

Despite the colour zonation observed in plane-polarised light, none of the elements analysed appeared to show any systematic variation from core to rim. This could therefore either be the result of elements which were not analysed, very small variations undetected by the EDS microprobe, or variations in Fe^{3+} or Fe^{2+} which were not determined for the biotites.

4.5: Fe-Ti Oxides

4.5.1 General

Small grains of 'opaques' occurring along the cleavages of biotites have been described in the previous section, though much larger, discrete oxide grains have been observed and analysed in all units of the complex apart from GS-B. In reflected light, they appear as strongly reflective, entirely homogeneous grains, showing none of the exsolution textures described from other Gardar centres.

4.5.2 Chemical variation

Fe^{3+} has been recalculated by the method of Carmichael (1967) by assuming that the deficiency when assigning the cations to eight oxygens is a result of Fe^{3+} alone. All analyses are plotted on a triangular diagram of $R^{2+}O$–$R_2^{3+}O_3$–$R^{4+}O_2$, where R^{2+}, R^{3+}, and R^{4+} are divalent, trivalent, and tetravalent cations respectively. These are mainly Fe^{2+}, Fe^{3+}, and Ti^{4+}, though minor elements (Ca, Mg, Mn, Al, and Si) account for a few percent of the cation totals.

As can be seen, all but one of the analyses lie on the ülvospinel-magnetite (*üsp-mgt*) solid-solution tie-line, the one exception being a single ilmenite grain from a pegmatite sample (138055.11). Thus although the Buddington and Lindsley (1964) geothermometer-oxygen barometer cannot be used, it is possible to generalise about the f_{O_2} of the magma from which the oxides crystallised from their overall composition. The exchange governing this series is simply $2Fe^{3+} \rightleftharpoons Fe^{2+} + Ti$ (*magt*⇌*üsp*), so that increasing oxidation will result in this equilibrium shifting to the left, and thus "for the same temperature, an increase in f_{O_2} results in a decrease in the percentage of TiO_2 in the magnetite" (Buddington and Lindsley 1964). The tendency of the oxides to plot towards the magnetite end of the series therefore suggests that compared to many other Gardar centres, the magmas at Grønnedal-Íka were relatively oxidising.

Fig. 4.5.1. Iron-Titanium oxides in the system RO-R_2O_3-RO_2, plotted on a molecular percent basis, recalculated by the method of Carmichael (1967).

All but one of the analyses are members of the ülvospinel-magnetite series, and tend to be relatively rich in magnetite.

Fig. 4.5.2. Trends of Ti, Fe^{2+} , and Fe^{3+} vs. Mn.
Ti, and Fe^{2+} increase, while Fe^{3+} decreases, suggesting an exchange such as:

$$Ti^{4+} + (Fe^{2+}, Mn) \rightleftharpoons Fe^{3+}$$

which controls the composition of the ülvospinel-magnetite series, to which all but one of the Grønnedal analyses belong.

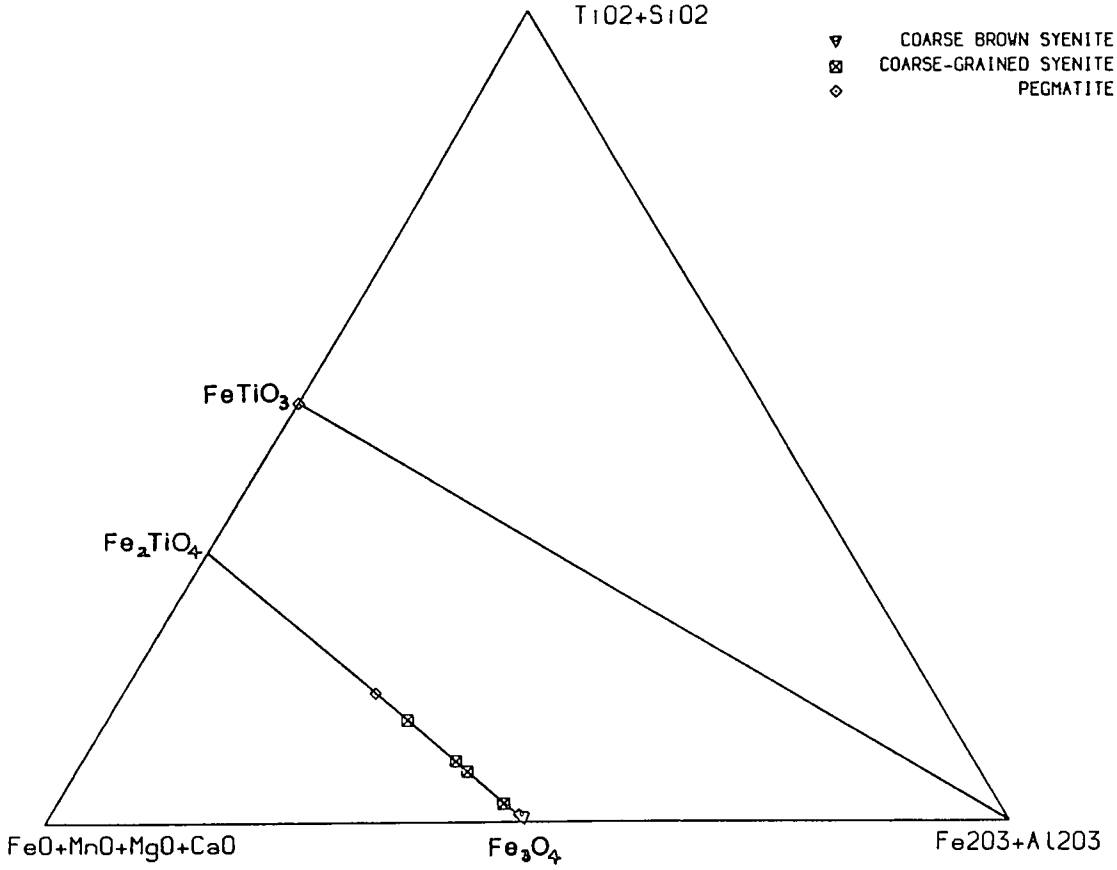
TiO2+SiO2
FeTiO3
Fe2TiO4
FeO+MnO+MgO+CaO
Fe3O4
Fe2O3+Al2O3
COARSE BROWN SYENITE
COARSE-GRAINED SYENITE
PEGMATITE

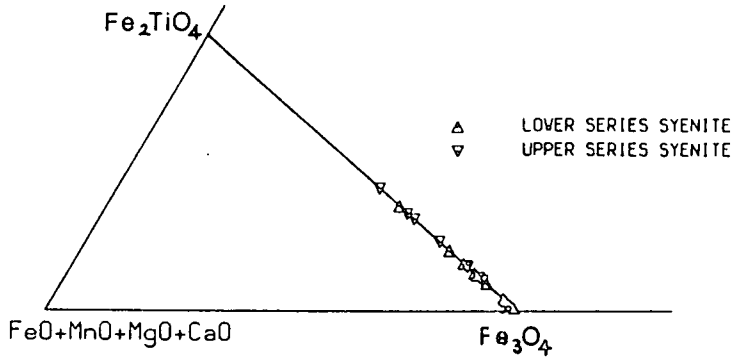
Fe2TiO4
FeO+MnO+MgO+CaO
Fe3O4
LOWER SERIES SYENITE
UPPER SERIES SYENITE

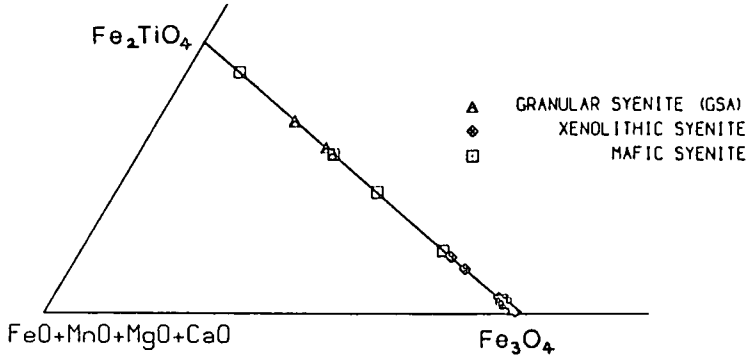
Fe2TiO4
FeO+MnO+MgO+CaO
Fe3O4
GRANULAR SYENITE (GSA)
XENOLITHIC SYENITE
MAFIC SYENITE

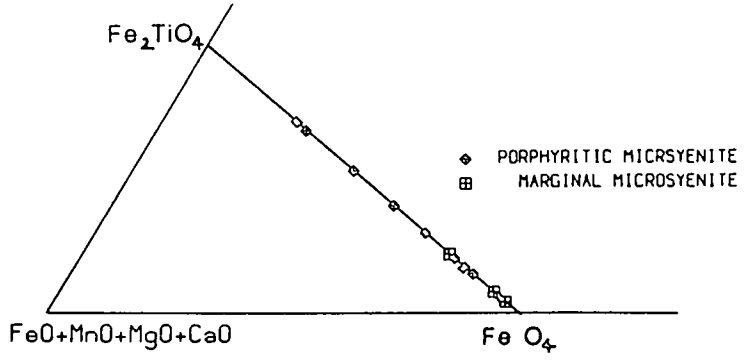
Fe2TiO4
FeO+MnO+MgO+CaO
Fe O4
PORPHYRITIC MICRSYENITE
MARGINAL MICROSYENITE

Fig. 4.5.1

Fig. 4.5.2

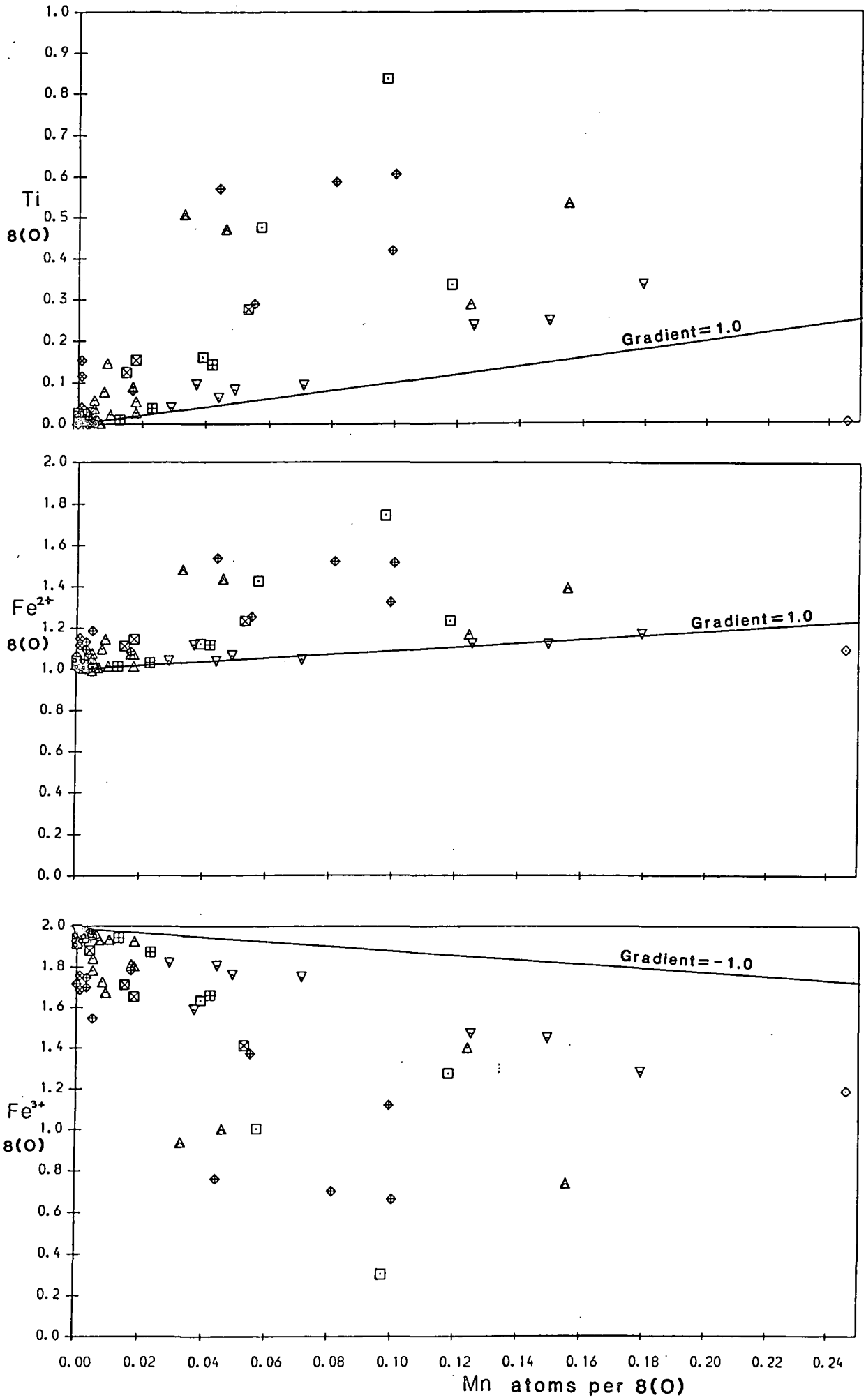
Ti
8(O)
Gradient = 1.0
Fe2+
8(O)
Gradient = 1.0
Fe3+
8(O)
Gradient = -1.0
Mn atoms per 8(O)

The remaining elements do not generally exceed about 1%, though Ca reaches 1.83% in GS-A, and Al 1.85% (oxides) in a Porphyritic Microsyenite dyke. Fig 4.5.2 shows variations of Fe^{3+}, Fe^{2+}, and Ti against Mn. Consistent trends are seen in the Upper Series Syenite, which marks the 'minimum' gradient of 1:1 for these variations. An exchange such as $(Mn,Fe^{2+})+Ti \rightleftharpoons 2Fe^{3+}$ is consistent with these variations, which would result in the different compositions of the *üsp-mgt* series, with Mn substituting for Fe^{2+}, as it does in the pyroxenes.

4.6 Nepheline and Gieseckite

4.6.1 Introduction

Nepheline is a major phase in all units of the complex except for the Xenolithic Porphyritic Syenite, where it was detected neither as a phenocryst nor in the groundmass. In all other units, it usually occurs as coarse-grained, millimetre-sized euhedral crystals, suggestive of an early crystallising, cumulus origin, frequently enclosed by alkali feldspar and cancrinite. Alteration is a common feature of the Grønnedal-Íka syenites, nepheline being one of the first minerals to be affected, resulting in the micaceous mineral gieseckite. This occurs as fine-grained aggregates, partially or wholly replacing the nepheline, but in the more altered rocks, forms larger, discrete crystals, which are colourless in plane-polarised light with high 2nd-order interference colours. It gives rise to the pale-pink colour of the nepheline in hand specimen, and is the characteristic mineral of the 'rotten' syenites which are so abundant at Grønnedal.

4.6.2 Chemical variation

The nepheline and gieseckite analyses are plotted in the system $Ne-Ks-Qz$ (fig. 4.6.1) on a molecular weight percent basis. All Na is assigned to nepheline, all K to kalsilite, and Ca to anorthite, while any excess Si after assignment to these molecules represents Qz. Molecular proportions were then converted to wt.% by multiplication by the relevant molecular weights.

Fig. 4.6.1A. All nepheline and gieseckite analyses plotted in the system $Ne - Ks - Qz$ on a molecular wt.% basis. Qz represents excess SiO_2 after assignment of this molecule to Ne, Ks, and An (anorthite). The gieseckite forms a distinct trend indicating loss of Na with gradually increasing Si/K ratio.

Fig. 4.6.1B. Expansion of lower left-hand portion of fig. 4.6.1A to show the variation in the nepheline compositions more clearly. The analyses form a distinctly elongated region as a result of slight alteration to gieseckite. Also shown are the ideal Morozewicz (M) and Buerger (B) compositions, in between which one would expect the analyses to lie after subsolidus re-equilibration.

Fig. 4.6.1C. A wide scatter in compositions is still apparent even when the compositions of only the cores are plotted, suggesting that the scatter in fig. 4.6.1B is not, for example, due to alteration of the rims, but is a genuine variation in the composition of the nepheline.

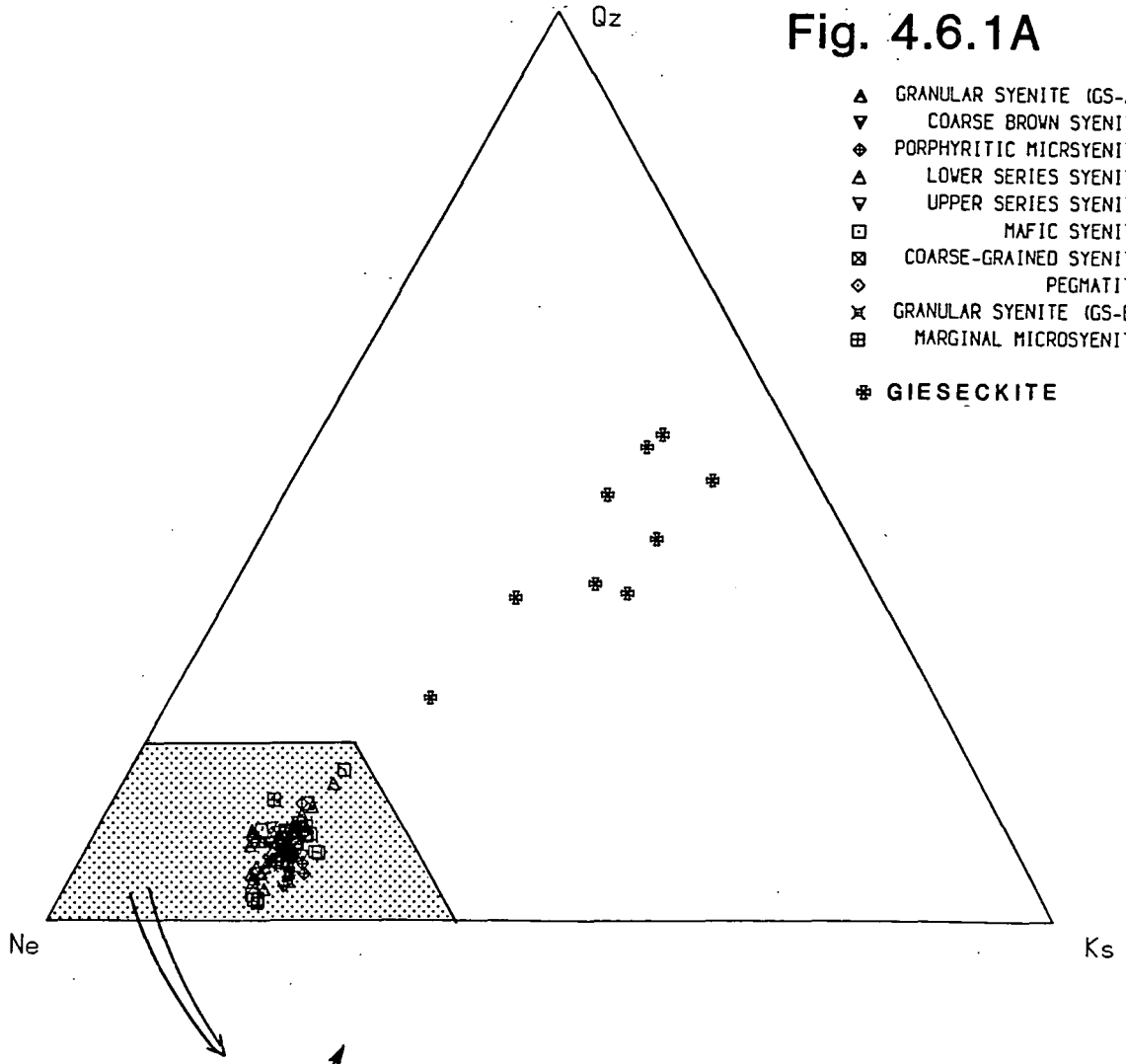
Fig. 4.6.1A
Qz
Ne
Ks
GRANULAR SYENITE (GS-A)
COARSE BROWN SYENITE
PORPHYRITIC MICRSYENITE
LOWER SERIES SYENITE
UPPER SERIES SYENITE
MAFIC SYENITE
COARSE-GRAINED SYENITE
PEGMATITE
GRANULAR SYENITE (GS-B)
MARGINAL MICROSYENITE
GIESECKITE

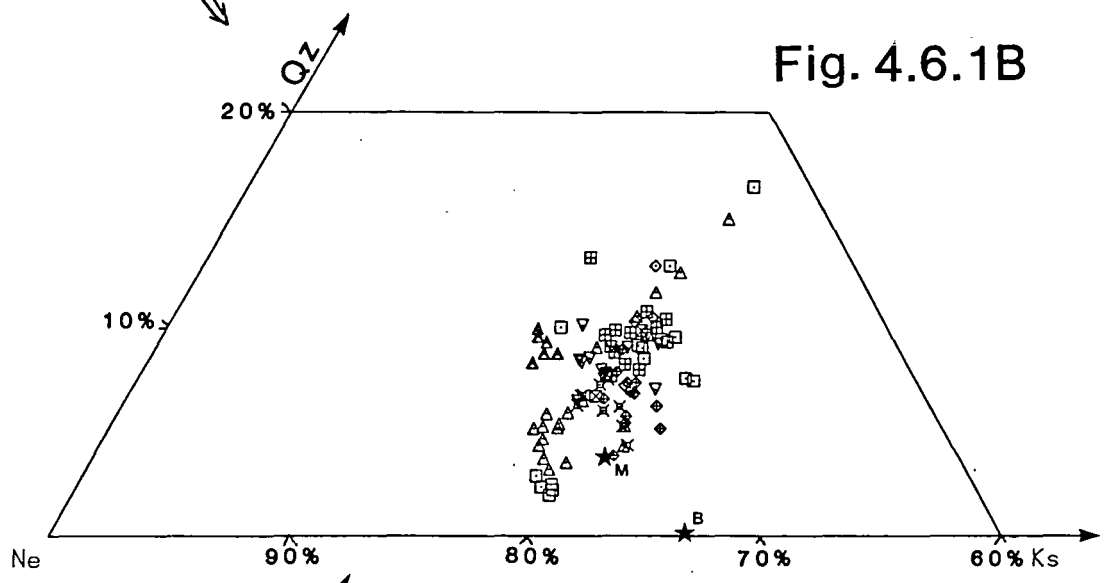
Fig. 4.6.1B
Qz
20%
10%
Ne
90%
80%
70%
60%
Ks
M
B

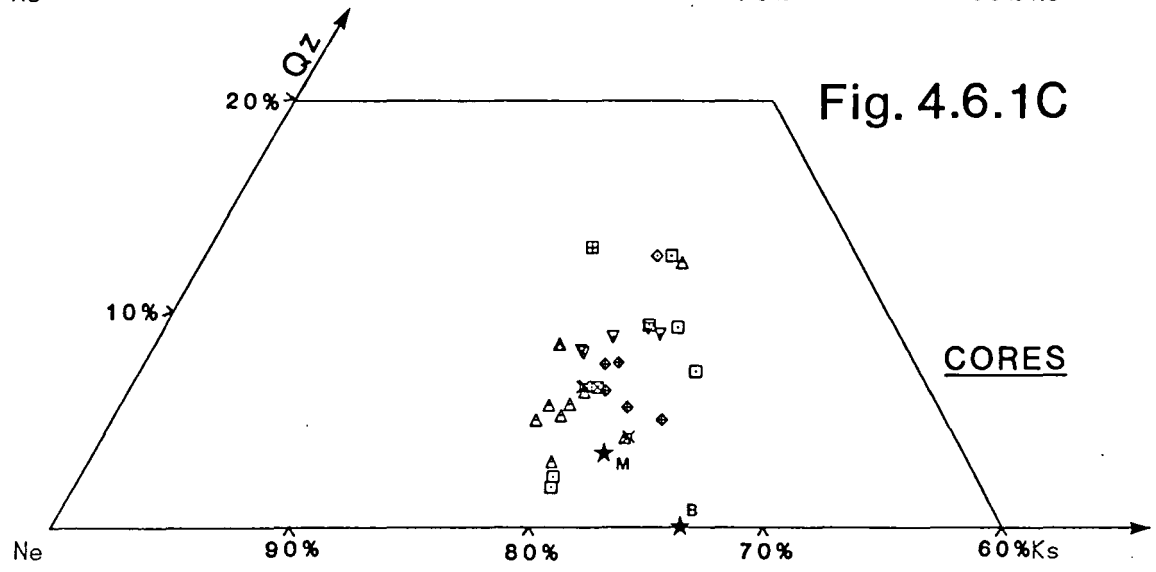
Fig. 4.6.1C
Qz
20%
10%
Ne
90%
80%
70%
60%
Ks
M
B
CORES

Nepheline analyses almost always show some solid solution with kalsilite and Qz, the latter a result of vacant sites in the lattice which would be filled by Na (Hamilton and MacKenzie 1960). The nephelines from Grønnedal-Íka are no exception to this. Also shown in fig. 4.6.1A are the gieseckite analyses, which form a trend almost perpendicular to the $Qz - Ks$ tie-line, suggesting loss of Na with slightly increasing Si/K, as suggested by Chambers (1976).

The lower left-hand corner of the plot is expanded in fig. 4.6.1B, which shows the analyses 'drawn-out' along the line of the gieseckite compositional trend, and strongly suggests that many of the nepheline analyses have been affected by the presence of gieseckite. Fig. 4.6.1C, showing analyses of only the cores of nepheline, indicates a similar spread of results to fig. 4.6.1B, suggesting that the cores are affected as much as the rims.

Tilley (1954) suggests that plutonic nephelines undergo subsolidus exchange of Na and K with alkali-feldspars, eventually resulting in nepheline with a higher proportion of Ks in solid solution than in the original crystal. This brings the composition into the area which lies between the ideal Buerger composition ($Na_3KAl_4Si_4O_{16}$) and the Morozewicz composition (the theoretical formula of most rock-forming nephelines, $Na_{6.1}K_{1.52}\square_{0.38}Al_{7.62}Si_{8.32}O_{32}$). However, as with nephelines from other Gardar complexes, those from Grønnedal-Íka appear to have undergone little, if any, subsolidus re-equilibration, no composition lying in the Morozewicz-Buerger convergence field (fig. 4.6.2). This is somewhat surprising considering the plutonic nature of the nephelines, and the relatively high volatile content of the magmas, which one might expect to assist with the subsolidus exchange (as in the case of alkali feldspar exsolution, Parsons 1978).

The Hamilton geothermometer, which enables the temperature of nepheline crystallising in equilibrium with alkali feldspar to be estimated (Hamilton 1961), is difficult to apply at Grønnedal-Íka for two principle reasons. Despite the apparent lack of subsolidus equilibration, the nephelines do show significant alteration to

Fig. 4.6.2. Nepheline compositions from the various syenite units, plotted in the system $Ne - Ks - Qz$ (molecular wt.%). No compositions lie in the convergence field between the Morozewicz (M) and Buerger (B) compositions, a feature which is also shown by nephelines from other Gardar centres. Also shown are the limits of solid solution of nepheline in equilibrium with alkali feldspar(at p_{H_2O}=1.034kb) after Hamilton (1961). As can be seen, several analyses lie outside the maximum theoretical limits of solid solution (1068°C), as a result of partial alteration to gieseckite, and largely because of this, the geothermometer cannot be used to give reliable temperature estimates.

Fig. 4.6.2

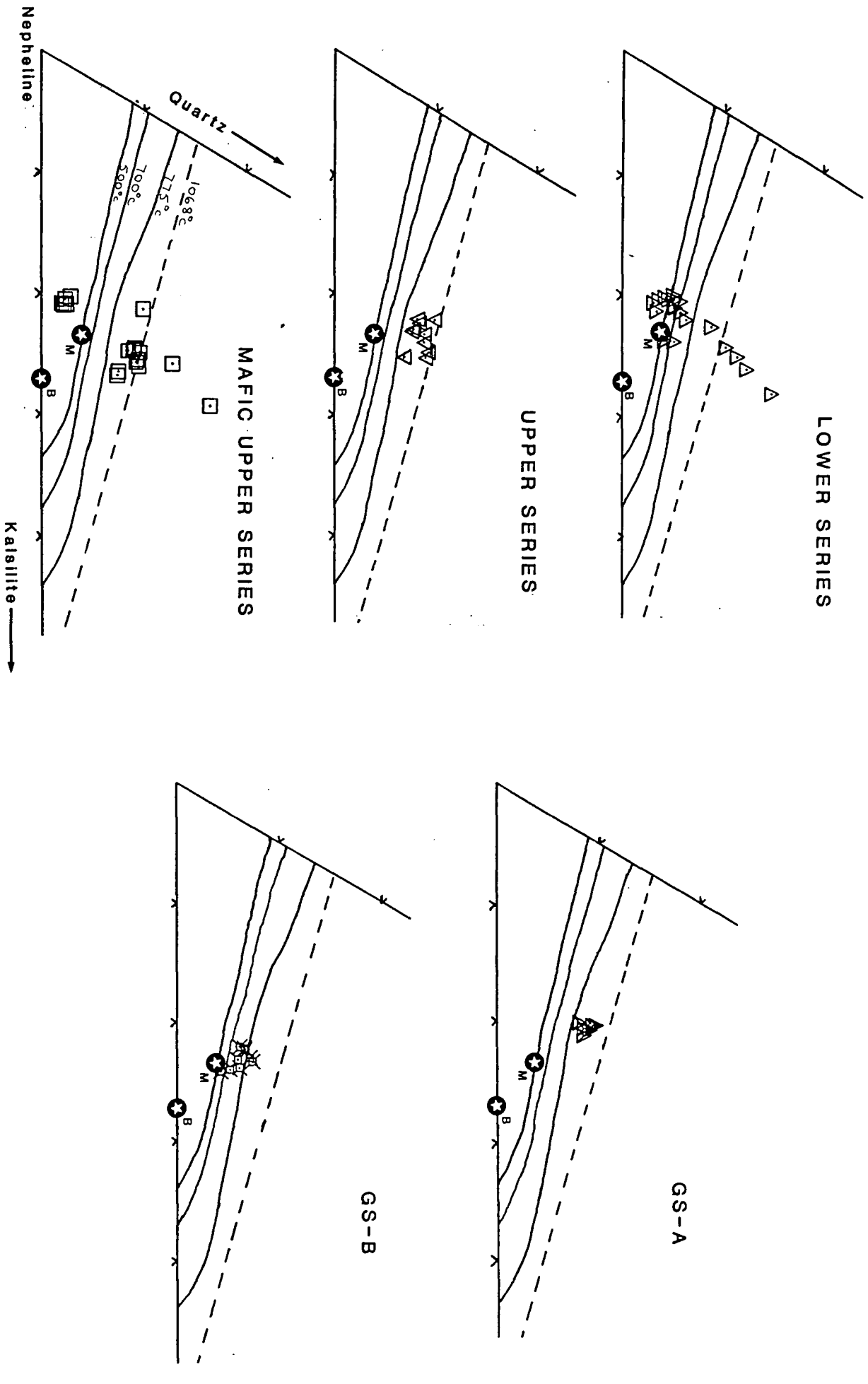
Nepheline
Quartz
Kalsilite
1098°C
1155°C
1100°C
590°C
M
B
LOWER SERIES
UPPER SERIES
MAFIC UPPER SERIES
GS-A
GS-B

Fig. 4.6.2 (cont.)

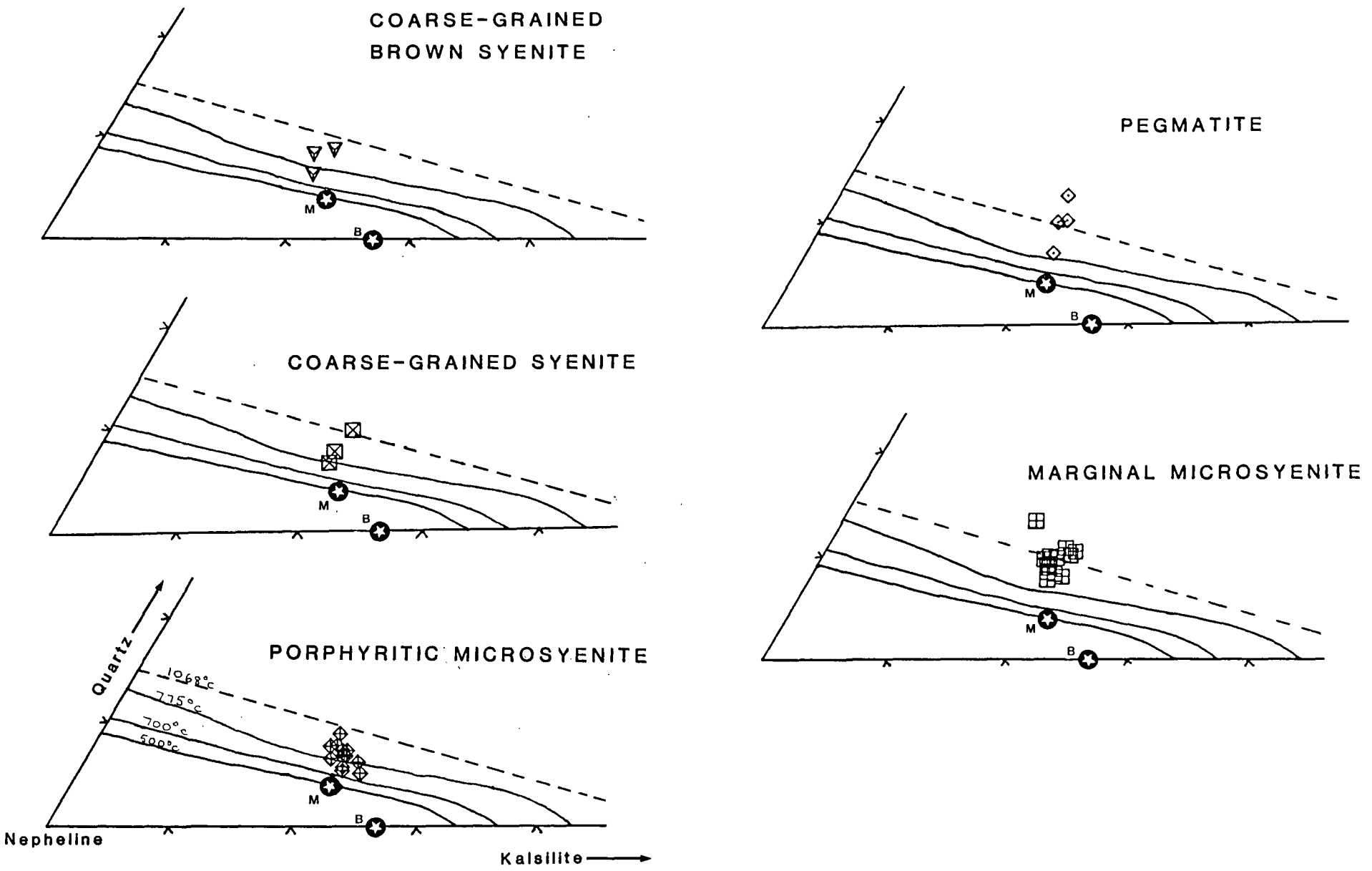
COARSE-GRAINED
BROWN SYENITE
M
B
PEGMATITE
M
B
COARSE-GRAINED SYENITE
M
B
MARGINAL MICROSYENITE
M
B
PORPHYRITIC MICROSYENITE
Quartz
1068°c
775°c
700°c
500°c
M
B
Nepheline
Kalsilite

gieseckite, which will result in a temperature estimate that is too high; only a slight deviation as a result of gieseckite being analysed could result in significant errors in the estimation of crystallisation temperature. The Lower Series Syenite is particularly affected in this way (fig. 4.6.2). Some units have very coherent plots, though, suggesting that the analyses have been little affected by alteration, and these give the following temperatures of crystallisation:

GS-A	800–900°C
GS-B	700–800°C
Porphyritic Microsyenite	700–1000°C
Upper Series Syenite	800–1050°C

However, Nash *et al.* (1969) suggest that the co-existance of sodalite increases the amount of 'excess SiO_2' in the nepheline, rendering the geothermometer inappropriate.

4.6.3 Minor elements

Nephelines are usually very poor in minor elements, the most significant being Fe, presumably substituting for Al as Fe_2O_3, which at Grønnedal-Íka generally lies in the range 0.5-1.0 wt%, though up to 1.34% (0.054 atoms per 8(O)) occurs in G178.09. This analysis also contains the greatest amounts of Mg and Mn (0.466% and 0.146% respectively), and may be the result of analysing some interstitial pyroxene which occurs as minute prismatic grains in thin-section (section 3.9, plates 3.9a,b). Ca is present (as anorthite), with up to 0.047 atoms per 8(O).

Gieseckite is richer in Si and K than nepheline, has an increasing Si/K ratio with decreasing Na, and lower Na in general (down to 1.55%). It is also richer in Fe (1.79% in G43) and generally poorer in Ca, with totals between 90% and 95%, the deficit presumably being made up by water (Chambers 1976).

4.7 Feldspars

4.7.1 General

Alkali feldspar is by far the most abundant mineral phase at Grønnedal-Íka, present in every sample of syenite collected, and occasionally making up nearly 100% of the rock, as in the pulaskitic facies at the top of the Lower Series Syenite. The crystals are somewhat variable in size, though generally of the order 12mm × 12mm × 2mm, with a strongly developed tabular habit and preferred orientation, resulting in the characteristic laminated appearance of the Upper and Lower Series Syenites. Upton (1964) noted that the (010) face becomes increasingly developed throughout the augite syenite - foyaite sequence of the Hviddal dyke on Tugtutôq, the most strongly fractionated rocks having very thin, tabular feldspars. Stephenson (1976) notes a similar effect with increasing fractionation of the South Qôroq centre, as do Kempe and Deer (1970) at Kangerdlugssuaq, and Nash *et al.* (1969) at Mount Suswa, Kenya. MacKenzie and Smith (1961) note that the very flat, tabular habit is characteristic of feldspars from nepheline syenite magmas, and suggest that it is a result of the metastable crystallisation of sanidine, with subsequent preservation of the sanidine habit. More recently, Smith (1974) proposes that feldspar habit in general is a result of anisotropic bonding within the lattice, the relative strengths of which vary according to the physical and chemical conditions of the environment in which the mineral is crystallising. The common occurrence of tabular alkali feldspars in nepheline syenites may be partly a result of the high alkali and/or volatile content, both features being characteristic of such rocks.

4.7.2 Exsolution

All of the alkali feldspars at Grønnedal are strongly and quite coarsely exsolved, resulting in considerable problems when trying to obtain a bulk analysis for a particular grain. In an attempt to overcome the problem, the electron beam

was rastered over a length of $c.150\mu$m, a compromise between using too large a distance, which would mean losing too much count-time during the fly-back, and a smaller distance which would not cover a sufficiently large area of the grain. Even so, totals of around 95% were obtained, though the stoichiometry of the feldspars was recorded accurately. Several analyses per grain were carried out, chosen so that the direction of raster would cross as many of the exsolution lamellae as possible.

In practise, it was found to be very difficult to obtain consistent readings even for a single grain, the results of which are shown in fig. 4.7.1. The wide range of compositions between *Or* and *Ab* may be a result of not rastering over a sufficiently large area of the sample, or a true scatter in the feldspar compositions. Both Stephenson (1973) and Chambers (1976) used a defocussed beam of only 50μm diameter for analysing feldspars, and seemed to obtain reasonable groupings of analyses. Rastering the beam over 150μm should, if orientated at a high angle to the exsolution lamellae, give a more homogenised analysis of the sample, so it would seem that the analyses do represent a true scatter in alkali feldspar compositions.

4.7.3 Chemical variation

As can be seen from fig. 4.7.1, little Ca is present (a maximum of 0.039 atoms per eight oxygens occurring in the Mafic Upper Series Syenite), and the overall grouping of analyses suggests a slight excess of *Or* over *Ab*, compositions scattered mainly on the *Or*-rich side of the 5kb eutectic (Yoder *et al.*, 1957). This lack of Ca suggests strongly evolved feldspar compositions, the Mafic Upper Series Syenite being somwhat less evolved, as also implied by the pyroxene compositions from this unit. Stephenson (1976) suggests that alkali feldspar compositions from the South Qôroq centre which lie to the *Or*-rich side of the 5kb eutectic are the result of nepheline co-precipitating with the feldspar. This would tend to increase the K/Na ratio of subsequent crystallising phases, and move the eutectic towards more

Fig. 4.7.1(two pages). Feldspar analyses for each syenite unit, plotted in the system $Ab - Or - An$ (wt.%). The 5kb eutectic (after Yoder *et al.*, 1957) is also shown.

Fig. 4.7.1

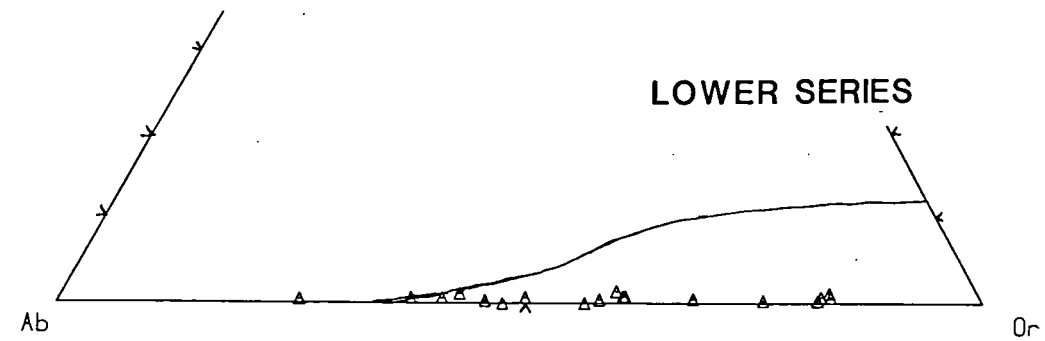
LOWER SERIES
Ab
Or

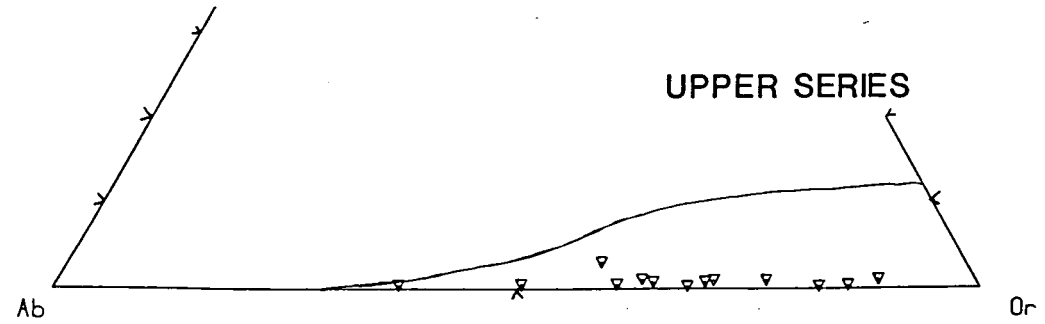
UPPER SERIES
Ab
Or

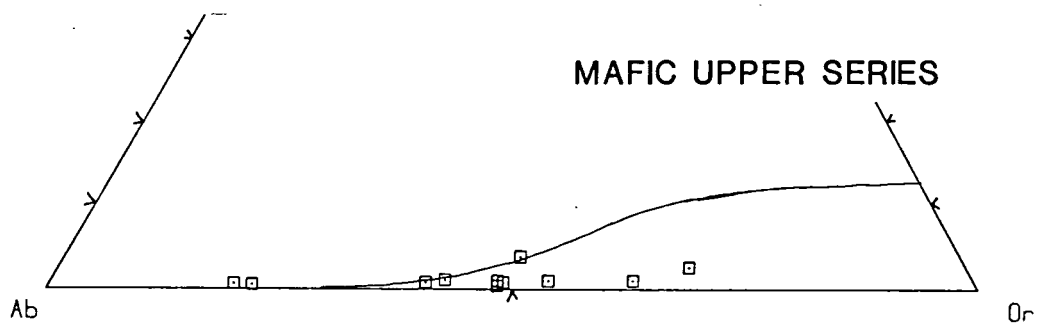
MAFIC UPPER SERIES
Ab
Or

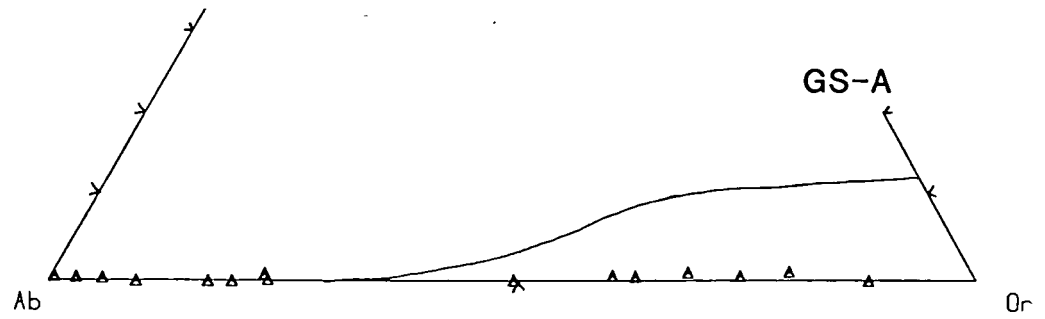
GS-A
Ab
Or

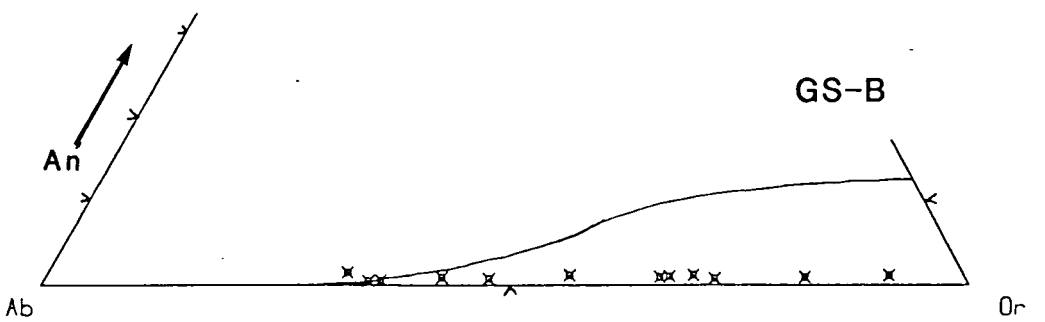
GS-B
An
Ab
Or

Fig. 4.7.1 (cont.)

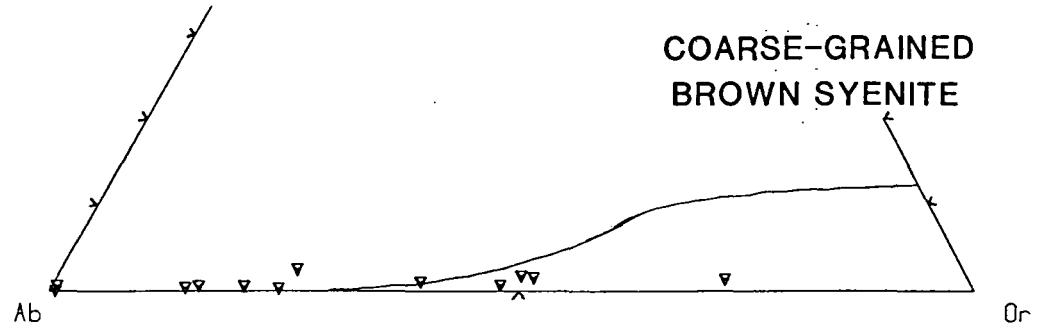
COARSE-GRAINED
BROWN SYENITE
Ab
Or

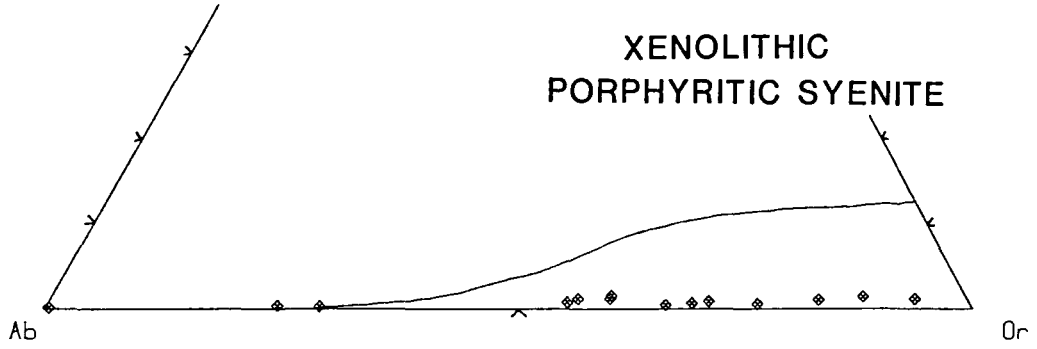
XENOLITHIC
PORPHYRITIC SYENITE
Ab
Or

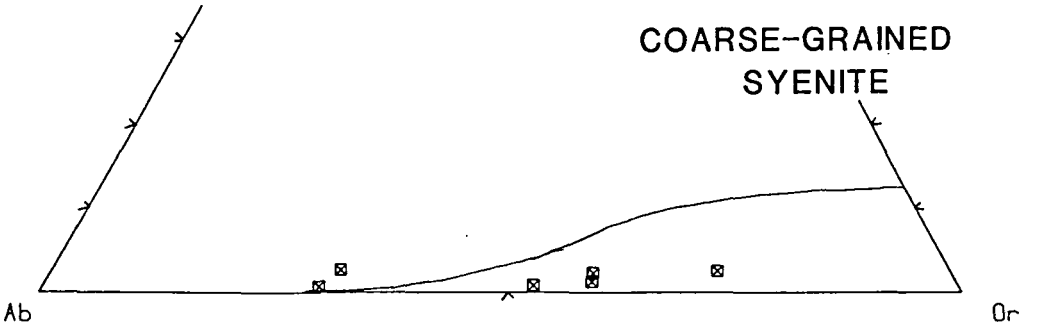
COARSE-GRAINED
SYENITE
Ab
Or

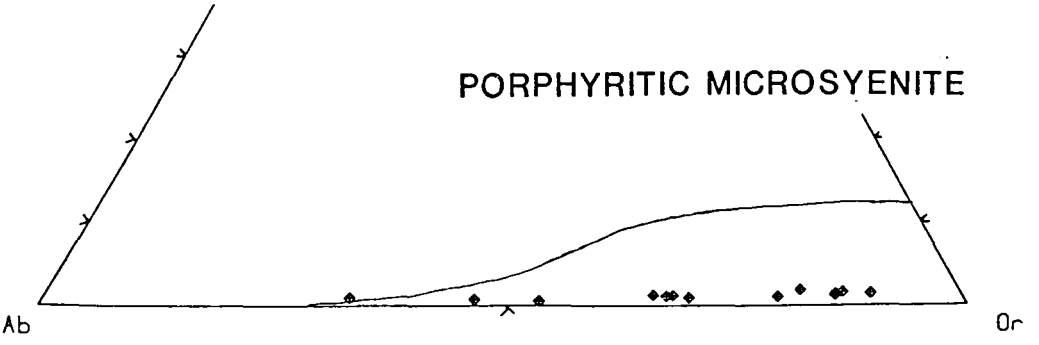
PORPHYRITIC MICROSYENITE
Ab
Or

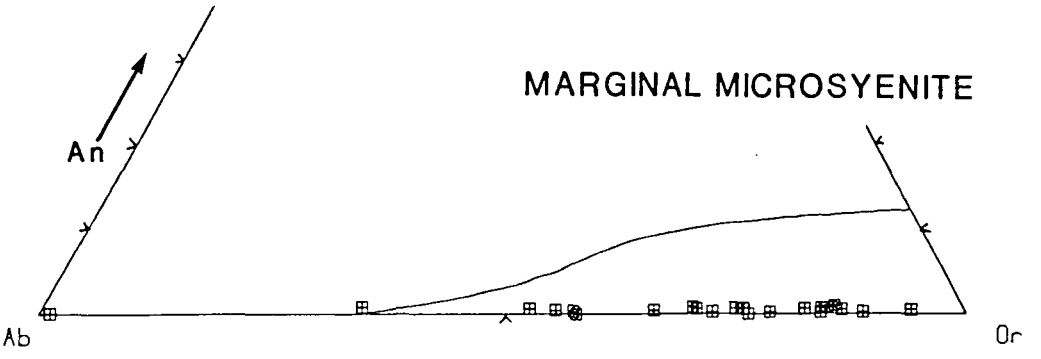
An
MARGINAL MICROSYENITE
Ab
Or

potassic compositions. The very variable amounts of nepheline which are observed in different samples of the same rock-unit (chapter 3) would suggest that different parts of the crystallising magma may have had separate crystallisation histories, developing a wide variety of feldspar compositions according to the amount of nepheline which was co-precipitating at the time.

The Mafic Upper Series Syenite feldspars are seen to be slightly more albitic than those from most of the other rock units, though the majority of analyses still plot on the *Or*-rich side of the eutectic. Similarly, the Coarse-Grained Brown Syenite contains relatively albitic feldspars, though here the majority of analyses are on the *Ab*-rich side of the eutectic. Feldspars from GS-A show a strong bimodal distribution, the two compositional groups apparently separated by the eutectic. The Coarse-Grained Brown Syenite and GS-A show evidence of having suffered some metasomatic alteration (sections 3.6 and 3.5.1 respectively), which could have given rise to more albitic compositions (cf. chapter 7). The Mafic Upper Series Syenite, however, appears to have experienced very little metasomatic alteration, and the feldspar compositions which lie closer to the eutectic could be explained by a smaller amount of co-precipitating nepheline. Samples of these rocks do appear to contain less nepheline when viewed in thin-section (section 3.4).

No consistent patterns regarding zonation were observed, other than overgrowths on feldspars from the Xenolithic Porphyritic Syenite being more K-rich than the cores. This contrasts with alkali feldspar from other Gardar centres, where K-rich rims frequently overgrow cores of more plagioclase-rich compositions. Additionally, there does not appear to be any clear difference between groundmass and phenocryst feldspars. It is possible that the compositions have been slightly affected by late-stage metasomatic alteration, as has been observed in feldspars of the North Qôroq centre by Rae and Chambers (1988). In this

respect, cathodoluminescence observations of the Grønnedal-Íka feldspars would no doubt be extremely interesting.

Minor elements

The only significant minor element is Fe, which does not usually exceed 0.5 wt% oxide, though higher values (up to 0.822%) occur in feldspars from the Xenolithic Porphyritic Syenite, in a potassic overgrowth on a more albitic core, as mentioned earlier. Ba reaches a maximum of 0.824% in the Coarse-Grained Syenite, though is generally present in amounts less than 0.1%, while Mn and Mg never exceed around 0.4% .

4.8 Zircons

Zircon is a surprisingly common phase in most of the syenite units of Grønnedal-Íka, particularly in the more altered samples, and occurs as interstitial and poikilitic grains up to three or four millimetres in diameter.

Little recent published work on the occurrence of zircons in igneous rocks is available, other than that which is concerned with radiometric dating, though it is a common accessory mineral, particularly in rocks which are rich in Na (Deer *et al.*, 1963). It is an early crystallising phase in granitic and dioritic magmas, becoming "increasingly delayed" in more alkaline magmas (Poldervaart 1956). The interstitial nature of the zircons in the Grønnedal syenites would appear to support this statement. Poldervaart also suggests that in 'agpaitic' (peralkaline) magmas, Zr occurs in the form of other zirconium silicates (such as eudialyte, catapleite), while in miaskitic (subalkaline) magmas, it occurs simply as the mineral zircon. Again, this appears to be true for the syenites at Grønnedal-Íka, which are generally subalkaline and contain no zirconium-rich minerals other than zircon itself. Jones (1980) suggests that the low a_{SiO_2} has prevented the formation of zircon in the Motzfeldt centre, though the presence of nepheline would suggest that the activity is equally low at Grønnedal-Íka.

The elements analysed in the zircons total almost exactly 100%, suggesting that rare-earth elements (REE) or hafnium (up to 24% HfO_2 having been reported in a zircon from Norway by Levinson and Bornup, 1959) are not present in any significant quantities. After Zr and Si, Na occurs in the greatest abundance (0.76%) while Ti, Fe, and Mg are all present in amounts less than 0.5%. Qualitative microprobe investigations of zircons from several of the syenite units have revealed that very small quantities of REE's were detectable using the EDS system at Durham. It is unfortunate that time was not available for a detailed investigation using the WDS system, as the occurrence of zircon in such quantities at Grønnedal appears most unusual.

4.9 Apatite

Apatite is a very abundant mineral at Grønnedal, occurring in most samples of all the syenites. It has also been reported in the Motzfeldt, South Qôroq, and North Qôroq centres (Jones 1980, Stephenson 1973, Chambers 1976 respectively), although no analyses were made. CaO and P_2O_5 comprise the bulk of the analysed oxides, and of the remaining elements, Si is the most abundant (1.165 wt.% SiO_2 in 27193, a Mafic Upper Series Syenite). Analytical totals lie in the range 92% - 96%, the deficit consisting mainly of F, Cl, and H_2O (generally around 4%, Deer *et al.*, 1966), with Rare Earth elements (REE's) and CO_2 making up the remainder. Four samples were partially analysed for REE's (La, Ce, Pr, Nd, and Sm) by Dr. J.A. Craven of Edinburgh University, the results of which are set out in the table below. Cerium is the most abundant REE in the apatites, occurring up to 1.94% CeO_2, followed by Nd (up to 0.98% Nd_2O_5), both from sample 138048 from the Lower Series Syenite.

REE apatites belong to the apatite-britholite series, the REE's possibly entering the lattice by the coupled substitution (After Speer and Ribbe 1982):

$$Si^{4+} + REE^{3+} \rightleftharpoons P^{5+} + Ca^{2+}$$

Sample no.	27259	31854	138048	138011
Rock-type	Mafic Syenite	Xenolithic Syenite	Lower Series	Coarse-Brown Syenite
No. of analyses	9	6	9	19
Average La_2O_3(wt.%)	0.590	0.161	0.532	0.245
Average CeO_2(wt.%)	1.485	0.471	1.375	0.669
Average Pr_2O_3(wt.%)	0.207	0.127	0.205	0.122
Average Nd_2O_5 (wt.%)	0.736	0.283	0.763	0.393
Average Sm_2O_3(wt.%)	0.161	0.054	0.137	0.089
Total (wt.%)	3.179	1.096	3.012	1.518

4.10 Other minerals

Cancrinite

Cancrinite is an abundant interstitial phase in the coarser syenite units, where the grains are less tightly packed together. Its occurrence at Grønnedal-Íka is highly suggestive of crystallisation from late-stage fluids, and often forms areas more than 1cm across, poikilitically enclosing euhedral nephelines (plate 3.3). It also occasionally partly replaces nepheline, suggesting that the paragenesis of cancrinite is not due to simple late-stage crystallisation, but may also be a result of reactions between volatile-rich fluids and nepheline.

The main substitution in cancrinite is SO_4^{2-} for CO_3^{2-}, giving rise to vishnevite. However, only very minute quantities of S were detected, suggesting that the samples are close to end-member cancrinite (Chambers 1976, Pearce 1988). Cancrinites also show exchange of Ca for Na, both of which show considerable variation in the samples from Grønnedal, though most tend to contain some Ca (up to 1.2 atoms per 24 oxygens), while samples from the Xenolithic Porphyritic Syenite are richest in Na, with around 5.5-6.0 atoms per 24(O).

K exceeded 1% in only one sample (138044.14), which was also the richest in Fe (1.57%). Of the other elements, only Mg was detected in any quantity (0.488% maximum), the greatest amounts occurring in the Xenolithic Porphyritic Syenite. Totals vary between about 84% and 88%, the remainder consisting of H_2O and CO_2. This compares quite favourably with amounts of volatiles (H_2O, CO_2, SO_3, Cl) given in Deer *et al.* (1982) of 13% from a cancrinite from Ontario, Canada.

Analcite

Analcite has the formula $NaAlSi_2O_6.H_2O$, and may be thought of as the Na analogue of leucite ($KAlSi_2O_6$). It is a difficult mineral to identify at Grønnedal-Íka by optical means, where it occurs as small interstitial grains, and was discovered by chance when analysing for nephelines.* Of the eleven analyses made, seven were from syenites and four from metasomatised rocks, though in general the mineral is more common in the more altered rocks.

Roux and Hamilton (1976) showed that primary analcite has a very limited stability field of 5–13Kb, and 600–640°C, so that most analcite will tend to be of secondary origin. Henderson and Gibb (1977) proposed that the analcite in the crinanite of the Dippin Sill in SW Arran is the result of a reaction between nepheline and albite, and in view of the minor interstitial occurrence of this mineral at Grønnedal-Íka, together with its greater abundance in the more altered rocks, a secondary origin is proposed here.

The major substitution in analcite is $Na+Al \rightleftharpoons Si$, becoming increasingly Si-rich with increasing fractionation (Kim and Burley, 1971). Si varies between 2.4 and 2.67 atoms per six oxygens, Kim and Burley (1971) suggesting that considerable amounts of excess SiO_2 can be taken up in solid solution (up to nearly three Si atoms per 6(O)). Na varies between 2.06 and 0.76 atoms, but is generally around 1.25 atoms per 6(O) (fig. 4.10.1). Little K and Ca are present (up to 0.298% and

* and have been recalculated on the basis of 8(O) in Appendix II.

Fig. 4.10.1

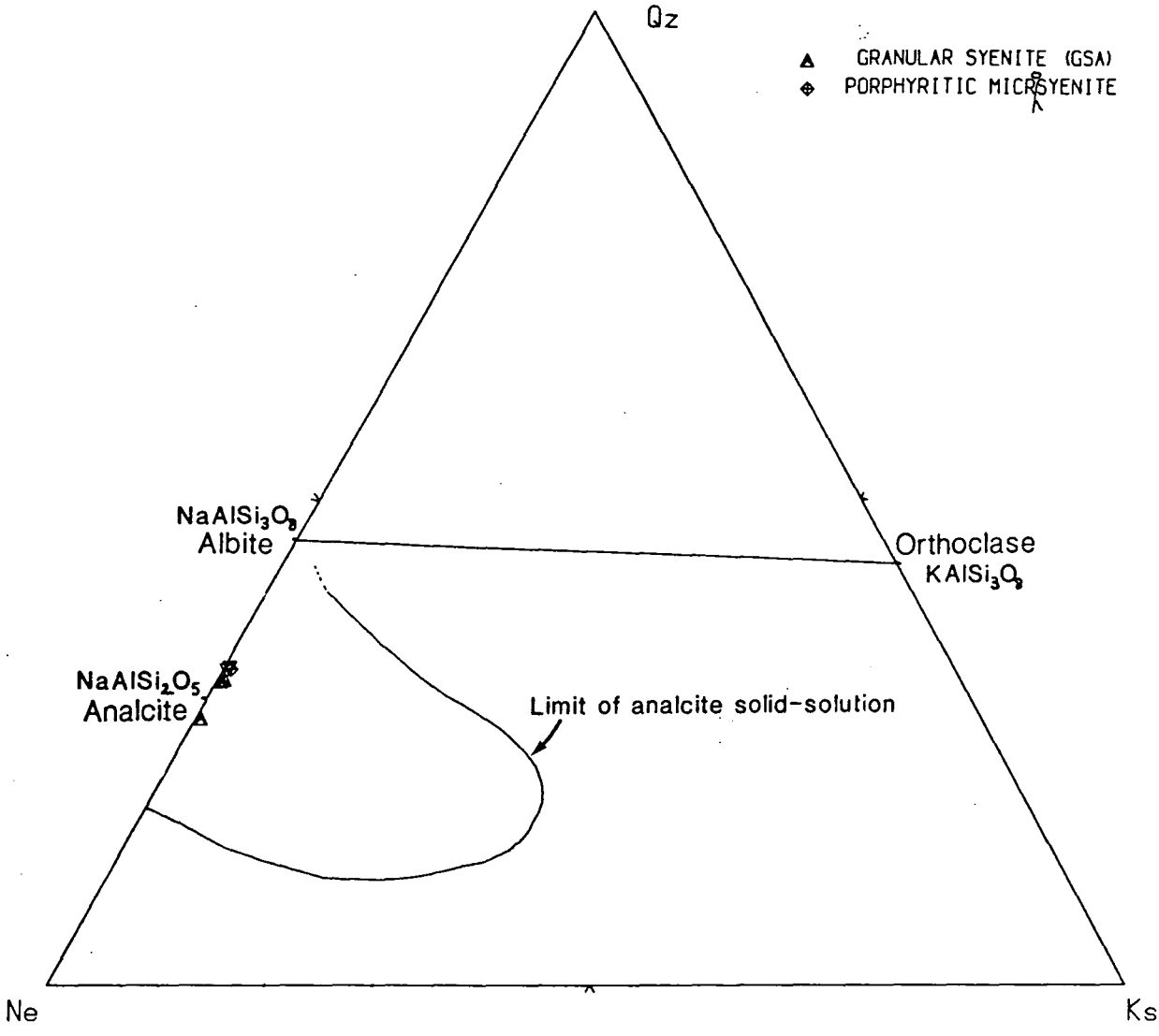

Fig. 4.10.1. Analcite analyses plotted in the system $Ne - Ks - Qz$ (wt.%) The extensive solid-solution field of analcite, as determined experimentally by Kim and Burley (1971), is shown.

0.747% respectively), with only minute quantities of the other elements analysed. Totals vary between 88% and 99%, the deficit being made up by water.

Sodalite

Only three analyses of sodalite from non-metasomatised rocks were made, though the mineral is much more common than this would suggest, occurring as distinct bright-blue aggregates in the region of the Radioelv gorge. Like analcite, it occurs most commonly in the more altered samples, and four analyses were made from metasomatised specimens. It is generally present as small, interstitial isotropic grains, and like analcite, is not easy to pick out when it occurs as such small grains.

The formula of sodalite is $3NaAlSiO_4.NaCl$, with chlorine an essential constituent of the mineral, occurring up to a maximum of 8.67% at Grønnedal. Little variation in composition was found, and negligible amounts of Fe, Mg, Mn, Ca, K, and S. Wellman (1970) suggests that sodalite is a liquidus mineral in the system $Ab - Or - Ne - Ks - NaCl - KCl - H_2O$ over a wide range of pressures, so that in contrast to the analcite and like the cancrinite, the sodalite may be of (late) primary origin.

Carbonate

Grains of interstitial carbonate in relatively unaltered syenites have already been mentioned and illustrated (plate 3.4). Only three analyses of carbonate in unmetasomatised syenites were made, and shown to be almost pure calcium carbonate, with up to 0.84% Mn, 0.449% Fe, and 0.163% Mg. They may have a significance out of all proportion to their abundance concerning the generation of the carbonatites, an aspect which is discussed more fully in chapter 6.

4.11 Conclusions

This section summarises much of what has already been discussed in earlier parts of the chapter regarding the physical and chemical properties of the magma from which the various phases crystallised.

The more obvious aspects of the magma chemistry, such as the high alkalinity and presence of volatiles, have been mentioned in chapter 3 since they are evident from petrographic observations. Microprobe analysis confirms that sodalite is indeed present, usually containing around 8% Cl, suggesting that chlorine-rich fluids were present in the later stages of the crystallisation history.

The lack of olivine in these rocks has already been referred to in chapter 3, and in view of the absence of this phase it is perhaps surprising that the pyroxenes and oxides are not significantly richer in Mn than those from the other Gardar complexes, which generally have similar whole-rock abundancies of MnO (0.2-0.6%).

Several other features of the mineral chemistry suggest that the f_{O_2} of the magma was relatively high compared to other Gardar centres. Pyroxene trends (section 4.2) show early enrichment of the acmite end-member, which could result from a high $a_{Fe^{3+}}$, possibly as a result of a high f_{O_2}, though as discussed in section 4.2.4, other factors may well be involved.

More conclusive evidence for a high f_{O_2} comes from the chemistry of the opaque oxides. With only one exception, they are members of the ülvospinel-magnetite series, and are predominantly magnetite-rich. According to Buddington and Lindsley (1964), "for a given temperature, at successively higher oxygen fugacities, the composition of magnetite-ülvospinel becomes successivly lower in TiO_2". This would therefore suggest crystallisation from magmas which are relatively oxidising at Grønnedal-Íka.

Indirect evidence for the f_{O_2} also comes from the lack of amphibole in most of the samples observed. Fig. 4.11.1 shows the stability curve for sodic amphiboles as determined experimentally by Ernst (1962), below which the amphiboles are stable, and above which they are unstable. The Quartz-Fayalite-Magnetite buffer is also shown, which separates assemblages containing quartz and fayalite (below) from magnetite (above). Combining the petrographic observations of chapter 3 with these curves, the region of $f_{O_2} - T$ space occupied by the Grønnedal-Íka magmas is suggested as the stippled area in fig. 4.11.1. It is unfortunate that a temperature estimate could not be obtained from the nepheline analyses (due to alteration) to define the conditions more accurately, though as can be seen, the f_{O_2} is probably greater than about 10^{-22} bars.

Fig. 4.11.1

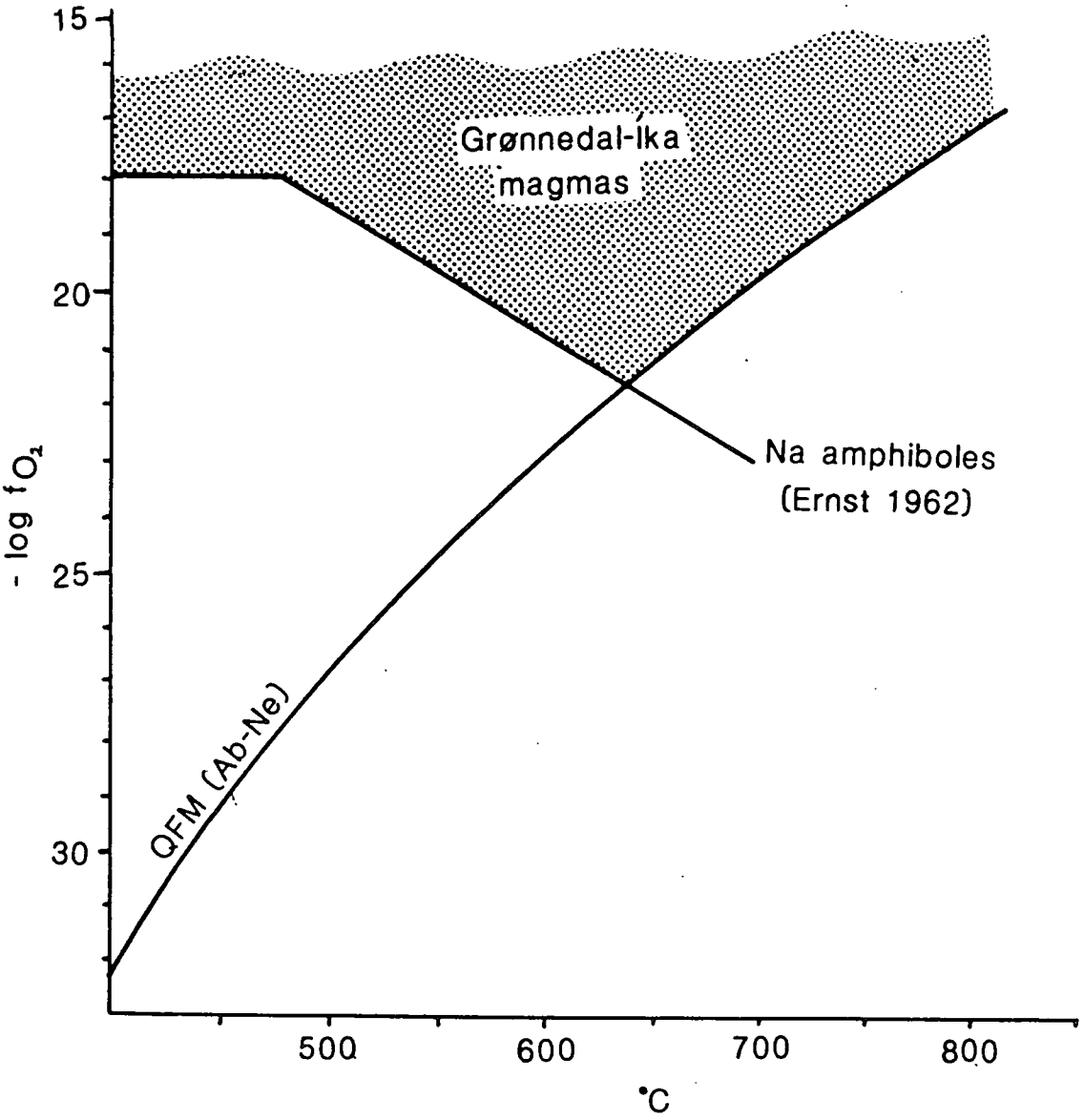

Fig. 4.11.1. Graph of $-\log(f_{O_2})$ against temperature (reproduced from Platt and Woolley, 1977). The quartz-fayalite-magnetite (QFM) buffer at the silica activity defined by the albite-nepheline buffer is shown, though variations in a_{SiO_2} affect the position of the curve only slightly. The stability curve of sodic amphiboles (Ernst 1962) is also shown, separating fields of amphibole-present (below) from amphibole-absent (above). From petrographic observations, it is suggested that the f_{O_2} of the Grønnedal-Íka magmas occupies the area above both of these curves, and is shown stippled.

CHAPTER 5: GEOCHEMISTRY

5.1: Introduction

Whole-rock chemical analyses were carried-out using X-ray fluorescence (XRF) techniques on fresh samples (where possible) from all units of the complex, collected over as wide a geographical area as possible. Carbonatites and metasomatised rocks are described in chapters six and seven respectively, while sample preparation and full XRF operating conditions are described in Appendix III.

Because of the restricted range of SiO_2 in the rock-types present at Grønnedal-Íka, analyses are plotted on variation diagrams using the 'Fractionation Index' (FI) of Macdonald (1969) as the abscissa. This is essentially a modification of the differentiation index of Thornton and Tuttle (1960) (normative $qz + ab + or + ne$), involving the addition of sodium metasilicate and acmite, the latter becoming increasingly important with increasing peralkalinity. Normative abundances were calculated using the program `NORM.PL1`, a modification of `NORMCAL` written by Gill (1972a), and using Fe^{2+}/Fe^{3+} ratios determined for the units at Grønnedal by Gill (*op. cit.*) using wet chemical methods.

Fig. 5.1.1A shows the range of fractionation indices for all analyses made on samples from the various rock units of the complex. Similar ranges in FI have been determined by Stephenson (1973) and Chambers (1976) for the South and North Qôroq centres respectively, but they omitted analyses containing normative corundum. This arises due to the alteration of nepheline to gieseckite, and they suggest that this gives anomalously low values of FI. Fig. 5.1.1B shows only corundum-free analyses, and illustrates that not only is the range of FI of each rock-type usually unaffected, but the distribution of fractionation indices is little different from that in fig. 5.1.1A. The two exceptions to this are the Coarse-Grained Syenite and Coarse-Grained Brown Syenite, which show greater amounts

Fig. 5.1.1. Range of Fractionation Indices of individual rock units at Grønnedal-Íka. The Fractionation Index, FI, (after Macdonald 1969) is calculated as the weight percent of normative components ($ab + or + an + ne + ac$) plus normative sodium metasilicate, as calculated using the program `NORM.PL1` (after Gill 1972b).

Fig. 5.1.1A shows all 229 syenite samples on which whole-rock analyses were carried out, while fig. 5.1.1B omits analyses containing normative corundum. For most of the units, there is little change in either the range or the distribution of FI's.

Fig. 5.1.1A

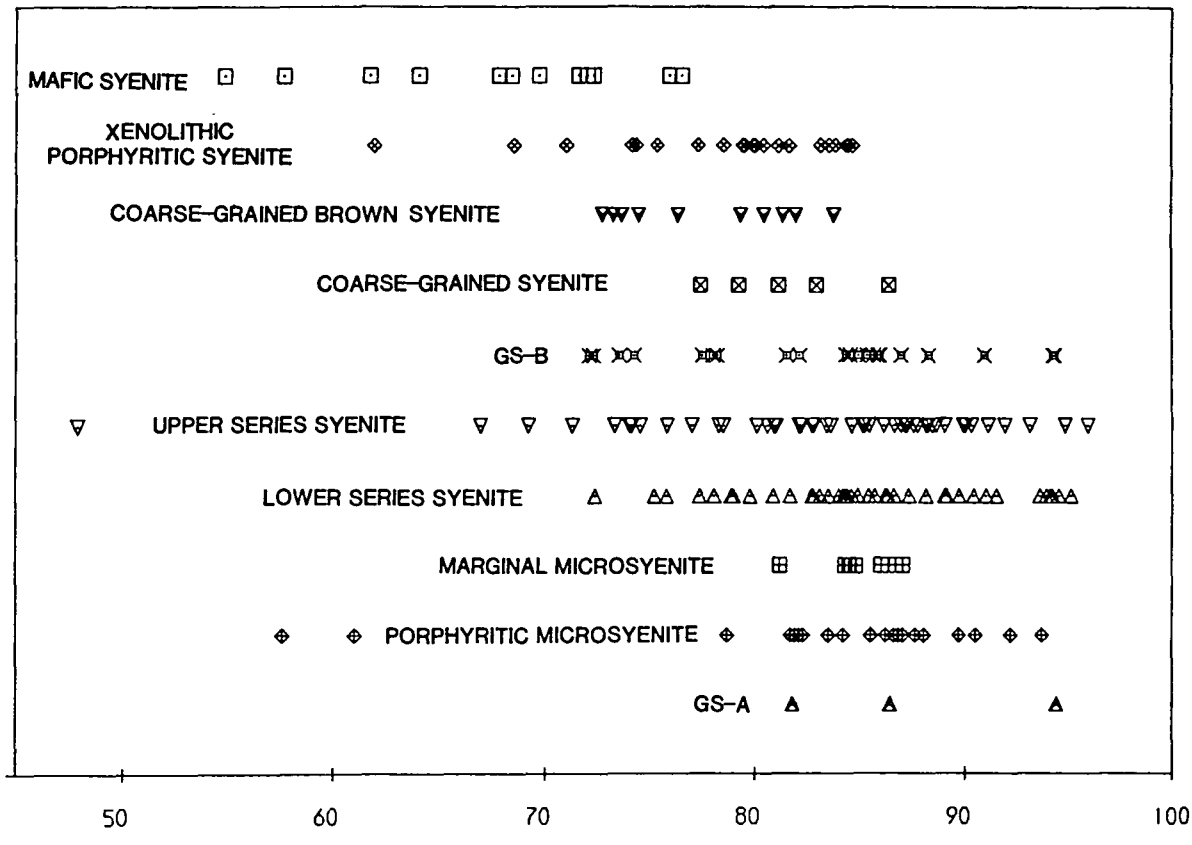

Fig. 5.1.1B

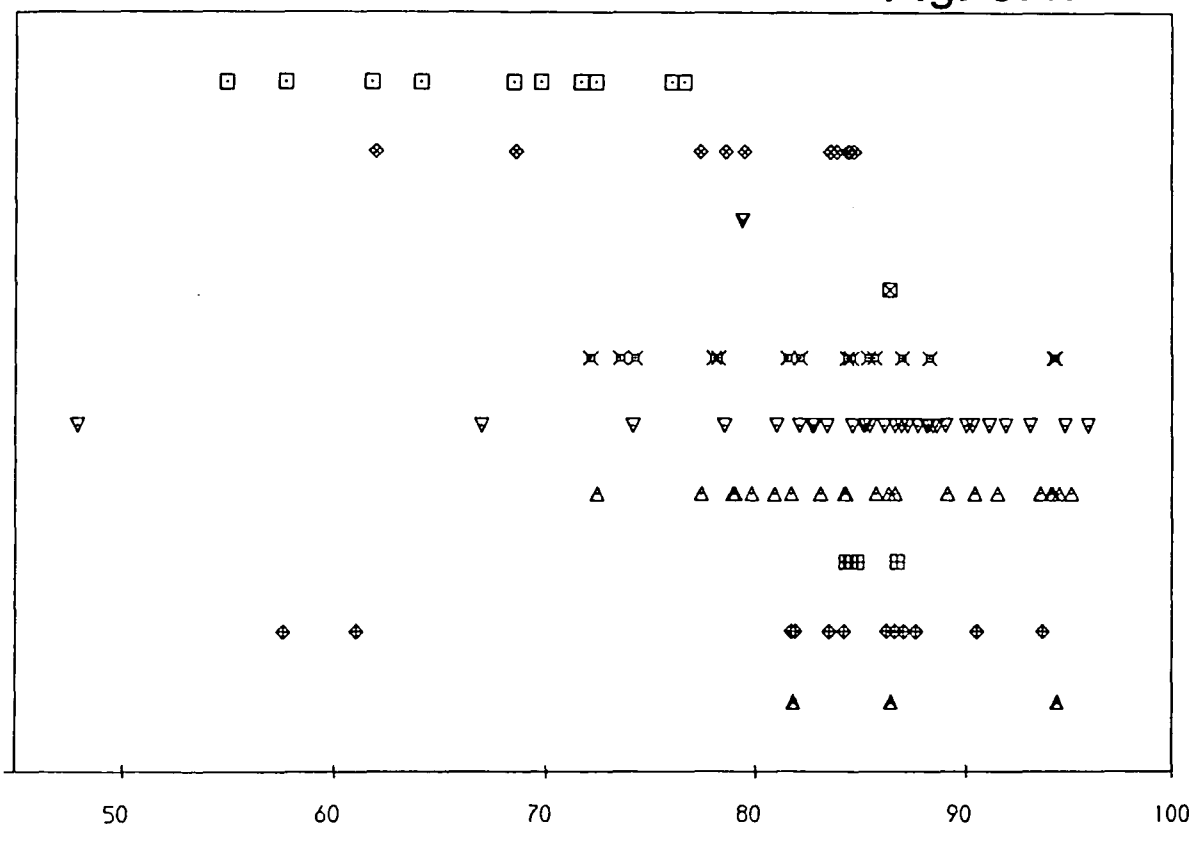

of alteration, resulting in a larger proportion of normative corundum. As useful information may be lost if samples with normative corundum are omitted, these analyses are retained in the major and trace element variation diagrams.

Petrographic evidence (chapter 3) suggests that a large number of samples, particularly those from the laminated units, contain minerals of cumulus origin. Thus in contrast to aphyric volcanic rocks, these samples are not representative of the liquids from which they crystallised.

In a study of the Skaergaard layered series, Paster *et al.* (1974) considered some of the possible causes of whole-rock compositional variations in cumulate rocks. They suggested that the composition of the interstitial liquids within an accumulating crystal pile remained in approximate equilibrium with the unconsolidated magma as long as circulation of magma through the crystal pile could take place. Once the intercrystalline areas were sealed-off, as a result of continued crystal growth, the intercumulus liquid would be trapped and crystallises *in situ.* The element concentrations within the interstitial liquid at the time of trapping will contribute to the bulk composition of the rock. Thus the final composition may be strongly dependent on the time that the interstitial liquids are trapped; the later in the evolution of the magma that this occurs, the more evolved will be the composition of the trapped liquids. The texture of the rock may be particularly significant in controlling the time of trapping (and therefore composition of the trapped liquid), with coarser grained, poorly laminated samples allowing magma circulation to continue for longer, and developing more evolved rock compositions. It has already been shown that variations in pyroxene composition may be controlled by the proportion of crystallisation that takes place from intercrystalline areas in the Lower Series (section 4.2.5, fig. 4.2.6B). Some of the observed scatter in the range of whole-rock compositions may similarly be controlled by variations in the textural arrangement of the cumulus phases, particularly alkali feldspars,

the tabular nature of which may act as a baffle to the migration of intercumulus liquids.

5.2: Major elements

Fig. 5.2.1 shows the ten major elements (Si, Al, Fe, Mg, Ca, Na, K, Ti, Mn, and P) plotted as weight per cent oxides, together with the loss-on-ignition (H_2O+) and peralkalinity (molecular Na_2O+K_2O/Al_2O_3), plotted against Fractionation Index (FI).

Elements such as Si, Al, Na, and K will naturally show an increase with FI, since these elements are present in the minerals which define the FI. The diagrams do serve to indicate the range of elements present, however, and enable comparisons with other complexes to be made.

The more fractionated samples from Grønnedal tend to be rather more siliceous than those with an equivalent FI from South and North Qôroq (Stephenson 1973, and Chambers 1976). Above FI=85, there is a weak suggestion of two trends, one of which shows a continuing increase in SiO_2, while the other remains virtually constant at around 55% SiO_2.

Al_2O_3 increases with FI up to FI$\approx$85, thereafter decreasing very slightly. Note that this decrease starts to occur at the same value of FI at which the two silica trends are discernible. The Coarse-Grained Brown Syenite shows some of the highest Al_2O_3 contents, at relatively low values of FI. The loss of Na from nepheline during alteration to gieseckite (see below) has resulted in a relative increase in the amount of Al_2O_3 in this unit.

Na_2O and K_2O show a considerable scatter of values, possibly as a result of nepheline alteration which would affect these elements more than any other, though a gradual increase with FI is suggested. The Coarse-Grained Brown Syenite, which contains relatively large amounts of Al_2O_3, is correspondingly poorer in Na_2O. As suggested above, this is a result of Na-loss during gieseckite formation.

Fig. 5.2.1(Three pages). Major element variation in terms of weight percent oxide against Fractionation Index (FI). Those elements present in the minerals which make up the FI (mainly Si, Al, Na, K) not surprisingly show an increase in weight percent oxide with increasing FI, while others generally decrease in abundance. Also shown are the loss-on-ignition (LOI) values for all samples, and the peralkalinity index (molecular Na_2O+K_2O/Al_2O_3).

Symbols as in fig. 5.1.1.

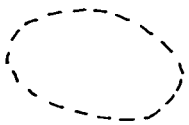

Coarse-Grained Brown Syenite.

Fig. 5.2.1

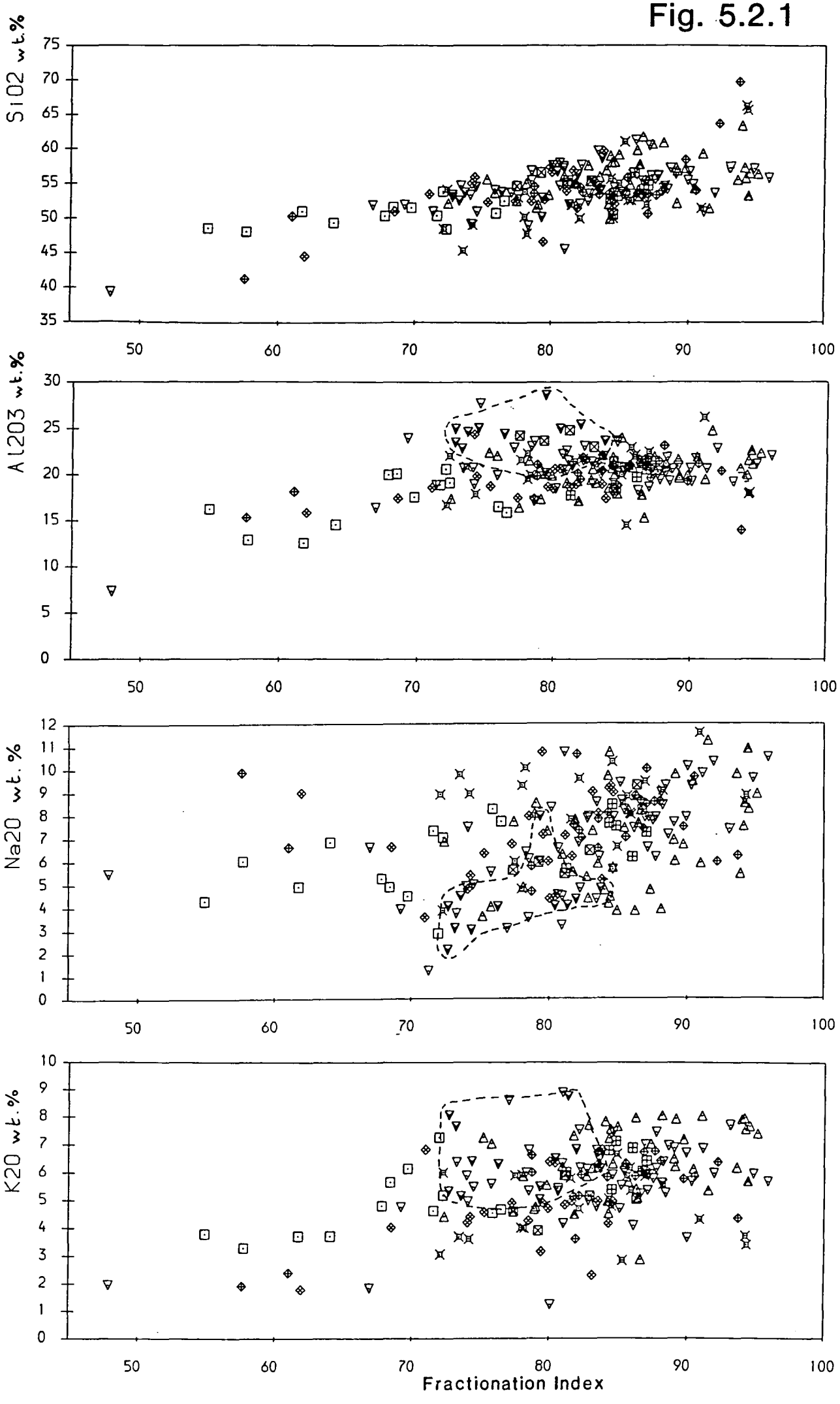
SiO2 wt.%
75
70
65
60
55
50
45
40
35
50
60
70
80
90
100
Al2O3 wt.%
30
25
20
15
10
5
0
Na2O wt.%
12
11
10
9
8
7
6
5
4
3
2
1
0
K2O wt.%
Fractionation Index

Fig. 5.2.1 (cont.)

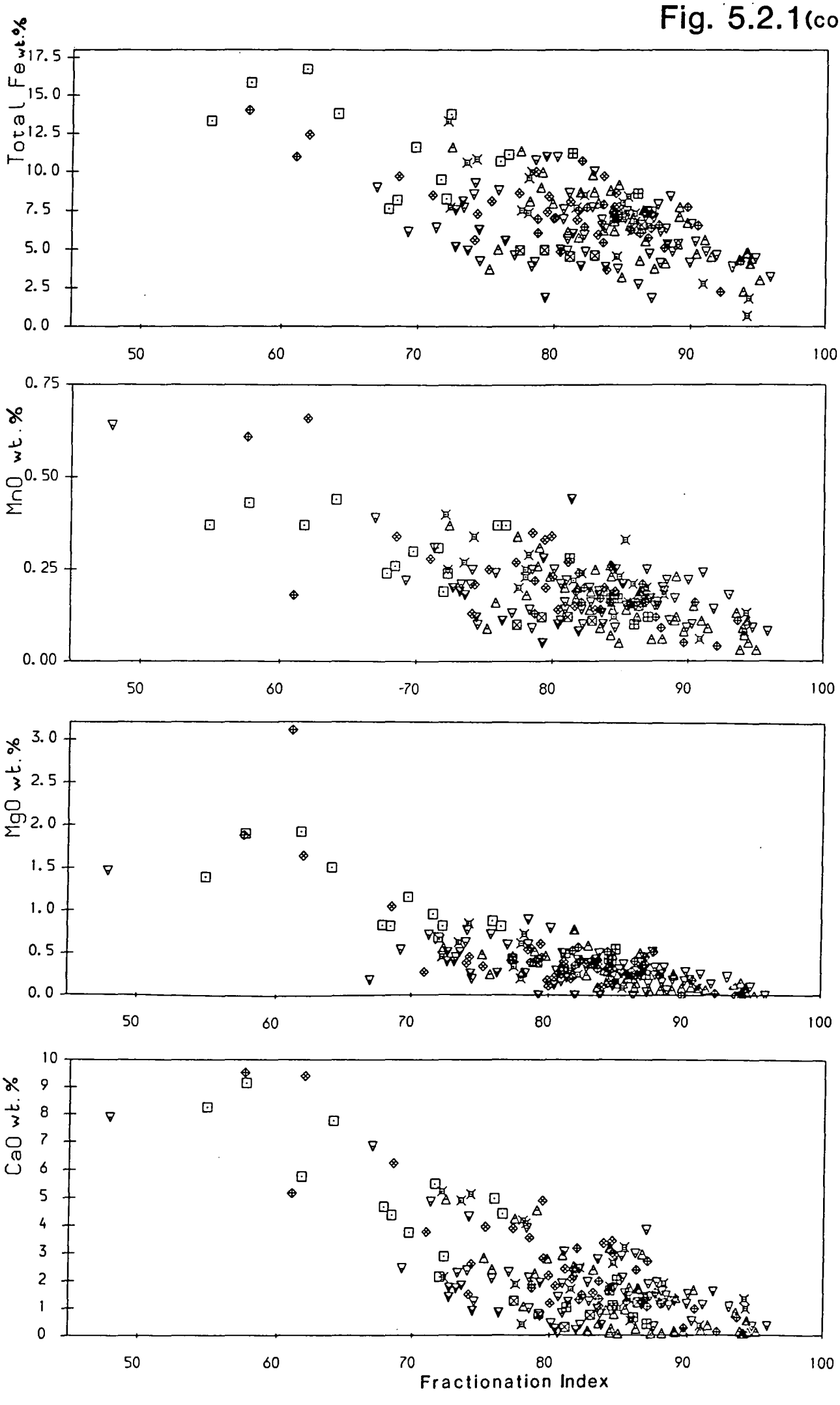
Total Fe wt.%
17.5
15.0
12.5
10.0
7.5
5.0
2.5
0.0
50
60
70
80
90
100
MnO wt.%
0.75
0.50
0.25
0.00
50
60
-70
80
90
100
MgO wt.%
3.0
2.5
2.0
1.5
1.0
0.5
0.0
50
60
70
80
90
100
CaO wt.%
10
9
8
7
6
5
4
3
2
1
0
50
60
70
80
90
100
Fractionation Index

Fig. 5.2.1(cont.)

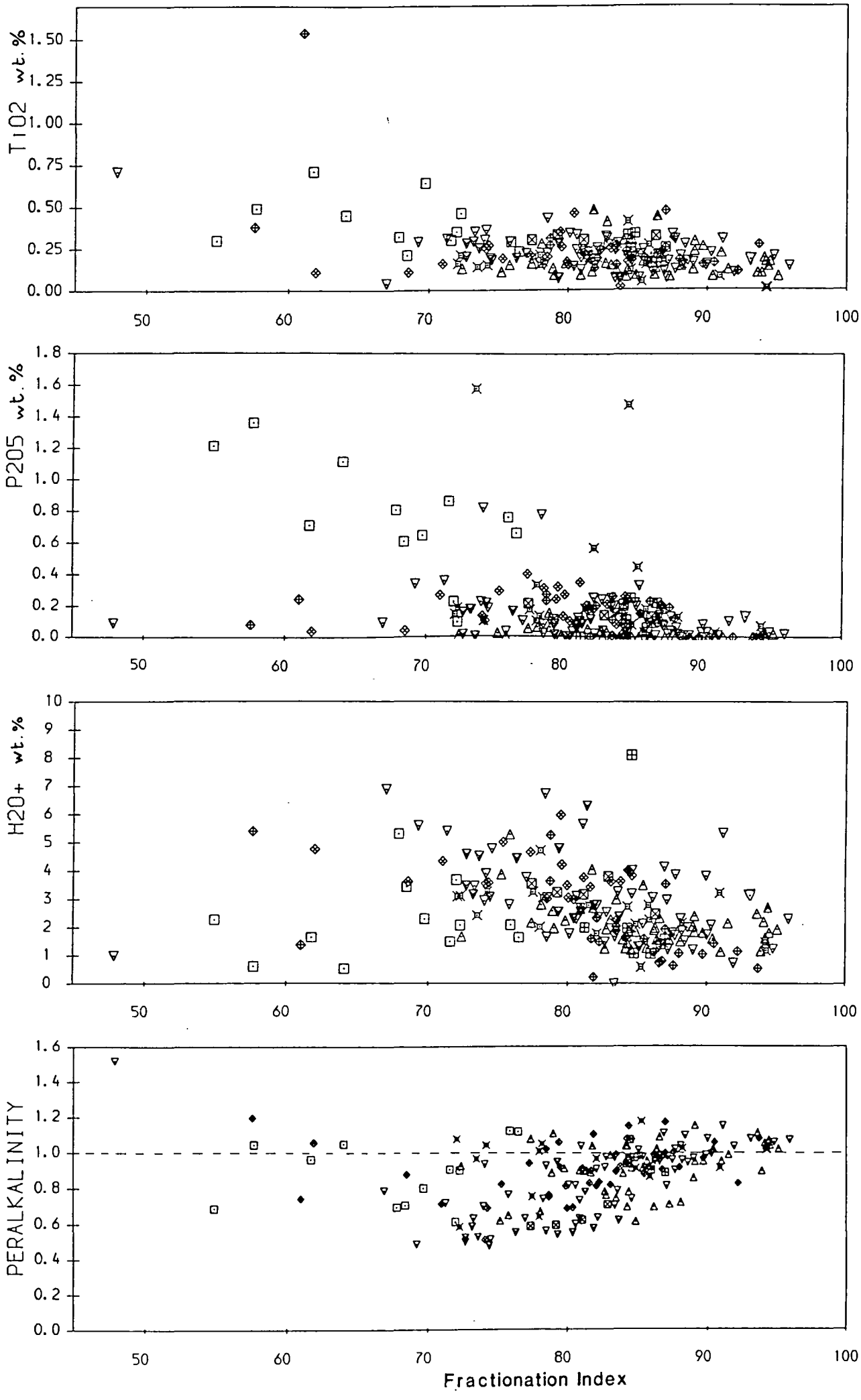
TiO2 wt.%
1.50
1.25
1.00
0.75
0.50
0.25
0.00
50
60
70
80
90
100
P2O5 wt.%
1.8
1.6
1.4
1.2
1.0
0.8
0.6
0.4
0.2
0.0
50
60
70
80
90
100
H2O+ wt.%
10
9
8
7
6
5
4
3
2
1
0
50
60
70
80
90
100
PERALKALINITY
1.6
1.4
1.2
1.0
0.8
0.6
0.4
0.2
0.0
50
60
70
80
90
100
Fractionation Index

Total Fe (as Fe_2O_3), MnO, and MgO all decrease with FI as the proportion of mafic minerals (mainly pyroxene) decreases, and generally have their highest values in the Mafic Upper Series Syenite as a result of the high proportion of pyroxene in this unit. Exceptions to this are the amount of MnO, which is greatest in G244 from the Xenolithic Porphyritic Syenite (0.66% MnO), and samples from the Upper Series Syenite and Porphyritic Microsyenite, both of which have anomalously high MnO contents.

CaO is present mainly in diopsidic and hedenbergitic pyroxenes at Grønnedal-Íka. The alkali feldspars contain very little anorthite, and thus the CaO content decreases rapidly with FI.

TiO_2 shows little variation, remaining buffered at around 0.1–0.4%, presumably by the presence of magnetite. Greater abundances are present in the Mafic Upper Series Syenites (up to about 0.75% TiO_2), controlled by the presence of pyroxene, and an exceptionally high value of 1.54% in G253, a Porphyritic Microsyenite. Petrographic observations suggest that this sample (from the south shore of Eqaluit, map 3), which also contains anomalously high Mg (MgO$\approx$3%) and Ca (CaO$\approx$10%), has lamprophyric affinities.

P_2O_5 shows a wide scatter of abundances, though a gradual decrease with FI is suggested. The highest values occur in the Mafic Upper Series Syenite (up to 1.4%), which contains relatively large quantites of modal apatite (cf. plate 3.6), although one sample from GS-B contains nearly 1.6% P_2O_5. These values compare well with the results of Morteani *et al.* (1986), who report values of less than 1.8% P_2O_5 in the syenites. The scatter in values suggests a cumulus origin for the apatites, an idea supported by the euhedral, prismatic nature of the crystals.

Loss-on-ignition values (H_2O+) are somewhat scattered, but at FI>75 seem to show a steady decrease. One might expect an increase with fractionation, as

the rising proportion of volatiles in the residual liquid increases, resulting in the crystallisation of a greater proportion of hydrous minerals. It is possible that the most fractionated rocks, which consist mainly of nepheline and alkali feldspar, are a result of crystal accumulation, and that compaction processes have expelled any intercumulus liquids which might have crystallised hydrous phases. Some of the Mafic Upper Series Syenite samples have quite low values of H_2O+, presumably as a result of their larger modal proportion of anhydrous mafic phases (pyroxenes).

Peralkalinity

With one exception, the peralkalinity of the Grønnedal-Íka syenites does not exceed 1.2, the majority being less than unity. The exception is G118D, a sample from the disturbed boundary zone between the Lower and Upper Series Syenite in the Radioelv, which has a peralkalinity index of 1.52. This sample shows several other peculiar chemical characteristics, with the lowest SiO_2 (39.3%) and Al_2O_3 (7.34%), low K_2O (1.96%), and very high TiO_2 (0.71%) and MnO (0.64%), with exceptionally high total Fe (34.2%). These unusual values are explained by the high modal proportion of aegirine-augite and low proportion of alkali feldspar in the sample. No strong trend is discernible at low values of fractionation, partly as a result of the paucity of data, but above FI$\approx$70, peralkalinity tends to increase, the most fractionated samples all having a peralkalinity index slightly greater than 1.0.

5.3: Trace elements

Trace element abundances in parts per million of the element by weight (ppm) for seventeen elements (Ba, Nb, Zr, Y, Sr, Rb, Zn, Cu, Ni, Pb, Th, V, Cr, Nd, Ga, La, Ce) are illustrated in fig. 5.3.1. U was analysed, but abundances rarely exceed the detection limit, and it is not therefore shown. When plotted against the fractionation index (FI) of Macdonald (1969) as for the major elements, a considerable scatter is evident. This is no doubt partly due to the cumulus origin of many of the rock-forming minerals into which various elements are preferentially

Fig. 5.3.1(Eight pages). Trace element abundances (in ppm by weight of element) plotted against Fractionation Index (FI). On the facing page of the corresponding variation diagram are the range of abundances in each individual rock unit.

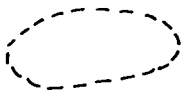

Compositional field of North Qôroq (Chambers 1976).

Compositional field of South Qôroq (Stephenson 1973).

Abbreviations for the rock units are as follows:

GSA = Granular Syenite (GS-A)	GSB = Granular Syenite (GS-B)
PMS = Porphyritic Microsyenite	CGS = Coarse-Grained Syenite
MMS = Marginal Microsyenite	CGBS = Coarse-Grained Brown Syenite
LSS = Lower Series Syenite	XPS = Xenolithic Porphyritic Syenite
USS = Upper Series Syenite	MUS = Mafic Upper Series Syenite

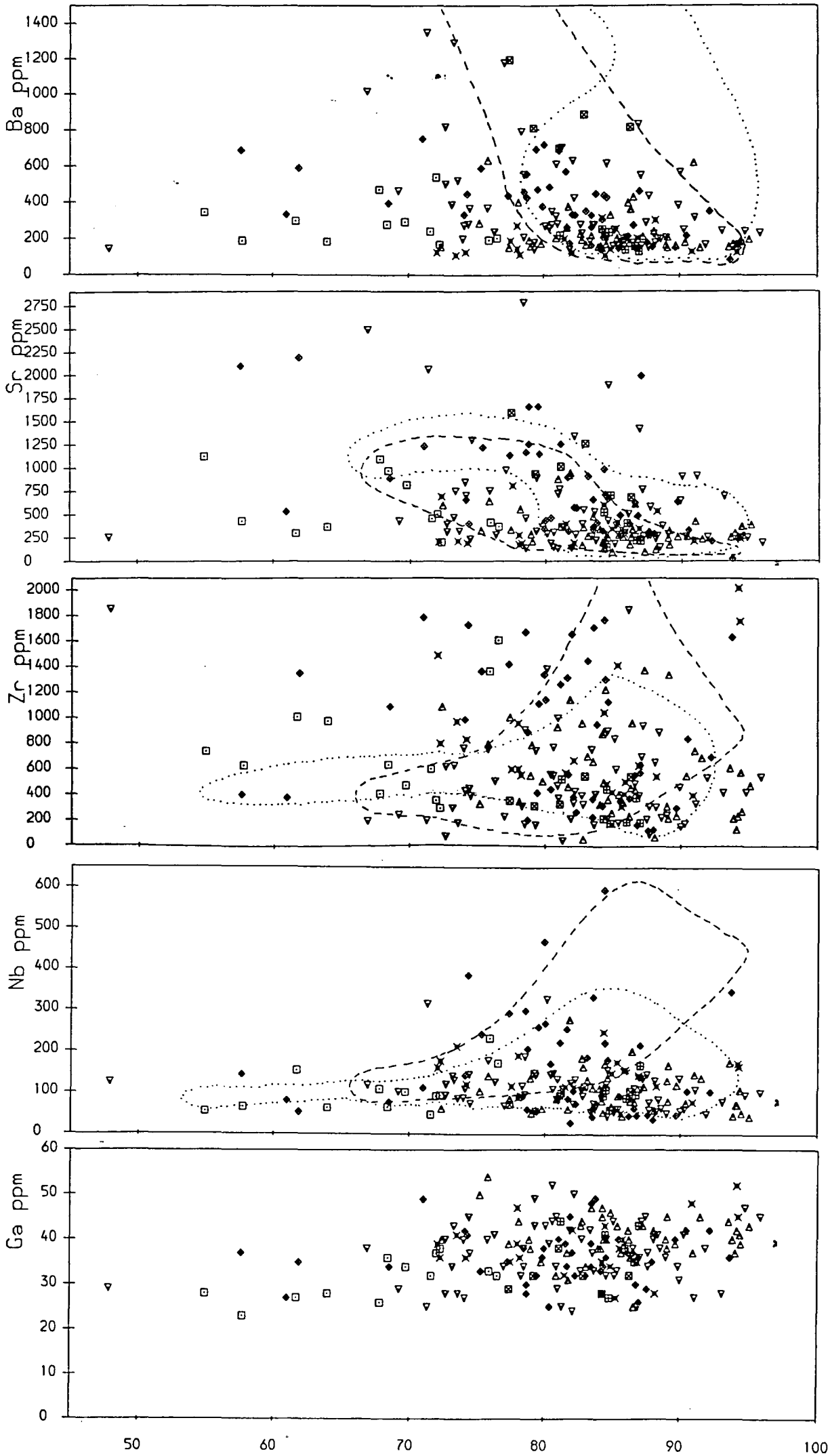
Ba ppm
0
200
400
600
800
1000
1200
1400
Sr ppm
0
250
500
750
1000
1250
1500
1750
2000
2250
2500
2750
Zr ppm
0
200
400
600
800
1000
1200
1400
1600
1800
2000
Nb ppm
0
100
200
300
400
500
600
Ga ppm
0
10
20
30
40
50
60
50
60
70
80
90
100
F. I.

Fig. 5.3.1

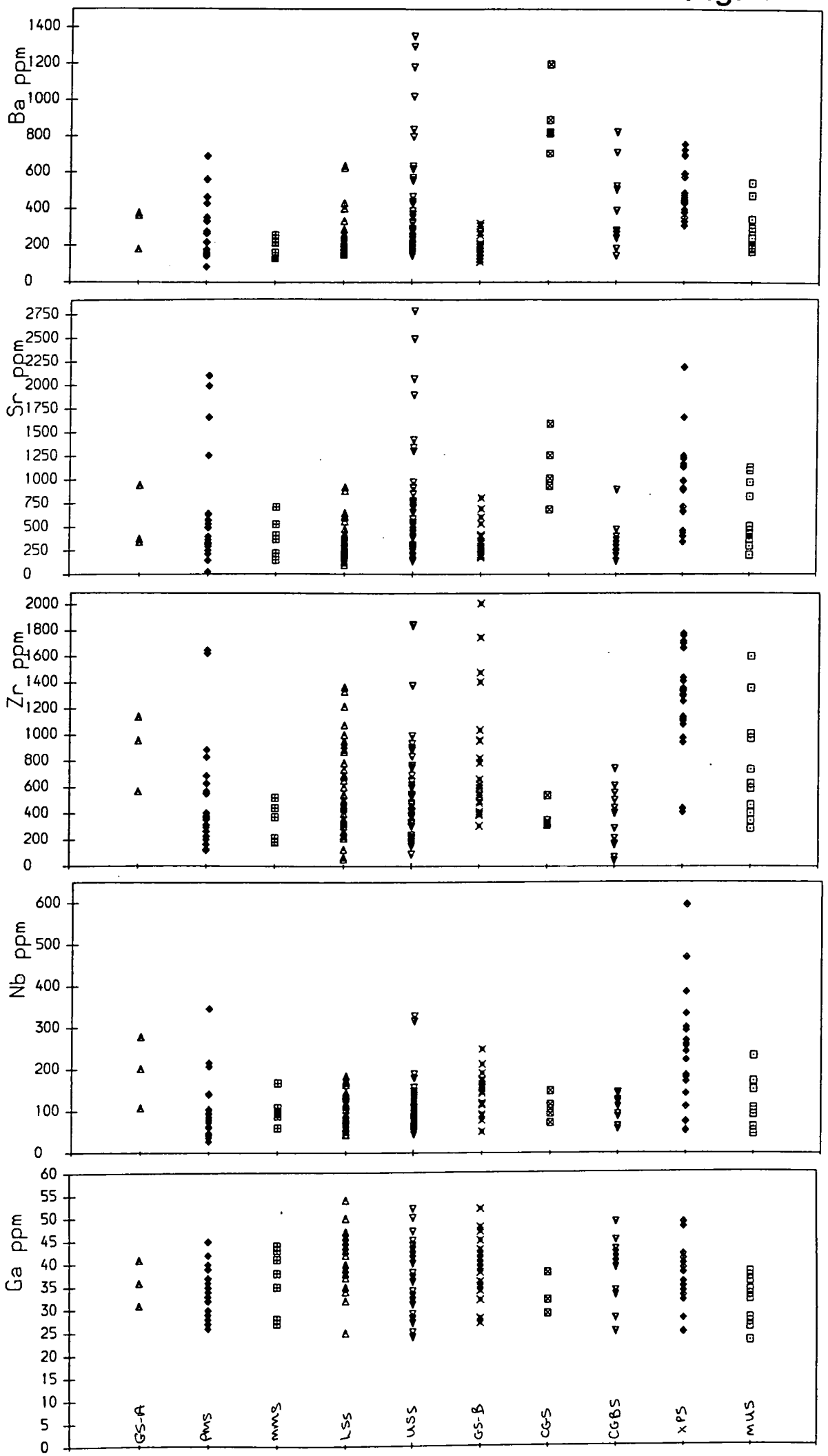
Ba ppm
0
200
400
600
800
1000
1200
1400
Sr ppm
0
250
500
750
1000
1250
1500
1750
2000
2250
2500
2750
Zr ppm
0
200
400
600
800
1000
1200
1400
1600
1800
2000
Nb ppm
0
100
200
300
400
500
600
Ga ppm
0
5
10
15
20
25
30
35
40
45
50
55
60
GS-A
AMS
MMS
LSS
USS
GS-B
CGS
CGBS
XPS
MUS

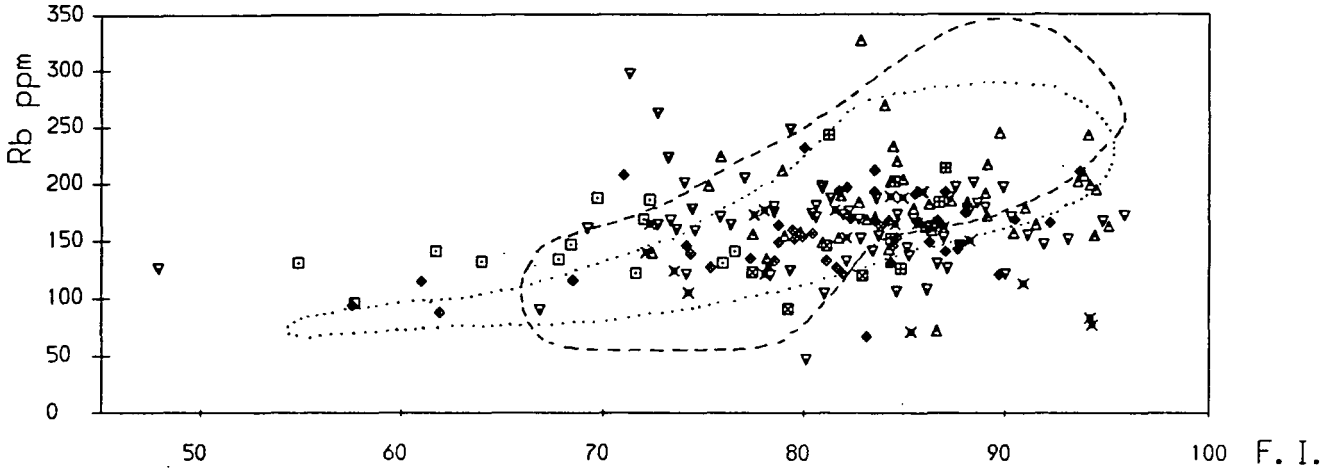
Rb ppm
350
300
250
200
150
100
50
0
50
60
70
80
90
100
F. I.

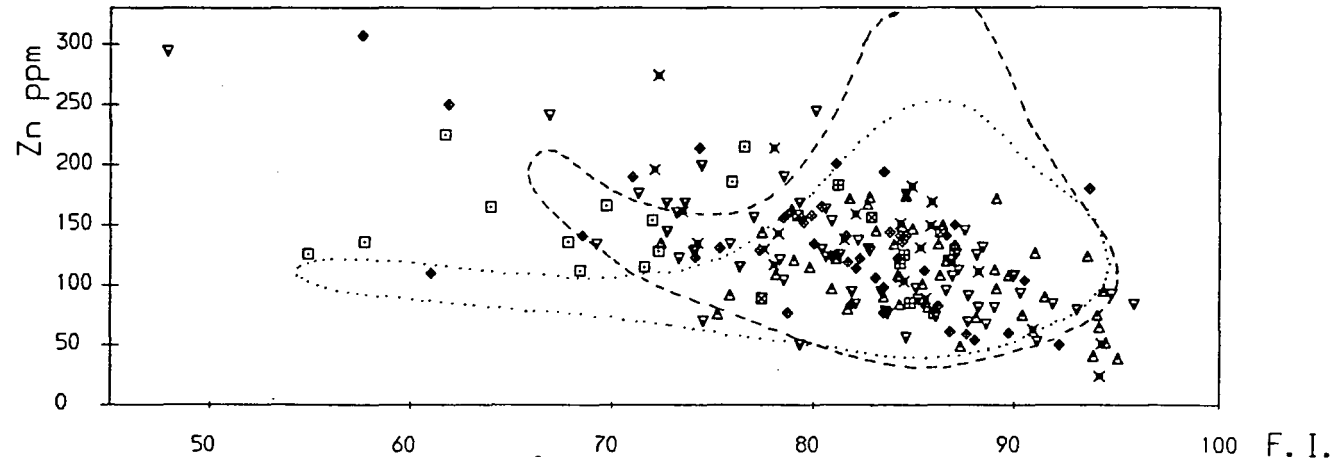
Zn ppm
300
250
200
150
100
50
0
50
60
70
80
90
100
F. I.

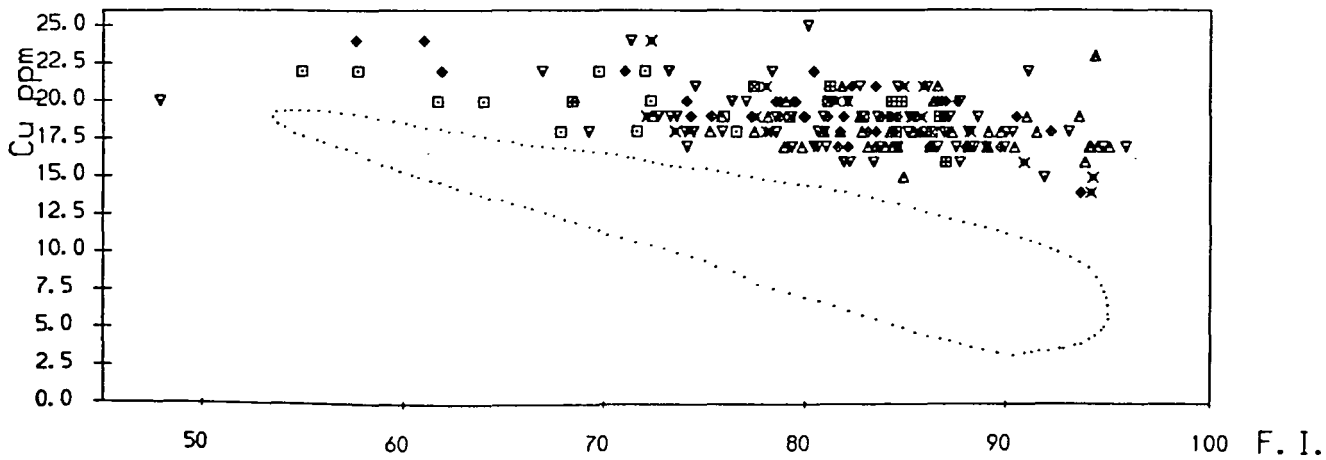
Cu ppm
25.0
22.5
20.0
17.5
15.0
12.5
10.0
7.5
5.0
2.5
0.0
50
60
70
80
90
100
F. I.

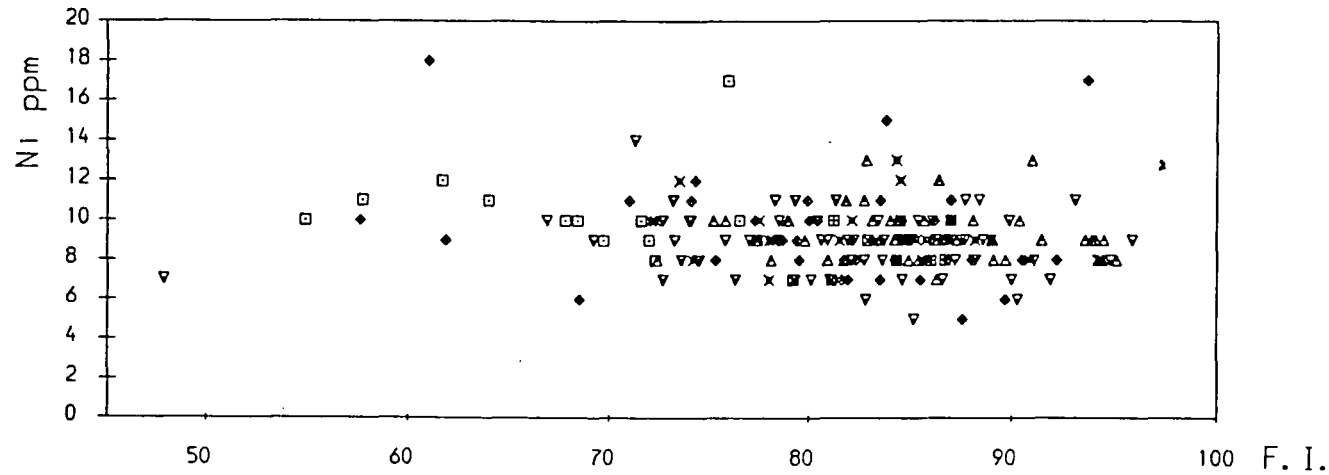
Ni ppm
20
18
16
14
12
10
8
6
4
2
0
50
60
70
80
90
100
F. I.

Fig. 5.3.1(cont.)

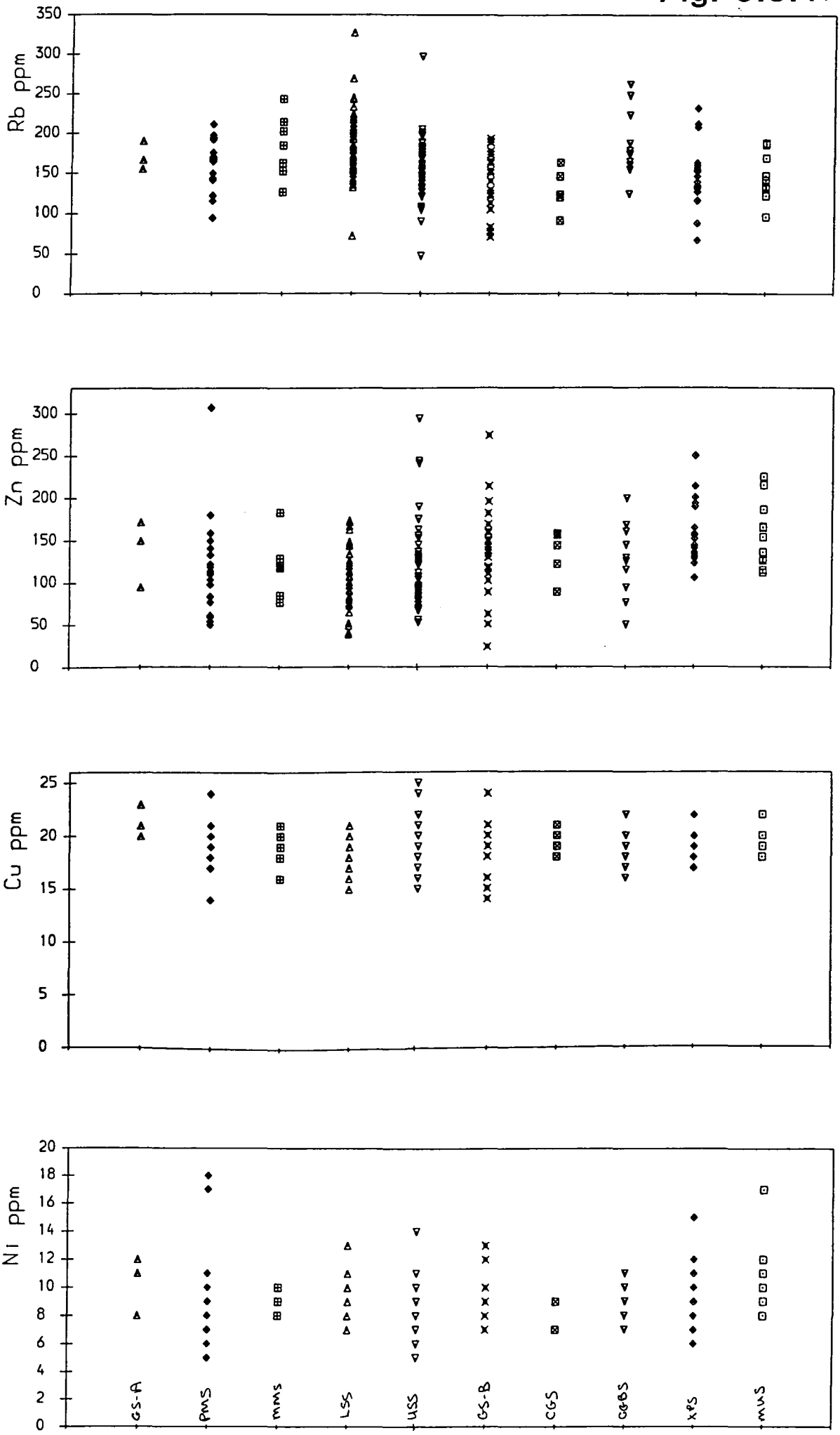
Rb ppm
350
300
250
200
150
100
50
0
Zn ppm
300
250
200
150
100
50
0
Cu ppm
25
20
15
10
5
0
Ni ppm
20
18
16
14
12
10
8
6
4
2
0
GS-A
PMS
MMS
LSS
USS
GS-B
CGS
GGBS
XPS
MUS

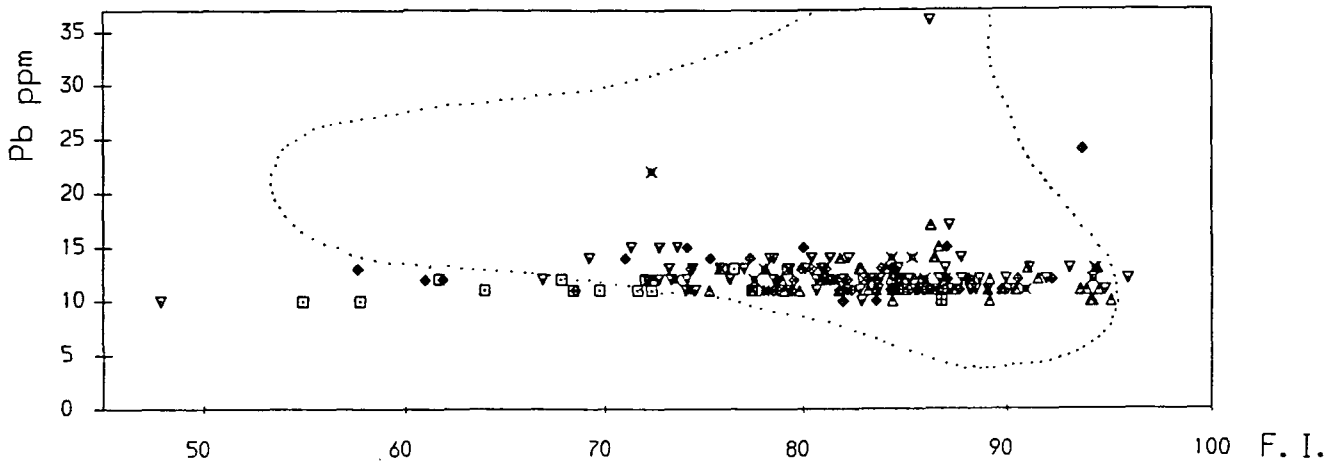
Pb ppm
35
30
25
20
15
10
5
0
50
60
70
80
90
100
F. I.

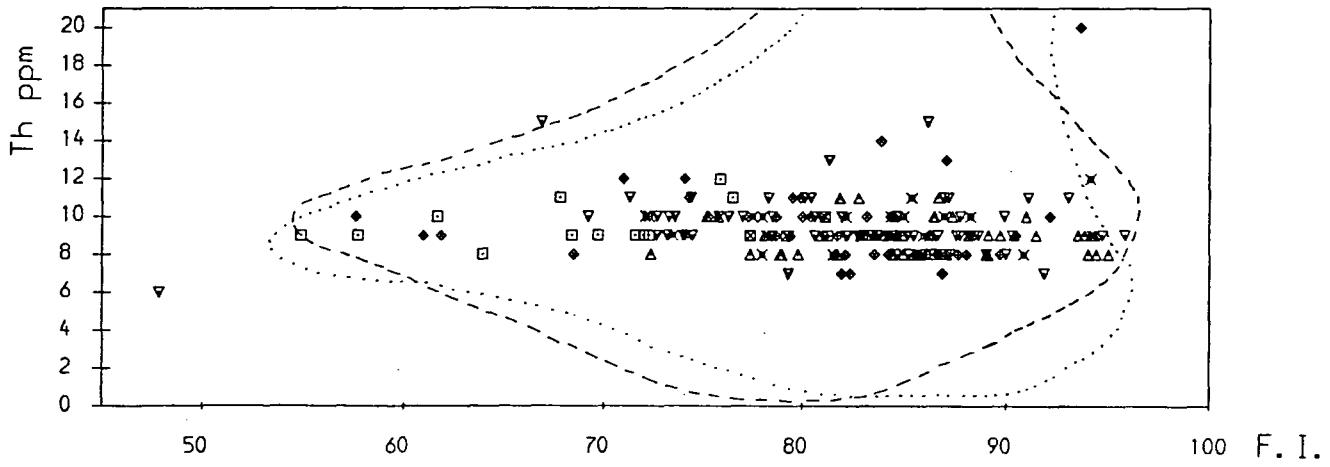
Th ppm
20
18
16
14
12
10
8
6
4
2
0
50
60
70
80
90
100
F. I.

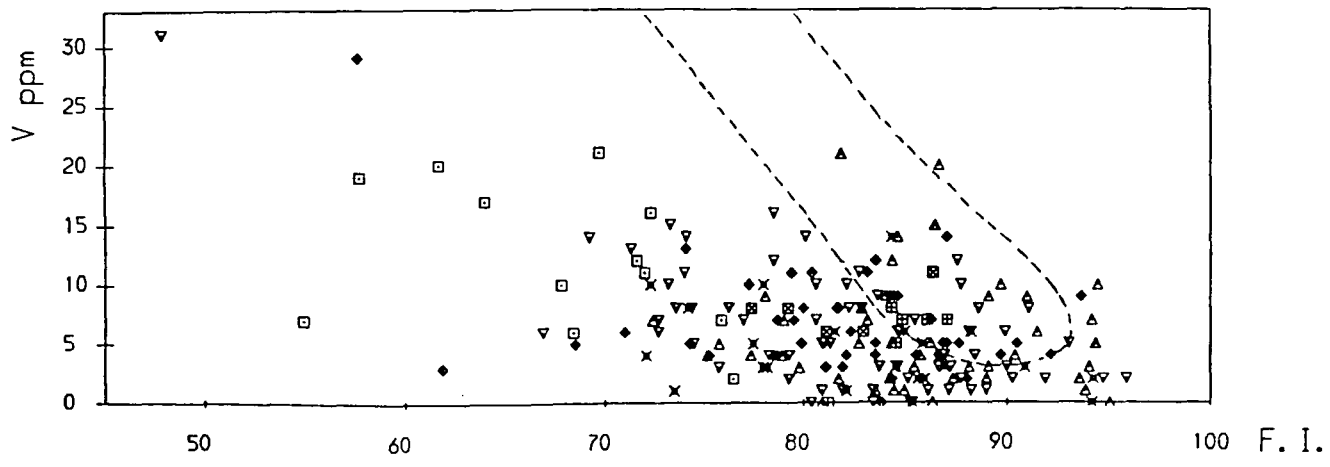
V ppm
30
25
20
15
10
5
0
50
60
70
80
90
100
F. I.

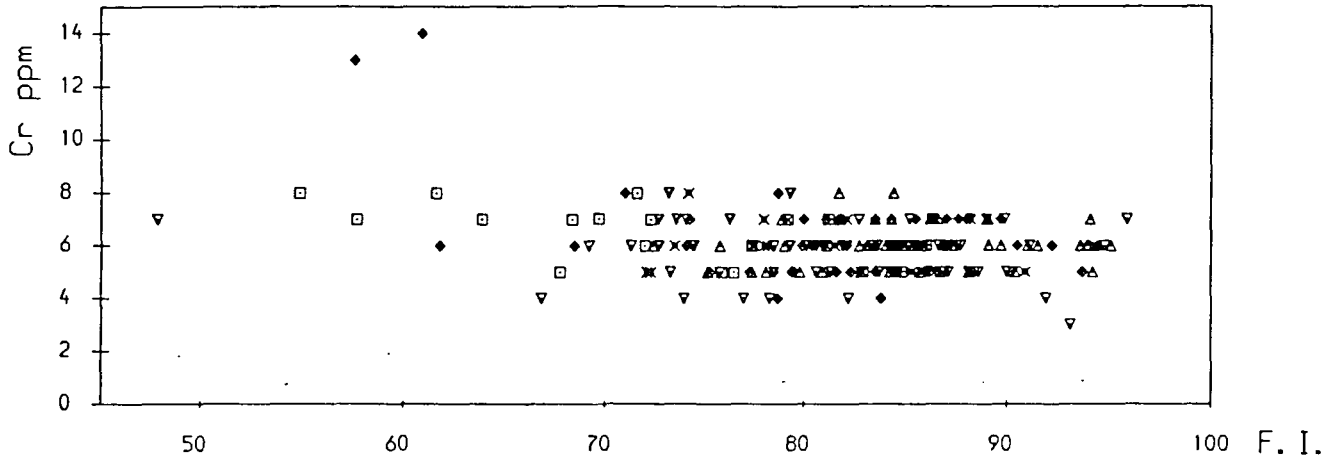
Cr ppm
14
12
10
8
6
4
2
0
50
60
70
80
90
100
F. I.

Fig. 5.3.1(cont.)

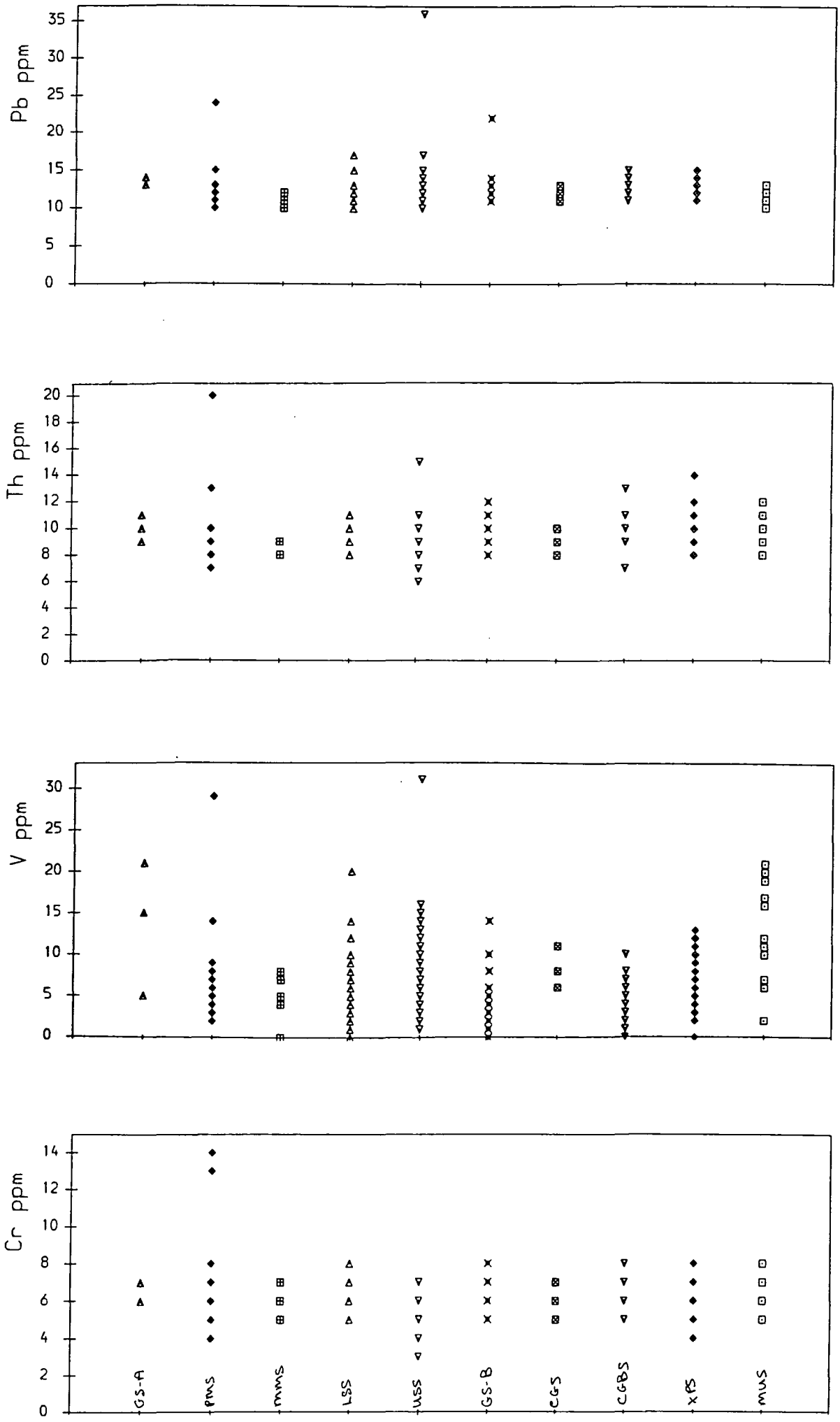
Pb ppm
0
5
10
15
20
25
30
35
Th ppm
0
2
4
6
8
10
12
14
16
18
20
V ppm
0
5
10
15
20
25
30
Cr ppm
0
2
4
6
8
10
12
14
GS-A
PMS
MMS
LSS
USS
GS-B
CGS
CGBS
XPS
MUS

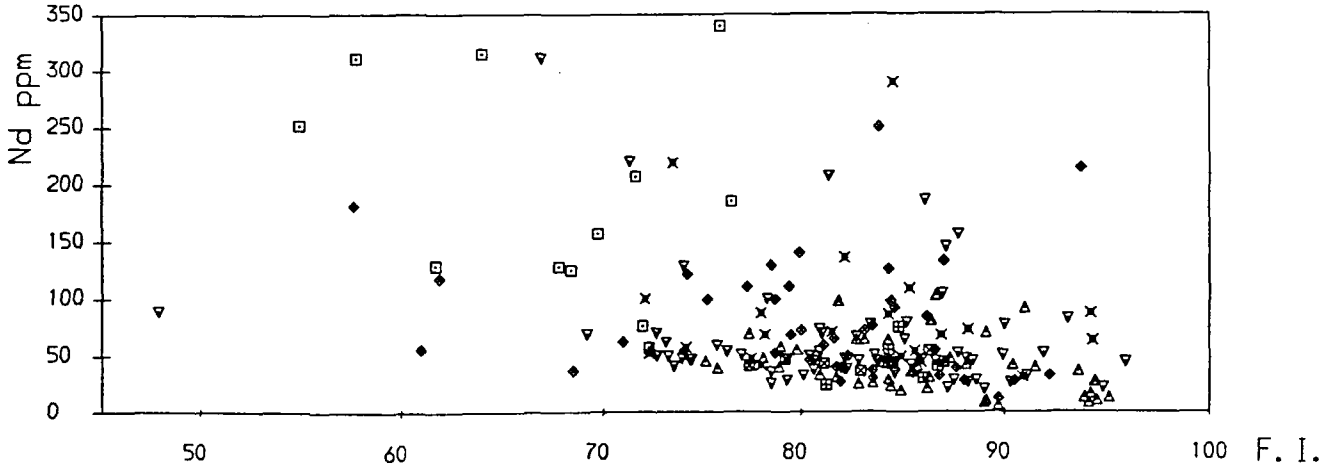
Nd ppm
350
300
250
200
150
100
50
0
50
60
70
80
90
100
F. I.

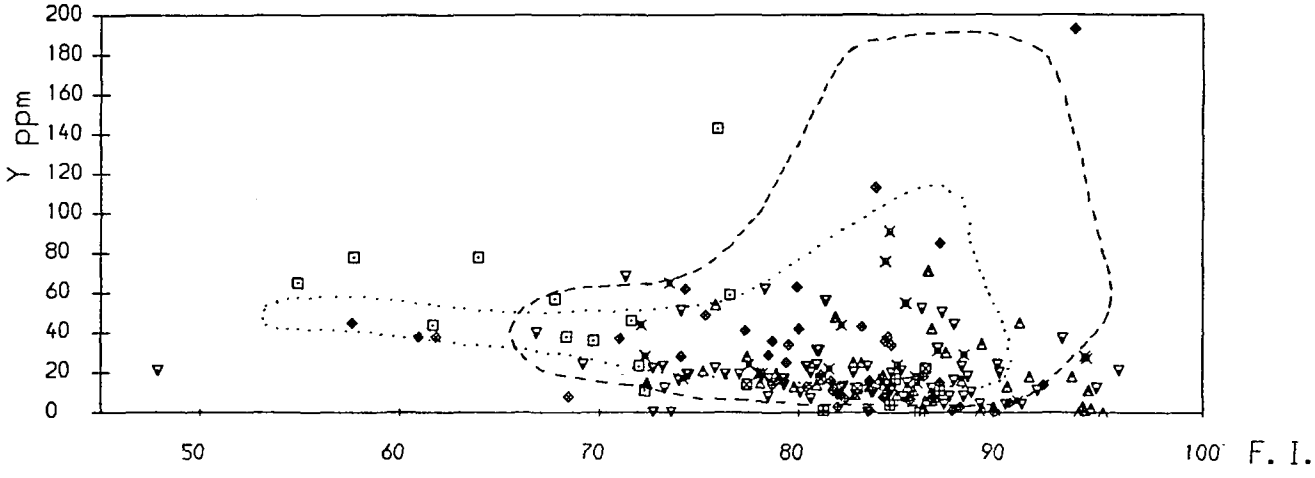
Y ppm
200
180
160
140
120
100
80
60
40
20
0
50
60
70
80
90
100
F. I.

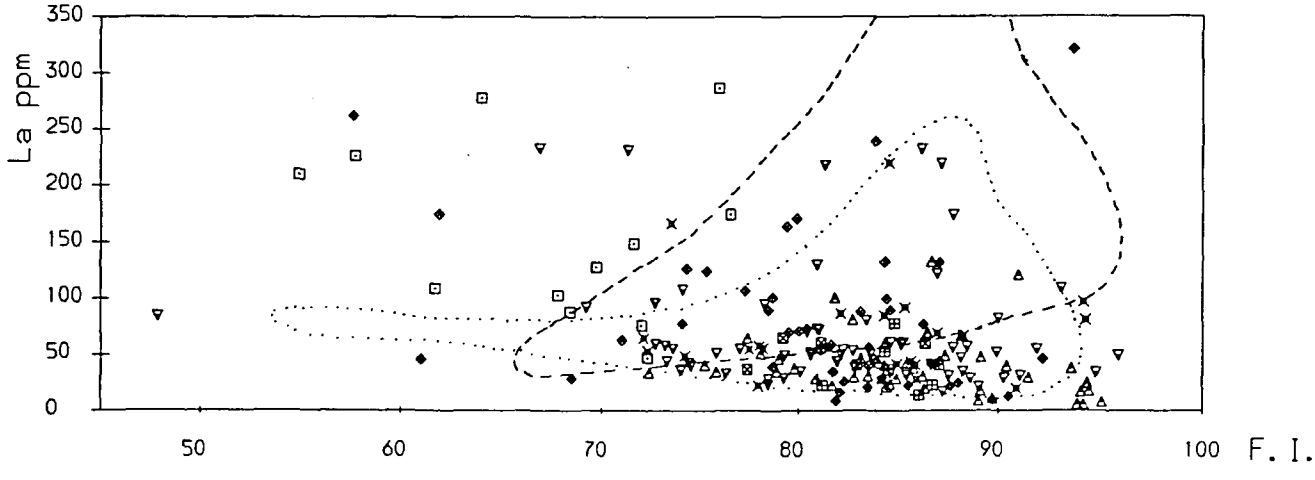
La ppm
350
300
250
200
150
100
50
0
50
60
70
80
90
100
F. I.

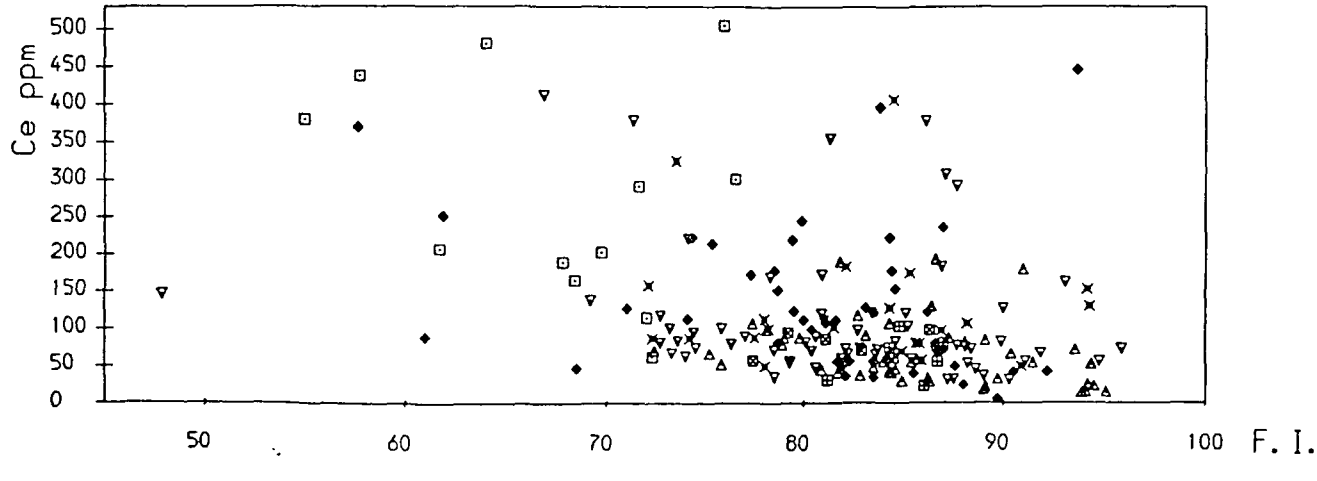
Ce ppm
500
450
400
350
300
250
200
150
100
50
0
50
60
70
80
90
100
F. I.

Fig. 5.3.1(cont.)

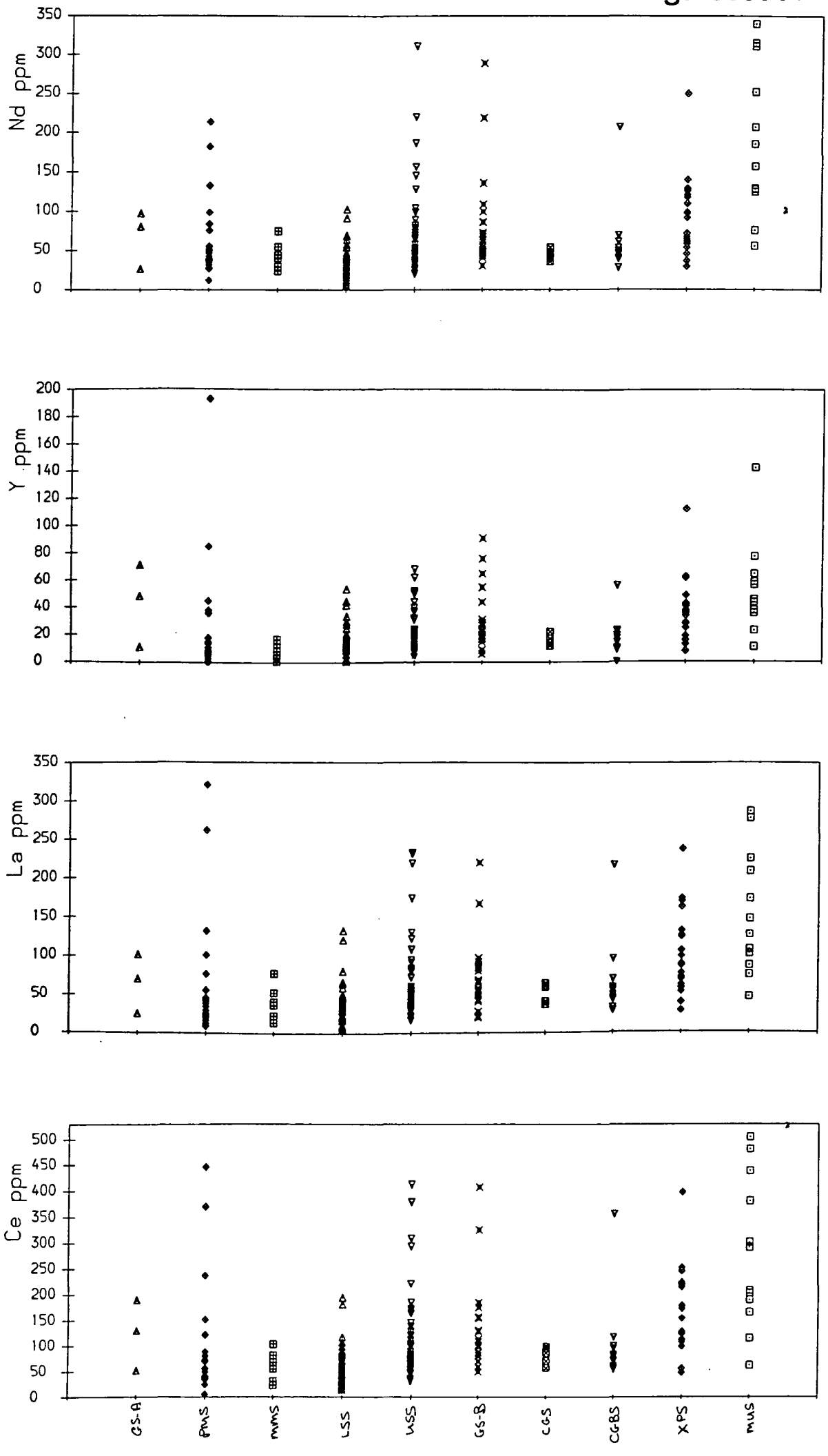
Nd ppm
0
50
100
150
200
250
300
350
Y ppm
0
20
40
60
80
100
120
140
160
180
200
La ppm
0
50
100
150
200
250
300
350
Ce ppm
0
50
100
150
200
250
300
350
400
450
500
GS-A
PMS
MMS
LSS
LSS
GS-B
CGS
CGBS
XPS
MUS

incorporated, but may also be a result of the metasomatic alteration which has affected all of the syenite units to varying degrees. Ba, Rb, Pb, Th, Zr, Nb, Y, La, and Zn in particular may all be mobilised by hydrothermal processes. Additionally, the sporadic occurrence of very small grains of phases such as monazite, rinkite, allanite, and låvenite, which contain large quantities of trace elements, although rarely observed in thin-section, could give anomalously high concentrations of these elements.

Trace element abundances plotted against FI do not show the range of concentrations in each rock type very clearly. This is shown in the diagrams on the pages facing the abundance *vs.* FI plots, by separating the individual rock-units. A similar method has been used by Gill (1972a) to illustrate the element variation between the Grønnedal-Íka syenites, and may be used to discriminate between some of the units on geochemical grounds.

Ba, Sr

The similar behaviour of these elements is evident in the relative compositional ranges of the different syenite units, where their abundances are set out separately in fig. 5.3.1. The Coarse-Grained Syenite and Xenolithic Porphyritic Syenite contain high levels of both of these elements, while a wide range of Ba and Sr abundances is apparent in the Upper Series Syenite, the Coarse-Grained Brown Syenite, and the Porphyritic Microsyenite. Overall concentrations of these elements contrast with those from South and North Qôroq (Stephenson 1973, and Chambers 1976, respectively), those from Grønnedal being richer in Sr and poorer in Ba, while a decrease in abundance with FI is not as obvious as in these two centres.

An exceptionally high Ba concentration of 2217ppm (not illustrated) was found in G255, a rather altered sample from a shear-zone at the margin of GS-B, which has evidently suffered some metasomatic alteration.

Nb, Zr

Concentrations of both of these elements are comparable to those from North Qôroq, though again, a wide scatter of values is apparent, particularly for Zr. Morteani *et al.* (1986) report similar values of Nb for the Grønnedal-Íka syenites, which appears to show a slight decrease with fractionation after FI=70, presumably as a result of fractionation of Zr-rich phases (such as zircon), contrasting with an increase with FI at both South and North Qôroq. A slight enrichment in both of these elements is apparent in the Xenolithic Porphyritic Syenite and GS-A, while Zr contents tend to be high in GS-B, and the exceptional value of 9706ppm Nb occurs in an altered Upper Series Syenite (sample G269, not illustrated). The Coarse-Grained Brown Syenite is comparatively poor in Zr, somewhat surprisingly considering that petrographic observations have shown this unit to contain prominent zircons. In the absence of Zr-rich minerals such as catapleite, eudialyte, and låvenite, which are not observed in the syenites at Grønnedal, zircon is probably the only significant host for this element

Ga

Although no rock-type shows significant enrichment in this element, the Mafic Upper Series Syenites are relatively depleted in Ga. The geochemistry of Ga shows a strong similarity to that of Al, which is also slightly depleted in the Mafic Syenites relative to the other units. The high modal proportion of alkali-rich pyroxene gives rise to a relatively high peralkalinity index, resulting in a relatively low overall abundance of Al, and hence Ga.

Rb

This element shows similar concentrations to other Gardar centres, and a slight increase with FI, reflecting the trend of K_2O, with which Rb is geochemically comparable. The Lower Series Syenite and Coarse-Grained Brown Syenite tend to be moderately enriched in this element relative to the other units.

Zn, Cu, Ni

All of these elements show a decrease with FI, the trend of Zn being the most marked. Abundancies are comparable to samples from North and South Qôroq, where by contrast these elements show a slight increase with fractionation.

Zn is strongly partitioned into amphibole (D_{Zn}^{amp}=7), and biotite (D_{Zn}^{biot} ≈20, Henderson 1982), so that fractionation of one or both of these phases prior to emplacement may be responsible for the observed trend at Grønnedal.

Cu is mainly controlled by the occurrence of sulphide minerals, the presence of which in samples of GS-A (eg. G168) would account for the relative enrichment of Cu in this unit. Ni and Cu may substitute for Mg in pyroxene (D_{Cu}^{cpx}=1.5-2.4, Irving 1978), early fractionation of which could result in the observed slight decrease with FI.

Pb

Pb shows virtually no variation with FI, and is buffered at very low values of around 10-12ppm, though G269 (an altered Upper Series Syenite), which was also enriched in Nb, shows the anomalously high value of 36ppm. This sample is also significantly enriched in U, containing 50ppm of this element. Overall abundances are far lower than at South and North Qôroq, which show several times the amount of Pb at Grønnedal-Íka. These two centres also show a larger scatter or even an increase in Pb in the more fractionated rocks.

Th

The low abundances of Th have resulted in marked discontinuities between samples with different element concentrations, a feature which is apparent in other plots where the maximum concentration is less than about 40ppm (eg. Cu, Ni, Pb, Th, Cr). Because of this, and particularly for elements with a fairly restricted

range, conclusions regarding trends in elemental abundance are difficult to draw, though Th seems to show a slight decrease with FI.

V

V shows a considerable scatter of values, but a slight decrease with FI is again suggested. Fractionation of magnetite and possibly pyroxene will preferentially remove V from the magma ($D_V^{magt} \approx 3.9$, Henderson 1982). The presence of this element in pyroxene is suggested by slightly elevated values in the Mafic Upper Series Syenites.

Cr

Cr shows similar behaviour to Ni, partitioning into pyroxene ($D_{Cr}^{cpx}=8.4$, Henderson 1982). Abundances are fairly constant at around 6ppm, though somewhat lower in the Lower Series Syenite. The low abundance of this element results in a rather 'discontinuous' plot, and conclusions regarding changing abundance with FI are difficult to draw.

Nd, Y, La, Ce

All of these elements are highly incompatible, and present in phases such as rinkite, låvenite, monazite, and allanite, as well as in solid solution in minerals such as apatite and zircon. In contrast to trends from other Gardar centres, where their incompatibility results in an increase with FI due to their increasing concentration in the residual magma, trends from Grønnedal-Íka show a tendency to decrease with FI. Early fractionation of phases, such as those above, which are rich in these elements, may have caused their depletion in the magma prior to emplacement. In order to test for the fractionation of apatite and zircon, these elements were plotted against P_2O_5 and Zr, some of the results of which are shown in fig. 5.3.2. Only Nd showed any sort of correlation, the strongest with P_2O_5, and suggests that apatite was probably significant in controlling the Nd concentration

Fig 5.3.2. Nd(ppm) vs. P_2O_5 (wt. %) and Zr(ppm).

A sympathetic variation of Nd with Zr and P_2O_5 is observed, suggesting that fractionation of zircon (or other Zr-rich phases) and/or apatite may have occurred to give the present distribution of REE's.

Symbols as in fig. 5.1.1 and 5.3.1.

Fig. 5.3.2

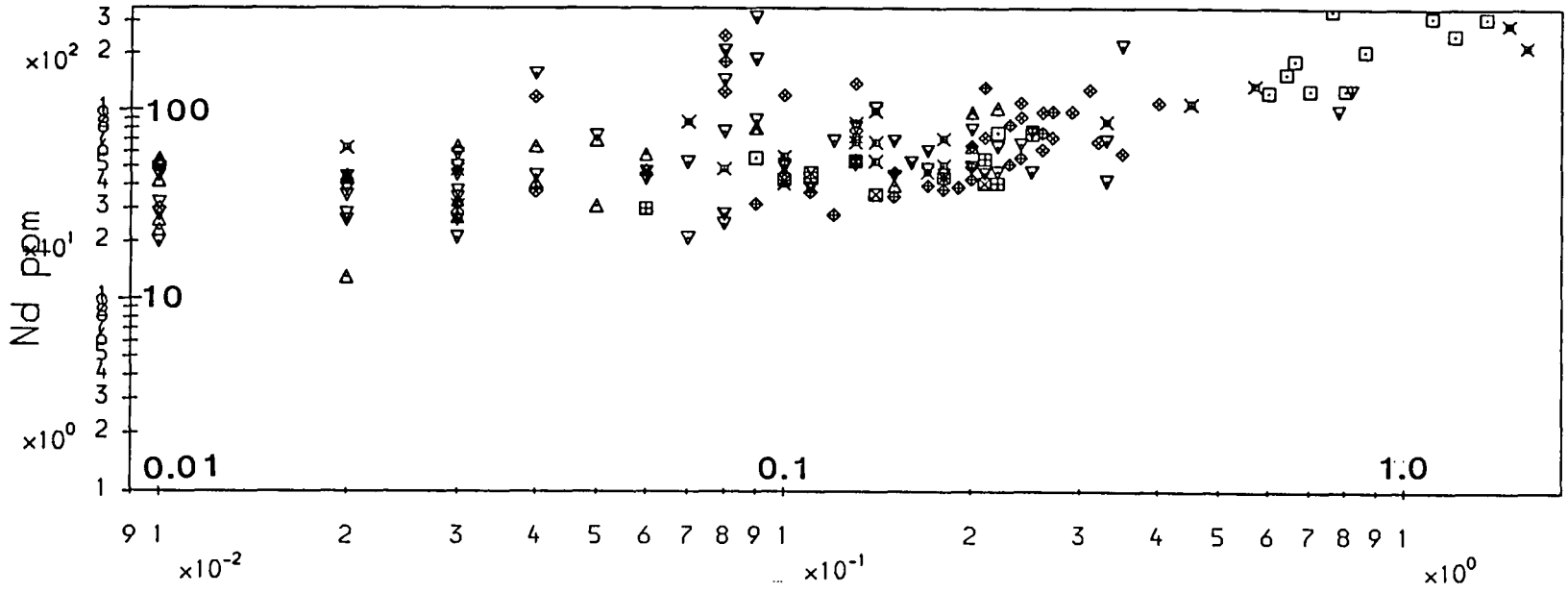

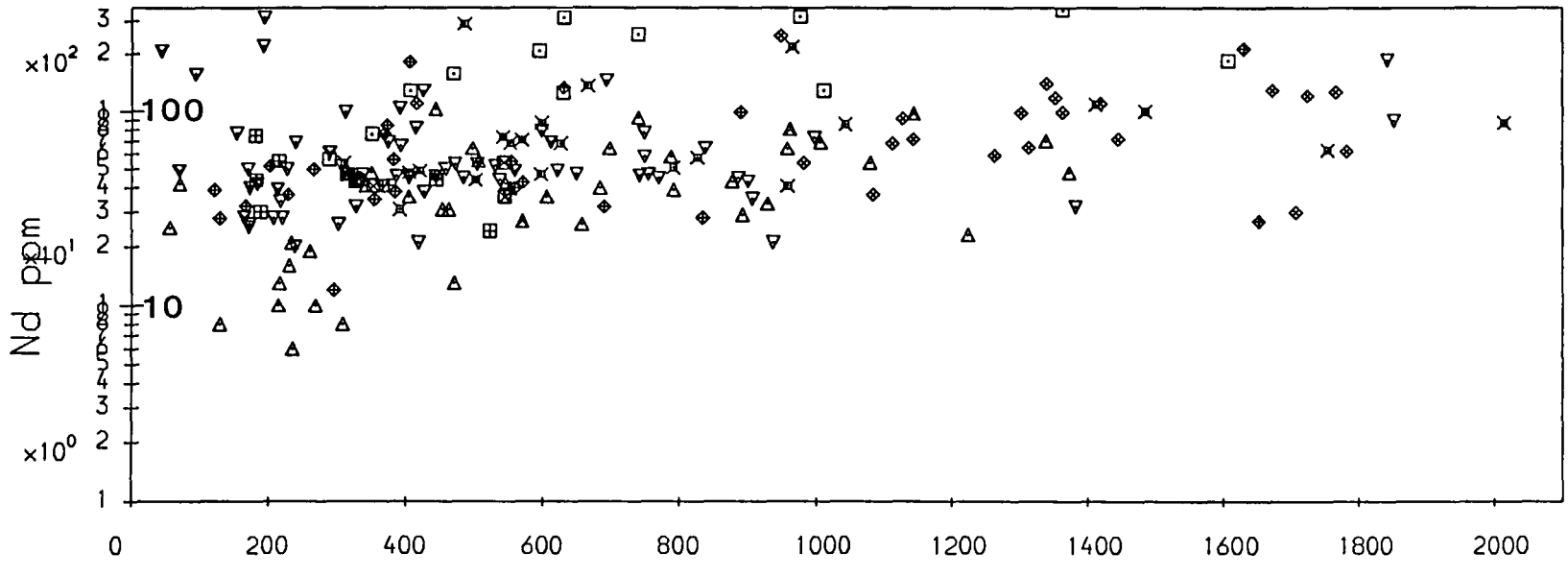

GS-A
CGBS
PMS
XPS
LOWER SERIES
UPPER SERIES
MAFIC U. SERIES
CGS
GS-B
MARG. MICROSY

of the syenites, while the weaker correlation with Zr suggests that zircon was less important.

None of the syenites have characteristic abundances of these elements other than the Mafic Upper Series Syenite, in which they tend to be slightly enriched.

There is obviously a considerable scatter in all of the trace elements analysed, which may be due to cumulus processess, though Chambers (1976) suggests that later remobilisation of some elements (Pb, Th, Zr, Nb, Y, and La in particular) and the sporadic occurrence of certain minerals may give rise to the scatter of abundances at North Qôroq. Stephenson (1973) also points to the ease of mobilisation of Zr, Nb, La, Y, and Zn in contributing to the scatter of concentrations of these elements at South Qôroq.

Certain features regarding the changing abundances of the trace elements with fractionation at Grønnedal-Íka appear to stand out, however. Most show a slight decrease in abundance with increasing FI (Zn, Cu, V, Nd, La, Ce, and Y more strongly; Nb, Sr, Ni, and Th less strongly), with only Ga and Rb showing a slight increase. This is in marked contrast to the trends from other Gardar centres, and may be a result of early fractionation and removal of phases which are rich in these elements, and accumulation of felsic phases (such as alkali feldspar and nepheline) which are not.

5.4: Normative mineralogy

5.4.1: The Residua system

Most of the Grønnedal-Íka syenites have normative $ab + or + ne$ greater than about 80%, and can be represented in 'Petrogeny's Residua' system ($Ne-Ks-Qz$, Bowen 1937). For rocks with a peralkalinity index of 1.0, the composition will be represented accurately, while for others, their position will be a projection onto the Na_2O–K_2O–SiO_2 plane from the Al_2O_3–Na_2O–K_2O–SiO_2 quaternary system.

All normative compositions are shown in fig. 5.4.1, together with the 1kb and 5kb eutectics (after Hamilton and MacKenzie 1965, and Morse 1969 respectively). These eutectics refer to conditions of water saturation (ie. $p_{H_2O} = p_{total}$), a situation rarely achieved in natural magmas except perhaps at a very late stage of crystallisation. Nearly all the units have some analyses which plot in the oversaturated region of the system, even though quartz was never observed in thin-section or detected during microprobe analysis. This may be a result of wall rock contamination, or nepheline alteration to gieseckite, the latter resulting in an increase in the Si/K ratio and a loss of Na (section 4.6). Some other compositions plot within the nepheline field at 1kb (and some even at 5kb), a feature noted by Gill (1972a) at Grønnedal-Íka, and Stephenson (1973) at South Qôroq. Kogarko (1974) has shown that an increase in the acid volatile content of a magma (such as HF, and particularly HCl) tends to displace the alkali feldspar-nepheline phase boundary towards the $Ne - Ks$ join. Henderson *et al.* (1989) suggest that the presence of silica-undersaturated phases such as biotite (a common mineral at Grønnedal) and alkali-amphibole, which do not appear in the norm, may increase the amount of normative nepheline following reassignment of the various oxides during the calculation.

A general trend towards the $ne - ksp$ minimum at 1kb from the Si-rich side of the eutectic is observed, compositions tending to cluster around a point just above the 1kb minimum. If crystallisation occurred at $p_{H_2O} <$ 1kb, final liquid compositions would be displaced slightly further towards the oversaturated part of the system, giving rise to the observed concentration of analyses. The more evolved rocks follow the 'unique fractionation curve' (Hamilton and MacKenzie 1965) quite closely, unlike trends from North and South Qôroq, which tend to be more strongly displaced towards orthoclase (*or*). The less evolved, more feldspathic rocks do tend to be more scattered, though slightly displaced towards *or*. James and Hamilton (1969) suggest that Ca may shift the 'thermal valley' towards the K-rich side of the system, while the presence of volatiles may have an affect

Fig. 5.4.1. All normative compositions plotted in the system $Ne - Ks - Qz$ ('Petrogeny's Residua', Bowen 1937). There is a tendency for the analyses to cluster around a point just above the 1kb $ne - ksp$ phase boundary, near to the undersaturated minimum temperature composition. Also shown are the 1kb and 5kb eutectics (after Hamilton and MacKenzie 1965, and Morse 1969), and the oversaturated, saturated, and undersaturated minima (at 1kb) shown as ⊙, and the normative compositional fields of North and South Qôroq.

Fig. 5.4.2(Two pages). Normative compositions from individual syenite units plotted in the $Ne - Ks - Qz$ system. The 1kb and (where appropriate) the 5kb eutectics are shown, as are the phase-boundary minima (⊙).

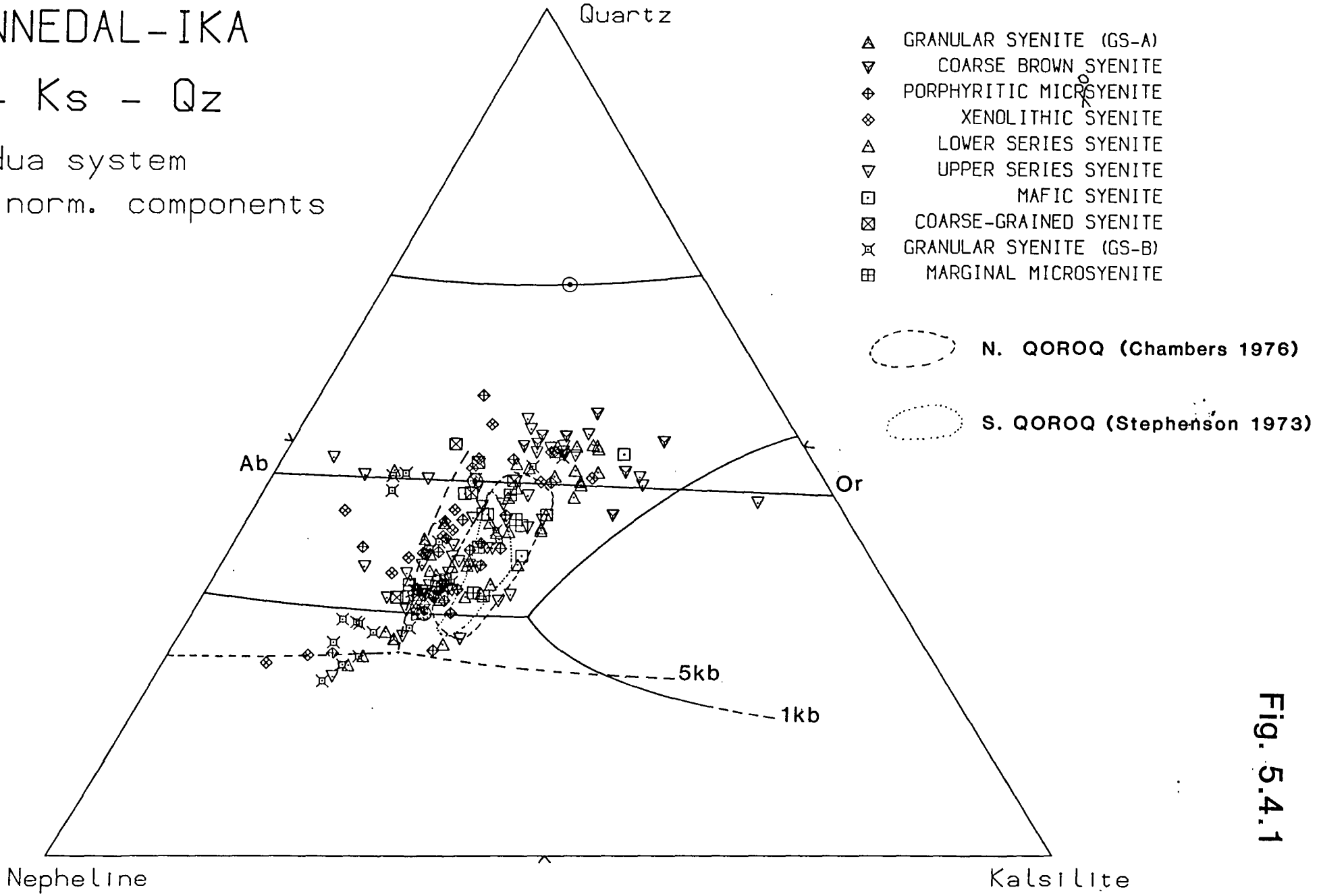
GRONNEDAL-IKA
Ne - Ks - Qz
Residua system
wt.% norm. components
Quartz
Nepheline
Kalsilite
Ab
Or
5kb
1kb
GRANULAR SYENITE (GS-A)
COARSE BROWN SYENITE
PORPHYRITIC MICROSYENITE
XENOLITHIC SYENITE
LOWER SERIES SYENITE
UPPER SERIES SYENITE
MAFIC SYENITE
COARSE-GRAINED SYENITE
GRANULAR SYENITE (GS-B)
MARGINAL MICROSYENITE
N. QOROQ (Chambers 1976)
S. QOROQ (Stephenson 1973)

Fig. 5.4.1

Fig. 5.4.2

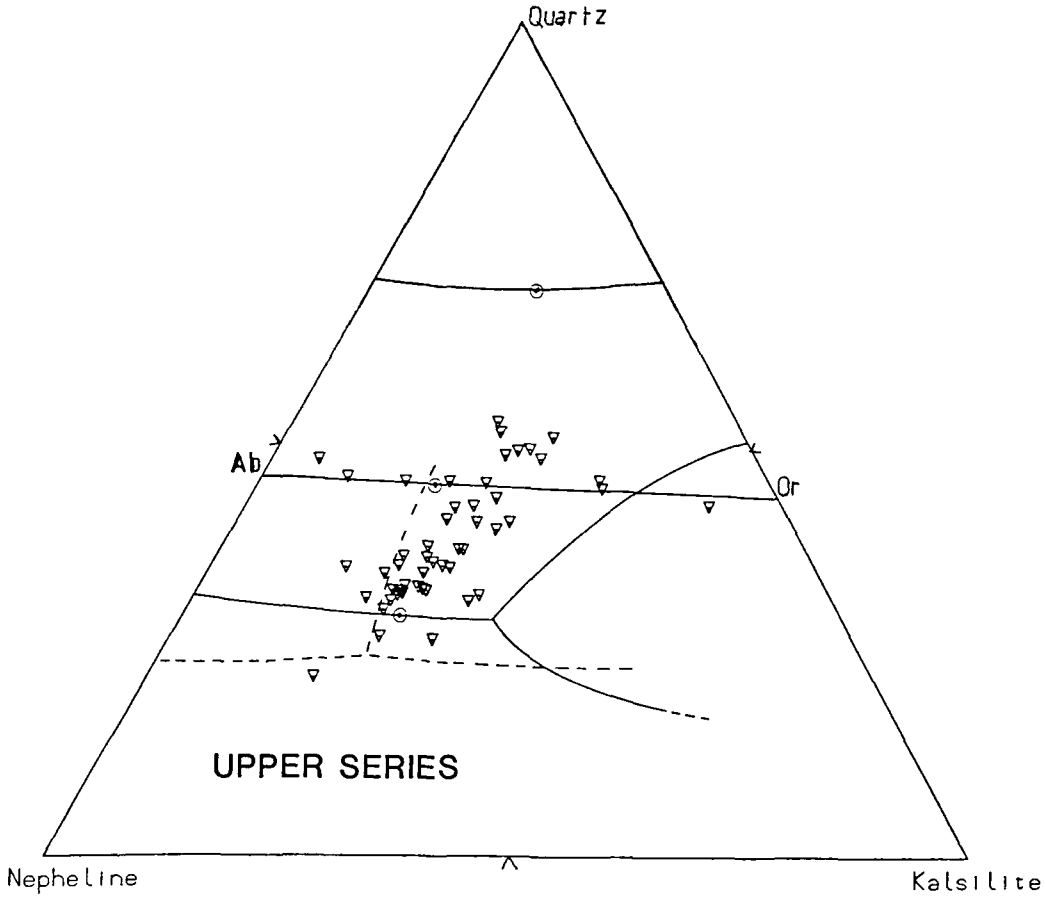
Quartz
Ab
Or
UPPER SERIES
Nepheline
Kalsilite

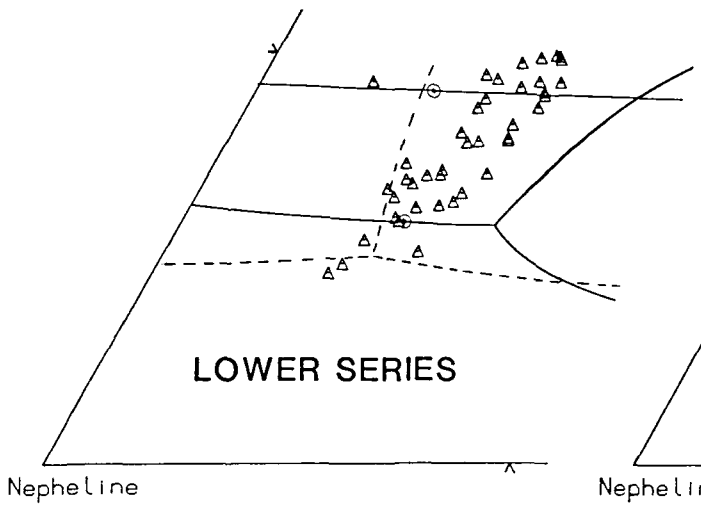
LOWER SERIES
Nepheline

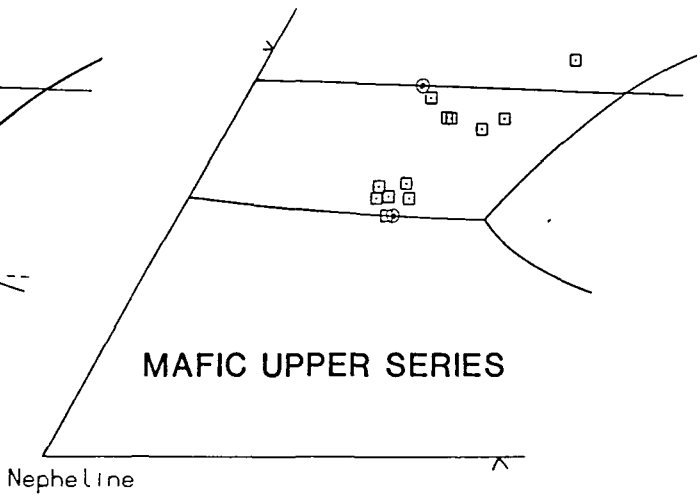
MAFIC UPPER SERIES
Nepheline

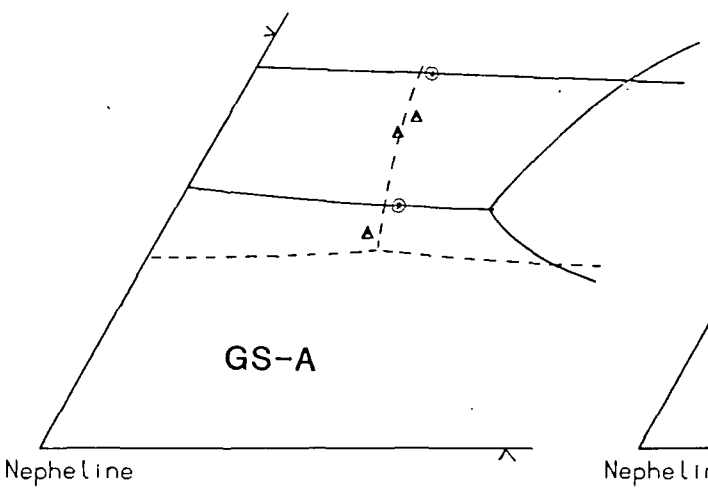
GS-A
Nepheline

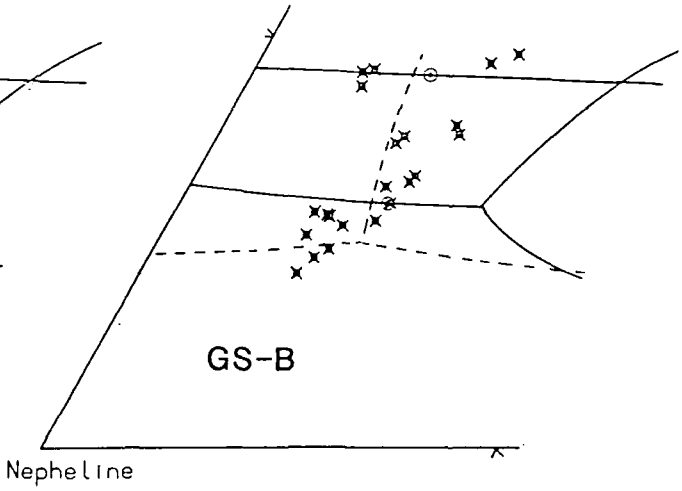
GS-B
Nepheline

Fig. 5.4.2 (cont.)

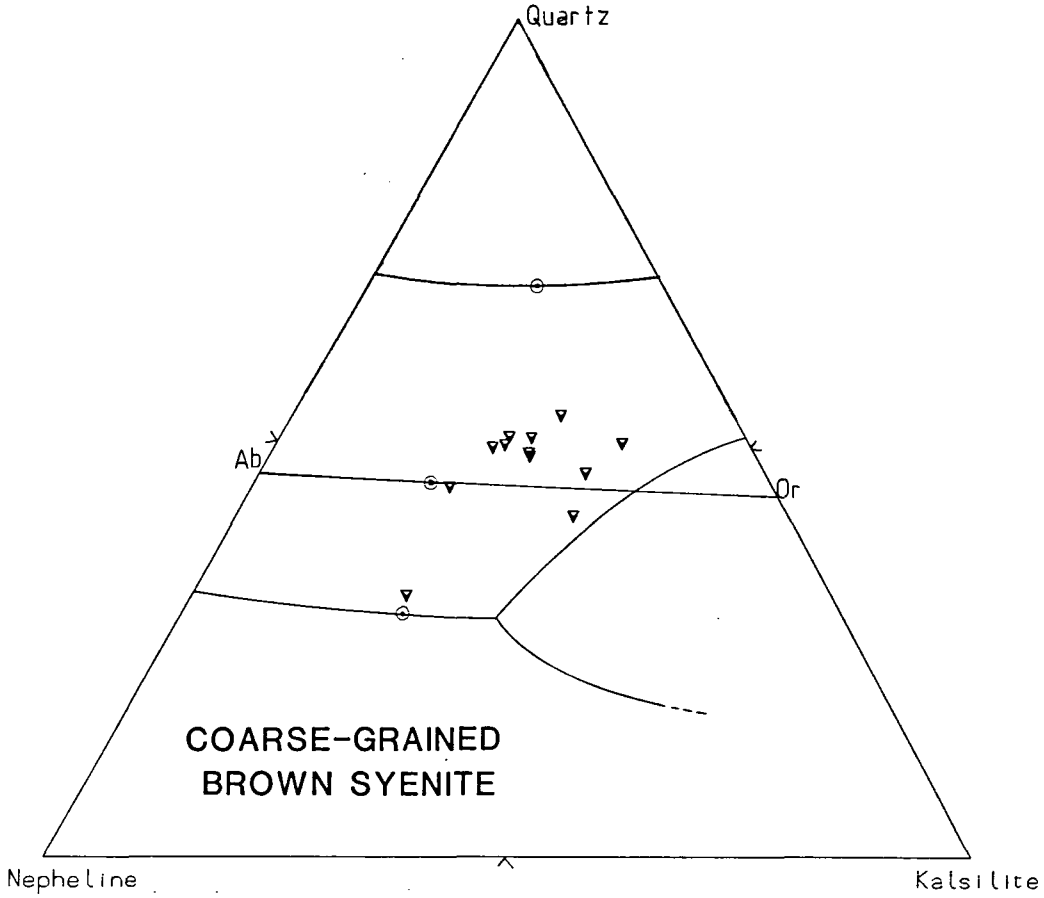
Quartz
Ab
Or
COARSE-GRAINED
BROWN SYENITE
Nepheline
Kalsilite

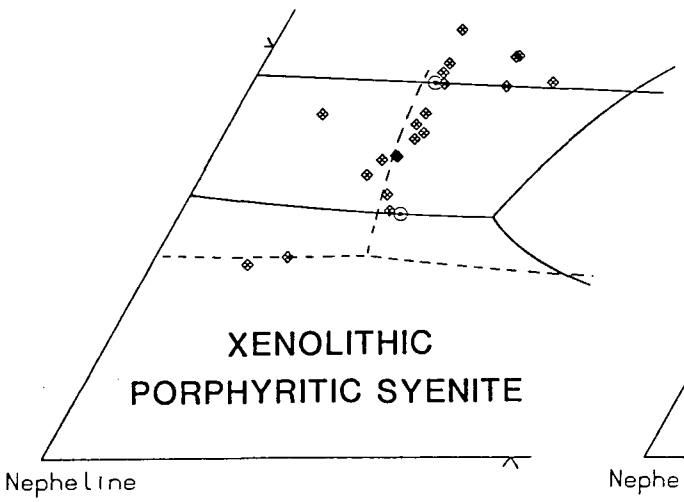
XENOLITHIC
PORPHYRITIC SYENITE
Nepheline

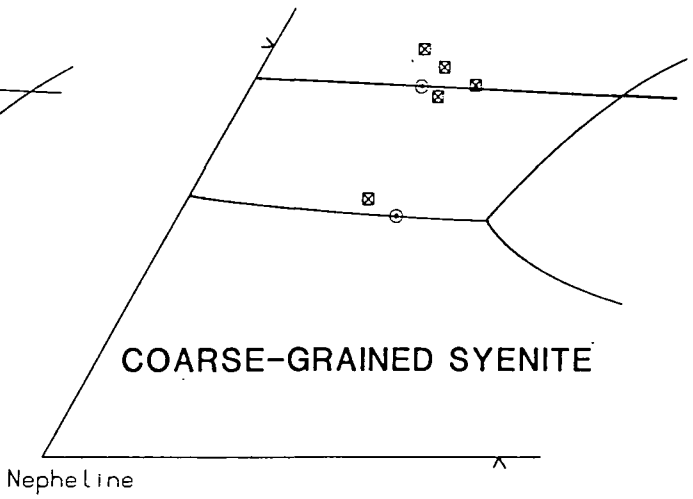
COARSE-GRAINED SYENITE
Nepheline

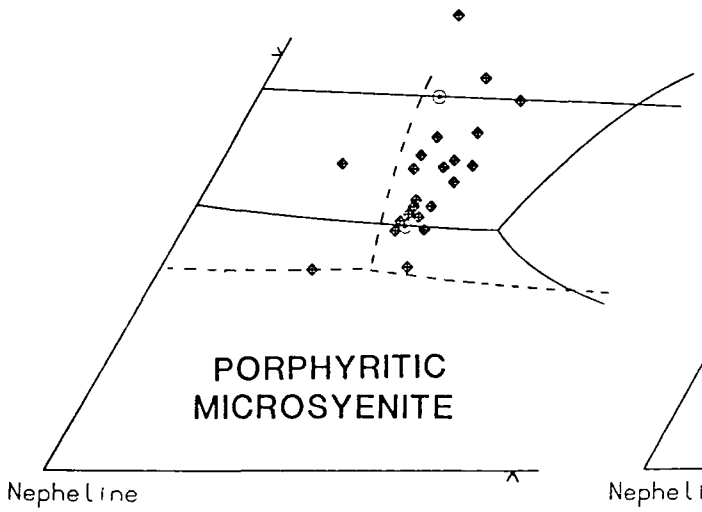
PORPHYRITIC
MICROSYENITE
Nepheline

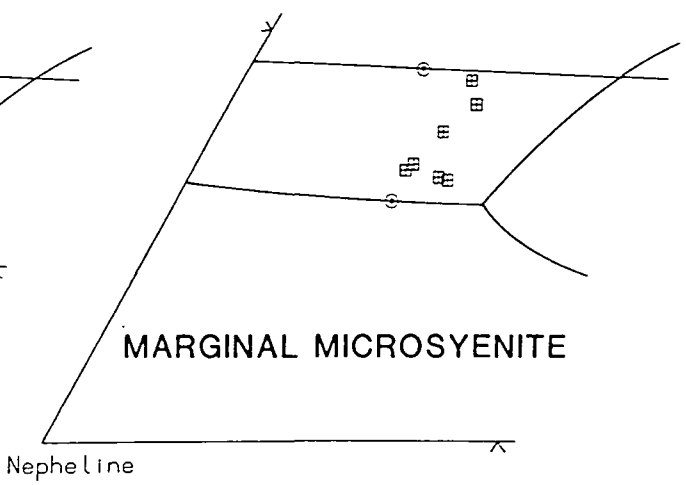
MARGINAL MICROSYENITE
Nepheline

on the shape of the liquidus surface as well as displacing the eutectics (Kogarko, *op. cit.*).

Fig 5.4.2 shows the felsic normative components of each sample from the different rock units plotted in the residua system, together with the 1kb and (where appropriate), the 5kb eutectics.

Lower Series Syenite

The Lower Series shows the most coherent set of compositions, with a continuous trend which converges on the 'thermal valley' with increasing fractionation. As with most units, some samples plot in the oversaturated part of the system; these tend to show the greatest amounts of alteration.

A few samples lie within the nepheline field at 1kb, and two even at 5kb. As described above, displacement of the phase boundaries is not simply due to varying p_{H_2O}, but other magmatic components, particularly acid volatiles, are important.

Upper Series Syenite

This unit shows a less coherent trend, possibly due to a larger number of slightly more altered samples, though compositions do tend to cluster around a point just above the minimum on the $ne - ksp$ boundary at 1kb.

Mafic Upper Series Syenite

Because of the lower proportion of felsic components, this unit may be expected to show the greatest distortion when plotted in the residua system. Several analyses still cluster around a point just above the $ne - ksp$ phase boundary, however, and are slightly displaced towards ab.

GS-A, GS-B

Only three samples from GS-A were collected and analysed, and these show a considerable spread of compositions. Petrographic observations (section 3.5.1) suggest that this unit has experienced some metasomatic alteration.

The trend for GS-B extends well into the nepheline field at 5kb, and is displaced towards the Na-rich side of the system. It is possible that volatile components may have become concentrated in these marginal rocks and displaced the $ne - ksp$ boundary towards the $Ne - Ks$ tie-line, allowing compositions to continue to evolve away from the alkali feldspar join, well into the nepheline field at 1kb.

Xenolithic Porphyritic Syenite

Most samples from this unit occupy a very narrow band along the thermal valley between the $Ab - Or$ tie-line and the 1kb $ne - ksp$ minimum, though a few samples show a marked departure from this trend. Only xenolith-free samples of Xenolithic Porphyritic Syenite were chosen for XRF analysis, though it is possible that some of the phenocrysts are xenocrysts, which may cause anomalies.

Coarse-Grained Brown Syenite

This unit generally shows oversaturated compositions, presumably as a result of nepheline alteration. Thought to be a continuation of the Lower Series Syenite (Emeleus 1964, and as a result of fieldwork carried out in 1987), the alteration renders comparison with the Lower Series virtually impossible.

Coarse-Grained Syenite

Only a few samples of this minor unit were collected and analysed, compositions generally varying from just oversaturated to just undersaturated, and slightly displaced towards *ab*. The very coarse grain-size and fairly altered nature of this unit may have resulted in rather imprecise analyses.

Porphyritic Microsyenite and Marginal Microsyenite

The fine grain-size of these rocks suggests that, in contrast to the other syenite units, they may represent chilled liquids. The variable proportion of phenocrysts in some samples of the Porphyritic Microsyenite, however, suggests that the Marginal Microsyenites maybe the best (and possibly only) representatives of chilled liquid compositions. Both units show fairly coherent sets of data, slightly displaced towards *or*, the Porphyritic Microsyenites converging on a point just above the 1kb $ne - ksp$ boundary, as with many of the other syenites.

5.4.2: Variation in normative composition with height

Sampling was carried out across the Lower and Upper Series Syenite along a series of transects, with a view to determining any systematic chemical variations within the units. The general dip of the lamination towards the centre of the complex results in samples taken from an increasing stratigraphic height when moving from the outer to inner margin of the units.

Fig. 5.4.3 shows the variations in normative compositions with increasing distance from the outer margin, corresponding to an increase in stratigraphic height within the Lower and Upper Series Syenite. The most interesting feature of these variations is that after an initial trend towards the undersaturated minimum with increasing height, three of the transects record an abrupt reversal of trend, and become increasingly feldspathic. The one exception to this is from the Upper Series, which shows the reversed trend immediately, with increasingly feldspathic compositions developed with continuously increasing height in the series. Gill (1972a) noted a similar increase in silica enrichment with height for samples in the Lower and Upper Series Syenite, though his work did not reveal the initial trend towards the undersaturated minimum that this work shows. His analyses were not performed on samples collected from transects, and thus may have

Fig. 5.4.3. Variations in normative composition with height in the laminated syenites (Lower and Upper Series). A trend towards generally more undersaturated (fractionated) compositions with increasing distance from the upper and lower margins is apparent, as a result of the development of a 'sandwich horizon' towards the centre of each unit. See text for further discussion of trends.

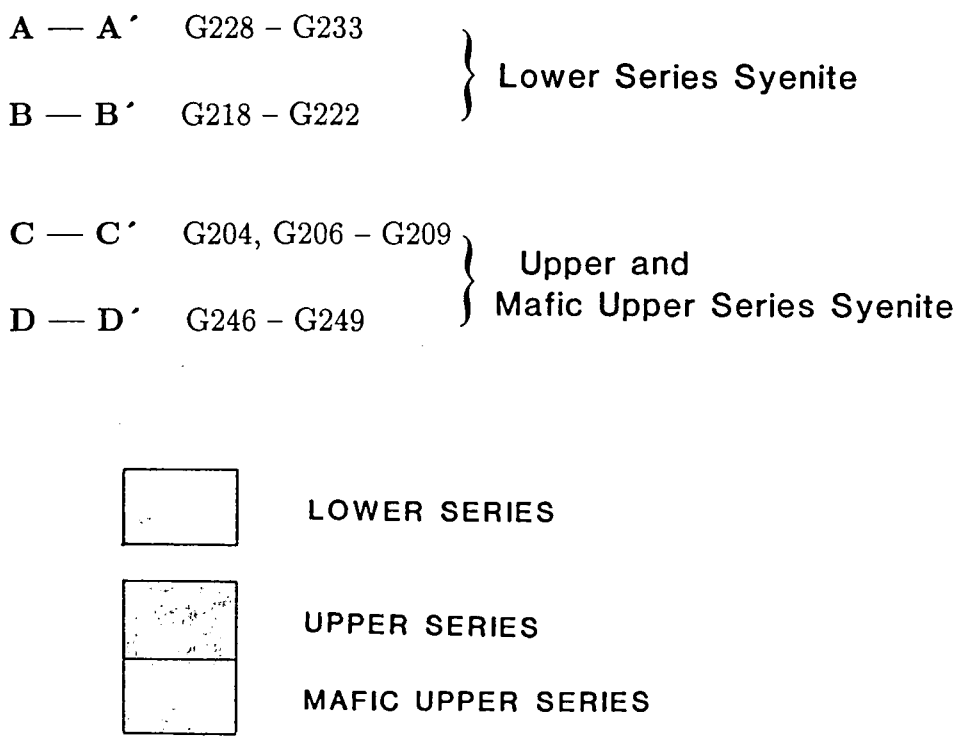

Fig. 5.4.3

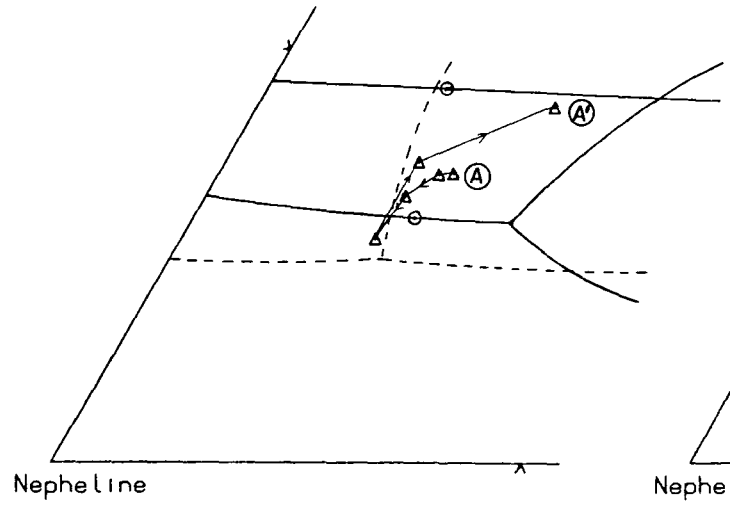
A'
A
Nepheline

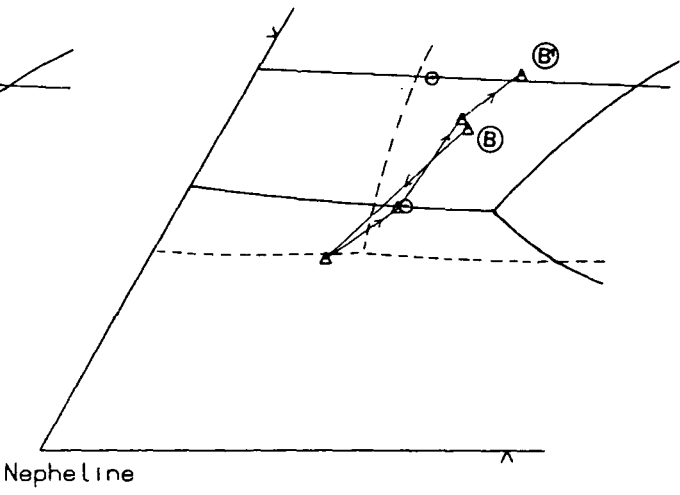
B'
B
Nepheline

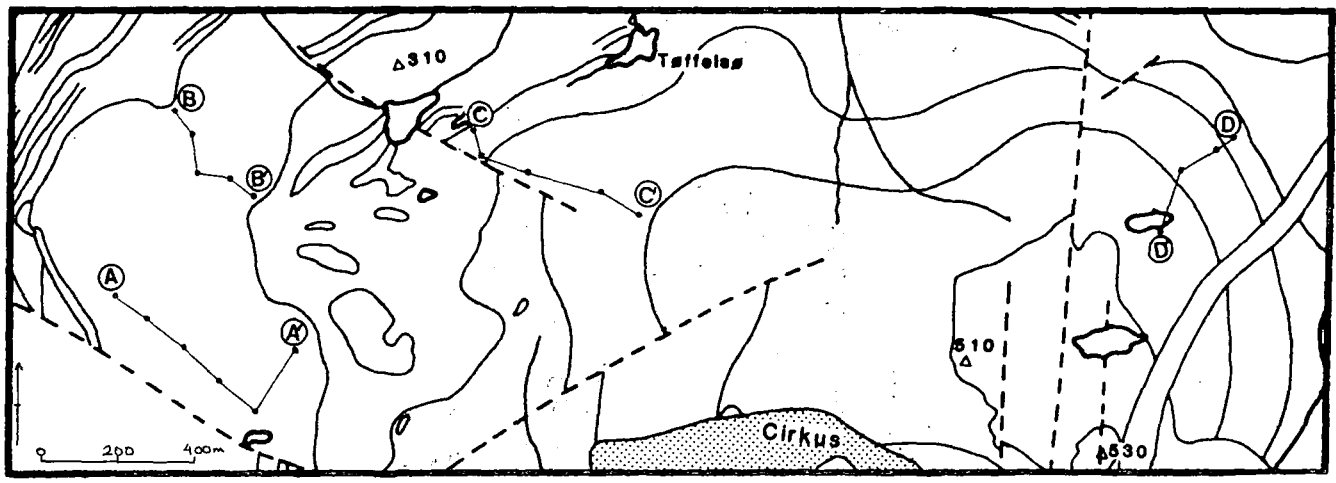
△310
Taffelen
B
B'
C
C'
A
A'
D
D'
510
Cirkus
530
200
400m

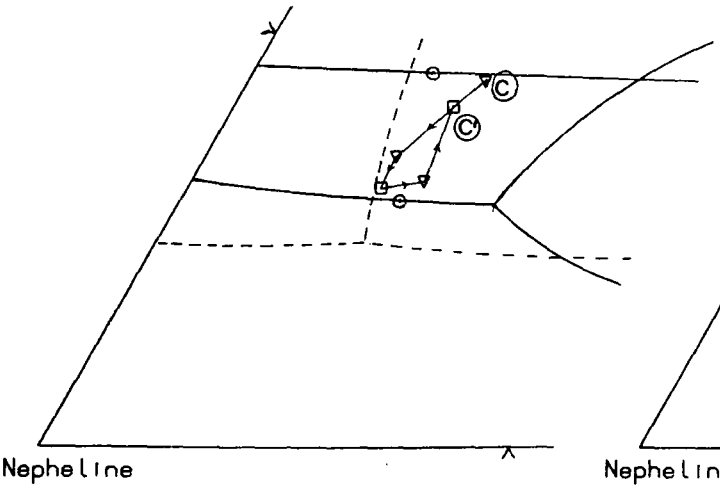
C
C'
Nepheline

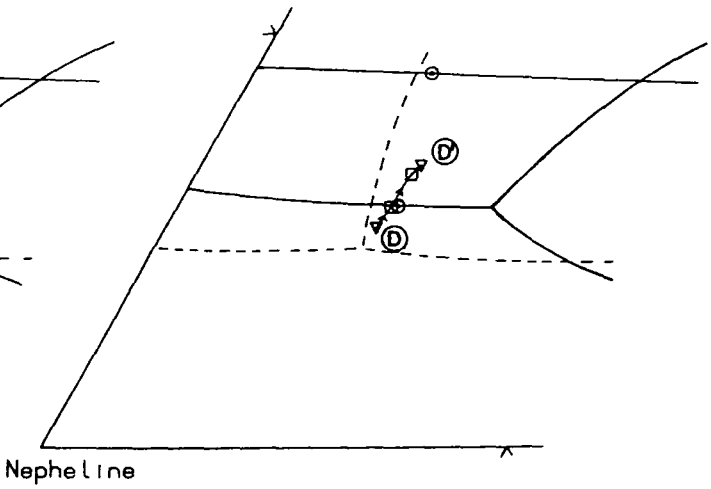
D'
D
Nepheline

missed the small compositional variations recorded from samples collected more systematically.

The initial trend of compositions towards the undersaturated minimum is comparable to that of other Gardar centres and silica undersaturated magmas in general. Fractionation of alkali feldspar, the composition of which is determined by the shape of the fractionation curve which intersects the liquid composition, drives the residual liquid towards the $ne - ksp$ phase boundary, at which point nepheline appears on the liquidus. In an ideal system of perfect fractional crystallisation, nepheline and alkali feldspar then crystallise simultaneously, the proportion of nepheline increasing until the undersaturated minimum is reached, where the proportion of minerals fractionating remains constant, and the liquid eventually solidifies. Magmas representing more evolved, silica undersaturated compositions thus plot nearer to the undersaturated minimum, and the initial trend of the Grønnedal-Íka syenites is generally of increasing fractionation with height in each unit. Compositions which plot in the nepheline field at 1kb could be a result of crystallisation under conditions of higher p_{H_2O}, though some plot in the nepheline field even at 5kb. It is likely that these rocks contain some cumulus nepheline, and petrographic evidence would appear to bear this out (chapter 3).

At stratigraphically higher levels within each unit, the rocks become increasingly feldspathic, and the trends turn back towards the $ab - or$ join; the entire trend of G246–G249 (D–D′) in the Upper Series Syenite is in this direction. The most feldspathic syenites in the Lower Series occur underneath the gneiss raft (map 1), a characteristic noted by Gill (1972a), where the rock is pulaskitic in places, consisting almost entirely of alkali feldspar.

The reversal of trend may simply be a result of approaching the inner margin of the Lower Series, ie. the contact with the gneiss raft. Initial crystallisation of the magma adjacent to the raft would result in rock compositions which plot near to the $ab - or$ join in the residua system, as in the case of samples from the

lower (outer) margin of the unit. Crystallisation then proceeds inwards (downwards) from the lower surface of the raft, and as the magma differentiates, more fractionated compositions are produced. The most evolved compositions thus occur towards the centre of the unit, with samples taken progressively closer to the margins (lower – outer, or upper – inner) being less evolved. The development of a 'sandwich horizon' such as this occurs during the evolution of many other intrusive bodies, eg. Skaergaard (Wager and Brown 1968), and the Palisades Sill (Shirley 1987). The highly feldspathic (pulaskitic) facies at the top of the Lower Series may be a result of the separation of nepheline from alkali feldspar due to their different settling velocities in the magma. Although their densities are almost identical (ρ_{ne}=2.56-2.67, ρ_{ksp}=2.55-2.63, Deer *et al.*, 1966), the tabular shape of the alkali feldspar, which presents a relatively large surface area and thus resistance to gravitational settling, would result in a slower rate of settling than the more equant nephelines.

It is harder to explain the Upper Series trends in a similar way to the Lower Series in the absence of an exposed gneiss raft. Upton (1974) suggests that emplacement of the Gardar central complexes may be a result of repeated foundering of 'rafts' of country rock from the roof of the intrusion, citing Grønnedal-Íka as an example. Only one such raft outcrops at Grønnedal, although it is possible that there may have been others at higher structural levels within the complex. This might be used to explain C–C′ in a similar way to the Lower Series trends, although D–D′ , where the whole trend is one of decreasing fractionation with height, remains problematic. If separation of nepheline from alkali feldspar does indeed occur by the process suggested above, the relative proportion of feldspar would be expected to increase upwards, nearer to the source of the cumulus phases, perhaps from the magma cooling adjacent to a gneiss raft.

Magmatic sorting is almost certainly responsible for some of the observed variations in composition with position (both laterally as well as vertically) in the

laminated syenites. The lamination itself may be a result of feldspar deposition from magmatic currents, and there is much evidence for slumping in parts of both the Lower and Upper Series in the form of swirled lamination and contorted mafic schlieren (plate 2.2). Redistribution of mineral phases would be assisted by such processes. In particular, alkali feldspars could be affected more strongly than other minerals due to their tabular shape, resulting in a relatively large surface area to mass ratio compared to the more equant phases, such as nepheline.

5.5: Rare-earth element geochemistry

Sixteen samples from each of the syenite units were analysed for rare-earth elements (REE's) by Instrumental Neutron Activation Analysis (INAA), the operating conditions of which are outlined by Leat *et al.* (1989, in press) and in Appendix IV. Samples were chosen on the basis of their La, Ce, and Nd contents as determined by XRF methods, taking those which contained 'average' abundances for these elements in each particular rock group. All units have at least one sample analysed for REE's, and from those which were thought to be of particular importance, two or more analyses were carried out.

Fig. 5.5.1 shows the data presented in the usual form, with REE concentrations normalised to chondritic abundances, using the values of Boynton (1984); missing data have been interpolated from the nearest analysed neighbours.

Several features are apparent from these diagrams:

1. All units show strong enrichment relative to chondritic values.
2. Light REE/Heavy REE (LREE/HREE) ratios are generally high.
3. Many samples show at least slight Eu anomalies.
4. Slight negative Yb anomalies are sometimes present.
5. A slight initial increase in normalised abundance with atomic number.

Each of these points is now considered in more detail.

Fig. 5.5.1. Rare-earth element (REE) distribution patterns for the syenite units, normalised using chondritic abundances of Boynton (1984). All show strong overall enrichment relative to chondritic abundances, and steep curves as a result of high light REE/heavy REE ratios, typical of liquids produced by small amounts of partial melting of mantle material (Cullers and Graf 1984).

Slight negative Eu anomalies are characteristic of most of the samples, although one from the Xenolithic Porphyritic Syenite (G245) shows a distinct positive anomaly.

Fig. 5.5.1

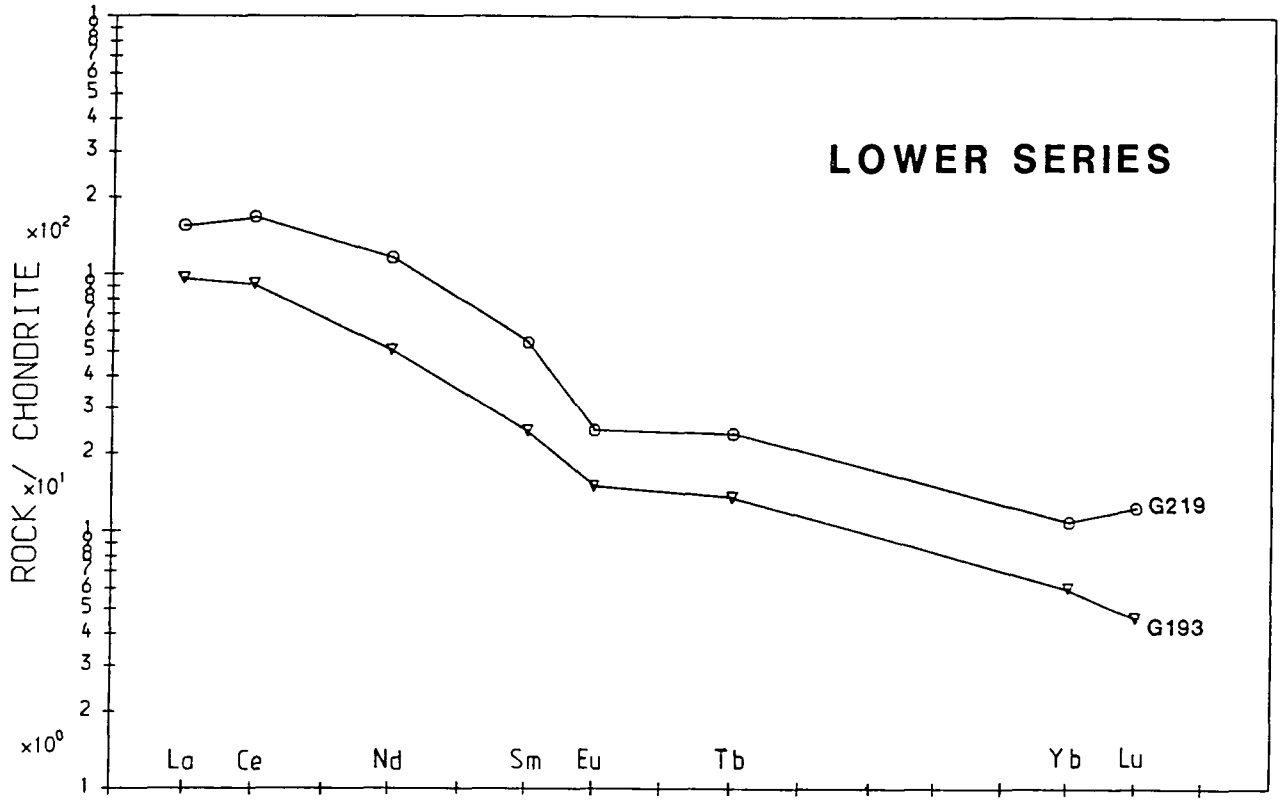
LOWER SERIES
ROCK / CHONDRITE
×10²
×10¹
×10⁰
G219
G193
La
Ce
Nd
Sm
Eu
Tb
Yb
Lu

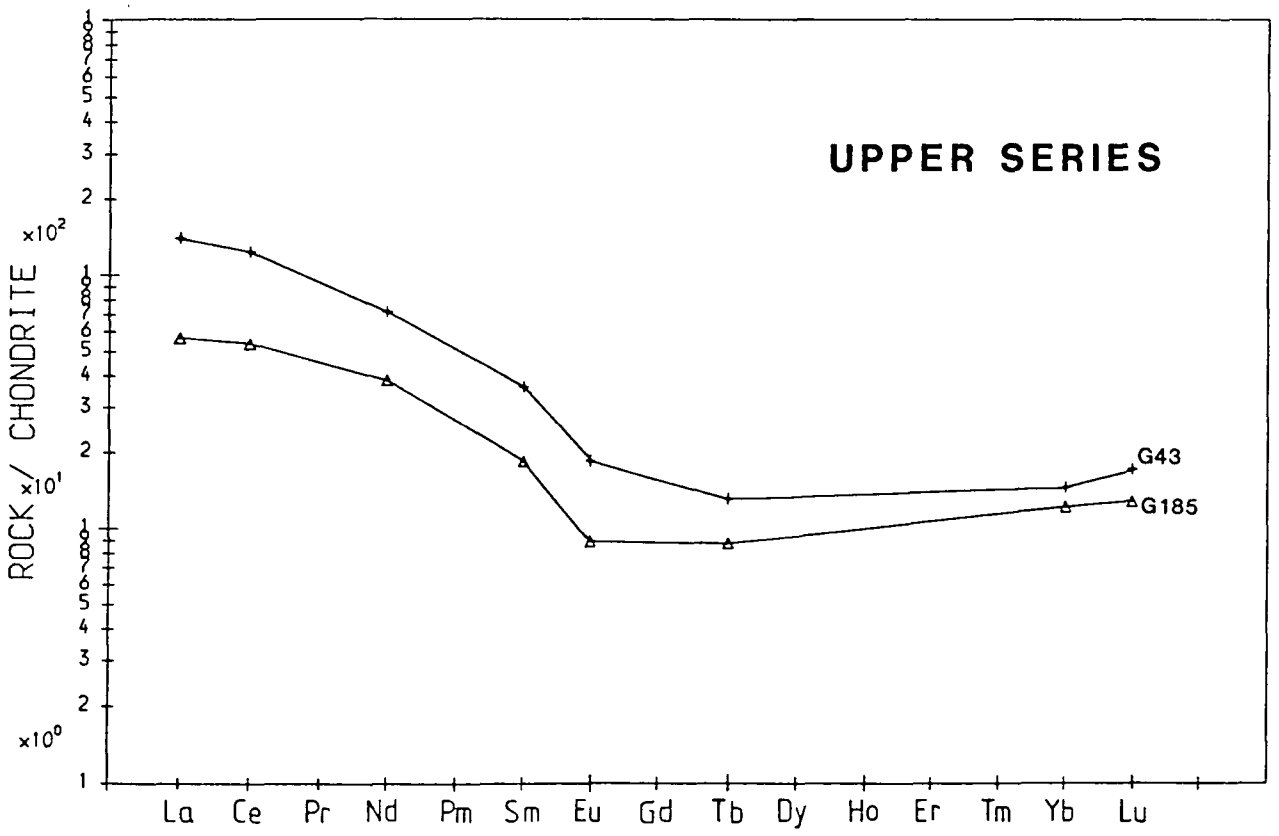
UPPER SERIES
ROCK / CHONDRITE
×10²
×10¹
×10⁰
G43
G185
La
Ce
Pr
Nd
Pm
Sm
Eu
Gd
Tb
Dy
Ho
Er
Tm
Yb
Lu

Fig. 5.5.1(cont.)

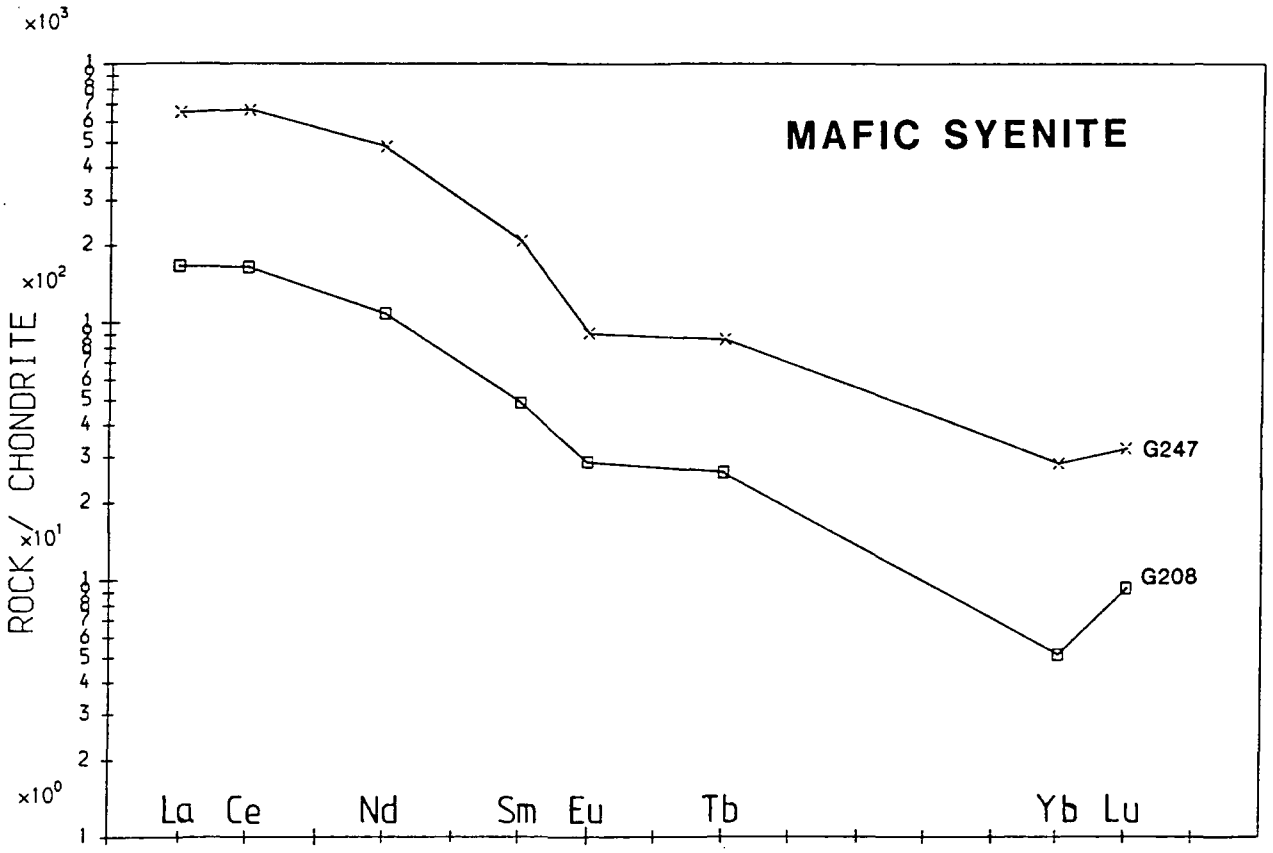
MAFIC SYENITE
ROCK/ CHONDRITE
×10³
×10²
×10¹
×10⁰
G247
G208
La Ce Nd Sm Eu Tb Yb Lu

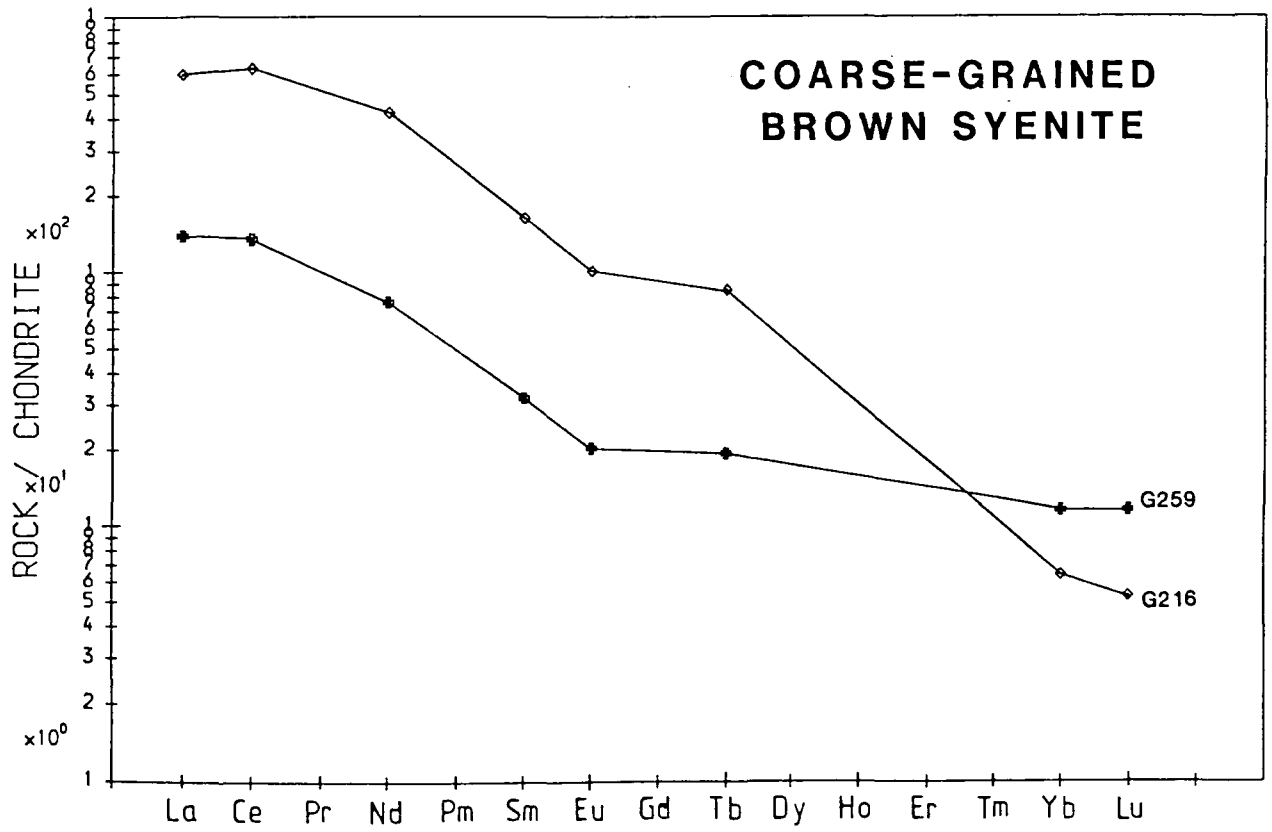
COARSE-GRAINED
BROWN SYENITE
ROCK/ CHONDRITE
×10²
×10¹
×10⁰
G259
G216
La Ce Pr Nd Pm Sm Eu Gd Tb Dy Ho Er Tm Yb Lu

Fig. 5.5.1(cont.)

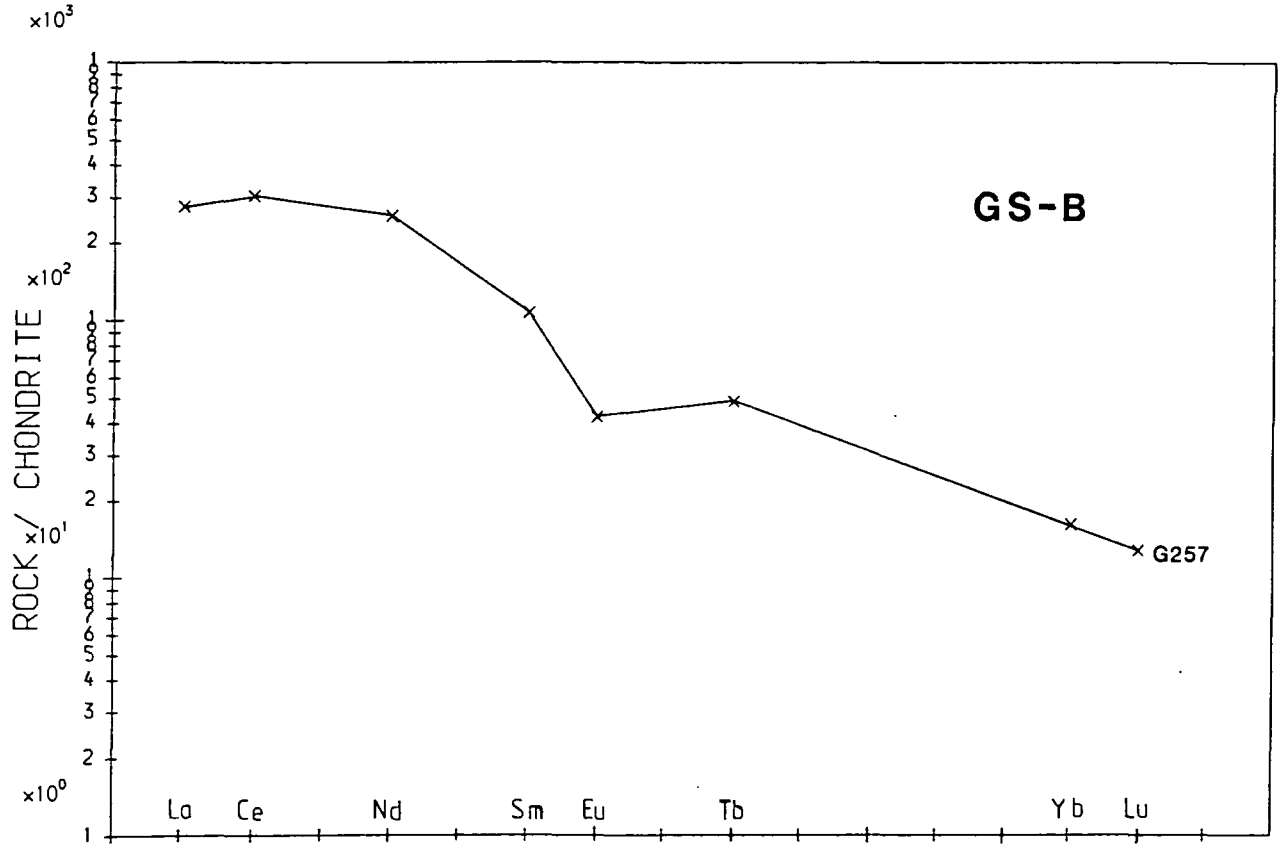
GS-B
ROCK/ CHONDRITE
×10³
×10²
×10¹
×10⁰
G257
La
Ce
Nd
Sm
Eu
Tb
Yb
Lu

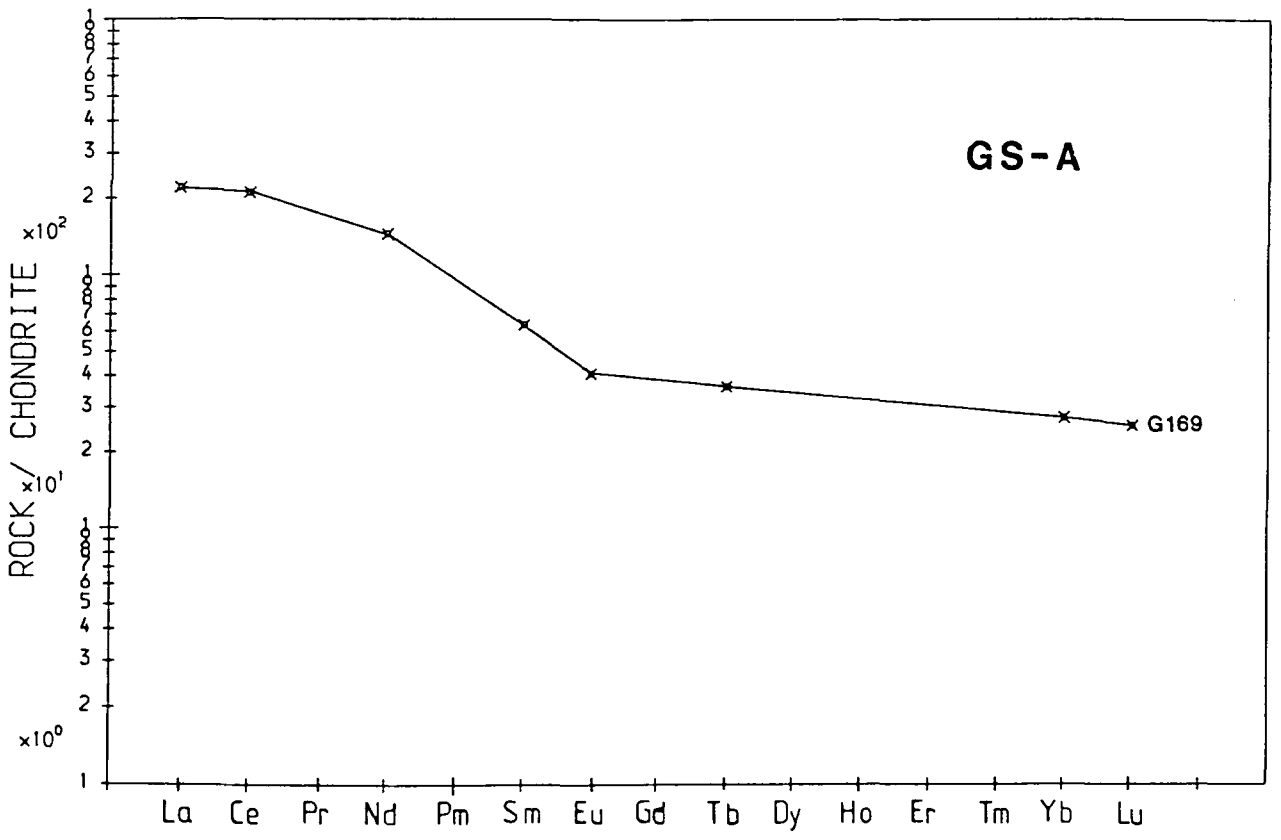
GS-A
ROCK/ CHONDRITE
×10²
×10¹
×10⁰
G169
La
Ce
Pr
Nd
Pm
Sm
Eu
Gd
Tb
Dy
Ho
Er
Tm
Yb
Lu

Fig. 5.5.1 (cont.)

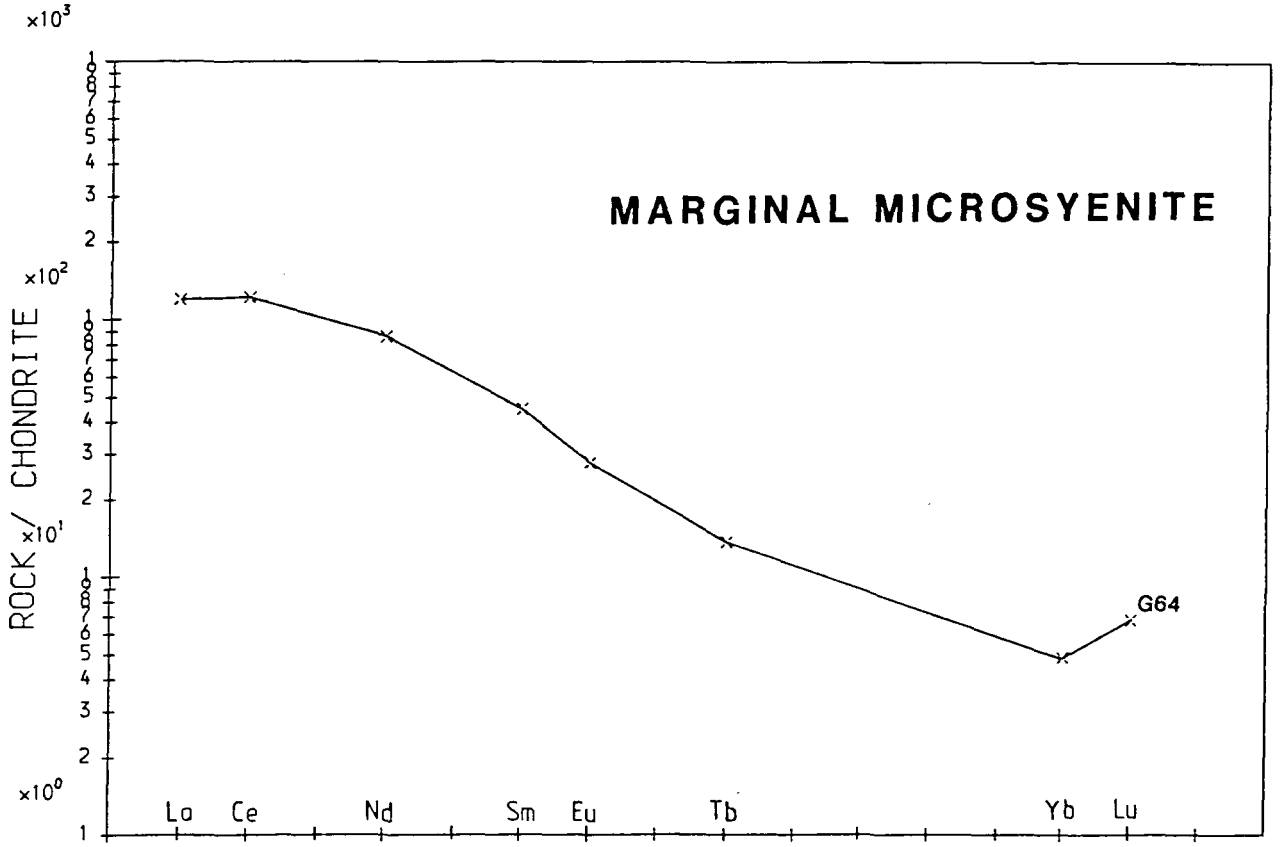
MARGINAL MICROSYENITE
ROCK / CHONDRITE
×10³
×10²
×10¹
×10⁰
G64
La
Ce
Nd
Sm
Eu
Tb
Yb
Lu

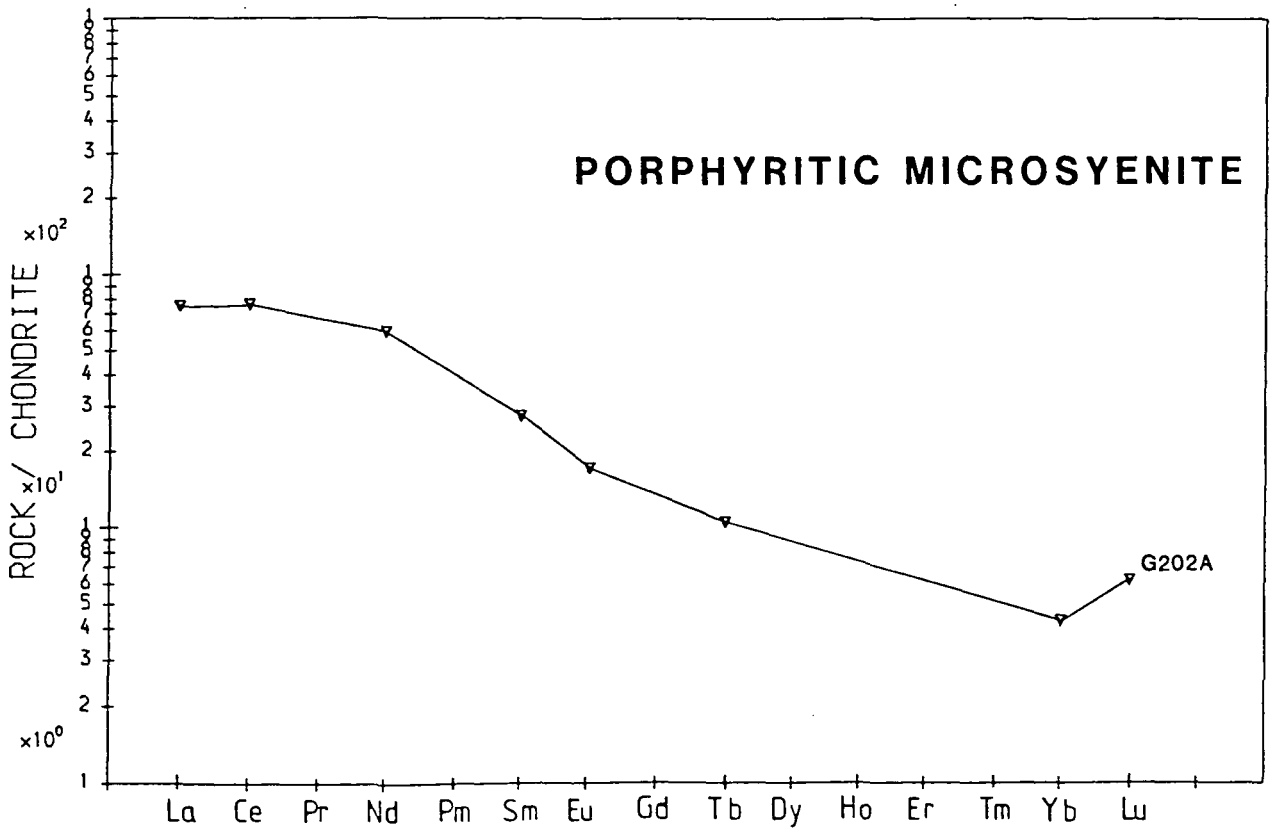
PORPHYRITIC MICROSYENITE
ROCK / CHONDRITE
×10²
×10¹
×10⁰
G202A
La
Ce
Pr
Nd
Pm
Sm
Eu
Gd
Tb
Dy
Ho
Er
Tm
Yb
Lu

Fig. 5.5.1 (cont.)

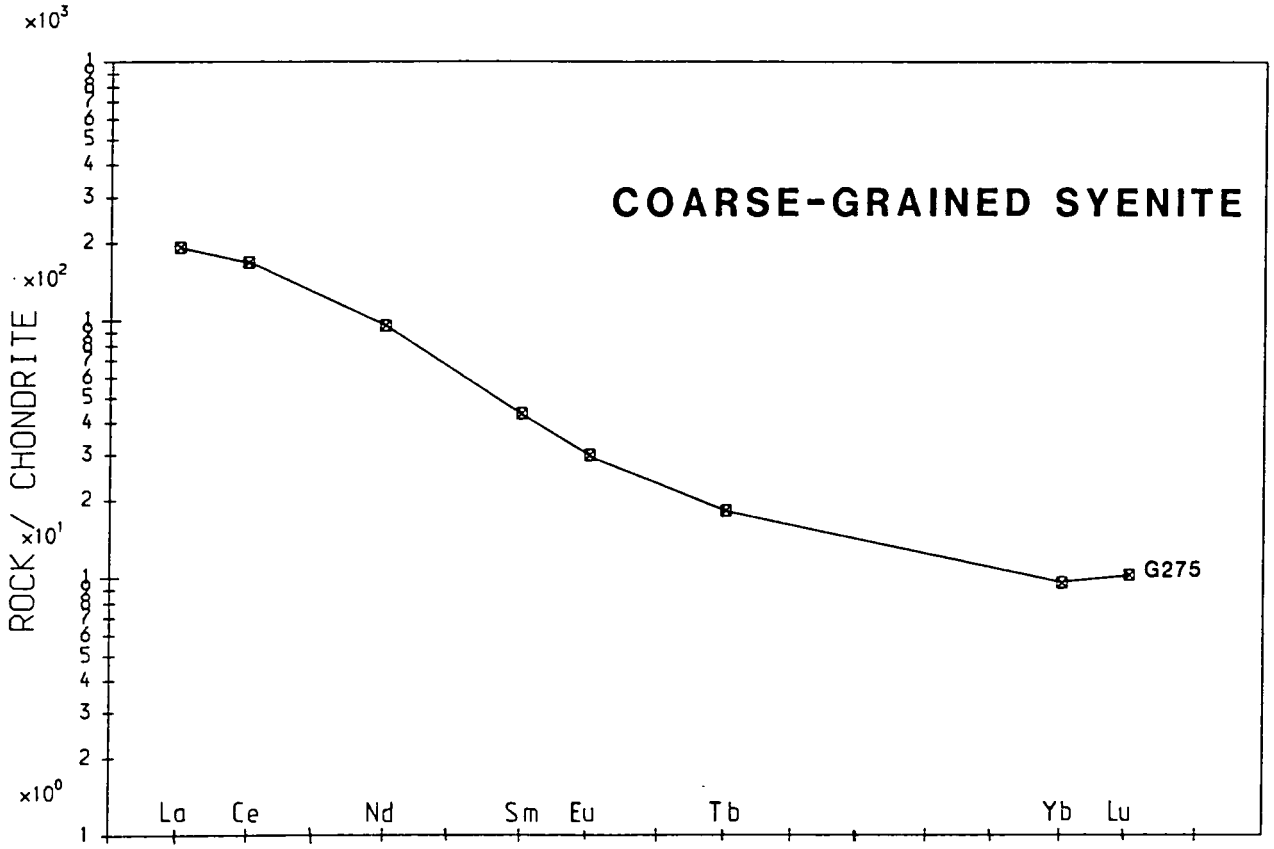
COARSE-GRAINED SYENITE
ROCK x/ CHONDRITE
x10³
x10²
x10¹
x10⁰
G275
La Ce Nd Sm Eu Tb Yb Lu

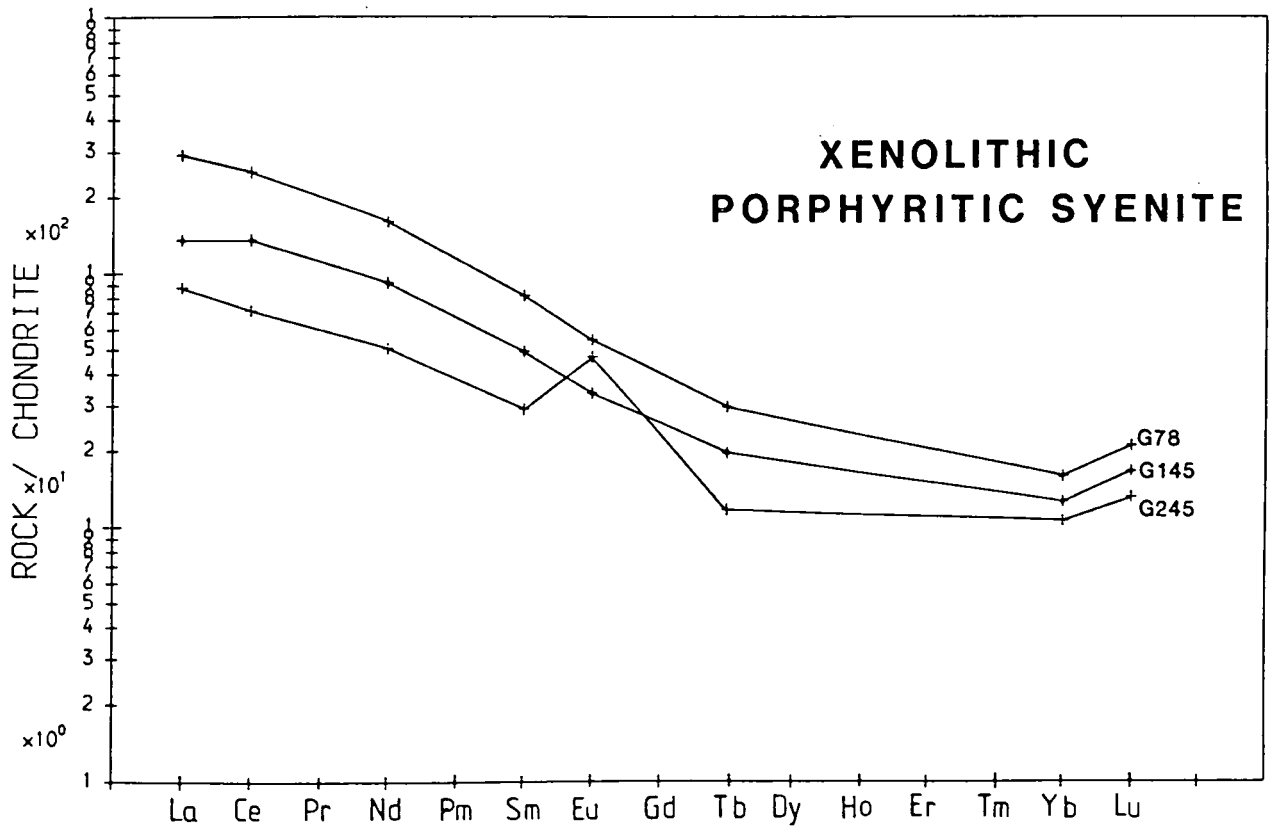
XENOLITHIC
PORPHYRITIC SYENITE
ROCK x/ CHONDRITE
x10²
x10¹
x10⁰
G78
G145
G245
La Ce Pr Nd Pm Sm Eu Gd Tb Dy Ho Er Tm Yb Lu

5.5.1: Overall enrichment

All the syenites show strong overall enrichment compared to chondritic abundances, with LREE's showing 55–650× chondrite and HREE's 5–30× chondrite. These enrichment factors are comparable to those of the phonolites of the Igaliko dyke swarm (Pearce 1988), though the latter are marginally richer in LREE's.

5.5.2: LREE/HREE ratios

All samples have moderately steep curves as a result of high LREE/HREE ratios. These are measured as $(La/Lu)_{cn}$ (where *cn*=chondrite normalised), and generally vary between 4 and 20, although G216, a Coarse-Grained Brown Syenite, has $(La/Lu)_{cn}$=113. The variation of $(La/Lu)_{cn}$ against overall REE enrichment is shown in fig. 5.5.2, and shows that with increasing LREE abundance, the LREE/HREE ratio increases, ie. the curves become 'steeper', although the Grønnedal-Íka syenites do not show such steep trends as the phonolites from the Igaliko dykes (Pearce, *op. cit.*). Allanite is one of the few minerals for which $D^{allan}_{HREE} > D^{allan}_{LREE}$ (Henderson 1984). Although not observed in thin section, the mineral does occur in syenites (Deer *et al.*, 1966), and in the Gardar, it has been reported from Ilímaussaq (Sørensen and Petersen 1981). Fractionation of this phase could potentially reduce the $(La/Lu)_{cn}$ of a phonolitic magma with a LREE/HREE trend, such as represented by the Igaliko dykes, giving rise to comparable trends in syenites such as occur at Grønnedal.

5.5.3: Eu anomalies

Although Gd, one of the elements used to fix the Eu anomaly, is unreliable when analysed using INAA methods (and has therefore been omitted from fig. 5.5.1), many samples show negative anomalies, with one sample from the Xenolithic Porphyritic Syenite (G245) showing a positive Eu anomaly. Fractionation of plagioclase commonly results in negative Eu anomalies, the presence or absence of which may be used to divide the syenite units at Grønnedal into two main groups:

Fig. 5.5.2. $(La/Lu)_{cn}$ vs. Ce and Yb.

The slope of the chondrite normalised REE distribution curve, $(La/La)_{cn}$, increases with total REE content. The correlation between gradient and REE content is stronger with light REE's (measured as Ce ppm) than with heavy REE's (Yb).

Fig. 5.5.2

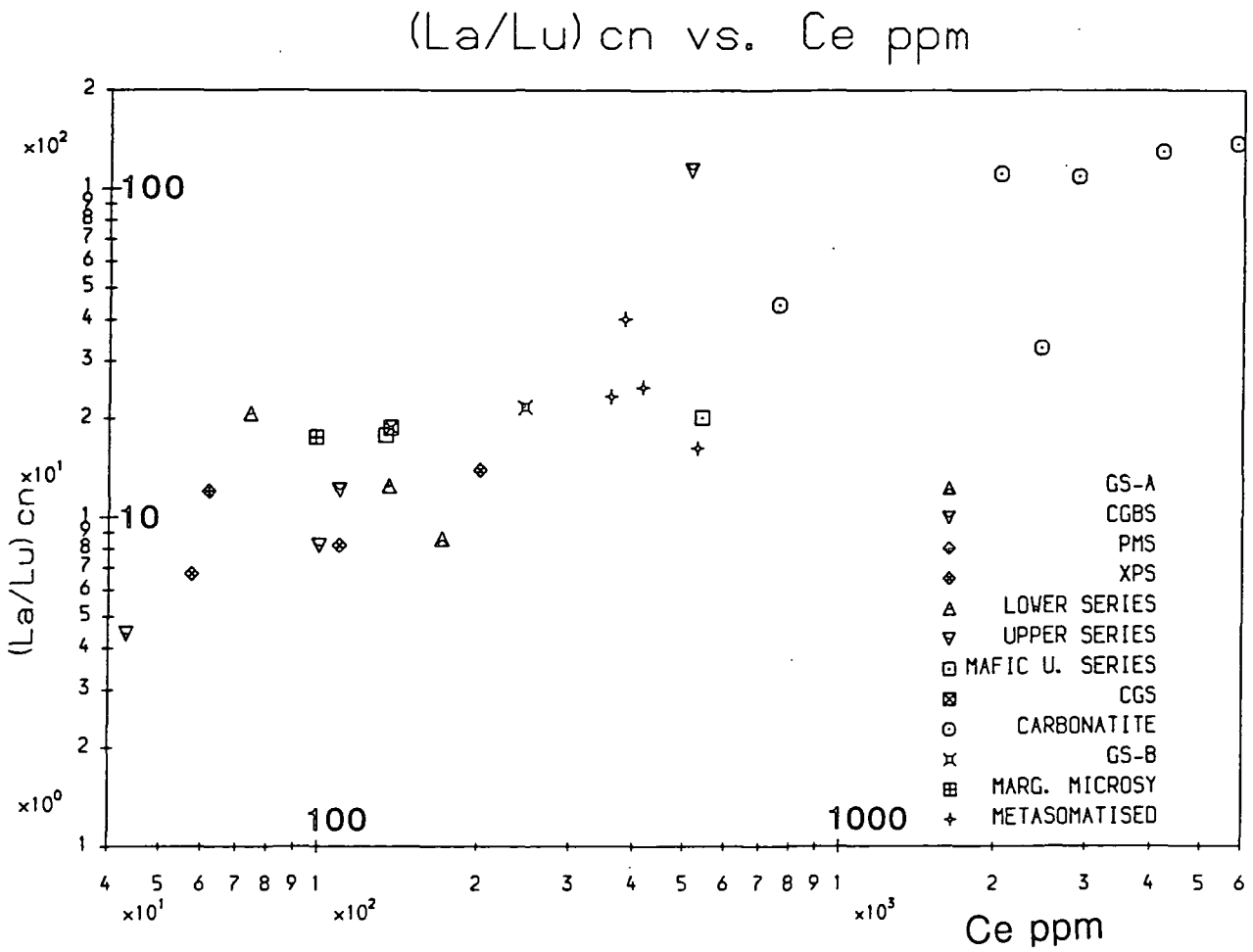
(La/Lu) cn vs. Ce ppm
(La/Lu) cn
Ce ppm
100
10
100
1000
GS-A
CGBS
PMS
XPS
LOWER SERIES
UPPER SERIES
MAFIC U. SERIES
CGS
CARBONATITE
GS-B
MARG. MICROSY
METASOMATISED

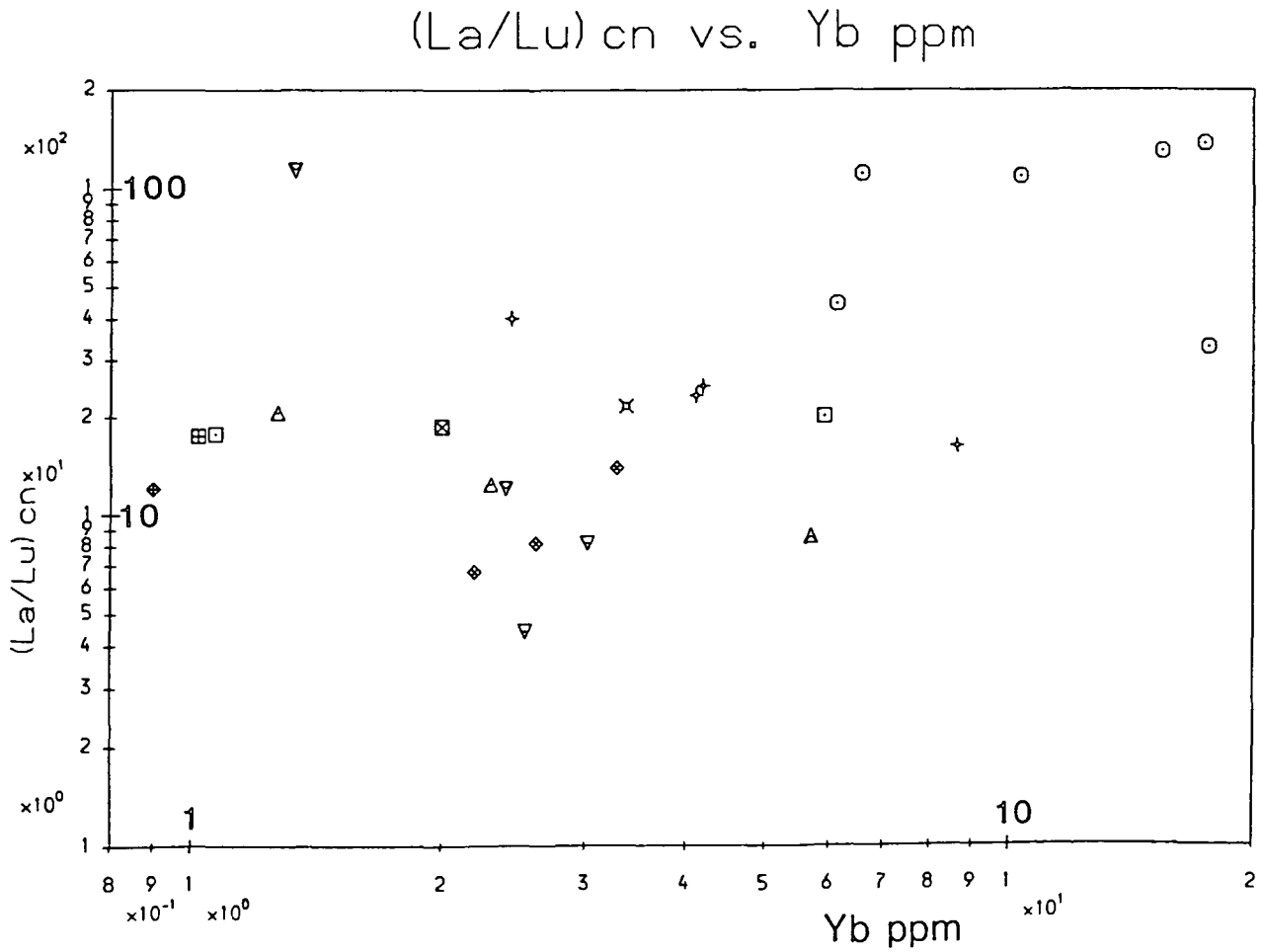
(La/Lu) cn vs. Yb ppm
(La/Lu) cn
Yb ppm
100
10
1
10

i) Negative Eu anomalies: Lower and Upper Series, Mafic Syenites, Coarse-Grained Brown Syenite, GS-B, and possibly GS-A.

This group includes the main laminated units as well as the marginal rocks, which appear to be coeval on the basis of field and petrographic evidence.

ii) No Eu anomaly or positive anomaly: Coarse-Grained Syenite, Xenolithic Syenite, microsyenites.

This group consists of the later, cross-cutting units (Coarse-Grained and Xenolithic Syenites), and the microsyenite dykes.

The lack of an anomaly in a marginal chilled facies has also been observed by Upton *et al.* (1985) in the border group of the Tugtutôq Older Giant Dyke Complex, samples from the internal part of which show negative Eu anomalies. They suggest that Eu enters the plagioclase structure but was not lost to the system by gravitational removal at the margins , and that in the central group (cf. the Upper Series Syenite at Grønnedal), depletion of the magma in Eu had occurred by the time crystallisation commenced.

The positive anomaly in sample G245 from the Xenolithic Porphyritic Syenite is a unique occurrence among the REE trends from Grønnedal, and it is possible that this sample was taken from a batch of magma which acted as the sink for the Eu-rich crystals. Alternatively, the absence of anomalies in any of the other samples analysed from this unit and lack of any obvious plagioclase in thin-section suggests a possible xenocrystic origin. Many of the xenoliths in this unit could not be matched with any of the syenites seen in the field, and have presumably been brought up from deeper levels of the complex. These may have been the 'sink' for any settling Eu-rich phases, and might have given rise to the positive anomaly following disaggregation and/or digestion of the Eu-enriched rock.

5.5.4: Negative Yb anomalies

Most analyses show a flattening of the HREE 'tail' ($Yb_{cn} \approx Lu_{cn}$), with some even having a slight negative Yb anomaly. While for many of the samples this may be due to analytical error (Leat, pers. comm.), for those which show quite pronounced anomalies the effect may be genuine (eg. Marginal Microsyenite G64 and Porphyritic Microsyenite G23, $(Lu/Yb)_{cn}$=1.40; Mafic Syenite G208, $(Lu/Yb)_{cn}$=1.82). A garnet-rich source rock is probably the most likely explanation for these slight anomalies, since $D^{gt}_{Yb} > D^{gt}_{Lu}$ (43 compared to 38, Henderson 1982). Very small amounts of partial melting (of the order of 1%) of such a source rock, in which garnet had not completed its melting, might give rise to a liquid relatively depleted in HREE's (Cullers and Graf 1984), but richer in the more incompatible of these two elements, ie. Lu.

5.5.5: Ce anomalies

Most samples show a flat region of the REE curve between La and Ce, some showing a slight positive Ce anomaly. This effect is much less pronounced than the Yb anomaly described previously, and may simply be due to analytical error (Leat, pers. comm., Appendix IV and table IV.1). Samples showing this effect most strongly are from the Lower Series (G219), GS-B (G257), and the Mafic Syenite (G247). Negative Ce anomalies may develop under strongly oxidising conditions (Cullers and Graf 1984) due to oxidation of Ce^{3+} to Ce^{4+}, the latter having a higher partition coefficient in many minerals (Goldschmidt 1954). The bulk of the mineralogical evidence, however, points to a relatively oxidising magmatic environment, although negative anomalies are not developed. Ce is less strongly partitioned into magnetite than either La or Nd (Paster *et al.* 1974), fractionation of which could result in a slight positive Ce anomaly.

5.6: Summary and conclusions

This section reviews the various points regarding the whole-rock geochemistry of the complex, described in earlier parts of this chapter.

Both major and trace-element abundances are comparable to those of other Gardar centres (eg. North and South Qôroq), though the variation in trace-element concentrations with fractionation is often markedly different (fig. 5.2.1).

Of the major elements, Na_2O, K_2O, Al_2O_3, and SiO_2 generally increase with fractionation, partly as a result of their presence in the phases which comprise the Fractionation Index (section 5.2), while a decrease in Ca, Mg, Fe, Mn, Ti, and P suggests fractionation of phases containing these elements (such as the mafic minerals, plagioclase, and apatite).

Many of the trace elements are seen to decrease in abundance with increasing fractionation (section 5.3), with only Ga (and possibly Rb) showing an increase. It is suggested that the fractionation of phases such as allanite, låvenite, monazite, and rinkite (which have occasionally been observed in thin-section) as well as apatite (in which the rare-earth elements are strongly partitioned, section 4.9) may have resulted in the observed decreasing trends.

The scatter in both major and trace element concentrations is often considerable, even when samples containing normative corundum (the amount of which increases with alteration, as a result of nepheline breakdown) are omitted. It appears that many of the samples contain a proportion of cumulus crystals, which accumulated on the floor of the magma chamber. As long as liquid was able to pass through the crystal pile, the intercrystalline fluid would remain in approximate equilibrium with the evolving magma (Paster *et al.* 1974). With continued cooling, entrapment of intercumulus liquid would inevitably occur, the precise time that this took place being important in determining the composition of the trapped material. Textural variations might significantly affect the time that this

occurred, and could ultimately control the composition of the rock sample. Many of the petrographic textures are highly suggestive of a cumulus origin, while field evidence indicates that magmatic currents (either as a result of magmatic convection or slumping) may have been responsible for redistributing the cumulus phases. Some trace elements are often compatible in many of the principle cumulus phases (eg alkali feldspar – Ba, Rb) while the sporadic occurrence of rare minerals which are very rich in certain elements (eg. monazite, which concentrates the rare-earth elements) could give rise to scatter in the analyses. Chambers (1976) accounts for the scatter in trace element abundances at North Qôroq as being due to the mobilisation and redistribution of many elements during metasomatism. This process also appears to have affected all of the syenites at Grønnedal-Íka to some extent, and may well have played a part in causing the observed scatter of abundances.

An attempt has been made to characterise the syenite units by their trace element abundances. This is not easy due to the range of concentrations observed for most of the syenites, as well as an insufficient number of samples for some units, though this was also attempted by Gill (1972a). The Mafic Upper Series is the least fractionated unit, and appears to be relatively enriched in many elements, particularly Ce, La, and Nd (possibly due to the high modal proportion of apatite), but also V and Ni (due to the presence of pyroxene). The Upper Series Syenite itself is also slightly enriched in most elements, particularly Ce, La, Nd, Sr, and Ba, while slightly depleted in Rb and Sr. The Xenolithic Porphyritic Syenite is also enriched in Sr and Ba, and particularly Zr, while the Coarse-Grained Syenite is likewise relatively enriched in Ba and Sr.

Normative compositions plot along a trend which is displaced towards the potassic part of the residua system. Experimental work (James and Hamilton 1969, and Kogarko 1974) suggests that additional components can alter the shape of the liquidus surface, and may displace the 'thermal valley'. Natural magmas

will be more complex still, and it is hardly surprising that the analyses do not lie in between the silica saturated and undersaturated minima.

Transects across the Lower and Upper Series Syenite generally show a trend towards increasing undersaturation with height, before an abrupt reversal occurs as the upper margin (exposed or inferred) is approached. Thus a 'sandwich horizon', such as occurs at Skaergaard (Wager and Brown 1968) and the Palisades Sill (Shirley 1987) seems to be developed in the laminated syenites at Grønnedal-Íka. The pulaskitic facies beneath the gneiss raft at the top of the Lower Series Syenite may be a result of the differential settling rates of the tabular alkali feldspars and equant nephelines.

Chondrite-normalised REE trends indicate strong overall enrichment, particularly for the LREE's, resulting in high $(La/Lu)_{cn}$ ratios and quite 'steep' curves, typical of magmas produced by small amounts of partial melting of a garnet-rich source. The presence of garnet may also have given rise to the negative Yb anomalies seen in many of the samples. Negative Eu anomalies occur in many, though by no means all of the samples, and enables a broad division of the syenite units into two main groups. Field evidence suggests that those with a negative Eu anomaly seem to have been emplaced first, while samples with no anomaly tend to show cross-cutting relationships, and appear to have been emplaced later. Samples thought to represent chilled liquids from the main units (the Porphyritic Microsyenite and the marginal microsyenites) also show no Eu anomalies, suggesting that separation of plagioclase occurred following emplacement of the main units. A similar feature has been noted by Upton *et al.* (1985) in the border group of the Tugtutôq Older Giant Dyke Complex. Fractionation of other phases, particularly REE minerals, apatite, and possibly allanite, may have substantially modified the shape of the REE curve of the parent magma, to give rise to the observed trends.

CHAPTER 6: THE CARBONATITES

The carbonatite plug at Grønnedal-Íka represents the most significant single occurrence of this rock-type in the Gardar. Because of its importance, the field appearance, mineralogy, geochemistry, and petrogenesis are described here in a separate chapter to the other rocks of the complex.

6.1: Field appearance

Thought to have been emplaced as a single, centrally located 'plug' (map 2), the carbonatite now forms three main separate outcrops within the syenite as a result of faulting (map 1), and is generally poorly exposed, weathering to a gravel over most of the outcrop. However, it is well-exposed in the east wall above the Cirkus, in Urdal, and in the Hyttelv both above and below the Jernhat, where a continuous section through the carbonatite and adjacent Xenolithic Porphyritic Syenite can be seen. In addition, minor bodies of carbonatite are very abundant throughout the complex as veins and dykes, up to 1m across, especially in faulted areas. Emeleus (1964) considered that the presence of carbonatite along fault-planes is a result of plastic deformation and flow of the rock due to compressive forces associated with the faulting. Fieldwork in 1987 confirmed that the faulting post-dates the carbonatite, though since the movement was predominantly strike-slip, the compressional component of stress may have been relatively unimportant. This carbonate may have been deposited from fluids injected along the fault-plane, possibly remobilising and redepositing some original carbonatite as well. Carbonatite dykes, in particular, are common in the south-east of the complex, where they occur on both the north-east and south-west shores of Íka fjord, cutting the Upper Series Syenite and country-rock (eg. sample G107). One interesting exposure occurs in a faulted area to the north of the Radio lakes, where a small pond has considerably receded, probably as a result of dissolution and leakage through the underlying carbonatite.

On weathered surfaces, the rock is typically buff coloured, but it varies from white through cream to dark grey-brown, while fresh surfaces tend to be correspondingly less brown and paler in colour. The grain size varies from millimetre-sized, giving a søvitic rock, to finer-grained areas of alvikite, one type grading into the other over as little as a few tens of centimetres. Pegmatitic patches occur near the Jernhat, with crystals up to 15mm in size (plate 6.1), while a possible quench texture, with elongated prismatic crystals was observed in a loose block (plate 6.2).

Mineralogically, the carbonatites are fairly simple, with white or glassy calcite prisms forming up to nearly 100% of the rock (eg. sample G102), though other minerals can usually be seen in hand specimen. The commonest of these is magnetite, frequently occurring as millimetre-sized octahedra which weather clear of the surface, forming up to 50% of the rock by volume. The magnetite is thought to be a secondary mineral after siderite, as a result of decarbonation and oxidation in the vicinity of thick dolerite dykes which post-date the carbonatite. Observations that the modal proportion of magnetite increases towards the dykes appear to bear this out, as does the magnetic survey carried out around the major NE-SW–trending dyke near the Jernhat by J. Espersen (Bøgvad 1951, and fig. 13 from Emeleus 1964). Even in the absence of magnetite, the presence of iron is indicated by an interstitial red or ochrous mineral (eg. sample G52), possibly haematite. Copper sulphides are present in carbonatite exposures in the Hyttelv, but the commonest accessory after magnetite is a pale-coloured mineral, forming prismatic crystals a few centimetres long, often growing in bunches. It is easily visible, weathering clear of the surface of the carbonatite, hard, brittle, and very difficult to sample, although the hardness suggests that it is an alkali feldspar rather than barytes.

A particularly prominent feature of the carbonatite in almost all exposures is the presence of xenoliths of varying sizes (millimetres to tens of centimetres) and

Plate 6.1. Coarse pegmatitic patch in carbonatite outcrops in the Hyttelv, just below the Jernhat. The coarser, paler rock forming the pegmatite is in sharp contact with finer, darker (more siderite-rich) rock. Hammer head is 12cm long.

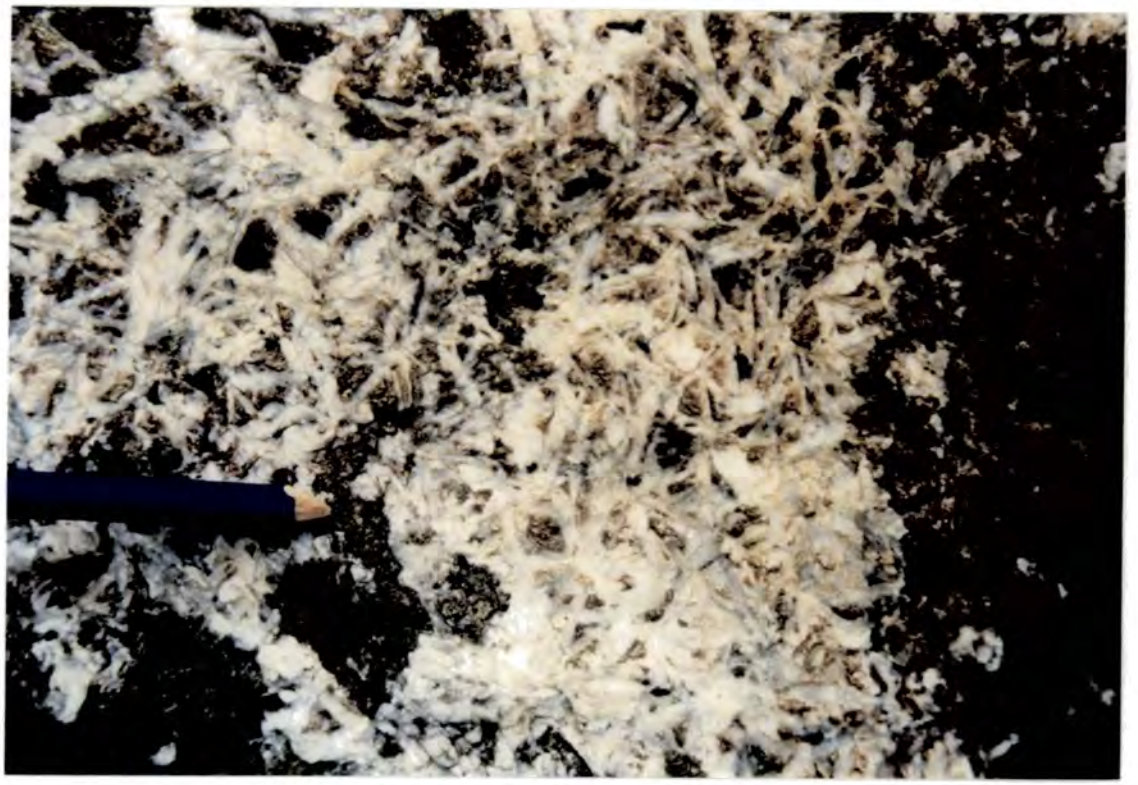

Plate 6.2. Bladed calcite crystals in loose block of carbonatite. This texture was not seen *in situ*, but is suggestive of a marginal quench facies, reminiscent of the harrisitic textures in the Isle of Rhum gabbros.

Plate 6.3. Flow-banded, xenolithic carbonatite (loose block). The xenoliths consist of recrystallised gneiss and syenite, while the flow-banding wrapping around the xenoliths is picked out by trails of magnetite. Hammer head is 12cm long.

Plate 6.4. Truncation of flow banding by thin basaltic dykes, 500m south-west of the Jernhat. The banding does not appear to be disrupted, suggesting that remobilisation, a common occurrence near the larger basic dykes, did not take place. Hammer shaft is 60cm long.

lithologies, the proportion of which increases towards the margins, where exposures show xenoliths in the process of being detached. The effects of carbonation are well seen here, with a network of very fine carbonate veins pervading and impregnating the country-rock (the areas shown as blue stipple on map 1). Both gneiss and syenite are present as xenoliths, though it is often difficult to distinguish between the two as a result of carbonation, recrystallisation, and staining. Rims of iron oxide around the xenoliths suggests strongly oxidising conditions in the carbonatite magma.

One other important feature of the carbonatites is the presence of flow-banding, picked out on weathered surfaces by trails of magnetite and iron-rich carbonate (siderite), wrapping around any xenoliths present (plate 6.3), which may themselves be entrained into layers. This flow-banding is occasionally highly contorted though usually straight or gently undulating in outcrop, and undisturbed by later small-scale dykes which cut straight across the magnetite trails (plate 6.4). Bailey (1966) suggests that banding and streaking-out of xenoliths in carbonatite plugs from Zambia is a result of solid-state emplacement.

6.2: Petrography

The dominant mineral of the carbonatites is calcium carbonate, forming almost 100% of the rock in places, with coarse crystals up to 5mm across, generally anhedral or subhedral, and occasional euhedral grains with rhomboid terminations (sample G53). As mentioned in the previous section, the rock is thus classified as a søvite (Streckeisen 1980). Polysynthetic twinning is commonly seen in the carbonate crystals, the twin lamellae are often curved, and the grains show shadowy extinction (plate 6.5). In addition, sample G74 shows a marked directional fabric, with elongation of the calcite grains up to five times the width of the crystal, and zones of reduced grain-size (down to 80μm) parallel to the direction of elongation. These all seem to suggest that the carbonatite has suffered a certain amount of

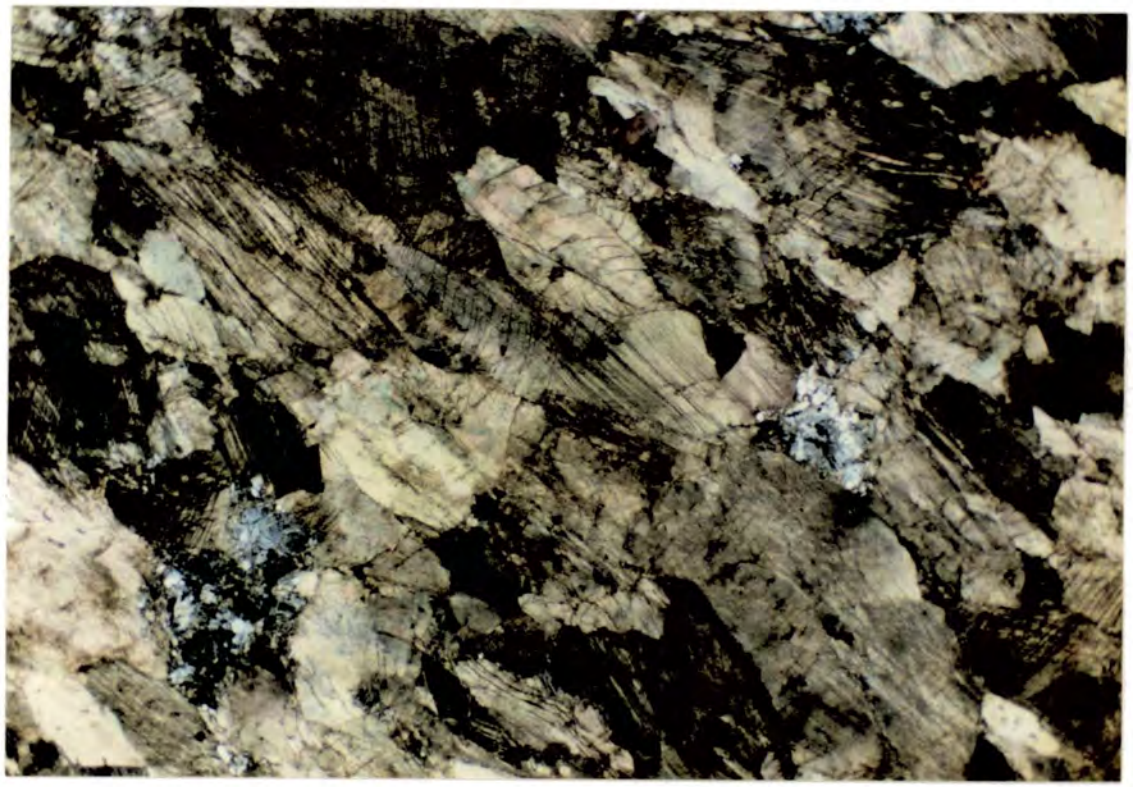

Plate 6.5. G52. ×11. XPL. Typical carbonatite, consisting mainly of calcite (note gently curved twin lamellae) and occasional interstitial silicates (alkali feldspar). There is a suggestion of a directional fabric, from top left to bottom right in this section.

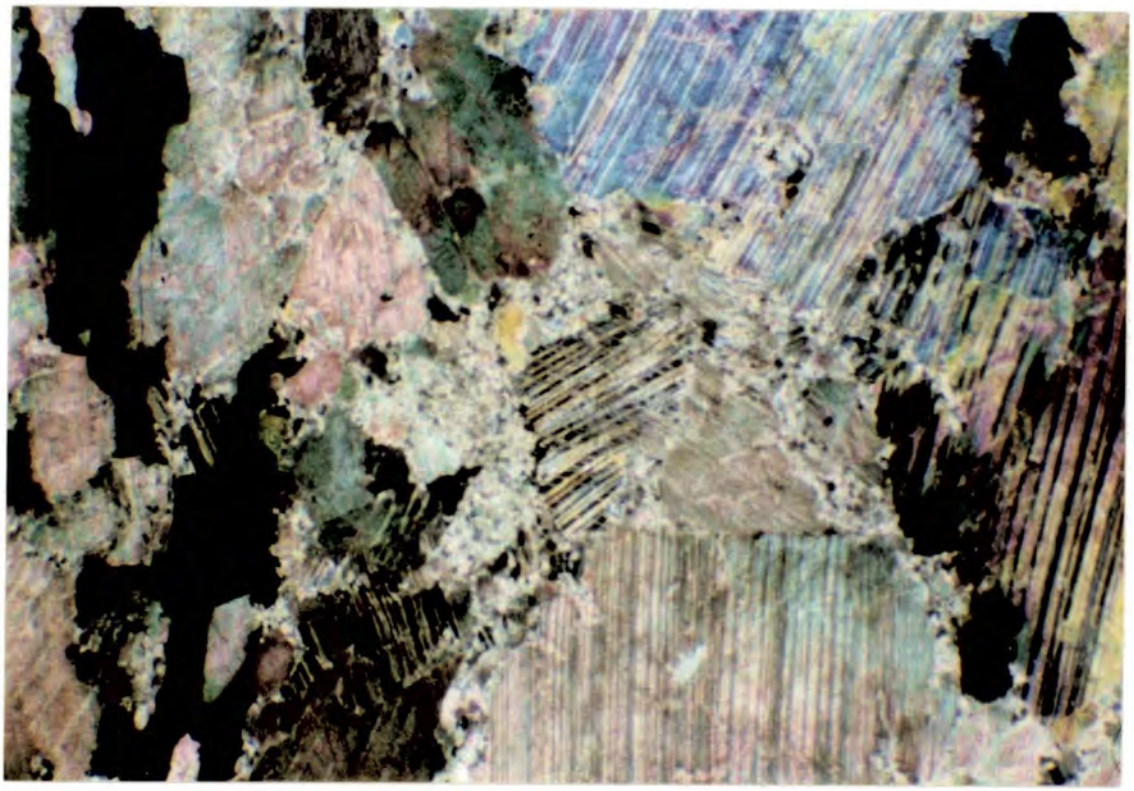

Plate 6.6. G47. ×35. XPL. Carbonatite from adjacent to an alkaline dyke. Opaque grains are visible on the left and right of the field of view, but the most important feature of this sample is the presence of grain-boundary recrystallisation and ductile fracture (see text for explanation).

deformation, either due to adjacent dyke emplacement (which could have produced the textures in G74, due to its proximity to a dyke), later fault movement, or intrusion of the carbonatite as a partly crystallised magma. As plate 6.4 shows, the dykes cut straight across the carbonatite flow-banding with apparently little effect, while if a result of faulting, rocks 300m away from the nearest fault zone are affected, and samples nearer to the same zone are less strongly deformed. The strain was thus probably imparted to the calcite crystals during emplacement of the magma in the majority of cases (cf. Bailey *op. cit.*).

Granoblastic recrystallisation textures are present in some samples, notably G56 and G133, which occur as carbonatite slivers in the large dolerite dyke to the west of the Langesø outlet. The recrystallised, polygonal grains are relatively small, most being in the range 200–300μm, though some coarser, relict calcite grains remain. Grain-boundary recrystallisation is evident in G47, a sample from an outcrop adjacent to an alkaline dyke to the north of the Radio lakes (map 3 and plate 6.6). Restriction of the recrystallisation to the intergranular areas suggests that it was fluid-enhanced, the fluids possibly emanating from the dyke. This type of recrystallisation is not observed adjacent to the much larger basic dykes, possibly due to their lower volatile content. In addition, G47 also shows gently curved calcite twin lamellae and ductile fracture due to work-hardening as a result of strain at relatively high temperatures.

As mentioned in section 6.1, magnetite (after siderite) is a common mineral seen at carbonatite outcrops, increasing in abundance in areas of dyke emplacement. In thin-section, the magnetite usually occurs as amorphous areas up to 1 or 2mm across, though it sometimes picks out the cleavages in grains of siderite (sample G55). In reflected light, however, these areas of magnetite are usually seen to consist of a mass of granular crystals, each around 20–500μm across. The siderite is sometimes difficult to distinguish from calcite, and occurs only sparingly, having usually been altered to magnetite. It commonly occurs as minute

grains 20–50μm across, or as euhedral rhombs in G55 and G30, and occasionally as coarser euhedral crystals in G55, comparable in size to the calcite (plate 6.7). It has a higher relief than the calcite, and can also be stained a rusty-brown due to slight alteration to oxides of iron, presumably at lower temperatures than are required for the formation of magnetite. In sample G30, the smaller siderite rhombs are concentrated along grain-boundaries between the calcite crystals. Iron-rich carbonatites (ferrocarbonatites) can be derived from carbonatite magmas by advanced fractional crystallisation, so the interstitial nature of the grains in G30 may be due to late-stage crystallisation. Alternatively, Le Bas (1987) suggests that the late-stage residue from carbonatite fractionation may be so rich in volatiles that it behaves not as a melt, but as a fluid which can penetrate along crystal boundaries, gradually replacing the primary calcites. The siderite grains in G30 do appear to be replacing the larger calcites, so that this mechanism may have operated, the residual iron-rich fluids affecting the earlier formed calcite-carbonatite.

Silicate minerals make up less than about 5% of most samples, the commonest being feldspar grains up to *c.*0.5mm across, with shadowy extinction, and plagioclase twinning. These are interstitial to the calcite grains, and appear to have crystallised from trapped residual liquids (plate 6.5). Very pale-green aegirine occurs as small subhedral grains *c.*300μm across, and as radiating acicular needles in bunches up to 1mm across (samples 39709 and G107 respectively, plate 6.8). Deep-blue, acicular needles of alkali amphibole also occur in 39709, while a green, chloritic alteration material, probably after original ferromagnesian silicates, occurs in many other samples.

Apatite is the only common non-silicate accessory mineral, occurring in bunches along the carbonate grain-boundaries, though in G101, interstitial barytes possibly occurs (colourless, high relief, prismatic cross-section).

In contrast with many carbonatites of the world, the rock at Grønnedal-Íka is surprisingly poor in U-Th-Nb-Zr-REE minerals, though zircon grains and an

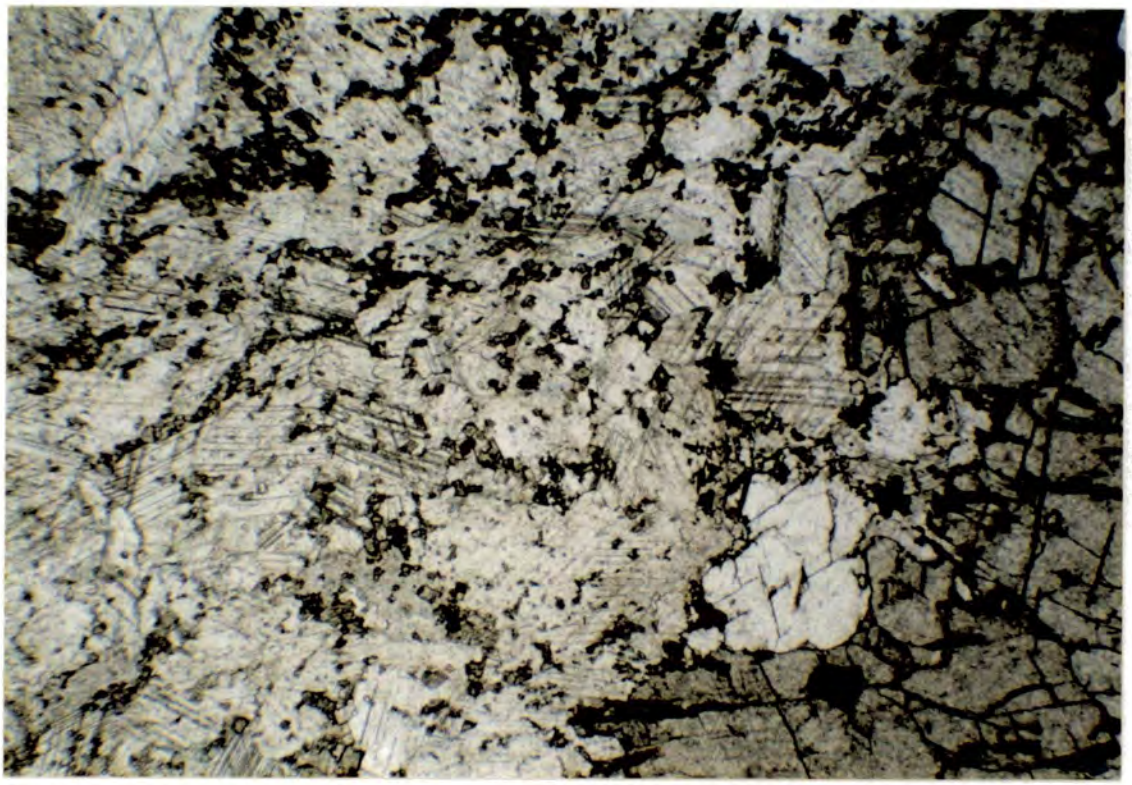

Plate 6.7. G55. ×11. PPL. Siderite (darker grey) with haematite along the cleavage planes. The paler coloured calcite can easily be distinguished, and much smaller rhombs of siderite within the calcite can just be made out.

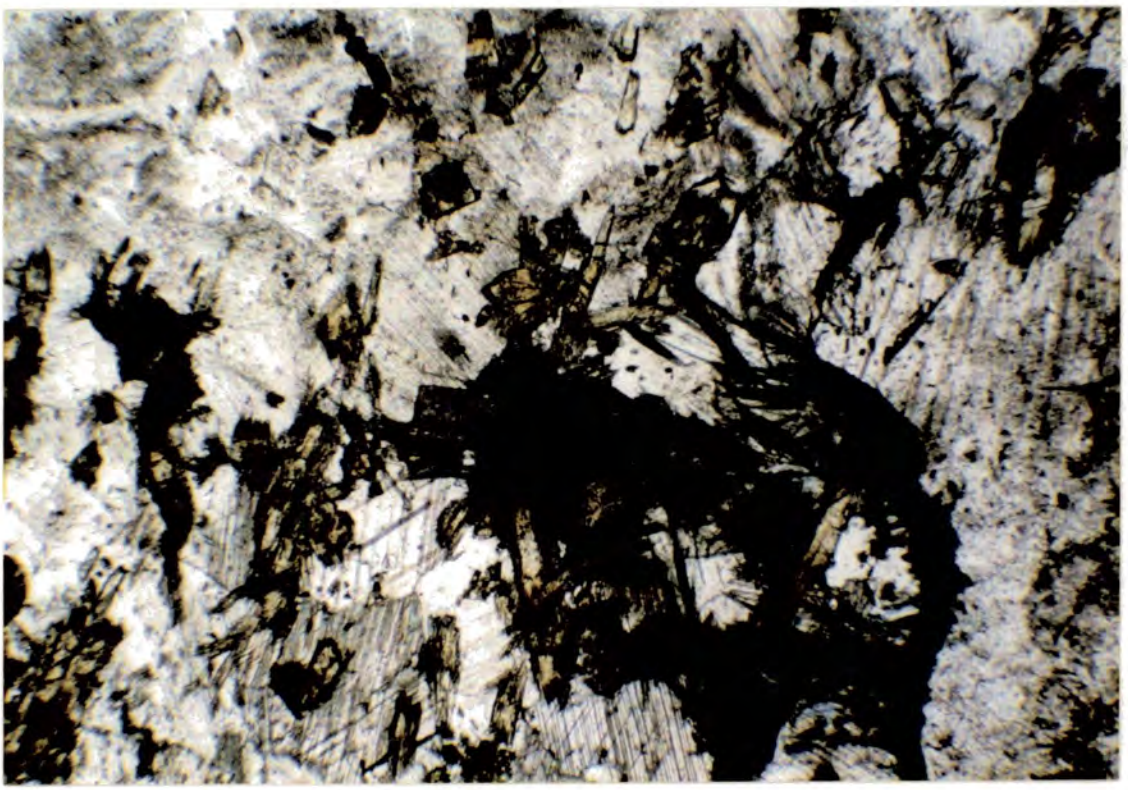

Plate 6.8. 39709. ×35. PPL. Ferromagnesian mineralogy of the carbonatites. Deep blue, acicular alkali-amphibole, and pale green-yellow pyroxene grains.

orange, isotropic, slightly zoned, rhombic grain 150μm across occurs in G265. Brown pleochroic haloes in micaceous grains in G74 indicate the presence of small radioactive element-bearing grains, though even these may simply be zircon.

6.3: Mineralogy

Analyses of the carbonatite minerals were carried out at Edinburgh and Durham, using the same operating conditions as for the syenites, which are described in Appendix II. Recalculations and site-assignments (for the amphiboles) were carried out using the programs described in chapter 4, and are illustrated in fig. 6.3.1.

6.3.1: Pyroxenes

Pyroxenes are the most abundant mafic phase in the carbonatites, though were observed in only two samples (39709 and G107). Very pale green-yellow in plane-polarised light, they are highly sodic and very restricted in composition, containing *Ac* >92 mol.%. This contrasts with trends from the Igaliko carbonatite dykes (Pearce 1988) which do not exceed Ac_{20}, and from the Fen complex (Andersen 1988), which show a wide range of compositions (fig. 6.3.1A).

Compared to the Grønnedal-Íka syenites, the carbonatite pyroxenes have very low Al contents (less than 0.1 atoms per six oxygens, ≈2.2% oxide), though not as low as the 0.2%–1.3% in the Fen carbonatite (Andersen *op. cit.*). In addition, those from Grønnedal also contain very low amounts of Mn (less than 0.16% MnO), contrasting with the pyroxenes from the Igaliko dykes, which contain up to 8.8% MnO (0.288 atoms per 6(O), Pearce *op. cit.*).

6.3.2: Amphiboles

Amphibole is an important phase in some carbonatites (Le Bas 1981), often occurring to the exclusion of pyroxene (eg. at Sarfartôq, Secher and Larsen 1980). However, Pearce (1988) found amphibole in only one sample of a carbonatite dyke from Igaliko, and it is not common at Grønnedal-Íka: only four analyses were made

Fig. 6.3.1. Carbonatite mineral analyses, plotted in terms of molecular proportions.

A. Pyroxenes. Mg–(Fe^{2+}+Mn)–Na. All are rich in Na, most compositions plotting at the evolved end of the 'average' trend of the syenitic pyroxenes. Compositional fields of pyroxenes from other carbonatite complexes (Igaliko and Fen) are shown for comparison.

B. Oxides. $RO–R_2O_3–RO_2$. Molecular end-members re-calculated using the method of Carmichael (1967). All analyses lie close to the magnetite-rich end of the *mgt-üsp* series.

C. Feldspars. $Ab–Or–An$. The majority of compositions are albitic, although a few orthoclase-rich analyses are present. One analysis contains roughly equal molecular proportions of Ab and Or.

D. Carbonates. Ca–Mg–Fe. Most compositions are almost pure calcite, although a few sideritic grains were analysed. The calcites contain only traces of Mg, while the siderites contain a few percent of this element.

Fig. 6.3.1

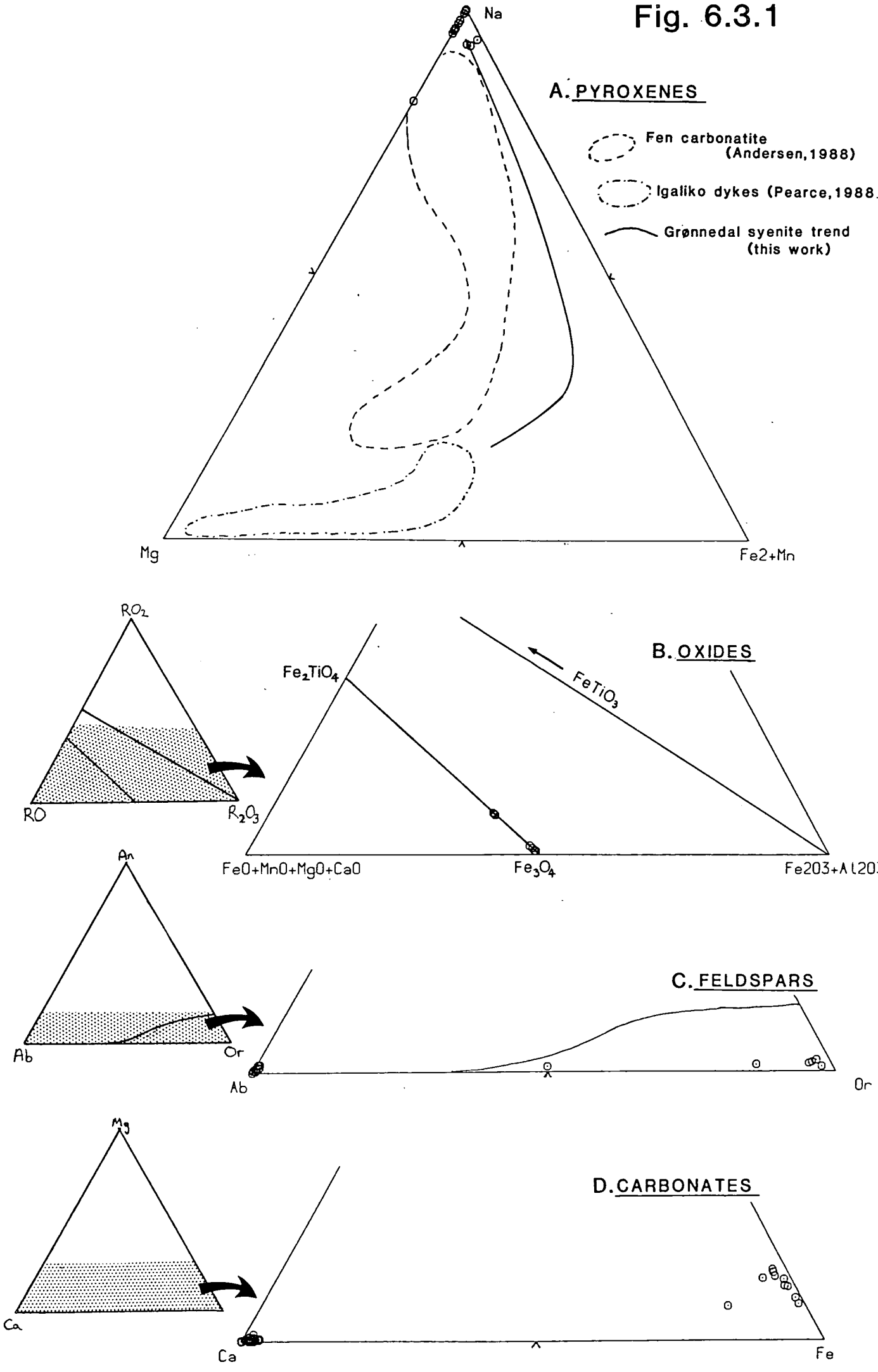
Na
A. PYROXENES
Fen carbonatite (Andersen,1988)
Igaliko dykes (Pearce,1988)
Grønnedal syenite trend (this work)
Mg
Fe2+Mn
RO2
RO
R2O3
B. OXIDES
Fe2TiO4
FeTiO3
FeO+MnO+MgO+CaO
Fe3O4
Fe2O3+Al2O
An
Ab
Or
C. FELDSPARS
Ab
Or
Mg
Ca
D. CARBONATES
Ca
Fe

from a single carbonatite sample (39709, plate 6.8). After recalculation and site assignment, these were found to be arfvedsonites/magnesio-arfvedsonites, which according to Heinrich (1966) are very rare in carbonatites, though they have been reported by Secher and Larsen (*op. cit.*) from Sarfartôq.

The amphiboles from Grønnedal are very siliceous (Si_T >7.9 atoms per 23 oxygens), and consequently poor in Al (Al_T <0.1 atoms per 23(O)), suggesting highly evolved compositions as a result of the exchange $Na_B+Si_T \rightleftharpoons Ca_B+Al_T$. Ti values are also very low compared to those in amphiboles from the syenites (Ti_C <0.03 atoms, compared to Ti_C ≈0.1-0.3 atoms per 23(O) in the syenites), also suggesting high degrees of fractionation, and according to Helz (1973) implies a low temperature of equilibration. Low Ti and Al contents are also characteristic of the amphiboles from the carbonatites of the Igaliko dykes (Pearce *op. cit.*) and Sarfartôq (Secher and Larsen *op. cit.*), though unlike those from Igaliko, the Grønnedal analyses are low in Mn.

6.3.3: Oxides

Seven analyses of opaque oxides from two samples (G103 and G265) were made, and found to be members of the magnetite-ülvospinel series (fig. 6.3.1B). Gaspar and Wyllie (1983) point out that oxide minerals ("compositionally close to pure magnetite", Mitchell (1979)) are characteristic of all carbonatites, though as discussed in section 6.1, the increase in proportion of magnetite nearer to the basic dykes suggests that it may be a secondary mineral, as a result of decarbonation and oxidation of siderite.

The analyses show a close grouping within each sample, those from G265 containing >96% *mgt* (molecular per cent), while those from G103 contain around 84% *mgt*. The latter is richer in Si and poorer in Mn, despite more of the ülvospinel component, presumably as a result of the substitution of these elements for Ti and Fe^{2+}. MnO is around 1.5% in G103, comparable to analyses from Jacupiranga

(Gaspar and Wyllie *op. cit.*), compared to negligible quantities in G265, while Mg abundances (typically around 0.5% MgO) are generally lower than those from Jacupiranga. TiO_2 does not exceed 1% in any of the analyses, which one might expect if the oxides were primarily derived from decarbonated siderite, as the latter contains negligible quantities of Ti (Deer *et al.*, 1966).

6.3.4: Feldspars

Alkali feldspar is a minor, but moderately common phase in the Grønnedal-Íka carbonatite, although Heinrich (1966) suggests that the mineral is generally widespread in carbonatites. Potassium feldspar is invariably present in the marginal carbonatite dykes at Sarfartôq (Secher and Larsen 1980), though the majority of alkali feldspars at Grønnedal are albitic, with Na>0.92 atoms per 8(O) (fig. 6.3.1C), reflecting the whole rock composition of the carbonatite ($Na_2O > K_2O$ in general, section 6.4.2). The remainder of compositions are potassium-rich, with one analysis showing $Ab \approx Or$ (Ab/Or=1.05). The occurrence of albite in the carbonatite at Grønnedal is rather unusual, although it has also been found in carbonatites from Ravelli county (Montana), and Seiland (Norway), but is generally a rather rare phase in this type of rock (Heinrich 1966). BaO and CaO are present in only trace quantities, neither exceeding 0.5% by weight.

6.3.5: Carbonates

Carbonate minerals comprise more than 50% of a true carbonatite (Streckeisen 1980), and at Grønnedal-Íka, the majority are calcites with little solid-solution with siderite (fig. 6.3.1D). Separate siderite crystals are present, however, although Heinrich (1966) suggests that this mineral is often destroyed during deuteric alteration, and as described in section 6.1, has usually been altered to magnetite. Very little MgO occurs in the calcites (generally <0.5%), while in the siderites, up to 4.7% MgO may be present. MnO occurs up to 4.9%, and shows

no preference for either siderite or calcite, while Na_2O and BaO are present in amounts less than 0.5%. Analysis of Sr was attempted, but difficulties were encountered due to the inability of the EDS detector to resolve the Sr L and Si K peaks.

No other separate carbonate phases, such as dolomite, witherite, ankerite, rhodochrosite, or strontianite, were observed.

6.3.6: Other minerals

REE Minerals

Exotic phases such as pyrochlore, monazite, and columbite, which are "moderately common" according to Heinrich (1966) are rather rare in the Grønnedal-Íka carbonatite. Whole-rock REE abundances are comparable to those of other intrusive carbonatites (Le Bas 1981), and are possibly present in minute interstitial grains of 'exotics', or in solid solution in apatite or calcite (eg. Maravic and Morteani 1980)

Discrete REE-rich grains of pyrochlore, which also contain Ca and Na, as well as U, Th, and Nb occur in G265 and G52. Whole-rock trace element abundances in these samples are consistent with the occurrence of such a mineral.

Apatite

Apatite occurs in a few of the carbonatites, although analyses were not carried out due to lack of time. REE determinations for this phase would be interesting, as Speer and Ribbe (1982) have shown that substantial amounts of REE's can enter the apatite lattice, giving rise to britholite (section 4.9). In view of the rarity of other possible host minerals, this could explain the high whole-rock REE contents observed in the carbonatites (section 6.4.4).

Sulphides

Pyrite is the most commonly occurring sulphide in carbonatites according to Heinrich (1966), and has been analysed in G46, while a solid-solution between Zn and Fe sulphides occurs in G107. A Co-Ni-Fe sulphide has also been analysed in the latter, although since the Durham microprobe was not standardised for sulphides, quantitative determinations could not be carried out.

Quartz

Very high SiO_2 contents (15.2%) in G107 reflect the presence of quartz, though the mineral is probably of secondary origin (Heinrich 1966). This sample is from a dyke within country rock metasediments on the south-east side of Íka fjord and also one of the very few carbonatites to contain pyroxenes. It thus seems likely that the quartz is a result of contamination by basement rocks.

6.4: Geochemistry

6.4.1: Introduction

Twenty-five samples of 'carbonatite', ie. rocks containing more than 50% carbonate minerals by weight (Streckeisen 1980), were analysed for ten major elements and eighteen trace elements, as for the syenites (Appendix III).

Major element analyses were carried out on fused beads made from samples which had been heated at 1050°C for two hours. The final analyses were then scaled-down accordingly, knowing the loss-on-ignition (LOI) values for the samples. Trace elements were analysed from pressed pellets made from powdered samples, as for the syenites. Seven carbonatites from the Igaliko dyke swarm with totals (including traces) of 100±0.3%, which were analysed by Pearce (1988), were used as standards, the compositions of which are listed in Appendix III, table III.3.

LOI values vary between 26% and 43% of the dry weight of the sample, and for comparison, pure $CaCO_3$ would have a LOI of 44.0%. Major element totals,

including LOI's, are less than 100% by up to 3%, as a result of the relatively large proportion of trace elements which are typical of carbonatites.

6.4.2: Major element variation

A classification of carbonatites based on whole-rock CaO, MgO, and total Fe was proposed by Woolley (1982), and all analyses are plotted using these parameters in fig. 6.4.1. More than three-quarters of the samples are classified as søvites using this scheme, the remainder being ferrocarbonatites, with generally very little enrichment in MgO. Sample G29 is somewhat anomalous, lying away from the main 'trend', and contains 10.8% MgO compared to a maximum of 1.26% MgO in the majority of carbonatite samples. Petrographic observations suggest that this sample is a highly carbonated rock, rather than a true carbonatite, although the LOI of 26.6% would imply that it probably contains more than 50% carbonate, and is therefore a carbonatite according to Streckeisen (*op. cit.*). Many other aspects of its geochemistry are similarly extreme, with the highest values of SiO_2, Al_2O_3, MgO, K_2O, and TiO_2 observed, together with low CaO. The petrography and geochemistry suggest that the original rock probably had basic affinities, and was possibly one of the Brown Dykes which are caught up in the intense faulting near the head of the Bryggerens Elv (map 1, and Emeleus 1964), and has been affected by later CO_2-rich fluids (cf. chapter 7). It is retained more for comparative purposes than as an attempt to relate its geochemistry to that of the other carbonatites.

The strong coherence of the analyses in this system is comparable to carbonatites from the Igaliko dykes (Pearce 1988), West Kenya (Le Bas 1977), and Tundulu, in Malawi (Garson 1962), though the Grønnedal carbonatites are less strongly enriched in MgO than in most of these examples. Field relationships at many localities tend to indicate a series from søvite to more Mg and Fe-rich carbonatites, Garson's (1962) data from Tundulu suggesting that the trend away from CaO corresponds with the order of emplacement (Woolley 1982). By way

Fig. 6.4.1. Carbonatite classification based on Fe_2O_3+MnO, MgO, and CaO whole-rock contents (after Woolley 1982). The majority of analyses are MgO-poor søvites, the remainder lying in the ferrocarbonatite field. Sample G29 is anomalous, and perhaps more akin to the metasomatised rocks described in chapter 7, although it probably contains more than 50% carbonate by weight. The trend of increasing iron enrichment is accompanied by a slight increase in MgO.

GRONNEDAL-IKA CARBONATITES

CLASSIFICATION

Fe2O3+MnO - MgO - CaO
weight %

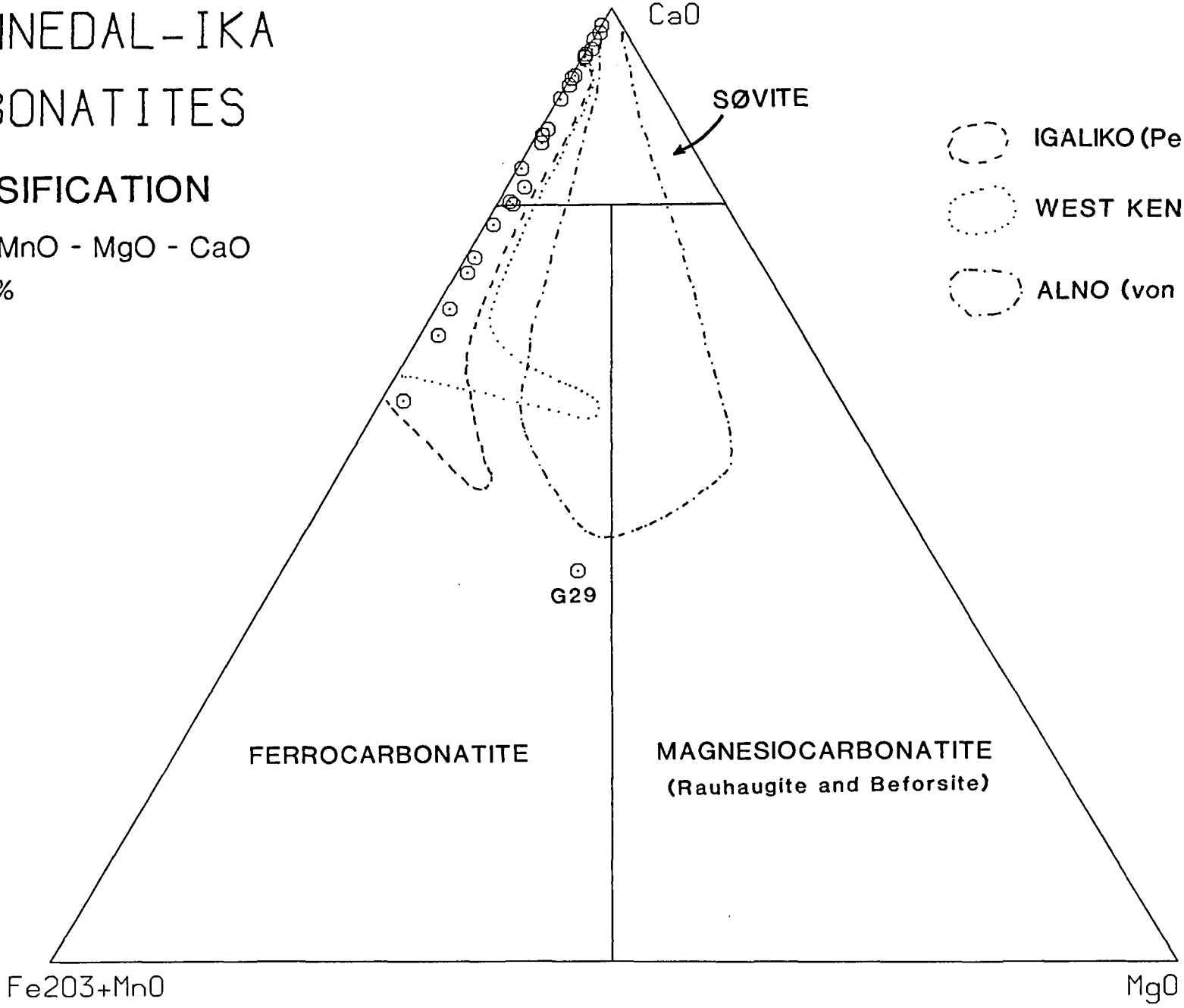

Fig. 6.4.1

of comparison, the very similar trend of analyses from the Grønnedal carbonatite could also be interpreted as one of increasing Fe and slight Mg enrichment, although field evidence for any order of emplacement is unclear due to faulting and poor exposure. However, following reconstruction of the complex (map 2), Emeleus (1964) suggested that the carbonatite within the plug becomes more sideritic towards the centre. Such an observation would be compatible with a model involving crystallisation which proceeds from the sides, with more fractionated, Fe-rich carbonatites occurring towards the core.

Le Bas (1981, 1987) describes the evolution of carbonatite compositions in the system ($MgO+\Sigma Fe$)–CaO–(Na_2O+K_2O), beginning from a hypothetical alkali-rich parent, comparable in composition to natrocarbonatite lava from Oldoinyo Lengai (fig. 6.4.2A). He suggests that this loses alkalis by fenitisation, and evolves towards more calcic (søvitic) compositions with increasing loss of alkalis. A change to evolution by a mechanism of fractional crystallisation is then suggested, giving rise to increasingly Fe and Mg-rich compositions as suggested by Woolley (1982) and described above.

Samples of the Grønnedal-Íka carbonatite are generally very poor in alkalis ($Na_2O+K_2O<1.3\%$, ignoring G29). According to Le Bas (1987), these would have been lost during fenitisation, while Twyman and Gittins (1987) take an opposing view, suggesting that they were not initially present. The trend towards increasing Fe enrichment shown by the Grønnedal carbonatites shown in fig. 6.4.2 would thus have been produced by fractional crystallisation according to Le Bas (*op. cit.*). These alternative ideas concerning the evolution of carbonatites in general are discussed more fully in section 6.5.

Other elements

Other major elements are present in small quantities, as set out in the table below (ignoring G29).

Fig. 6.4.2A. Evolution of carbonatite magmas from parental natrocarbonatite (after Le Bas 1981). Alkali-loss gives rise to wall-rock fenitisation, and is followed by fractional crystallisation leading to iron enrichment. Carbonatite analyses from Grønnedal plot on the alkali-free base line, and extend from CaO-rich (søvitic) to Fe-rich (ferrocarbonatite) compositions. The dominant process in the development of different carbonatite compositions at Grønnedal thus seems to be fractional crystallisation.

Fig. 6.4.2B. Variation of Al_2O_3 against SiO_2. The sympathetic variation between these two parameters probably reflects the presence of alumino-silicates in the rock, mainly as alkali feldspar.

Fig. 6.4.2A

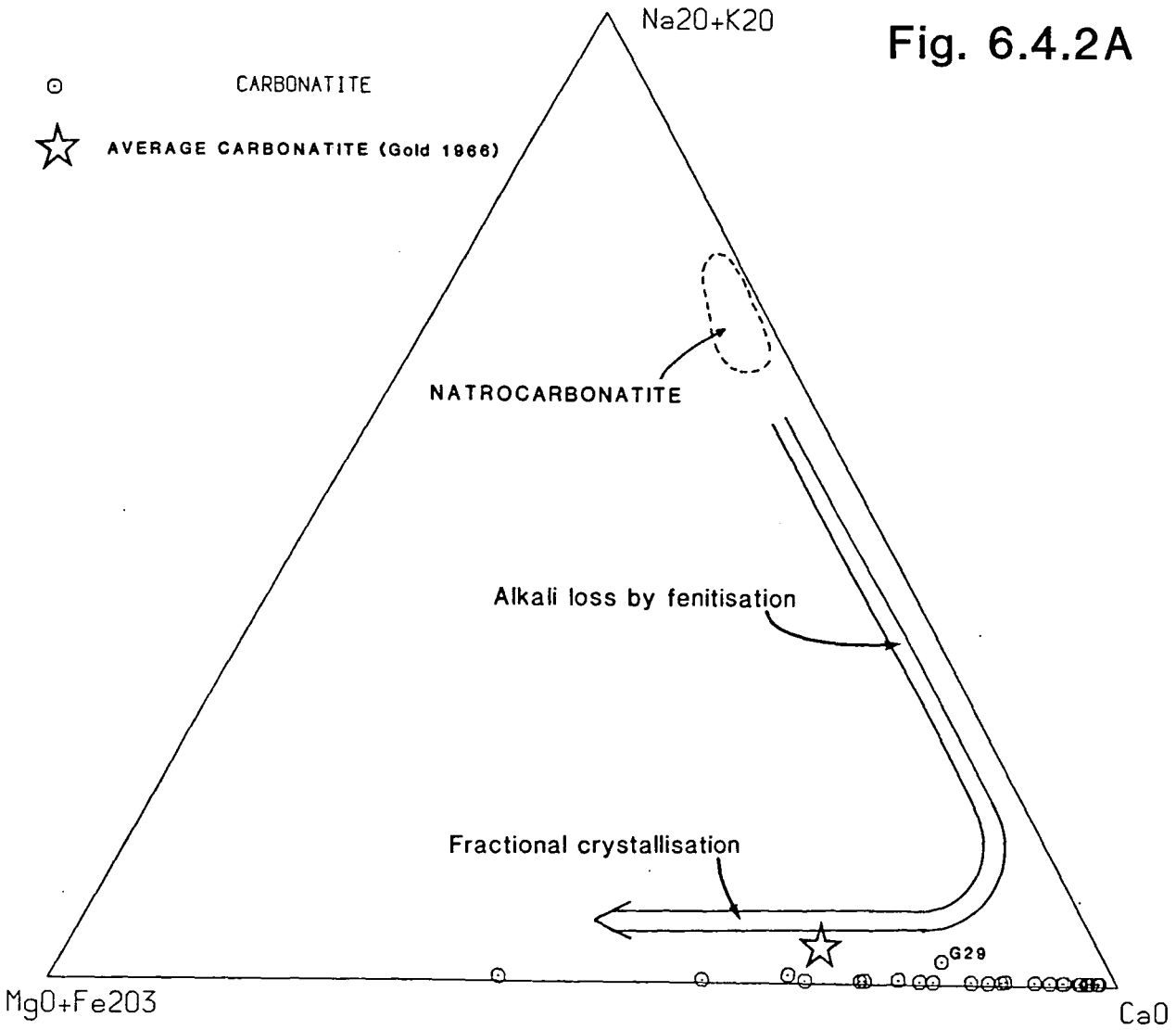

Fig. 6.4.2B

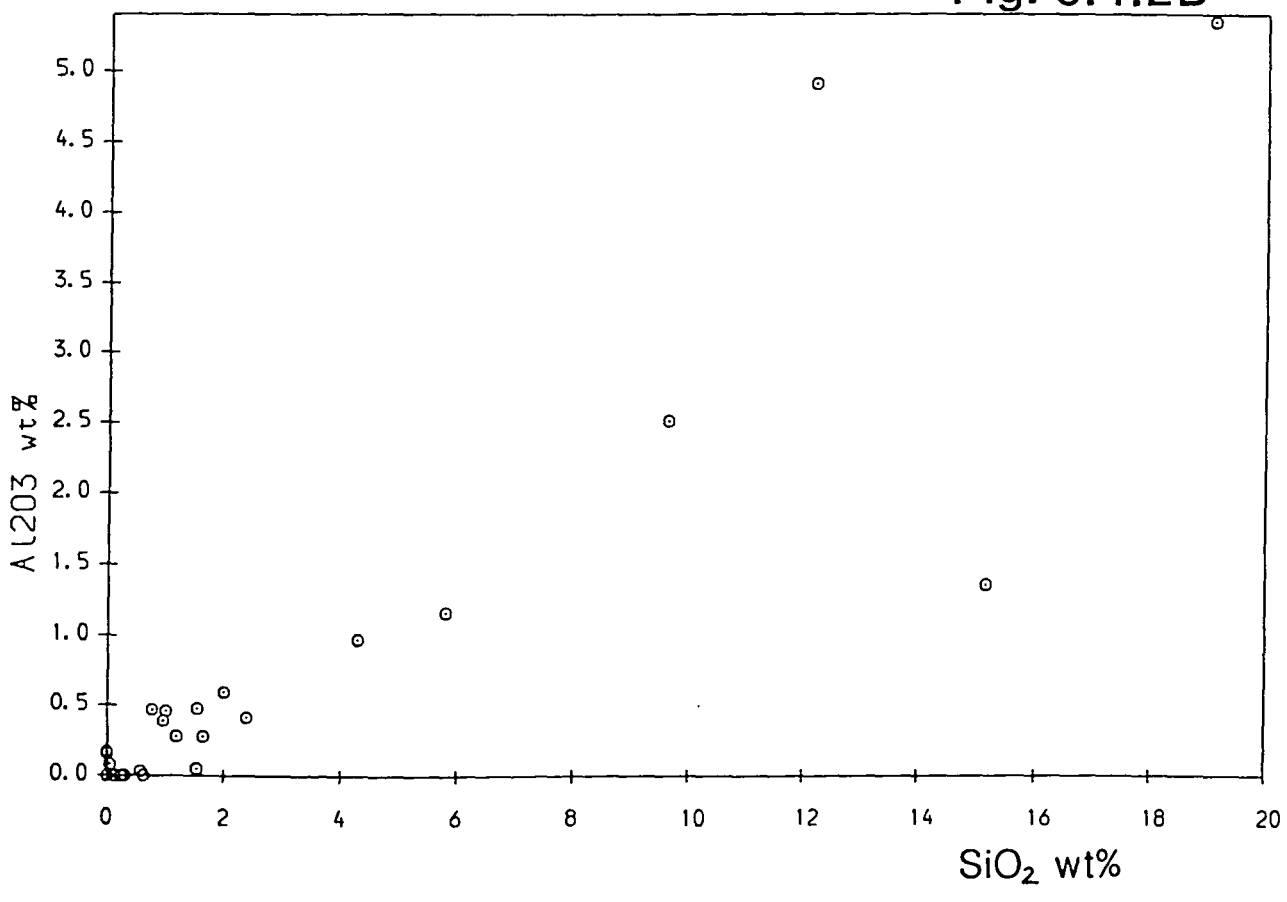

Oxide (wt.%)	Average carbonatite (Gold 1963)	W.Kenya Le Bas (1977)	Grønnedal (maximum)	Grønnedal (average)
SiO_2	12.10	0.83	15.16	2.59
Al_2O_3	3.55	0.65	4.91	0.62
TiO_2	0.80	0.07	0.10	0.04
MnO	0.61	5.53	2.93	1.27
P_2O_5	2.06	0.42	3.64	1.27

As can be seen, the 'average' abundances of these elements from the Grønnedal-Íka carbonatite are comparable to the two examples given above.

When plotted against SiO_2 (a good parameter, as it shows a relatively large range of values), only Al_2O_3 shows any correlation, showing an increase with increasing SiO_2 (fig. 6.4.2B). Al and Si are probably present mainly in alkali feldspars in carbonatites, and therefore not surprisingly show a sympathetic variation, controlled mainly by the modal abundance of this phase.

6.4.3: Trace element and incompatible element variations

Trace elements may be usefully illustrated in the form of 'spidergrams' (fig. 6.4.3), which show ten of the eighteen trace elements and three of the 'major elements' (P, K, and Ti) normalised to chondritic abundances (taken from Thompson 1982). Elements on the abscissa are arranged roughly in order of increasing compatibility in a four phase lherzolite ($ol + cpx + opx + gt$) undergoing partial melting (Wilson 1989) from left to right.

Those trace elements not shown on the spidergrams (Zn, Cu, Ni, Pb, U, V, Cr, and Ga) are, apart from Zn and U, generally present in insignificant quantities of only a few ppm. Occasional anomalies do occur, however, usually in sample G29, which contains the greatest amounts of Ni, Cu, V, Cr, Pb, and Ga. Cu is a difficult element to analyse accurately, all samples (apart from G29) giving

Fig. 6.4.3

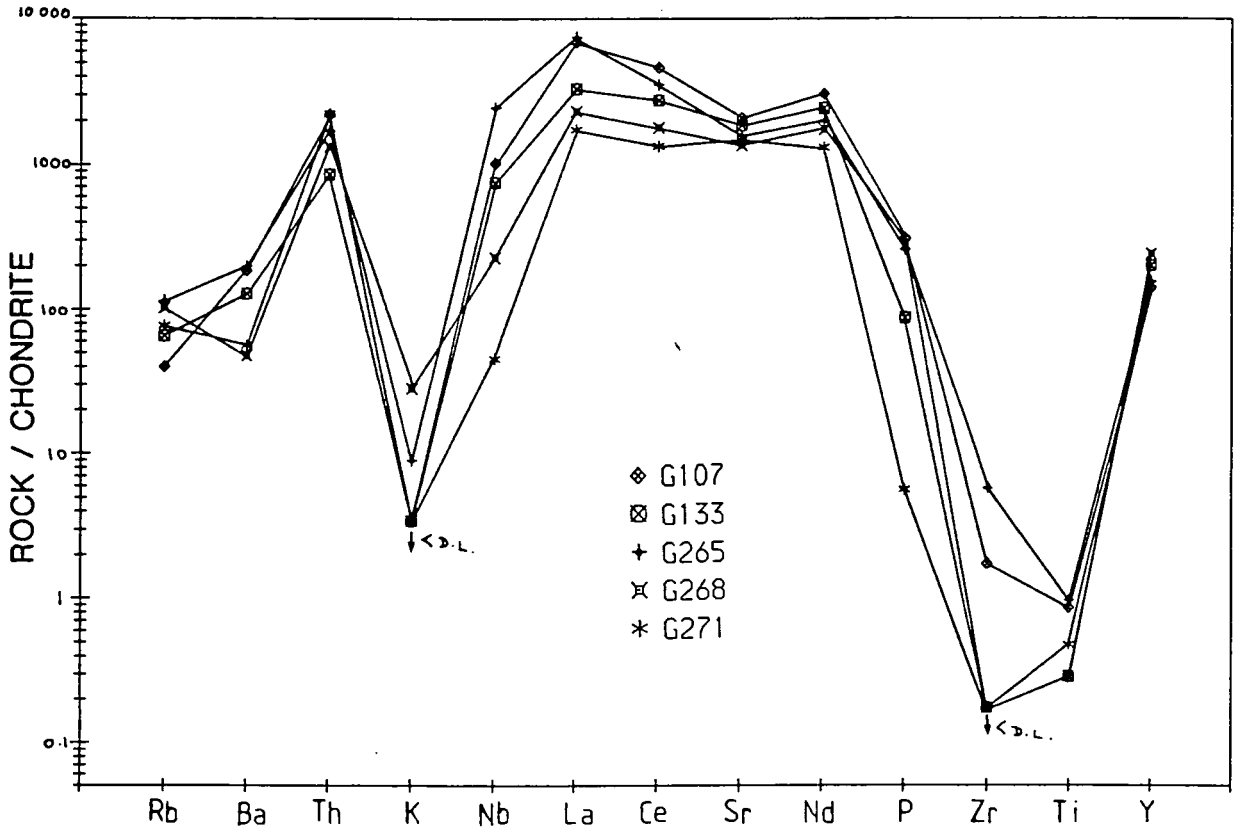

Fig. 6.4.3.(three pages) Incompatible element 'spidergrams' for all 25 carbonatite samples analysed, normalised using chondritic abundances of Thompson (1982). All show comparable trends, which are characterised by high Ba, Sr, Th, Nb, REE's, and Y, and very low K, Zr, and Ti. Where the abundance of these elements falls below detection limit, this is indicated by ↓<D.L.

Fig. 6.4.3 (cont.)

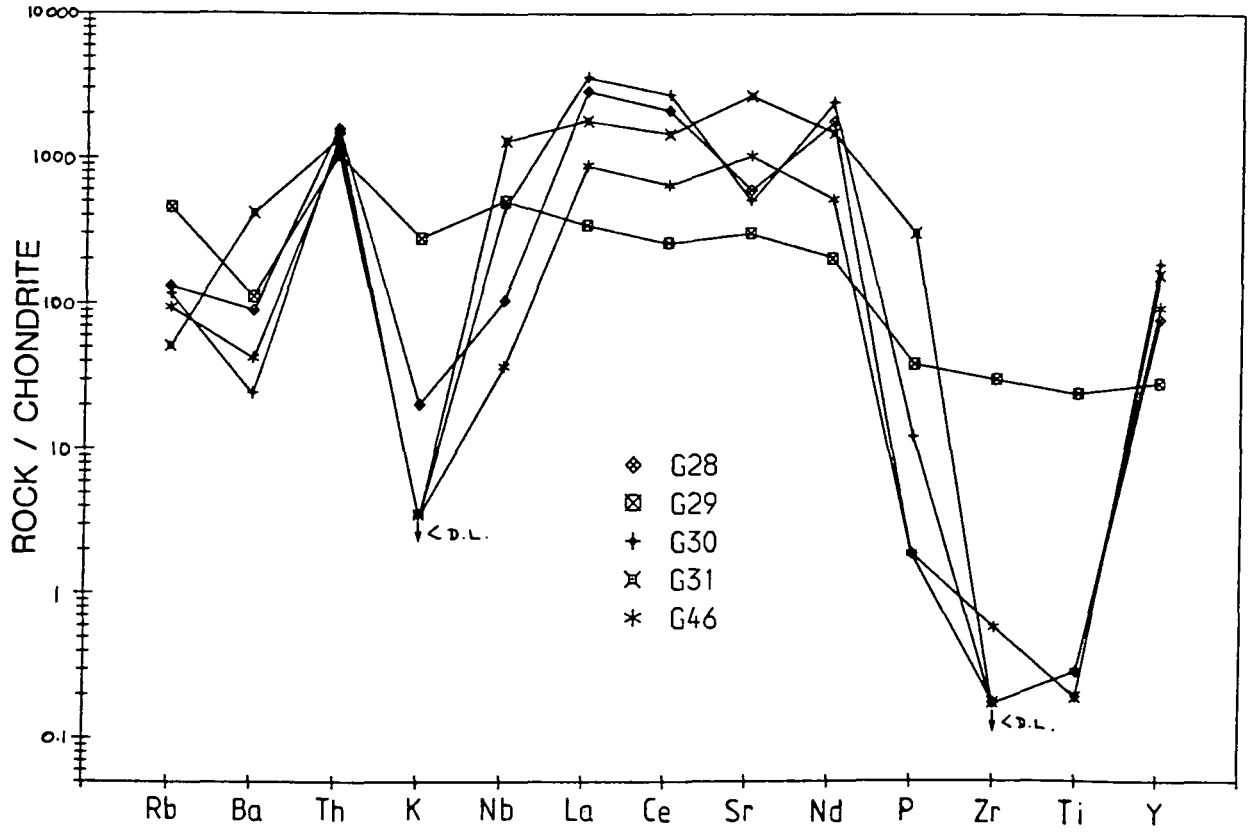
ROCK / CHONDRITE
10000
1000
100
10
1
0.1
G28
G29
G30
G31
G46
<D.L.
<D.L.
Rb
Ba
Th
K
Nb
La
Ce
Sr
Nd
P
Zr
Ti
Y

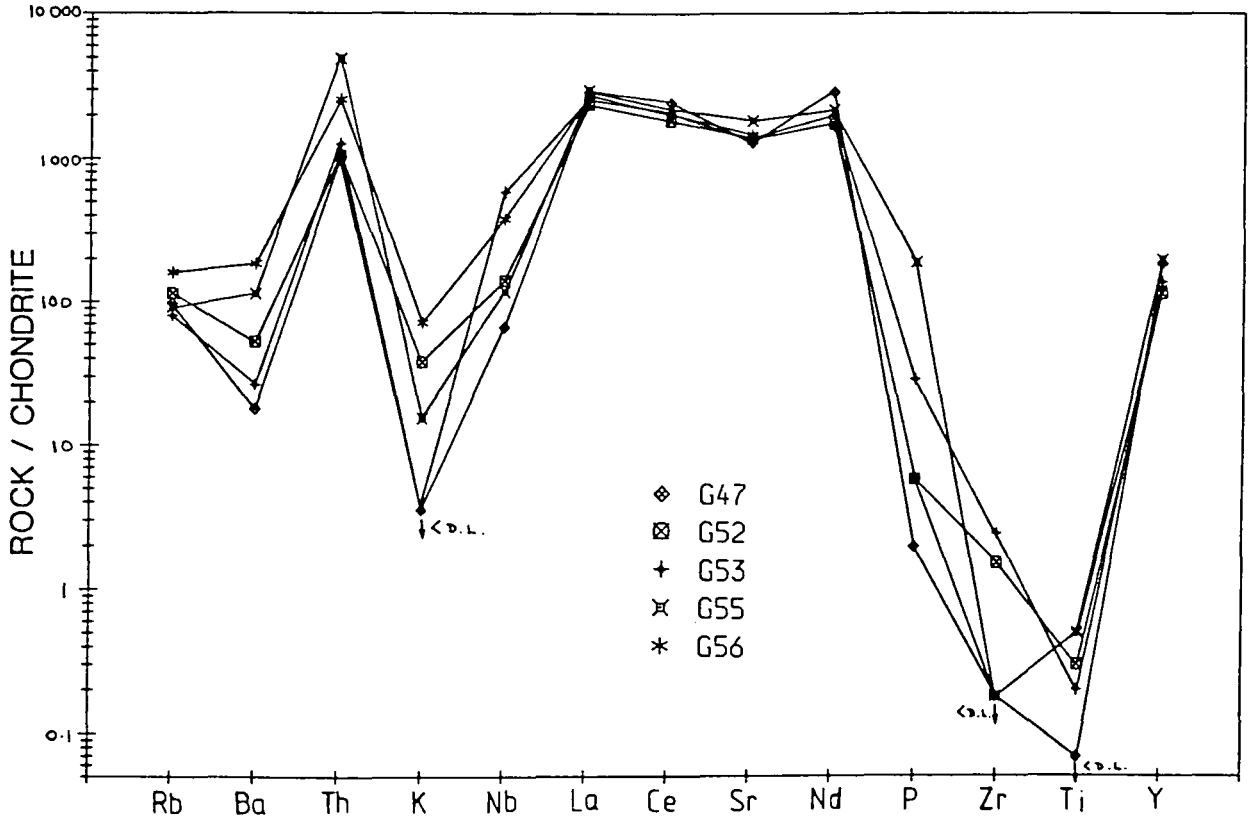
ROCK / CHONDRITE
10 000
1000
100
10
1
0.1
G47
G52
G53
G55
G56
<D.L.
<D.L.
<D.L.
Rb
Ba
Th
K
Nb
La
Ce
Sr
Nd
P
Zr
Ti
Y

Fig. 6.4.3 (cont.)

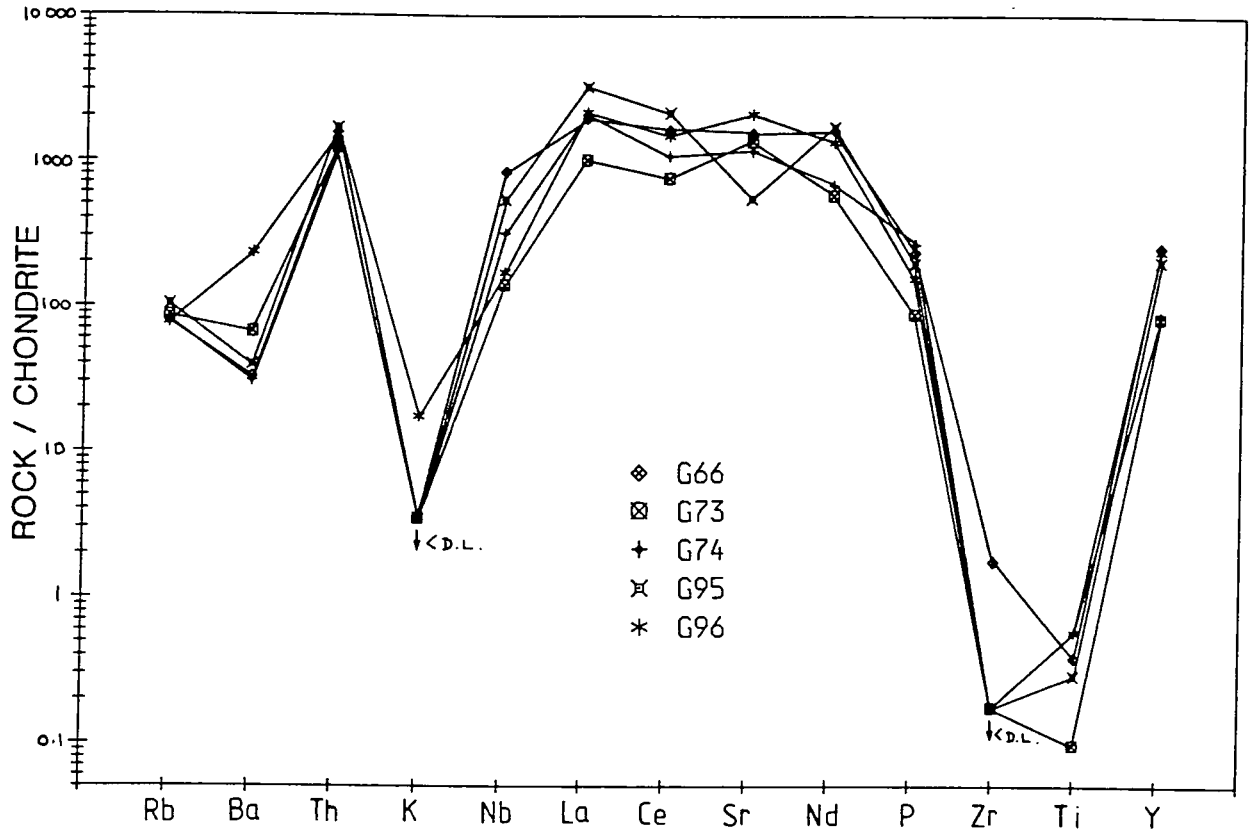
ROCK / CHONDRITE
10 000
1000
100
10
1
0.1
G66
G73
G74
G95
G96
<D.L.
<D.L.
Rb
Ba
Th
K
Nb
La
Ce
Sr
Nd
P
Zr
Ti
Y

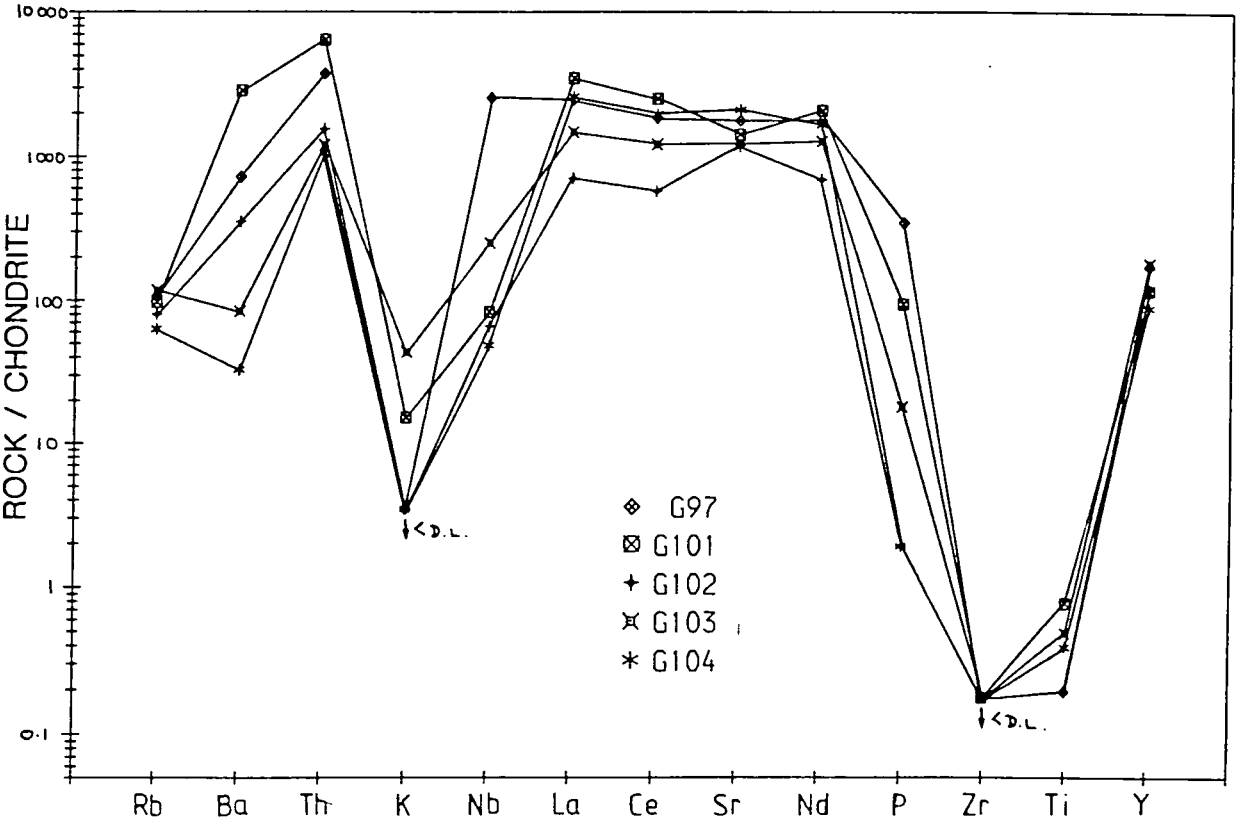
ROCK / CHONDRITE
10 000
1000
100
10
1
0.1
G97
G101
G102
G103
G104
<D.L.
<D.L.
Rb
Ba
Th
K
Nb
La
Ce
Sr
Nd
P
Zr
Ti
Y

values of 0ppm, an unrealistically low amount considering that many samples were observed to contain sulphide minerals.

U is commonly present in carbonatites in phases such as pyrochlore, perovskite, monazite, and sphene (Heinrich 1966), though only pyrochlore has been identified in the Grønnedal samples (G265). It is present in abundances of the order of several tens of ppm, reaching a maximum of 41ppm in G265. These values exceed those of the Sarfartôq carbonatite (Secher and Larsen 1980), but are comparable to abundances from the Igaliko dykes (Pearce 1988).

The abundance of Zn is probably controlled by the presence of sulphide minerals, which have been observed in the carbonatites. The lack of reliable data for Cu and Pb, which might show sympathetic variations, preclude the testing of this idea.

Returning now to the incompatible element 'spidergrams' (fig. 6.4.3), a number of characteristic features are apparent:

1. Marked troughs at K, Ti, and Zr.

2. High REE's, Th, and Y (up to 800–8000× chondrite).

3. Positive or negative Sr anomalies.

These features are broadly similar to those of the Igaliko carbonatite dykes (Pearce 1988), and are not artefacts as a result of using some of these samples as standards. Count-rates show that the low abundances of these elements are genuine, and have been checked using international standards. Zr suffers from interference by Sr and has been determined by recalculation after determining the extent of the interference in Zr-poor standards.

Sample G29 is again different from the carbonate-rich carbonatites, showing a much smoother trend with less pronounced peaks and troughs, and a decrease in enrichment with increasing compatibility.

In contrast to the Igaliko carbonatites, Rb is quite strongly enriched in the Grønnedal-Íka carbonatite, with tens to several hundred times chondritic abundance. Ba is generally less strongly enriched than at Igaliko and this, together with the higher Rb contents, frequently results in an initial 'dip' in the normalised abundance curve. Exceptions to this are most pronounced in samples G31 and G101, which show positive Ba anomalies. Baryte has been observed in the latter, resulting in a whole-rock value of nearly 20 000ppm Ba, an order of magnitude greater than in any other carbonatite sample.

One of the most interesting features of these diagrams is the presence of negative or positive Sr anomalies compared to the adjacent elements (Ce and Nd). Most samples show a negative anomaly (eg. G28, G30, G95), though a few show rather less pronouncd positive anomalies (eg. G31, G73, G102). The former group are frequently more enriched in the REE's (La, Ce, Nd), suggesting that the negative anomaly may be a result of increasing fractionation. Le Bas (1981) and Woolley (1982) suggest that Fe content increases with fractionation, although no relationship between the abundance of this element and the Sr anomaly is observed. One might expect that fractionation of Sr-rich phases such as alkali feldspar (Pearce 1988) or apatite (Deer *et al.*, 1966) would give rise to a negative anomaly, but the Al_2O_3 and P abundances do not appear to reflect this. In the absence of data regarding the partitioning of Sr between potential fractionating phases (such as calcite and siderite) and carbonate melts, it is unreasonable to draw any definite conclusions regarding the nature of this anomaly.

Ta and Hf

INAA data for Ta and Hf for the syenites, carbonatites, and metasomatised rocks are shown in fig. 6.4.4. Ta is generally the more abundant of the two elements, varying from 0.47 to 8.60 ppm in the carbonatites, and up to 26.3 ppm in the syenites (the Xenolithic Porphyritic Syenite), although 60 ppm was recorded in a metasomatised syenite (G90). Hf shows a similar pattern to Ta, being more

Fig. 6.4.5A. REE data for the six carbonatite samples analysed using INAA methods (Appendix IV), normalised using values of Boynton (1984). All show high overall enrichments compared to chondrite abundances, and steep trends as a result of high light REE/heavy REE ratios. These REE patterns are typical of carbonatites in general (eg. Cullers and Graf 1984).

Fig. 6.4.5B. Comparison between carbonatite and syenite REE trends at Grønnedal-Íka.

Fig. 6.4.4. Ta and Hf whole-rock data for all samples. Not only do the carbonatites have lower Ta and Hf than the syenitic rocks, but the Hf/Ta ratio is lower in the carbonatites than the syenites. Such a distribution of these elements is characteristic of rocks produced by carbonate-silicate liquid immiscibility (Hamilton *et al.* 1989).

Fig. 6.4.4A

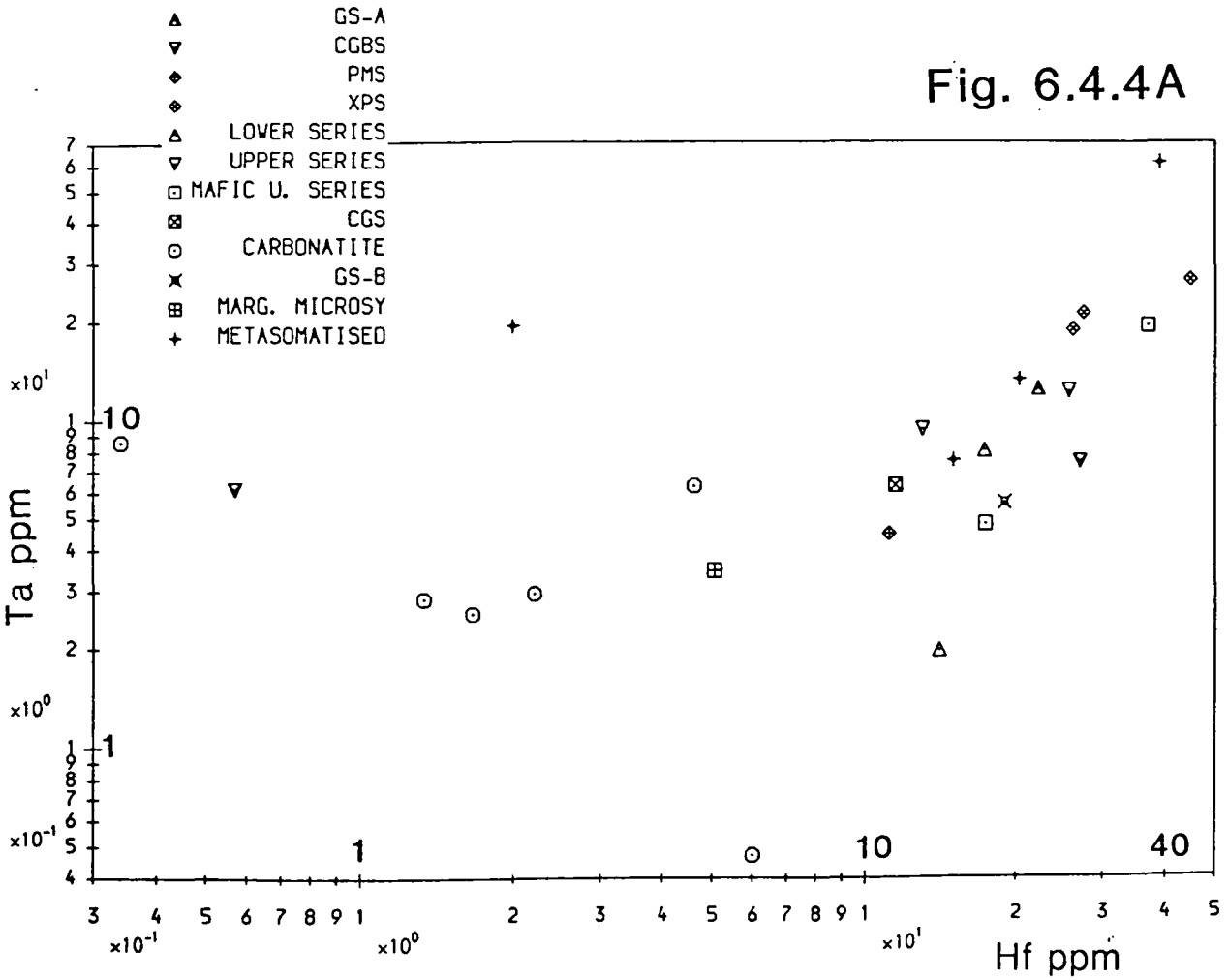

Fig. 6.4.4B

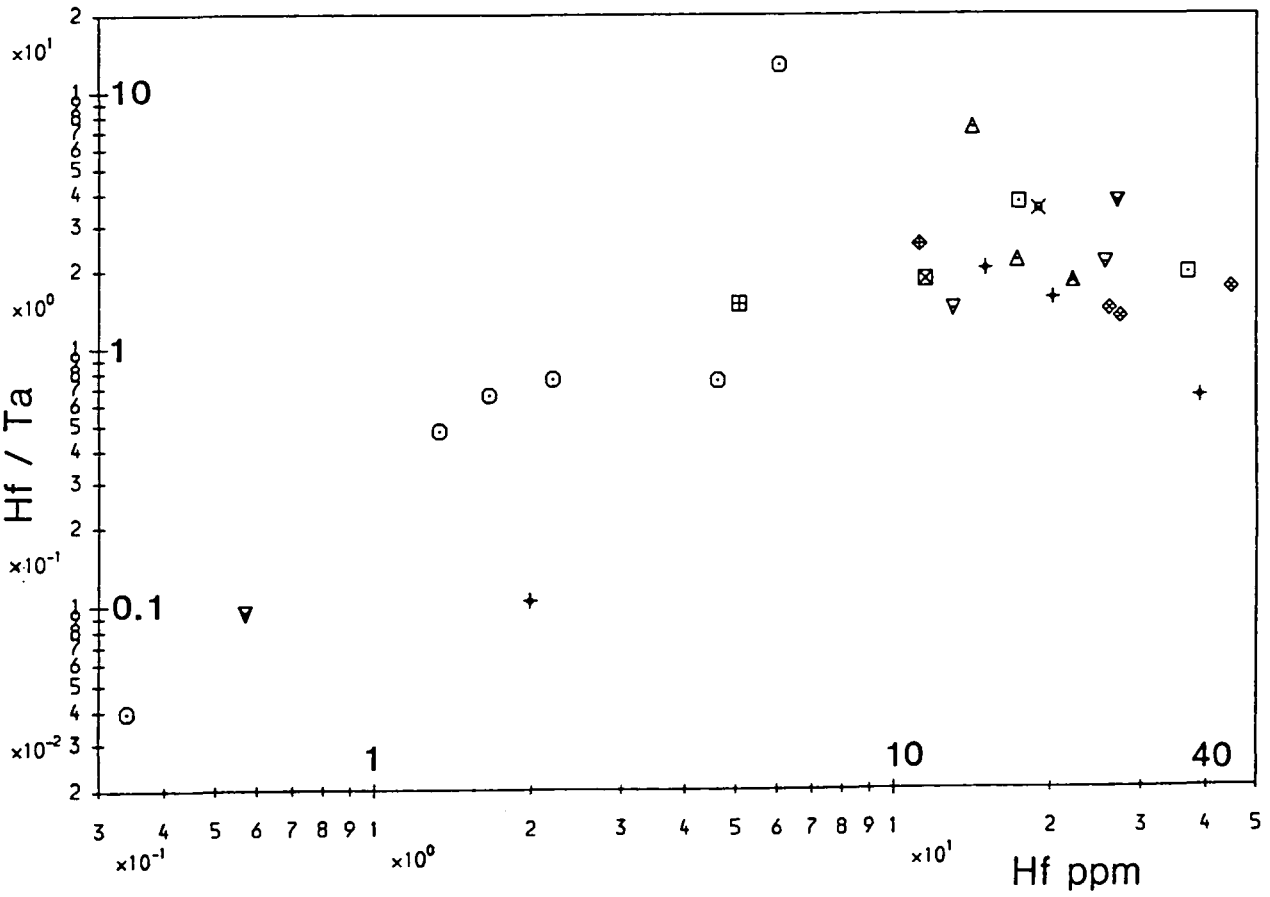

Fig. 6.4.5A

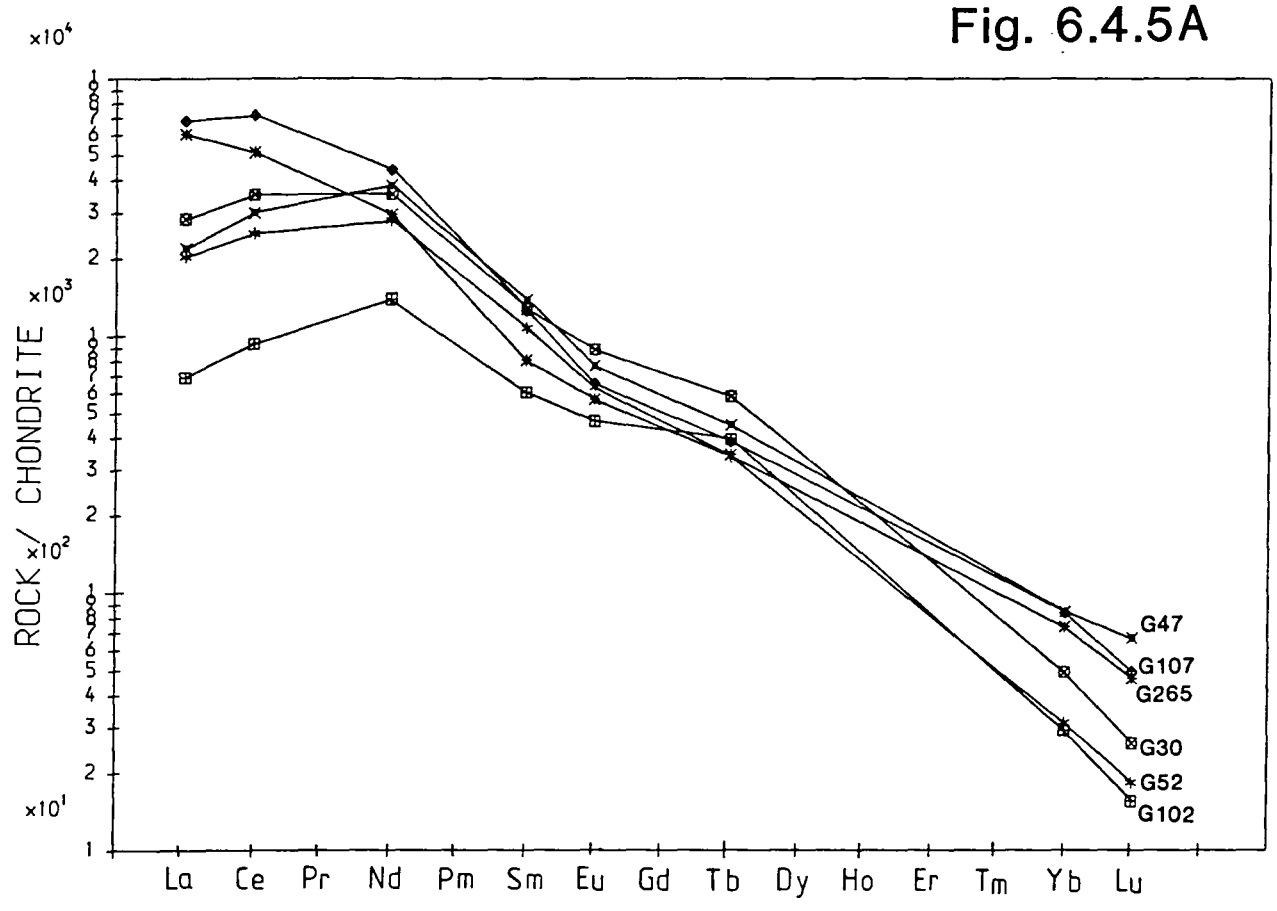

Fig. 6.4.5B

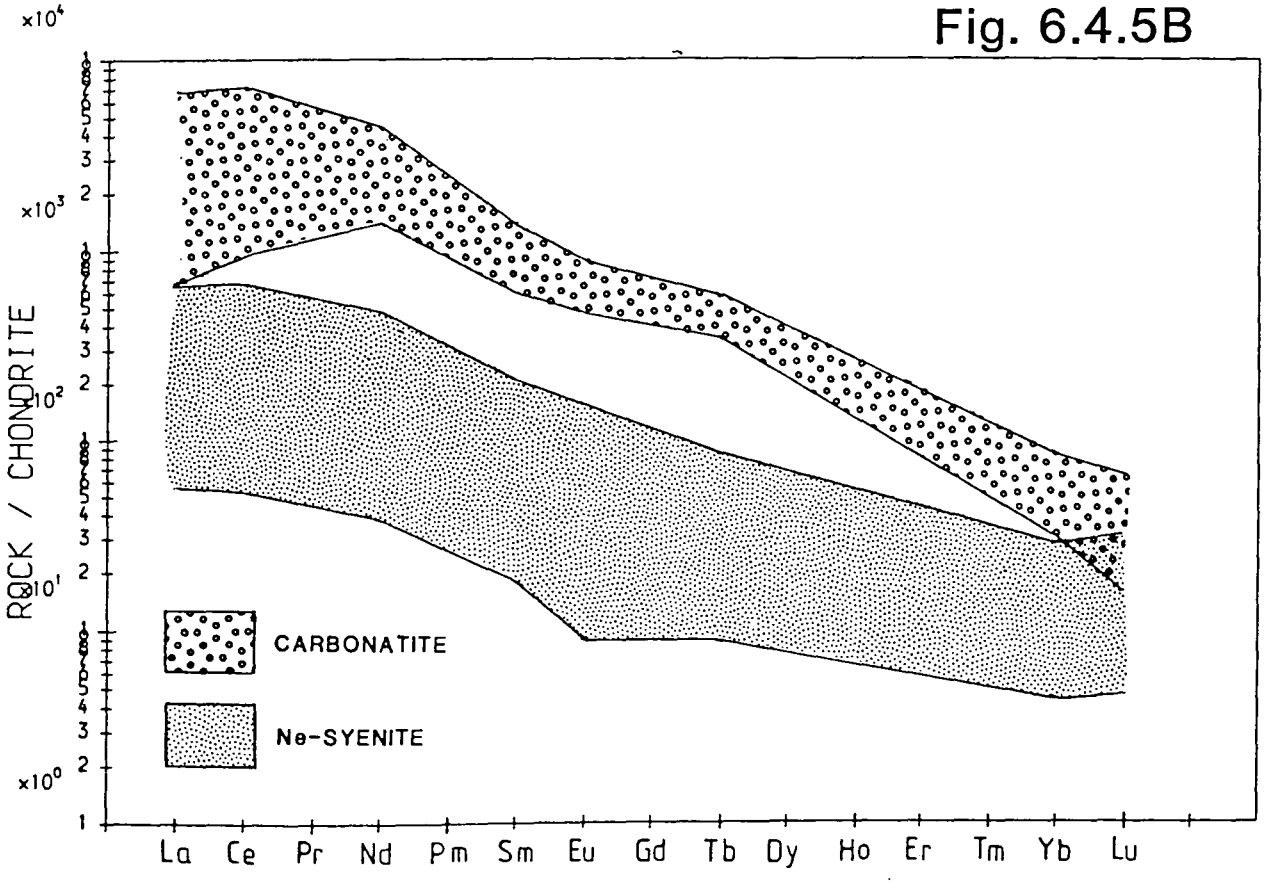

abundant in the syenites (up to 44.7 ppm) and less enriched in the carbonatites (up to 6ppm). Thus the Hf/Ta ratio of the carbonatites as a group tends to be less than that of the syenites, as shown in fig. 6.4.4B.

The relevance of these features of the incompatible element geochemistry to the petrogenesis of the carbonatite will be discussed in section 6.5.

6.4.4: REE geochemistry

REE distribution patterns of carbonatites are reviewed by Möller *et al.* (1980) and are shown for six samples of the Grønnedal carbonatite in fig. 6.4.5A. All samples show very high overall REE enrichment, with LREE's 700–7000× chondrite, and HREE's 15–70× chondrite, comparable to enrichments reported by Cullers and Graf (1984). Fig. 6.4.5B compares carbonatite and syenite REE trends, and shows that for the heaviest element (Lu) there is a slight overlap with the range of the most enriched syenites. However, LREE/HREE ratios, measured as $(La/Lu)_{cn}$ (where *cn*=chondrite normalised) are generally very high compared to the syenites (cf. fig. 5.5.2 and 6.4.5B), with $(La/Lu)_{cn}$ generally in excess of 100.

The sample with the highest $(La/Lu)_{cn}$ ratio (G107, $(La/Lu)_{cn}$=137) may have been affected by metasomatic alteration, as it contains stellate growths of radiating acicular pyroxene (section 6.2), and on the basis of their texture are possibly of secondary origin. Conversely, the very pure nature of G102 (which consists almost entirely of $CaCO_3$) probably accounts for the relatively low REE abundances in this sample.

All but one of the samples have $Ce_{cn} > La_{cn}$, three of which also have $Nd_{cn} > Ce_{cn}$, before abundances decrease with increasing atomic number. It is possible that these anomalies may be the result of analytical error, though the effect is so pronounced in G47 and G102 ($Nd_{cn} \approx 2 \times La_{cn}$), that for these it is probably genuine.

Eu anomalies are generally absent from carbonatites (Cullers and Graf 1984), although samples from Grønnedal-Íka seem to show a slight negative anomaly. Eby (1975) has reported positive and negative Eu anomalies from Oka, Quebec, and suggests that these are caused by competition between fractionating phases for Eu^{2+}.

The significance of the REE trends and the incompatible element variations to the petrogenesis of the carbonatites will now be discussed.

6.5: Carbonatite petrogenesis and conclusions

Although carbonatites are now almost universally accepted as being of igneous origin, their petrogenesis and the formation of carbonatite complexes have been much debated since Brøgger (1921) described the Fen carbonatites as having crystallised from a primary carbonate magma. Many hypotheses have since been proposed, some of which were reviewed by Pecora (1956), and include ideas such as differentiation from an alkaline magma, precipitation from hydrothermal fluids, and alteration of xenoliths. More recently, two contrasting theories for the origin of carbonatites have been proposed, either of which has to account for their characteristic enrichment in trace elements compared to the silicate rocks with which they are often associated.

McKenzie (1984, 1985) suggested that the separation of very small amounts of partial melt (as low as tenths of a percent) from the mantle could give rise to nephelinitic magmas, which then fractionate to give the wide range of associated rock-types (including carbonatite) found in many alkaline complexes. Recently, the possibility that carbonatites are primary mantle melts has been demonstrated by Wallace and Green (1989) who produced alkali-rich dolomitic melts from CO_2-rich peridotites at pressures of 21–30kb, although the potential of this process to produce large incompatible element enrichments has not yet been evaluated (Gittins 1989).

The idea that liquid immiscibilty could play an important role in carbonatite petrogenesis was first demonstrated experimentally by Koster van Groos and Wyllie (1966), who showed that a miscibility gap between albite-rich and Na_2CO_3-rich liquids existed down to 870°C at 1kb. Later work (Koster van Groos and Wyllie 1968) indicated that the addition of H_2O did not destroy the 2-liquid field, although it tends to decrease in size at >20% H_2O, and that the two liquids are stable down to 725°C. Using natural lavas, Freestone and Hamilton (1980) provided further information concerning the genesis of carbonatites, showing that increasing pressure (0.7–7.6kb) and decreasing temperature (1250–1050°C) caused the 2-liquid field to expand in the system (SiO_2+Al_2O_3)–CaO–(Na_2O+K_2O) (fig. 6.5.1A). They also suggested that the 2-liquid field closed off at alkali-poor compositions, ie. despite field and petrographic evidence to the contrary (eg. the Benfontein sill, Dawson and Hawthorne 1973), nephelinitic and kimberlitic compositions were apparently miscible with carbonate-rich liquids.

However, reinvestigation of the system containing SiO_2, Al_2O_3, CaO, Na_2O, and CO_2 by Kjarsgaard and Hamilton (1988) demonstrated that between 1100°C and 1250°C at 5kb, the miscibility gap does not close off, but extends to the alkali-free base-line (fig. 6.5.1B). A pure $CaCO_3$ melt was thus immiscible with a silicate melt. Later work (Kjarsgaard and Hamilton 1989) showed that this 2-liquid field extended to at least 15kb, increasing in size with increasing pressure and decreasing temperature.

Having established that silicate and carbonate liquids are immiscible over a wide range of $P-T-x$ space, the next problem is to determine how the observed compositions of carbonatites seen in the field are derived from this initial parental carbonate-rich magma. The two contrasting opinions on this matter have already been referred to in section 6.4.2. Le Bas (1981, 1987) suggests that alkali-poor carbonatites, common in many complexes (eg. Grønnedal-Íka) are derived from an alkali-rich parent, similar in composition to the natrocarbonatite

Fig. 6.5.1. Experimental evidence for carbonate-silicate liquid immiscibility.

A. The extent of liquid immiscibility in the system (SiO_2+Al_2O_3)–CaO–Na_2O, showing the effect of pressure on the solvus, which appeared to close-off towards alkali-poor compositions (after Freestone and Hamilton 1980).

B. Later re-investigation of the same system suggested that the two-liquid field continued to the alkali-free base line, so that kimberlitic and nephelinitic compositions were shown to be immiscible with calcite carbonatite (søvitic) compositions. (After Kjarsgaard and Hamilton 1988).

Fig. 6.5.1A

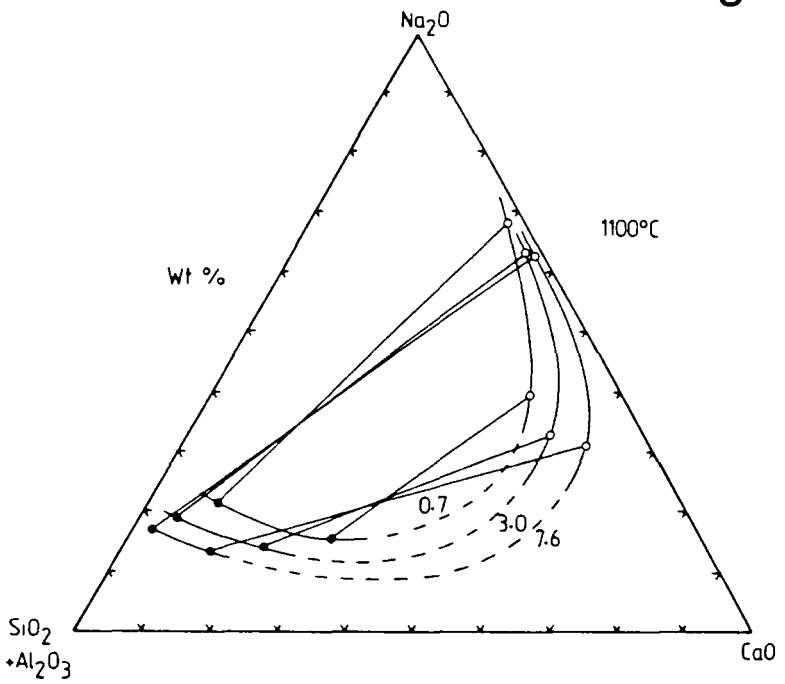

Effect of pressure on solvus at 1,100° C. $P_{total} = P_{CO_2}$ is indicated in kb

Fig. 6.5.1B

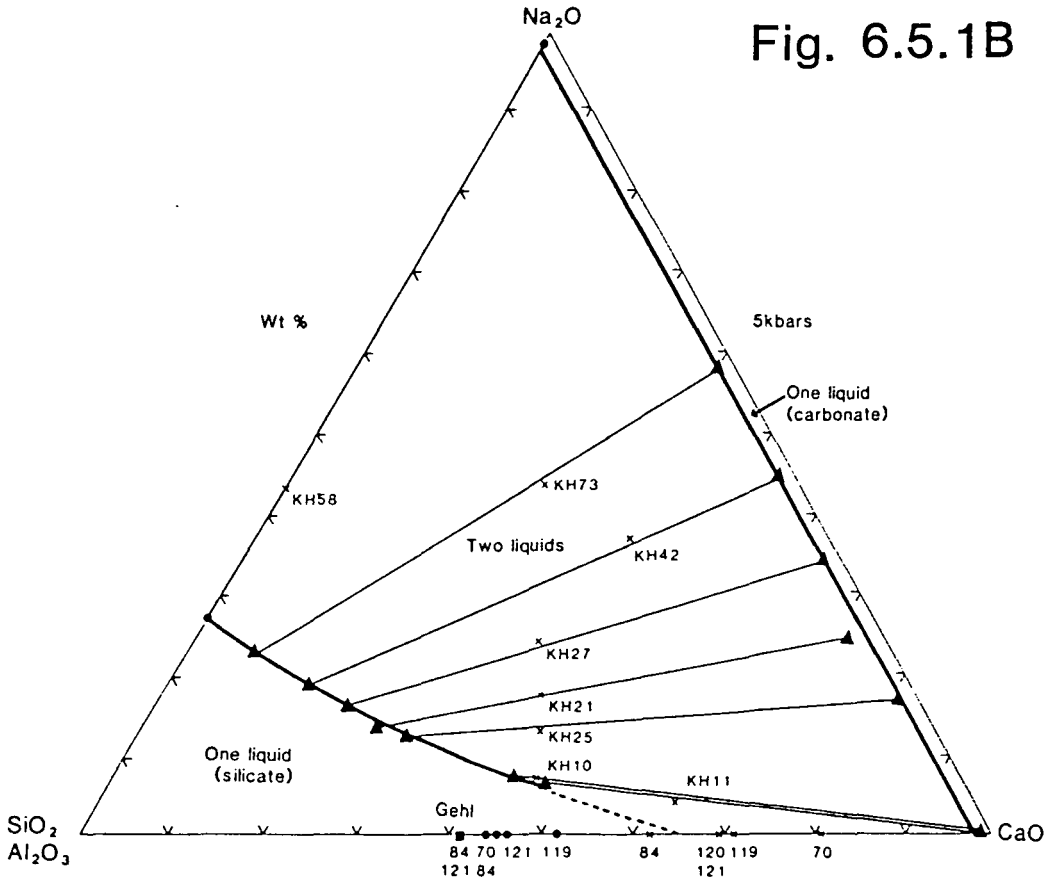

The experimentally determined two-liquid field at 5 kbar and 1250 C for Na_2O-bearing compositions. The crosses mark the starting composition and the run members are also shown. A number of Na_2O-free starting compositions and their subsequent silicate-rich melt composition formed at 5 kbar and in the temperature range 1100 to 1250 C are shown on the base line; [illegible]. GEHL is the composition of gehlenite crystals observed in some Na_2O-free runs. Weight per cent.

lavas of Oldoinyo Lengai, produced by unmixing of a CO_2-saturated phonolitic magma. Progressive loss of alkalis through fenitisation thus gives rise to a Ca-rich, alkali-poor søvite (fig. 6.4.2A). Twyman and Gittins (1987), however, proposed that immiscibility occurred much earlier in the petrogenetic history, within the mantle, involving separation of a carbonate-rich liquid from an olivine-nephelinite parent. Crystallisation of dominantly anhydrous minerals, initially of low alkali content (eg. calcite, dolomite, apatite, and Fe-Ti oxides) increases the alkali and H_2O content, and progressively reduces its viscosity. Extreme alkali enrichment may thus result, with fenitisation occurring through the loss of a hydrous phase following water saturation in the magma. The natrocarbonatite lavas of Oldoinyo Lengai are thus explained as being the result of crystal fractionation, rather than representing a primary magmatic composition.

It is probably not possible to generalise about the origin of carbonatites as a whole, with one mechanism perhaps dominating a particular complex or related suite of rocks. The most realistic approach is probably one such as that of Pearce (1989, in prep.), concerning the carbonatites of the Gardar province. He suggests that late-stage carbonatites, such as those from the Igaliko dykes, may be dominantly the result of CO_2-saturation in a silicate magma with increasing evolution followed by immiscibility, while the early carbonatites forming small plugs, such as at Qagssiarssuk, may be a result of primary mantle melting.

The occurrence of cancrinite and calcite in the syenites (chapter 3) seems to indicate the presence of carbonate-rich late stage liquids, and in view of the late-stage origin of the carbonatite at Grønnedal-Íka and the considerable evidence from other silicate-carbonatite complexes, an origin by liquid immiscibilty is proposed here. As suggested in chapter 4, most of the syenites have been affected by cumulus processes to some extent and do not therefore represent chilled liquids. However, there are a number of lines of geochemical evidence to support an origin by liquid immiscibilty. Although Koster van Groos (1975) found that Sr was not

strongly partitioned into a carbonate liquid in equilibrium with a silicate liquid, Pearce (*op. cit.*) reports that Kjarsgaard has found Sr to be ten to twenty times enriched in the carbonate liquid compared to the conjugate silicate liquid. The majority of carbonatite samples from Grønnedal-Íka contain between 10 000ppm and 25 000ppm Sr and could thus have equilibrated with syenites containing Sr abundances of 500–2500ppm. All units have some samples within this range, though the slightly elevated abundances in the Coarse-Grained Syenite and Xenolithic Porphyritic Syenite means that the majority of samples from these units lie within these limits.

Bedson (1983, 1984) and Hamilton *et al.* (1989) have investigated the distribution of REE's and other elements (Ba, Cr, Mn, Cu, Zr, Hf, and Ta) between natrocarbonatite-phonolite and nephelinite-calcite carbonatite immiscible pairs at a variety of pressures (1–6kb) and temperatures (1050–1250°C). Their results showed that for the natrocarbonatite-phonolite pair at higher pressures, most of these elements (though significantly, not Ta and Hf) are consistently more strongly partitioned into the carbonate rather than the silicate liquid (fig. 6.5.2, 6.5.3). Additionally it was shown that the LREE's are more strongly enriched in the carbonate phase than the HREE's. This is in contrast to the results of Wendlandt and Harrison (1979), who investigated the REE distribution in the sanidine–K_2CO_3 system, and found that HREE's partitioned into the carbonate roughly three times more strongly than into the silicate liquid. These results contrast with the bulk of carbonatite-alkali silicate REE abundances, which show the LREE/HREE ratio in the carbonatite to be greater than that of the co-existing silicate (eg. Cullers and Graf 1984). The bulk compositions used in these experiments probably do not apply to many carbonatite and carbonatite-silicate complexes, however, including Grønnedal-Íka.

$(La/Lu)_{cn}$ ratios against overall REE enrichment are illustrated in fig. 5.5.2, and clearly show that the carbonatites are more strongly enriched in LREE's than

Fig. 6.5.2. Variation of REE distribution coefficients for silicate-carbonate conjugate liquids in equilibrium, with pressure (6.5.2A) and temperature (6.5.2B), in the phonolite natrocarbonatite system.

$$K_D = \frac{Concentration\ of\ element\ in\ silicate}{Concentration\ of\ element\ in\ carbonate}$$

(After Hamilton *et al.* 1989).

Fig. 6.5.3. Variation of distribution coefficients of Ta, Mn, and Ba with pressure (6.5.3A) and temperature (6.5.3B) for phonolite-silicate immiscible liquids in equilibrium. Significantly, only Ta is preferentially enriched in the silicate phase at all conditions of pressure and temperature.

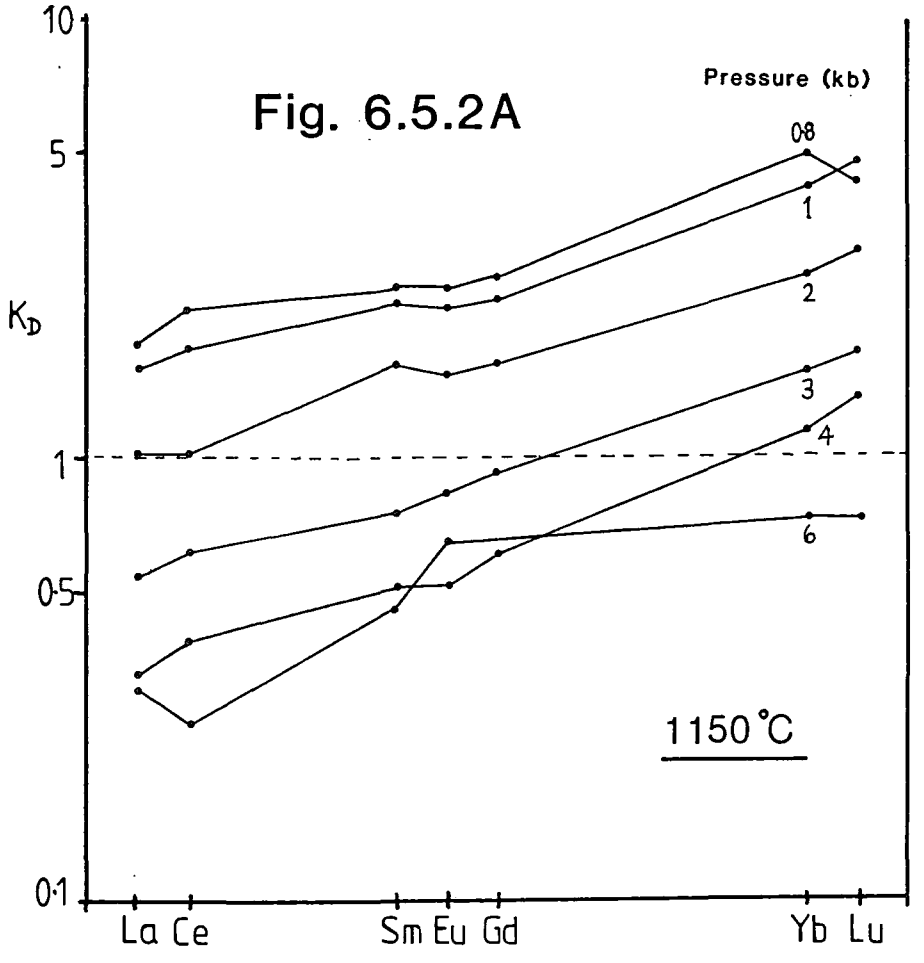
Fig. 6.5.2A
Pressure (kb)
08
1
2
3
4
6
K_D
10
5
1
0·5
0·1
1150 °C
La Ce
Sm Eu Gd
Yb Lu

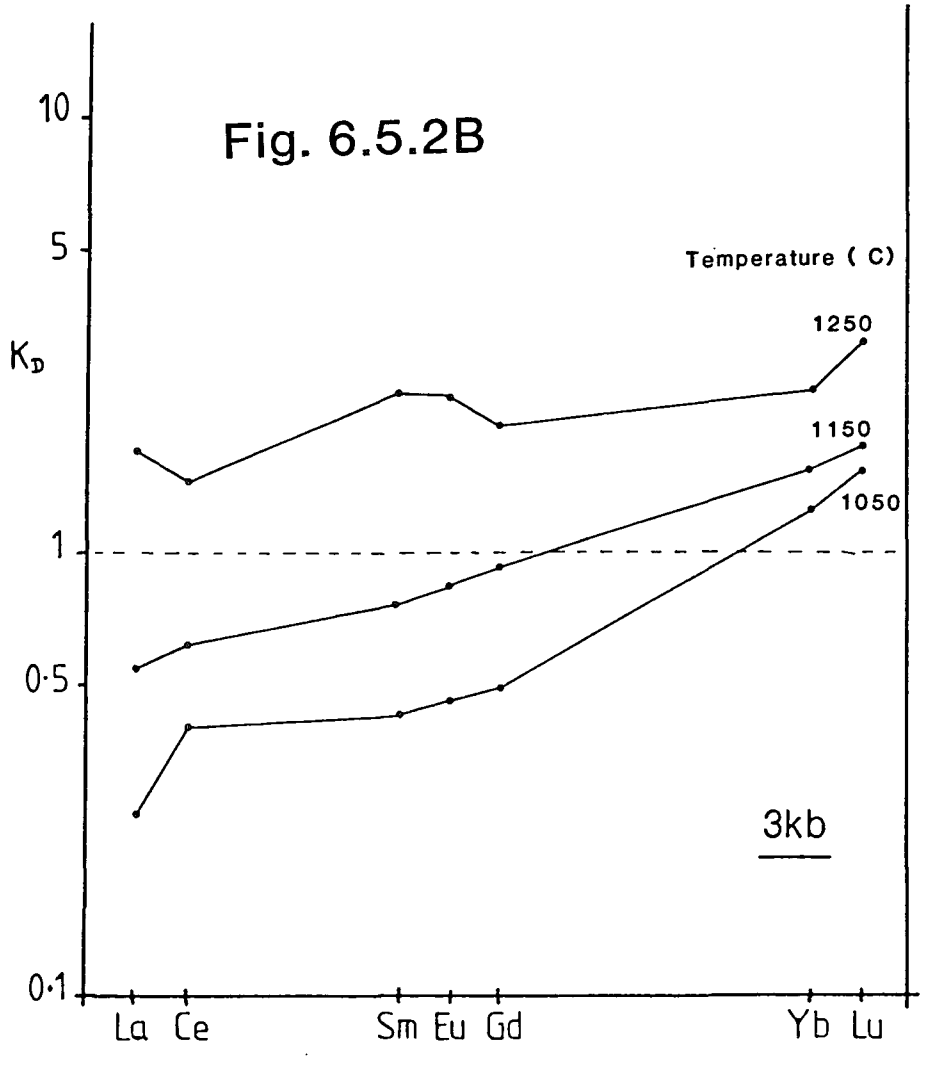
Fig. 6.5.2B
Temperature (C)
1250
1150
1050
K_D
10
5
1
0·5
0·1
3kb
La Ce
Sm Eu Gd
Yb Lu

Fig. 6.5.3A

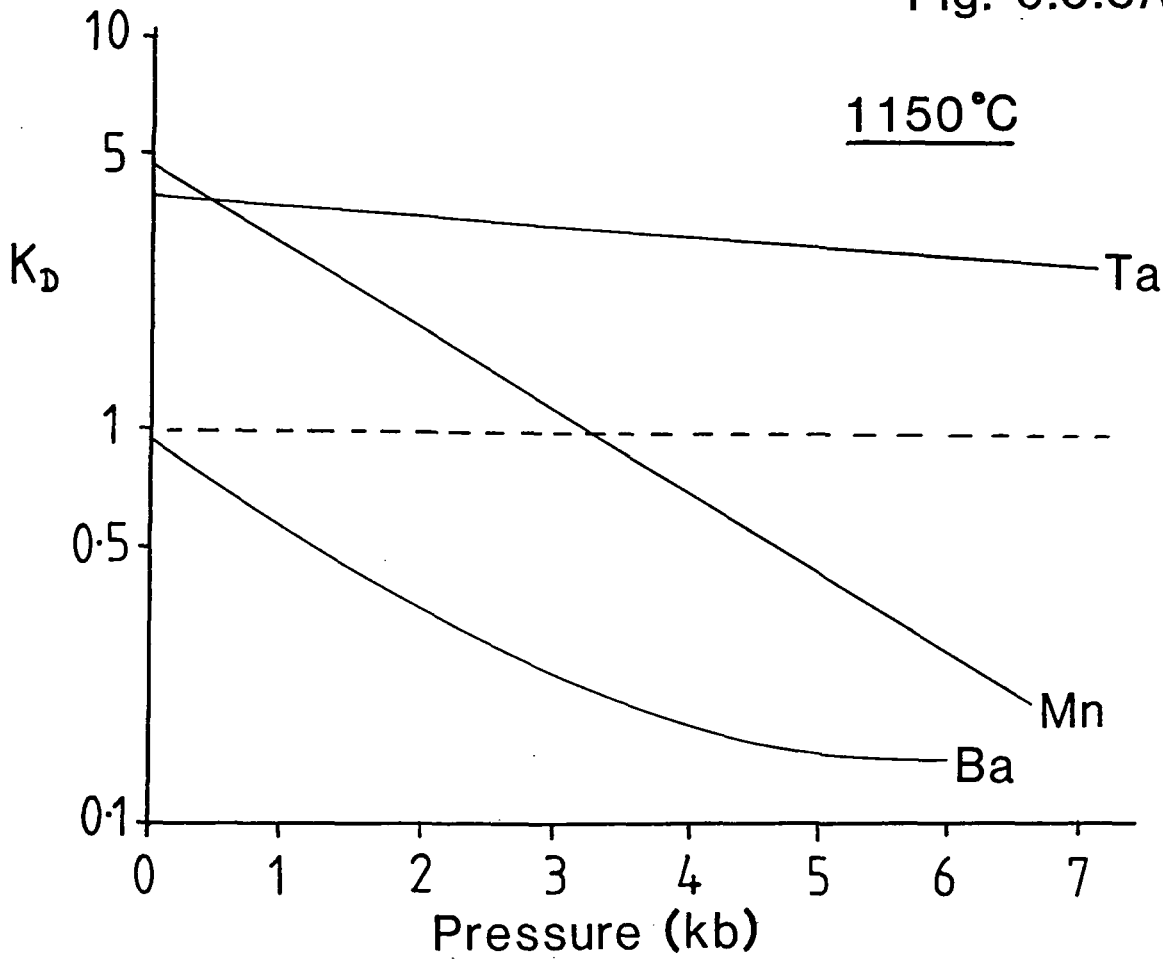

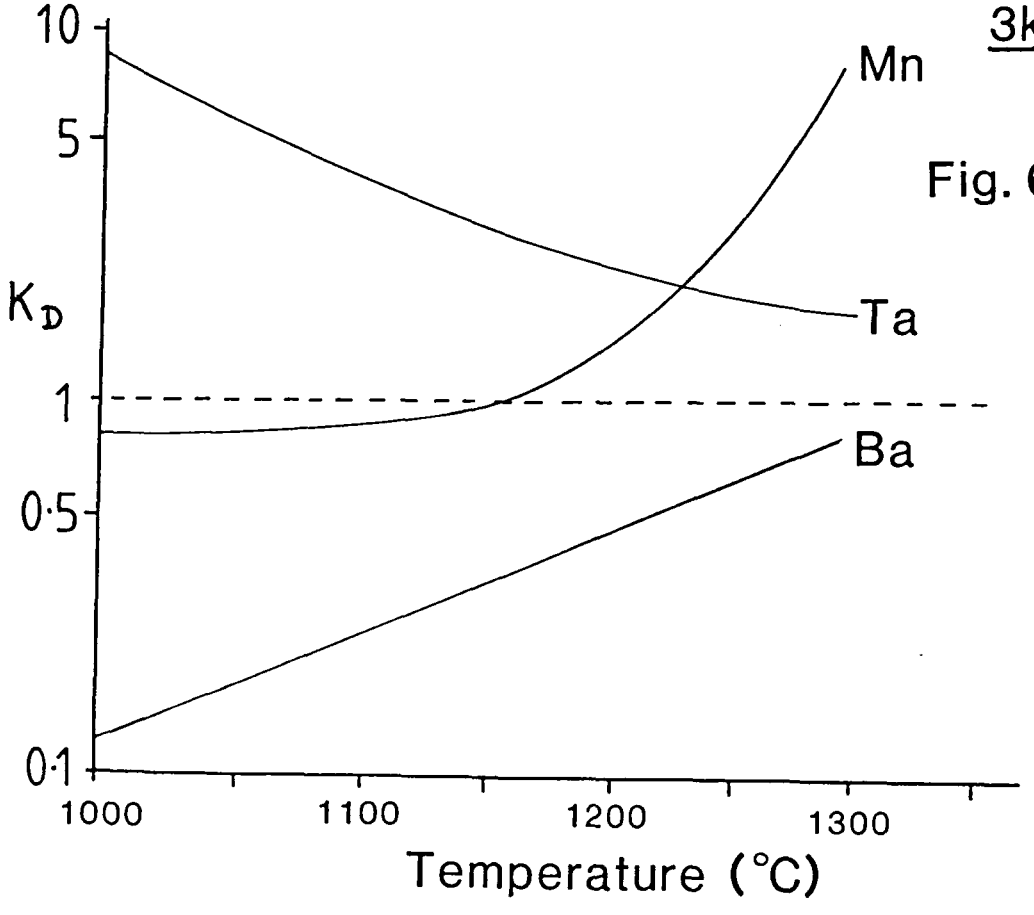

Fig. 6.5.3B

HREE's compared to most of the syenites. This agrees with the results of Hamilton *et al.* (1989) for the phonolite-natrocarbonatite system, results for the nephelinite-calcite carbonatite pair showing no consistent pattern. The higher Ce and Nd normalised abundances seen in the carbonatite REE trends may be explained if separation occurred at $p \approx$6kb, due to a 'dip' in the REE distribution curve at Ce (fig. 6.5.2A). The distribution coefficient for Nd was not determined, but it is possible that this element partitions more strongly into the carbonate than its REE neighbours.

Mn and Ba are also strongly partitioned into the carbonate phase in the phonolite system, particularly at higher pressures ($p >$5kb, fig. 6.5.3A), while in the nephelinite system, no obvious correlation between distribution and physical conditions are apparent. Mn contents in the carbonatite (generally 0.5–1.5% MnO) could be produced by immiscibility, enriched some 3 to 5 times compared to the conjugate silicate liquid (0.15–0.3% MnO in the syenites). Ba contents do not agree so well, with several hundred ppm of this element occurring in both the syenites and carbonatite. Occasional extreme values in the carbonatite (nearly 20 000ppm in G101) suggest that accumulation of Ba-rich phases such as baryte or witherite may have occurred, following fractionation. The high density ($\rho_{baryte} \approx$4.5, $\rho_{witherite} \approx$4.3, Deer *et al.*, 1966) and the low viscosity and density of the carbonatite magma (Twyman and Gittins 1987) would have facilitated gravitational separation.

The relative depletion of Zr in the Grønnedal carbonatite is rather problematic, since although the results of Hamilton *et al.* (1989) are somewhat scattered, they generally predict that similar amounts of Zr would occur in the phonolite and natrocarbonatite if they formed as an immiscible pair. Pearce (1989, in prep.) suggests that a similar situation in the carbonatites of the Igaliko dykes is a result of the Zr being retained as peralkaline zirconium complexes in the residual silicate liquid. Similarly, Zr may also have been carried away in peralkaline metasomatic

fluids as the carbonatite evolved, resulting in the crystallisation of zircon in the metasomatic rocks (chapter 7). It is also possible that fractionation of zirconium silicates has occurred prior to emplacement, the low viscosity and density of the carbonatite magma resulting in efficient gravitational separation.

Perhaps the most convincing evidence for the origin of the Grønnedal-Íka carbonatite comes from the relative abundances of Ta and Hf in the syenite and carbonatite samples (fig. 6.4.4). Hamilton *et al.* (1989) showed that in both the nephelinite and phonolite systems, at all conditions of temperature and pressure under examination, Ta was preferentially partitioned into the silicate phase. During normal fractionation processes, Ta might be expected to be more concentrated in the residual carbonate-rich liquid (being an incompatible element), so that the relative abundance of this element in associated silicate and carbonate rocks may indicate the mode of genesis. In addition, Bedson (1983) suggests that Hf may be used to test for immiscibility, and although not illustrated, Hamilton *et al.* (1989) found that Hf was enriched in the silicate phase more than ten times, and commonly more than a hundred times the abundances in the conjugate carbonate phase. Fig. 6.4.4 clearly shows that not only Ta, but particularly Hf, are much less abundant in the carbonatites than the syenites, but the Hf/Ta ratio is much lower in the carbonatite samples. With the relatively small amount of data available, the analytical errors involved, and the rocks almost certainly unrepresentative of the liquid compositions at the time of unmixing, these data strongly suggest that liquid immiscibilty has played a major role in the formation of the carbonatite at Grønnedal-Íka.

Having established that the carbonatite is almost certainly related to the syenites by immiscibility, is it possible to determine which unit, or groups of units were derived from the original conjugate silicate liquid? Field evidence suggests that the most likely unit is the Xenolithic Porphyritic Syenite, having been emplaced distinctly later than the laminated syenites, and therefore much closer in age to

the even later carbonatite plug. The composition of the carbonatite samples are compared with those of the Xenolithic Porphyritic Syenite and the other syenites in the (SiO_2+TiO_2+Al_2O_3)–(CaO+MgO+ΣFe)–(Na_2O+K_2O) system in fig. 6.5.5 (after Kjarsgaard 1988). The syenites plot close to the proposed 7kb solvus, while the carbonatites plot on a line parallel to the projected tie-line to the hypothetical conjugate carbonate-rich liquid. It is thus possible that the carbonatite represents a primary immiscible phase from the syenitic rocks. However, fractionation will have shifted the silicate compositions away from the CaO+MgO+Fe_2O_3 apex of fig. 6.5.4, and the carbonatites are almost certainly not representative of a quenched liquid composition. It would thus be unconvincing to attempt to relate the two rock types by this method.

However, REE data (fig. 6.4.5) show an insignificant Eu anomaly in the carbonatite samples, and apart from one (G245), these are absent from the Xenolithic Porphyritic Syenite as well. The data of Hamilton *et al.* (1989) show no strong fractionation of Eu relative to Sm, so that a Eu anomaly-free silicate would exist in equilibrium with an anomaly-free carbonatite. Hf and Ta data constrain the identity of the conjugate silicate phase more accurately. Hf contents in the Xenolithic Porphyritic Syenite are of the order of tens of times the carbonatite abundances, while Ta contents are generally enriched some five to ten times that of the carbonatite. These enrichment factors both agree with the results of Hamilton *et al.* (1989) more closely than with any of the other units at Grønnedal.

Fig. 6.5.4. Syenite and carbonatite analyses in the system investigated by Kjarsgaard and Hamilton (1988), showing the extent of the two-liquid field at 5kb. Most of the carbonatite compositions plot very close to the $CaO+MgO+Fe_2O_3$ apex, the presence of alumino-silicates giving rise to the spread of analyses. The proposed 7kb solvus is also shown, and the relationship of the Xenolithic Porphyritic Syenite to the carbonatite is discussed in the text.

GRONNEDAL-IKA CARBONATITES

AFTER KJARSGAARD AND HAMILTON, 1988

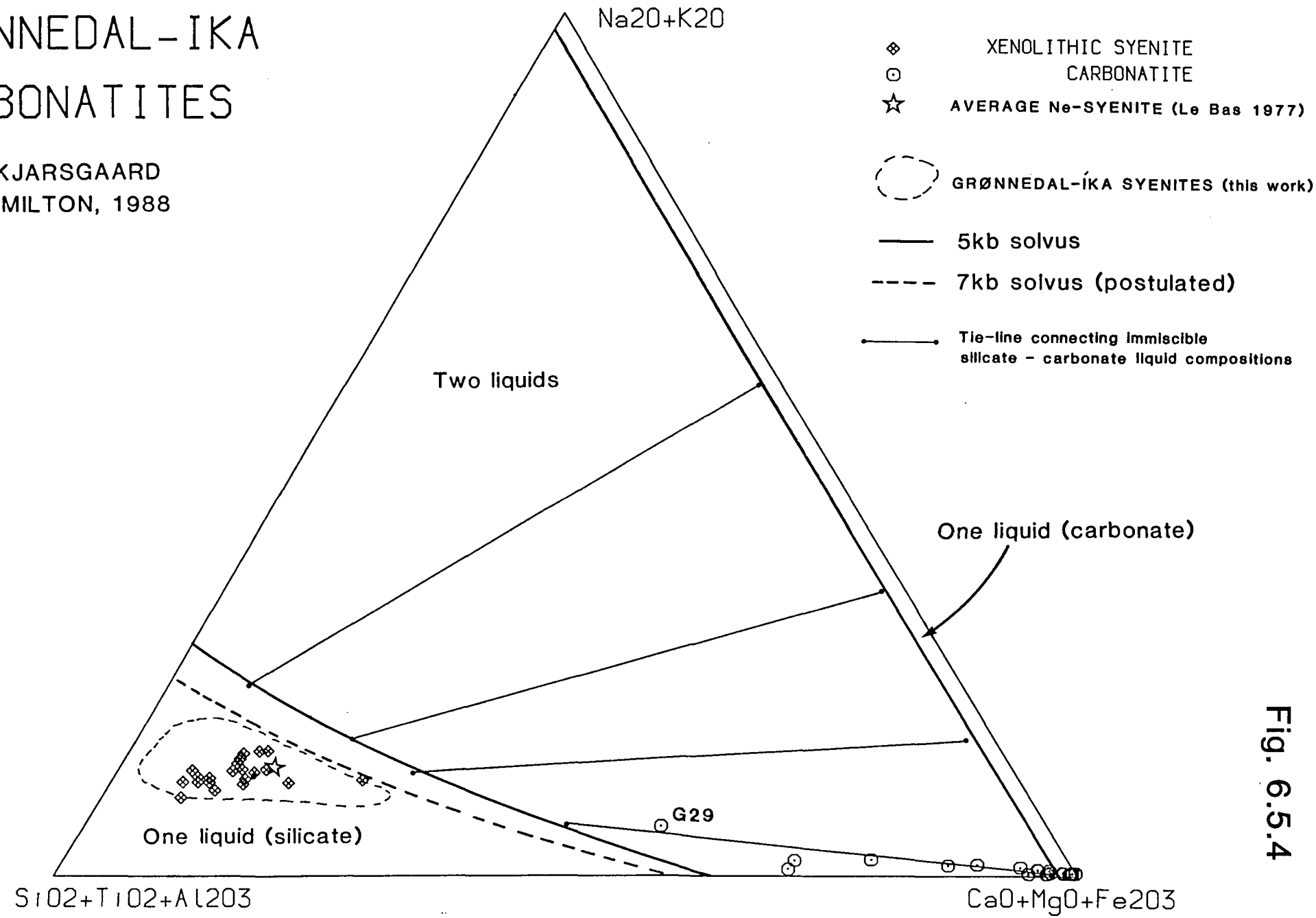

Fig. 6.5.4

CHAPTER 7: METASOMATISM AND ALTERATION ASSOCIATED WITH THE COMPLEX

Metasomatic alteration is an important aspect of the geology of many of the Gardar igneous centres. In the North Qôroq centre, metasomatism of older syenite units adjacent to younger units has occurred, as well as alteration of the Julianehåb Granite country rock next to the outer margins of the intrusion (Chambers 1976, Rae and Chambers 1988). In the Motzfeldt Centre, metasomatic alteration of the roof zone has resulted in extensive Th-U-Zr-Nb-REE mineralisation, and high Ta contents (up to 0.6%), possibly of economic importance (Tukiainen *et al.*, 1983). Ferguson (1964) and Larsen (1977) have described the alteration effects of the Ilímaussaq intrusion on the adjacent country rock sandstones and lavas of the Eriksfjord Formation, and in view of the significance of metasomatised rocks at Grønnedal-Íka, they are described here in a separate chapter.

Alteration affects country-rock gneisses as well as the syenites, and has led to significant changes in the mineralogy of both of these rock-types. However, as mentioned in section 2.7, the Coarse-Grained Brown Syenite is considered to be the result of alteration of Lower and Upper Series Syenite, and since this unit was originally mapped separately, it is not considered here. This chapter is therefore restricted to those rocks in which metasomatic alteration is considered to have played a significant part in the production of the observed textures and mineralogies. Though it is often possible to distinguish such a rock on field evidence alone, it is usually necessary to confirm such predictions by thin-section examination. Rock-types which make-up this group generally fall into two broad categories:

Altered syenites

Very strongly altered syenites, which frequently effervesce with dilute HCl due to the presence of secondary carbonate. They occur *in situ* in areas affected by the carbonatite, and as xenoliths in the Xenolithic Porphyritic Syenite.

Altered gneisses

Metasomatised country-rock, either adjacent to the intrusion, though more commonly as fragments up to tens of metres across within the syenites.

7.1: Field appearance

7.1.1: General

On a small-scale, late-stage veins or aggregates of bright-blue sodalite are associated with alteration of the syenite over a distance of several centimetres on either side of the vein, rendering the nephelines more strongly coloured, either deep-pink, or more usually white in colour, due to an increase in the amount of gieseckite (plate 7.1). Sodalite is common in the Radioelv, an area well-known to the occupants of the Naval Base at Grønnedal for collecting this mineral. Late-stage growth of bright-green pyroxene along with the sodalite also occurs, eg. on the north-west shore of Íka fjord. In the Upper Series Syenite in the upper parts of the Radioelv, the rock appears to have been brecciated, and the angular fragments, down to the size of individual crystals, appear to have been re-cemented by green pyroxene (G126, and plate 7.2).

7.1.2: Altered syenites

Both within and adjacent to the carbonatite, large areas of syenite have undergone extreme alteration and impregnation by carbonate to form rocks which are here termed 'carbosyenites'. Apart from effervescing with acid, these rocks are characterized by a fine (millimetre-sized) grain-size, even in samples located several hundred metres from the contact, and are therefore probably the result of recrystallisation. They are also very pale in colour, being predominantly feldspathic, with occasional resinous-brown zircons up to 4mm in size, and bear little resemblance to either gneiss or unaltered syenite. This type of alteration is particularly well developed around the carbonatite outcrops at the head of Urdal.

Plate 7.1. Discolouration of syenite adjacent to a sodalite vein (bright blue), mainly as a result of nepheline alteration to gieseckite. Hammer head is 12cm long.

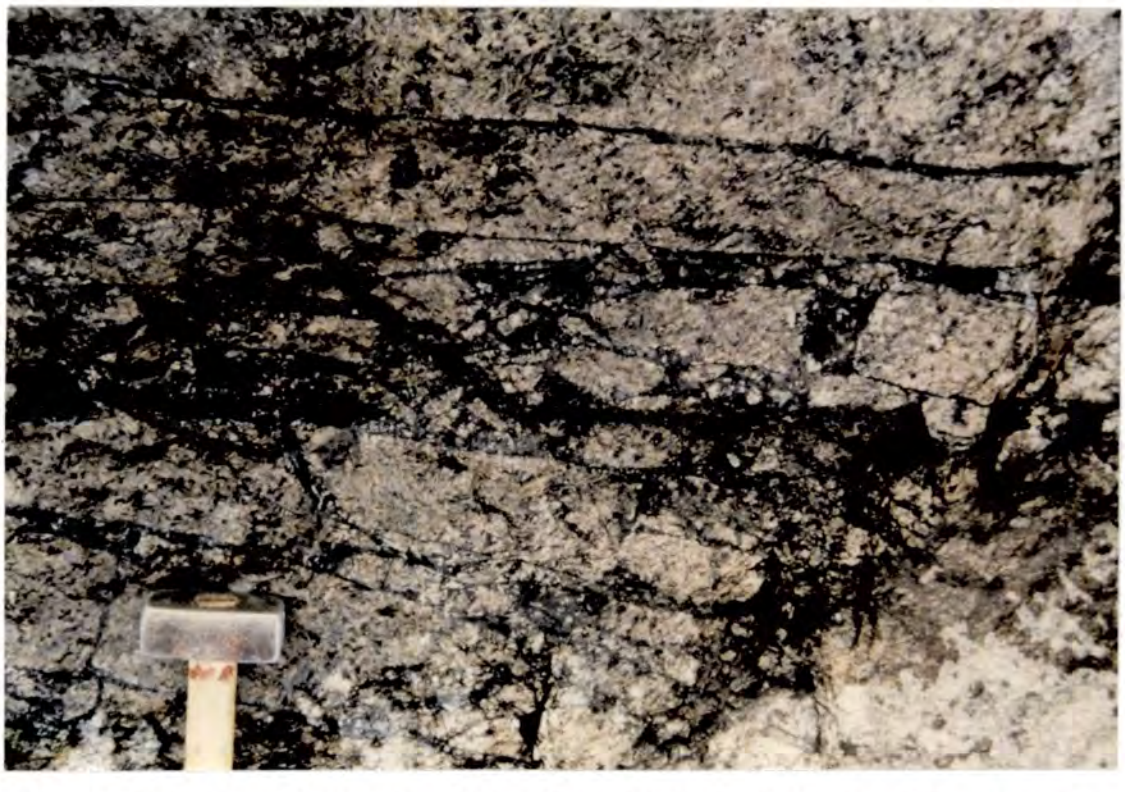

Plate 7.2. Veining and brecciation of Upper Series Syenite by dark-green alkali pyroxene as a result of soda-metasomatism (eg. G126). Hammer head is 12cm long.

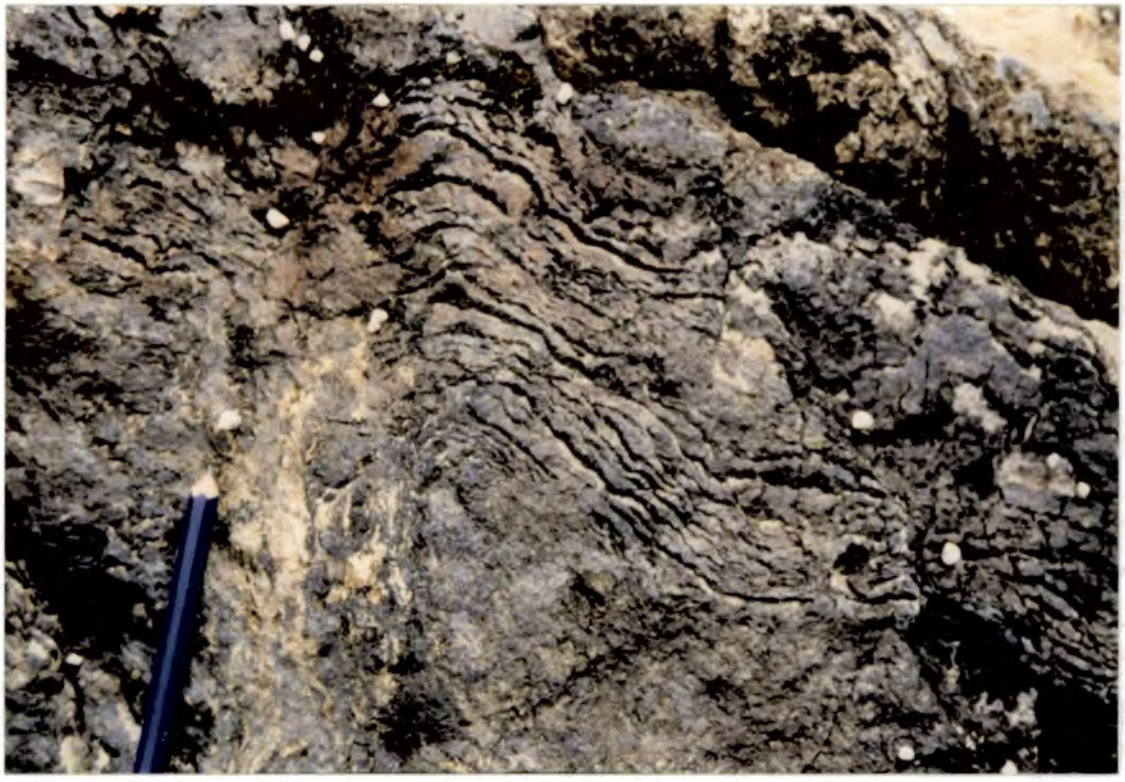

Plate 7.3. Metasomatised metasediments at the extreme south-east end of the complex, on the south-east shore of Íka fjord. The pale blue tinge is due to the replacement of the original mafic mineralogy by alkali amphibole (eg. sample G108).

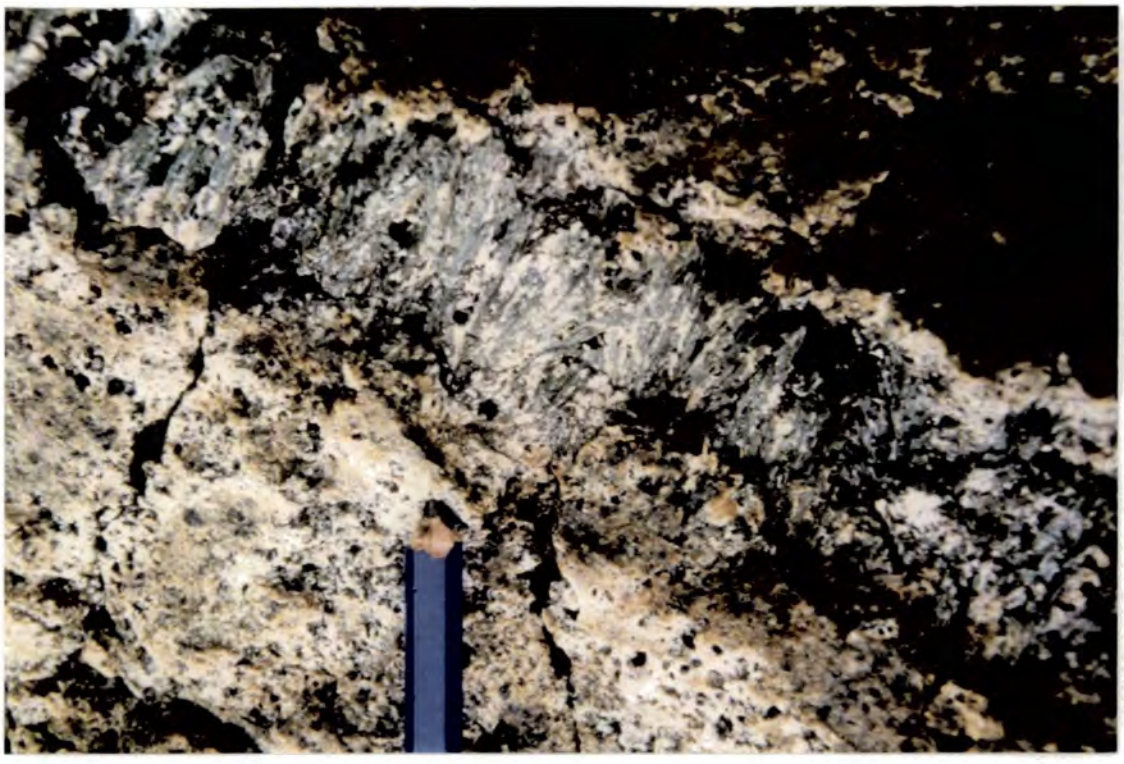

Plate 7.4. Metasomatised gneiss, with a 3cm-thick band of acicular pyroxene, growing perpendicular to the original foliation, preferentially replacing the mineralogy of this layer (eg. sample G139).

7.1.3: Altered gneisses

Metasomatism of gneiss, either adjacent to the intrusion or as detached blocks within the syenites, commonly results in the rock developing a bluish tinge due to the growth of alkali amphibole (plate 7.3), and occasional bright-green acicular pyroxenes. Bright-blue amphibole occurs along fracture surfaces in the gneiss adjacent to the marginal syenites in the north-west of the complex, although the rock as a whole does not appear to be altered here. Because of their large surface area/volume ratio, it is the isolated blocks, tens of centimetres to tens of metres in size, which occur mainly in the Bryggerens Elv (shown on map 1) and Radioelv (not shown) which are more susceptible to metasomatic alteration. Another good example occurs just to the north of the 530m peak in the area of the Xenolithic Porphyritic Syenite. Green acicular pyroxenes are here concentrated into centimetre-thick sub-parallel bands, possibly pseudomorphing the original mineralogy of a banded gneiss (samples G139, and G145; plate 7.4).

In the absence of secondary amphibole and pyroxene, it is very difficult to determine whether the gneisses have suffered metasomatism, so that the wall rocks, and parts of the gneiss raft (which should show considerable alteration, especially at its base), may have been more affected than is apparent in the field. Thin-section examination, however, usually reveals any alteration that has occurred.

7.2: Petrography

7.2.1: General

Before the individual characteristics of the altered syenites and gneisses are described, several features of the petrography which are common to both will be mentioned.

i) Zircon – The presence of this mineral has been noted in chapter 3, occurring sporadically as small grains in the 'less fresh' syenites. In the metasomatised rocks described here, this mineral is a common groundmass phase.

ii) Radiating feldspars – Stellate and felted plagioclase laths up to 3mm long (though usually smaller) with narrow twin lamellae (later identified as albite, section 7.3.5) are very abundant in both metasomatised rock-types (plate 7.5).

iii) Carbonate – This occurs in both rock-types as an interstitial phase, but is particularly abundant in some of the altered syenites ('carbosyenites').

7.2.2: Altered syenites

Carbonate minerals, mainly calcite with some siderite, can form up to 30% of the rock by volume, and in extreme cases (G94) approaches the 50% carbonate needed for the rock to be termed a carbonatite (Streckeisen 1980), and are referred to in this work as 'carbosyenites'. Zircon is prominent, occurring as subhedral grains up to 4mm across (eg. G180), and very often as poikilitic crystals up to 3mm in size. In sample G27, apparently isolated zircon grains are seen to be in optical continuity, and the three-dimensional form of the crystal may be a quite complex structure.

Separate laths of secondary plagioclase *c.*1mm long are quite common in addition to the stellate growths already mentioned, and although some relict alkali feldspar is usually preserved, all other minerals are entirely altered (nepheline to gieseckite and white mica, pyroxene to chlorite and opaques; plate 7.6). Secondary pyroxene occurs in G180 as a mass of grassy-green to yellow-brown acicular crystals, and in the 'pyroxene-breccia' (G126) described in section 7.1.2. Though the latter is not carbonated and surprisingly fresh-looking, the rock has clearly suffered the effects of metasomatism, with the aegirine-augites occurring along grain-boundaries as small, clean, bottle-green, equant grains 100-500μm in size, apparently replacing nepheline and alkali feldspar in the rock. The latter two minerals are commonly 400-500μm across, and frequently and show granoblastic recrystallisation textures.

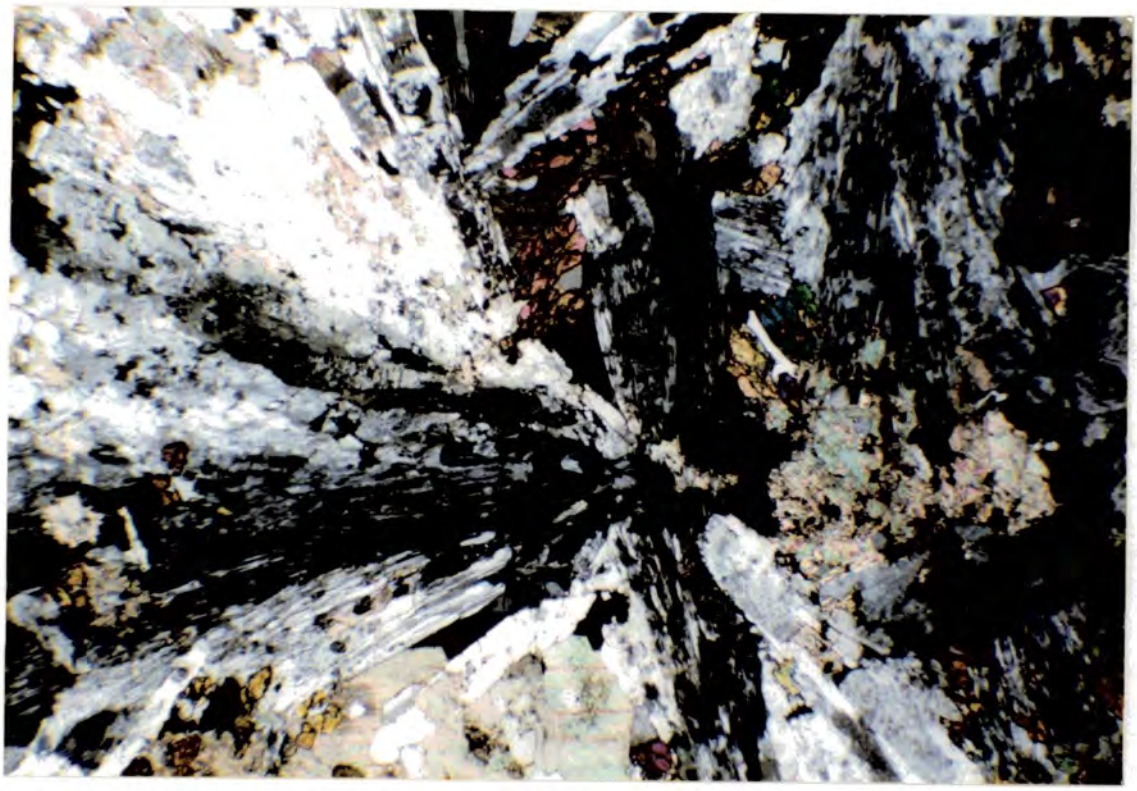

Plate 7.5. G146. ×35. XPL. Radiating alkali feldspars in altered gneiss as a result of metasomatic recrystallsation. Also present are grains of carbonate (bottom centre), with amphibole and zircon grains to the left and right respectively.

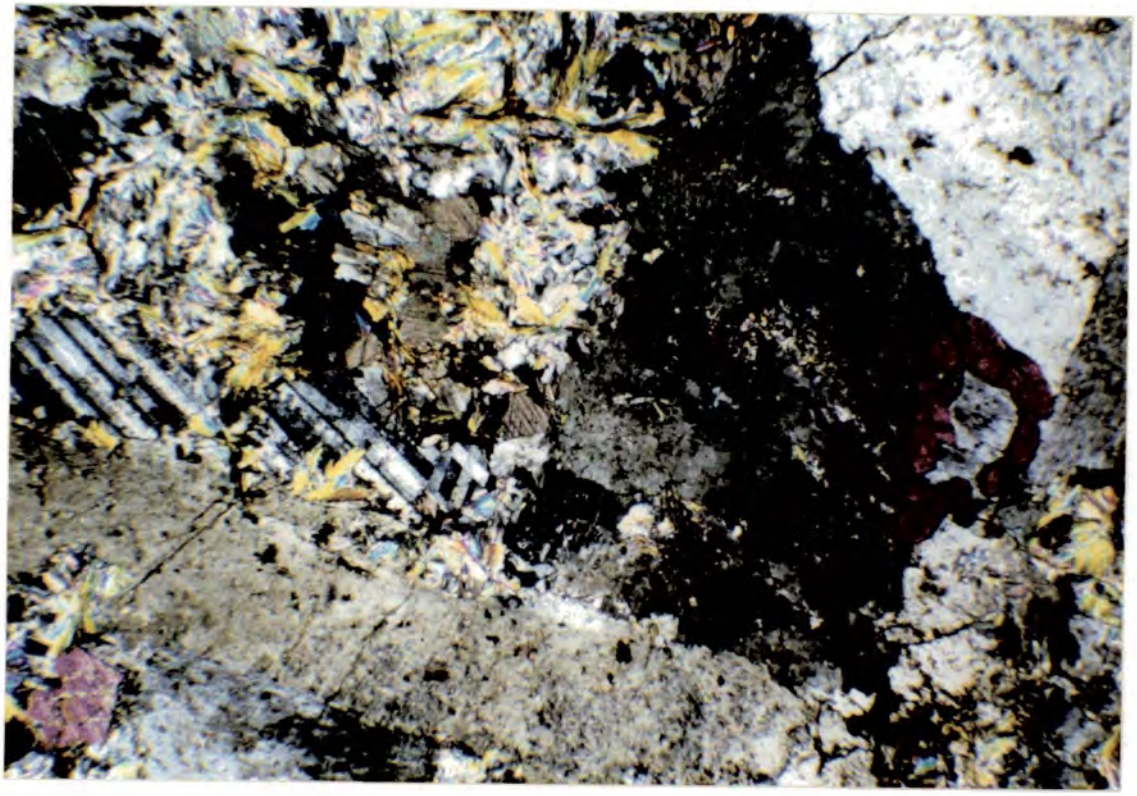

Plate 7.6. G272. ×35. XPL. Carbosyenite. Relict alkali feldspar (centre) with carbonate and white mica to the left, and a zircon grain to the right, possibly replacing the feldspar which it surrounds.

7.2.3: Altered gneisses

Though these rocks retain many characteristics of the original lithology (relict quartz and plagioclase), they show some very interesting secondary textures and mineralogies which are highly suggestive of metasomatic alteration.

Interstitial zircon and carbonate grains are present, as mentioned in section 7.2.1, but the most characteristic mineral of this group of rocks is amphibole, occurring in a variety of forms and colours. In sample G108, a metasediment adjacent to the outer margin of the complex, the rock consist almost entirely of felted masses of alkali amphibole (α sky-blue, β lilac, γ pale-yellow), with individual grains often zoned to a darker-blue rim. More commonly, though, the amphibole occurs as fresh, equant grains up to $c.800\mu$m across, (α pale green-brown, β deep red-brown, γ pale-brown) sometimes with smaller felsic inclusions, and occasionally fringed with a deep-blue amphibole (α blue, β purple, γ pale-yellow), as in sample G239 (plate 7.7). Small grains of aegirine-augite, $c.100\mu$m across occur in G197, and appear to be partly replacing primary quartz grains in the gneiss (plate 7.8). These intergranular pyroxenes can be fairly coarse, up to 800μm $\times$ 300μm in G14, where the replacement of quartz is more obvious. Very pale acicular or prismatic pyroxene grains up to 1.5mm long occur in several samples, most notably G198. Rowbotham (1973) has described a sample of metasomatised amphibolite dyke from basement rocks in the Bryggerens Elv (sample 27281) containing zoned amphiboles, which electron microprobe studies showed to be magnesioarfvedsonite, becoming increasingly iron-rich towards the rim. The rims have a similar pleochroic scheme to the amphiboles in G108, but in contrast, sample 27281 also contains unzoned, euhedral, prismatic alkali pyroxenes.

Biotite occurs quite commonly, though from petrographic observations alone it is impossible to determine whether its presence is due to recrystallisation of original biotites, or entirely of secondary origin. A rusty red-brown to pale-brown pleochroism is characteristic, but most striking are those in G26, which occur

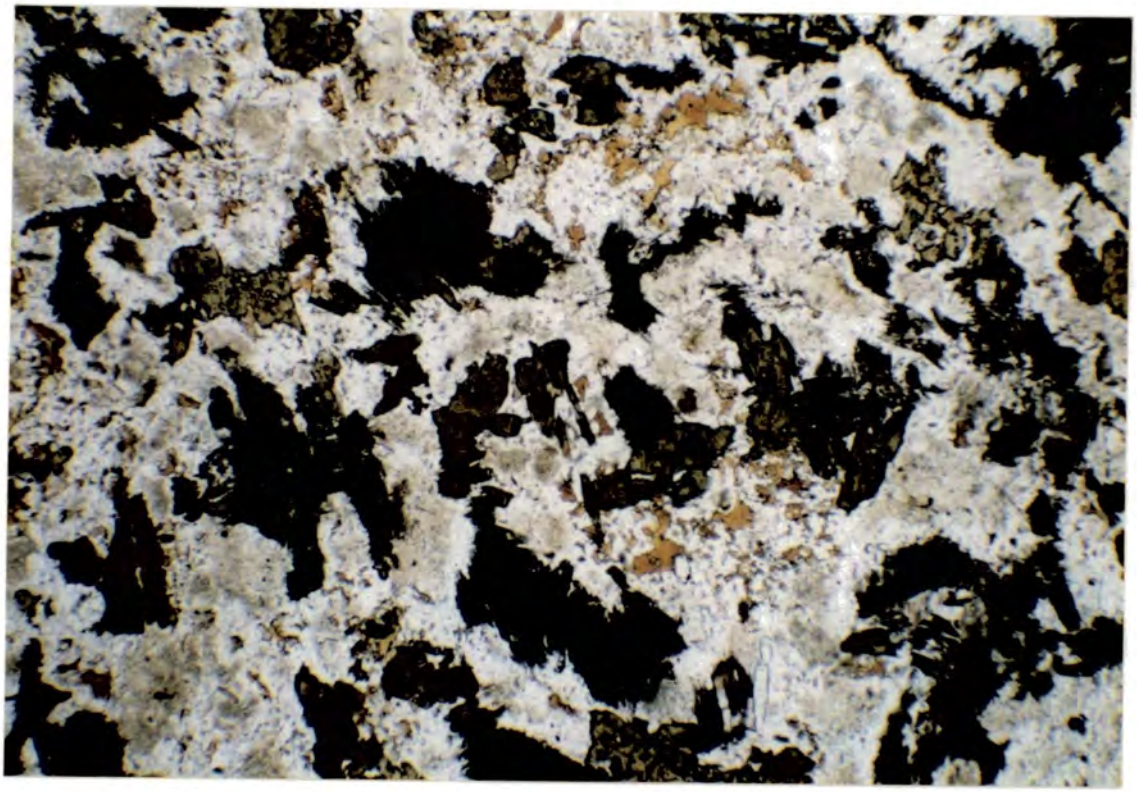

Plate 7.7. G239. ×35. PPL. Secondary amphibole with deep blue fringes to brown-green cores, and pale-orange biotite. The white mineral is alkali feldspar.

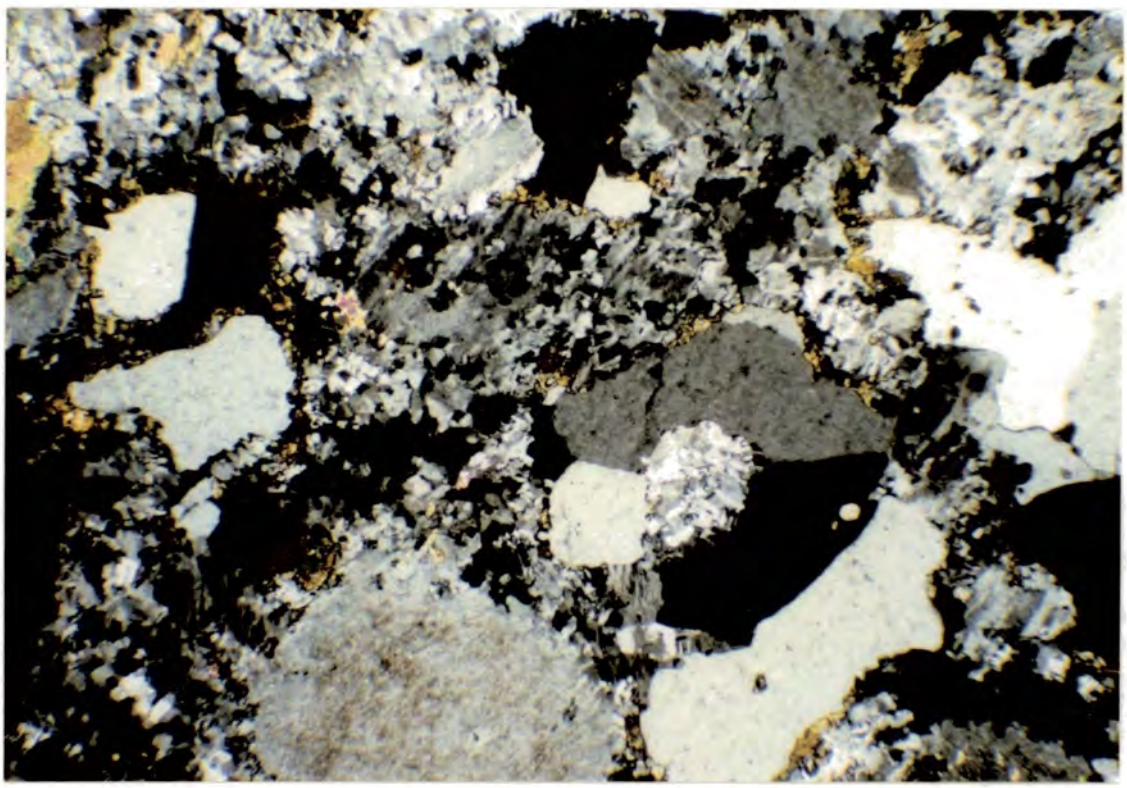

Plate 7.8. G197. ×35. XPL. Intergranular pyroxene (yellow interference colours) growing along the grain-boundaries between much coarser quartz grains, possibly partly replacing them.

up to 2mm × 3mm in size. These biotites show unusual pleochroism (α pale-brown; β, γ emerald-green, green-brown) zoned from brown cores to green rims. Kink-bands in the cleavages, possibly the result of later deformation, show up prominently. Phlogopite has been recorded by Rowbotham in 27281 (α pale-yellow; β, γ orange-brown), together with patches of tetraferriphlogopite, which has a 'reversed' pleochroic scheme (ie. α orange-brown; β, γ pale-yellow). The latter has also been found in G239, though phlogopite itself is entirely absent in this sample.

7.3: Mineralogy

7.3.1: Introduction

Analyses of minerals from the metasomatised rocks were carried out at Manchester and Durham. Electron microprobe operating conditions are described in Appendix II.

The products of alkali-metasomatism ('fenitisation') tend to be mineralogically syenitic, and Le Bas (1987) suggests that these rocks are commonly misidentified as igneous syenites. Where the effects of alteration were not distinguished in the field, petrographic evidence was used to determine the extent of the metasomatism.

To a large extent, the mineralogy (and hence also the whole-rock composition) depends on the composition of the original rock. Thus at Grønnedal-Íka, there are generally two distinct metasomatic rock types: the altered/carbonated syenites, which were originally igneous syenites of the complex, and altered gneisses, from the basement country rock (section 7.1).

Many workers (eg. Rubie 1982, Mian and Le Bas 1986, 1987) have related changing mineralogical compositions to increasing distance from the contact with the source of the metasomatic fluids. At Grønnedal-Íka this would not be practical, as field evidence did not suggest any systematic variation in degree of alteration

with position in the complex. This section therefore examines the mineralogy of the altered rocks, paying particular attention to any mineral zonation which may be present, and makes some comparisons with the mineralogy of the unaltered syenites, and with metasomatic rocks from other alkaline complexes.

7.3.2: Pyroxenes

Fig. 7.3.1A shows pyroxene compositions from the altered rocks plotted in the system Mg–(Fe^{2+}+Mn)–Na after recalculation to atomic proportions using the program `IRON3.STOIC` as described in section 4.2.2. There is a certain resemblance to the trend of pyroxenes from the unaltered syenites (fig. 4.2.1B), though most compositions from the altered rocks tend to be rather more sodic. Similar ranges in composition have also been noted by Chambers (1976) in fenitic rocks from North Qôroq, and by Andersen (1989) in altered rocks from the Fen complex in southern Norway. Both authors note the trend from aegirine-augite to aegirine, culminating in highly acmitic compositions (eg. Na>93% from Fen, Andersen *op. cit.*). The most sodic analyses from Grønnedal contain Na>95% from G26, an altered metabasite, while a sodium-poor group (Na_{18}–Na_{40}) occurs in G197, a sample from the gneiss raft, near the contact with the Lower Series Syenite (map 4 and plate 7.8).

An optically zoned pyroxene grain in an altered syenite (G9) was systematically probed from the core to the rim, the four analyses of which are joined by arrows in fig. 7.3.1. A large increase in Na and a slight decrease in Mg from core to rim is apparent. Rubie and Gunter (1983) reviewed the evidence for the compositional change from aegirine-augite to aegirine in metasomatic pyroxenes, and suggest that this is due to decreasing temperature with increasing evolution of the metasomatic fluids. This process appears to have given rise to the observed increase in Na content towards the rim. However, as reviewed in section 4.2.4, such changes may also be the result of crystallisation from an increasingly oxidising magma (eg. Larsen 1976, Jones 1980, Stephenson and Upton 1982). Le Bas

Fig. 7.3.1A. Pyroxene analyses from the metasomatised rocks in the system Mg–(Fe^{2+}+Mn)–Na. Although most are Na-rich, a relatively Na-poor group of compositions were analysed from G197. The compositional fields of fenitic pyroxenes from North Qôroq (Chambers 1976) and Fen (Andersen 1989) are shown for comparison. The core-rim variations in a zoned pyroxene from G9 are illustrated by joining the analyses with arrows.

Fig. 7.3.1B(two pages). Element variations in terms of atoms per formula unit (6 oxygens) plotted against Na-Mg as a fractionation index (Stephenson 1972). Core-rim compositions are joined by arrows, as in fig. 7.3.1A.

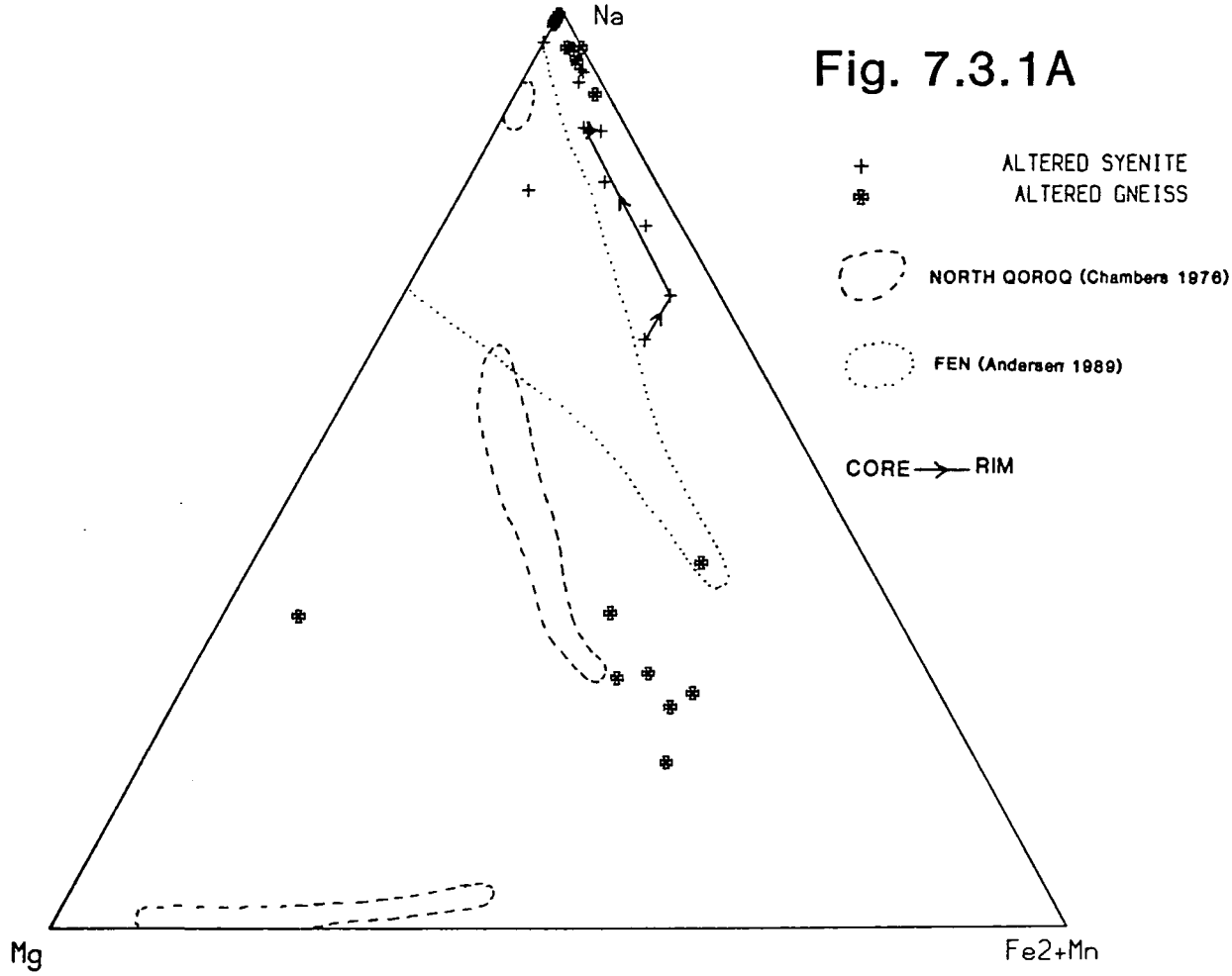

Fig. 7.3.1A

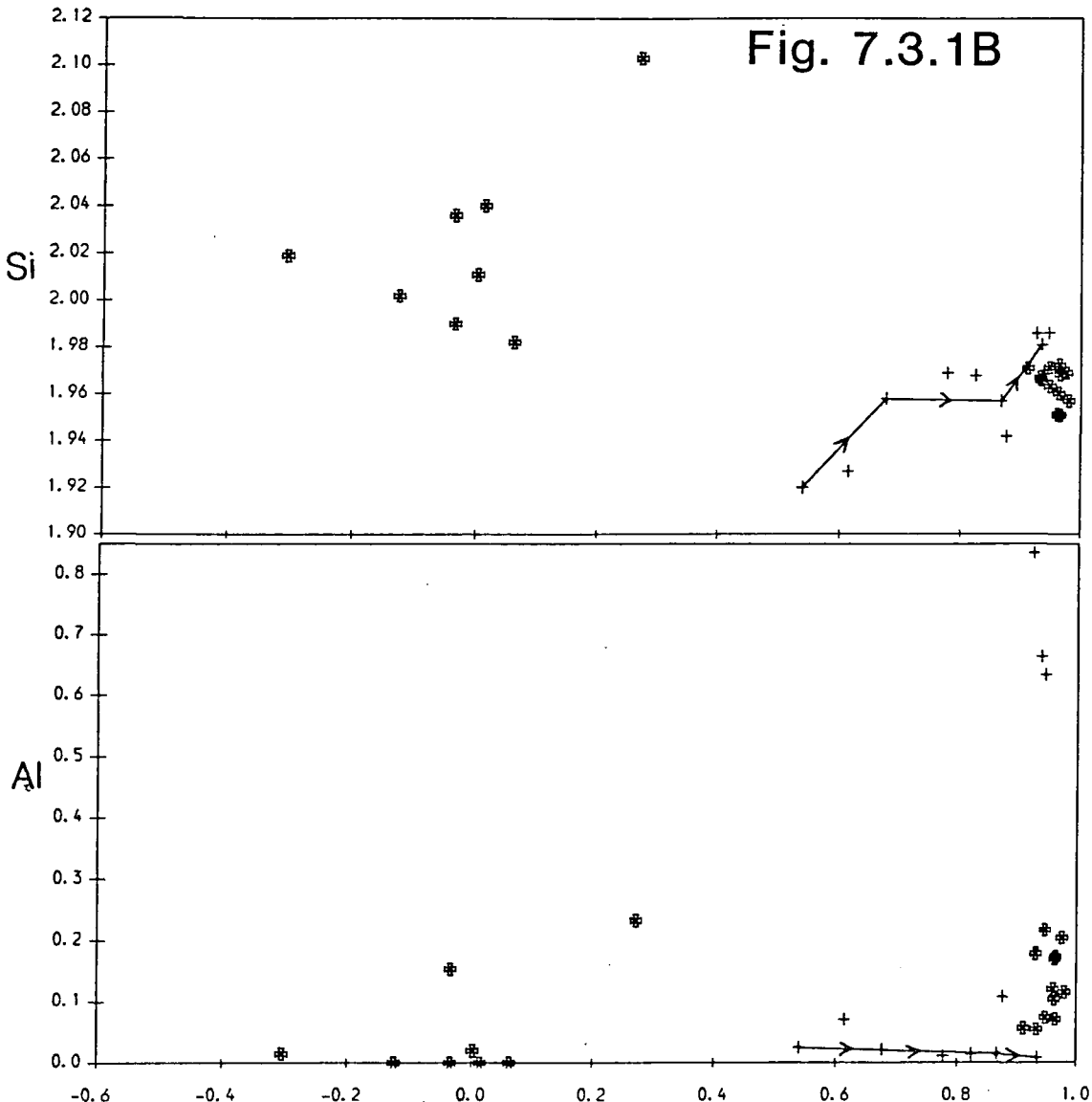

Fig. 7.3.1B

Fig. 7.3.1B (cont.)

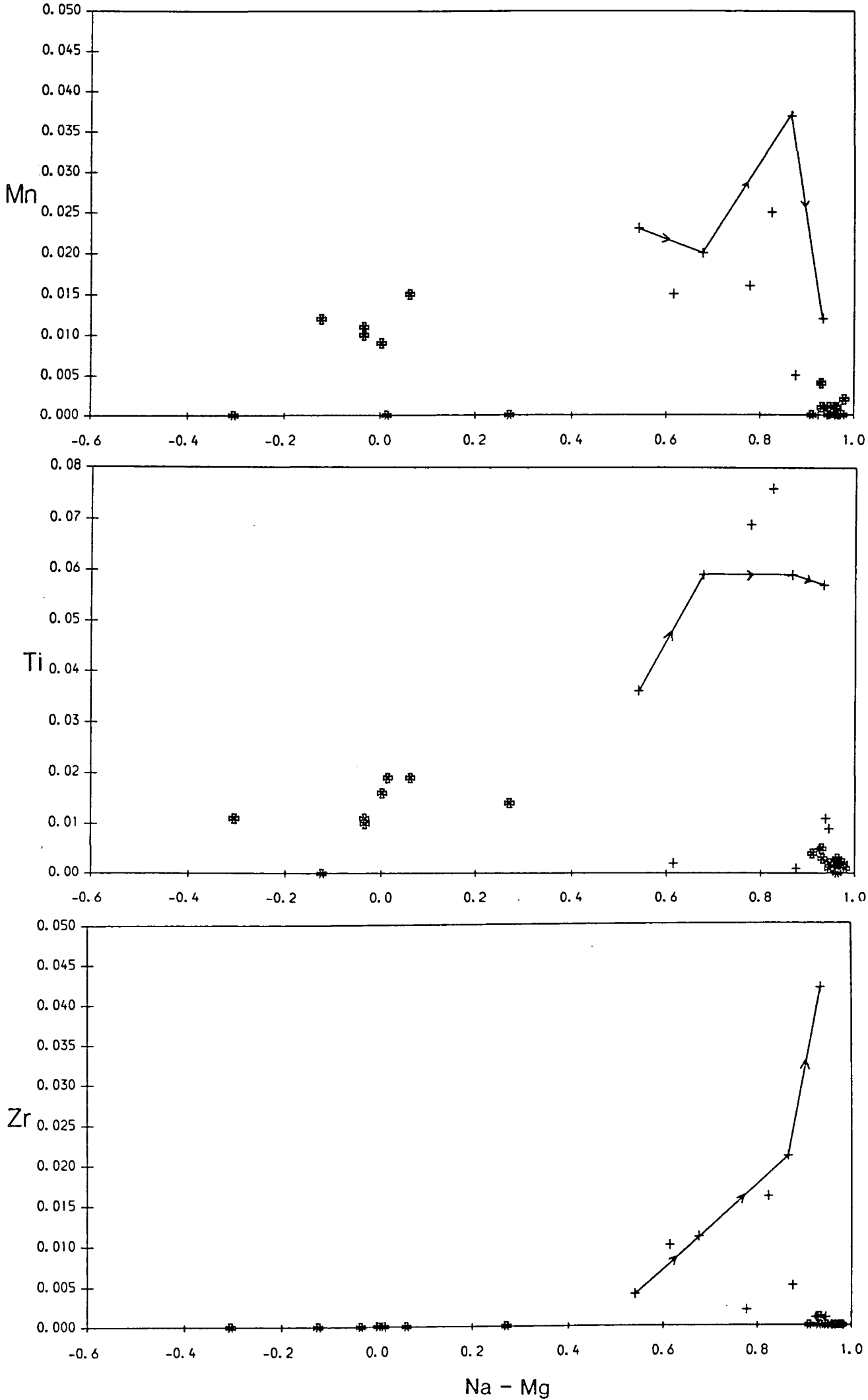

(1977) suggests that $a_{Fe^{3+}}$ of the fluids emanating from a carbonatite increases with fractionation, giving rise to increasingly 'oxidised' fenites. However, primary magmatic variation, and variation produced by post-magmatic (ie. metasomatic) alteration are frequently difficult to distinguish (Chambers, pers. comm.), and other mineralogical and petrographic information must be sought.

Other elements

The use of the parameter Na-Mg as an index of fractionation (Stephenson 1973) was described in section 4.2.7. The metasomatic pyroxenes are generally more strongly fractionated than those of magmatic origin, and a larger scatter of elements with increasing fractionation is evident (fig. 7.3.1B). Very high Al contents (>0.8 atoms per six oxygens) occur in G180, an altered syenite, suggesting a high proportion of jadeite, with a small amount of Fe^{3+} (in octahedral co-ordination), giving $Na(Al,Fe^{3+})Si_2O_6$. The four analyses from the zoned pyroxene in G9 show an increase in Si, Zr, and Ti, and a decrease in Al from core to rim. Mn shows erratic behaviour, but a general decrease is suggested from core to rim.

7.3.3: Amphiboles

Amphiboles are common constituents of a wide variety of fenites associated with carbonatites and silicate-dominated alkaline rocks (eg. Sutherland 1969, Woolley *et al.* 1972, Chambers 1976, Mian and Le Bas 1986, Andersen 1989). Analyses of amphiboles from two altered gneisses (G239, and G108) and one altered syenite (G9) were carried out, and although generally sodium-rich, the other elements show much variation. More than half of the analyses are classified as 'sodic amphiboles' according to Leake (1978), ie. Na_B >1.34, and occur mainly in the altered gneisses. Most of these are magnesio-arfvedsonites or riebeckites, the exception being a ferro-eckermannite from the altered syenite (G9), and are similar to amphibole compositions found in other fenites (cf. the above authors).

All other compositions are sodic-calcic (ferro-richterite and silicic edenite) or calcic (ferro-edenite and ferro-edenitic hornblende) according to Leake (*op. cit.*).

Plate 7.7 shows the marked zonation of amphiboles in G239. The pale-yellow cores consist of ferro-edenite or ferro-edenitic hornblende (richer in Si), which pass rapidly into purple-blue rims of riebeckite. Most elements show a consistent variation in abundance from core to rim:

Cores: richer in Ti, Al. Slightly richer in Fe^{2+}, Mn, Mg, Ca.

Rims: richer in Fe^{3+}, total Na, K, Zr.

These variations suggest that the metasomatising fluids became more alkali-rich with time, which in turn may have affected the activities of the other elements. Ernst (1962) showed that alkali amphiboles are stabilised by a high f_{O_2}, which would also give rise to a high $a_{Fe^{3+}}/a_{Fe^{2+}}$, although Carmichael and Nicholls (1967) suggested that high $a_{Fe^{3+}}$ may be a result of increasing alkali activity (the 'alkali ferric-iron effect', see also section 4.2.4). Watson (1979) showed that the solubility of Zr increases with peralkalinity in felsic melts, due to the formation of complexes such as Na_4ZrSiO_6. This effect may also occur in peralkaline metasomatic fluids, with complex formation possibly assisted by the halogens (particularly F) and CO_2 (eg. Pointer *et al.*, 1988). Higher Zr concentrations towards the rims of the amphiboles may thus be a result of crystallisation from increasingly peralkaline and/or halogen- or CO_2-rich fluids, which were able to transport more Zr in the form of zircono-fluoro-carbonate-silicate complexes.

Chemical variation

Comparisons with metasomatic amphiboles from other areas of the world are difficult due to the variety of different rock-types in which they occur, the composition of which must have affected the type of amphibole that may be present. Fig. 7.3.2A compares igneous and metasomatic amphiboles from Grønnedal-Íka in the

Fig. 7.3.2A. Amphibole analyses from the metasomatised rocks compared with compositions from the 'unaltered' syenites, plotted in the system Ca-Na-K (atomic proportions). Also shown are the compositional fields of amphiboles from fenitised gneisses associated with the Sarfartôq carbonatite complex in west Greenland (Secher and Larsen 1980). The core and rim compositions of the same amphibole crystal from G239 are joined by an arrow. Most notable is the difference between amphibole compositions from the altered gneisses and altered syenite (G9), the latter containing a considerably lower atomic proportion of K.

Fig. 7.3.2B(three pages). Amphibole element variations in terms of atoms per 23 oxygens, plotted using Na_B-Al_T as a fractionation index (Stephenson 1972), and compared with amphibole compositions from 'unaltered' syenites. Core-rim analyses from G239 are again joined by an arrow, and show an increase from core to rim in Si, Fe^{3+}, and Zr, and a decrease in the remaining elements. Although total Na increases considerably from core to im (fig. 7.3.2A), Na_A decreases.

Compositional field of amphiboles from unaltered syenites.

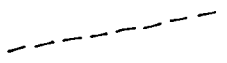

Trend of amphiboles from unaltered syenites.

Fig. 7.3.2A

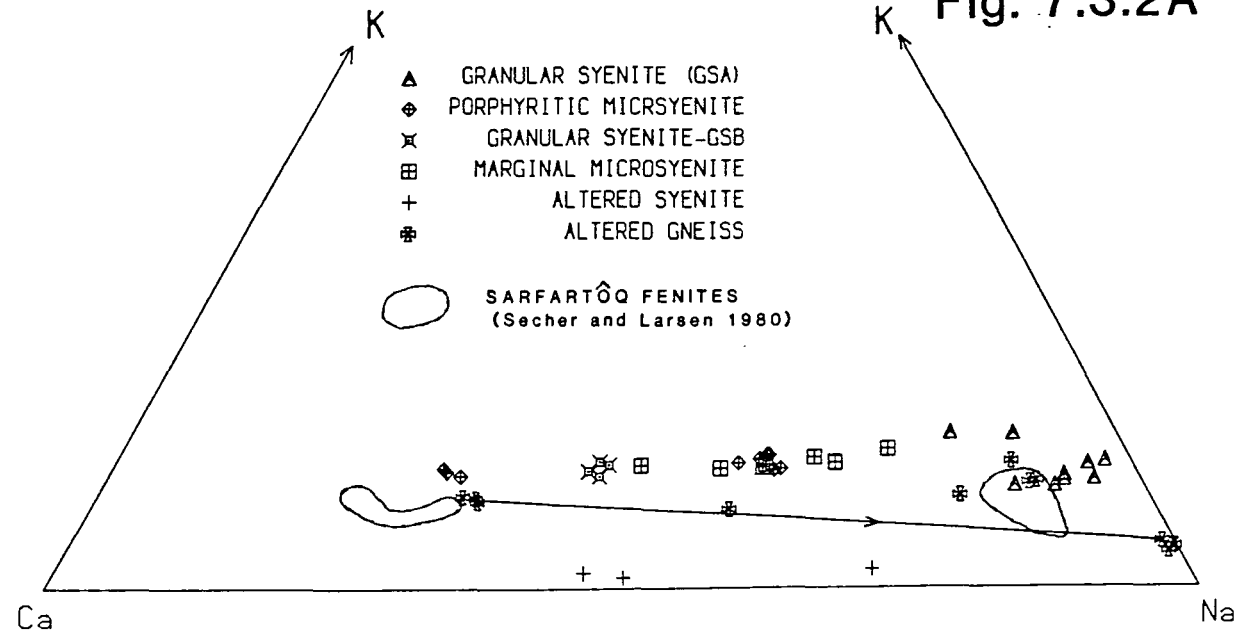

Fig. 7.3.2B

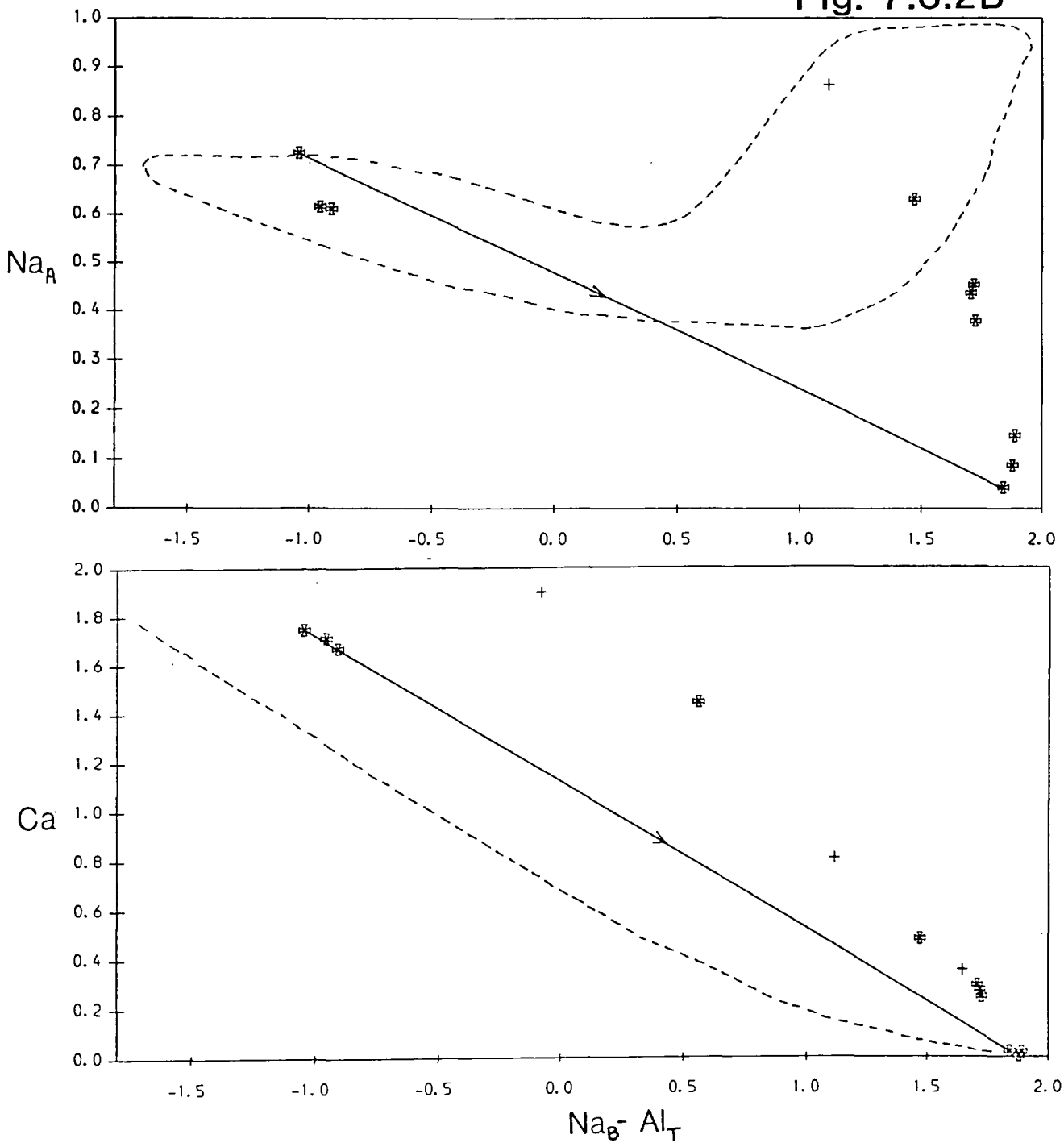

Fig. 7.3.2B (cont.)

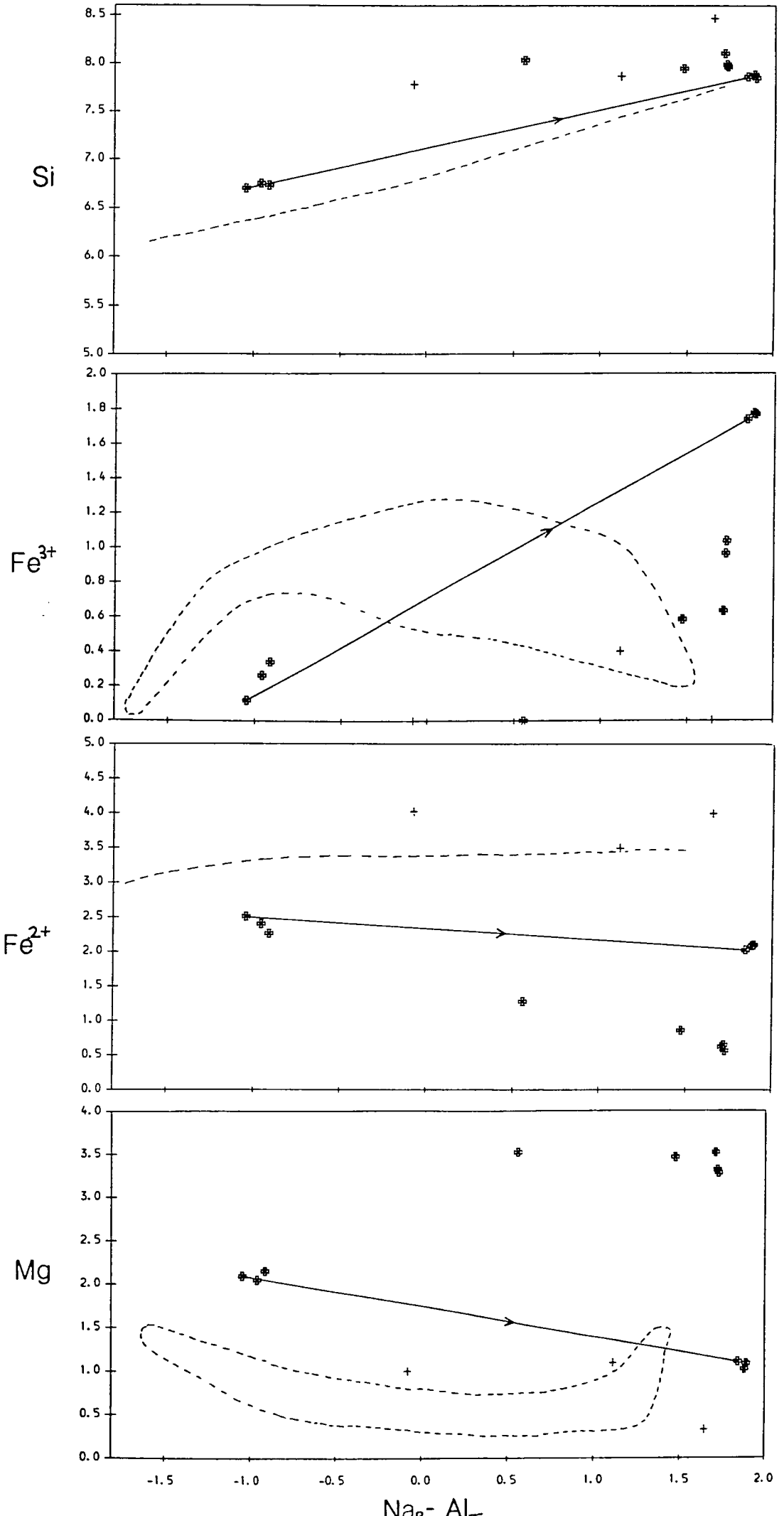

system Ca–Na–K with compositions from fenitised basement gneisses from Sarfartôq (Secher and Larsen 1980). Compositions from Sarfartôq are also magnesio-arfvedsonites (as well as some riebeckites), and have similar compositions to amphiboles from both the altered gneisses and unaltered syenites, while those from the altered syenites are consistently poorer in K. The core-rim compositions in G239 are connected by arrows and show strong enrichment in Na relative to Ca from the cores to the rims.

Element variation is also shown using Na_B-Al_T as an index of fractionation (Stephenson 1973) in fig. 7.3.2B, which compares the compositions of the igneous and metasomatic amphiboles. The wide range of values for most elements compared to the igneous amphiboles is probably a reflection of the variety of original rock compositions, and only Si shows a consistent increase with fractionation. However, some general comparisons with the compositions of igneous amphiboles can be made, the latter having lower Si, Mg, and Fe^{2+}, higher K, Ca, and Mn, and comparable Fe^{3+} and Ti. Some consistent variations occur between the altered syenite and gneiss amphiboles, those from the syenite having higher Fe^{2+} and lower K and Mg than those from the gneisses. The strong zonation in amphiboles from G239 is also shown in fig. 7.3.2B, and shows quantitatively the core-rim variations discussed above. Interestingly, although total Na content increases from core to rim, Na_A decreases. This is probably a result of a decrease in cations other than Na which occupy the B-site (particularly Ca), which Na will enter in preference to the A-site.

7.3.4: Micas

Based on petrographic observations, the majority of micas in the metasomatic rocks were identified as 'biotites', the compositions of which are illustrated in fig. 7.3.3A (after Deer *et al.*, 1966). All analyses plot in the biotite field, ie. Fe/Fe+Mg>0.333, although they tend to be slightly more magnesian than the 'igneous' biotites. Even so, none of the micas would be termed 'phlogopites', though

Fig. 7.3.3A. Classification of metasomatic micas using Fe/Fe+Mg vs. Al_T (Deer *et al.*, 1966). All analyses plot in the field of biotites, and most are comparable to the compositions from 'unaltered' syenites, although a few are slightly more magnesian. Four analyses of white mica from the 'carbosyenite' G272 are shown circled, and core-rim compositions for zoned biotites from G26 are joined by arrows.

Fig. 7.3.3B. MnO (wt.%) vs. Al_T. Biotites from the altered syenites are considerably richer in MnO than those from the gneisses.

Symbols as in figs. 7.3.1 and 7.3.2.

Compositional field of biotites from unaltered syenites.

Fig. 7.3.4A. TiO_2 (wt.%) vs. Al_T. The zonation in biotites from G26 shows a decrease in TiO_2 from core to rim. White micas from G272 are circled, and the compositional field of biotites from unaltered syenites shown dashed.

Fig. 7.3.4B. Mg–ΣFe–Ti (atomic proportions). Ti contents are generally lower in biotites from the altered rocks at a similar degree of fractionation (measured as Fe/Mg) compared to those from unaltered syenites.

Fig. 7.3.3A

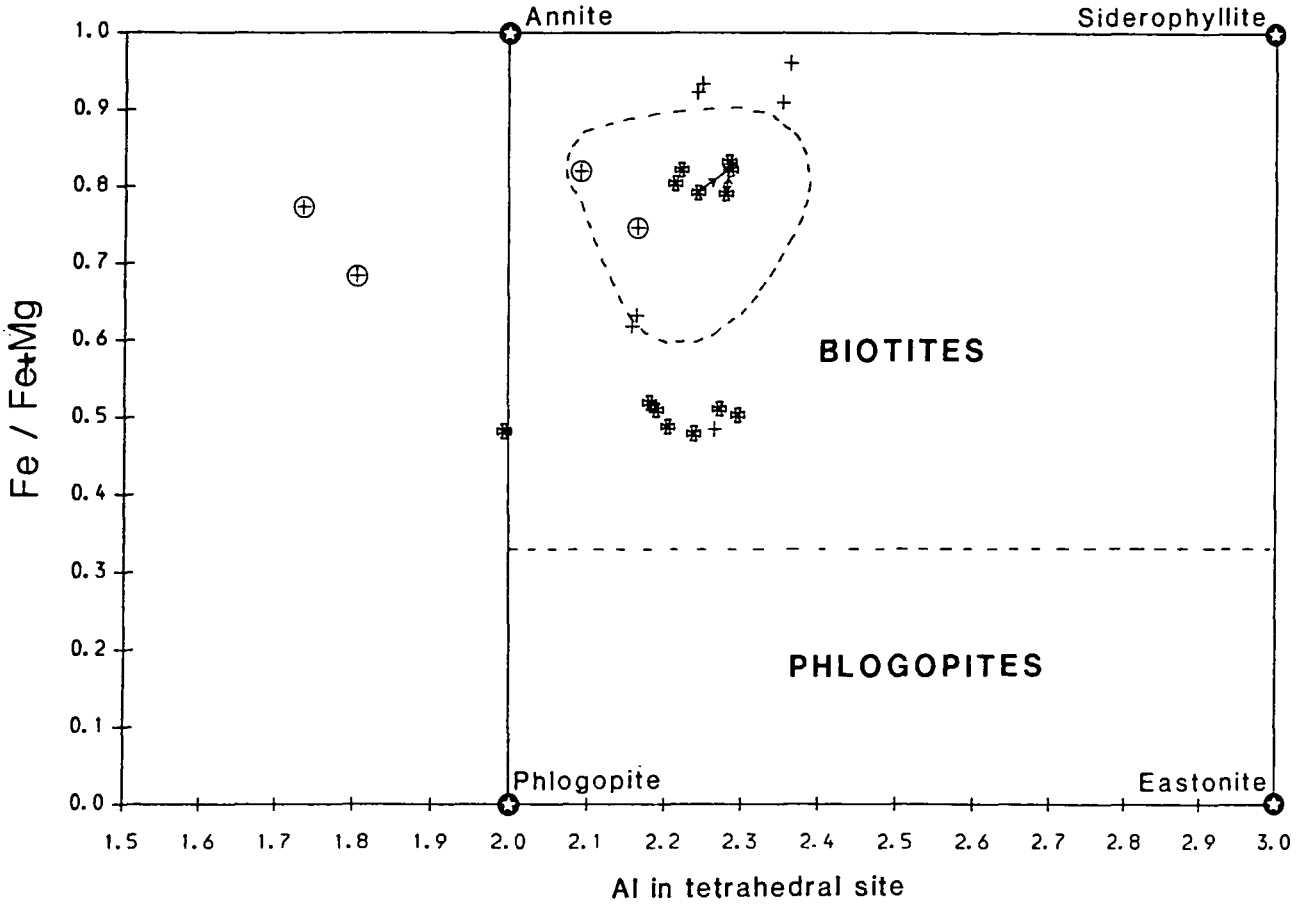

Fig. 7.3.3B

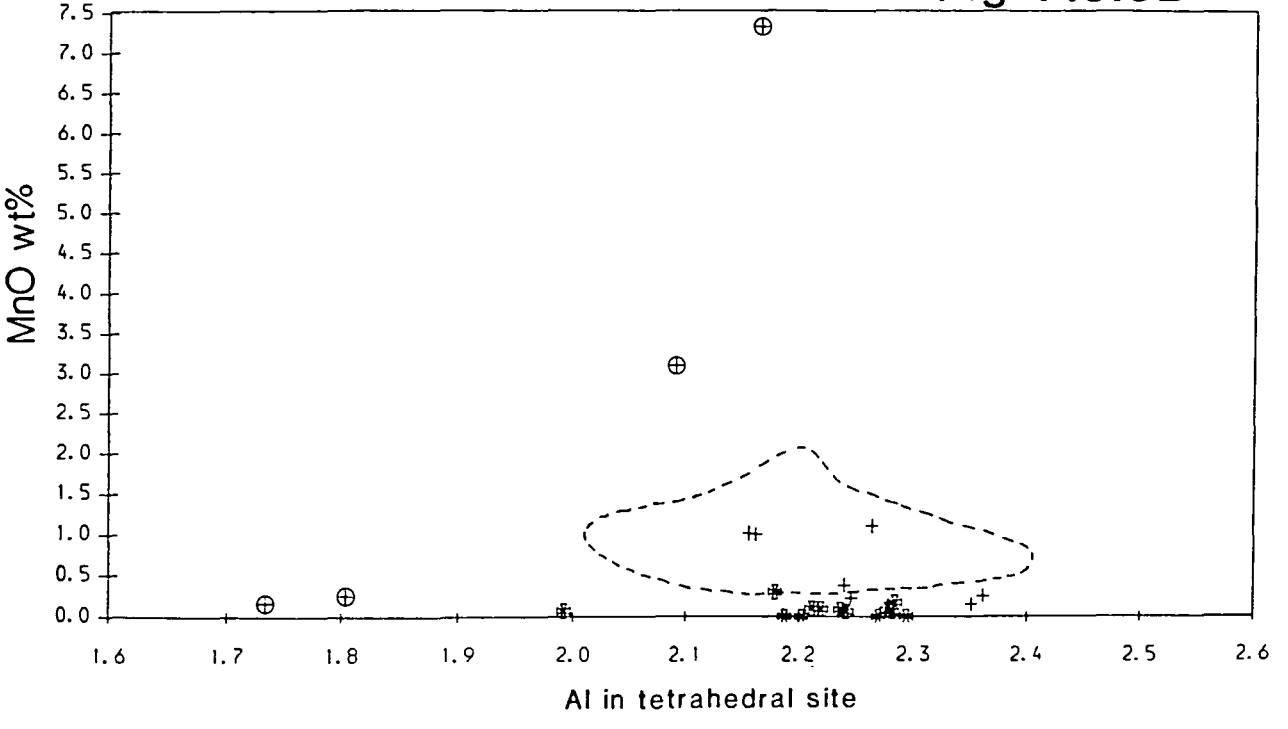

Fig. 7.3.4A

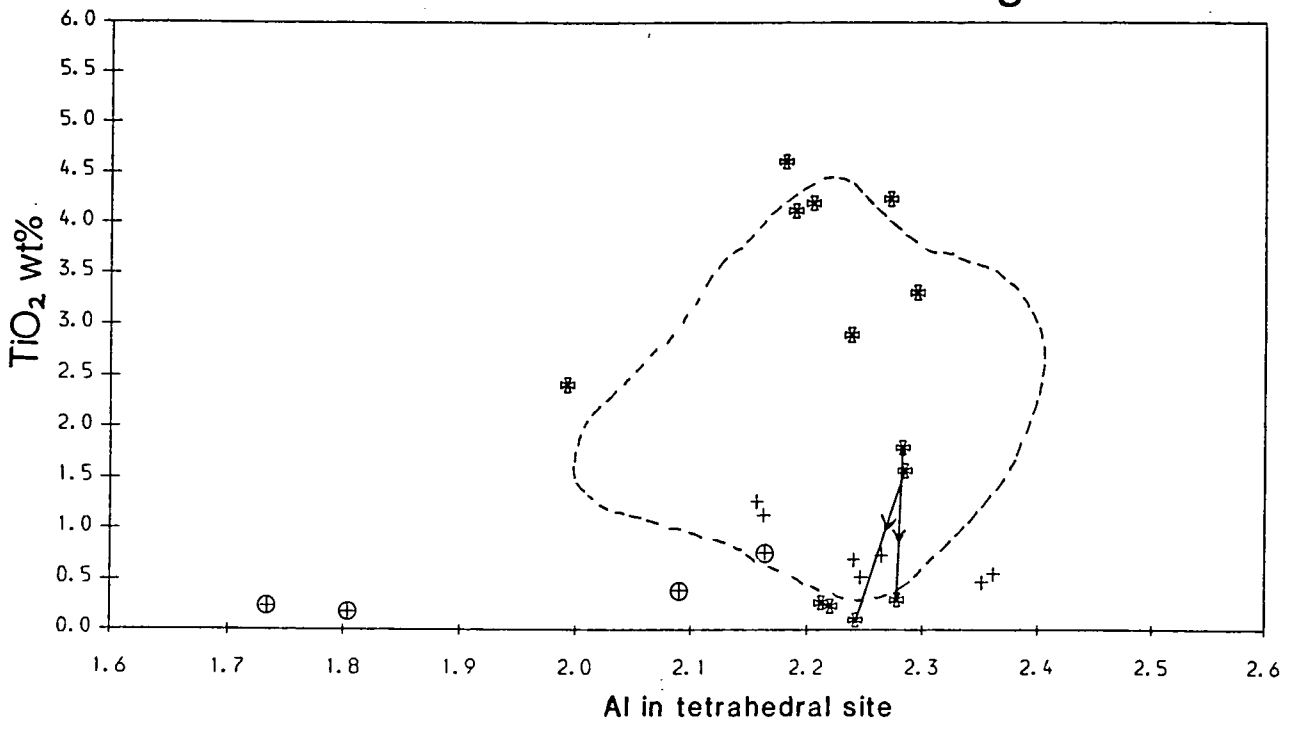

Fig. 7.3.4B

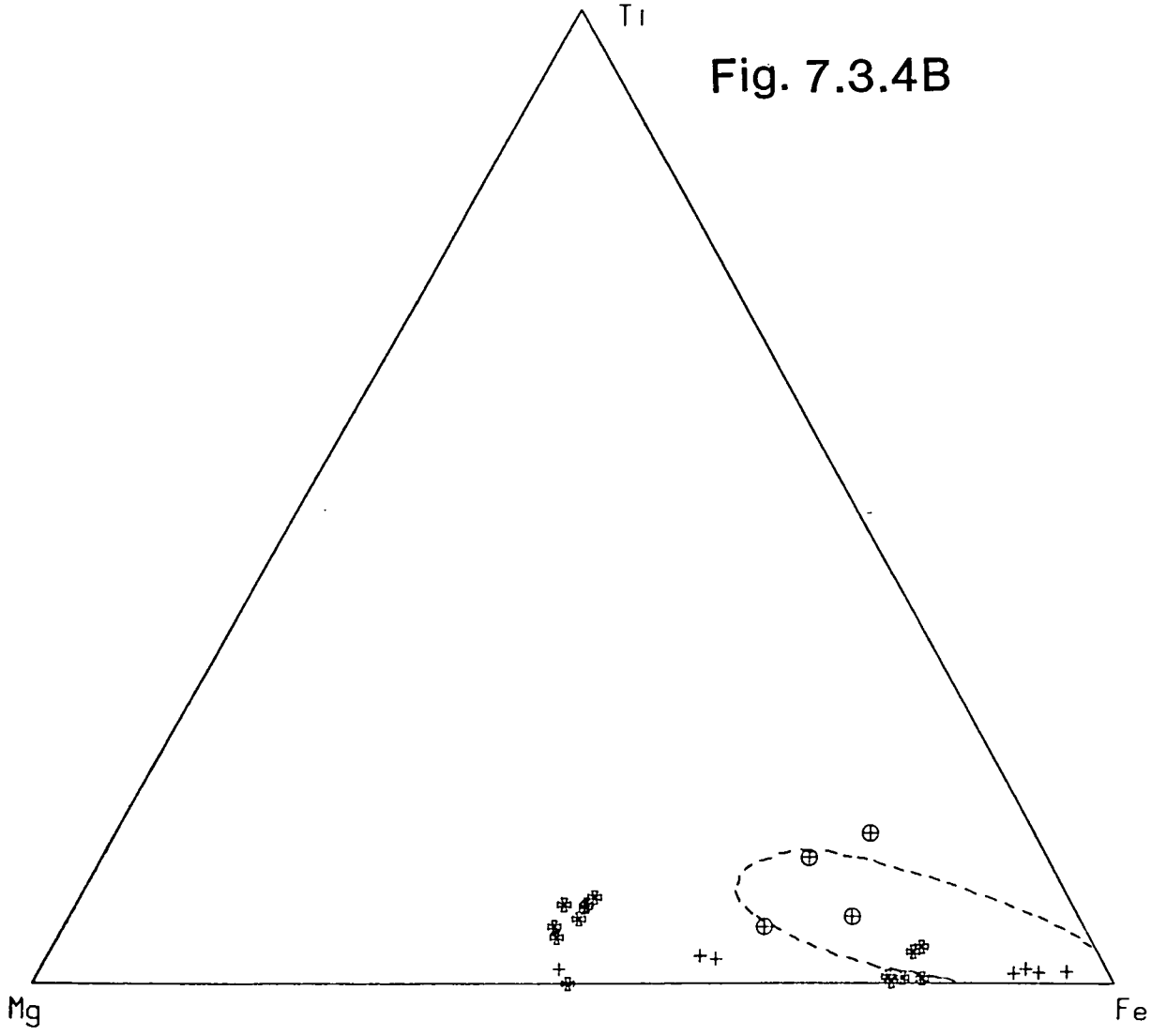

this mineral has been reported from fenites of the North Qôroq centre (Chambers 1976) and the Loe Shilman carbonatite complex, Pakistan (Mian and Le Bas 1987). The latter contains increasingly magnesian compositions as the contact with the carbonatite is approached, giving rise to a complete series from biotite to phlogopite. These micas occur in fenitised argillaceous rocks, however, so it is possible that the presence of phlogopite is dependent on host rock composition, although a lower temperature of metasomatism may be responsible for its absence at Grønnedal.

Four analyses of white micas from the carbosyenite G272 are shown circled in fig. 7.3.3A, which microprobe determinations have shown to be muscovitic in composition, containing around 5.5 Al atoms per 22 oxygens, occupying the Y (octahedral) site. Fig. 7.3.3B shows the very high values of Mn reported from these micas (MnO up to 7.3 wt%, equivalent to nearly one atom per 22(O)), far in excess of the maximum 2% described by Deer *et al.* (1966). It is possible that some of the oxide alteration material associated with these rocks has been incorporated into the analyses, but even for an oxide, this is a high value. MnO contents in the biotites (*sensu stricto*) are generally lower than in those from the unaltered rocks (fig. 7.3.3B), and are usually less than about 1%. Ti contents also tend to be lower in biotites from the altered rocks (fig. 7.3.4A), with a maximum of 4.6% TiO_2 in G197. The variation in Ti content is also shown in the Mg–Fe–Ti system (fig. 7.3.4B), and as for the igneous biotites, tend to show a decrease in Ti with increasing Fe/Mg, ie. increasing fractionation.

Zonation

Biotites from sample G26, an altered metabasic xenolith in the Upper Series Syenite, show prominent colour zoning from brown cores to green rims. Microprobe investigations have shown that the cores are richer in TiO_2 than the rims (fig. 7.4.4A), the opposite of the variations in biotites from the Sarfartôq fenites (Secher and Larsen 1980). Other elements showing a consistent core-rim variation

are Mg, Ca, and Na, which are all slightly more abundant in the green biotite rims. Deer *et al.* (1966) suggest that the brown colour of biotites is due to Ti, while Fe^{3+} gives rise to green biotites. Although Fe^{3+} cannot be accurately determined due to the non-stoichiometric composition of the biotites, the very low Ti contents of the rims in G26 (TiO_2 <0.35%) suggests that it may be a lack of Ti, rather than excessive amounts of Fe^{3+} which allows the green colour to be seen.

7.3.5: Oxides

Oxide mineral compositions are shown in fig. 7.3.5A. As for all but one of the analyses in the syenites and carbonatites, those from the metasomatic rocks are magnetite-rich members of the magnetite-ülvospinel series. Three distinct groups of analyses are apparent, reflecting the results from three different samples (G26, G136, and G146). Elements other than Fe are very scarce, the next most abundant being Ti (up to 4.4% TiO_2) followed by Si (up to 4.3% SiO_2), while of the remainder, only MnO exceeds 1% by weight.

7.3.6: Feldspars

Microprobe analysis of the feldspars was carried out using a rastered electron beam in an attempt to overcome the analytical problems associated with perthitic exsolution (cf. section 4.7.2). The results are illustrated in the system Albite-Orthoclase-Anorthite ($Ab - Or - An$, fig. 7.3.5B). This gives a rather misleading impression of the distribution of analyses, however, as the great majority of compositions are almost certainly very rich in Ab, although more grains were tested which were obviously not albitic. Two analyses from a carbosyenite (G272) plot quite close to Or, however, and there is some scatter towards Ab. Up to 0.21 atoms of Ca per eight oxygens occur in one sample of altered gneiss (G239), the composition of which has probably been influenced by the presence of plagioclase in the original rock. Of the remaining elements, Fe does not usually exceed 1% by

Fig. 7.3.5A. Oxide compositions in the system RO–R_2O_3–RO_2, with end members calculated using the method of Carmichael, *et al.* (1967). All compositions are magnetite-rich members of the *mgt-üsp* series.

Fig. 7.3.5B. Feldspar compositions in the system *Ab–Or–An* (molecular wt%). Although the majority of analyses are highly albitic, a range of compositions between albite and orthoclase is apparent.

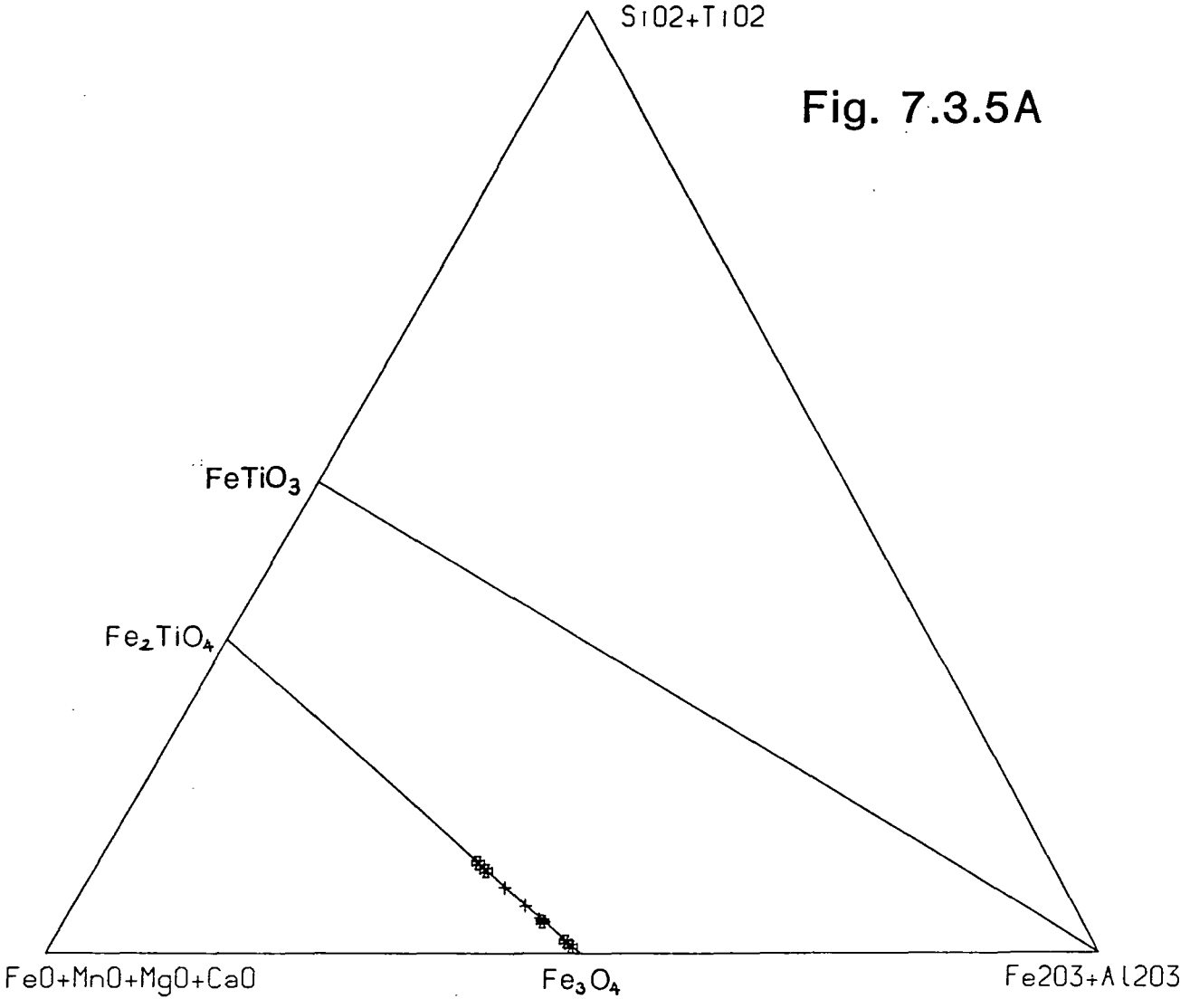

Fig. 7.3.5A

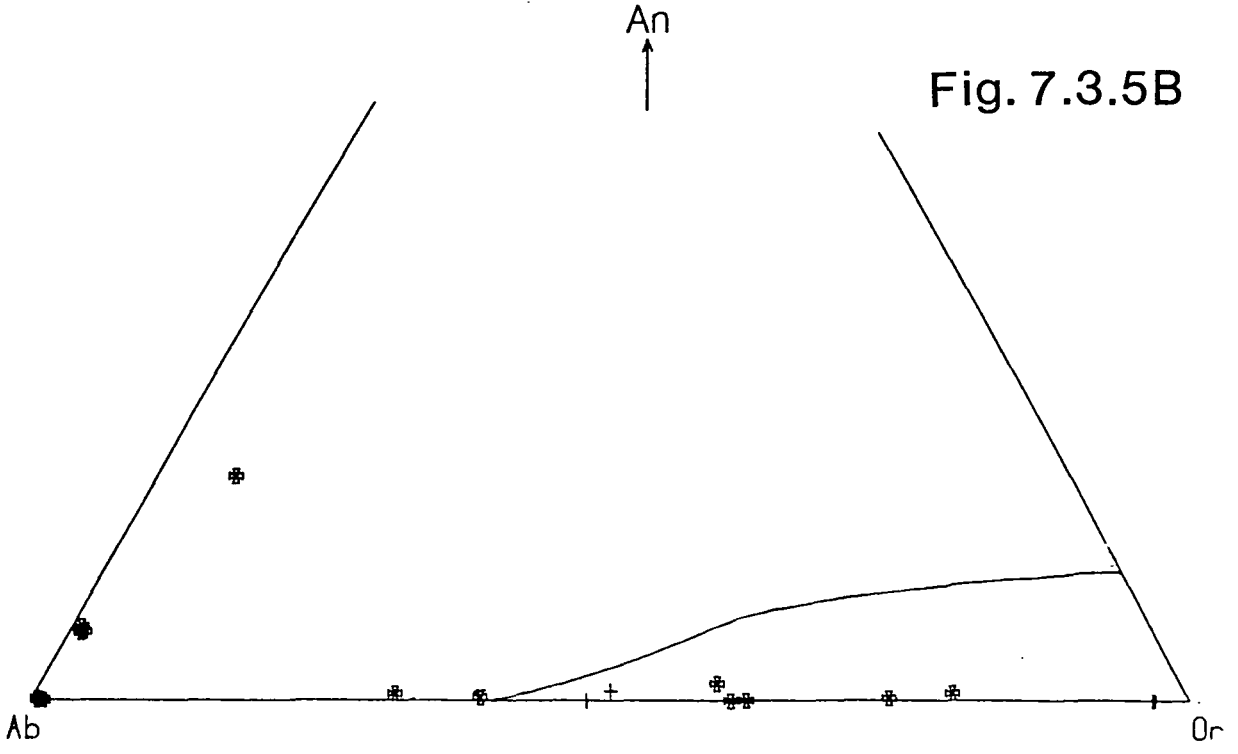

Fig. 7.3.5B

weight of oxide, and is not significantly different from amounts in the feldspars of the unaltered syenites, while Ba reaches a maximum of 0.7% BaO in G197.

Rae and Chambers (1988) suggest that discrete grains of albite and orthoclase, present in metasomatised syenites from the North Qôroq centre, are a result of extreme unmixing assisted by fluids, with little or no addition of Na. Sample G272 contains separate orthoclase and albite end-member phases, although some intermediate compositions (with $ab \approx or$) also occur. Rae and Chambers (*op. cit.*) also note that against the outer margins of North Qôroq, the country rock has experienced strong albitisation, and contains up to 85% modal albite. Although such extreme alteration has not been recorded at Grønnedal-Íka, it does appear that the large quantities of albite in some of the altered gneisses may be a result of the addition of Na, whereas the syenites already contained sufficient quantities of the appropriate phases, and the albite is a result of unmixing and recrystallisation.

7.3.6: Zircon

The occurrence of zircon has already been noted in the Coarse-Grained Brown Syenite, considered to be a less strongly altered facies than the syenites described here, and the mineral is a relatively common phase in both the metasomatised syenites and gneisses. As with the zircons in the less altered and unaltered rocks, very little variation in composition was detected, and after Si and Zr, only Na appears to be present in more than trace amounts (up to 0.76% in G180), and thus only a few analyses were made. A reconnaissance of the REE content was carried out, but found to be present in insignificant quantities (generally below the detection limit of the EDS microprobe).

The occurrence of zircon in metasomatic rocks from the roof zone of the Motzfeldt Centre has been noted by Tukiainen *et al.* (1983), and also by Pointer *et al.* (1988) and Rustamov *et al.* (1988), in altered rocks from Nigeria and the

Caucasus respectively. The latter note "granite-granosyenites....having metasomatic (post-magmatic) zircons in their apical portions", while Pointer *et al.* (*op. cit.*) found zircons in albitised rocks, and propose that they crystallised from F-bearing metasomatic fluids.

Although no fluorite was found in any of the samples at Grønnedal-Íka (altered or unaltered) in this study, Emeleus (1964) found this mineral occurring as interstitial grains in the Lower Series Syenite. The presence of sodalite and carbonate (below) points to the existance of Cl- and CO_2-bearing fluids which may also have assisted with the transport of Zr during metasomatism. In addition, Zr becomes increasingly soluble with increasing peralkalinity (Watson 1979). The presence of alkali amphiboles and pyroxenes suggests that the metasomatic fluids were peralkaline in character, and could have carried Zr in the form of complexes such as Na_4ZrSiO_6.

7.3.7: Other minerals

Carbonate

Le Bas (1987) suggests that carbonate minerals are rare in fenites unless associated with a carbonatite. Their abundance in many of the altered rocks (eg. the 'carbosyenites') thus points to the carbonatite as an important source of the metasomatising fluids.

The compositions of the carbonate minerals from the metasomatised rocks are very comparable to those from the unaltered syenites, being predominantly Ca-rich. After CaO, FeO and MnO are the next most abundant components, although neither exceeds 2% by weight. BaO reaches 0.25% in G136, while SiO_2 is commonly around 0.2% in most of the analyses. None of the other elements exceed about 0.15% by weight of oxide.

Sodalite

Three sodalite analyses from G180 were made, which contain around 8% Cl. This is equivalent to around one atom per twelve oxygens, and corresponds well with the theoretical formula of sodalite ($3NaAlSiO_4.NaCl$).

Analcite

The presence of analcite has already been noted in the unaltered syenites (section 4.10). Three analyses from the altered syenite G136 were made, and show that only Si, Al, and Na exceed 0.5% (oxide) in abundance.

A secondary origin for analcite has been suggested by Henderson and Gibb (1977) to account for the presence of this mineral in the crinanite of the Dippin Sill on Arran, by a reaction between albite and nepheline. A secondary origin seems highly likely at Grønnedal in view of the altered nature of the rocks in which this mineral commonly occurs.

Quartz

Two quartz analyses were made while analysing for felsic phases in the altered syenite G9. The close proximity of this sample to the contact with the country-rock gneisses (around 3m) suggests that the presence of this mineral may be a result of wall-rock contamination.

7.4: Geochemistry

7.4.1: Introduction

XRF analyses for major and trace elements were carried out on strongly altered samples of syenite and gneiss, using the methods described in Appendix III. Some samples were collected (eg. G113, G114) which at the time were were thought to be good representatives of unaltered gneiss, with which the altered gneisses could have been compared. However, later petrographic examination

showed that these samples had in fact experienced the effects of metasomatism. There are numerous analyses of 'unaltered' syenites, however (chapter 5), the compositional field of which is shown on all the element variation diagrams in this section.

Direct comparison between altered and unaltered rocks in terms of weight % of oxide is unsatisfactory. For example, if the metasomatism is primarily an additive process, with an overall increase in rock mass and no exchange taking place, some elements may appear to decrease in abundance. McKie (1966) assumed that exchange was dominantly cationic, and recalculated analyses to a standard cell of 100 oxygens. This concept of immobile oxygen has since been questioned by Rubie (1982), who considered metasomatic gains and losses in terms of a range of possible volume changes (after Gresens 1967). Field and petrographic observations from Grønnedal-Íka show no evidence for a volume change during metasomatism, and thus the method of McKie (*op. cit.*) is preferred, with major element analyses recalculated to a 100 oxygen cell.

Many authors (eg. Woolley *et al.* 1972, Rubie *op. cit.*, Rubie and Gunter 1983) describe whole rock geochemical changes in terms of the distance from the contact with the source of the metasomatism. Such an approach is impractical here, as the alteration is extremely patchy, and like many other regions of metasomatic alteration, probably strongly dependent on, for example, initial rock composition, permeability, and texture. As the process of metasomatism generally involves loss of Si and gain of Na (eg. McKie 1966, Woolley *et al.* 1972, Chambers 1976), and for which there is good petrographic evidence at Grønnedal (eg. sample G197, plate 7.8), chemical variations are plotted using Na-Si (atoms per 100(O)) as a fractionation index.

7.4.2: Major elements

Major element compositions of metasomatised gneiss and syenite samples are shown in fig. 7.4.1, and compared with the compositions of unaltered syenites. Sample G75, a carbonated basic dyke from the Hyttelv (map 3) lies out of the range of these diagrams, with Na-Si=-5.75. It is remarkably rich in Ca (37.6% CaO) and P (13.3% P_2O_5), containing a large proportion of modal apatite and calcite, and of the other elements, only Fe exceeds 6% (9.16% total FeO). To include this sample would skew the diagrams unrealistically.

A large amount of scatter is evident, presumably at least partly as a result of the heterogenous nature of the original rocks, and although a few elements show a constant trend, this too may be a reflection of the original rock composition. For example, total Fe and Ca+Mg+Fe+Al all increase with increasing degree of alteration (Na-Si), a feature which also occurs in metasomatic rocks from Oldonyo Dili (McKie 1966), Callander Bay (Currie and Ferguson 1971), and North Qôroq (Chambers 1976). Such a change might also be expected in the unaltered equivalents, since during fractionation of igneous rocks, silica generally increases, and the ferromagnesian elements tend to decrease. Thus the fenites derived from igneous rocks at the above localities may show a similar variation, which might be interpreted as being a result of metasomatic alteration. Mn also shows a slight increase with Na-Si, a feature common to many fenites, though possibly for the reasons described above rather than any metasomatic changes, while K decreases slightly, as at Oldonyo Dili (McKie *op. cit.*).

Other elements show no consistent variation, although some comparisons can be made between the altered gneisses and syenites. The latter tend to be slightly richer in K and Al than the gneisses, which may again be related to original compositional differences rather than any metasomatic changes. Somewhat surprisingly, perhaps, the gneisses are richer in Na, possibly due to the breakdown

Fig. 7.4.1(three pages). Major elements, Na+K, and Ca+Mg+Fe+Al, recalculated to a 100 oxygen cell, following the method of McKie (1966), and plotted against Na-Si (100(O)) as an index of fractionation (see text).

Compositional field of unaltered syenites (recalculated to 100(O)).

Fig. 7.4.1

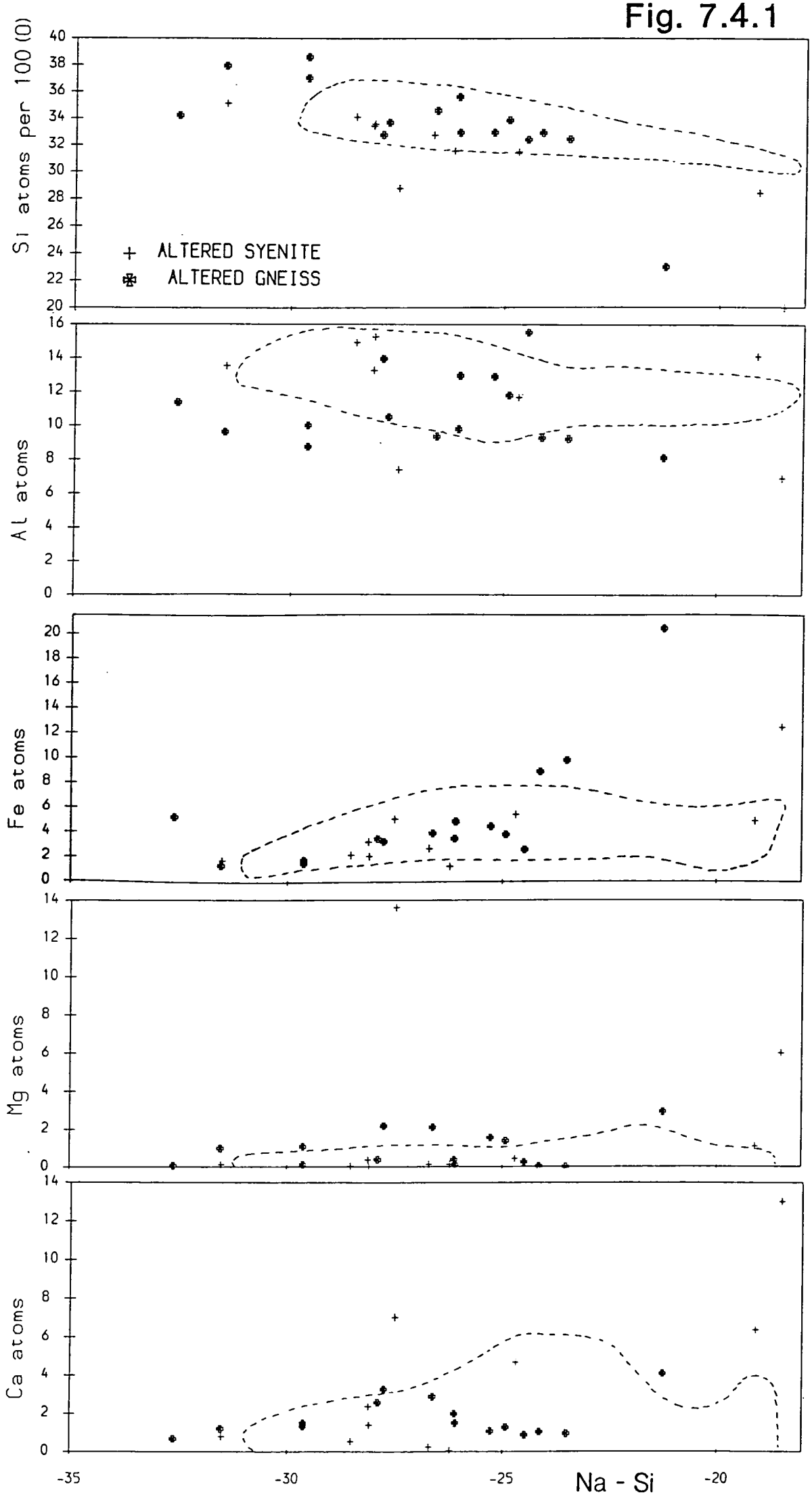
Si atoms per 100 (O)
+ ALTERED SYENITE
ALTERED GNEISS
Al atoms
Fe atoms
Mg atoms
Ca atoms
-35
-30
-25
Na - Si
-20

Fig. 7.4.1 (cont.)

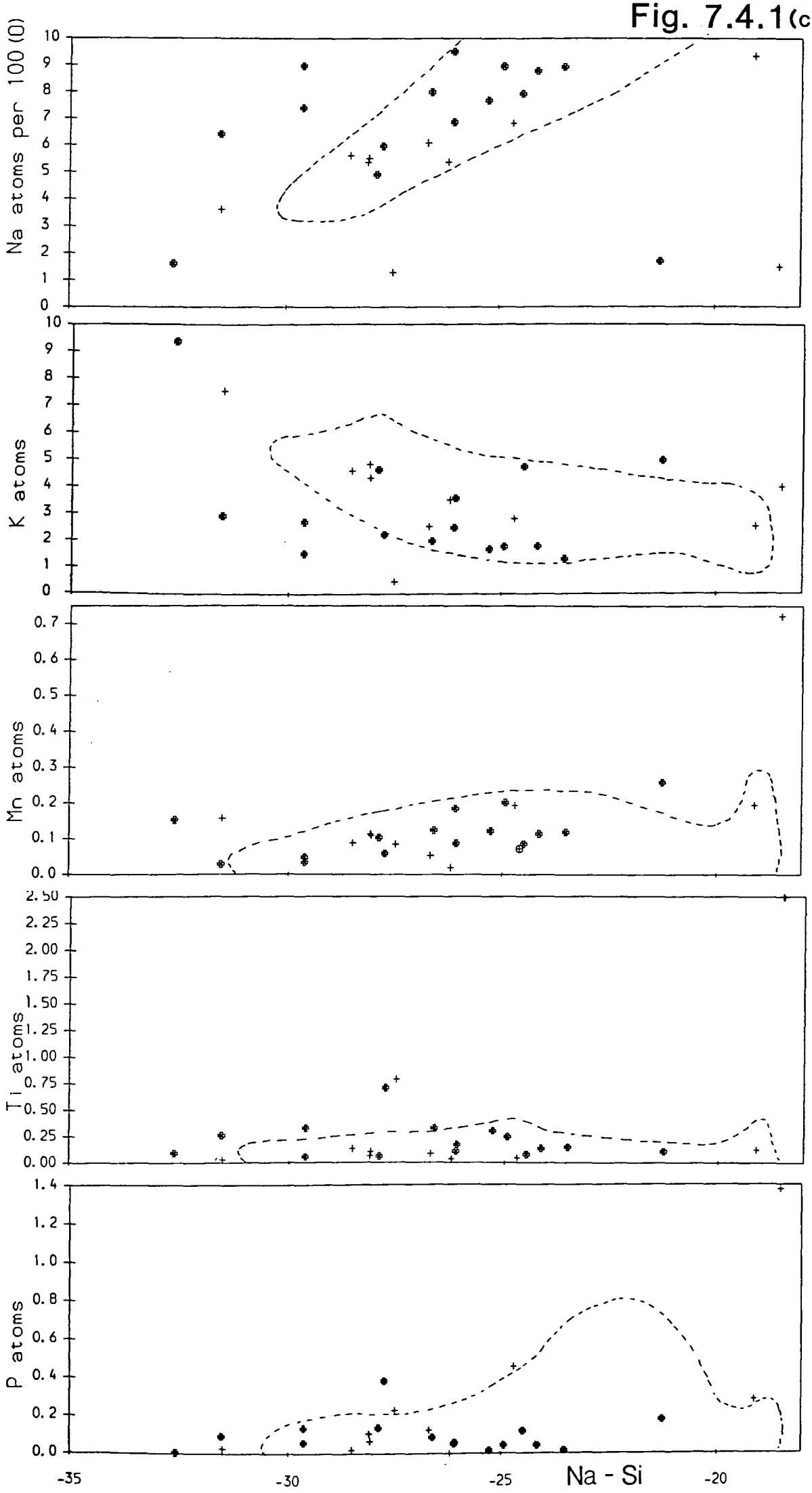
Na atoms per 100 (O)
K atoms
Mn atoms
Ti atoms
P atoms
Na - Si
-35
-30
-25
-20

Fig. 7.4.1(cont.)

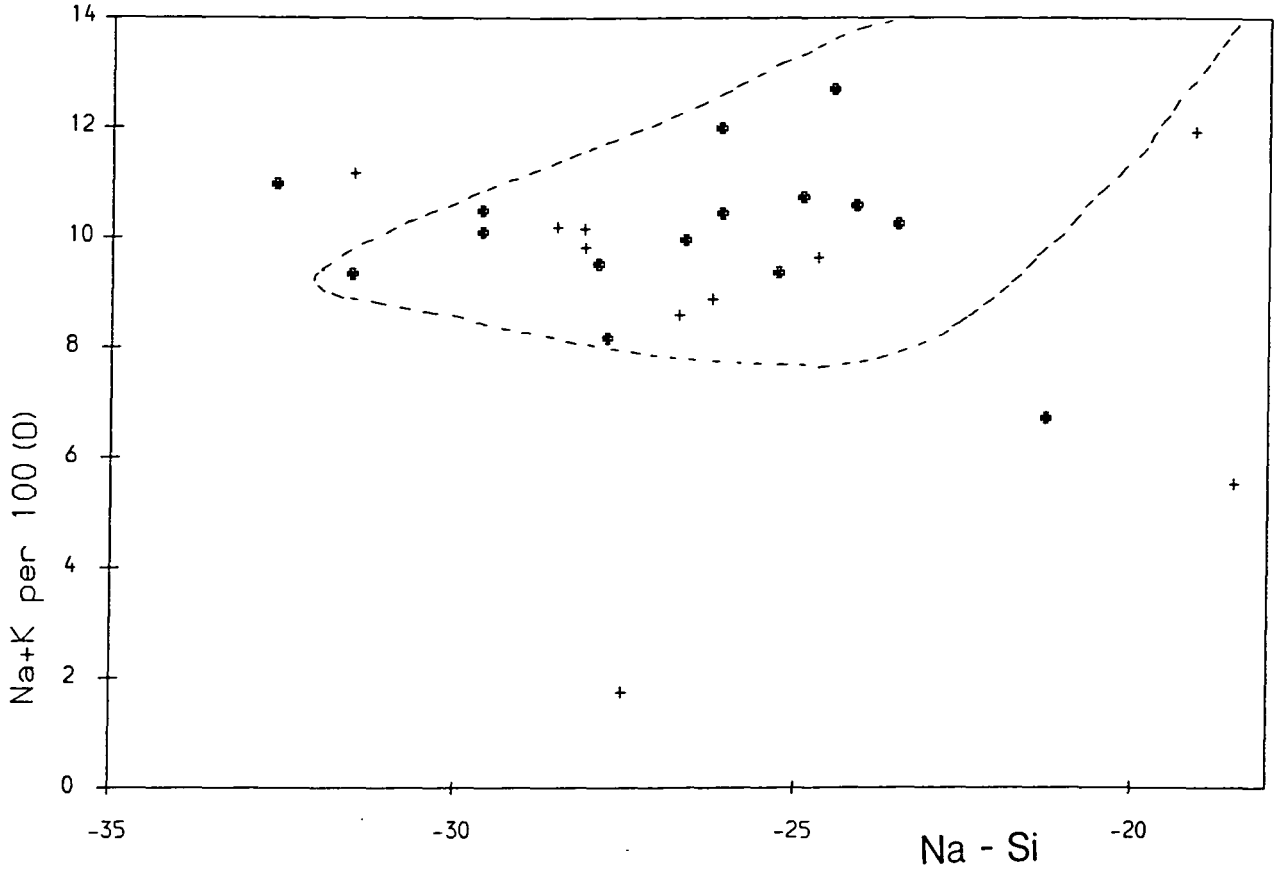
14
12
10
8
6
4
2
0
Na+K per 100 (O)
-35
-30
-25
-20
Na - Si

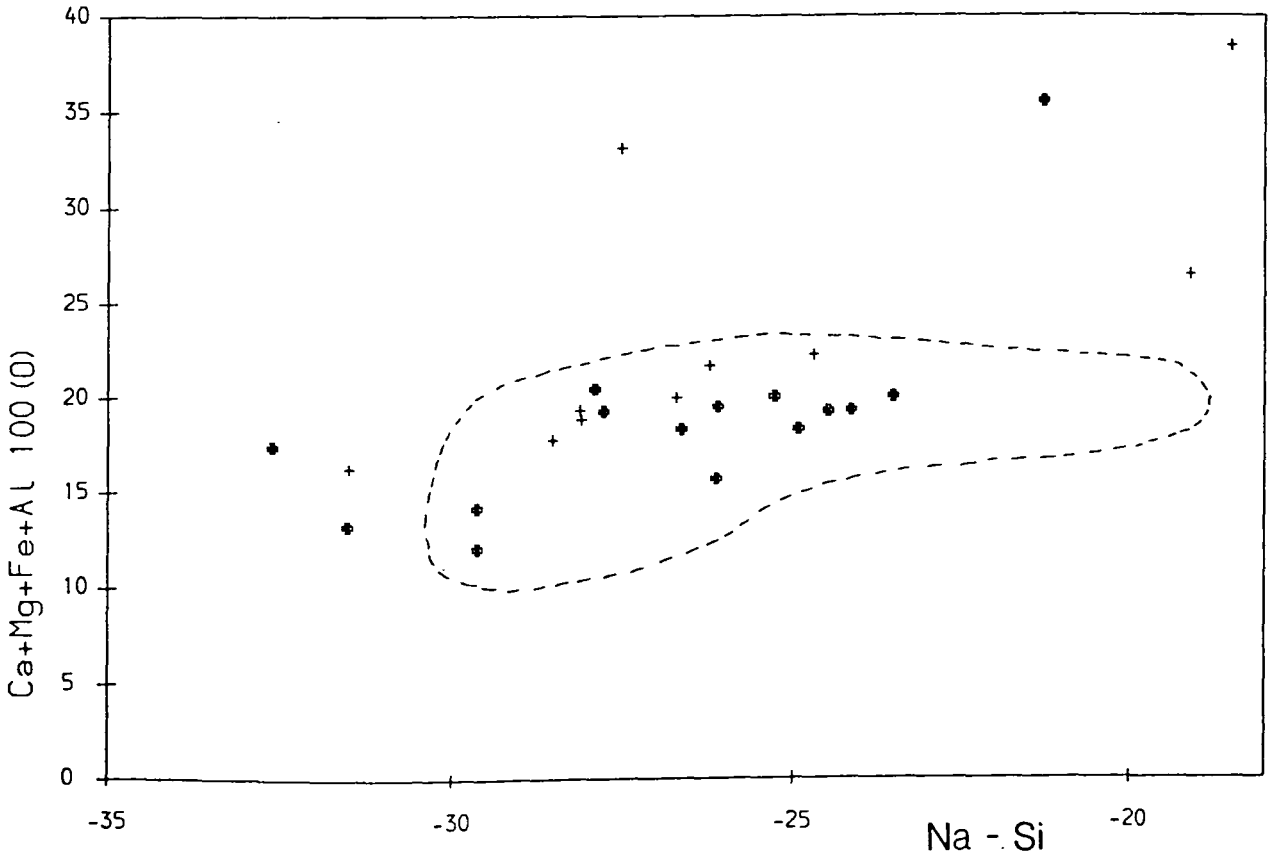
40
35
30
25
20
15
10
5
0
Ca+Mg+Fe+Al 100 (O)
-35
-30
-25
-20
Na - Si

of nepheline (a major Na-bearing phase) and loss of this element from the syenites. Although alkali feldspar is present in both the altered gneisses and syenites, the gneisses frequently contain a high modal proportion of alkali pyroxene and amphibole. These minerals are generally less abundant in the syenites, and may be the principle cause of the different whole-rock Na contents. Chambers (1976) suggests that Na may be fixed by reaction with quartz to give alkali amphiboles and pyroxenes, evidence for which is shown in plate 7.8, where pyroxene appears to be replacing primary quartz along the grain-boundaries. The absence of quartz in the syenites means that Na cannot be fixed by such a reaction, and does not reach such elevated abundances.

7.4.3: Trace elements

Trace element variations (in ppm by weight of element) are shown in fig. 7.4.2, again using Na-Si as an index of fractionation. As for the major elements, a large scatter of values is evident, and no real trends can be made out, although some interesting comparisons with the unaltered syenites can be made. Sample G75 is again omitted for the reasons outlined in the previous section, but contains some extreme trace element abundances compared to the other metasomatised samples:

	Y	Sr	Rb	U	Th	Nd	La	Ce
G75 (ppm)	905	8957	29	16	80	3755	4274	7174
Others (range)	3-124	158-4686	45-879	2-13	8-40	13-264	0-223	29-422

The high REE and Y contents may be accounted for by the high proportion of modal apatite, while carbonate minerals and apatite are the most likely host for Sr. The radioactive elements (U, Th) may be hosted by occasional small, very dark-brown grains which occur in G75. Sample G276, a calc-silicate rock (?altered basic dyke) from the vicinity of the Jernhat, is markedly enriched in the transition metal elements compared to other samples:

Fig. 7.4.2(two pages). Trace element compositions of the altered rocks (in ppm) plotted against Na-Si as an index of fractionation. Only those elements which show features of significance are illustrated (see text), and are compared with the compositions of unaltered syenites (dashed field).

Fig. 7.4.2

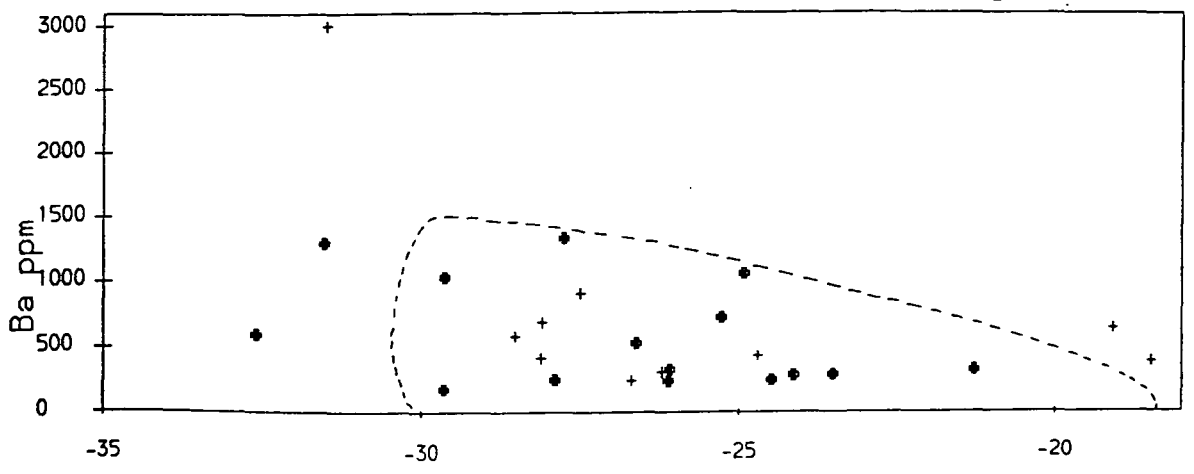
Ba ppm
3000
2500
2000
1500
1000
500
0
-35
-30
-25
-20

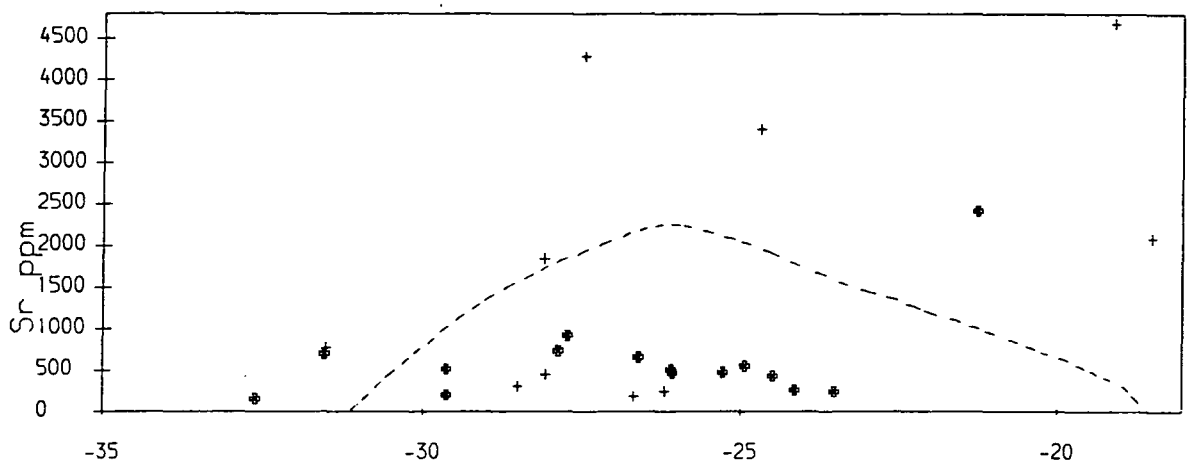
Sr ppm
4500
4000
3500
3000
2500
2000
1500
1000
500
0
-35
-30
-25
-20

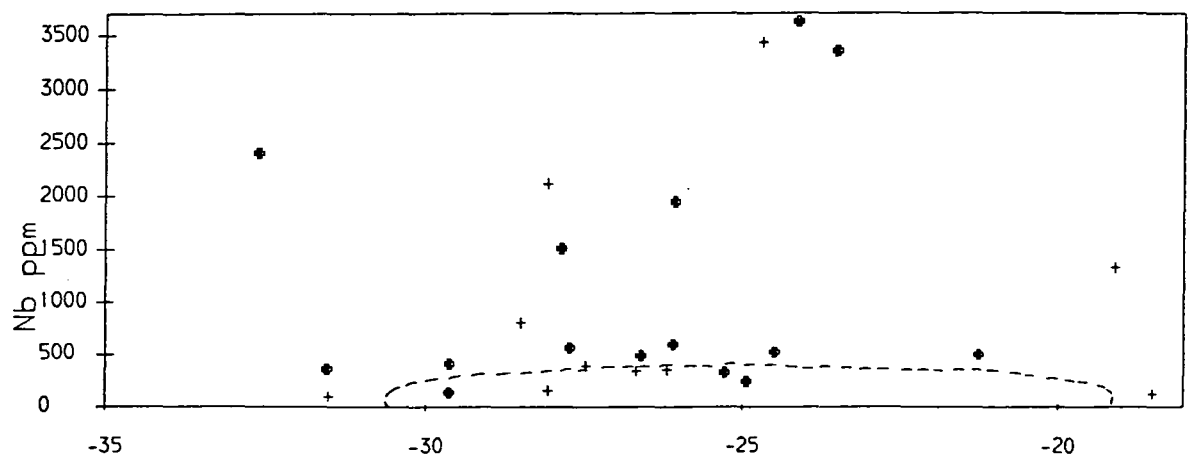
Nb ppm
3500
3000
2500
2000
1500
1000
500
0
-35
-30
-25
-20

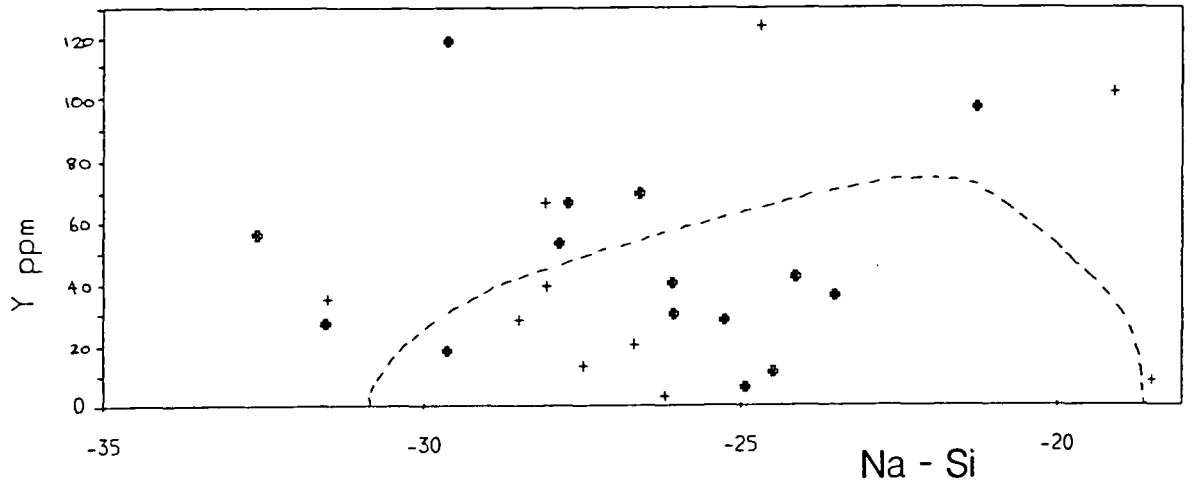
Y ppm
120
100
80
60
40
20
0
-35
-30
-25
-20
Na - Si

Fig. 7.4.2 (cont.)

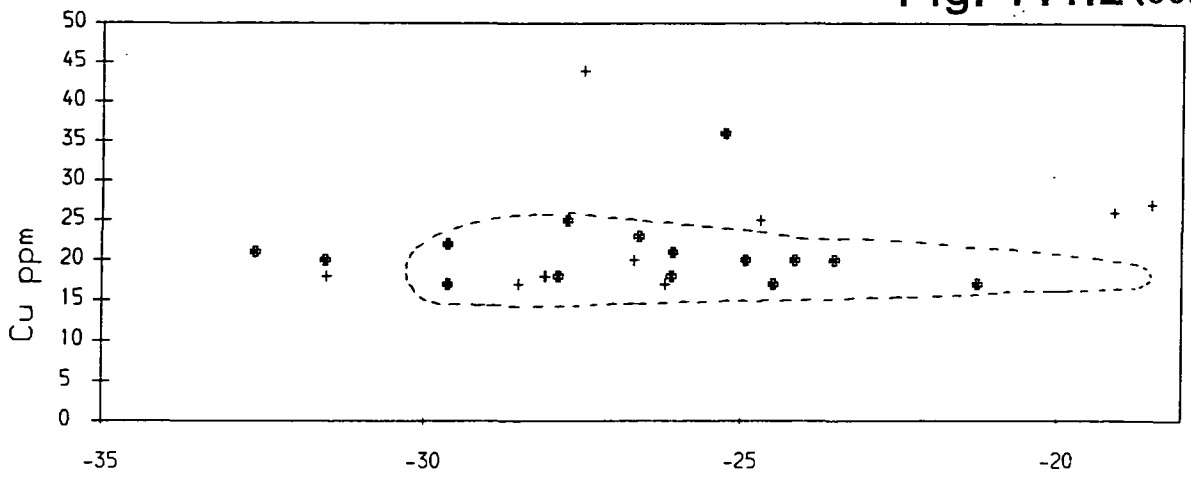
Cu ppm
50
45
40
35
30
25
20
15
10
5
0
-35
-30
-25
-20

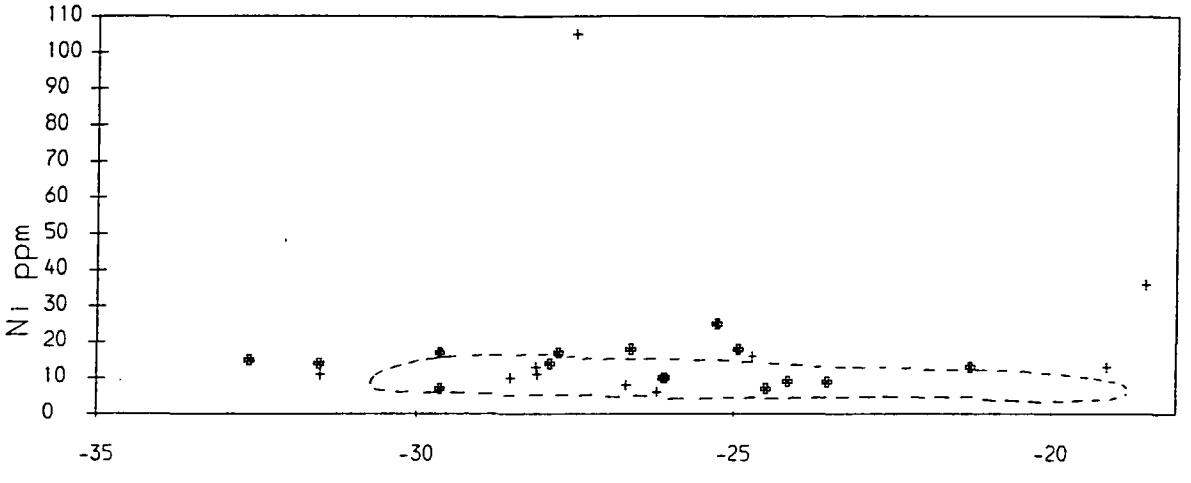
Ni ppm
110
100
90
80
70
60
50
40
30
20
10
0
-35
-30
-25
-20

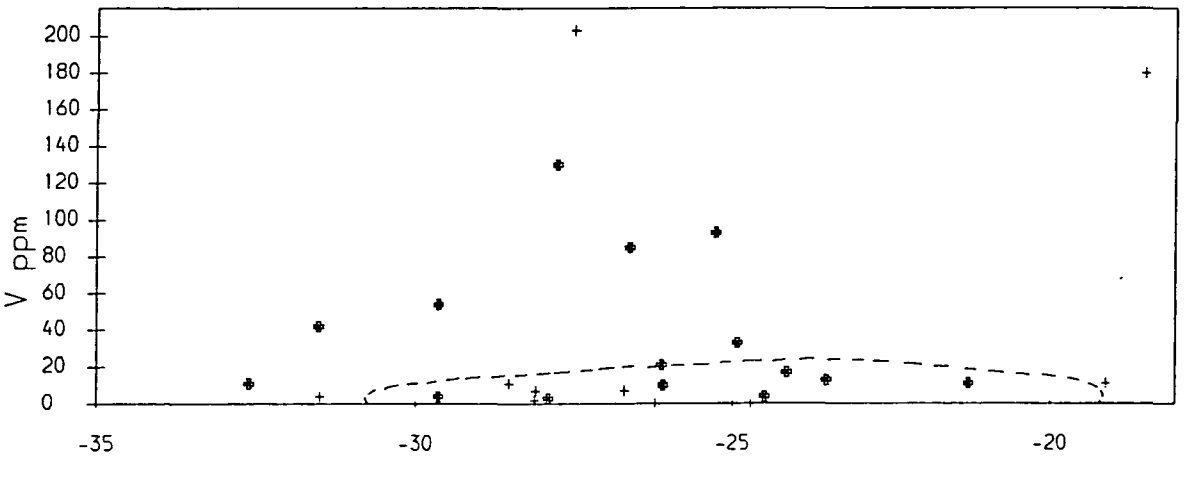
V ppm
200
180
160
140
120
100
80
60
40
20
0
-35
-30
-25
-20

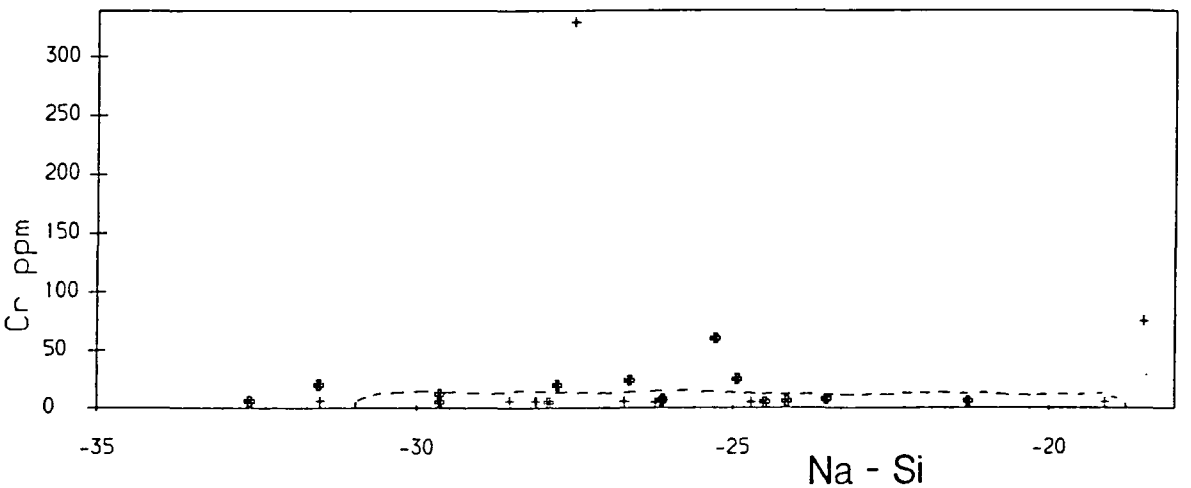
Cr ppm
300
250
200
150
100
50
0
-35
-30
-25
-20
Na - Si

	Cu	Ni	V	Cr
G276 (ppm)	44	105	203	330
Others	17-36	6-43	0-75	0-75

These values may be due to the original rock being fairly mafic in composition, containing comparable abundances to other basic rock compositions (eg. Middlemost 1985). Small specks of sulphide minerals are are also occasionally visible on freshly broken surfaces of this specimen, and may well be acting as the host for some of these elements.

In comparison to the unaltered rocks, Y is slightly enriched in both the metasomatised gneisses and syenites, while Sr tends to be richer in the latter, presumably due to a greater proportion of interstitial carbonate. Ni, Cu, Cr, and V are marginally enriched in some of the gneisses compared to the altered syenites, though this may be due to original compositional differences.

The only element to show significant enrichment compared to the unaltered syenites is Nb. This occurs in abundances greater than 3000ppm in G146A and B (altered gneisses) and G27 (carbosyenite), and is generally more than ten times enriched in the altered compared to the unaltered rocks. Increased Nb contents have been reported from fenites associated with the North Qôroq centre (Chambers 1976) and Sarfartôq (Secher and Larsen 1980), though Zr enrichment is also important in these areas, a feature not apparent in the altered rocks of Grønnedal. No single phase has been identified which may be acting as a host for the Nb, although it may be concentrated in patches of deep red-brown alteration material which occurs in many of the altered rocks (Emeleus, pers. comm.).

7.4.4: Rare-earth element geochemistry

Four samples were analysed for REE's (fig. 7.4.3), the positions of which are shown on map 3. These are as follows:

G26 – Biotite-rich metabasic gneiss xenolith from the Upper Series.

Fig. 7.4.3. Rare-earth element (REE) abundances of four altered rocks, normalised using the chondritic abundances of Boynton (1982). Note the higher light REE/heavy REE ratios of the altered syenites (G136, G90) compared to the gneisses, possibly as a result of original differences in abundance of these elements.

Fig. 7.4.4A. Comparison between chondrite normalised REE from the syenites, carbonatite, and altered rocks from Grønnedal. The elevated REE content of the altered rocks compared to the bulk of the unaltered syenites is obvious.

Fig. 7.4.4B. Comparison between normalised REE trends of an acid gneiss xenolith (G57) and the Xenolithic Porphyritic Syenite host rock, showing the slight enrichment in the xenolith. Light REE/heavy REE ratios are also marginally greater than in the host rock.

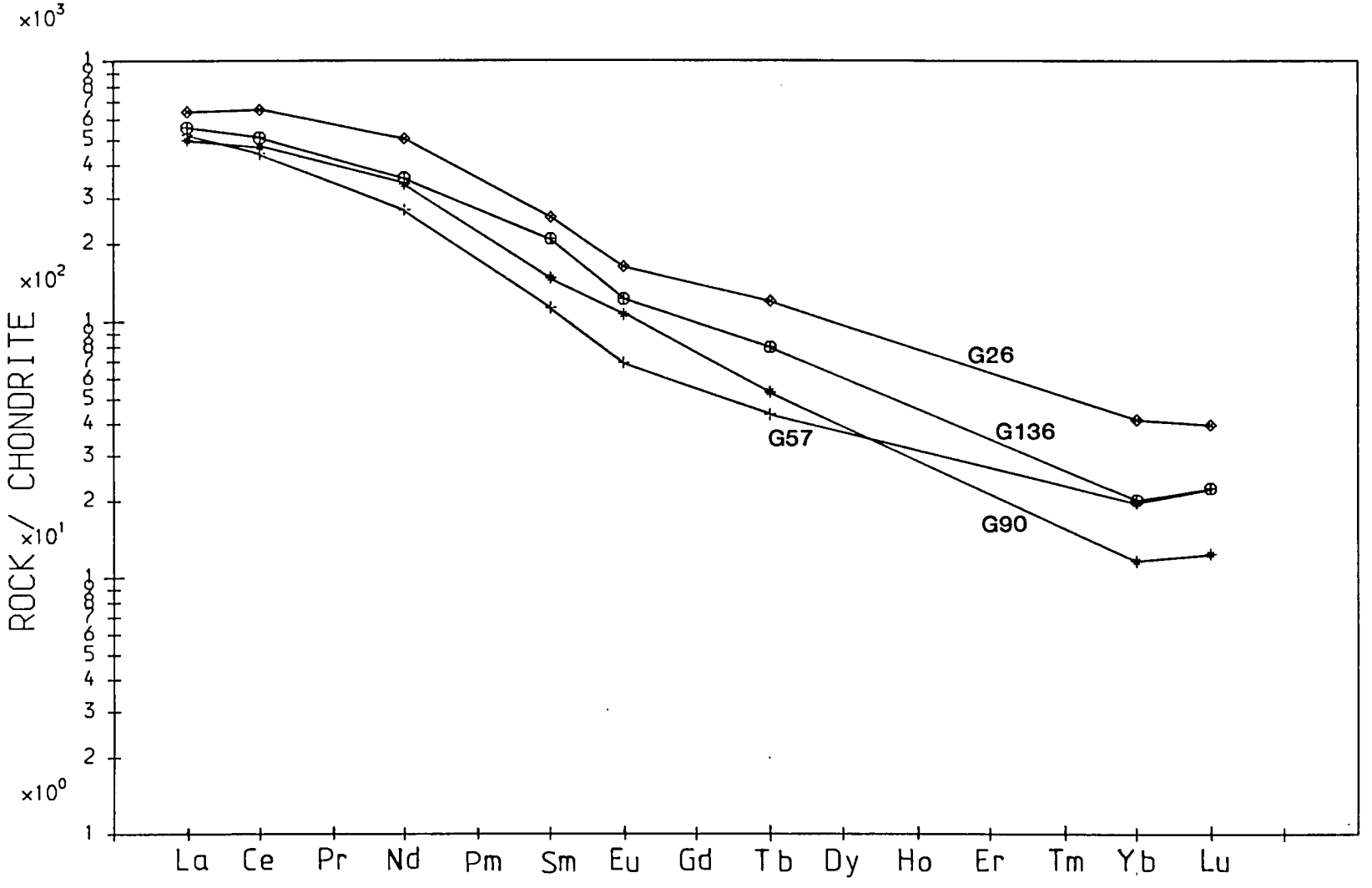
ROCK / CHONDRITE
×10³
×10²
×10¹
×10⁰
1
2
3
4
5
6
8
La
Ce
Pr
Nd
Pm
Sm
Eu
Gd
Tb
Dy
Ho
Er
Tm
Yb
Lu
G26
G136
G57
G90

Fig. 7.4.3

Fig. 7.4.4A

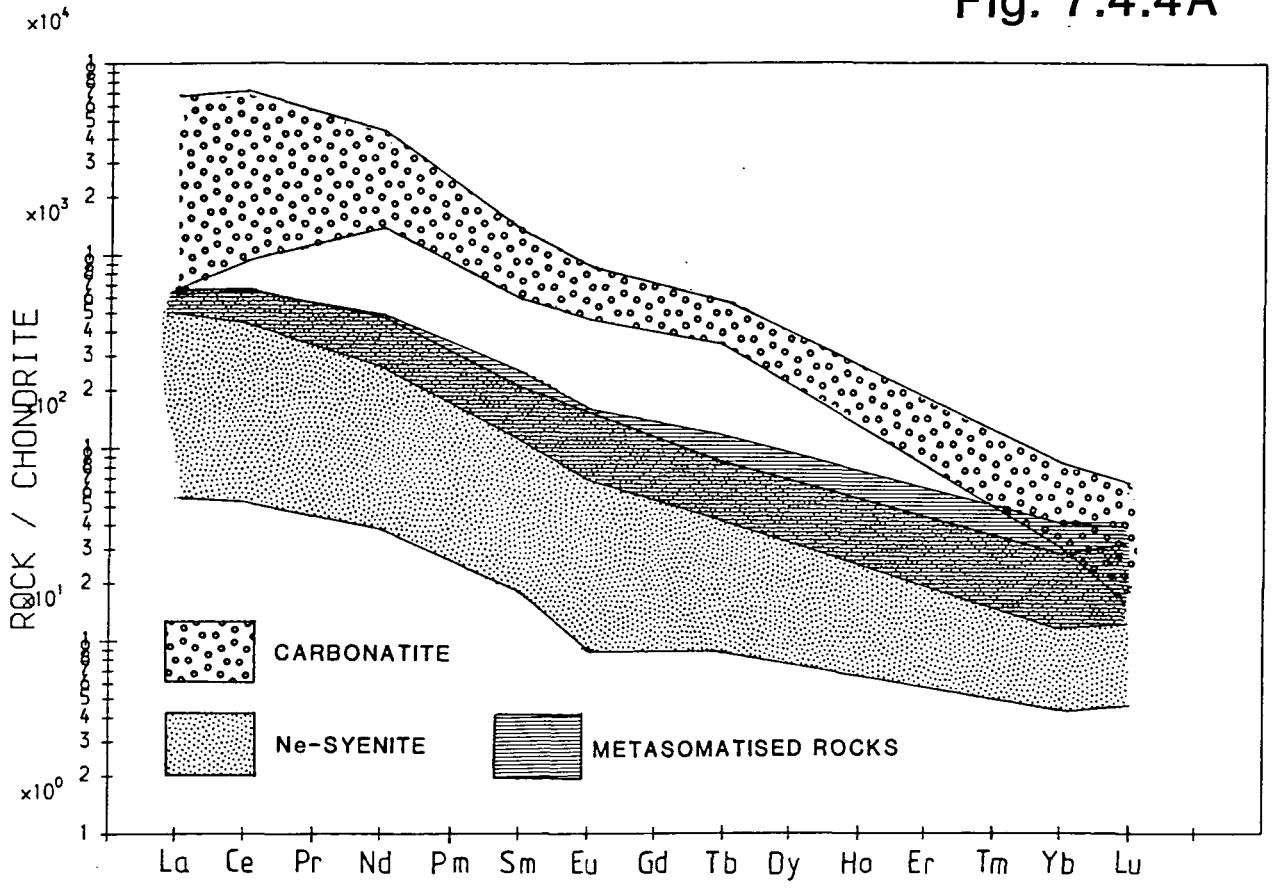

Fig. 7.4.4B

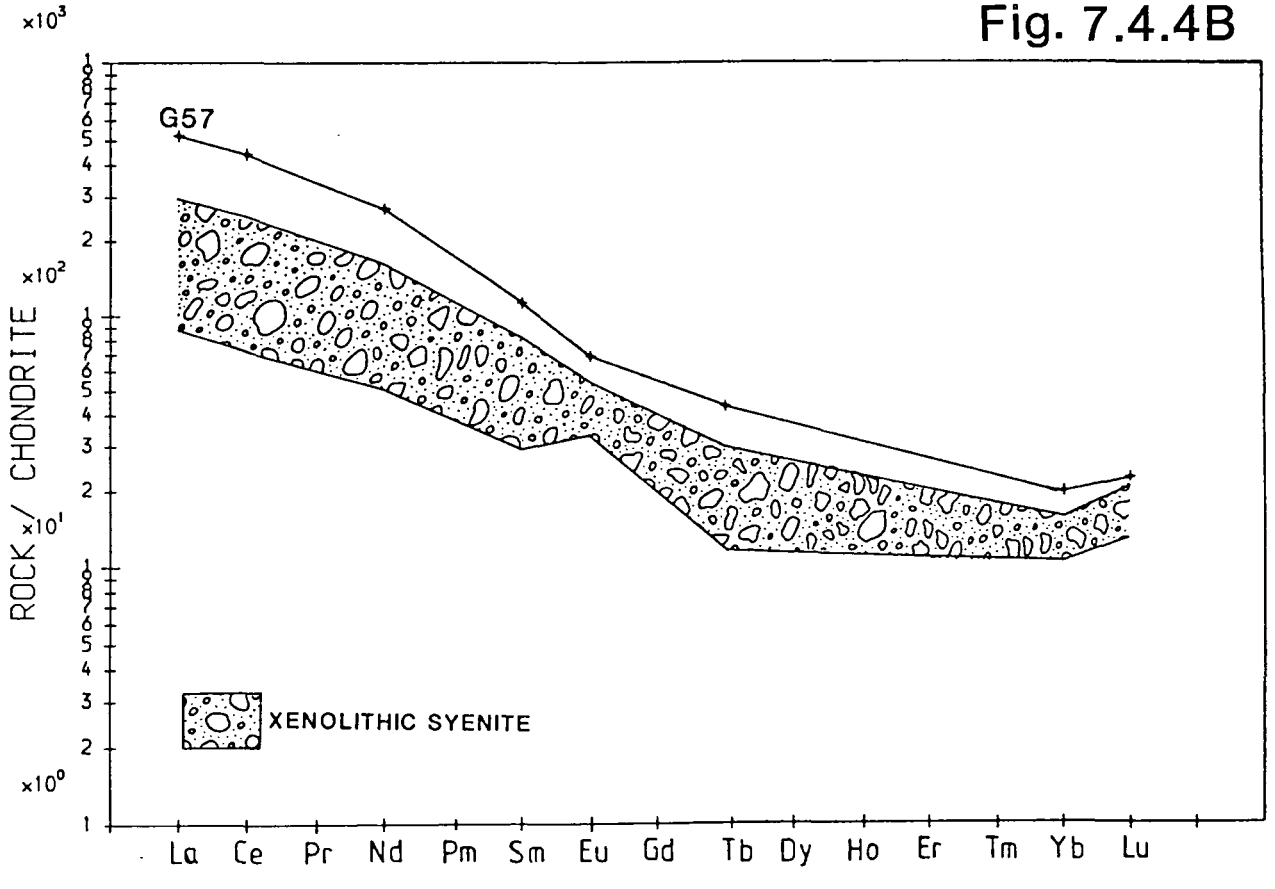

G57 – Acid gneiss xenolith from the Xenolithic Porphyritic Syenite.

G90 – Strongly carbonated syenite from the Hyttelv.

G136 – Carbonated xenolithic syenite from above the Cirkus.

Overall REE abundances relative to chondrite are intermediate to those of the syenites and carbonatites (fig. 7.4.4A), while LREE/HREE ratios (measured as $(La/Lu)_{cn}$ behave similarly (fig. 5.5.2). The two altered syenites (G90 and G136) show steeper trends, probably as a result of higher initial $(La/Lu)_{cn}$ ratios, although overall abundances are fairly comparable to the altered gneisses.

Compared to REE trends of fenites from Sarfartôq (Secher and Larsen 1980) and Loch Borralan (Martin *et al.* 1978), those of Grønnedal-Íka are relatively smooth, and generally show very slight negative Eu anomalies as opposed to pronounced positive anomalies in the 'radioactive shear-zone rocks' from Sarfartôq. Sample G57, a xenolith from the Xenolithic Porphyritic Syenite, is compared with the range of REE contents in samples of xenolith-free host rock in fig. 7.4.4B. The xenolith is moderately enriched in overall abundances compared to the host rock, with a slightly higher LREE/HREE ratio. Martin *et al.* (*op. cit.*) report LREE enriched fenitised quartzites adjacent to the Loch Borralan complex, although they did not have sufficient data to determine whether this is a result of original source rock enrichment, or preferential uptake of LREE's from the source by the metasomatising fluids. In view of the parallel trend of G57 and the host rock, it is suggested that the enrichment reflects the composition of the source, rather than being due to any significant fractionation of REE's by the metasomatic process in this case.

7.5: Conclusions: nature and origin of the metasomatising fluids

According to Rubie and Gunter (1983), "fenitisation is a process of alkali metasomatism that occurs around intrusions of ijolite, nepheline syenite, carbonatite,

and related rock-types". Mineralogical changes that occur include the loss or replacement of quartz, growth of alkali-rich amphiboles and pyroxenes, and growth or recrystallisation of alkali feldspar. All of these features have been observed at Grønnedal-Íka (sections 7.2, 7.3), and the rocks may thus be termed fenites according to this definition. Rubie and Gunter (*op. cit.*) also suggest that the composition of fenites is temperature dependent, becoming more potassic as the temperature decreases with time and/or distance from the source of the fluids, and that aegirine forms at lower temperatures than aegirine-augite. The majority of metasomatic pyroxenes at Grønnedal-Íka are aegirines or Na-rich aegirine-augites, suggestive of a low temperature of formation. In addition, the zonation of some mineral grains (sections 7.3.2, 7.3.3) suggests that the metasomatic fluids probably became more sodic with time. However, as described previously (sections 4.2.5, 7.3.3, Carmichael and Nicholls 1967), the activity of Na^+ appears to be partly dependent on $a_{Fe^{3+}}$, which may increase with fractionation in fluids associated with a carbonatite (Le Bas 1977). Fluids from the carbonatite may thus have given rise to the observed mineral zonations.

Le Bas (1981, 1987) reviewed the types of fenites associated with different source rock-types. He suggests that alkali silicate-dominated complexes give rise to fenites characterised by pyroxenes which grade from aegirine-augite to aegirine with increasing distance from the contact, and alkali feldspars of intermediate composition (Ab_{60-40}, Or_{40-60}). Carbonate minerals are generally rare unless later carbonatite intrusions are present. In contrast, carbonatites give rise to more varied fenites than those associated with silicate intrusions. Potassic metasomatism tends to occur towards the roof of the carbonatite, while deeper levels are characterised by sodic fenites. The latter, which are only exposed in more deeply eroded areas, typically contain albite, magnesio-arfvedsonite, aegirine, and iron oxides, all of which occur in the fenites at Grønnedal. In contrast to those adjacent to silicate-rocks, feldspars produced by metasomatic fluids emanating from a carbonatite tend to be either albitic ($Ab_{>90}$) or potassic ($Or_{>85}$) rather than

of intermediate composition. While the majority of feldspars at Grønnedal are albitic (fig. 7.3.5B), some show intermediate compositions. Rae and Chambers (1988), however, suggest that metasomatism of the North Qôroq nepheline syenites has simply resulted in enhanced unmixing of the feldspars, eventually giving rise to separate *Ab*-rich and *Or*-rich grains, similar to compositions produced by carbonatitic fenites. Incomplete unmixing may have occurred in the Grønnedal syenites, giving rise to the range of intermediate compositions analysed.

Based on these observations, is it possible to determine the nature and origin (whether from the syenites or the carbonatite) of the fenitising fluids at Grønnedal? In summary, the significant characteristics of the altered rocks are as follows:

Syenites

- Interstitial carbonate (giving rise to high whole-rock Sr).
- Recrystallised alkali feldspar.
- Alteration of nepheline to gieseckite (resulting in Na depletion).

Gneisses

- Secondary alkali pyroxenes and amphiboles.
- ?Growth of new albite

Significant features common to both are an increase in Ca+Mg+Fe+Al, Nb and REE enrichment, and increased LREE/HREE ratios in the altered compared to the unaltered rocks.

The variety of mineralogical and whole-rock compositions of the altered syenites and gneisses, ie. which elements are 'fixed' and which pass through, appears to be controlled largely by the original rock composition in many cases. For example, the abundance of sodic amphibole, pyroxene, and feldspar in the gneisses may in part be due to the presence of quartz in this rock, which reacts with the metasomatic fluids, as in the formation of aegirine, for example:

$$2H_2O+Na^+ + Fe^{3+} + 2SiO_2 \rightleftharpoons 4H^+ + NaFe^{3+}Si_2O_6$$

(After Rubie and Gunter 1983).

The lack of quartz in the syenites means that such a reaction cannot occur, and Na cannot be retained by this process, so that the gneisses tend to have slightly higher whole-rock abundances of this element. Other factors which may control the composition of the fenite include the texture of the rock, which may affect the permeability, and therefore resistance to the passage of metasomatic fluids. The greater amounts of alteration on the Coarse-Grained Brown Syenite compared to the Lower Series Syenite may be attributed to the lack of lamination and more open framework of feldspar laths in the former, as well as a coarser grain size (section 2.7). The distance from the source of fenitising fluids (eg. Rubie and Gunter *op. cit.*) and depth in the complex (Le Bas 1987), as described earlier, may also be important, although these would be difficult to test at Grønnedal without further fieldwork.

It does appear, however, that the metasomatising fluid was particularly rich in Na, CO_2, Nb, and REE's, as the presence of these elements, or phases containing them, characterise the Grønnedal fenites. REE's may form complexes with CO_2 and halogens, particularly F (Möller *et al.*, 1980), giving rise to complexes such as $RE(CO_3)_n^{3-2n}$, $(RE)F^{2+}$, $(RE)F_2^+$, etc. Although not found in the course of this work, Emeleus (1964) reports interstitial fluorite in some of the syenites from Grønnedal. Sodalite occurs fairly commonly in the altered rocks, so that Cl presumably occurred in the metasomatising fluids, and could also have formed REE complexes. Based on fluid inclusion studies, Sobolev *et al.* (1974) and Roedder (1984) suggest that such fluids may indeed be highly saline.

Returning to the problem of the source of the metasomatism, one is inclined to agree with Rubie and Gunter (1983) that "fenitisation around some carbonatites is little different from fenitisation around ijolite and nepheline syenite". Without more field data, it is not possible to be certain whether the carbonatite or the

syenites were the dominant source of the metasomatic fluids. There is evidence that both gave rise to metasomatism at the time of their intrusion, with country-rock gneisses far removed from the carbonatite as well as xenoliths within the carbonatite both showing evidence of alteration. In addition, the metasomatic effects of the syenite will have been 'overprinted' by those of the carbonatite, and will thus be difficult to distinguish. Andersen (1988) has recently proposed that a third, alkali-rich, immiscible phase may be generated during the unmixing of a carbonate liquid from a silicate liquid (for which there is strong evidence at Grønnedal, section 6.5). He suggests that fluid inclusion data show that an alkali-chloride rich aqueous fluid such as this may have existed at Fen at an early stage in the evolution of the complex, but that more experimental work is needed to clarify the possible immiscible relationships.

Of particular significance may be the carbonated samples G75 and G276. Petrographic and field observations suggest that these samples originally had basic igneous affinities, and show relict textural affinities with dykes of the later olivine-dolerite (BD) dyke swarms, which post-date the complex. Some of the alteration may thus have occurred after emplacement of the final unit of the complex (the carbonatite). Igneous activity in this area continued sporadically throughout the remainder of the Gardar, with emplacement of late alkaline dykes representing a resurgence of alkaline activity (Gill 1972a,b). Leaching of elements from the earlier units of the complex may have occurred during this episode, resulting in the growth and recrystallisation of many mineral phases. In addition, the faulting which has affected the complex may also have been important in contributing to the alteration of the syenites and country rocks, acting as channels for the migration of metasomatic fluids. Secher and Larsen (1980) describe intense fenitisation in fault zones associated with the Sarfartôq carbonatite complex, while the faulted areas of Grønnedal-Íka certainly seem to have experienced substantial amounts of carbonation and fenitisation.

All of the features described in this section have no doubt contributed to the alteration, but the most significant feature is probably the age of the complex. At 1299±17Ma (Blaxland *et al.*, 1978), Grønnedal-Íka is the oldest of the Gardar centres, and in a tectonically active province such as this, experiencing repeated cycles of igneous activity, the age of this complex is probably the single most important aspect.

CHAPTER 8: CONCLUSIONS

This chapter essentially summarises and integrates the conclusions reached in the preceding chapters, and brings them together into a petrogenentic and evolutionary model for the complex.

8.1: Magma genesis

The Gardar period was characterised by repeated episodes of continental rifting and alkaline magma genesis (eg. Upton and Emeleus 1987), possibly as a result of continental plate movement between the North American and Grenvillian plates.

Rare-earth element (REE) trends from the different syenite units of the Grønnedal-Íka complex are typically steep, with high $(La/Lu)_{cn}$ ratios, typical of magmas derived by a few percent of partial melting of a garnet-lherzolite mantle source (eg. Cullers and Graf 1984). This parental magma, which was probably of alkali basaltic affinity, gave rise to phonolitic compositions as a result of plagioclase and clinopyroxene fractionation (Upton and Emeleus, *op. cit*). Most units show REE trends with slight negative Eu anomalies. The later cross-cutting Xenolithic Porphyritic Syenite and minor bodies of Coarse-Grained Syenite which were emplaced subsequently, tend to show no such anomaly.

8.2: Emplacement

The original ellipsoidal outline of the complex is evident from the reconstructed geological map (map 2, after Emeleus 1964). Stephenson (1976b) suggests that the elongation was produced as a result of emplacement during sinistral ductile shearing, and thus approximates to a strain ellipse for the deformation. Emplacement appears to have occurred into relatively hot country rock, as suggested by the very narrow or complete lack of chilled margins to the complex.

8.3: Marginal rocks

Both in terms of petrographic variations and field relationships, the marginal rocks are highly complex. They are particularly well-developed in the north-west of the complex, where three different facies, originally distinguished by Emeleus (1964), were identified during fieldwork undertaken in 1987.

i. *Coarse-Grained Brown Syenite.* Although commonly developed around the margins of the complex, this alteration facies was found to be more widespread than the original geological map suggested (map 1, after Emeleus, *op. cit.*). The coarse, open texture of the alkali feldspar tablets may have rendered this type of rock more susceptible to alteration than the better laminated syenites of the Lower and Upper Series. Zircon appears to be a relatively common phase in this rock.

ii. *GS-B* (GS-1 of Emeleus, *op. cit.*). This granular, unlaminated facies occurs as discontinuous sheets at the outer margin of the complex, within the Lower Series and country rocks.

iii. *GS-A* (GS-2 of Emeleus, *op. cit.*). This occurs as an elongated body (possibly a partial ring-dyke) around the north-west part of the complex, cutting across the Lower Series and GS-B, against which it shows a chilled margin. Petrographically, this unit is very distinctive, characterised by clean, prismatic alkali pyroxenes, generally showing extreme zonation, and Zr enrichment.

8.4 Physical and chemical properties of the magma

Superficially, the bulk of the syenites at Grønnedal-Íka (the Lower and Upper Series) are very similar to the rocks which make up other undersaturated Gardar complexes (eg. North and South Qôroq, Motzfeldt). Petrographic and textural evidence shows that most samples contain cumulus nepheline, alkali feldspar, and pyroxene. The characteristic tabular shape of the feldspars has assisted the development of a well defined lamination in the Lower and Upper Series, which

often shows evidence of slumping. Magmatic currents, rather than compaction due to the weight of overlying material, are suggested as the principle cause of the lamination, as some of the strongest lamination occurs towards the top of the Lower Series. Pyroxene compositions are strongly affected by the amount of postcumulus growth which takes place, which is in turn largely controlled by the composition of the trapped interstitial liquids, and the overall texture of the rock; a more open mineral framework allows a greater proportion of intercrystalline liquid to be trapped.

The Grønnedal-Íka syenites show some striking mineralogical differences to other undersaturated Gardar centres. The lack of amphibole from all but a few microsyenite dykes, marginal rocks, and one sample of Mafic Syenite (Emeleus 1964), may be due to a low p_{H_2O}, while the absence of olivine points to an oxygen fugacity above the Fayalite-Magnetite-Quartz buffer. The composition of the oxide minerals, which are dominantly magnetite-rich end members of the *mgt-üsp* series, provides further evidence for a relatively oxidising magma ("for the same temperature, an increase in f_{O_2} results in a decrease in the percentage of TiO_2 in the magnetite", Buddington and Lindsley 1964). Ernst (1962) also suggests that alkali amphiboles of the riebeckite-arfvedsonite series are unstable at high oxygen fugacities, and may account for the scarcity of this phase at Grønnedal. In addition, enrichment in the acmite end member begins at a relatively early stage in the evolution of the pyroxenes, a feature which has been related to increasing f_{O_2}, although other physico-chemical controls may well be important (section 4.2.5).

The presence of zircon as interstitial or poikilitic grains in samples from all of the syenite units is unusual, though it may be taking the place of other Zr-bearing phases, such as eudialyte, which are not present in these rocks. Its presence is more usually regarded as being the result of metasomatic alteration, and increases in modal abundance with alteration at Grønnedal (section 8.8).

8.5: Chemical evolution

Major and trace element trends from the different rock units of the complex are very difficult to distinguish due to the large amount of scatter in abundances. Two suggestions are proposed to account for this:

i. Alteration. Metasomatic alteration has affected all of the syenites to some extent, resulting in the redistribution of many elements. For example, the Coarse-Grained Brown Syenite analyses show elevated Al_2O_3 and lower Na_2O values than the bulk of the syenites, principally as a result of all of the nepheline being altered to gieseckite in this rock.

ii. Texture. The arrangement of the consituent minerals of the rock, particularly the alkali feldspars, may determine the quantity, and indirectly, the composition of the trapped interstitial liquid. For example, the intercrystalline liquid in a poorly laminated rock with a more open framework may remain in equilibrium with the evolving, unconsolidated magma for a longer period of time than in a well laminated syenite, where pockets of liquid may be sealed off relatively soon after 'deposition' of the cumulus minerals. Liquids which are trapped at different times in the evolution of the magma will contain different abundances of elements, these contributing to the overall composition of the rock. The texture may vary considerably from one sample to another within the same unit, and may thus give rise to large differences in the whole-rock composition (Paster *et al.*, 1974).

Some trends can be made out, however. Based on normative compositions, the different units show a range of Fractionation Indices (FI, after Macdonald 1969), against which element abundances have been compared. Few trends can be made out, however, though among the trace elements, some show a decrease with increasing FI, presumably due to fractionation of phases containing these elements. In particular, the REE's (Nd, La, Ce) all show a decrease with FI, and

a positive correlation with P_2O_5 and Zr, suggesting that fractionation of apatite and zircon took place.

Although it is difficult to draw conclusions regarding variations in normative composition, most samples define a trend towards the undersaturated minimum in the residua system, but are increasingly displaced towards the potassium-rich side of the diagram with increasing silica saturation. This effect has been recognised at North and South Qôroq (Chambers 1976, Stephenson 1973), and is probably an effect of additional components in the magma (eg. Kogarko 1974, James and Hamilton 1969), resulting in a distortion when compositions are projected onto the three-phase surface. When plotted in the residua system, normative compositions of samples taken from transects across the Lower and Upper Series show evidence for the existence of an extensive 'sandwich horizon'. Simultaneous crystallisation of magma from the upper and lower margins of both units has given rise to the most evolved compositions occurring in the central parts of the unit, as in the Skaergaard Layered Series (Wager and Brown 1968), and the Palisades Sill (Shirley 1987).

8.6: The carbonatite

The final phase of intrusive activity at Grønnedal-Íka was the emplacement of a plug of xenolithic carbonatite. Prominent flow-banding, as defined by siderite and secondary magnetite, and petrographic evidence which shows that the constituent minerals have undergone ductile deformation, suggest that the rock was emplaced largely in the solid state (cf. Bailey 1966).

Mineralogically, the rock consists dominantly of calcite (ie. a søvite), with siderite occurring in small quantities, although this mineral has usually been altered to magnetite, particularly adjacent to the later, cross-cutting dykes. Apatite, alkali feldspar, and barytes are also occasionally present, though compared to many carbonatites (eg. Le Bas 1977), the rock at Grønnedal is very poor in

'exotic' minerals. Occasional alkali mafic minerals occur, and are always highly sodic (eg. aegirine, and arfvedsonitic amphiboles).

Major element geochemical variations show a trend of increasing iron enrichment with slight enrichment in MgO. This is similar to many carbonatite complexes of the world (eg. Woolley 1982), and is a result of fractionation of Ca-rich carbonate minerals, resulting in a magma of ferrocarbonatitic composition (Le Bas 1981). Some trace elements are frequently enriched in the carbonatite compared to the syenites, particularly Th, Sr, REE's, and Y, while other elements are relatively depleted. In addition, the REE trends show high LREE/HREE ratios, with $(La/Lu)_{cn}$ commonly exceeding 100.

8.7: Relationship of the carbonatite to the syenites

Many features of the trace element geochemistry of the carbonatite may be accounted for by envoking an origin by liquid immiscibility from a CO_2-saturated phonolitic magma, at a temperature of less than about 1100°C and pressures of 5–6kb or more. Using partition coefficients for elements distributed between co-existing carbonate and silicate liquids (from Bedson *et al.*, 1989), a genetic relationship between the syenitic and carbonatite rocks of the complex is suggested by the following:

- Overall REE abundances and $(La/Lu)_{cn}$ are greater in the carbonatite than the syenites.
- Enrichment of Mn in the carbonatite some 3–5 times compared to the syenites.
- Enrichment of Ta and Hf, and lower Hf/Ta ratios in the *syenites* compared to the carbonatite. This is particularly significant, as these distributions could not be produced simply by fractional crystallisation.

On the basis of field evidence alone, the Xenolithic Porphyritic Syenite would seem to be the most likely single candidate for the conjugate silicate phase to the

carbonate. Both were intruded relatively late in the evolution of the complex, and the large proportion of xenolithic material in these rocks suggests that they were both emplaced forcibly. Ta and Hf ratios between these units agree with the silicate/carbonate distribution coefficients of Hamilton, *et al.* (1989) more closely than with any other of the silicate units of the complex.

8.8: Alteration

The effects of mild alteration are are evident in all units of the complex, as shown by the formation of gieseckite after nepheline, and the development of sodalite-rich veins. More intense alteration has given rise to the Coarse-Grained Brown Syenite, which shows alteration of pyroxenes to opaque oxides and micaceous material, interstitial carbonate, and frequently zircon. Recrystallisation of the alkali feldspars may also have occurred.

The most intense effects of metasomatic alteration generally affect gneiss xenoliths within the syenites, and areas of syenite intruded by the carbonatite. Secondary alkali amphibole is a characteristic mineral of the altered gneisses, while carbonation, and complete recrystallisation of alkali feldspar have occurred in the syenites. Alkali pyroxenes commonly occur in both, varying in composition from aegirine-augite to aegirine, and often partially replace quartz in the gneisses. Zircon occurs in both types of altered rock, generally as poikilitic or interstitial grains, although euhedral crystals up to 10mm across were found in a carbonated syenite. Metasomatic zircons have been reported from the roof zone of the Motzfeldt centre (Tukiainen *et al.*, 1983) and in many other parts of the world (eg. Pointer *et al.*, 1988; Rustamov *et al.*, 1988). The chemistry of the mafic minerals of the altered rocks suggests that the metasomatic fluids were peralkaline in nature, which would have enabled Zr to be carried in solution (Watson 1979). Significantly, the carbonatite, which was probably a source of the metasomatic fluids, is exceptionally depleted in Zr compared to the other rocks of the complex.

Consistent trends in element variations from the altered rocks are not easy to distinguish, principally on account of the large variation in original rock composition. With increasing alteration (measured as Na-Si atoms per 100 oxygens, after McKie 1966), total Fe, Mn, and 'cafemics' (Ca+Fe+Mg+Al) tend to increaese, while K decreases slightly. Compared to the altered syenites, the gneisses tend to be richer in Na, possibly as a result of this element being fixed by reaction with quartz to form alkali mafic minerals. Trace elements show a wide scatter of values, although compared to the unaltered rocks, Sr is enriched in the altered syenites (due to the abundance of carbonate), while Nb and the REE's show a slight enrichment in both altered rock types.

It is probable that both the syenites and the carbonatites produced late-stage, peralkaline, Cl- and CO_2-rich residual fluids, which gave rise to the observed effects of the metasomatism.

Some of the later olivine-dolerite dykes which cross-cut all units of the complex also appear to show the effects of metasomatism and carbonation, particularly in faulted areas. Remobilisation and deposition of carbonate may have occurred along the fault zones, which acted as channels for the migration of metasomatic fluids, possibly associated with the late Gardar resurgence of alkaline activity which gave rise to trachyte and phonolite dykes in this region.

As Grønnedal-Íka is the oldest of the Gardar centres, it is perhaps not surprising that that it has experienced a considerable amount of post magmatic alteration.

8.9: Summary

The most significant features of the complex thus appear to be:

- Parental magmas produced by small amounts of partial melting of a garnet lherzolite mantle source.

- Emplacement of magmas with a relatively high f_{O_2} in a region undergoing sinistral shear.

- Crystallisation of cumulus nepheline, alkali feldspar, and pyroxene, and development of 'sandwich horizons'.

- Development of a wide range of major and trace element abundances as a result of variable amounts of crystallisation from trapped intercrystalline liquids.

- Emplacement of a carbonatite derived by liquid immiscibility from a CO_2-saturated phonolite magma. The conjugate silicate phase was probably emplaced as the Xenolithic Porphyritic Syenite.

- Alteration of xenolithic material, country rock, and rocks of the complex itself by metasomatic fluids derived from the syenites, carbonatite, and later alkaline activity in the area.

APPENDIX I

Samples

Samples used for analysis or referred to throughout this thesis are listed here, and separated according to the collector, as follows:

Collector(s):	Years:
C.H. Emeleus	1956–1958
R.C.O. Gill and D. Stephenson	1973
C.M. Bedford	1987

Only those collected in 1987 were used for whole-rock analysis, while samples for microprobe work have been taken from all of the above collections.

Sampling in 1987 was carried out with the aim of covering as wide a geographical area of the complex as possible. In general, every effort was made to obtain fresh samples, although highly altered specimens were sometimes collected deliberately. Where possible, transects across the syenite units were made; these are indicated by a vertical line in the sample tables. The localities of samples collected during the 1987 field season are shown on map 3, while the positions of samples used for microprobe analysis are shown on map 4.

The data is set out as follows:

Column 1: Collector and sample number.

Column 2: Rock type, abbreviated as follows:

LSS=Lower Series Syenite
USS=Upper Series Syenite
MUS=Mafic Upper Series
GS-A=Granular Syenite (GS-A)
GS-B=Granular Syenite (GS-B)
CBT=Carbonatite
ALSY=Altered syenite
ALGN=Altered gneiss
CGBS=Coarse-Grained Brown Syenite
CGS=Coarse-Grained Syenite
PMS=Porphyritic Microsyenite
MMS=Marginal Microsyenite
XPS=Xenolithic Porphyritic Syenite
PEG=Pegmatite
MISC=Miscellaneous

Column 3: If used for whole-rock (XRF) analysis (marked by *).

Column 4: If used for microprobe analysis (E=Edinburgh probe; M=Manchester probe; D=Durham probe).

Column 5: If used for neutron-activation analysis (marked by *).

Column 6: Any field relationships or petrographic features of interest.

SAMPLE NUMBER	ROCK-TYPE	XRF	MICROPROBE	INAA	NOTES
Emeleus					
27056	XPS		E		
27113	LSS		E		Typical laminated syenite.
27193	MUS		E		
27259	MUS		E		
31846	XPS		D		
39709	CBT		E		Alkali px and amphibole.
Gill and Stephenson					
138001	CGBS		E		
138007	GSA		E		Acicular aegirines.
138012	CGBS		E		
138025	LSS		E		
138027	CGBS		M		
138044	LSS		E		
138046	LSS		E		
138048	LSS		E		
138055	PEG		M		
Bedford					
G1	LSS	*			
G2	LSS	*			
G3	LSS	*			
G4	LSS	*			
G5	LSS	*			
G6	LSS	*			
G7	LSS	*			
G8	MISC	*			Pyroxene-rich vein in LSS.
G9	ALSY		D		3m from contact.
G10	CGBS	*			
G11	LSS	*			
G12	GSB	*			
G13	LSS	*			Zircons.
G14	ALGN	*			
G15	LSS	*			
G16	USS	*			
G17	USS	*			Large zircons.
G18	ALSY				Px-veined PMS dyke.
G19	USS	*			Zircons.
G20	USS	*	D		
G21	MUS	*	D		
G22	MUS	*			
G23	PMS	*			
G24	USS	*			Nepheline-rich; Zircons.
G25	USS	*			
G26	ALGN	*	D	*	Biotite-rich alt'd metabasite.
G27	ALSY	*			Zircon and some sulphide.
G28	CBT	*			Very pure CBT.
G29	CBT	*			
G30	CBT	*		*	
G31	CBT	*			
G32	USS	*			
G33	XPS	*			
G34	XPS	*			
G35	USS	*			
G36	PMS	*			

SAMPLE NUMBER	ROCK TYPE	XRF	MICROPROBE	INAA	NOTES
G37	MMS	*	M		15cm from contact.
G38	MMS	*	M		50cm from contact.
G39	MISC				Xenolith in USS.
G40	PMS	*			
G41	XPS		D		Loose block of XPS.
G42	ALGN				Gneiss xenolith in XPS.
G43	USS	*	M	*	
G44	MMS	*	M		Amphibole-rich 'dyke'.
G45A	CGS	*			Very coarse CGS, two
G45B	CGS	*			samples taken.
G46	CBT	*	D		
G47	CBT	*	D	*	
G48	USS?				Zircon.
G49	USS	*			
G50	USS				Difficult to sample.
G51	ALGN	*			Zircon.
G52	CBT	*	D	*	
G53	CBT	*			
G54	ALGN	*			Zircon.
G55	CBT	*			Pyrite-rich.
G56	CBT	*			Magnetite-rich.
G57	ALGN	*		*	
G58	MISC				Carbonated ?XPS.
G59	USS	*			
G60	GSB	*			
G61	GSB	*			
G62	CGBS	*			Zircon.
G63	MMS				
G64	MMS	*	M,D	*	
G64A	MMS	*			Slightly coarser than G64.
G65					Xenolithic basic dyke.
G66	CBT	*			
G67A	XPS				Selection of XPS
G67B	XPS				samples from same
G67C	XPS				locality. Only G67D
G67D	XPS	*			free of xenoliths.
G68A	XPS	*			Xenolith free.
G68B	XPS				
G69	CGS				Sheared CGS, near Xenolithsø.
G70	CGS	*			
G71	CGS	*			
G72	USS	*			Nepheline-rich.
G73	CBT	*			
G74	CBT	*	D		Enclave in large basic dyke.
G75	ALSY	*			
G76	CBT				?Quench texture.
G77	PMS	*			
G78	XPS	*		*	
G79	XPS	*			
G80	XPS	*	D		
G81	GSB	*			
G82	CGBS	*			Poikilitic zircons.
G83	MISC	*			
G84	GSB	*	D		
G85	CGBS	*			
G86	MISC	*			
G87	GSB	*			

SAMPLE NUMBER	ROCK TYPE	XRF	MICROPROBE	INAA	NOTES
G88	XPS	*			Zircons.
G89	XPS	*			
G90	ALSY	*		*	Zircons.
G91	USS	*			
G92	XPS	*			
G93	XPS	*			
G94	ALSY	*			
G95	CBT	*			
G96	CBT	*			
G97	CBT	*			Magnetite-rich.
G98	MISC				Highly oxidised
G99	MISC				xenoliths from CBT
G100	MISC				above Jernhat.
G101	CBT	*			Possible barytes.
G102	CBT	*		*	
G103	CBT	*	D		
G104	CBT	*			
G105	ALGN	*			
G106	ALGN	*			
G107	CBT	*	D	*	Radiating acicular aegirines
G108	ALGN		D		Altered metasediment.
G109	USS	*			
G110	MMS	*			Amphibole-rich 'dyke'.
G111	USS	*			
G112	USS	*			
G113	ALGN	*			
G114	ALGN	*			
G115	USS	*			
G116	USS	*			
G117	LSS	*			
G118A	USS	*	D		Mafic clots/veins
G118B	USS				from zone of
G118C	USS				disturbance between
G118D	USS	*			USS and LSS.
G119	USS	*			
G120	USS	*			
G121	MISC				Dolerite dyke.
G122	PMS	*			
G123	PMS	*			
G124	PMS	*			Zircon.
G125	PMS	*			
G126	ALSY				Px-veined USS.
G127	USS	*			
G128	USS	*			
G129	USS	*			
G130	USS	*			
G131	USS	*			
G132	USS	*			
G133	CBT	*			Pyrite-rich.
G134	XPS	*			
G135	USS	*	D		
G136	ALGN	*	D	*	
G137	XPS	*			
G138	XPS	*			Zircons.
G139	XPS	*			
G140	XPS	*			Zircons.
G141	XPS	*			
G142	USS	*			

SAMPLE NUMBER	ROCK TYPE	XRF	MICROPROBE	INAA	NOTES
G143	PMS	*			
G144	XPS	*			
G145	XPS	*	D	*	
G146A	ALGN	*	D		Altered foliated gneiss
G146B	ALGN	*			with poikilitic zircons.
G147	MISC				Feldspathic rock.
G148	MUS	*			
G149	USS	*			
G150	MUS	*			
G151	USS	*			
G152	PMS	*	D		
G153	USS	*			
G154	USS	*			Zircons.
G155	ALGN	*			
G156	USS	*	D		
G157	PMS	*			
G158	USS	*			
G159	PMS	*			
G160	USS	*			
G161	CGBS	*			
G162	GSB	*			
G163	GSB	*			
G164	GSB	*			Large euhedral zircons.
G165	GSB	*			Zircons.
G166	GSB	*			
G167	PMS	*			
G168	GSA	*	D		Zircons and pyrite.
G169	GSA	*	D	*	Zoned acicular pyroxenes.
G170	GSB	*			
G171	GSB	*			
G172	GSA	*	D		Zoned acicular pyroxenes.
G173	MISC				Loose block of dyke.
G174	GSB	*			
G175	LSS	*			
G176	LSS	*			
G177	LSS	*			
G178	PMS	*	D		
G179	PEG				Resistant PEG dyke.
G180	ALSY	*	D		
G181	LSF	*			Very feldspathic.
G182	LSS				Crumbly LSS with zircons.
G183	PEG		D		1m-wide dyke.
G184	PMS	*			
G185	USS	*		*	
G186	USS	*	D		
G187	MUS	*			
G188	MUS	*	M,D		
G189	MUS	*			From Emeleus'
G190	MUS				layered locality.
G191	USS	*	M		
G192	USS	*			
G193	LSS	*		*	Zircons.
G194	LSS	*			
G195	LSS	*			Zircons.
G196	LSS	*			
G197	ALGN	*	M		Samples from base of
G198	ALGN	*			gneiss raft.
G199	PMS	*			

SAMPLE NUMBER	ROCK TYPE	XRF	MICROPROBE	INAA	NOTES
G200	PMS				Blebs of coarser syenite.
G201	LSS	*			
G202A	PMS	*	D	*	
G202B	PMS	*			
G203	LSS	*			
G204	USS	*	M		
G205	MISC				LSS+PMS intermingled.
G206	USS	*			
G207	MUS	*	M		
G208	USS	*		*	
G209	MUS	*			
G210	MUS	*			
G211	GSB	*			
G212	GSB	*			
G213	CGBS	*			
G214	GSB	*			
G215	CGBS	*			
G216	CGBS	*		*	
G217	CGBS	*			
G218	LSS	*			
G219	LSS	*		*	
G220	LSS	*	M		Zircons.
G221	LSS	*			
G222	LSS	*			
G223	PMS	*			
G224	PMS	*			
G225	LSS	*			
G226	GSB	*			
G227	GSB	*			
G228	LSS	*			
G229	LSS	*			
G230	LSS	*			
G231	LSS	*			
G232	LSS	*			
G233	LSS	*			
G234A	PMS				
G234B	PMS	*			
G235	USS	*			
G236A	CGBS	*			
G236B	CGBS	*			
G237	MISC	*			?Altered dolerite.
G238	USS	*			Nepheline-rich.
G239	ALGN	*	D		Zoned amphiboles.
G240	MUS	*			
G241	ALGN				Brecciated gneiss.
G242	ALGN	*			
G243	MISC				Felsic xenolithic dyke.
G244	XPS	*			
G245	XPS	*		*	
G246	USS	*			Amphibole.
G247	MUS	*		*	
G248	MUS	*	M		
G249	USS	*			
G250	XPS	*			
G251	USS	*			
G252	USS	*			
G253	PMS	*	D		ol+amphibole. Lamprophyric?
G254	GSB	*			

SAMPLE NUMBER	ROCK TYPE	XRF	MICROPROBE	INAA	NOTES
G255	GSB	*			Sheared rock, near margin.
G256	CGBS	*			
G257	GSB	*	D	*	
G258	CGBS				mm-sized zircons.
G259	LSS	*		*	
G260	LSS	*			
G261	LSS	*			
G262	LSS	*			
G263	LSS	*			
G264	MISC				Sheared phyllitic rock.
G265	CBT	*	D	*	Sulphide.
G266	ALSY	*			
G267	USS	*			
G268	CBT	*			
G269	USS	*			Zircons.
G270	MISC				Carbonatite breccia.
G271	CBT	*			
G272	ALSY	*	D		Strongly carbonated. Zircons
G273	ALSY	*			
G274	PMS	*			
G275	CGS	*	D	*	
G276	ALSY	*			Carbonated ?basic dyke.

APPENDIX II

Electron-probe microanalysis

Mineral analyses were carried out using microprobes fitted with Wavelength Dispersive Spectrometers (WDS; at Edinburgh), and Energy Dispersive Spectrometers (EDS; at Durham and Manchester). A comparison between the two types of detector is given in table II.1, while table II.2 shows the standards used, the X-ray peaks measured, and where relevant, the 2θ angle and the spectrometer crystal used for each element.

Edinburgh

A Cameca Camebax microprobe fitted with four wavelength spectrometers was used for initial mineralogical work. An electron beam of 23nA at a voltage of 20kV was used, with peak and background count times between 5s and 40s, using longer count times for smaller element abundances. Count-times were automatically selected having chosen a particular mineral phase to analyse. REE's in apatites were kindly analysed by Dr. J.A. Craven using a defocussed electron beam, and standardised using a REE-spiked glass.

Durham and Manchester

Modified Cambridge Instruments Geoscan microprobes, fitted with EDS detectors, were used at both of these departments, using similar operating conditions and methods in each case. Both were operated at a beam current of 5nA with an accelerating voltage of 15kV, and use Li-doped Si-detectors, maintained at the temperature of liquid nitrogen to reduce electronic noise. A 'live-time' of 100s was used for each analysis, processing carried out using a Harwell 2010 pulse-processor and Link Systems 290 electronics at Manchester, while at Durham, a Link Systems AN 10/56AS unit was used. Spectra of the standards are held on hard disc in the on-line computer. These are compared with the unknown spectra, calibrated

using a cobalt metal standard for the calculation of element concentrations. The Co analysis thus corrects for any long-term drift, acting as a 'monitor' sample.

ZAF corrections are carried out using a procedure based on the `TIM1` program of Duncumb and Jones (1969). The atomic number correction described by Duncumb and Reed (1968) is used, together with Reed's (1965) fluorescence correction. The absorbtion effects are calculated using Philibert's (1963) equation, using Heinrich's (1967) absorbtion coefficients, and bulk mass absorbtion coefficients as calculated by Yakowitz *et al.* (1973).

The large number of analyses carried out in the course of this work meant that the quicker method of EDS analysis was preferred. However, there are some disadvantages, as outlined in table II.1, the most notable of which is the poor peak resolution. In particular, it was not possible to analyse for Sr in calcite due to the overlap of SiK on SrL using an EDS detector. There is no doubt that WDS is to be preferred for more detailed and precise mineralogical work, once an initial survey using EDS analysis has been carried out.

Mineral recalculations

The following programs, written by N.J.G. Pearce, and listed in Pearce (1988) were used for recalculation purposes:

`IRON3.STOIC` – Calculates Fe^{3+}, Fe^{2+}, and atomic proportions where stoichiometry can be assumed. In this work, the program was only used for recalculating pyroxene analyses.

`IRON3.OX` – Calculates Fe^{3+} and Fe^{2+} for oxides, and reports end-member compositions in terms of *mgt-üsp* and *ht-il*.

`IRON3.AMP` – Calculates Fe^{3+} and Fe^{2+} for amphiboles, by assuming that the octahedral and tetrahedral cations total to 13.000, and assigns elements to the different cation sites (after Leake 1978).

MINAT.F77 – Calculates atomic proportions without determining Fe^{3+} and Fe^{2+}. Used for all other phases.

AMPH.CLAS – Used for naming the amphiboles, using the method of Leake (*op. cit.*) after site assignment has been carried out using IRON3.AMP.

Pyroxene end-members were calculated using the program PYROXENE.F4B, written by Dr. A. Peckett, which allows recalculation of Fe^{3+} and Fe^{2+} ratios from analyses where all Fe is reported as FeO. Initially, enough Fe^{3+} is assigned to produce acmite and K-acmite, giving a minimum Fe^{3+} value, after which various pyroxene end-member molecules are extracted from the atomic composition. The Fe^{3+}/Fe^{2+} ratio is adjusted at various stages to account for excess Na and K by forming more acmite and K-acmite, while $CaFe^{3+}AlSiO_6$ (ferri-Tschermak's molecule) is not permitted in this calculation, with all Fe^{3+} forming acmite. Other options are allowed, which include fixing Fe^{3+}/Fe^{2+}, allowing Si to vary to use up all the cations as end-members, and permitting $CaFe^{3+}AlSiO_6$. The file PYROXENE.HLP gives full details of the pyroxene end-members and the various options available.

Element compositions for all mineral phases analysed (in terms of weight % oxide and atomic proportions), are given in the following tables. Where a particular element was not determined, this is indicated by 'nd.'.

(N.B. Analysis numbers less than about 300.00 refer to samples belonging to the 'G' series, ie. those collected during the 1987 field season).

* indicates that analysis was carried out using a WDS microprobe (Edinburgh)

Table II.1

Comparison between E.D. and W.D. spectrometers

E.D.S. Energy dispersive spectrometers	W.D.S. Wavelength dispersive spectrometers
Solid state device.	Mechanical device.
Has the ability to acquire and display and entire x-ray spectrum simultaneously.	Can measure only one x-ray peak (or background) position at a time ∴ multiple spectrometers are often employed.
Detects major elements only Detection limit 0.1% dep. on El'mt (e.g. Ti, Ca). Has 'poor' Pk/Bg ratio.	Detects major and trace elements. Detection limits:- 0.02% (200ppm) typically, down to 50ppm with effort. Has 10 times (typ) higher Pk/Bg ratio than E.D.S.
Elemental ranges typically Na → U Down to B with special windowless detector	B → U Range depends on diffracting crystals available. Full coverage requires 4 crystals interchangable in use. F routinely analysed
'poor' resolving power serious overlaps:- Sr, Rb, L radiation with SiK BaL/TiK AgL/CdL SK/BiM/Pb M R.E.E.	'good' resolution all resolved by W.D.S. { analysis of Ba/Ti in micas, complex sulphides and sulphosalts, det of Sr/Rb in Feldspars, are all possible.
Rapid assimilation of mineral type from the spectrum display	Information from only one element acquired at a time. This can be useful in determining a particular phase with a key element, via rate meter display and audio output.

(Taken from electron-probe microanalysis course notes, April 1987, Univ. of Manchester)

Table II.2

Electron microprobe operating conditions

Element	Line	Crystal*	$2\theta°$*	Standard
Si	K	TAP	32.22	Wollastonite or Forsterite
Ti	K	PET	36.60	Rutile
Al	K	TAP	37.91	Corundum
Fe	K	LIF	57.49	Fayalite
Mn	K	LIF	62.94	Tephroite
Mg	K	TAP	45.26	Periclase or Forsterite
Ca	K	PET	45.13	Wollastonite
Na	K	TAP	55.21	Jadeite or Albite
K	K	PET	50.60	Orthoclase
Ba	L	PET	36.96	Barytes
Zr	L	TAP	27.36	Zr metal
Cl	K	PET	65.40	Halite
S	K	PET	75.76	Pyrite
P	K	TAP	27.74	Apatite
Cu	L	—	—	Cu metal
Ni	K	—	—	Ni metal
Zn	L	—	—	Zn metal
Co	K	—	—	Co metal
La	L	PET	35.44	REE glass
Ce	L	PET	34.01	REE glass
Pr	L	PET	29.86	REE glass
Nd	L	PET	31.40	REE glass
Sm	L	LIF	66.21	REE glass

* relevant to the Edinburgh probe only (WDS).

— indicates not analysed at Edinburgh.

ANALYSIS LOCATION

As well as showing the chemical composition of the phases analysed, the following tables also give an indication of the texture of the grain, and for coarse grains, the position within the crystal.

Crystal Type

1 = Groundmass	9 = Overgrowth (eg. amph on px)
2 = Xenocryst	10 = Inclusion
3 = Poikiloblast	11 = Reaction rim (eg. biotite on opaque)
4 = Crystal #1	12 = Relic cores (eg. pyroxenes in XPS)
5 = Crystal #2	13 = Crystal #5
6 = Crystal #3	14 = Interstitial/poikilitic
7 = Crystal #4	15 = Exsolution
8 = Alteration product	

Position in crystal

1 . Core	8 = Groundmass
2 .	9 = Overgrowth
3 .	10 = Inclusion
4 . Intermediate	-1 = Miscellaneous
5 .	
6 .	
7 . Rim	

AMPHIBOLES

The naming of amphiboles in this thesis has been carried out according to the method of Leake (1978), based on site assignments (following recalcula to T+C cations totalling 13.00). The names are given in the tables of amphibole analyses using the following abbreviations:

Mg-	= Magnesio-	Arf	= Arfvedsonite
Mg'an-	= Magnesian	Pg	= Pargasite
Fe-	= Ferro-	Kat	= Katophorite
Fe'n-	= Ferroan-	Hast	= Hastingsite
Ca-	= Calcic	Richt	= Richterite
Ca'n-	= Calcian	Eck	= Eckermanite
Sub-Ca-	= Sub-calcic	Hb	= Hornblende
Ed-	= Edenite/Edenitic	Rieb	= Riebeckite
Si'ic-	= Silicic		
H'ic-	= Hastingsitic		

PYROXENE ANALYSES

	27113.01*	27113.02*	27113.03*	27113.04*	27113.07*	27113.08*	27113.09*	27113.10*	27193.01*	27193.02*	27193.03*	27193.04*	27193.05*	27193.06*	27193.09*	138044.01*	138044.02*
Weight % oxide																	
SiO2	50.574	50.544	50.399	49.934	50.177	50.424	50.365	49.821	51.154	50.931	50.744	50.375	50.987	50.112	51.319	50.547	50.258
TiO2	0.109	0.115	0.091	1.020	0.116	0.118	0.099	0.117	0.399	0.342	0.323	0.274	0.362	0.301	0.455	0.138	0.138
Al2O3	1.113	1.175	1.066	1.263	1.239	1.148	1.203	1.102	1.115	1.146	0.970	1.146	1.094	1.006	1.168	1.237	1.234
FeO	24.180	24.430	23.460	23.172	24.166	24.289	24.481	23.475	23.194	23.092	22.879	22.554	22.607	23.170	22.730	23.619	23.780
MnO	0.980	0.955	0.937	0.959	0.978	0.924	0.967	0.957	0.874	0.833	0.931	0.891	0.833	0.869	0.887	0.752	0.731
MgO	1.536	1.547	2.218	2.400	1.514	1.611	1.465	2.171	2.472	2.417	2.523	2.732	2.660	2.765	2.678	2.139	2.125
CaO	14.117	14.051	16.007	17.019	14.640	15.004	14.917	15.775	14.461	14.664	14.778	16.079	14.729	17.074	14.388	13.885	13.556
Na2O	6.018	6.066	4.900	4.361	5.674	5.600	5.719	5.085	6.097	5.990	5.701	4.836	6.072	4.197	6.066	6.352	6.534
K2O	0.019	0.0	0.010	0.0	nd.	nd.	nd.	nd.	nd.	nd.	nd.	nd.	nd.	nd.	nd.	nd.	nd.
ZrO2	nd.	nd.	nd.	nd.	nd.	nd.	nd.	nd.	nd.	nd.	nd.	nd.	nd.	nd.	nd.	nd.	nd.
Total	98.646	98.883	99.088	100.128	98.504	99.118	99.216	98.503	99.766	99.415	98.849	98.887	99.344	99.494	99.691	98.669	98.356
Atoms per 6 oxygens																	
Si	1.981	1.975	1.974	1.946	1.973	1.972	1.967	1.961	1.969	1.969	1.976	1.971	1.967	1.961	1.974	1.965	1.958
Ti	0.003	0.003	0.003	0.030	0.003	0.003	0.003	0.003	0.012	0.010	0.009	0.008	0.011	0.009	0.013	0.004	0.004
Al	0.051	0.054	0.049	0.058	0.057	0.053	0.055	0.051	0.051	0.052	0.045	0.053	0.050	0.046	0.053	0.057	0.057
Fe3	0.439	0.449	0.369	0.320	0.422	0.421	0.437	0.409	0.443	0.440	0.414	0.356	0.449	0.331	0.424	0.484	0.513
Fe2	0.353	0.349	0.399	0.435	0.373	0.373	0.362	0.364	0.304	0.307	0.331	0.382	0.280	0.427	0.307	0.284	0.261
Mn	0.033	0.032	0.031	0.032	0.033	0.031	0.032	0.032	0.028	0.027	0.031	0.030	0.027	0.029	0.029	0.025	0.024
Mg	0.090	0.090	0.129	0.139	0.089	0.094	0.085	0.127	0.142	0.139	0.146	0.159	0.153	0.161	0.154	0.124	0.123
Ca	0.592	0.588	0.672	0.711	0.617	0.629	0.624	0.665	0.596	0.607	0.617	0.674	0.609	0.716	0.593	0.578	0.566
Na	0.457	0.460	0.372	0.329	0.433	0.425	0.433	0.388	0.455	0.449	0.431	0.367	0.454	0.319	0.453	0.479	0.494
K	0.001	0.0	0.0	0.0	0.0	0.0	0.0	0.0	0.0	0.0	0.0	0.0	0.0	0.0	0.0	0.0	0.0
Zr	0.0	0.0	0.0	0.0	0.0	0.0	0.0	0.0	0.0	0.0	0.0	0.0	0.0	0.0	0.0	0.0	0.0
Rock Type	LSS	LSS	LSS	LSS	LSS	LSS	LSS	LSS	MUS	MUS	MUS	MUS	MUS	MUS	MUS	LSS	LSS
Crystal	4.	4.	4.	4.	5.	5.	6.	6.	1.	1.	4.	4.	5.	5.	14.	14.	14.
Position	7.	7.	1.	1.	7.	1.	7.	1.	-1.	-1.	7.	1.	7.	1.	-1.	1.	6.
Atomic percent																	
Mg	9.6	9.7	13.9	14.9	9.6	10.2	9.3	13.9	15.3	15.1	15.5	17.0	16.7	17.2	16.3	13.6	13.6
Fe2+Mn	41.4	40.9	46.2	49.9	43.8	43.8	43.2	43.5	35.7	36.2	38.6	43.9	33.6	48.7	35.6	33.9	31.6
Na	49.0	49.4	40.0	35.2	46.7	46.0	47.5	42.6	49.0	48.7	45.9	39.1	49.7	34.1	48.0	52.5	54.8

PYROXENE ANALYSES

	* 138044.03	* 138044.04	* 138044.05	* 138044.15	* 138044.17	* 138044.18	* 138048.01	* 138048.02	* 138048.03	* 138048.04	* 138048.05	* 138048.06	* 27056.01	* 27056.02	* 27056.03	* 27056.04	* 27056.05
Weight % oxide																	
SiO2	50.431	50.824	50.642	51.757	51.394	50.226	50.142	50.045	50.180	49.980	49.336	50.266	50.298	50.373	50.374	49.017	47.247
TiO2	0.104	0.122	0.154	0.274	0.189	0.152	0.208	0.151	0.135	0.125	0.109	0.090	0.223	0.344	0.243	0.245	0.208
Al2O3	1.232	1.203	1.167	1.717	1.400	0.979	1.113	1.362	1.215	1.208	1.624	1.174	2.316	2.571	2.392	2.300	1.053
FeO	23.406	23.784	24.193	25.623	25.388	24.971	23.893	22.693	22.267	22.719	23.367	23.472	17.199	18.574	16.990	17.403	23.655
MnO	0.917	0.821	0.647	0.446	0.502	0.722	1.008	0.983	0.951	0.940	0.965	0.984	0.495	0.638	0.590	0.545	0.750
MgO	2.132	2.233	1.982	0.955	1.087	1.495	1.897	2.757	3.128	2.839	2.050	2.279	6.881	5.764	6.876	6.355	1.094
CaO	15.351	13.824	13.044	8.232	9.455	12.833	16.398	17.825	17.501	18.125	15.858	16.753	19.446	18.909	19.387	19.931	11.670
Na2O	5.189	6.392	6.653	9.984	9.414	6.783	4.762	3.668	4.133	3.584	4.728	4.491	2.610	3.052	2.586	2.625	8.907
K2O	nd.	nd.	nd.	nd.	nd.	nd.	nd.	nd.	nd.	nd.	nd.	nd.	nd.	nd.	nd.	nd.	nd.
ZrO2	nd.	nd.	nd.	0.362	0.476	0.723	0.236	0.217	0.228	0.173	0.276	0.254	0.117	0.136	0.123	0.111	0.702
Total	98.762	99.203	98.482	99.350	99.305	98.884	99.657	99.701	99.738	99.693	98.313	99.763	99.585	100.361	99.561	98.532	95.286
Atoms per 6 oxygens																	
Si	1.978	1.965	1.972	1.961	1.956	1.961	1.963	1.963	1.955	1.960	1.953	1.964	1.931	1.927	1.934	1.905	1.875
Ti	0.003	0.004	0.005	0.008	0.005	0.004	0.006	0.004	0.004	0.004	0.003	0.003	0.006	0.010	0.007	0.007	0.006
Al	0.057	0.055	0.054	0.077	0.063	0.045	0.051	0.063	0.056	0.056	0.076	0.054	0.105	0.116	0.108	0.105	0.049
Fe3	0.376	0.487	0.497	0.706	0.691	0.511	0.363	0.274	0.330	0.282	0.364	0.343	0.211	0.232	0.197	0.263	0.847
Fe2	0.392	0.282	0.291	0.106	0.117	0.304	0.419	0.471	0.395	0.463	0.410	0.424	0.341	0.362	0.348	0.303	-0.062
Mn	0.030	0.027	0.021	0.014	0.016	0.024	0.033	0.033	0.031	0.031	0.032	0.033	0.016	0.021	0.019	0.018	0.025
Mg	0.125	0.129	0.115	0.054	0.062	0.087	0.111	0.161	0.182	0.166	0.121	0.133	0.394	0.329	0.393	0.368	0.065
Ca	0.645	0.573	0.544	0.334	0.386	0.537	0.688	0.749	0.731	0.762	0.673	0.701	0.800	0.775	0.798	0.830	0.496
Na	0.395	0.479	0.502	0.733	0.695	0.513	0.361	0.279	0.312	0.273	0.363	0.340	0.194	0.226	0.193	0.198	0.685
K	0.0	0.0	0.0	0.0	0.0	0.0	0.0	0.0	0.0	0.0	0.0	0.0	0.0	0.0	0.0	0.0	0.0
Zr	0.0	0.0	0.0	0.007	0.009	0.014	0.005	0.004	0.004	0.003	0.005	0.005	0.002	0.003	0.002	0.002	0.014
Rock Type	LSS	LSS	LSS	LSS	LSS	LSS	LSS	LSS	LSS	LSS	LSS	LSS	XPS	XPS	XPS	XPS	XPS
Crystal	4.	4.	5.	14.	14.	14.	4.	4.	5.	5.	14.	14.	10.	10.	10.	10.	1.
Position	2.	7.	6.	7.	2.	4.	6.	1.	7.	2.	7.	1.	7.	1.	7.	1.	-1.
Atomic percent																	
Mg	13.3	14.1	12.4	6.0	7.0	9.4	12.0	17.1	19.8	17.8	13.1	14.3	41.7	35.1	41.2	41.5	8.7
Fe2+Mn	44.8	33.7	33.6	13.2	14.9	35.3	48.9	53.4	46.3	52.9	47.7	49.1	37.8	40.8	38.5	36.2	0.0
Na	41.9	52.2	54.0	80.8	78.1	55.3	39.1	29.6	33.9	29.3	39.2	36.6	20.5	24.1	20.3	22.3	91.3

PYROXENE ANALYSES

	* 27056.08	* 27056.09	* 27056.10	* 138046.01	* 138046.02	* 138046.03	* 138046.04	* 27259.01	* 27259.02	* 27259.03	* 27259.04	* 27259.05	* 138007.01	* 138007.02	* 138007.03	* 138007.04	* 138007.05
Weight % oxide																	
SiO2	51.078	51.135	50.470	50.537	50.397	50.165	50.018	51.064	50.317	50.664	50.213	50.402	52.718	52.413	51.041	50.434	52.875
TiO2	0.250	0.179	0.167	0.103	0.098	0.114	0.098	0.173	0.152	0.136	0.186	0.202	2.165	1.152	0.464	0.422	2.567
Al2O3	1.084	1.097	1.143	1.339	1.249	1.113	1.232	1.155	1.084	1.127	1.051	1.157	1.746	1.353	1.949	1.319	0.780
FeO	25.198	25.246	25.154	24.292	23.733	24.795	23.526	22.894	21.331	20.575	21.496	21.563	25.027	25.865	13.599	16.730	25.036
MnO	0.607	0.720	0.709	0.986	0.943	0.935	0.928	0.862	1.020	0.869	1.018	0.907	0.237	0.263	0.399	0.515	0.545
MgO	1.176	1.139	1.053	1.609	2.125	1.422	2.276	2.818	4.041	4.400	3.781	3.667	0.588	0.744	9.771	7.494	0.947
CaO	7.746	8.674	8.386	14.570	16.052	14.658	16.787	15.865	18.787	18.778	18.300	18.008	2.157	3.998	21.252	19.972	1.457
Na2O	10.447	9.794	10.188	5.927	4.970	5.874	4.596	4.994	2.915	3.093	3.100	3.608	14.082	12.683	1.042	1.961	14.512
K2O	nd.	nd.	nd.	nd.	nd.	nd.	nd.	nd.	nd.	nd.	nd.	nd.	nd.	nd.	nd.	nd.	nd.
ZrO2	0.717	0.873	0.812	0.746	0.487	0.431	0.297	0.320	0.203	0.166	0.203	0.251	0.674	0.673	0.087	0.097	0.556
Total	98.303	98.857	98.082	100.109	100.054	99.507	99.758	100.145	99.850	99.808	99.348	99.765	99.394	99.144	99.604	98.944	99.275
Atoms per 6 oxygens																	
Si	1.950	1.954	1.936	1.959	1.960	1.957	1.953	1.974	1.967	1.971	1.973	1.965	1.946	1.959	1.948	1.956	1.949
Ti	0.007	0.005	0.005	0.003	0.003	0.003	0.003	0.005	0.004	0.004	0.005	0.006	0.060	0.032	0.013	0.012	0.071
Al	0.049	0.049	0.052	0.061	0.057	0.051	0.057	0.053	0.050	0.052	0.049	0.053	0.076	0.060	0.088	0.060	0.034
Fe3	0.784	0.726	0.794	0.433	0.373	0.455	0.368	0.351	0.220	0.224	0.222	0.268	0.895	0.853	0.063	0.147	0.943
Fe2	0.020	0.081	0.013	0.355	0.399	0.354	0.400	0.389	0.477	0.445	0.484	0.435	-0.123	-0.045	0.371	0.395	-0.171
Mn	0.020	0.023	0.023	0.032	0.031	0.031	0.031	0.028	0.034	0.029	0.034	0.030	0.007	0.008	0.013	0.017	0.017
Mg	0.067	0.065	0.060	0.093	0.123	0.083	0.132	0.162	0.235	0.255	0.221	0.213	0.032	0.041	0.556	0.433	0.052
Ca	0.317	0.355	0.345	0.605	0.669	0.613	0.702	0.657	0.787	0.783	0.771	0.752	0.085	0.160	0.869	0.830	0.058
Na	0.773	0.726	0.758	0.445	0.375	0.444	0.348	0.374	0.221	0.233	0.236	0.273	1.008	0.919	0.077	0.147	1.037
K	0.0	0.0	0.0	0.0	0.0	0.0	0.0	0.0	0.0	0.0	0.0	0.0	0.0	0.0	0.0	0.0	0.0
Zr	0.013	0.016	0.015	0.014	0.009	0.008	0.006	0.006	0.004	0.003	0.004	0.005	0.012	0.012	0.002	0.002	0.010
Rock Type	XPS	XPS	XPS	LSS	LSS	LSS	LSS	MUS	MUS	MUS	MUS	MUS	GS-A	GS-A	GS-A	GS-A	GS-A
Crystal	1.	1.	1.	4.	4.	5.	5.	4.	4.	5.	5.	14.	9.	9.	12.	1.	9.
Position	-1.	-1.	-1.	7.	1.	7.	1.	7.	1.	7.	1.	-1.	7.	4.	-1.	-1.	7.
Atomic percent																	
Mg	7.6	7.3	7.0	10.1	13.3	9.1	14.5	17.0	24.3	26.5	22.7	22.4	3.1	4.3	54.7	43.6	4.8
Fe2+Mn	4.5	11.6	4.2	41.8	46.3	42.2	47.3	43.8	52.8	49.3	53.1	48.9	0.0	0.0	37.8	41.5	0.0
Na	87.8	81.1	88.8	48.1	40.4	48.7	38.2	39.2	22.9	24.2	24.2	28.7	96.9	95.7	7.6	14.8	95.2

PYROXENE ANALYSES

	* 138007.06	* 138007.07	* 138001.01	* 138001.02	* 138001.03	* 138025.01	* 138025.02	* 138025.03	* 138025.04	* 39709.03	* 39709.05	* 39709.08	* 39709.09	* 39709.10	* 39709.11	* 39709.12	* 39709.13
Weight % oxide																	
SiO2	51.913	51.467	50.434	50.896	48.771	50.340	50.143	49.919	50.009	49.353	50.856	50.432	50.339	52.676	52.951	52.716	52.852
TiO2	0.735	0.310	0.080	0.074	0.087	0.073	0.063	0.082	0.103	0.442	0.310	0.579	0.105	0.025	0.057	0.028	0.039
Al2O3	0.916	0.848	1.190	1.063	1.296	1.200	1.354	1.254	1.279	0.820	0.738	1.854	0.571	0.355	2.207	0.326	1.776
FeO	25.974	23.679	23.828	23.893	22.181	23.371	23.076	23.074	23.029	24.761	27.665	25.501	27.632	29.589	27.431	29.545	27.842
MnO	0.332	0.739	0.800	0.736	0.965	0.970	0.984	0.949	0.994	0.158	0.049	0.111	0.073	0.017	0.011	0.034	0.019
MgO	1.043	2.446	2.188	2.295	2.578	2.507	2.570	2.513	2.418	3.387	0.741	0.918	0.809	0.041	0.004	0.048	0.033
CaO	6.388	12.090	13.732	13.229	15.519	14.901	15.289	14.857	16.293	1.883	0.405	0.950	0.622	0.233	0.048	0.312	0.105
Na2O	11.137	7.470	6.586	6.831	6.092	5.530	5.261	5.568	4.521	12.330	15.075	14.848	14.973	15.753	15.783	15.702	15.745
K2O	nd.	nd.	nd.	nd.	nd.	nd.	nd.	nd.	nd.	0.443	0.012	0.028	0.011	nd.	nd.	nd.	nd.
ZrO2	0.821	0.458	0.410	0.469	0.333	0.0	0.0	0.0	0.0	nd.	nd.	nd.	nd.	0.024	0.062	0.019	0.012
Total	99.259	99.507	99.248	99.486	97.822	98.892	98.740	98.216	98.646	93.577	95.851	95.221	95.135	98.713	98.554	98.730	98.423
Atoms per 6 oxygens																	
Si	1.960	1.971	1.950	1.960	1.909	1.959	1.955	1.954	1.968	1.916	1.921	1.909	1.914	1.938	1.939	1.940	1.940
Ti	0.021	0.009	0.002	0.002	0.003	0.002	0.002	0.002	0.003	0.013	0.009	0.016	0.003	0.001	0.002	0.001	0.001
Al	0.041	0.038	0.054	0.048	0.060	0.055	0.062	0.058	0.059	0.038	0.033	0.083	0.026	0.015	0.095	0.014	0.077
Fe3	0.782	0.539	0.519	0.520	0.566	0.440	0.421	0.452	0.344	1.055	1.213	1.158	1.244	1.231	1.142	1.225	1.161
Fe2	0.038	0.219	0.251	0.249	0.160	0.320	0.332	0.303	0.413	-0.251	-0.339	-0.351	-0.365	-0.320	-0.302	-0.316	-0.306
Mn	0.011	0.024	0.026	0.024	0.032	0.032	0.033	0.031	0.033	0.005	0.002	0.004	0.002	0.001	0.0	0.001	0.001
Mg	0.059	0.140	0.126	0.132	0.150	0.145	0.149	0.147	0.142	0.196	0.042	0.052	0.046	0.002	0.0	0.003	0.002
Ca	0.258	0.496	0.569	0.546	0.651	0.621	0.639	0.623	0.687	0.078	0.016	0.039	0.025	0.009	0.002	0.012	0.004
Na	0.815	0.555	0.494	0.510	0.462	0.417	0.398	0.423	0.345	0.928	1.104	1.090	1.104	1.124	1.121	1.120	1.121
K	0.0	0.0	0.0	0.0	0.0	0.0	0.0	0.0	0.0	0.022	0.001	0.001	0.001	0.0	0.0	0.0	0.0
Zr	0.015	0.009	0.008	0.009	0.006	0.0	0.0	0.0	0.0	0.0	0.0	0.0	0.0	0.0	0.001	0.0	0.0
Rock Type	GS-A	GS-A	CGBS	CGBS	CGBS	LSS	LSS	LSS	LSS	CBT	CBT	CBT	CBT	CBT	CBT	CBT	CBT
Crystal	9.	9.	1.	1.	1.	4.	4.	5.	5.	1.	1.	1.	1.	1.	1.	1.	1.
Position	4.	1.	-1.	-1.	-1.	7.	1.	7.	1.	-1.	-1.	-1.	-1.	-1.	-1.	-1.	-1.
Atomic percent																	
Mg	6.4	14.9	14.0	14.4	18.7	15.9	16.3	16.3	15.2	17.4	3.7	4.6	4.0	0.2	0.0	0.3	0.2
Fe2+Mn	5.3	25.9	30.9	29.8	23.9	38.5	40.0	36.9	47.8	0.0	0.0	0.0	0.0	0.0	0.0	0.0	0.0
Na	88.3	59.2	55.1	55.7	57.5	45.6	43.6	46.8	37.0	82.6	96.3	95.4	96.0	99.8	100.0	99.7	99.8

PYROXENE ANALYSES

	* 39709.14	* 39709.15	* 39709.16	* 39709.17	* 39709.18	* 39709.19	38.01	38.03	38.04	38.05	38.06	38.07	38.08	38.09	38.10	197.01	197.06
Weight % oxide																	
SiO2	51.704	52.005	52.198	52.170	52.133	51.169	51.857	51.443	51.192	50.295	50.793	51.228	50.808	50.800	50.517	50.588	51.143
TiO2	0.199	0.059	1.317	0.045	0.099	0.379	0.0	0.0	0.0	0.0	0.0	0.0	0.0	0.0	0.0	0.0	0.630
Al2O3	0.785	0.438	0.451	0.375	0.317	0.501	1.194	1.154	0.985	3.402	1.325	1.177	1.057	1.404	1.142	0.0	0.0
FeO	27.614	28.984	27.113	29.199	28.886	26.852	25.837	25.509	26.794	29.191	26.311	25.473	25.949	26.403	25.102	20.526	20.752
MnO	0.063	0.024	0.109	0.0	0.024	0.056	0.794	0.860	0.871	0.586	1.002	0.772	1.020	0.831	1.041	0.366	0.0
MgO	0.724	0.062	0.405	0.059	0.148	0.741	1.859	2.121	1.115	1.033	0.872	1.203	1.390	1.184	2.058	5.166	4.333
CaO	0.731	0.206	0.270	0.326	0.865	0.815	15.873	15.274	14.421	7.314	12.225	13.887	15.134	14.463	15.737	19.351	16.824
Na2O	15.270	15.306	15.313	15.366	15.007	14.982	6.087	4.940	5.845	8.749	6.651	5.675	5.136	5.652	4.580	2.348	3.517
K2O	0.003	nd.	nd.	nd.	nd.	nd.	0.0	0.0	0.0	0.492	0.0	0.0	0.0	0.0	0.0	0.0	0.0
ZrO2	nd.	0.178	0.193	0.087	0.400	0.162	nd.	nd.	nd.	nd.	nd.	nd.	nd.	nd.	nd.	nd.	nd.
Total	97.093	97.262	97.369	97.627	97.879	95.657	103.501	101.301	101.223	101.062	99.179	99.415	100.494	100.737	100.177	98.345	97.199
Atoms per 6 oxygens																	
Si	1.926	1.946	1.948	1.944	1.945	1.937	1.936	1.979	1.970	1.895	1.982	2.004	1.976	1.964	1.970	2.002	2.040
Ti	0.006	0.002	0.037	0.001	0.003	0.011	0.0	0.0	0.0	0.0	0.0	0.0	0.0	0.0	0.0	0.0	0.019
Al	0.034	0.019	0.020	0.016	0.014	0.022	0.053	0.052	0.045	0.151	0.061	0.054	0.048	0.064	0.053	0.0	0.0
Fe3	1.206	1.190	1.111	1.200	1.161	1.175	0.516	0.358	0.452	0.722	0.478	0.368	0.387	0.432	0.353	0.175	0.154
Fe2	-0.346	-0.283	-0.264	-0.290	-0.260	-0.325	0.291	0.463	0.411	0.197	0.381	0.465	0.457	0.422	0.466	0.504	0.538
Mn	0.002	0.001	0.003	0.0	0.001	0.002	0.025	0.028	0.028	0.019	0.033	0.026	0.034	0.027	0.034	0.012	0.0
Mg	0.040	0.003	0.023	0.003	0.008	0.042	0.103	0.122	0.064	0.058	0.051	0.070	0.081	0.068	0.120	0.305	0.258
Ca	0.029	0.008	0.011	0.013	0.035	0.033	0.635	0.630	0.595	0.295	0.511	0.582	0.631	0.599	0.658	0.821	0.719
Na	1.103	1.110	1.108	1.110	1.086	1.100	0.441	0.369	0.436	0.639	0.503	0.430	0.387	0.424	0.346	0.180	0.272
K	0.0	0.0	0.0	0.0	0.0	0.0	0.0	0.0	0.0	0.024	0.0	0.0	0.0	0.0	0.0	0.0	0.0
Zr	0.0	0.003	0.004	0.002	0.007	0.003	0.0	0.0	0.0	0.0	0.0	0.0	0.0	0.0	0.0	0.0	0.0
Rock Type	CBT	CBT	CBT	CBT	CBT	CBT	PMS	MMS	MMS	MMS	MMS	MMS	MMS	MMS	MMS	ALGN	ALGN
Crystal	1.	1.	1.	1.	1.	1.	12.	1.	1.	1.	1.	1.	1.	1.	1.	14.	1.
Position	-1.	-1.	7.	4.	1.	-1.	-1.	8.	8.	8.	8.	8.	8.	8.	7.	-1.	3.
Atomic percent																	
Mg	3.5	0.3	2.0	0.3	0.7	3.7	12.0	12.4	6.8	6.4	5.3	7.1	8.4	7.2	12.4	30.5	24.2
Fe2+Mn	0.0	0.0	0.0	0.0	0.0	0.0	36.7	50.0	46.8	23.7	42.8	49.5	51.2	47.7	51.8	51.5	50.4
Na	96.5	99.7	98.0	99.7	99.3	96.3	51.3	37.6	46.4	70.0	52.0	43.4	40.4	45.1	35.8	18.0	25.5

PYROXENE ANALYSES

	197.07	197.08	197.09	197.10	197.11	197.12	220.01	220.02	220.03	220.04	220.05	44.06	44.07	44.11	44.12	37.01	37.02
Weight % oxide																	
SiO2	51.885	52.613	52.239	55.481	52.900	56.830	52.301	52.160	52.266	50.745	50.565	52.415	51.938	51.802	52.203	52.349	51.398
TiO2	0.537	0.673	0.351	0.384	0.389	0.506	0.0	0.0	0.0	0.0	0.0	0.0	0.367	0.332	0.440	0.0	0.0
Al2O3	0.441	0.0	0.0	0.357	3.369	5.323	1.166	1.225	1.590	0.943	0.861	1.479	1.120	1.181	1.238	1.297	0.865
FeO	20.779	21.912	20.621	16.794	18.872	16.500	26.302	25.985	27.253	25.407	25.907	26.868	27.536	26.735	27.043	23.967	22.610
MnO	0.284	0.484	0.339	0.0	0.294	0.0	0.976	1.261	1.175	1.013	1.026	0.0	0.408	0.582	0.528	1.649	1.186
MgO	4.953	4.885	5.237	13.319	5.404	3.403	2.008	2.238	1.094	2.182	1.885	1.106	1.346	0.963	1.240	3.678	3.599
CaO	16.768	16.925	18.914	5.843	13.820	12.446	14.730	15.230	13.877	16.335	14.550	11.006	11.291	10.766	10.806	16.874	15.022
Na2O	3.629	4.596	3.551	5.911	3.683	6.403	5.327	5.309	5.786	4.309	5.262	6.758	7.372	7.132	6.840	3.992	4.766
K2O	0.0	0.0	0.0	1.656	0.591	0.0	0.0	0.0	0.0	0.0	0.0	0.0	0.0	0.0	0.0	0.0	0.0
ZrO2	nd.	nd.	nd.	nd.	nd.	nd.	nd.	nd.	nd.	nd.	nd.	nd.	nd.	nd.	nd.	nd.	nd.
Total	99.476	102.088	101.252	99.745	99.322	101.411	102.810	103.408	103.041	100.934	100.056	99.632	101.378	99.493	100.338	103.806	99.446
Atoms per 6 oxygens																	
Si	2.011	1.982	1.990	2.019	2.036	2.103	1.981	1.962	1.979	1.969	1.969	2.032	1.973	2.010	2.013	1.964	1.995
Ti	0.016	0.019	0.010	0.011	0.011	0.014	0.0	0.0	0.0	0.0	0.0	0.0	0.010	0.010	0.013	0.0	0.0
Al	0.020	0.0	0.0	0.015	0.153	0.232	0.052	0.054	0.071	0.043	0.040	0.068	0.050	0.054	0.056	0.057	0.040
Fe3	0.214	0.334	0.262	0.420	0.057	0.0	0.377	0.409	0.396	0.343	0.420	0.376	0.526	0.443	0.404	0.305	0.328
Fe2	0.459	0.357	0.395	0.091	0.550	0.511	0.456	0.408	0.467	0.482	0.424	0.495	0.349	0.424	0.468	0.447	0.406
Mn	0.009	0.015	0.011	0.0	0.010	0.0	0.031	0.040	0.038	0.033	0.034	0.0	0.013	0.019	0.017	0.052	0.039
Mg	0.286	0.274	0.297	0.722	0.310	0.188	0.113	0.125	0.062	0.126	0.109	0.064	0.076	0.056	0.071	0.206	0.208
Ca	0.696	0.683	0.772	0.228	0.570	0.493	0.598	0.614	0.563	0.679	0.607	0.457	0.460	0.448	0.446	0.678	0.625
Na	0.288	0.336	0.262	0.417	0.275	0.459	0.391	0.387	0.425	0.324	0.397	0.508	0.543	0.537	0.511	0.290	0.359
K	0.0	0.0	0.0	0.077	0.029	0.0	0.0	0.0	0.0	0.0	0.0	0.0	0.0	0.0	0.0	0.0	0.0
Zr	0.0	0.0	0.0	0.0	0.0	0.0	0.0	0.0	0.0	0.0	0.0	0.0	0.0	0.0	0.0	0.0	0.0
Rock Type	ALGN	ALGN	ALGN	ALGN	ALGN	ALGN	LSS	LSS	LSS	LSS	LSS	MMS	MMS	MMS	MMS	MMS	MMS
Crystal	1.	1.	1.	1.	1.	1.	4.	4.	5.	5.	5.	12.	12.	12.	12.	1.	1.
Position	1.	1.	8.	8.	8.	8.	7.	1.	7.	1.	4.	-1.	-1.	-1.	-1.	8.	8.
Atomic percent																	
Mg	27.4	27.9	30.8	58.7	27.1	16.2	11.4	13.0	6.3	13.1	11.3	6.0	7.7	5.4	6.7	20.7	20.6
Fe2+Mn	44.9	37.9	42.1	7.4	48.9	44.1	49.1	46.7	50.9	53.4	47.5	46.4	36.9	42.8	45.5	50.2	44.0
Na	27.6	34.2	27.2	33.9	24.0	39.6	39.5	40.3	42.8	33.6	41.2	47.6	55.4	51.8	47.9	29.1	35.5

PYROXENE ANALYSES

	37.03	37.04	37.05	37.06	138055.01	138055.02	138055.03	138055.04	138055.05	138055.06	64.02	64.03	64.04	64.05	204.01	204.02	204.03
Weight % oxide																	
SiO2	51.008	52.186	50.995	51.137	55.197	57.029	54.223	55.200	54.494	54.554	50.379	49.843	50.676	50.694	50.169	49.271	49.829
TiO2	0.0	0.0	0.0	0.0	1.006	0.311	0.0	0.241	0.0	0.0	0.0	0.256	0.0	0.0	0.0	0.0	0.0
Al2O3	1.105	1.302	1.449	1.274	4.896	7.249	1.353	2.489	3.985	1.427	1.029	0.973	1.697	1.050	0.867	1.167	1.080
FeO	22.712	24.738	22.730	22.555	26.386	24.931	30.092	30.196	29.317	30.620	24.422	24.868	24.859	24.679	25.152	24.518	24.793
MnO	1.474	0.859	1.644	1.340	0.0	0.0	0.367	0.0	0.0	0.0	0.853	0.997	0.750	0.898	0.925	1.180	1.187
MgO	3.377	2.413	2.931	3.113	0.0	0.0	0.0	0.0	0.0	0.0	2.114	2.360	2.331	1.849	1.512	1.723	1.711
CaO	16.529	11.565	16.231	16.997	0.0	0.0	2.095	0.0	0.0	0.0	16.287	16.296	15.962	15.766	15.665	16.231	15.995
Na2O	3.672	6.660	3.742	3.871	13.937	14.176	12.534	13.577	13.386	13.466	4.141	3.601	4.258	4.004	5.861	5.278	5.322
K2O	0.0	0.0	0.0	0.0	0.0	0.0	0.0	0.0	0.0	0.0	0.0	0.0	0.0	0.0	0.0	0.0	0.0
ZrO2	nd.	nd.	nd.	nd.	nd.	nd.	nd.	nd.	nd.	nd.	nd.	nd.	nd.	nd.	nd.	nd.	nd.
Total	99.877	99.723	99.722	100.287	101.422	103.696	100.664	101.703	101.182	100.067	99.225	99.194	100.533	98.940	100.151	99.368	99.917
Atoms per 6 oxygens																	
Si	1.992	2.006	1.997	1.986	1.992	1.998	2.011	2.009	1.988	2.021	1.988	1.978	1.969	2.013	1.941	1.926	1.938
Ti	0.0	0.0	0.0	0.0	0.027	0.008	0.0	0.007	0.0	0.0	0.0	0.008	0.0	0.0	0.0	0.0	0.0
Al	0.051	0.059	0.067	0.058	0.208	0.299	0.059	0.107	0.171	0.062	0.048	0.046	0.078	0.049	0.040	0.054	0.050
Fe3	0.243	0.425	0.222	0.261	0.728	0.650	0.820	0.820	0.800	0.862	0.293	0.260	0.305	0.234	0.519	0.495	0.476
Fe2	0.499	0.371	0.522	0.471	0.069	0.080	0.114	0.099	0.094	0.086	0.513	0.565	0.503	0.586	0.295	0.307	0.330
Mn	0.049	0.028	0.055	0.044	0.0	0.0	0.012	0.0	0.0	0.0	0.029	0.034	0.025	0.030	0.030	0.039	0.039
Mg	0.197	0.138	0.171	0.180	0.0	0.0	0.0	0.0	0.0	0.0	0.124	0.140	0.135	0.109	0.087	0.100	0.099
Ca	0.692	0.476	0.681	0.707	0.0	0.0	0.083	0.0	0.0	0.0	0.689	0.693	0.665	0.671	0.649	0.680	0.667
Na	0.278	0.496	0.284	0.291	0.975	0.963	0.901	0.958	0.947	0.967	0.317	0.277	0.321	0.308	0.440	0.400	0.401
K	0.0	0.0	0.0	0.0	0.0	0.0	0.0	0.0	0.0	0.0	0.0	0.0	0.0	0.0	0.0	0.0	0.0
Zr	0.0	0.0	0.0	0.0	0.0	0.0	0.0	0.0	0.0	0.0	0.0	0.0	0.0	0.0	0.0	0.0	0.0
Rock Type	MMS	MMS	MMS	MMS	PEG	PEG	PEG	PEG	PEG	PEG	MMS	MMS	MMS	MMS	USS	USS	USS
Crystal	1.	1.	1.	1.	14.	1.	14.	14.	14.	14.	1.	1.	1.	1.	4.	4.	5.
Position	8.	8.	8.	8.	-1.	8.	7.	2.	6.	-1.	-1.	-1.	-1.	-1.	1.	7.	6.
Atomic percent																	
Mg	19.3	13.4	16.6	18.3	0.0	0.0	0.0	0.0	0.0	0.0	12.6	13.8	13.7	10.6	10.2	11.8	11.4
Fe2+Mn	53.6	38.6	55.9	52.2	6.6	7.7	12.3	9.4	9.0	8.2	55.1	59.0	53.7	59.6	38.1	40.9	42.5
Na	27.2	48.0	27.5	29.5	93.4	92.3	87.7	90.6	91.0	91.8	32.2	27.3	32.6	29.8	51.6	47.3	46.1

PYROXENE ANALYSES

	204.04	204.05	204.06	207.02	207.01	207.03	207.06	207.05	207.04	207.09	20.01	20.02	20.04	20.05	20.07	20.08	191.01
Weight % oxide																	
SiO2	50.177	51.192	50.140	49.409	51.635	50.663	51.340	51.401	51.760	51.786	51.687	51.899	50.963	49.220	52.099	50.416	49.945
TiO2	0.0	0.0	0.261	0.420	0.0	0.414	0.0	0.0	0.0	0.0	0.0	0.0	0.251	0.0	0.0	0.0	0.0
Al2O3	1.254	1.186	1.258	3.538	1.127	1.328	1.775	0.860	1.789	0.911	1.266	0.844	0.874	1.189	1.089	4.011	0.912
FeO	24.014	25.917	24.233	21.572	23.469	18.987	18.969	23.987	19.622	23.564	25.372	24.333	25.980	25.744	25.465	23.186	24.807
MnO	0.996	1.038	1.205	0.930	0.935	0.601	0.790	0.963	0.522	1.054	0.769	1.064	0.922	0.946	0.828	0.734	1.201
MgO	2.548	1.816	2.278	5.179	2.973	5.654	5.825	2.901	6.030	3.344	1.730	2.622	1.604	1.435	1.882	2.009	1.913
CaO	16.892	15.569	14.882	15.351	16.307	20.461	21.217	16.701	20.500	17.557	13.568	14.855	14.186	13.208	14.164	13.776	16.129
Na2O	4.516	5.639	6.044	4.068	4.529	2.381	1.610	4.351	2.160	3.492	5.501	5.177	5.384	5.325	5.254	4.069	3.941
K2O	0.0	0.0	0.0	0.413	0.0	0.0	0.0	0.0	0.0	0.0	0.0	0.0	0.0	0.0	0.0	0.0	0.0
ZrO2	nd.	nd.	nd.	nd.	nd.	nd.	nd.	nd.	nd.	nd.	nd.	nd.	nd.	nd.	nd.	nd.	nd.
Total	100.397	102.357	100.301	100.880	100.975	100.489	101.526	101.164	102.383	101.708	99.893	100.794	100.164	97.067	100.781	98.201	98.848
Atoms per 6 oxygens																	
Si	1.944	1.942	1.925	1.877	1.985	1.951	1.965	1.978	1.956	1.991	2.011	1.996	1.985	1.977	2.013	2.001	1.987
Ti	0.0	0.0	0.008	0.012	0.0	0.012	0.0	0.0	0.0	0.0	0.0	0.0	0.007	0.0	0.0	0.0	0.0
Al	0.057	0.053	0.057	0.158	0.051	0.060	0.080	0.039	0.080	0.041	0.058	0.038	0.040	0.056	0.050	0.188	0.043
Fe3	0.394	0.479	0.527	0.384	0.317	0.192	0.109	0.330	0.167	0.237	0.336	0.356	0.383	0.404	0.319	0.124	0.288
Fe2	0.384	0.343	0.251	0.302	0.437	0.419	0.498	0.442	0.453	0.521	0.490	0.427	0.463	0.461	0.504	0.645	0.537
Mn	0.033	0.033	0.039	0.030	0.030	0.020	0.026	0.031	0.017	0.034	0.025	0.035	0.030	0.032	0.027	0.025	0.040
Mg	0.147	0.103	0.130	0.293	0.170	0.324	0.332	0.166	0.340	0.192	0.100	0.150	0.093	0.086	0.108	0.119	0.113
Ca	0.701	0.633	0.612	0.625	0.672	0.844	0.870	0.689	0.830	0.723	0.566	0.612	0.592	0.569	0.586	0.586	0.687
Na	0.339	0.415	0.450	0.300	0.338	0.178	0.119	0.325	0.158	0.260	0.415	0.386	0.407	0.415	0.394	0.313	0.304
K	0.0	0.0	0.0	0.020	0.0	0.0	0.0	0.0	0.0	0.0	0.0	0.0	0.0	0.0	0.0	0.0	0.0
Zr	0.0	0.0	0.0	0.0	0.0	0.0	0.0	0.0	0.0	0.0	0.0	0.0	0.0	0.0	0.0	0.0	0.0
Rock Type	USS	USS	USS	MUS	MUS	MUS	MUS	MUS	MUS	MUS	USS	USS	USS	USS	USS	USS	USS
Crystal	5.	6.	6.	4.	4.	5.	6.	6.	5.	7.	4.	4.	5.	5.	6.	1.	14.
Position	1.	6.	1.	1.	7.	7.	1.	7.	2.	6.	7.	1.	7.	1.	1.	8.	7.
Atomic percent																	
Mg	16.3	11.5	14.9	31.7	17.4	34.4	34.1	17.2	35.1	19.1	9.7	15.0	9.4	8.7	10.5	10.8	11.4
Fe2+Mn	46.2	42.1	33.3	35.9	47.9	46.7	53.7	49.1	48.6	55.1	50.0	46.3	49.6	49.6	51.4	60.8	58.0
Na	37.5	46.4	51.7	32.4	34.7	18.9	12.2	33.7	16.3	25.8	40.3	38.7	41.0	41.8	38.1	28.4	30.6

PYROXENE ANALYSES

	191.02	191.03	191.04	191.05	21.02	21.03	21.04	21.05	21.07	21.06	43.01	43.02	43.03	43.04	43.05	43.06	248.01
Weight % oxide																	
SiO2	50.867	51.339	50.640	51.349	52.009	52.054	50.885	50.741	50.448	52.562	53.891	54.163	53.958	52.934	52.745	52.974	54.055
TiO2	0.0	0.241	0.0	0.0	0.236	0.295	0.0	0.268	0.245	0.0	0.283	0.385	0.434	0.278	0.350	0.343	0.524
Al2O3	0.982	1.014	0.834	0.599	0.880	0.723	0.775	0.783	0.766	1.036	1.123	0.879	0.944	0.718	0.797	0.891	1.013
FeO	24.138	24.545	25.157	26.134	24.274	24.078	23.208	23.495	19.987	25.350	27.554	26.450	27.253	26.271	24.551	25.637	26.394
MnO	1.305	1.356	1.286	1.308	0.884	0.854	0.813	0.858	0.991	0.454	0.866	0.861	1.134	1.094	0.781	0.833	0.890
MgO	2.559	2.465	1.820	1.243	3.168	3.015	3.264	2.983	4.732	1.719	0.648	1.013	1.006	0.915	2.323	1.890	1.513
CaO	16.830	16.486	14.976	12.685	14.611	14.583	15.447	15.879	18.601	9.988	9.480	9.181	9.547	9.419	12.390	11.148	10.733
Na2O	3.823	4.352	4.812	5.971	5.175	4.984	4.327	4.250	3.409	7.841	8.966	8.862	8.498	7.917	6.539	7.231	7.880
K2O	0.0	0.0	0.0	0.0	0.0	0.0	0.0	0.0	0.0	0.0	0.0	0.0	0.0	0.0	0.0	0.0	0.0
ZrO2	nd.	nd.	nd.	nd.	nd.	nd.	nd.	nd.	nd.	nd.	nd.	nd.	nd.	nd.	nd.	nd.	nd.
Total	100.504	101.798	99.525	99.289	101.237	100.586	98.719	99.257	99.179	98.950	102.811	101.794	102.774	99.546	100.476	100.947	103.002
Atoms per 6 oxygens																	
Si	1.984	1.971	1.989	2.013	1.987	2.006	2.001	1.991	1.965	2.025	2.001	2.027	2.010	2.042	2.018	2.014	2.011
Ti	0.0	0.007	0.0	0.0	0.007	0.009	0.0	0.008	0.007	0.0	0.008	0.011	0.012	0.008	0.010	0.010	0.015
Al	0.045	0.046	0.039	0.028	0.040	0.033	0.036	0.036	0.035	0.047	0.049	0.039	0.041	0.033	0.036	0.040	0.044
Fe3	0.277	0.321	0.350	0.400	0.356	0.310	0.291	0.289	0.278	0.489	0.578	0.528	0.527	0.460	0.393	0.445	0.472
Fe2	0.510	0.467	0.476	0.456	0.420	0.467	0.472	0.482	0.374	0.328	0.278	0.300	0.322	0.388	0.392	0.370	0.349
Mn	0.043	0.044	0.043	0.043	0.029	0.028	0.027	0.029	0.033	0.015	0.027	0.027	0.036	0.036	0.025	0.027	0.028
Mg	0.149	0.141	0.107	0.073	0.180	0.173	0.191	0.174	0.275	0.099	0.036	0.057	0.056	0.053	0.132	0.107	0.084
Ca	0.703	0.678	0.630	0.533	0.598	0.602	0.651	0.668	0.776	0.412	0.377	0.368	0.381	0.389	0.508	0.454	0.428
Na	0.289	0.324	0.366	0.454	0.383	0.373	0.330	0.323	0.257	0.586	0.646	0.643	0.614	0.592	0.485	0.533	0.568
K	0.0	0.0	0.0	0.0	0.0	0.0	0.0	0.0	0.0	0.0	0.0	0.0	0.0	0.0	0.0	0.0	0.0
Zr	0.0	0.0	0.0	0.0	0.0	0.0	0.0	0.0	0.0	0.0	0.0	0.0	0.0	0.0	0.0	0.0	0.0
Rock Type	USS	USS	USS	USS	MUS	MUS	MUS	MUS	MUS	MUS	USS	USS	USS	USS	USS	USS	MUS
Crystal	14.	14.	14.	14.	1.	1.	1.	1.	1.	1.	1.	1.	1.	1.	1.	1.	4.
Position	1.	7.	1.	-1.	7.	1.	1.	7.	1.	7.	7.	1.	7.	1.	1.	7.	7.
Atomic percent																	
Mg	15.0	14.4	10.8	7.1	17.8	16.6	18.7	17.3	29.3	9.6	3.6	5.6	5.4	5.0	12.8	10.3	8.2
Fe2+Mn	55.8	52.4	52.3	48.6	44.4	47.6	48.9	50.7	43.3	33.4	30.9	31.8	34.8	39.7	40.3	38.3	36.6
Na	29.2	33.2	36.9	44.2	37.8	35.8	32.4	32.0	27.4	57.0	65.5	62.6	59.7	55.4	46.9	51.4	55.2

PYROXENE ANALYSES

	248.02	248.03	248.04	248.05	188.02	188.03	188.04	188.05	188.06	172.01	172.02	172.03	172.04	172.05	172.06	172.11	172.12
Weight % oxide																	
SiO2	51.246	53.910	52.505	52.902	53.636	51.270	51.235	51.189	51.135	49.804	53.150	52.757	50.636	51.240	52.813	50.036	49.055
TiO2	0.263	0.0	0.335	0.357	0.0	0.0	0.0	0.0	0.0	0.375	1.456	1.864	0.429	0.662	1.737	0.384	0.286
Al2O3	0.683	0.814	0.695	0.675	0.743	1.041	0.523	0.830	0.583	2.550	1.903	1.451	1.796	1.483	1.591	1.231	0.684
FeO	24.329	24.654	24.530	24.956	24.272	23.734	23.490	24.066	23.384	19.391	28.407	27.408	17.074	28.554	27.267	16.995	22.621
MnO	0.983	1.082	0.662	0.987	1.080	1.015	1.108	0.913	1.115	0.643	0.278	0.437	0.650	0.142	0.493	0.392	0.744
MgO	1.864	2.679	2.294	1.961	2.993	2.991	3.202	2.423	3.286	6.606	0.523	0.695	8.084	0.644	0.532	7.561	3.381
CaO	11.468	12.394	12.282	11.145	16.706	15.035	16.510	15.848	16.647	17.625	2.296	1.372	20.476	7.408	1.306	21.082	19.307
Na2O	6.952	6.944	6.474	6.946	4.368	5.100	3.889	4.221	3.939	2.815	12.609	13.192	1.674	9.412	13.071	1.454	2.171
K2O	0.147	0.140	0.0	0.0	0.0	0.0	0.135	0.0	0.0	0.230	0.034	0.006	0.030	0.0	0.0	0.0	0.0
ZrO2	nd.	nd.	nd.	nd.	nd.	nd.	nd.	nd.	nd.	0.107	0.620	0.623	0.018	0.703	1.026	0.0	0.204
Total	97.935	102.617	99.777	99.929	103.798	100.186	100.092	99.490	100.089	100.146	101.276	99.805	100.867	100.248	99.836	99.135	98.453
Atoms per 6 oxygens																	
Si	2.006	2.009	2.024	2.035	2.013	1.978	1.997	2.010	1.992	1.908	1.959	1.962	1.926	1.952	1.970	1.943	1.969
Ti	0.008	0.0	0.010	0.010	0.0	0.0	0.0	0.0	0.0	0.011	0.040	0.052	0.012	0.019	0.049	0.011	0.009
Al	0.032	0.036	0.032	0.031	0.033	0.047	0.024	0.038	0.027	0.115	0.083	0.064	0.081	0.067	0.070	0.056	0.032
Fe3	0.475	0.454	0.386	0.398	0.258	0.378	0.282	0.262	0.287	0.263	0.799	0.837	0.168	0.660	0.801	0.144	0.174
Fe2	0.321	0.314	0.405	0.405	0.504	0.388	0.484	0.528	0.474	0.359	0.077	0.015	0.375	0.250	0.049	0.408	0.586
Mn	0.033	0.034	0.022	0.032	0.034	0.033	0.037	0.030	0.037	0.021	0.009	0.014	0.021	0.005	0.016	0.013	0.025
Mg	0.109	0.149	0.132	0.112	0.167	0.172	0.186	0.142	0.191	0.377	0.029	0.039	0.458	0.037	0.030	0.438	0.202
Ca	0.481	0.495	0.507	0.459	0.672	0.622	0.690	0.667	0.695	0.724	0.091	0.055	0.834	0.302	0.052	0.877	0.830
Na	0.528	0.502	0.484	0.518	0.318	0.382	0.294	0.321	0.297	0.209	0.901	0.951	0.123	0.695	0.945	0.109	0.169
K	0.007	0.007	0.0	0.0	0.0	0.0	0.007	0.0	0.0	0.011	0.002	0.0	0.001	0.0	0.0	0.0	0.0
Zr	0.0	0.0	0.0	0.0	0.0	0.0	0.0	0.0	0.0	0.002	0.011	0.011	0.0	0.013	0.019	0.0	0.004
Rock Type	MUS	MUS	MUS	MUS	MUS	MUS	MUS	MUS	MUS	GS-A	GS-A	GS-A	GS-A	GS-A	GS-A	GS-A	GS-A
Crystal	4.	4.	1.	1.	1.	1.	1.	1.	1.	1.	1.	1.	1.	1.	1.	1.	1.
Position	4.	1.	7.	1.	1.	4.	4.	7.	1.	1.	4.	7.	1.	4.	7.	1.	7.
Atomic percent																	
Mg	11.0	14.9	12.7	10.5	16.3	17.6	18.6	13.9	19.1	39.0	2.9	3.8	46.9	3.7	2.9	45.2	20.6
Fe2+Mn	35.7	34.8	40.9	41.0	52.6	43.2	52.0	54.7	51.2	39.3	8.5	2.8	40.5	25.8	6.3	43.5	62.2
Na	53.3	50.3	46.4	48.5	31.1	39.2	29.4	31.4	29.7	21.6	88.7	93.3	12.6	70.4	90.9	11.3	17.2

PYROXENE ANALYSES

	169.01	169.02	169.04	169.05	169.06	169.07	169.09	169.10	169.11	169.12	169.13	169.14	169.15	169.18	169.19	169.20	169.21
Weight % oxide																	
SiO2	49.265	49.658	48.851	50.548	51.539	51.738	51.672	51.259	49.749	49.605	49.346	47.912	49.239	50.981	51.008	50.487	50.753
TiO2	0.921	0.021	0.330	0.209	0.561	0.920	0.312	0.262	0.116	0.193	0.510	0.559	0.620	0.600	0.473	0.364	0.308
Al2O3	2.075	0.964	1.330	0.849	0.898	0.939	2.192	1.232	1.060	0.872	1.172	2.060	3.457	0.853	0.691	1.030	1.025
FeO	21.467	27.349	24.250	27.128	27.037	27.317	28.546	28.731	27.622	27.734	23.953	21.293	20.771	27.720	27.527	27.390	28.744
MnO	0.612	0.625	0.705	0.426	0.307	0.754	0.249	0.377	0.447	0.560	0.791	0.680	0.642	0.316	0.279	0.297	0.305
MgO	4.740	0.562	2.599	0.381	0.343	0.118	0.356	0.563	0.487	0.924	3.280	4.629	4.291	0.340	0.325	0.421	0.310
CaO	20.569	13.389	18.248	9.869	3.455	1.484	4.953	7.552	10.793	15.678	20.567	20.393	21.413	3.123	3.768	4.775	6.185
Na2O	1.373	5.906	3.129	8.081	11.339	12.694	10.590	9.426	7.104	4.166	1.614	0.965	1.945	11.885	11.307	10.188	9.797
K2O	0.0	0.0	0.0	0.0	0.0	0.0	0.036	0.0	0.049	0.0	0.0	0.059	0.055	0.037	0.0	0.0	0.0
ZrO2	0.220	0.678	0.320	0.986	2.537	2.577	0.688	0.702	0.816	0.673	0.081	0.0	0.078	2.354	2.210	1.827	1.963
Total	101.242	99.152	99.762	98.477	98.016	98.541	99.594	100.104	98.243	100.405	101.314	98.550	102.511	98.209	97.588	96.779	99.390
Atoms per 6 oxygens																	
Si	1.918	1.963	1.931	1.981	1.995	1.977	1.962	1.956	1.968	1.964	1.937	1.920	1.877	1.961	1.982	1.989	1.961
Ti	0.027	0.001	0.010	0.006	0.016	0.026	0.009	0.008	0.003	0.006	0.015	0.017	0.018	0.017	0.014	0.011	0.009
Al	0.095	0.045	0.062	0.039	0.041	0.042	0.098	0.055	0.049	0.041	0.054	0.097	0.155	0.039	0.032	0.048	0.047
Fe3	0.110	0.454	0.284	0.562	0.691	0.795	0.715	0.688	0.523	0.314	0.162	0.108	0.198	0.804	0.745	0.660	0.674
Fe2	0.589	0.450	0.518	0.327	0.184	0.079	0.191	0.229	0.391	0.605	0.625	0.606	0.464	0.088	0.149	0.242	0.255
Mn	0.020	0.021	0.024	0.014	0.010	0.024	0.008	0.012	0.015	0.019	0.026	0.023	0.021	0.010	0.009	0.010	0.010
Mg	0.275	0.033	0.153	0.022	0.020	0.007	0.020	0.032	0.029	0.055	0.192	0.276	0.244	0.019	0.019	0.025	0.018
Ca	0.858	0.567	0.773	0.415	0.143	0.061	0.202	0.309	0.458	0.665	0.865	0.875	0.875	0.129	0.157	0.202	0.256
Na	0.104	0.453	0.240	0.614	0.851	0.941	0.780	0.698	0.545	0.320	0.123	0.075	0.144	0.886	0.852	0.778	0.734
K	0.0	0.0	0.0	0.0	0.0	0.0	0.002	0.0	0.002	0.0	0.0	0.003	0.003	0.002	0.0	0.0	0.0
Zr	0.004	0.013	0.006	0.019	0.048	0.048	0.013	0.013	0.016	0.013	0.002	0.0	0.001	0.044	0.042	0.035	0.037
Rock Type	GS-A	GS-A	GS-A	GS-A	GS-A	GS-A	GS-A	GS-A	GS-A	GS-A	GS-A	GS-A	GS-A	GS-A	GS-A	GS-A	GS-A
Crystal	1.	1.	1.	1.	1.	1.	1.	1.	1.	1.	1.	1.	1.	1.	1.	1.	1.
Position	1.	4.	1.	4.	7.	-1.	7.	6.	5.	5.	4.	3.	2.	7.	6.	5.	4.
Atomic percent																	
Mg	27.8	3.4	16.4	2.3	1.9	0.7	2.0	3.3	3.0	5.5	19.9	28.2	27.9	1.9	1.8	2.4	1.8
Fe2+Mn	61.6	49.2	58.0	34.9	18.2	9.8	19.9	24.8	41.4	62.5	67.4	64.2	55.6	9.8	15.4	23.9	26.1
Na	10.5	47.3	25.7	62.8	79.9	89.5	78.1	71.9	55.6	32.0	12.7	7.7	16.5	88.3	82.8	73.7	72.2

PYROXENE ANALYSES

	169.22	169.23	169.24	169.25	84.01	84.02	84.03	84.04	257.02	257.03	257.04	41.01	41.02	41.03	41.04	41.05	41.06
Weight % oxide																	
SiO2	49.778	48.206	47.692	48.465	50.726	49.640	49.183	50.660	51.070	51.736	51.262	49.369	50.580	50.809	50.373	49.728	49.547
TiO2	0.318	0.309	0.416	0.399	0.203	0.176	0.057	0.078	0.0	0.195	0.127	0.180	0.231	0.376	0.399	0.377	0.314
Al2O3	1.309	1.187	1.724	1.755	1.493	1.257	1.158	1.352	1.229	1.417	1.354	0.964	2.518	2.816	0.941	1.302	2.533
FeO	27.829	24.095	24.554	23.633	23.995	25.304	4.238	25.224	26.154	26.144	25.002	25.763	18.217	17.556	25.094	22.622	25.331
MnO	0.483	0.613	0.641	0.610	0.965	0.815	1.201	1.070	1.111	1.130	1.228	0.821	0.592	0.542	1.050	0.939	0.909
MgO	0.506	2.367	2.620	2.913	3.065	2.589	2.268	1.970	1.583	1.437	2.244	1.487	6.580	7.043	2.150	3.537	1.452
CaO	10.491	19.634	17.330	19.316	16.517	17.783	16.581	14.785	13.574	12.521	12.350	10.464	19.170	20.132	13.052	13.899	8.103
Na2O	7.267	2.670	4.835	2.710	4.304	3.187	3.759	5.041	6.010	6.707	6.954	6.943	2.395	2.229	6.011	5.246	8.769
K2O	0.0	0.0	0.040	0.035	0.038	0.0	0.0	0.047	0.0	0.0	0.0	0.040	0.012	0.0	0.0	0.351	0.046
ZrO2	0.979	0.169	0.367	0.127	0.037	0.198	0.388	0.539	0.373	0.493	0.259	0.552	0.027	0.0	0.532	0.365	0.679
Total	98.960	99.250	100.219	99.963	101.343	100.949	78.833	100.766	101.104	101.780	100.780	96.583	100.322	101.503	99.602	98.366	97.683
Atoms per 6 oxygens																	
Si	1.956	1.922	1.849	1.910	1.947	1.941	2.348	1.964	1.963	1.968	1.951	1.973	1.936	1.918	1.961	1.946	1.925
Ti	0.009	0.009	0.012	0.012	0.006	0.005	0.002	0.002	0.0	0.006	0.004	0.005	0.007	0.011	0.012	0.011	0.009
Al	0.061	0.056	0.079	0.082	0.068	0.058	0.065	0.062	0.056	0.064	0.061	0.045	0.114	0.125	0.043	0.060	0.116
Fe3	0.525	0.282	0.551	0.279	0.347	0.284	0.0	0.367	0.452	0.466	0.533	0.516	0.177	0.180	0.445	0.428	0.653
Fe2	0.389	0.522	0.245	0.499	0.423	0.544	0.169	0.451	0.388	0.365	0.263	0.345	0.406	0.375	0.371	0.313	0.170
Mn	0.016	0.021	0.021	0.020	0.031	0.027	0.049	0.035	0.036	0.036	0.040	0.028	0.019	0.017	0.035	0.031	0.030
Mg	0.030	0.141	0.151	0.171	0.175	0.151	0.161	0.114	0.091	0.081	0.127	0.089	0.375	0.396	0.125	0.206	0.084
Ca	0.442	0.839	0.720	0.816	0.679	0.745	0.848	0.614	0.559	0.510	0.504	0.448	0.786	0.814	0.544	0.583	0.337
Na	0.554	0.206	0.363	0.207	0.320	0.242	0.348	0.379	0.448	0.495	0.513	0.538	0.178	0.163	0.454	0.398	0.661
K	0.0	0.0	0.002	0.002	0.002	0.0	0.0	0.002	0.0	0.0	0.0	0.002	0.001	0.0	0.0	0.018	0.002
Zr	0.019	0.003	0.007	0.002	0.001	0.004	0.009	0.010	0.007	0.009	0.005	0.011	0.001	0.0	0.010	0.007	0.013
Rock Type	GS-A	GS-A	GS-A	GS-A	GS-B	GS-B	GS-B	GS-B	GS-B	GS-B	GS-B	XPS	XPS	XPS	XPS	XPS	XPS
Crystal	1.	1.	1.	1.	1.	1.	10.	10.	10.	1.	1.	4.	4.	5.	5.	1.	1.
Position	3.	2.	1.	0.	7.	1.	10.	10.	10.	8.	8.	7.	1.	1.	7.	8.	8.
Atomic percent																	
Mg	3.0	15.8	19.4	19.1	18.4	15.7	22.1	11.6	9.4	8.3	13.5	8.9	38.3	41.6	12.7	21.7	8.9
Fe2+Mn	41.0	61.0	34.1	57.9	47.8	59.2	30.0	49.6	44.0	41.0	32.1	37.3	43.5	41.2	41.2	36.3	21.2
Na	56.0	23.1	46.5	23.1	33.7	25.1	47.9	38.7	46.5	50.7	54.4	53.8	18.2	17.1	46.1	42.0	69.9

PYROXENE ANALYSES

	80.03	80.04	145.01	145.02	145.05	145.07	145.08	145.09	145.10	145.13	145.14	145.18	145.19	145.20	145.21	145.23	186.01
Weight % oxide																	
SiO2	46.335	50.365	50.746	51.252	47.741	48.580	51.534	50.197	49.197	50.939	50.374	48.602	50.331	51.334	50.717	54.369	50.756
TiO2	0.192	0.070	0.314	0.152	1.523	0.271	0.293	0.905	1.613	0.341	0.334	1.527	0.344	0.371	0.300	0.364	0.330
Al2O3	3.084	1.283	1.177	1.568	3.908	2.328	1.255	3.580	3.754	4.566	1.038	4.419	1.056	2.198	3.299	6.287	1.840
FeO	17.342	18.879	27.545	27.832	13.481	19.970	27.660	13.712	16.873	23.024	25.987	13.432	25.609	25.440	25.316	20.072	28.074
MnO	0.932	0.873	0.223	0.340	0.298	0.463	0.462	0.141	0.401	0.627	0.802	0.367	0.835	0.737	0.546	0.490	0.523
MgO	7.549	6.078	0.986	0.577	8.289	5.207	1.164	8.831	7.303	0.852	1.866	8.267	2.142	0.985	0.825	0.824	0.948
CaO	20.235	20.741	3.835	2.998	20.927	17.842	5.756	20.709	17.592	7.941	10.319	21.219	12.658	8.210	5.927	5.689	6.330
Na2O	1.209	1.495	11.113	11.719	1.556	2.640	10.200	1.970	3.063	8.230	7.681	1.677	6.411	8.630	9.718	9.695	10.385
K2O	0.0	0.0	0.0	0.030	0.0	0.080	0.102	0.045	0.481	0.0	0.0	0.0	0.005	0.0	0.069	0.064	0.116
ZrO2	1.580	0.008	0.587	0.709	0.0	0.0	0.694	0.0	0.038	0.580	0.726	0.0	0.572	0.568	0.890	0.394	0.373
Total	98.458	99.792	96.526	97.177	97.723	97.381	99.120	100.090	100.315	97.100	99.127	99.510	99.963	98.473	97.607	98.248	99.675
Atoms per 6 oxygens																	
Si	1.827	1.963	1.971	1.972	1.857	1.929	1.965	1.896	1.864	1.990	1.950	1.855	1.946	1.986	1.962	2.058	1.920
Ti	0.006	0.002	0.009	0.004	0.045	0.008	0.008	0.026	0.046	0.010	0.010	0.044	0.010	0.011	0.009	0.010	0.009
Al	0.143	0.059	0.054	0.071	0.179	0.109	0.056	0.159	0.168	0.210	0.047	0.199	0.048	0.100	0.150	0.281	0.082
Fe3	0.223	0.124	0.801	0.825	0.134	0.224	0.730	0.144	0.260	0.391	0.583	0.128	0.498	0.532	0.607	0.282	0.813
Fe2	0.349	0.491	0.093	0.070	0.304	0.440	0.152	0.289	0.275	0.362	0.258	0.301	0.330	0.292	0.212	0.353	0.075
Mn	0.031	0.029	0.007	0.011	0.010	0.016	0.015	0.005	0.013	0.021	0.026	0.012	0.027	0.024	0.018	0.016	0.017
Mg	0.444	0.353	0.057	0.033	0.481	0.308	0.066	0.497	0.412	0.050	0.108	0.470	0.123	0.057	0.048	0.046	0.053
Ca	0.855	0.866	0.160	0.124	0.872	0.759	0.235	0.838	0.714	0.332	0.428	0.868	0.525	0.340	0.246	0.231	0.257
Na	0.092	0.113	0.837	0.874	0.117	0.203	0.754	0.144	0.225	0.623	0.576	0.124	0.481	0.647	0.729	0.712	0.762
K	0.0	0.0	0.0	0.001	0.0	0.004	0.005	0.002	0.023	0.0	0.0	0.0	0.0	0.0	0.003	0.003	0.006
Zr	0.030	0.0	0.011	0.013	0.0	0.0	0.013	0.0	0.001	0.011	0.014	0.0	0.011	0.011	0.017	0.007	0.007
Rock Type	XPS	XPS	XPS	XPS	XPS	XPS	XPS	XPS	XPS	XPS	XPS	XPS	XPS	XPS	XPS	XPS	PMS
Crystal	1.	1.	1.	1.	12.	12.	9.	12.	9.	9.	9.	12.	9.	9.	9.	1.	4.
Position	8.	8.	8.	8.	-1.	-1.	9.	-1.	9.	9.	9.	-1.	9.	9.	9.	8.	7.
Atomic percent																	
Mg	48.5	35.8	5.7	3.3	52.7	31.9	6.7	53.2	44.5	4.7	11.2	51.8	12.8	5.6	4.8	4.1	5.8
Fe2+Mn	41.5	52.7	10.1	8.2	34.4	47.2	16.9	31.4	31.1	36.3	29.3	34.5	37.1	31.0	22.8	32.7	10.1
Na	10.0	11.5	84.2	88.5	12.8	21.0	76.4	15.4	24.3	59.0	59.5	13.7	50.1	63.4	72.4	63.2	84.0

PYROXENE ANALYSES

	186.02	186.05	178.13	178.14	178.15	178.16	178.18	178.19	64.08	64.09	64.10	64.11	180.01	180.02	180.03	26.01	26.02
Weight % oxide																	
SiO2	51.040	50.108	50.777	50.595	50.438	50.450	50.750	50.540	49.140	49.327	49.347	48.798	53.718	53.542	52.771	52.304	52.065
TiO2	0.191	0.167	0.239	0.234	0.187	0.118	0.262	0.240	0.625	0.180	0.704	0.323	0.308	0.175	0.387	0.015	0.075
Al2O3	1.167	1.112	1.332	1.308	1.447	1.332	1.362	1.286	3.136	1.217	3.316	0.975	14.543	19.110	15.099	2.365	2.716
FeO	23.112	27.625	27.867	27.739	27.398	27.342	27.599	27.516	14.880	25.243	15.016	25.277	12.783	6.298	12.262	29.951	29.735
MnO	0.963	0.998	0.791	0.569	0.839	1.007	0.658	0.782	0.432	0.881	0.462	0.808	0.0	0.0	0.024	0.0	0.029
MgO	3.792	1.100	1.029	1.111	1.154	0.889	1.107	1.086	8.702	2.183	8.787	2.235	0.228	0.420	0.254	0.295	0.249
CaO	15.685	12.546	11.029	11.107	10.890	10.215	10.336	10.467	21.427	15.877	21.243	17.633	0.0	0.0	0.0	0.0	0.056
Na2O	4.830	6.422	7.225	7.136	7.192	7.505	7.467	7.437	1.036	4.212	1.293	3.307	13.385	13.178	13.173	13.467	13.423
K2O	0.0	0.015	0.003	0.0	0.0	0.0	0.0	0.0	0.0	0.0	0.0	0.012	0.068	0.147	0.078	0.024	0.070
ZrO2	0.039	0.693	0.638	0.456	0.629	1.905	0.419	0.717	0.0	0.164	0.0	0.150	0.081	0.041	0.0	0.0	0.011
Total	100.819	100.786	100.930	100.255	100.174	100.763	99.960	100.071	99.378	99.284	100.168	99.518	95.114	92.911	94.048	98.421	98.429
Atoms per 6 oxygens																	
Si	1.953	1.939	1.950	1.953	1.948	1.948	1.959	1.953	1.889	1.947	1.878	1.938	1.986	1.986	1.970	1.960	1.951
Ti	0.005	0.005	0.007	0.007	0.005	0.003	0.008	0.007	0.018	0.005	0.020	0.010	0.009	0.005	0.011	0.0	0.002
Al	0.053	0.051	0.060	0.060	0.066	0.061	0.062	0.059	0.142	0.057	0.149	0.046	0.634	0.836	0.664	0.104	0.120
Fe3	0.388	0.519	0.541	0.537	0.541	0.526	0.547	0.552	0.121	0.355	0.150	0.309	0.337	0.136	0.331	0.954	0.953
Fe2	0.352	0.375	0.354	0.358	0.344	0.357	0.344	0.338	0.357	0.478	0.328	0.530	0.058	0.059	0.052	-0.015	-0.021
Mn	0.031	0.033	0.026	0.019	0.027	0.033	0.022	0.026	0.014	0.029	0.015	0.027	0.0	0.0	0.001	0.0	0.001
Mg	0.216	0.063	0.059	0.064	0.066	0.051	0.064	0.063	0.499	0.128	0.498	0.132	0.013	0.023	0.014	0.016	0.014
Ca	0.643	0.520	0.454	0.459	0.451	0.423	0.428	0.433	0.883	0.671	0.866	0.750	0.0	0.0	0.0	0.0	0.002
Na	0.358	0.482	0.538	0.534	0.539	0.562	0.559	0.557	0.077	0.322	0.095	0.255	0.959	0.948	0.953	0.979	0.975
K	0.0	0.001	0.0	0.0	0.0	0.0	0.0	0.0	0.0	0.0	0.0	0.001	0.003	0.007	0.004	0.001	0.003
Zr	0.001	0.013	0.012	0.009	0.012	0.036	0.008	0.014	0.0	0.003	0.0	0.003	0.001	0.001	0.0	0.0	0.0
Rock Type	PMS	PMS	PMS	PMS	PMS	PMS	PMS	PMS	MMS	MMS	MMS	MMS	ALSY	ALSY	ALSY	ALGN	ALGN
Crystal	4.	1.	1.	1.	4.	4.	1.	1.	12.	9.	12.	9.	1.	1.	1.	1.	1.
Position	1.	8.	8.	8.	7.	1.	8.	8.	-1.	9.	-1.	9.	8.	8.	8.	8.	8.
Atomic percent																	
Mg	22.6	6.6	6.0	6.6	6.8	5.1	6.5	6.4	52.7	13.4	53.2	14.0	1.3	2.2	1.4	1.6	1.4
Fe2+Mn	40.0	42.8	38.9	38.7	38.0	38.9	37.0	37.0	39.2	53.0	36.6	59.0	5.6	5.7	5.2	0.0	0.0
Na	37.4	50.6	55.1	54.8	55.2	56.0	56.5	56.6	8.1	33.6	10.1	27.0	93.1	92.0	93.4	98.4	98.6

PYROXENE ANALYSES

	26.03	26.04	26.05	26.06	26.13	26.14	9.01	9.02	9.03	9.04	9.05	9.06	275.01	275.02	275.03	275.04	275.05
Weight % oxide																	
SiO2	52.421	52.633	52.599	53.693	52.534	52.190	49.550	51.234	51.951	51.971	51.467	51.461	51.182	50.991	49.868	50.641	50.882
TiO2	0.054	0.083	0.177	0.036	0.104	0.050	1.233	2.067	2.069	2.004	2.650	2.382	0.429	0.406	0.321	0.194	0.309
Al2O3	3.907	4.632	4.053	5.013	3.837	2.601	0.556	0.457	0.339	0.169	0.302	0.251	1.771	1.055	1.026	1.916	1.838
FeO	27.571	26.719	27.985	27.027	28.192	29.205	28.785	28.557	27.875	28.265	27.132	28.907	15.566	19.078	24.626	18.807	17.187
MnO	0.0	0.0	0.113	0.0	0.027	0.061	0.708	0.630	1.161	0.380	0.780	0.494	0.583	0.827	0.878	0.736	0.589
MgO	0.153	0.097	0.238	0.301	0.025	0.204	1.698	0.920	0.785	0.531	0.957	0.649	8.500	5.967	2.569	5.319	6.885
CaO	0.097	0.009	0.0	0.0	0.075	0.176	7.777	5.805	1.910	0.119	2.422	3.841	21.379	19.676	16.098	18.751	19.173
Na2O	13.381	13.521	13.022	13.535	13.259	13.627	8.486	9.831	12.456	13.038	11.851	10.978	1.209	2.413	4.111	3.046	2.808
K2O	0.109	0.041	0.273	0.034	0.0	0.0	0.0	0.0	0.053	0.0	0.0	0.0	0.067	0.108	0.012	0.032	0.049
ZrO2	0.0	0.0	0.0	0.0	0.0	0.0	0.186	0.584	1.163	2.248	0.865	0.110	0.124	0.043	0.343	0.190	0.058
Total	97.693	97.735	98.460	99.639	98.053	98.114	98.979	100.085	99.762	98.725	98.426	99.073	100.810	100.564	99.852	99.632	99.778
Atoms per 6 oxygens																	
Si	1.968	1.969	1.967	1.971	1.972	1.957	1.920	1.958	1.957	1.981	1.968	1.969	1.947	1.961	1.958	1.958	1.948
Ti	0.002	0.002	0.005	0.001	0.003	0.001	0.036	0.059	0.059	0.057	0.076	0.069	0.012	0.012	0.009	0.006	0.009
Al	0.173	0.204	0.179	0.217	0.170	0.115	0.025	0.021	0.015	0.008	0.014	0.011	0.079	0.048	0.047	0.087	0.083
Fe3	0.867	0.836	0.835	0.804	0.845	0.959	0.693	0.652	0.824	0.795	0.744	0.725	0.091	0.190	0.318	0.208	0.212
Fe2	-0.001	0.0	0.041	0.026	0.040	-0.044	0.240	0.261	0.054	0.106	0.124	0.200	0.405	0.423	0.490	0.400	0.338
Mn	0.0	0.0	0.004	0.0	0.001	0.002	0.023	0.020	0.037	0.012	0.025	0.016	0.019	0.027	0.029	0.024	0.019
Mg	0.009	0.005	0.013	0.016	0.001	0.011	0.098	0.052	0.044	0.030	0.055	0.037	0.482	0.342	0.150	0.306	0.393
Ca	0.004	0.0	0.0	0.0	0.003	0.007	0.323	0.238	0.077	0.005	0.099	0.157	0.871	0.811	0.677	0.777	0.786
Na	0.974	0.981	0.944	0.963	0.965	0.991	0.638	0.728	0.910	0.964	0.879	0.814	0.089	0.180	0.313	0.228	0.208
K	0.005	0.002	0.013	0.002	0.0	0.0	0.0	0.0	0.003	0.0	0.0	0.0	0.003	0.005	0.001	0.002	0.002
Zr	0.0	0.0	0.0	0.0	0.0	0.0	0.004	0.011	0.021	0.042	0.016	0.002	0.002	0.001	0.007	0.004	0.001
Rock Type	ALGN	ALGN	ALGN	ALGN	ALGN	ALGN	ALSY	ALSY	ALSY	ALSY	ALSY	ALSY	CGS	CGS	CGS	CGS	CGS
Crystal	1.	1.	1.	1.	1.	1.	1.	1.	1.	1.	1.	1.	4.	4.	4.	1.	1.
Position	8.	7.	1.	8.	8.	8.	1.	4.	6.	7.	7.	4.	1.	4.	7.	8.	1.
Atomic percent																	
Mg	0.9	0.5	1.3	1.6	0.1	1.1	9.8	4.9	4.2	2.7	5.1	3.5	48.4	35.2	15.3	31.9	41.0
Fe2+Mn	0.0	0.0	4.5	2.6	4.1	0.0	26.3	26.5	8.7	10.6	13.8	20.2	42.6	46.3	52.9	44.3	37.3
Na	99.1	99.5	94.2	95.8	95.8	98.9	63.9	68.6	87.1	86.7	81.2	76.3	8.9	18.5	31.9	23.8	21.7

PYROXENE ANALYSES

	275.06	183.01	183.02	183.03	183.04	183.09	183.10	31846.01	31846.02	31846.03	135.01	135.02	135.03	118.05	118.06	118.07	118.08
Weight % oxide																	
SiO2	50.977	52.086	51.989	51.695	52.295	50.880	51.513	47.754	48.027	50.662	50.781	49.743	50.281	51.675	51.396	53.541	54.216
TiO2	0.124	0.090	0.236	0.073	0.075	0.413	0.625	1.653	1.699	0.238	0.125	0.066	0.062	0.391	0.250	0.843	1.450
Al2O3	1.162	2.095	1.628	2.055	1.845	1.746	2.200	5.948	6.247	1.164	1.114	1.161	1.183	1.088	0.987	1.270	2.254
FeO	19.559	28.122	29.011	27.980	28.913	27.157	27.081	12.959	11.948	26.102	24.815	23.548	25.138	25.773	26.560	30.342	28.972
MnO	0.761	0.013	0.006	0.0	0.261	0.612	0.543	0.361	0.274	0.736	1.218	0.909	1.046	1.026	1.247	0.214	0.0
MgO	5.804	0.158	0.024	0.118	0.191	0.295	0.219	8.272	8.888	1.143	2.497	2.856	2.166	1.901	1.907	0.288	0.142
CaO	19.276	0.107	0.271	0.262	0.497	3.593	3.388	21.352	21.240	8.878	16.861	16.790	15.492	12.209	11.968	0.850	0.256
Na2O	2.334	13.583	13.354	13.027	13.397	11.370	11.366	1.661	1.742	7.953	4.037	3.817	4.785	6.529	6.951	13.396	13.711
K2O	0.005	0.022	0.0	0.023	0.039	0.0	0.0	0.0	0.0	0.0	0.071	0.083	0.066	0.021	0.004	0.0	0.0
ZrO2	0.138	0.153	0.196	0.111	0.264	1.647	1.196	0.0	0.006	0.650	0.446	0.822	0.742	0.116	0.184	0.0	0.020
Total	100.140	96.429	96.715	95.344	97.777	97.713	98.131	99.960	100.071	97.526	101.965	99.795	100.961	100.729	101.454	100.744	101.021
Atoms per 6 oxygens																	
Si	1.973	1.985	1.987	2.000	1.975	1.964	1.976	1.809	1.808	1.994	1.955	1.955	1.949	1.981	1.953	1.973	1.985
Ti	0.004	0.003	0.007	0.002	0.002	0.012	0.018	0.047	0.048	0.007	0.004	0.002	0.002	0.011	0.007	0.023	0.040
Al	0.053	0.094	0.073	0.094	0.082	0.079	0.100	0.266	0.277	0.054	0.051	0.054	0.054	0.049	0.044	0.055	0.097
Fe3	0.164	0.929	0.922	0.876	0.936	0.757	0.713	0.144	0.138	0.526	0.320	0.296	0.379	0.448	0.541	0.909	0.826
Fe2	0.469	-0.033	0.006	0.030	-0.023	0.119	0.156	0.267	0.238	0.334	0.479	0.478	0.436	0.378	0.304	0.026	0.061
Mn	0.025	0.0	0.0	0.0	0.008	0.020	0.018	0.012	0.009	0.025	0.040	0.030	0.034	0.033	0.040	0.007	0.0
Mg	0.335	0.009	0.001	0.007	0.011	0.017	0.013	0.467	0.499	0.067	0.143	0.167	0.125	0.109	0.108	0.016	0.008
Ca	0.799	0.004	0.011	0.011	0.020	0.149	0.139	0.867	0.857	0.374	0.696	0.707	0.644	0.502	0.487	0.034	0.010
Na	0.175	1.004	0.990	0.977	0.981	0.851	0.845	0.122	0.127	0.607	0.301	0.291	0.360	0.485	0.512	0.957	0.973
K	0.0	0.001	0.0	0.001	0.002	0.0	0.0	0.0	0.0	0.0	0.003	0.004	0.003	0.001	0.0	0.0	0.0
Zr	0.003	0.003	0.004	0.002	0.005	0.031	0.022	0.0	0.0	0.012	0.008	0.016	0.014	0.002	0.003	0.0	0.0
Rock Type	CGS	PEG	PEG	PEG	PEG	PEG	PEG	XPS	XPS	XPS	USS	USS	USS	PEG	PEG	PEG	PEG
Crystal	1.	1.	1.	1.	1.	1.	1.	4.	4.	9.	1.	1.	1.	4.	4.	1.	1.
Position	7.	8.	8.	8.	8.	8.	8.	1.	5.	9.	8.	8.	8.	7.	1.	8.	8.
Atomic percent																	
Mg	33.4	0.9	0.1	0.7	1.1	1.7	1.3	53.8	57.2	6.5	14.8	17.3	13.1	10.8	11.2	1.6	0.8
Fe2+Mn	49.2	0.0	0.6	3.0	0.0	13.8	16.9	32.1	28.3	34.8	53.9	52.6	49.2	40.9	35.7	3.3	5.9
Na	17.4	99.1	99.3	96.4	98.9	84.5	81.9	14.1	14.5	58.8	31.3	30.1	37.7	48.3	53.1	95.1	93.4

PYROXENE ANALYSES

	156.01	156.02	156.03	202.03	202.04	253.09	253.10	253.11	152.05	152.06	136.17	136.18	107.01	107.02	107.03	107.04	146.01
Weight % oxide																	
SiO2	49.606	49.838	51.061	49.259	50.121	48.011	49.853	50.612	50.350	50.290	50.526	50.295	52.525	52.202	52.773	52.877	52.507
TiO2	0.237	0.0	0.233	0.032	0.475	1.877	1.177	0.855	0.276	0.204	0.037	0.067	1.228	0.605	0.801	1.159	0.066
Al2O3	1.175	1.114	1.171	1.150	1.843	4.700	3.426	3.274	1.309	1.228	2.394	1.575	2.072	1.138	0.984	2.474	1.617
FeO	23.159	19.877	23.347	25.013	18.824	12.033	10.714	10.982	23.334	24.227	27.716	26.530	28.764	30.604	31.626	28.130	31.639
MnO	0.950	0.942	0.900	1.032	0.458	0.360	0.281	0.300	0.809	1.450	0.155	0.473	0.041	0.0	0.0	0.0	0.0
MgO	3.544	5.565	3.993	2.294	6.006	9.710	10.619	10.933	3.098	3.079	0.591	2.123	0.580	0.466	0.164	0.483	0.191
CaO	17.879	20.544	15.473	15.754	19.290	21.906	22.027	22.323	18.117	17.809	2.408	6.042	0.440	0.390	0.079	0.444	0.160
Na2O	3.029	1.705	4.661	4.219	2.862	1.123	0.963	1.099	3.342	3.249	12.205	9.893	13.185	13.362	13.323	13.222	13.549
K2O	0.001	0.045	0.004	0.015	0.032	0.0	0.086	0.053	0.040	0.108	0.098	0.399	0.0	0.058	0.057	0.046	0.013
ZrO2	0.253	0.109	0.257	0.699	0.0	0.113	0.0	0.062	0.258	0.174	0.262	0.524	0.0	0.0	0.203	0.059	0.0
Total	99.833	99.739	101.100	99.467	99.911	99.833	99.146	100.493	100.933	101.818	96.392	97.921	98.835	98.825	100.010	98.894	99.742
Atoms per 6 oxygens																	
Si	1.950	1.949	1.953	1.946	1.928	1.820	1.892	1.892	1.956	1.942	1.942	1.927	1.966	1.956	1.967	1.975	1.951
Ti	0.007	0.0	0.007	0.001	0.014	0.054	0.034	0.024	0.008	0.006	0.001	0.002	0.035	0.017	0.022	0.033	0.002
Al	0.054	0.051	0.053	0.054	0.084	0.210	0.153	0.144	0.060	0.056	0.108	0.071	0.091	0.050	0.043	0.109	0.071
Fe3	0.254	0.178	0.365	0.350	0.248	0.121	0.070	0.103	0.257	0.290	0.910	0.805	0.865	0.977	0.936	0.834	1.001
Fe2	0.508	0.472	0.382	0.476	0.357	0.261	0.270	0.240	0.501	0.493	-0.019	0.045	0.035	-0.017	0.050	0.044	-0.018
Mn	0.032	0.031	0.029	0.035	0.015	0.012	0.009	0.010	0.027	0.047	0.005	0.015	0.001	0.0	0.0	0.0	0.0
Mg	0.208	0.324	0.228	0.135	0.344	0.549	0.601	0.609	0.179	0.177	0.034	0.121	0.032	0.026	0.009	0.027	0.011
Ca	0.753	0.861	0.634	0.667	0.795	0.890	0.896	0.894	0.754	0.737	0.099	0.248	0.018	0.016	0.003	0.018	0.006
Na	0.231	0.129	0.346	0.323	0.213	0.083	0.071	0.080	0.252	0.243	0.910	0.735	0.957	0.971	0.963	0.957	0.976
K	0.0	0.002	0.0	0.001	0.002	0.0	0.004	0.003	0.002	0.005	0.005	0.020	0.0	0.003	0.003	0.002	0.001
Zr	0.005	0.002	0.005	0.013	0.0	0.002	0.0	0.001	0.005	0.003	0.005	0.010	0.0	0.0	0.004	0.001	0.0
Rock Type	MUS	MUS	MUS	PMS	PMS	PMS	PMS	PMS	PMS	PMS	ALSY	ALSY	CBT	CBT	CBT	CBT	ALGN
Crystal	1.	1.	1.	1.	1.	1.	1.	1.	1.	1.	1.	1.	1.	1.	1.	1.	1.
Position	7.	1.	8.	7.	1.	8.	8.	8.	8.	8.	8.	8.	8.	8.	8.	8.	7.
Atomic percent																	
Mg	21.2	33.9	23.1	13.9	37.0	60.7	63.2	64.9	18.7	18.4	3.6	13.2	3.1	2.6	0.9	2.6	1.1
Fe2+Mn	55.2	52.6	41.7	52.7	40.0	30.2	29.3	26.6	55.1	56.3	0.0	6.6	3.5	0.0	4.9	4.3	0.0
Na	23.6	13.5	35.1	33.3	22.9	9.2	7.5	8.5	26.3	25.3	96.4	80.2	93.4	97.4	94.2	93.1	98.9

PYROXENE ANALYSES

	146.02	146.03	146.04	146.05	31846.06	31846.07	145.24	145.25	145.27	41.15	145.30
Weight % oxide											
SiO2	52.538	52.309	52.541	52.838	51.123	51.275	50.770	52.573	50.735	50.655	49.792
TiO2	0.058	0.150	0.093	0.105	0.150	0.121	0.433	0.474	0.346	0.560	0.961
Al2O3	1.676	1.278	1.248	1.253	0.920	0.896	1.752	2.103	1.061	1.283	2.391
FeO	31.582	31.715	31.691	31.418	28.445	28.789	23.963	27.487	27.377	24.247	21.570
MnO	0.016	0.0	0.025	0.130	0.747	0.807	0.896	0.436	0.706	0.783	0.746
MgO	0.191	0.226	0.212	0.258	1.144	0.997	2.823	1.128	0.894	3.018	4.641
CaO	0.126	0.736	0.642	0.949	9.734	11.189	12.537	5.070	8.916	11.754	16.240
Na2O	13.236	12.648	13.034	12.839	7.728	7.150	7.201	10.714	8.303	7.691	4.173
K2O	0.0	0.030	0.0	0.001	0.003	0.0	0.079	0.0	0.0	0.066	0.263
ZrO2	0.0	0.0	0.078	0.0	0.776	1.171	0.418	0.949	0.706	0.555	0.257
Total	99.423	99.092	99.564	99.791	100.770	102.395	100.872	100.934	99.044	100.612	101.034
Atoms per 6 oxygens											
Si	1.963	1.971	1.966	1.974	1.961	1.952	1.918	1.963	1.969	1.913	1.899
Ti	0.002	0.004	0.003	0.003	0.004	0.003	0.012	0.013	0.010	0.016	0.028
Al	0.074	0.057	0.055	0.055	0.042	0.040	0.078	0.093	0.049	0.057	0.108
Fe3	0.956	0.918	0.951	0.921	0.573	0.534	0.577	0.696	0.591	0.630	0.351
Fe2	0.031	0.082	0.040	0.060	0.340	0.383	0.180	0.163	0.297	0.136	0.337
Mn	0.001	0.0	0.001	0.004	0.024	0.026	0.029	0.014	0.023	0.025	0.024
Mg	0.011	0.013	0.012	0.014	0.065	0.057	0.159	0.063	0.052	0.170	0.264
Ca	0.005	0.030	0.026	0.038	0.400	0.456	0.508	0.203	0.371	0.476	0.664
Na	0.959	0.924	0.945	0.930	0.575	0.528	0.528	0.776	0.625	0.563	0.309
K	0.0	0.001	0.0	0.0	0.0	0.0	0.004	0.0	0.0	0.003	0.013
Zr	0.0	0.0	0.001	0.0	0.015	0.022	0.008	0.017	0.013	0.010	0.005
Rock Type	ALGN	ALGN	ALGN	MET	XPS	XPS	XPS	XPS	XPS	XPS	XPS
Crystal	1.	1.	1.	1.	9.	9.	9.	9.	9.	9.	9.
Position	1.	7.	7.	1.	9.	9.	9.	9.	9.	9.	9.
Atomic percent											
Mg	1.1	1.3	1.2	1.4	6.5	5.7	17.7	6.2	5.2	19.0	28.3
Fe2+Mn	3.2	8.0	4.1	6.3	36.3	41.1	23.3	17.4	32.1	18.0	38.7
Na	95.7	90.7	94.7	92.3	57.3	53.1	58.9	76.4	62.7	63.0	33.1

AMPHIBOLE ANALYSES

	* 138007.08	* 138007.09	* 138007.10	* 138007.11	* 39709.01	* 39709.02	* 39709.04	* 39709.06	44.01	44.02	44.03	44.04	44.05	44.08	44.09	44.10	169.31
Weight % oxide																	
SiO2	48.764	45.622	46.351	45.875	51.663	52.304	51.773	52.098	46.422	45.667	45.814	46.376	45.696	45.897	46.189	46.050	45.187
TiO2	0.910	2.004	2.920	1.862	0.156	0.239	0.299	0.177	1.344	1.803	1.730	1.319	1.521	1.673	1.513	2.101	1.808
Al2O3	2.116	3.501	2.862	3.090	0.292	0.305	0.570	0.347	4.744	5.569	5.554	4.661	4.840	5.409	5.433	5.815	5.308
FeO	25.558	28.989	27.855	29.241	24.137	23.642	26.228	24.946	32.560	29.321	31.751	31.507	32.270	31.663	30.037	31.957	33.736
MnO	1.326	0.807	1.069	0.899	0.270	0.261	0.204	0.254	1.146	0.920	1.093	0.876	0.973	1.141	1.083	0.896	1.233
MgO	4.967	3.058	3.584	3.107	8.262	8.739	5.625	7.882	2.469	4.151	2.766	2.757	2.338	2.941	3.919	2.838	1.126
CaO	1.378	2.216	1.311	1.573	0.187	0.133	0.253	0.192	3.689	7.286	4.929	4.650	4.628	5.604	6.749	5.947	2.689
Na2O	9.457	8.534	9.261	9.175	7.846	8.013	9.495	7.983	6.517	4.286	5.960	6.178	6.139	5.365	5.434	5.781	7.245
K2O	1.783	1.610	1.825	1.653	1.498	1.640	1.088	1.584	1.975	1.689	1.875	1.795	1.796	1.672	1.798	1.836	2.290
BaO	nd.	nd.	nd.	nd.	nd.	nd.	nd.	nd.	nd.	nd.	nd.	nd.	nd.	nd.	nd.	nd.	nd.
ZrO2	nd.	nd.	nd.	nd.	nd.	nd.	nd.	nd.	nd.	nd.	nd.	nd.	nd.	nd.	nd.	nd.	nd.
Total	96.259	96.341	97.038	96.475	94.311	95.276	95.535	95.463	100.866	100.692	101.472	100.119	100.201	101.365	102.155	103.221	100.622
Atoms per 23 oxygens. T+C cations=13.00																	
Si	7.746	7.345	7.397	7.384	7.915	7.919	8.093	7.925	7.108	6.978	6.985	7.172	7.085	6.990	7.014	6.945	7.015
Ti	0.109	0.243	0.350	0.225	0.018	0.027	0.035	0.020	0.155	0.207	0.198	0.153	0.177	0.192	0.173	0.238	0.211
Al	0.396	0.665	0.538	0.586	0.053	0.054	0.105	0.062	0.856	1.003	0.998	0.850	0.885	0.971	0.973	1.034	0.971
Fe3	0.152	0.400	0.282	0.449	1.396	1.340	0.458	1.324	1.088	0.641	0.898	0.752	0.851	0.928	0.510	0.634	1.048
Fe2	3.243	3.504	3.436	3.487	1.696	1.653	2.971	1.850	3.081	3.106	3.151	3.323	3.333	3.105	3.305	3.396	3.332
Mn	0.178	0.110	0.144	0.123	0.035	0.033	0.027	0.033	0.149	0.119	0.141	0.115	0.128	0.147	0.139	0.114	0.162
Mg	1.176	0.734	0.852	0.745	1.886	1.972	1.310	1.787	0.563	0.945	0.629	0.635	0.540	0.668	0.887	0.638	0.261
Ca	0.235	0.382	0.224	0.271	0.031	0.022	0.042	0.031	0.605	1.193	0.805	0.771	0.769	0.914	1.098	0.961	0.447
Na	2.913	2.664	2.866	2.863	2.331	2.352	2.878	2.354	1.935	1.270	1.762	1.852	1.846	1.584	1.600	1.690	2.181
K	0.361	0.331	0.372	0.339	0.293	0.317	0.217	0.307	0.386	0.329	0.365	0.354	0.355	0.325	0.348	0.353	0.454
Ba	0.0	0.0	0.0	0.0	0.0	0.0	0.0	0.0	0.0	0.0	0.0	0.0	0.0	0.0	0.0	0.0	0.0
Zr	0.0	0.0	0.0	0.0	0.0	0.0	0.0	0.0	0.0	0.0	0.0	0.0	0.0	0.0	0.0	0.0	0.0
Rock Type	GS-A	GS-A	GS-A	GS-A	CBT	CBT	CBT	CBT	MMS	MMS	MMS	MMS	MMS	MMS	MMS	MMS	GS-A
Crystal	1.	1.	1.	1.	1.	1.	1.	1.	14.	14.	14.	14.	14.	14.	14.	14.	9.
Position	-1.	-1.	7.	1.	-1.	-1.	-1.	-1.	7.	1.	4.	6.	5.	7.	4.	1.	9.
Leake (1978) classification	Arf	Arf	Arf	Arf	Mg-Arf	Mg-Arf	Arf	Arf	Ca'n-Arf	Kat	Kat	Kat	Kat	Kat	Kat	Kat	Arf

AMPHIBOLE ANALYSES

	169.33	169.34	169.35	169.36	84.05	84.06	84.07	84.08	186.06	186.07	186.08	186.09	186.10	186.11	108.03	108.04	108.06
Weight % oxide																	
SiO2	46.919	45.864	46.738	47.613	40.688	40.156	41.258	40.762	42.576	43.071	43.431	42.640	43.102	43.138	57.071	56.890	56.827
TiO2	0.984	1.022	1.192	2.821	0.520	0.441	0.407	0.363	1.183	1.174	1.154	1.065	1.086	1.189	0.226	0.125	0.343
Al2O3	3.917	5.677	3.501	2.927	8.508	8.041	8.171	8.044	5.258	5.289	5.467	5.408	5.518	5.435	0.511	0.181	0.464
FeO	32.188	31.764	32.052	31.972	32.032	30.556	31.728	31.602	33.065	32.403	33.090	33.453	32.904	33.200	13.728	13.728	12.333
MnO	1.241	1.126	1.212	1.101	0.986	1.121	1.089	0.911	1.244	1.515	1.252	1.070	1.311	1.255	0.321	0.312	0.244
MgO	1.509	1.382	1.403	1.587	2.228	2.376	2.351	2.325	2.055	1.896	2.102	2.238	2.116	2.148	15.754	15.832	16.603
CaO	0.725	1.573	0.713	0.419	8.492	8.333	8.164	8.150	5.474	5.813	5.620	5.720	5.406	5.610	1.639	1.805	3.196
Na2O	8.469	7.329	8.567	8.888	4.071	4.176	4.088	4.229	5.391	5.044	5.584	5.739	5.588	5.319	7.879	8.007	7.934
K2O	1.560	2.141	1.827	1.908	1.687	1.607	1.800	1.782	1.859	1.698	1.909	1.715	1.671	1.793	1.507	1.522	1.418
BaO	nd.	nd.	nd.	nd.	nd.	nd.	nd.	nd.	nd.	nd.	nd.	nd.	nd.	nd.	nd.	nd.	nd.
ZrO2	1.655	1.773	1.719	0.094	0.198	0.428	0.344	0.290	0.283	0.222	0.237	0.298	0.287	0.211	0.0	0.0	0.064
Total	99.167	99.651	98.924	99.330	99.410	97.235	99.400	98.458	98.388	98.125	99.846	99.346	98.989	99.298	98.636	98.402	99.426
Atoms per 23 oxygens. T+C cations=13.00																	
Si	7.322	7.118	7.363	7.433	6.439	6.507	6.515	6.516	6.785	6.870	6.825	6.745	6.804	6.792	7.971	7.992	7.950
Ti	0.115	0.119	0.141	0.331	0.062	0.054	0.048	0.044	0.142	0.141	0.136	0.127	0.129	0.141	0.024	0.013	0.036
Al	0.721	1.039	0.650	0.539	1.587	1.536	1.521	1.516	0.988	0.995	1.013	1.009	1.027	1.009	0.084	0.030	0.077
Fe3	1.037	1.067	0.853	0.707	0.912	0.736	0.922	0.854	1.201	1.058	1.052	1.157	1.186	1.218	1.033	0.962	0.580
Fe2	3.164	3.056	3.369	3.468	3.328	3.405	3.268	3.371	3.206	3.265	3.297	3.269	3.158	3.154	0.570	0.651	0.863
Mn	0.164	0.148	0.162	0.146	0.132	0.154	0.146	0.123	0.168	0.205	0.167	0.143	0.175	0.167	0.038	0.037	0.029
Mg	0.351	0.320	0.329	0.369	0.525	0.574	0.553	0.554	0.488	0.451	0.492	0.528	0.498	0.504	3.279	3.315	3.461
Ca	0.121	0.262	0.120	0.070	1.440	1.447	1.381	1.396	0.935	0.993	0.946	0.970	0.914	0.946	0.245	0.272	0.479
Na	2.563	2.205	2.617	2.691	1.249	1.312	1.252	1.311	1.666	1.560	1.701	1.760	1.710	1.624	2.134	2.181	2.152
K	0.311	0.424	0.367	0.380	0.341	0.332	0.363	0.363	0.378	0.346	0.383	0.346	0.337	0.360	0.269	0.273	0.253
Ba	0.0	0.0	0.0	0.0	0.0	0.0	0.0	0.0	0.0	0.0	0.0	0.0	0.0	0.0	0.0	0.0	0.0
Zr	0.126	0.134	0.132	0.007	0.015	0.034	0.026	0.023	0.022	0.017	0.018	0.023	0.022	0.016	0.0	0.0	0.004
Rock Type	GS-A	GS-A	GS-A	GS-A	GS-B	GS-B	GS-B	GS-B	PMS	PMS	PMS	PMS	PMS	PMS	ALGN	ALGN	ALGN
Crystal	1.	1.	1.	1.	14.	14.	14.	14.	1.	1.	14.	14.	14.	14.	1.	1.	1.
Position	1.	7.	8.	8.	-1.	-1.	-1.	-1.	6.	1.	7.	1.	7.	2.	8.	8.	8.
Leake (1978) classification	Arf	Arf	Arf	Arf	Sub-Ca H'ic-Hb	Sub-Ca Fe-Ed-Hb	Sub-Ca Fe-Ed-Hb	Sub-Ca Fe-Ed-Hb	Kat	Kat	Kat	Kat	Kat	Kat	Mg-Arf	Mg-Arf	Mg-Arf

AMPHIBOLE ANALYSES

	108.07	108.08	239.01	239.02	239.03	239.04	239.05	239.07	9.07	9.08	9.15	253.06	253.07	253.08
Weight % oxide														
SiO2	57.712	50.602	44.399	44.746	53.450	45.011	52.488	52.777	51.498	48.005	41.800	39.825	40.270	39.370
TiO2	0.167	0.123	1.778	1.798	0.834	1.534	0.623	0.499	0.810	0.234	0.216	2.752	2.415	2.938
Al2O3	0.330	0.513	7.458	6.999	0.814	7.332	0.501	0.688	0.478	0.413	0.370	11.184	11.456	11.111
FeO	10.709	9.641	20.810	20.702	30.587	21.242	30.905	30.891	29.050	28.410	25.817	22.454	22.861	22.654
MnO	0.369	0.334	0.329	0.427	0.0	0.490	0.022	0.195	0.095	0.152	0.522	0.390	0.364	0.460
MgO	16.805	14.902	9.304	9.580	5.077	9.156	4.896	4.620	1.353	4.510	3.593	6.474	6.493	5.947
CaO	1.943	8.483	10.812	10.356	0.149	10.657	0.133	0.031	2.010	4.586	10.754	10.846	10.677	10.951
Na2O	7.873	6.945	3.340	3.225	7.081	3.106	7.334	7.191	11.393	6.469	5.913	2.852	3.038	2.919
K2O	1.859	1.439	1.344	1.239	0.496	1.327	0.393	0.443	0.052	0.248	0.191	1.747	1.645	1.715
BaO	nd.	nd.	nd.	nd.	nd.	nd.	nd.	nd.	nd.	nd.	nd.	nd.	nd.	nd.
ZrO2	0.015	0.0	0.056	0.089	0.321	0.0	0.392	0.312	0.0	0.0	0.0	0.410	0.610	0.595
Total	97.782	92.982	99.630	99.161	98.809	99.855	97.687	97.647	96.739	93.027	89.176	98.934	99.829	98.660
Atoms per 23 oxygens.	T+C cations=13.00													
Si	8.107	8.037	6.703	6.737	7.866	6.754	7.852	7.886	8.468	7.872	7.787	6.161	6.159	6.154
Ti	0.018	0.015	0.202	0.204	0.092	0.173	0.070	0.056	0.100	0.029	0.030	0.320	0.278	0.345
Al	0.055	0.096	1.327	1.242	0.141	1.297	0.088	0.121	0.093	0.080	0.081	2.040	2.066	2.048
Fe3	0.632	0.0	0.119	0.343	1.736	0.264	1.765	1.771	0.0	0.399	0.0	0.141	0.247	0.0
Fe2	0.626	1.281	2.509	2.264	2.028	2.402	2.101	2.089	3.995	3.498	4.022	2.764	2.677	2.961
Mn	0.044	0.045	0.042	0.054	0.0	0.062	0.003	0.025	0.013	0.021	0.082	0.051	0.047	0.061
Mg	3.518	3.527	2.093	2.150	1.113	2.048	1.092	1.029	0.332	1.102	0.997	1.493	1.480	1.385
Ca	0.292	1.444	1.749	1.671	0.023	1.713	0.021	0.005	0.354	0.806	2.147	1.798	1.750	1.834
Na	2.144	2.139	0.978	0.941	2.020	0.904	2.127	2.083	3.632	2.057	2.136	0.855	0.901	0.885
K	0.333	0.292	0.259	0.238	0.093	0.254	0.075	0.084	0.011	0.052	0.045	0.345	0.321	0.342
Ba	0.0	0.0	0.0	0.0	0.0	0.0	0.0	0.0	0.0	0.0	0.0	0.0	0.0	0.0
Zr	0.001	0.0	0.004	0.007	0.023	0.0	0.029	0.023	0.0	0.0	0.0	0.031	0.045	0.045
Rock Type	ALGN	ALGN	ALGN	ALGN	ALGN	ALGN	ALGN	ALGN	ALSY	ALSY	ALSY	PMS	PMS	PMS
Crystal	1.	1.	1.	1.	1.	1.	1.	1.	1.	1.	1.	1.	1.	1.
Position	8.	8.	1.	1.	7.	1.	7.	8.	8.	8.	8.	8.	8.	8.
Leake (1978) classification	Mg-Arf	Sub-Ca Si'ic-Ed	Fe-Ed-Hb	Fe-Ed-Hb	Rieb	Fe-Ed	Rieb	Rieb	Fe-Eck	Fe-Richt	Si'ic Fe-Ed	Fe'n-Pg	Mg-Hast	Fe'n-Pg

BIOTITE ANALYSES - Total Fe as FeO

	* 27113.13	* 27113.14	* 27113.15	* 27113.16	* 27193.07	* 27193.08	* 27193.10	* 27193.13	* 138044.06	* 138044.07	* 138044.08	* 138044.19	* 138044.20	* 138044.21	* 138044.22	* 138044.23	* 138048.07
Weight % oxide																	
SiO2	43.175	36.164	36.129	37.314	35.488	35.666	37.102	36.549	36.099	36.288	35.978	45.896	49.063	45.062	36.256	36.250	35.286
TiO2	2.127	1.839	1.471	1.455	3.350	2.867	2.802	2.789	2.085	1.988	2.238	1.236	1.270	1.624	2.132	2.221	1.106
Al2O3	15.229	13.963	13.022	13.912	12.161	11.535	12.106	12.458	13.454	13.448	13.384	15.470	16.253	15.417	12.681	14.269	13.967
FeO	18.477	25.312	29.546	27.362	27.366	29.301	29.328	27.082	26.298	26.232	25.398	21.213	19.788	17.779	24.931	25.128	28.166
MnO	1.783	2.173	1.632	1.617	0.903	0.947	0.993	1.027	1.296	1.297	1.283	0.595	0.580	0.806	1.256	1.420	2.134
MgO	4.370	5.647	3.401	3.734	7.104	5.490	5.214	6.118	6.554	6.490	6.395	2.919	2.872	3.873	8.075	6.523	4.699
CaO	0.004	0.006	0.009	0.024	0.042	0.147	0.058	0.075	0.125	0.059	0.167	0.133	0.072	0.071	0.143	0.012	0.021
Na2O	0.253	0.172	0.222	0.671	0.170	0.216	0.457	0.236	0.138	0.113	0.311	6.342	8.121	5.957	0.347	0.055	0.295
K2O	11.396	9.720	9.534	9.253	9.292	8.827	8.982	9.575	9.246	9.422	9.118	4.240	3.824	5.985	9.376	9.620	9.273
Total	96.814	94.996	94.966	95.342	95.876	94.996	97.042	95.909	95.295	95.337	94.272	98.044	101.843	96.574	95.197	95.498	94.947
Atoms per 22 oxygens																	
Si	6.441	5.783	5.889	5.957	5.662	5.790	5.864	5.811	5.749	5.775	5.771	6.617	6.726	6.573	5.756	5.729	5.728
Ti	0.239	0.221	0.180	0.175	0.402	0.350	0.333	0.333	0.250	0.238	0.270	0.134	0.131	0.178	0.255	0.264	0.135
Al	2.678	2.632	2.502	2.618	2.287	2.207	2.256	2.335	2.526	2.523	2.531	2.629	2.627	2.651	2.374	2.658	2.673
Fe	2.305	3.385	4.028	3.653	3.651	3.978	3.876	3.601	3.502	3.491	3.407	2.558	2.269	2.169	3.310	3.321	3.824
Mn	0.225	0.294	0.225	0.219	0.122	0.130	0.133	0.138	0.175	0.175	0.174	0.073	0.067	0.100	0.169	0.190	0.293
Mg	0.972	1.346	0.826	0.888	1.689	1.328	1.228	1.450	1.555	1.539	1.529	0.627	0.587	0.842	1.911	1.536	1.137
Ca	0.0	0.001	0.002	0.004	0.007	0.026	0.010	0.013	0.021	0.010	0.029	0.021	0.011	0.011	0.024	0.002	0.004
Na	0.073	0.053	0.070	0.208	0.053	0.068	0.140	0.073	0.043	0.035	0.097	1.773	2.159	1.685	0.107	0.017	0.093
K	2.169	1.983	1.983	1.884	1.891	1.828	1.811	1.942	1.878	1.913	1.866	0.780	0.669	1.114	1.899	1.940	1.920
Rock Type	LSS	LSS	LSS	LSS	MUS	MUS	MUS	MUS	LSS	LSS	LSS	LSS	LSS	LSS	LSS	LSS	LSS
Crystal	4.	4.	5.	5.	14.	14.	14.	14.	14.	14.	14.	14.	14.	14.	14.	14.	14.
Position	4.	6.	2.	6.	-1.	-1.	-1.	-1.	1.	7.	6.	-1.	-1.	-1.	-1.	-1.	-1.

BIOTITE ANALYSES - Total Fe as FeO

	* 138048.08	* 138048.09	* 27259.06	* 27259.07	* 27259.08	* 138007.12	* 138007.13	* 138001.04	* 138001.05	* 138001.06	* 138001.07	* 138001.08	* 138025.05	* 138025.06	38.11	38.12	38.23
Weight % oxide																	
SiO2	35.563	35.689	35.827	35.957	35.945	36.138	33.185	34.713	34.384	33.594	33.196	33.773	35.738	36.578	35.364	36.735	36.544
TiO2	0.943	1.255	2.842	2.801	2.298	1.566	2.099	1.138	1.497	0.836	0.670	0.753	1.648	2.102	1.387	1.687	1.508
Al2O3	13.999	13.263	12.961	13.295	12.793	11.273	10.506	11.623	12.213	13.279	11.985	12.259	14.519	16.487	11.076	12.053	12.665
FeO	27.053	27.002	27.954	27.596	28.494	30.480	27.028	35.198	34.115	33.882	35.235	35.160	22.653	18.158	32.997	34.639	34.492
MnO	2.069	2.149	0.926	0.933	1.075	1.458	1.309	0.576	0.748	0.722	0.733	0.730	3.035	2.670	1.254	1.118	0.973
MgO	5.802	5.836	4.929	4.774	4.894	5.290	5.288	2.968	2.772	2.363	2.618	2.611	7.488	8.759	4.591	4.712	2.330
CaO	0.011	0.005	0.058	0.0	0.004	0.364	0.034	0.014	0.052	0.293	0.181	0.055	0.009	0.051	0.429	0.569	0.0
Na2O	0.184	0.387	0.237	0.271	0.244	0.212	0.110	0.317	0.247	0.352	0.780	0.343	0.307	0.192	0.744	0.0	1.148
K2O	9.368	9.559	9.350	9.576	9.468	8.628	8.805	9.163	8.953	8.014	7.448	8.815	9.579	9.294	8.782	8.985	8.586
Total	94.992	95.145	95.084	95.203	95.215	95.409	88.364	95.710	94.981	93.335	92.846	94.499	94.976	94.291	96.624	100.498	98.246
Atoms per 22 oxygens																	
Si	5.732	5.761	5.770	5.774	5.803	5.877	5.819	5.776	5.734	5.678	5.693	5.703	5.668	5.661	5.777	5.748	5.848
Ti	0.114	0.152	0.344	0.338	0.279	0.192	0.277	0.142	0.188	0.106	0.086	0.096	0.197	0.245	0.170	0.199	0.181
Al	2.660	2.524	2.461	2.517	2.435	2.161	2.172	2.280	2.401	2.646	2.423	2.440	2.715	3.008	2.133	2.223	2.389
Fe	3.647	3.645	3.765	3.706	3.847	4.146	3.964	4.898	4.758	4.789	5.054	4.965	3.005	2.350	4.508	4.533	4.616
Mn	0.282	0.294	0.126	0.127	0.147	0.201	0.194	0.081	0.106	0.103	0.106	0.104	0.408	0.350	0.174	0.148	0.132
Mg	1.394	1.404	1.183	1.143	1.177	1.282	1.382	0.736	0.689	0.595	0.669	0.657	1.770	2.020	1.118	1.099	0.556
Ca	0.002	0.0	0.010	0.0	0.0	0.063	0.006	0.002	0.009	0.053	0.033	0.010	0.002	0.008	0.075	0.095	0.0
Na	0.058	0.121	0.074	0.084	0.076	0.067	0.037	0.102	0.080	0.115	0.259	0.112	0.094	0.058	0.236	0.0	0.356
K	1.926	1.968	1.921	1.962	1.950	1.790	1.970	1.945	1.905	1.728	1.630	1.899	1.938	1.835	1.830	1.794	1.753
Rock Type	LSS	LSS	MUS	MUS	MUS	GS-A	GS-A	CGBS	CGBS	CGBS	CGBS	CGBS	LSS	LSS	MMS	MMS	MMS
Crystal	14.	10.	14.	14.	14.	1.	1.	14.	14.	14.	14.	14.	14.	14.	1.	1.	1.
Position	-1.	-1.	-1.	-1.	-1.	-1.	-1.	-1.	-1.	-1.	-1.	-1.	-1.	-1.	8.	8.	8.

BIOTITE ANALYSES - Total Fe as FeO

	38.24	38.25	38.26	197.14	197.15	197.16	197.17	220.16	220.17	220.18	220.19	37.07	37.08	37.12	37.13	37.14	37.16
Weight % oxide																	
SiO2	35.882	35.470	35.710	38.517	38.948	38.667	39.136	14.787	35.192	34.357	35.555	34.319	35.839	32.293	35.926	34.251	34.029
TiO2	1.722	2.829	1.838	4.198	4.608	4.122	4.238	0.653	1.315	1.693	1.294	1.248	1.934	0.622	0.491	0.723	1.648
Al2O3	11.948	13.083	12.395	12.535	12.521	12.485	13.165	6.219	13.071	13.632	13.331	12.188	12.978	12.992	14.006	11.951	12.313
FeO	36.432	32.871	36.348	20.898	22.180	22.043	22.034	68.158	35.687	36.009	36.401	35.342	35.953	33.480	30.716	38.274	37.233
MnO	0.944	1.211	1.026	0.0	0.298	0.0	0.0	0.0	0.516	0.545	0.466	1.597	1.060	1.559	1.902	0.758	1.091
MgO	2.541	2.762	2.799	12.288	11.555	11.911	11.850	1.086	1.779	2.444	1.640	1.716	1.566	5.278	4.855	1.521	1.517
CaO	0.0	0.0	0.0	0.0	0.0	0.0	0.0	2.177	0.0	0.0	0.0	0.177	0.0	0.0	0.0	0.0	0.225
Na2O	0.0	0.561	0.521	0.0	0.0	0.0	0.0	0.470	0.0	0.0	0.0	0.0	0.0	0.0	0.0	0.0	0.0
K2O	9.559	9.414	9.445	9.880	9.478	9.734	9.995	3.567	9.225	9.152	9.452	9.164	9.408	8.617	9.608	8.767	8.857
Total	99.028	98.201	100.082	98.316	99.588	98.962	100.418	97.117	96.785	97.832	98.139	95.751	98.738	94.841	97.504	96.245	96.913
Atoms per 22 oxygens																	
Si	5.777	5.675	5.690	5.741	5.749	5.747	5.725	3.091	5.765	5.581	5.754	5.738	5.762	5.416	5.726	5.742	5.649
Ti	0.209	0.340	0.220	0.471	0.512	0.461	0.466	0.103	0.162	0.207	0.157	0.157	0.234	0.078	0.059	0.091	0.206
Al	2.268	2.468	2.328	2.203	2.179	2.188	2.270	1.533	2.524	2.611	2.543	2.403	2.460	2.569	2.632	2.362	2.410
Fe	4.906	4.398	4.844	2.605	2.738	2.740	2.696	11.916	4.889	4.892	4.927	4.942	4.834	4.696	4.095	5.366	5.169
Mn	0.129	0.164	0.138	0.0	0.037	0.0	0.0	0.0	0.072	0.075	0.064	0.226	0.144	0.221	0.257	0.108	0.153
Mg	0.610	0.659	0.665	2.729	2.542	2.639	2.583	0.338	0.434	0.592	0.396	0.428	0.375	1.319	1.153	0.380	0.375
Ca	0.0	0.0	0.0	0.0	0.0	0.0	0.0	0.488	0.0	0.0	0.0	0.032	0.0	0.0	0.0	0.0	0.040
Na	0.0	0.174	0.161	0.0	0.0	0.0	0.0	0.191	0.0	0.0	0.0	0.0	0.0	0.0	0.0	0.0	0.0
K	1.964	1.921	1.920	1.879	1.785	1.846	1.865	0.951	1.928	1.897	1.952	1.955	1.930	1.844	1.954	1.875	1.876
Rock Type	MMS	MMS	MMS	ALGN	ALGN	ALGN	ALGN	LSS	LSS	LSS	LSS	MMS	MMS	MMS	MMS	MMS	MMS
Crystal	1.	1.	1.	1.	1.	1.	1.	14.	14.	14.	14.	9.	9.	14.	14.	1.	9.
Position	8.	8.	8.	8.	8.	8.	8.	-1.	-1.	-1.	-1.	9.	9.	-1.	-1.	8.	9.

BIOTITE ANALYSES - Total Fe as FeO

	64.06	64.07	204.07	204.08	204.09	204.10	207.07	207.10	207.11	207.12	191.15	191.14	191.16	191.17	21.08	21.09	21.10
Weight % oxide																	
SiO2	24.389	35.957	35.964	36.286	36.505	40.182	36.808	37.153	36.416	42.164	37.332	37.343	38.194	45.581	36.646	36.471	36.918
TiO2	2.286	3.063	1.542	1.706	1.939	2.082	3.047	3.303	3.082	3.263	1.970	5.048	1.419	2.197	3.191	3.339	3.516
Al2O3	9.599	14.039	12.037	13.147	13.600	15.788	11.751	11.097	11.074	13.144	12.508	13.686	11.984	16.699	11.808	11.177	11.868
FeO	51.213	31.162	31.903	30.627	27.803	22.765	34.039	32.152	33.559	26.343	35.179	34.584	38.483	16.921	31.181	31.795	31.449
MnO	0.719	0.866	1.353	1.358	1.648	1.062	0.772	0.970	0.803	0.417	1.296	2.321	0.340	0.688	0.559	0.814	0.632
MgO	2.502	3.385	5.070	5.603	6.093	5.993	4.096	4.514	4.084	2.324	1.869	0.403	0.0	2.692	4.617	4.316	4.550
CaO	0.0	0.0	0.354	0.248	0.0	0.0	0.0	0.0	0.0	0.0	0.0	0.0	0.0	0.0	0.0	0.0	0.0
Na2O	0.0	0.444	0.739	0.0	0.0	2.284	0.0	0.0	0.541	0.0	1.522	7.339	0.685	7.964	0.554	0.0	0.0
K2O	6.299	9.207	8.235	8.591	9.856	8.668	9.367	9.636	9.116	10.686	7.872	0.956	9.126	3.676	9.420	9.399	9.344
Total	97.007	98.123	97.197	97.566	97.444	98.824	99.880	98.825	98.675	98.341	99.548	101.680	100.231	96.418	97.976	97.311	98.277
Atoms per 22 oxygens																	
Si	4.457	5.671	5.764	5.733	5.737	5.972	5.777	5.860	5.796	6.391	5.885	5.639	6.059	6.562	5.802	5.838	5.814
Ti	0.314	0.363	0.186	0.203	0.229	0.233	0.360	0.392	0.369	0.372	0.234	0.573	0.169	0.238	0.380	0.402	0.416
Al	2.068	2.610	2.274	2.449	2.520	2.766	2.174	2.063	2.078	2.349	2.325	2.436	2.241	2.834	2.204	2.109	2.204
Fe	7.828	4.110	4.276	4.047	3.654	2.830	4.468	4.241	4.467	3.339	4.638	4.367	5.106	2.037	4.129	4.256	4.142
Mn	0.111	0.116	0.184	0.182	0.219	0.134	0.103	0.130	0.108	0.054	0.173	0.297	0.046	0.084	0.075	0.110	0.084
Mg	0.681	0.796	1.211	1.319	1.427	1.327	0.958	1.061	0.969	0.525	0.439	0.091	0.0	0.578	1.089	1.030	1.068
Ca	0.0	0.0	0.061	0.042	0.0	0.0	0.0	0.0	0.0	0.0	0.0	0.0	0.0	0.0	0.0	0.0	0.0
Na	0.0	0.136	0.230	0.0	0.0	0.658	0.0	0.0	0.167	0.0	0.465	2.149	0.211	2.223	0.170	0.0	0.0
K	1.469	1.853	1.684	1.732	1.976	1.644	1.875	1.939	1.851	2.066	1.583	0.184	1.847	0.675	1.903	1.919	1.877
Rock Type	MMS	MMS	USS	USS	USS	USS	MUS	MUS	MUS	MUS	USS	USS	USS	USS	MUS	MUS	MUS
Crystal	1.	1.	14.	14.	14.	14.	14.	14.	14.	14.	14.	14.	14.	14.	1.	1.	1.
Position	-1.	-1.	-1.	-1.	-1.	-1.	-1.	-1.	-1.	-1.	-1.	-1.	-1.	-1.	8.	8.	8.

BIOTITE ANALYSES - Total Fe as FeO

	21.11	43.07	43.08	43.09	43.10	248.06	248.07	248.08	188.07	188.08	172.07	172.08	172.09	172.10	169.26	169.27	169.32
Weight % oxide																	
SiO2	37.152	23.561	43.271	39.656	44.411	40.237	45.813	42.540	34.950	34.172	37.006	35.609	35.229	35.390	34.067	34.010	34.497
TiO2	3.446	3.708	2.696	2.302	1.798	1.943	0.744	1.800	1.496	2.620	3.247	3.413	4.408	4.141	3.298	3.485	3.396
Al2O3	11.696	8.079	13.654	13.344	10.357	12.716	13.100	14.760	10.081	12.029	10.511	11.528	11.437	11.390	10.993	11.012	11.115
FeO	31.096	46.025	19.275	28.876	27.636	17.089	30.946	27.049	37.912	32.781	30.033	29.666	29.899	30.703	36.533	37.361	36.876
MnO	0.819	2.686	1.673	1.461	0.611	3.534	0.557	1.570	1.022	1.511	1.677	1.748	1.651	0.490	0.857	1.099	1.038
MgO	4.719	5.778	5.236	2.008	1.689	11.839	0.0	2.344	4.689	5.428	5.477	5.123	4.592	5.060	1.195	1.293	1.825
CaO	0.0	0.0	0.0	0.0	0.0	0.0	0.0	0.0	0.0	0.0	0.232	0.088	0.184	0.176	0.383	0.379	0.200
Na2O	0.0	0.0	6.763	8.557	10.453	0.0	0.0	6.293	4.489	0.0	0.387	0.379	0.626	0.817	0.406	0.433	0.498
K2O	9.589	5.350	4.356	1.673	1.078	10.312	10.745	3.316	4.578	8.852	9.110	9.073	8.726	8.509	7.771	8.086	8.494
Total	98.517	95.187	96.924	97.877	98.033	97.670	101.905	99.672	99.217	97.393	97.680	96.627	96.752	96.676	95.503	97.158	97.939
Atoms per 22 oxygens																	
Si	5.837	4.328	6.371	6.054	6.655	6.006	6.759	6.258	5.620	5.528	5.873	5.722	5.660	5.675	5.704	5.633	5.651
Ti	0.407	0.512	0.299	0.264	0.203	0.218	0.083	0.199	0.181	0.319	0.388	0.412	0.533	0.499	0.415	0.434	0.418
Al	2.166	1.749	2.370	2.402	1.830	2.238	2.279	2.560	1.911	2.294	1.967	2.184	2.166	2.153	2.170	2.150	2.146
Fe	4.086	7.070	2.373	3.687	3.464	2.133	3.818	3.328	5.099	4.435	3.986	3.987	4.017	4.117	5.115	5.175	5.052
Mn	0.109	0.418	0.209	0.189	0.078	0.447	0.070	0.196	0.139	0.207	0.225	0.238	0.225	0.067	0.122	0.154	0.144
Mg	1.105	1.582	1.149	0.457	0.377	2.634	0.0	0.514	1.124	1.309	1.295	1.227	1.100	1.209	0.298	0.319	0.446
Ca	0.0	0.0	0.0	0.0	0.0	0.0	0.0	0.0	0.0	0.0	0.039	0.015	0.032	0.030	0.069	0.067	0.035
Na	0.0	0.0	1.931	2.533	3.037	0.0	0.0	1.795	1.400	0.0	0.119	0.118	0.195	0.254	0.132	0.139	0.158
K	1.922	1.254	0.818	0.326	0.206	1.964	2.022	0.622	0.939	1.827	1.845	1.860	1.789	1.741	1.660	1.709	1.775
Rock Type	MUS	USS	USS	USS	USS	MUS	MUS	MUS	MUS	MUS	GS-A	GS-A	GS-A	GS-A	GS-A	GS-A	CGBS
Crystal	1.	14.	14.	14.	14.	14.	14.	14.	14.	14.	1.	1.	1.	1.	1.	1.	1.
Position	8.	-1.	-1.	-1.	-1.	-1.	-1.	-1.	-1.	-1.	1.	7.	4.	7.	8.	8.	9.

BIOTITE ANALYSES - Total Fe as FeO

	84.09	84.10	84.11	257.05	257.06	257.07	41.07	41.08	41.09	80.01	80.05	168.01	168.02	168.03	168.17	168.18	186.12
Weight % oxide																	
SiO2	34.892	35.296	35.869	35.825	34.863	36.174	36.340	36.365	35.098	40.490	42.379	32.301	31.847	32.476	33.172	33.606	42.669
TiO2	0.804	0.625	1.726	1.474	1.061	1.366	1.138	1.228	2.835	0.076	0.010	0.487	0.378	0.386	0.558	1.582	1.966
Al2O3	12.968	13.444	14.319	12.886	11.714	13.749	13.434	13.382	13.562	11.062	10.776	15.094	15.260	16.224	15.323	11.784	15.576
FeO	32.372	30.020	28.044	29.882	34.026	30.754	28.435	26.875	22.704	20.937	15.939	34.534	36.030	35.344	36.161	36.452	15.503
MnO	1.200	1.300	0.729	2.431	1.882	2.265	1.987	0.522	0.420	0.445	0.128	0.208	0.183	0.021	0.052	0.255	1.402
MgO	3.542	4.681	5.779	3.849	2.804	3.811	5.682	8.130	9.073	12.249	15.414	0.842	0.808	1.004	1.764	2.527	6.882
CaO	0.118	0.348	0.314	0.130	0.029	0.232	0.089	0.107	0.143	0.540	0.447	0.524	0.198	0.627	0.407	0.270	0.089
Na2O	0.464	0.701	0.656	0.562	0.405	0.387	0.569	0.252	0.320	0.443	0.291	0.058	0.223	0.081	0.264	0.425	5.830
K2O	9.122	8.807	9.488	9.523	9.170	9.739	9.346	9.297	9.125	8.801	8.912	7.990	9.241	7.242	8.790	7.866	5.984
Total	95.482	95.222	96.924	96.562	95.954	98.477	97.020	96.158	93.280	95.043	94.296	92.038	94.168	93.405	96.491	94.767	95.901
Atoms per 22 oxygens																	
Si	5.742	5.743	5.662	5.787	5.787	5.731	5.764	5.732	5.610	6.205	6.355	5.549	5.429	5.468	5.467	5.659	6.266
Ti	0.100	0.076	0.205	0.179	0.132	0.163	0.136	0.146	0.341	0.009	0.001	0.063	0.048	0.049	0.069	0.200	0.217
Al	2.516	2.579	2.665	2.454	2.292	2.568	2.512	2.487	2.556	1.998	1.905	3.057	3.067	3.220	2.977	2.339	2.697
Fe	4.455	4.085	3.702	4.037	4.723	4.075	3.772	3.543	3.035	2.683	1.999	4.962	5.136	4.977	4.984	5.133	1.904
Mn	0.167	0.179	0.097	0.333	0.265	0.304	0.267	0.070	0.057	0.058	0.016	0.030	0.026	0.003	0.007	0.036	0.174
Mg	0.869	1.135	1.360	0.927	0.694	0.900	1.343	1.910	2.161	2.797	3.445	0.216	0.205	0.252	0.433	0.634	1.506
Ca	0.021	0.061	0.053	0.023	0.005	0.039	0.015	0.018	0.024	0.089	0.072	0.096	0.036	0.113	0.072	0.049	0.014
Na	0.148	0.221	0.201	0.176	0.130	0.119	0.175	0.077	0.099	0.132	0.085	0.019	0.074	0.026	0.084	0.139	1.660
K	1.915	1.828	1.911	1.962	1.942	1.968	1.891	1.870	1.861	1.721	1.705	1.751	2.010	1.556	1.848	1.690	1.121
Rock Type	GS-B	GS-B	GS-B	GS-B	GS-B	GS-B	XPS	XPS	XPS	XPS	XPS	GS-B	GS-B	GS-B	XPS	XPS	PMS
Crystal	14.	14.	14.	1.	1.	1.	1.	1.	1.	1.	4.	1.	1.	1.	1.	1.	1.
Position	-1.	-1.	-1.	8.	8.	8.	8.	8.	8.	8.	7.	8.	8.	8.	7.	1.	8.

BIOTITE ANALYSES - Total Fe as FeO

	178.20	178.21	178.22	178.23	64.12	64.12	64.13	180.15	180.16	180.17	180.18	26.07	26.08	26.09	26.10	26.11	26.12
Weight % oxide																	
SiO2	34.646	35.206	33.940	34.324	34.203	35.011	34.131	33.273	32.977	33.082	33.570	35.034	34.267	34.699	34.202	35.121	34.390
TiO2	1.719	1.861	1.740	1.763	3.507	2.693	2.461	0.558	0.477	0.527	0.698	0.306	1.803	0.100	1.577	0.275	0.241
Al2O3	11.274	11.409	10.538	11.613	12.604	12.676	12.497	12.149	11.890	11.125	11.229	12.638	11.681	11.494	11.761	11.410	11.261
FeO	36.090	36.446	36.538	36.140	31.207	30.978	33.083	39.699	37.587	39.839	39.318	33.498	34.661	34.872	35.044	34.906	35.582
MnO	1.326	1.094	1.366	1.299	1.113	1.180	0.928	0.261	0.154	0.226	0.383	0.080	0.056	0.062	0.171	0.101	0.091
MgO	2.552	2.693	2.562	2.259	4.182	3.788	3.140	0.915	2.102	1.593	1.847	4.990	3.941	5.145	4.274	4.791	4.339
CaO	0.213	0.250	0.119	0.292	0.133	0.073	0.183	0.153	0.336	0.132	0.168	0.078	0.001	0.070	0.006	0.023	0.150
Na2O	0.471	0.374	0.527	0.420	0.246	0.922	0.314	0.510	0.273	0.418	0.382	0.304	0.229	0.254	0.193	0.104	0.226
K2O	9.158	9.344	9.193	9.020	9.453	9.121	9.327	8.615	8.477	8.465	8.549	9.292	8.991	9.207	9.303	9.579	9.087
Total	97.449	98.677	96.523	97.130	96.648	96.442	96.064	96.133	94.273	95.407	96.144	96.220	95.630	95.903	96.531	96.310	95.367
Atoms per 22 oxygens																	
Si	5.712	5.720	5.693	5.678	5.547	5.668	5.618	5.639	5.649	5.666	5.681	5.722	5.678	5.742	5.635	5.788	5.752
Ti	0.213	0.227	0.219	0.219	0.428	0.328	0.305	0.071	0.061	0.068	0.089	0.038	0.225	0.012	0.195	0.034	0.030
Al	2.191	2.185	2.084	2.265	2.410	2.419	2.425	2.427	2.401	2.246	2.240	2.433	2.282	2.242	2.284	2.217	2.220
Fe	4.976	4.953	5.125	5.000	4.233	4.194	4.555	5.627	5.385	5.706	5.564	4.576	4.803	4.826	4.829	4.811	4.977
Mn	0.185	0.151	0.194	0.182	0.153	0.162	0.129	0.037	0.022	0.033	0.055	0.011	0.008	0.009	0.024	0.014	0.013
Mg	0.627	0.652	0.640	0.557	1.011	0.914	0.770	0.231	0.537	0.407	0.466	1.215	0.973	1.269	1.049	1.177	1.082
Ca	0.038	0.044	0.021	0.052	0.023	0.013	0.032	0.028	0.062	0.024	0.030	0.014	0.0	0.012	0.001	0.004	0.027
Na	0.151	0.118	0.171	0.135	0.077	0.289	0.100	0.168	0.091	0.139	0.125	0.096	0.074	0.081	0.062	0.033	0.073
K	1.926	1.937	1.967	1.904	1.956	1.884	1.959	1.863	1.853	1.850	1.846	1.936	1.901	1.944	1.955	2.014	1.939
Rock Type	PMS	PMS	PMS	PMS	MMS	MMS	MMS	ALSY	ALSY	ALSY	ALSY	ALGN	ALGN	ALGN	ALGN	ALGN	ALGN
Crystal	1.	1.	1.	1.	1.	1.	1.	1.	1.	1.	1.	1.	1.	1.	1.	1.	1.
Position	8.	8.	8.	8.	8.	8.	8.	8.	7.	1.	7.	7.	1.	7.	1.	8.	8.

BIOTITE ANALYSES - Total Fe as FeO

	239.08	239.09	239.10	272.04	272.05	272.06	272.13	275.07	275.08	275.09	275.10	275.11	183.12	183.13	156.04	156.05	202.01
Weight % oxide																	
SiO2	37.919	37.269	38.823	41.659	44.929	45.422	39.641	35.060	34.969	34.519	35.809	36.168	34.460	35.425	35.813	35.445	35.089
TiO2	2.904	3.315	2.417	0.395	0.183	0.237	0.766	3.629	3.504	3.429	3.064	3.303	0.360	0.341	3.357	3.385	1.323
Al2O3	12.812	12.725	11.094	33.835	33.671	33.045	29.659	12.012	11.207	11.094	11.597	12.212	11.667	11.258	11.765	11.810	11.405
FeO	20.161	20.980	21.046	1.606	1.818	2.276	3.510	30.778	31.659	32.444	29.436	28.646	37.289	36.843	29.119	28.491	34.289
MnO	0.084	0.0	0.071	3.109	0.255	0.166	7.325	0.441	0.577	0.444	0.852	0.820	0.170	0.0	0.798	0.915	0.808
MgO	12.302	11.646	12.703	0.199	0.474	0.376	0.672	4.761	4.364	4.221	5.594	5.495	2.767	2.800	6.147	6.622	3.778
CaO	0.152	0.132	0.195	0.110	0.058	0.149	0.349	0.210	0.159	0.153	0.123	0.053	0.080	0.205	0.045	0.226	0.041
Na2O	0.398	0.484	0.496	0.314	0.279	0.047	0.265	0.372	0.574	0.682	0.621	0.494	0.103	0.289	0.355	0.644	0.406
K2O	9.451	9.836	9.650	10.403	11.112	11.006	8.941	8.794	8.757	8.407	9.006	9.162	8.454	9.011	8.818	9.288	9.043
Total	96.183	96.387	96.495	91.630	92.779	92.724	91.128	96.057	95.770	95.393	96.102	96.353	95.350	96.172	96.217	96.826	96.182
Atoms per 22 oxygens																	
Si	5.763	5.698	5.912	5.910	6.196	6.266	5.837	5.662	5.707	5.676	5.755	5.761	5.782	5.879	5.722	5.645	5.781
Ti	0.332	0.381	0.277	0.042	0.019	0.025	0.085	0.441	0.430	0.424	0.370	0.396	0.045	0.043	0.403	0.405	0.164
Al	2.296	2.294	1.992	5.659	5.474	5.375	5.149	2.287	2.156	2.150	2.197	2.293	2.308	2.203	2.216	2.218	2.215
Fe	2.563	2.683	2.680	0.191	0.210	0.263	0.432	4.157	4.321	4.461	3.956	3.816	5.232	5.113	3.891	3.795	4.725
Mn	0.011	0.0	0.009	0.374	0.030	0.019	0.914	0.060	0.080	0.062	0.116	0.111	0.024	0.0	0.108	0.123	0.113
Mg	2.787	2.654	2.883	0.042	0.097	0.077	0.147	1.146	1.061	1.034	1.340	1.304	0.692	0.692	1.464	1.572	0.928
Ca	0.025	0.022	0.032	0.017	0.009	0.022	0.055	0.036	0.028	0.027	0.021	0.009	0.014	0.036	0.008	0.039	0.007
Na	0.117	0.143	0.146	0.086	0.075	0.013	0.076	0.116	0.182	0.217	0.194	0.153	0.034	0.093	0.110	0.199	0.130
K	1.833	1.919	1.875	1.883	1.955	1.937	1.680	1.812	1.823	1.764	1.847	1.862	1.810	1.908	1.798	1.887	1.901
Rock Type	ALGN	ALGN	ALGN	ALSY	ALSY	ALSY	ALSY	CGS	CGS	CGS	CGS	CGS	PEG	PEG	MUS	MUS	PMS
Crystal	1.	1.	1.	1.	1.	1.	1.	1.	1.	1.	1.	1.	1.	1.	1.	1.	1.
Position	8.	8.	8.	8.	8.	8.	8.	1.	7.	1.	7.	1.	8.	8.	8.	8.	7.

BIOTITE ANALYSES - Total Fe as FeO

	202.02	253.12	253.13	253.14	152.07	152.08	136.11	136.13	136.13
Weight % oxide									
SiO2	35.490	36.290	35.428	34.910	36.371	34.991	37.011	37.474	36.906
TiO2	1.358	5.623	5.799	5.169	2.425	2.016	1.272	1.139	0.741
Al2O3	11.117	13.479	13.437	13.531	13.184	11.676	13.155	13.390	12.666
FeO	34.356	24.694	25.818	25.723	26.714	32.515	24.021	25.041	21.222
MnO	0.723	0.332	0.410	0.392	1.423	0.951	1.024	1.009	1.120
MgO	3.976	7.667	6.982	6.689	5.434	3.949	8.356	8.198	12.676
CaO	0.156	0.018	0.0	0.0	0.158	0.127	0.204	0.142	0.254
Na2O	0.510	0.778	0.700	0.525	0.920	0.483	0.943	0.798	0.559
K2O	9.070	8.964	8.949	9.045	9.349	9.244	8.751	9.311	9.059
Total	96.756	97.845	97.523	95.984	95.978	95.952	94.737	96.502	95.203
Atoms per 22 oxygens									
Si	5.803	5.555	5.486	5.501	5.783	5.743	5.844	5.838	5.736
Ti	0.167	0.647	0.675	0.613	0.290	0.249	0.151	0.133	0.087
Al	2.143	2.432	2.453	2.514	2.471	2.259	2.449	2.459	2.321
Fe	4.698	3.161	3.344	3.390	3.552	4.463	3.172	3.263	2.759
Mn	0.100	0.043	0.054	0.052	0.192	0.132	0.137	0.133	0.147
Mg	0.969	1.749	1.611	1.571	1.288	0.966	1.966	1.903	2.936
Ca	0.027	0.003	0.0	0.0	0.027	0.022	0.035	0.024	0.042
Na	0.162	0.231	0.210	0.160	0.284	0.154	0.289	0.241	0.168
K	1.892	1.751	1.768	1.818	1.896	1.936	1.763	1.851	1.796
Rock Type	PMS	PMS	PMS	PMS	PMS	PMS	ALSY	ALSY	ALSY
Crystal	1.	1.	1.	1.	1.	1.	1.	1.	1.
Position	1.	8.	8.	8.	8.	8.	8.	8.	8.

OXIDE ANALYSES

	* 27113.12	* 27113.22	* 138048.16	* 138048.17	* 138048.18	* 138048.19	* 27056.24	* 27056.25	* 27056.26	* 27259.14	* 27259.15	* 27259.16	* 138001.12	* 138001.13	* 138001.14	* 138025.13
Weight % oxide																
SiO2	0.933	1.155	0.986	0.780	0.048	0.318	0.016	0.103	0.005	0.105	0.512	0.150	0.128	0.100	0.158	0.082
TiO2	1.754	2.568	1.920	1.240	2.952	4.805	1.354	3.783	5.043	0.821	11.508	28.241	0.226	0.194	0.238	0.435
Al2O3	0.248	0.530	0.421	0.373	0.055	0.136	0.042	0.038	0.095	0.038	0.233	0.152	0.073	0.084	0.137	0.127
FeO	84.062	84.040	84.519	85.143	85.281	83.030	87.306	84.289	83.733	91.309	77.444	62.191	90.866	90.884	90.968	90.768
MnO	0.519	0.245	0.150	0.155	0.486	0.270	0.020	0.036	0.042	0.063	3.603	2.905	0.044	0.063	0.088	0.112
MgO	0.059	0.299	0.251	0.201	0.028	0.051	0.0	0.020	0.023	0.020	0.016	0.003	0.031	0.019	0.0	0.028
CaO	0.021	0.0	0.033	0.0	0.014	0.028	0.007	0.017	0.012	0.0	0.026	0.004	0.0	0.003	0.013	0.005
Total	87.596	88.837	88.280	87.892	88.864	88.638	88.745	88.286	88.953	92.356	93.342	93.646	91.368	91.347	91.602	91.557
Atoms per 4 oxygens																
Si	0.038	0.046	0.040	0.032	0.002	0.013	0.001	0.004	0.0	0.004	0.020	0.006	0.005	0.004	0.006	0.003
Ti	0.054	0.078	0.058	0.038	0.090	0.147	0.041	0.116	0.154	0.024	0.336	0.838	0.007	0.006	0.007	0.013
Al	0.012	0.025	0.020	0.018	0.003	0.007	0.002	0.002	0.005	0.002	0.011	0.007	0.003	0.004	0.006	0.006
Fe3	1.804	1.727	1.783	1.843	1.814	1.674	1.914	1.758	1.688	1.942	1.278	0.305	1.973	1.977	1.967	1.962
Fe2	1.070	1.098	1.077	1.052	1.073	1.146	1.041	1.117	1.151	1.025	1.235	1.746	1.008	1.006	1.010	1.010
Mn	0.018	0.008	0.005	0.005	0.017	0.009	0.001	0.001	0.001	0.002	0.118	0.097	0.001	0.002	0.003	0.004
Mg	0.004	0.018	0.015	0.012	0.002	0.003	0.0	0.001	0.001	0.001	0.001	0.0	0.002	0.001	0.0	0.002
Ca	0.001	0.0	0.001	0.0	0.001	0.001	0.0	0.001	0.001	0.0	0.001	0.0	0.0	0.0	0.001	0.0
Rock Type	LSS	LSS	LSS	LSS	LSS	LSS	XPS	XPS	XPS	MUS	MUS	MUS	CGBS	CGBS	CGBS	LSS
Crystal	1.	10.	8.	10.	8.	8.	1.	1.	1.	10.	10.	15.	14.	14.	14.	4.
Position	-1.	-1.	-1.	-1.	10.	10.	-1.	-1.	-1.	7.	1.	-1.	-1.	7.	1.	1.
End members																
Mgt	90.8	87.6	90.2	93.0	90.8	84.0	95.8	88.0	84.6	97.2	64.4	15.6	98.8	99.0	98.7	98.4
Usp	9.2	12.4	9.8	7.0	9.2	16.0	4.2	12.0	15.4	2.8	35.6	84.4	1.2	1.0	1.3	1.6

OXIDE ANALYSES

	* 138025.14	* 138025.15	* 138025.16	* 138025.17	* 138025.18	* 138025.19	* 138027.07	* 138027.08	37.10	37.11	37.15	37.17	138055.11	138055.13	43.12	172.13	172.22
Weight % oxide																	
SiO2	0.088	0.132	0.010	0.149	0.123	0.122	0.341	0.226	0.797	0.461	0.433	0.462	0.233	0.481	2.335	0.603	0.293
TiO2	0.718	0.377	0.268	9.698	0.790	0.932	0.0	0.0	0.0	0.388	5.142	1.344	55.105	0.0	3.351	16.318	0.0
Al2O3	0.112	0.178	0.102	0.211	0.196	0.194	0.0	0.0	0.0	0.0	0.392	0.347	0.0	0.0	0.907	0.082	0.448
FeO	90.477	87.838	87.958	77.972	90.303	89.798	97.647	97.993	96.090	95.658	89.195	93.681	45.048	89.556	85.197	75.929	89.238
MnO	0.089	0.167	0.061	3.723	0.310	0.528	0.0	0.0	0.0	0.411	1.327	0.727	1.024	0.0	1.138	1.412	0.151
MgO	0.002	0.027	0.0	0.002	0.013	0.007	0.0	0.0	0.0	0.0	0.0	0.0	0.0	0.0	0.534	0.0	0.116
CaO	0.0	0.0	0.0	0.001	0.014	0.009	0.0	0.0	0.0	0.0	0.0	0.0	0.0	0.0	0.0	0.274	0.133
Total	91.486	88.719	88.399	91.756	91.749	91.590	97.988	98.219	96.887	96.918	96.489	96.561	101.410	90.037	93.462	94.618	90.379
Atoms per 4 oxygens																	
Si	0.003	0.005	0.0	0.006	0.005	0.005	0.012	0.008	0.029	0.017	0.016	0.017	0.009	0.019	0.089	0.023	0.012
Ti	0.021	0.011	0.008	0.288	0.023	0.027	0.0	0.0	0.0	0.011	0.144	0.038	1.550	0.0	0.096	0.472	0.0
Al	0.005	0.008	0.005	0.010	0.009	0.009	0.0	0.0	0.0	0.0	0.017	0.015	0.0	0.0	0.041	0.004	0.021
Fe3	1.946	1.958	1.978	1.403	1.935	1.927	1.975	1.984	1.941	1.944	1.662	1.876	0.0	1.962	1.590	1.005	1.956
Fe2	1.022	1.009	1.006	1.169	1.016	1.014	1.012	1.008	1.029	1.015	1.118	1.032	1.409	1.019	1.118	1.438	0.994
Mn	0.003	0.006	0.002	0.124	0.010	0.018	0.0	0.0	0.0	0.013	0.042	0.023	0.032	0.0	0.037	0.046	0.005
Mg	0.0	0.002	0.0	0.0	0.001	0.0	0.0	0.0	0.0	0.0	0.0	0.0	0.0	0.0	0.030	0.0	0.007
Ca	0.0	0.0	0.0	0.0	0.001	0.0	0.0	0.0	0.0	0.0	0.0	0.0	0.0	0.0	0.0	0.011	0.006
Rock Type	LSS	LSS	LSS	LSS	LSS	LSS	CGBS	CGBS	MMS	MMS	MMS	MMS	PEG	PEG	USS	GS-A	GS-A
Crystal	4.	15.	15.	10.	10.	10.	8.	8.	9.	9.	12.	1.	1.	1.	10.	10.	1.
Position	3.	-1.	-1.	-1.	-1.	-1.	-1.	-1.	9.	9.	-1.	8.	8.	8.	10.	10.	8.
End members																	
Mgt	97.5	98.3	99.1	70.6	97.2	96.8	98.8	99.2	97.1	97.2	84.0	94.5	0.0(Ht)	98.1	81.5	50.5	98.8
Usp	2.5	1.7	0.9	29.4	2.8	3.2	1.2	0.8	2.9	2.8	16.0	5.5	100.0(Il)	1.9	18.5	49.5	1.2

OXIDE ANALYSES

	172.23	169.38	169.41	168.15	168.16	26.15	26.16	26.17	275.19	275.20	275.21	275.22	183.08	135.15	135.16	135.17	118.01
Weight % oxide																	
SiO2	0.600	0.273	2.432	0.377	0.157	0.350	1.865	0.625	0.239	0.248	0.342	0.471	7.973	1.016	0.572	0.613	0.791
TiO2	0.054	18.127	19.136	0.053	0.0	0.077	0.0	0.062	4.287	5.310	9.515	1.013	0.078	1.412	2.299	3.351	2.899
Al203	0.265	0.608	0.144	1.257	0.131	0.063	0.574	0.049	0.335	0.355	0.110	0.284	0.835	0.487	0.398	0.268	0.163
FeO	89.477	77.726	68.986	87.939	91.382	94.392	92.275	94.126	87.286	86.816	81.778	90.771	57.752	91.446	92.626	89.692	89.336
MnO	0.209	1.058	4.939	0.0	0.103	0.0	0.0	0.0	0.459	0.547	1.603	0.136	6.127	0.911	1.426	2.249	1.534
MgO	0.190	0.013	0.034	0.083	0.026	0.105	0.183	0.0	0.100	0.024	0.044	0.0	0.167	0.065	0.008	0.0	0.0
CaO	0.014	0.009	1.832	0.094	0.0	0.295	0.118	0.0	0.070	0.0	0.036	0.0	0.530	0.098	0.075	0.0	0.0
Total	90.809	97.814	97.503	89.803	91.799	95.282	95.015	94.862	92.776	93.300	93.428	92.675	73.462	95.435	97.404	96.173	94.723
Atoms per 4 oxygens																	
Si	0.024	0.010	0.090	0.015	0.006	0.013	0.070	0.024	0.009	0.010	0.013	0.018	0.378	0.038	0.021	0.023	0.030
Ti	0.002	0.508	0.533	0.002	0.0	0.002	0.0	0.002	0.125	0.154	0.277	0.029	0.003	0.040	0.064	0.094	0.083
Al	0.012	0.027	0.006	0.059	0.006	0.003	0.025	0.002	0.015	0.016	0.005	0.013	0.047	0.022	0.017	0.012	0.007
Fe3	1.933	0.938	0.742	1.908	1.981	1.966	1.830	1.947	1.713	1.655	1.414	1.882	1.190	1.823	1.809	1.752	1.764
Fe2	1.009	1.483	1.396	1.008	1.002	0.998	1.057	1.026	1.112	1.145	1.234	1.048	1.097	1.041	1.039	1.047	1.065
Mn	0.007	0.033	0.155	0.0	0.003	0.0	0.0	0.0	0.015	0.018	0.053	0.004	0.246	0.029	0.044	0.071	0.049
Mg	0.011	0.001	0.002	0.005	0.002	0.006	0.010	0.0	0.006	0.001	0.003	0.0	0.012	0.004	0.0	0.0	0.0
Ca	0.001	0.0	0.073	0.004	0.0	0.012	0.005	0.0	0.003	0.0	0.001	0.0	0.027	0.004	0.003	0.0	0.0
Rock Type	GS-A	GS-A	GS-A	XPS	XPS	ALGN	ALGN	ALGN	CGS	CGS	CGS	CGS	PEG	USS	USS	USS	USS
Crystal	1.	1.	1.	1.	1.	1.	1.	1.	4.	4.	4.	4.	1.	1.	1.	1.	1.
Position	8.	8.	8.	8.	8.	8.	8.	8.	7.	1.	7.	1.	8.	8.	8.	8.	8.
End members																	
Mgt	97.5	48.2	37.5	98.3	99.4	98.5	93.0	97.5	86.6	83.6	71.0	95.2	61.9	92.2	91.5	88.3	88.7
Usp	2.5	51.8	62.5	1.7	0.6	1.5	7.0	2.5	13.4	16.4	29.0	4.8	38.1	7.8	8.5	11.7	11.3

OXIDE ANALYSES

	118.02	118.03	118.04	156.06	156.07	156.08	156.09	202.09	202.10	202.11	253.01	253.02	253.04	253.05	152.01	152.02	152.03
Weight % oxide																	
SiO2	0.593	0.402	0.464	0.222	0.282	0.399	0.373	4.792	2.826	3.284	0.453	0.942	2.704	0.505	0.620	0.553	0.518
TiO2	8.766	8.312	11.735	0.939	5.674	0.716	16.903	0.090	0.0	0.0	20.175	20.689	0.191	21.661	2.894	10.219	0.659
Al203	0.169	0.518	0.288	0.078	0.370	0.268	0.210	0.165	0.122	0.097	1.228	1.064	0.600	1.848	0.176	0.081	0.135
FeO	82.176	81.996	77.911	91.857	87.599	92.387	77.476	71.110	77.892	75.361	73.124	70.443	78.750	70.080	92.379	83.304	94.298
MnO	4.688	3.903	5.588	0.0	1.236	0.0	1.800	0.129	0.089	0.067	1.394	2.543	0.0	3.163	0.545	1.707	0.0
MgO	0.002	0.0	0.0	0.001	0.161	0.023	0.151	0.085	0.184	0.065	0.112	0.201	0.365	0.091	0.029	0.0	0.0
CaO	0.018	0.071	0.0	0.035	0.095	0.092	0.0	0.533	0.281	0.186	0.049	0.207	0.848	0.075	0.026	0.031	0.054
Total	96.412	95.202	95.986	93.132	95.417	93.885	96.913	76.904	81.394	79.060	96.535	96.089	83.458	97.423	96.669	95.895	95.664
Atoms per 4 oxygens																	
Si	0.022	0.015	0.018	0.009	0.011	0.015	0.014	0.220	0.123	0.148	0.017	0.036	0.114	0.019	0.023	0.021	0.019
Ti	0.247	0.237	0.333	0.027	0.161	0.021	0.477	0.003	0.0	0.0	0.571	0.588	0.006	0.607	0.081	0.290	0.019
Al	0.007	0.023	0.013	0.004	0.016	0.012	0.009	0.009	0.006	0.005	0.054	0.047	0.030	0.081	0.008	0.004	0.006
Fe3	1.452	1.473	1.286	1.924	1.636	1.915	1.005	1.545	1.747	1.700	0.764	0.705	1.718	0.667	1.785	1.374	1.914
Fe2	1.121	1.124	1.172	1.035	1.122	1.032	1.427	1.186	1.095	1.132	1.538	1.523	1.065	1.518	1.084	1.255	1.038
Mn	0.149	0.125	0.179	0.0	0.039	0.0	0.057	0.005	0.003	0.003	0.044	0.081	0.0	0.100	0.017	0.055	0.0
Mg	0.0	0.0	0.0	0.0	0.009	0.001	0.008	0.006	0.012	0.004	0.006	0.011	0.023	0.005	0.002	0.0	0.0
Ca	0.001	0.003	0.0	0.001	0.004	0.004	0.0	0.026	0.013	0.009	0.002	0.008	0.038	0.003	0.001	0.001	0.002
Rock Type	USS	USS	USS	MUS	MUS	MUS	MUS	PMS	PMS	PMS	PMS	PMS	PMS	PMS	PMS	PMS	PMS
Crystal	1.	1.	1.	1.	1.	1.	1.	11.	11.	11.	1.	1.	11.	1.	1.	1.	1.
Position	8.	8.	8.	8.	8.	8.	8.	-1.	-1.	-1.	8.	8.	-1.	8.	8.	8.	8.
End members																	
Mgt	73.1	74.8	65.0	96.4	82.8	96.4	50.8	77.7	87.7	85.2	41.0	37.6	87.9	37.4	89.6	68.9	96.2
Usp	26.9	25.2	35.0	3.6	17.2	3.6	49.2	22.3	12.3	14.8	59.0	62.4	12.1	62.6	10.4	31.1	3.8

OXIDE ANALYSES

	152.04	136.01	136.03	136.04	136.05	103.01	103.02	103.03	265.01	265.02	265.03	265.04	146.06	146.07
Weight % oxide														
SiO2	0.329	0.487	0.358	0.238	0.569	3.489	3.545	3.356	0.207	0.331	0.267	0.190	4.305	3.930
TiO2	14.936	2.959	4.408	2.032	1.910	0.049	0.012	0.072	0.939	0.117	0.552	0.230	0.019	0.097
Al2O3	0.282	0.107	0.176	0.316	0.363	0.023	0.457	0.003	0.052	0.076	0.060	0.055	0.357	0.455
FeO	78.354	87.207	82.412	88.823	89.171	68.626	66.273	68.721	91.866	96.620	96.033	93.968	64.134	63.922
MnO	3.120	0.0	0.016	0.0	0.051	1.476	1.373	1.257	0.0	0.0	0.0	0.068	1.341	3.629
MgO	0.059	0.064	0.0	0.040	0.109	0.399	0.536	0.413	0.091	0.0	0.0	0.0	0.416	0.246
CaO	0.085	0.191	0.027	0.079	0.113	0.795	0.781	0.561	0.149	0.083	0.048	0.0	0.493	0.453
Total	97.165	91.015	87.397	91.528	92.286	74.857	72.977	74.383	93.304	97.227	96.960	94.511	71.065	72.732
Atoms per 4 oxygens														
Si	0.012	0.019	0.015	0.009	0.022	0.164	0.171	0.159	0.008	0.012	0.010	0.007	0.213	0.190
Ti	0.420	0.088	0.137	0.060	0.056	0.002	0.0	0.003	0.027	0.003	0.015	0.007	0.001	0.004
Al	0.012	0.005	0.009	0.015	0.017	0.001	0.026	0.0	0.002	0.003	0.003	0.002	0.021	0.026
Fe3	1.123	1.781	1.688	1.847	1.828	1.664	1.628	1.671	1.927	1.959	1.945	1.970	1.552	1.586
Fe2	1.327	1.095	1.150	1.064	1.065	1.040	1.038	1.056	1.024	1.015	1.024	1.012	1.101	1.004
Mn	0.099	0.0	0.001	0.0	0.002	0.059	0.056	0.051	0.0	0.0	0.0	0.002	0.056	0.149
Mg	0.003	0.004	0.0	0.002	0.006	0.028	0.038	0.029	0.005	0.0	0.0	0.0	0.031	0.018
Ca	0.003	0.008	0.001	0.003	0.005	0.040	0.040	0.029	0.006	0.003	0.002	0.0	0.026	0.024
Rock Type	PMS	ALSY	ALSY	ALSY	ALSY	CBT	CBT	CBT	CBT	CBT	CBT	CBT	ALGN	ALGN
Crystal	1.	1.	1.	1.	1.	14.	1.	14.	1.	1.	1.	1.	1.	1.
Position	8.	8.	8.	8.	8.	-1.	8.	-1.	8.	8.	8.	8.	8.	8.
End members														
Mgt	56.8	89.3	84.9	93.1	92.2	83.4	82.9	83.8	96.5	98.5	97.5	98.6	78.6	80.6
Usp	43.2	10.7	15.1	6.9	7.8	16.6	17.1	16.2	3.5	1.5	2.5	1.4	21.4	19.4

NEPHELINE ANALYSES

	* 27113.05	* 27113.06	* 27113.24	* 27113.25	* 27193.11	* 27193.12	* 138048.20	* 138048.21	* 138048.22	* 138048.23	* 138048.26	* 27259.12	* 27259.13	* 27259.18	* 27259.19	* 27259.20	* 27259.21
Weight % oxide																	
SiO2	45.001	45.175	44.082	45.217	46.324	44.952	44.882	44.044	44.296	45.090	44.277	43.771	44.195	43.525	43.671	43.795	43.987
TiO2	0.026	0.012	0.0	0.0	0.013	0.022	0.0	0.009	0.0	0.018	0.0	0.023	0.025	0.026	0.023	0.029	0.023
Al2O3	32.699	32.867	33.102	33.137	33.592	33.155	32.410	32.955	32.541	32.476	32.526	33.096	33.080	33.604	33.197	33.349	33.089
FeO	0.706	0.748	0.827	0.502	0.660	0.804	0.600	0.538	0.787	0.744	0.561	0.655	0.592	0.413	0.536	0.349	0.471
MnO	0.005	0.017	0.029	0.0	0.010	0.027	0.029	0.002	0.015	0.008	0.0	0.025	0.005	0.020	0.0	0.018	0.0
MgO	0.011	0.0	0.020	0.017	0.009	0.007	0.019	0.018	0.017	0.005	0.018	0.003	0.006	0.016	0.005	0.012	0.014
CaO	0.012	0.013	0.013	0.035	0.053	0.077	0.053	0.025	0.016	0.022	0.030	0.028	0.036	0.282	0.026	0.041	0.039
Na2O	16.769	16.268	16.978	16.564	15.050	11.988	16.856	17.200	17.188	17.071	16.538	17.463	17.472	14.606	17.480	17.395	17.396
K2O	5.607	5.685	6.007	5.617	6.152	5.539	5.392	5.851	5.705	5.346	5.539	5.902	5.770	4.440	6.081	6.075	6.032
BaO	0.0	0.0	0.012	0.0	0.002	0.027	0.040	0.045	0.011	0.025	0.031	0.0	0.017	0.013	0.048	0.0	0.031
Total	100.836	100.785	101.070	101.089	101.865	96.598	100.281	100.687	100.576	100.805	99.520	100.973	101.198	96.948	101.143	101.063	101.085
Atoms per 8 oxygens																	
Si	2.139	2.144	2.102	2.138	2.164	2.186	2.144	2.106	2.120	2.144	2.132	2.092	2.103	2.121	2.087	2.089	2.098
Ti	0.0	0.0	0.0	0.0	0.0	0.0	0.0	0.0	0.0	0.0	0.0	0.0	0.0	0.0	0.0	0.001	0.0
Al	1.832	1.839	1.861	1.848	1.850	1.901	1.825	1.858	1.836	1.820	1.846	1.865	1.856	1.930	1.870	1.875	1.861
Fe	0.028	0.030	0.033	0.020	0.026	0.033	0.024	0.022	0.032	0.030	0.023	0.026	0.024	0.017	0.021	0.014	0.019
Mn	0.0	0.0	0.001	0.0	0.0	0.001	0.001	0.0	0.0	0.0	0.0	0.001	0.0	0.0	0.0	0.0	0.0
Mg	0.0	0.0	0.001	0.001	0.0	0.0	0.001	0.001	0.001	0.0	0.001	0.0	0.0	0.001	0.0	0.0	0.0
Ca	0.0	0.0	0.0	0.002	0.003	0.004	0.003	0.001	0.0	0.001	0.002	0.001	0.002	0.015	0.001	0.002	0.002
Na	1.545	1.497	1.570	1.519	1.363	1.130	1.561	1.595	1.595	1.574	1.544	1.618	1.612	1.380	1.620	1.609	1.609
K	0.340	0.344	0.365	0.339	0.367	0.344	0.329	0.357	0.348	0.324	0.340	0.360	0.350	0.276	0.371	0.370	0.367
Ba	0.0	0.0	0.0	0.0	0.0	0.0	0.0	0.0	0.0	0.0	0.0	0.0	0.0	0.0	0.0	0.0	0.0
Rock Type	LSS	LSS	LSS	LSS	MUS	MUS	LSS	LSS	LSS	LSS	LSS	MUS	MUS	MUS	MUS	MUS	MUS
Crystal	4.	1.	5.	5.	14.	14.	4.	4.	5.	5.	14.	4.	4.	4.	4.	5.	5.
Position	1.	1.	7.	2.	-1.	-1.	7.	1.	7.	1.	-1.	3.	7.	7.	2.	7.	2.

NEPHELINE ANALYSES

	* 138007.18	* 138007.19	* 138001.14	* 138001.15	* 138001.16	* 138025.09	* 138025.10	* 138025.21	* 138025.22	38.15	38.17	38.19	38.20	220.10	220.13	220.14	220.15
Weight % oxide																	
SiO2	46.145	46.147	44.809	45.647	45.129	45.542	45.892	44.208	44.274	46.032	45.370	46.353	45.856	45.910	46.817	47.154	46.418
TiO2	0.028	0.021	0.019	0.003	0.025	0.014	0.019	0.029	0.0	0.0	0.0	0.0	0.0	0.0	0.0	0.0	0.0
Al203	31.947	32.095	32.740	32.356	32.990	32.506	32.376	32.464	32.267	32.889	33.296	32.844	32.613	32.836	33.360	33.574	33.468
FeO	0.605	0.571	0.771	0.840	0.533	0.585	0.594	0.665	0.676	0.550	0.521	0.621	0.698	0.732	0.607	0.760	1.020
MnO	0.018	0.015	0.009	0.014	0.003	0.015	0.0	0.0	0.0	0.0	0.0	0.0	0.0	0.0	0.0	0.0	0.0
MgO	0.020	0.023	0.011	0.005	0.008	0.007	0.020	0.006	0.006	0.0	0.0	0.0	0.0	0.0	0.0	0.0	0.0
CaO	0.030	0.015	0.0	0.006	0.015	0.023	0.007	0.027	0.022	0.0	0.0	0.0	0.0	0.0	0.0	0.0	0.0
Na2O	16.434	16.040	15.110	15.849	16.304	15.477	17.041	16.955	16.843	15.162	15.398	15.362	15.463	14.847	14.657	13.210	14.065
K2O	4.750	4.727	5.578	5.267	5.606	5.330	5.452	5.479	5.469	5.672	6.082	5.507	5.541	5.571	5.684	5.866	5.721
BaO	0.028	0.008	0.045	0.010	0.002	0.020	0.0	0.005	0.014	0.0	0.0	0.0	0.0	0.0	0.0	0.0	0.0
Total	100.022	99.665	99.092	99.997	100.615	99.541	101.401	99.870	99.571	100.305	100.667	100.687	100.171	99.896	101.125	100.564	100.692
Atoms per 8 oxygens																	
Si	2.192	2.195	2.154	2.174	2.143	2.175	2.165	2.125	2.133	2.179	2.149	2.185	2.177	2.180	2.191	2.208	2.182
Ti	0.001	0.0	0.0	0.0	0.0	0.0	0.0	0.001	0.0	0.0	0.0	0.0	0.0	0.0	0.0	0.0	0.0
Al	1.789	1.800	1.855	1.817	1.847	1.830	1.800	1.840	1.833	1.835	1.860	1.825	1.826	1.839	1.840	1.853	1.855
Fe	0.024	0.023	0.031	0.033	0.021	0.023	0.023	0.027	0.027	0.022	0.021	0.024	0.028	0.029	0.024	0.030	0.040
Mn	0.0	0.0	0.0	0.0	0.0	0.0	0.0	0.0	0.0	0.0	0.0	0.0	0.0	0.0	0.0	0.0	0.0
Mg	0.001	0.002	0.0	0.0	0.0	0.0	0.001	0.0	0.0	0.0	0.0	0.0	0.0	0.0	0.0	0.0	0.0
Ca	0.002	0.0	0.0	0.0	0.0	0.001	0.0	0.001	0.001	0.0	0.0	0.0	0.0	0.0	0.0	0.0	0.0
Na	1.514	1.479	1.408	1.464	1.501	1.433	1.559	1.581	1.574	1.392	1.414	1.404	1.424	1.367	1.330	1.199	1.282
K	0.288	0.287	0.342	0.320	0.340	0.325	0.328	0.336	0.336	0.343	0.368	0.331	0.336	0.338	0.339	0.350	0.343
Ba	0.0	0.0	0.0	0.0	0.0	0.0	0.0	0.0	0.0	0.0	0.0	0.0	0.0	0.0	0.0	0.0	0.0
Rock Type	GS-A	GS-A	CGBS	CGBS	CGBS	LSS	LSS	LSS	LSS	MMS	MMS	MMS	MMS	LSS	LSS	LSS	LSS
Crystal	14.	14.	4.	4.	5.	4.	4.	4.	4.	1.	1.	1.	1.	4.	6.	7.	7.
Position	-1.	-1.	7.	1.	7.	6.	1.	7.	4.	8.	8.	8.	8.	4.	3.	7.	1.

NEPHELINE ANALYSES

	44.19	44.20	44.21	44.22	44.23	37.24	37.25	37.26	138055.14	138055.15	138055.16	207.13	207.14	207.15	207.16	207.17	191.06
Weight % oxide																	
SiO2	45.628	45.967	42.781	46.186	45.508	46.213	45.674	46.322	45.186	45.380	45.739	46.942	46.337	46.628	46.402	43.467	46.860
TiO2	0.0	0.0	0.0	0.0	0.0	0.0	0.0	0.0	0.0	0.0	0.0	0.0	0.0	0.0	0.0	0.0	0.0
Al2O3	33.145	32.916	34.691	32.515	33.013	33.457	33.651	33.485	32.420	32.328	32.082	33.394	33.845	33.246	33.158	31.561	33.176
FeO	0.821	0.518	0.482	0.355	0.652	0.492	0.549	0.437	0.687	0.764	0.683	0.589	0.679	0.657	0.596	0.537	0.689
MnO	0.0	0.0	0.0	0.0	0.0	0.0	0.0	0.0	0.0	0.0	0.0	0.0	0.0	0.0	0.0	0.0	0.0
MgO	0.0	0.0	0.0	0.0	0.0	0.0	0.0	0.0	0.0	0.0	0.0	0.0	0.0	0.0	0.0	0.0	0.0
CaO	0.0	0.0	0.0	0.0	0.0	0.0	0.758	0.0	0.0	0.0	0.0	0.0	0.266	0.0	0.0	0.268	0.0
Na2O	15.817	14.726	13.462	15.456	15.402	14.935	14.060	15.758	14.702	14.567	13.968	14.224	15.195	15.248	15.403	13.965	15.680
K2O	5.831	5.659	4.142	5.406	5.611	5.972	5.729	5.970	5.517	5.716	5.273	5.597	5.939	5.989	5.946	5.810	5.890
BaO	0.0	0.0	0.0	0.0	0.0	0.0	0.0	0.0	0.0	0.0	0.0	0.0	0.0	0.0	0.0	0.0	0.0
Total	101.242	99.786	95.558	99.918	100.186	101.069	100.421	101.972	98.512	98.755	97.745	100.746	102.261	101.768	101.505	95.608	102.295
Atoms per 8 oxygens																	
Si	2.152	2.183	2.100	2.191	2.161	2.171	2.157	2.163	2.177	2.183	2.208	2.199	2.156	2.179	2.175	2.164	2.181
Ti	0.0	0.0	0.0	0.0	0.0	0.0	0.0	0.0	0.0	0.0	0.0	0.0	0.0	0.0	0.0	0.0	0.0
Al	1.843	1.843	2.007	1.819	1.848	1.853	1.873	1.844	1.841	1.833	1.826	1.844	1.857	1.832	1.832	1.852	1.820
Fe	0.032	0.021	0.020	0.014	0.026	0.019	0.022	0.017	0.028	0.031	0.028	0.023	0.026	0.026	0.023	0.022	0.027
Mn	0.0	0.0	0.0	0.0	0.0	0.0	0.0	0.0	0.0	0.0	0.0	0.0	0.0	0.0	0.0	0.0	0.0
Mg	0.0	0.0	0.0	0.0	0.0	0.0	0.0	0.0	0.0	0.0	0.0	0.0	0.0	0.0	0.0	0.0	0.0
Ca	0.0	0.0	0.0	0.0	0.0	0.0	0.038	0.0	0.0	0.0	0.0	0.0	0.013	0.0	0.0	0.014	0.0
Na	1.447	1.356	1.281	1.422	1.418	1.360	1.287	1.427	1.373	1.358	1.308	1.292	1.371	1.382	1.400	1.348	1.415
K	0.351	0.343	0.259	0.327	0.340	0.358	0.345	0.356	0.339	0.351	0.325	0.334	0.353	0.357	0.356	0.369	0.350
Ba	0.0	0.0	0.0	0.0	0.0	0.0	0.0	0.0	0.0	0.0	0.0	0.0	0.0	0.0	0.0	0.0	0.0
Rock Type	MMS	MMS	MMS	MMS	MMS	MMS	MMS	MMS	PEG	PEG	PEG	MUS	MUS	MUS	MUS	MUS	USS
Crystal	1.	1.	1.	1.	1.	1.	1.	1.	4.	4.	4.	4.	4.	5.	5.	6.	4.
Position	8.	7.	1.	4.	8.	8.	8.	8.	7.	4.	1.	1.	7.	1.	7.	7.	6.

NEPHELINE ANALYSES

	191.07	191.08	191.09	248.11	248.12	248.13	248.14	172.14	172.17	169.37	169.39	84.12	84.13	84.14	84.18	257.08	257.09
Weight % oxide																	
SiO2	46.017	45.251	46.203	45.567	44.676	45.435	44.479	46.459	46.187	47.163	47.554	44.884	45.545	45.177	45.592	44.121	42.919
TiO2	0.0	0.0	0.0	0.0	0.0	0.0	0.0	0.0	0.101	0.0	0.0	0.001	0.0	0.015	0.0	0.061	0.0
Al2O3	33.125	33.614	33.706	34.433	33.847	33.000	33.384	31.175	30.945	32.641	32.129	32.598	32.364	33.098	33.141	32.606	32.508
FeO	0.747	0.598	0.880	0.317	0.0	0.611	0.0	0.781	0.647	0.632	0.803	0.674	0.740	0.439	0.403	0.364	0.423
MnO	0.0	0.0	0.0	0.0	0.0	0.0	0.0	0.049	0.008	0.0	0.0	0.0	0.072	0.0	0.105	0.131	0.0
MgO	0.0	0.0	0.0	0.0	0.0	0.0	0.0	0.307	0.328	0.355	0.314	0.277	0.287	0.272	0.289	0.129	0.231
CaO	0.0	0.0	0.0	0.0	0.0	0.0	0.0	0.214	0.114	0.181	0.164	0.139	0.132	0.104	0.209	0.053	0.183
Na2O	15.110	15.506	15.146	15.193	14.870	15.220	14.344	16.173	15.851	16.335	16.393	15.834	16.231	16.170	15.722	15.891	15.601
K2O	5.942	6.501	6.162	6.804	6.798	6.045	6.078	4.791	4.469	5.042	4.666	6.133	5.611	6.017	5.781	6.313	6.361
BaO	0.0	0.0	0.0	0.0	0.0	0.0	0.0	0.0	0.0	0.0	0.0	0.0	0.0	0.0	0.0	0.0	0.0
Total	100.941	101.470	102.097	102.314	100.191	100.311	98.285	100.054	98.679	102.480	102.102	100.739	101.166	101.292	101.242	99.682	98.281
Atoms per 8 oxygens																	
Si	2.170	2.134	2.157	2.127	2.128	2.159	2.146	2.210	2.218	2.189	2.209	2.137	2.157	2.135	2.148	2.125	2.101
Ti	0.0	0.0	0.0	0.0	0.0	0.0	0.0	0.0	0.004	0.0	0.0	0.0	0.0	0.0	0.0	0.002	0.0
Al	1.841	1.869	1.855	1.895	1.901	1.849	1.899	1.748	1.752	1.786	1.760	1.830	1.807	1.844	1.841	1.852	1.876
Fe	0.029	0.024	0.034	0.012	0.0	0.024	0.0	0.031	0.026	0.025	0.031	0.027	0.029	0.017	0.016	0.015	0.017
Mn	0.0	0.0	0.0	0.0	0.0	0.0	0.0	0.002	0.0	0.0	0.0	0.0	0.003	0.0	0.004	0.005	0.0
Mg	0.0	0.0	0.0	0.0	0.0	0.0	0.0	0.022	0.023	0.025	0.022	0.020	0.020	0.019	0.020	0.009	0.017
Ca	0.0	0.0	0.0	0.0	0.0	0.0	0.0	0.011	0.006	0.009	0.008	0.007	0.007	0.005	0.011	0.003	0.010
Na	1.381	1.418	1.371	1.375	1.373	1.402	1.342	1.492	1.476	1.470	1.477	1.462	1.491	1.481	1.436	1.484	1.481
K	0.357	0.391	0.367	0.405	0.413	0.366	0.374	0.291	0.274	0.299	0.277	0.373	0.339	0.363	0.347	0.388	0.397
Ba	0.0	0.0	0.0	0.0	0.0	0.0	0.0	0.0	0.0	0.0	0.0	0.0	0.0	0.0	0.0	0.0	0.0
Rock Type	USS	USS	USS	MUS	MUS	MUS	MUS	GS-A	GS-A	GS-A	GS-A	GS-B	GS-B	GS-B	GS-B	GS-B	GS-B
Crystal	4.	5.	6.	4.	4.	5.	5.	14.	1.	4.	5.	1.	1.	1.	14.	4.	4.
Position	1.	4.	1.	7.	1.	7.	1.	-1.	8.	1.	6.	7.	1.	-1.	-1.	7.	1.

NEPHELINE ANALYSES

	257.10	257.11	257.15	186.16	186.17	178.03	178.04	178.05	178.08	178.09	178.10	178.11	275.16	275.17	275.18	135.04	135.05
Weight % oxide																	
SiO2	44.469	44.946	44.819	44.189	43.112	44.017	43.295	43.486	43.746	45.341	43.690	43.083	44.852	44.748	44.589	45.771	45.447
TiO2	0.147	0.0	0.0	0.0	0.0	0.119	0.0	0.0	0.052	0.035	0.038	0.057	0.015	0.0	0.0	0.065	0.004
Al2O3	32.095	32.468	31.827	32.334	33.119	32.623	32.325	32.328	32.997	31.352	32.754	32.409	32.106	32.009	32.305	32.471	32.757
FeO	0.757	0.504	0.633	0.512	0.292	0.510	0.323	0.307	0.706	1.348	0.555	0.294	0.679	0.712	0.423	0.944	0.736
MnO	0.069	0.0	0.064	0.057	0.0	0.0	0.0	0.051	0.007	0.146	0.061	0.060	0.0	0.040	0.101	0.006	0.0
MgO	0.330	0.314	0.408	0.365	0.373	0.352	0.279	0.232	0.367	0.466	0.453	0.331	0.277	0.201	0.397	0.253	0.278
CaO	0.052	0.083	0.247	0.036	0.089	0.358	0.893	0.190	0.381	0.532	0.145	0.195	0.094	0.016	0.005	0.038	0.110
Na2O	16.075	16.032	15.568	15.246	15.221	15.560	15.457	15.390	14.926	15.356	15.650	15.701	15.497	14.624	15.886	15.831	15.243
K2O	5.554	5.570	5.612	5.900	6.650	6.203	6.134	6.107	6.353	5.541	6.250	6.341	5.642	5.632	5.719	5.741	5.473
BaO	0.0	0.0	0.0	0.0	0.0	0.0	0.0	0.0	0.0	0.0	0.0	0.0	0.0	0.0	0.0	0.0	0.0
Total	99.735	99.917	99.258	98.649	99.018	99.823	98.738	98.121	99.641	100.148	99.704	98.659	99.170	98.051	99.487	101.153	100.253
Atoms per 8 oxygens																	
Si	2.139	2.148	2.159	2.140	2.093	2.117	2.108	2.124	2.108	2.171	2.107	2.102	2.159	2.172	2.143	2.163	2.160
Ti	0.005	0.0	0.0	0.0	0.0	0.004	0.0	0.0	0.002	0.001	0.001	0.002	0.0	0.0	0.0	0.002	0.0
Al	1.820	1.829	1.807	1.846	1.896	1.850	1.856	1.861	1.875	1.769	1.862	1.864	1.822	1.831	1.830	1.809	1.836
Fe	0.030	0.020	0.025	0.021	0.012	0.021	0.013	0.013	0.028	0.054	0.022	0.012	0.027	0.029	0.017	0.037	0.029
Mn	0.003	0.0	0.003	0.002	0.0	0.0	0.0	0.002	0.0	0.006	0.002	0.002	0.0	0.002	0.004	0.0	0.0
Mg	0.024	0.022	0.029	0.026	0.027	0.025	0.020	0.017	0.026	0.033	0.033	0.024	0.020	0.015	0.028	0.018	0.020
Ca	0.003	0.004	0.013	0.002	0.005	0.018	0.047	0.010	0.020	0.027	0.007	0.010	0.005	0.0	0.0	0.002	0.006
Na	1.500	1.486	1.454	1.432	1.433	1.451	1.459	1.457	1.395	1.425	1.464	1.486	1.446	1.376	1.480	1.451	1.405
K	0.341	0.340	0.345	0.365	0.412	0.381	0.381	0.381	0.391	0.338	0.385	0.395	0.346	0.349	0.351	0.346	0.332
Ba	0.0	0.0	0.0	0.0	0.0	0.0	0.0	0.0	0.0	0.0	0.0	0.0	0.0	0.0	0.0	0.0	0.0
Rock Type	GS-B	GS-B	GS-B	PMS	PMS	PMS	PMS	PMS	PMS	PMS	LSS	LSS	CGS	CGS	CGS	USS	USS
Crystal	10.	10.	1.	4.	4.	4.	4.	4.	5.	5.	6.	6.	1.	4.	4.	1.	1.
Position	7.	1.	8.	7.	1.	6.	4.	1.	7.	1.	7.	1.	8.	7.	1.	7.	1.

NEPHELINE ANALYSES

	135.06	135.07	118.09	118.10	118.11	202.14	202.15	152.12	152.13	152.14	152.15
Weight % oxide											
SiO2	45.007	46.130	45.616	46.352	47.283	44.340	43.902	44.507	45.283	44.583	45.251
TiO2	0.0	0.0	0.0	0.023	0.0	0.0	0.0	0.039	0.008	0.012	0.0
Al2O3	32.548	32.091	31.655	32.583	31.937	32.091	32.494	32.627	32.584	32.049	32.455
FeO	0.558	0.776	1.006	1.063	0.896	0.631	0.443	0.527	0.374	0.739	0.674
MnO	0.114	0.0	0.029	0.0	0.059	0.0	0.0	0.0	0.039	0.0	0.042
MgO	0.0	0.078	0.204	0.175	0.184	0.225	0.168	0.046	0.322	0.075	0.260
CaO	0.055	0.0	0.003	0.083	0.024	0.172	0.0	0.033	0.099	0.008	0.012
Na2O	15.578	16.035	15.730	15.998	15.869	14.783	15.286	15.292	16.025	15.507	15.579
K2O	6.017	5.370	5.373	5.704	5.142	5.483	6.015	6.066	5.929	6.179	5.814
BaO	0.0	0.0	0.0	0.0	0.0	0.0	0.0	0.0	0.0	0.0	0.0
Total	99.910	100.518	99.751	102.086	101.394	97.863	98.378	99.168	100.676	99.152	100.092
Atoms per 8 oxygens											
Si	2.154	2.187	2.184	2.170	2.215	2.159	2.134	2.145	2.151	2.154	2.159
Ti	0.0	0.0	0.0	0.0	0.0	0.0	0.0	0.001	0.0	0.0	0.0
Al	1.837	1.793	1.786	1.799	1.763	1.842	1.863	1.854	1.824	1.826	1.825
Fe	0.022	0.031	0.040	0.042	0.035	0.026	0.018	0.021	0.015	0.030	0.027
Mn	0.005	0.0	0.001	0.0	0.002	0.0	0.0	0.0	0.002	0.0	0.002
Mg	0.0	0.006	0.015	0.012	0.013	0.016	0.012	0.003	0.023	0.005	0.018
Ca	0.003	0.0	0.0	0.004	0.001	0.009	0.0	0.002	0.005	0.0	0.0
Na	1.446	1.474	1.460	1.452	1.441	1.395	1.441	1.429	1.476	1.453	1.441
K	0.367	0.325	0.328	0.341	0.307	0.341	0.373	0.373	0.359	0.381	0.354
Ba	0.0	0.0	0.0	0.0	0.0	0.0	0.0	0.0	0.0	0.0	0.0
Rock Type	PEG	USS	USS	USS	USS	PMS	PMS	PMS	PMS	PMS	PMS
Crystal	1.	1.	1.	1.	1.	4.	4.	4.	4.	5.	5.
Position	7.	1.	8.	8.	8.	7.	3.	7.	1.	7.	1.

GIESECKITE ANALYSES

	138048.27*	138046.17*	20.14	20.15	21.17	21.18	43.20	43.21	248.20
Weight % oxide									
SiO2	44.281	46.108	49.778	50.441	48.184	49.943	48.322	48.002	47.618
TiO2	0.0	0.006	0.0	0.0	0.0	0.0	0.0	0.0	0.0
Al2O3	30.299	34.469	32.961	33.738	35.001	32.831	34.361	34.910	32.028
FeO	0.563	0.673	1.084	1.095	0.727	0.808	1.221	1.792	1.035
MnO	0.047	0.033	0.0	0.0	0.0	0.217	0.0	0.0	0.0
MgO	0.015	0.018	0.0	0.0	0.0	0.0	0.0	0.0	0.0
CaO	0.056	0.185	0.956	0.242	0.576	1.027	0.0	0.0	0.465
Na2O	8.721	2.930	2.213	1.954	1.549	3.304	4.670	4.246	5.978
K2O	6.106	8.258	6.664	7.070	8.508	6.697	8.260	9.186	6.455
BaO	0.029	0.010	0.0	0.0	0.0	0.0	0.0	0.0	0.0
Total	90.117	92.690	93.656	94.540	94.545	94.827	96.834	98.136	93.579
Atoms per 8 oxygens									
Si	2.284	2.275	2.397	2.400	2.316	2.387	2.298	2.269	2.360
Ti	0.0	0.0	0.0	0.0	0.0	0.0	0.0	0.0	0.0
Al	1.843	2.005	1.871	1.893	1.984	1.850	1.926	1.946	1.852
Fe	0.024	0.028	0.044	0.044	0.029	0.032	0.049	0.071	0.042
Mn	0.002	0.001	0.0	0.0	0.0	0.009	0.0	0.0	0.0
Mg	0.001	0.001	0.0	0.0	0.0	0.0	0.0	0.0	0.0
Ca	0.003	0.010	0.049	0.012	0.030	0.053	0.0	0.0	0.024
Na	0.872	0.280	0.207	0.180	0.144	0.306	0.431	0.389	0.568
K	0.402	0.520	0.409	0.429	0.522	0.408	0.501	0.554	0.404
Ba	0.001	0.0	0.0	0.0	0.0	0.0	0.0	0.0	0.0
Rock Type	LSS	LSS	USS	USS	MUS	MUS	USS	USS	MUS
Crystal	8.	8.	8.	8.	8.	8.	1.	1.	8.
Position	-1.	-1.	-1.	-1.	-1.	-1.	7.	1.	-1.

FELDSPAR ANALYSES

	138044.26	138044.27	138044.28	138044.29	138044.30	138048.31	138048.28	138048.29	138048.30	138048.31	138048.32	138048.33	191.18	191.19	191.20	191.21	191.22
Weight % oxide																	
SiO2	60.624	63.763	62.258	64.027	61.178	63.177	63.566	62.793	63.363	64.852	63.158	63.524	61.845	61.574	64.036	63.326	63.921
TiO2	0.0	0.0	0.0	0.0	0.004	0.033	0.008	0.008	0.052	0.033	0.0	0.0	0.0	0.0	0.107	0.0	0.023
Al2O3	16.771	17.723	17.192	17.841	16.993	17.195	17.668	17.707	17.797	18.312	17.970	17.960	17.469	17.224	17.951	18.056	18.151
FeO	0.159	0.405	0.075	0.262	0.079	0.283	0.030	0.143	0.164	0.150	0.243	0.0	0.395	0.273	0.117	0.240	0.169
MnO	0.059	0.0	0.0	0.017	0.003	0.023	0.056	0.042	0.016	0.0	0.021	0.040	0.190	0.112	0.136	0.026	0.045
MgO	0.148	0.090	0.113	0.196	0.036	0.0	0.137	0.065	0.183	0.225	0.155	0.115	0.271	0.171	0.245	0.105	0.109
CaO	0.130	0.063	0.275	0.014	0.234	0.066	0.079	0.002	0.052	0.090	0.116	0.123	0.195	0.213	0.201	0.156	0.096
Na2O	1.856	2.047	4.410	5.896	1.799	2.651	4.661	4.740	6.040	8.165	6.413	6.795	2.518	3.948	3.303	4.014	4.560
K2O	12.798	13.709	9.711	7.778	13.407	12.274	9.475	9.014	7.379	4.098	6.482	5.967	12.057	9.775	11.711	10.463	10.024
BaO	0.011	0.029	0.0	0.150	0.0	0.0	0.004	0.145	0.0	0.0	0.136	0.0	0.301	0.137	0.007	0.017	0.041
Total	92.556	97.829	94.034	96.181	93.733	95.702	95.684	94.659	95.046	95.925	94.694	94.524	95.241	93.427	97.814	96.403	97.139
Atoms per 8 oxygens																	
Si	3.005	2.998	3.002	2.998	3.001	3.017	3.003	2.998	2.994	2.995	2.988	2.997	2.982	2.994	2.988	2.985	2.986
Ti	0.0	0.0	0.0	0.0	0.0	0.001	0.0	0.0	0.002	0.001	0.0	0.0	0.0	0.0	0.004	0.0	0.0
Al	0.980	0.982	0.977	0.985	0.983	0.968	0.984	0.997	0.991	0.997	1.002	0.999	0.993	0.987	0.988	1.003	1.000
Fe	0.007	0.016	0.003	0.010	0.003	0.011	0.001	0.006	0.006	0.006	0.010	0.0	0.016	0.011	0.005	0.009	0.007
Mn	0.002	0.0	0.0	0.0	0.0	0.0	0.002	0.002	0.0	0.0	0.0	0.002	0.008	0.005	0.005	0.001	0.002
Mg	0.011	0.006	0.008	0.014	0.003	0.0	0.010	0.005	0.013	0.015	0.011	0.008	0.019	0.012	0.017	0.007	0.008
Ca	0.007	0.003	0.014	0.0	0.012	0.003	0.004	0.0	0.003	0.004	0.006	0.006	0.010	0.011	0.010	0.008	0.005
Na	0.178	0.187	0.412	0.535	0.171	0.245	0.427	0.439	0.553	0.731	0.588	0.622	0.235	0.372	0.299	0.367	0.413
K	0.809	0.822	0.597	0.465	0.839	0.748	0.571	0.549	0.445	0.241	0.391	0.359	0.742	0.606	0.697	0.629	0.597
Ba	0.0	0.0	0.0	0.003	0.0	0.0	0.0	0.003	0.0	0.0	0.003	0.0	0.006	0.003	0.0	0.0	0.0
Rock Type	LSS	LSS	LSS	LSS	LSS	LSS	LSS	LSS	LSS	LSS	LSS	LSS	USS	USS	USS	USS	USS
Crystal	4.	4.	5.	5.	6.	6.	4.	4.	14.	14.	14.	14.	4.	4.	5.	5.	6.
Position	1.	1.	7.	1.	7.	1.	1.	7.	-1.	-1.	-1.	-1.	1.	7.	1.	7.	1.
Molecular percent																	
Ab	17.1	17.6	38.9	52.0	15.9	23.5	41.2	43.0	53.8	73.8	58.3	61.6	22.8	36.2	28.5	35.2	39.3
Or	82.2	82.1	59.7	48.0	82.9	76.2	58.4	57.0	45.9	25.8	41.1	37.7	76.2	62.6	70.5	64.0	60.2
An	0.7	0.3	1.4	0.0	1.2	0.3	0.4	0.0	0.3	0.4	0.6	0.6	1.0	1.1	1.0	0.8	0.5

FELDSPAR ANALYSES

	191.23	220.20	220.21	220.22	220.23	220.24	220.25	138012.12	138012.13	13012.14	138012.15	138012.16	138012.17	207.22	207.23	207.24	207.25
Weight % oxide																	
SiO2	64.486	64.360	64.274	61.708	64.996	64.110	64.762	63.349	64.748	64.698	64.424	65.428	65.010	64.774	65.580	64.878	64.173
TiO2	0.0	0.0	0.0	0.092	0.006	0.0	0.0	0.0	0.0	0.010	0.031	0.0	0.153	0.0	0.004	0.0	0.0
Al2O3	17.922	18.013	17.971	17.582	18.206	17.973	18.175	18.082	18.439	18.193	18.625	18.578	18.482	18.221	18.453	18.387	18.486
FeO	0.229	0.197	0.110	0.500	0.208	0.298	0.184	0.012	0.277	0.173	0.184	0.225	0.061	0.091	0.255	0.744	0.159
MnO	0.0	0.0	0.0	0.088	0.0	0.119	0.073	0.0	0.0	0.106	0.209	0.0	0.039	0.0	0.110	0.0	0.0
MgO	0.194	0.267	0.052	0.235	0.006	0.349	0.273	0.178	0.298	0.268	0.273	0.228	0.271	0.162	0.332	0.234	0.329
CaO	0.107	0.169	0.167	0.092	0.222	0.140	0.139	0.119	0.103	0.058	0.0	0.099	0.046	0.219	0.174	0.132	0.194
Na2O	5.609	4.391	4.383	3.493	6.513	1.855	5.797	5.695	8.699	9.607	10.556	9.583	8.509	6.517	6.871	9.038	4.200
K2O	8.048	10.024	9.912	11.036	7.109	13.868	8.467	7.619	3.221	2.306	0.100	2.561	3.935	6.894	6.659	3.171	10.192
BaO	0.308	0.001	0.079	0.023	0.0	0.264	0.021	0.0	0.078	0.0	0.0	0.111	0.0	0.159	0.098	0.162	0.082
Total	96.903	97.422	96.948	94.849	97.266	98.976	97.891	95.054	95.863	95.419	94.402	96.813	96.506	97.037	98.536	96.746	97.815
Atoms per 8 oxygens																	
Si	3.000	2.994	3.002	2.973	2.998	2.986	2.987	2.991	2.987	2.991	2.981	2.986	2.985	2.994	2.985	2.979	2.977
Ti	0.0	0.0	0.0	0.003	0.0	0.0	0.0	0.0	0.0	0.0	0.001	0.0	0.005	0.0	0.0	0.0	0.0
Al	0.983	0.988	0.990	0.999	0.990	0.987	0.988	1.006	1.003	0.991	1.016	0.999	1.000	0.993	0.990	0.995	1.011
Fe	0.009	0.008	0.004	0.020	0.008	0.012	0.007	0.0	0.011	0.007	0.007	0.009	0.002	0.004	0.010	0.029	0.006
Mn	0.0	0.0	0.0	0.004	0.0	0.005	0.003	0.0	0.0	0.004	0.008	0.0	0.002	0.0	0.004	0.0	0.0
Mg	0.013	0.019	0.004	0.017	0.0	0.024	0.019	0.013	0.020	0.018	0.019	0.016	0.019	0.011	0.023	0.016	0.023
Ca	0.005	0.008	0.008	0.005	0.011	0.007	0.007	0.006	0.005	0.003	0.0	0.005	0.002	0.011	0.008	0.006	0.010
Na	0.506	0.396	0.397	0.326	0.582	0.168	0.518	0.521	0.778	0.861	0.947	0.848	0.758	0.584	0.606	0.805	0.378
K	0.478	0.595	0.591	0.678	0.418	0.824	0.498	0.459	0.190	0.136	0.006	0.149	0.231	0.406	0.387	0.186	0.603
Ba	0.006	0.0	0.001	0.0	0.0	0.005	0.0	0.0	0.001	0.0	0.0	0.002	0.0	0.003	0.002	0.003	0.001
Rock Type	USS	LSS	LSS	LSS	LSS	LSS	LSS	CGBS	CGBS	CGBS	CGBS	CGBS	CGBS	MUS	MUS	MUS	MUS
Crystal	6.	4.	4.	14.	14.	5.	5.	1.	1.	1.	1.	1.	1.	1.	1.	4.	4.
Position	7.	1.	7.	-1.	-1.	1.	7.	7.	1.	8.	8.	8.	8.	7.	1.	1.	7.
Molecular percent																	
Ab	49.7	38.2	38.5	31.0	56.1	16.0	49.2	51.4	79.0	85.4	99.3	83.9	75.4	56.9	59.1	79.8	36.8
Or	49.8	60.9	60.7	68.5	42.8	83.3	50.1	48.0	20.5	14.3	0.7	15.6	24.4	42.0	40.0	19.6	62.2
An	0.5	0.8	0.8	0.5	1.1	0.7	0.7	0.6	0.5	0.3	0.0	0.5	0.2	1.1	0.8	0.6	1.0

FELDSPAR ANALYSES

	207.26	207.27	188.15	188.16	188.17	188.18	188.19	138001.22	138001.23	138001.24	138001.25	138001.26	138001.27	275.23	275.24	275.25	275.26
Weight % oxide																	
SiO2	64.005	62.596	62.974	64.983	64.091	62.580	66.382	65.698	64.540	64.057	63.888	63.780	63.120	61.484	63.724	62.905	63.253
TiO2	0.028	0.168	0.003	0.168	0.030	0.0	0.078	0.0	0.0	0.0	0.0	0.0	0.153	0.0	0.0	0.091	0.0
Al203	17.957	17.708	18.074	18.433	18.041	17.606	18.910	18.763	18.028	18.265	18.226	17.789	17.735	17.666	17.959	18.694	17.792
FeO	0.165	0.183	0.291	0.204	0.285	0.189	0.143	0.090	0.094	0.023	0.459	0.221	0.202	0.090	0.275	0.276	0.131
MnO	0.073	0.041	0.069	0.0	0.0	0.0	0.069	0.045	0.005	0.0	0.042	0.0	0.103	0.0	0.067	0.059	0.0
MgO	0.085	0.153	0.186	0.148	0.228	0.230	0.329	0.257	0.054	0.213	0.308	0.121	0.256	0.137	0.192	0.357	0.206
CaO	0.192	0.774	0.155	0.088	0.198	0.513	0.103	0.112	0.484	0.195	0.336	0.297	0.258	0.518	0.133	0.168	0.536
Na2O	5.719	5.456	5.727	5.858	5.251	3.370	8.966	10.639	8.171	6.680	5.578	5.437	3.078	2.954	7.683	5.070	7.444
K2O	7.589	7.983	7.783	7.760	8.656	10.951	3.564	0.094	4.103	6.294	8.172	8.423	11.878	11.914	4.688	8.308	4.998
BaO	0.065	0.017	0.0	0.0	0.023	0.0	0.133	0.0	0.164	0.192	0.045	0.181	0.012	0.578	0.109	0.824	0.079
Total	95.878	95.079	95.262	97.642	96.803	95.439	98.677	95.698	95.643	95.919	97.054	96.249	96.795	95.341	94.830	96.752	94.439
Atoms per 8 oxygens																	
Si	2.999	2.974	2.978	2.989	2.989	2.987	2.981	2.994	2.998	2.988	2.974	2.994	2.982	2.968	2.992	2.951	2.987
Ti	0.0	0.006	0.0	0.006	0.001	0.0	0.003	0.0	0.0	0.0	0.0	0.0	0.005	0.0	0.0	0.003	0.0
Al	0.992	0.992	1.008	1.000	0.992	0.991	1.001	1.008	0.987	1.004	1.000	0.985	0.988	1.005	0.994	1.034	0.991
Fe	0.006	0.007	0.012	0.008	0.011	0.008	0.005	0.003	0.004	0.0	0.018	0.009	0.008	0.004	0.011	0.011	0.005
Mn	0.003	0.002	0.003	0.0	0.0	0.0	0.003	0.002	0.0	0.0	0.002	0.0	0.004	0.0	0.003	0.002	0.0
Mg	0.006	0.011	0.013	0.010	0.016	0.016	0.022	0.017	0.004	0.015	0.021	0.008	0.018	0.010	0.013	0.025	0.014
Ca	0.010	0.039	0.008	0.004	0.010	0.026	0.005	0.005	0.024	0.010	0.017	0.015	0.013	0.027	0.007	0.008	0.027
Na	0.520	0.503	0.525	0.522	0.475	0.312	0.781	0.940	0.736	0.604	0.503	0.495	0.282	0.276	0.699	0.461	0.682
K	0.454	0.484	0.470	0.455	0.515	0.667	0.204	0.005	0.243	0.375	0.485	0.504	0.716	0.734	0.281	0.497	0.301
Ba	0.001	0.0	0.0	0.0	0.0	0.0	0.002	0.0	0.003	0.004	0.0	0.003	0.0	0.011	0.002	0.015	0.001
Rock Type	MUS	MUS	MUS	MUS	MUS	MUS	MUS	CGBS	CGBS	CGBS	CGBS	CGBS	CGBS	CGS	CGS	CGS	CGS
Crystal	5.	5.	4.	4.	4.	5.	5.	1.	1.	1.	1.	1.	1.	1.	1.	1.	1.
Position	1.	7.	1.	4.	7.	1.	7.	7.	4.	7.	1.	7.	1.	1.	7.	1.	7.
Molecular percent																	
Ab	51.4	47.6	50.9	51.7	46.0	29.8	77.9	98.9	72.2	59.7	48.6	47.3	26.7	25.5	69.6	46.3	66.2
Or	47.6	48.5	48.3	47.8	52.9	67.6	21.6	0.6	25.3	39.3	49.7	51.1	72.0	71.9	29.7	52.9	31.0
An	1.0	3.9	0.8	0.4	1.0	2.6	0.5	0.6	2.5	1.0	1.7	1.5	1.3	2.6	0.7	0.9	2.8

FELDSPAR ANALYSES

	275.27	275.28	43.22	43.23	43.24	43.25	43.26	43.27	43.28	38.29	38.30	38.31	38.32	38.33	38.34	38.35	64.22
Weight % oxide																	
SiO2	62.738	62.356	60.885	62.115	59.544	61.679	62.392	62.513	62.090	63.119	62.902	62.562	61.234	62.392	61.959	61.074	64.431
TiO2	0.0	0.192	0.040	0.018	0.0	0.0	0.0	0.0	0.0	0.0	0.063	0.049	0.0	0.0	0.0	0.0	0.0
Al2O3	17.658	17.820	17.165	17.431	18.206	17.472	17.624	17.431	17.388	17.403	17.564	17.627	17.067	17.615	17.531	17.038	17.934
FeO	0.093	0.195	0.190	0.0	0.117	0.095	0.090	0.188	0.063	0.301	0.135	0.166	0.021	0.102	0.056	0.283	0.264
MnO	0.108	0.068	0.0	0.0	0.038	0.084	0.020	0.0	0.0	0.0	0.160	0.039	0.072	0.0	0.0	0.0	0.0
MgO	0.178	0.344	0.0	0.127	0.106	0.190	0.164	0.123	0.046	0.126	0.031	0.230	0.167	0.064	0.179	0.184	0.032
CaO	0.250	0.471	0.048	0.085	0.670	0.146	0.220	0.077	0.062	0.072	0.069	0.165	0.122	0.062	0.124	0.134	0.137
Na2O	4.393	4.437	1.933	1.601	4.679	3.339	1.187	6.812	3.540	3.859	4.877	3.458	2.735	4.770	5.310	1.746	1.854
K2O	9.321	9.487	13.154	13.945	9.682	11.254	14.379	5.718	10.865	10.627	8.593	11.671	12.211	9.063	8.343	13.789	14.245
BaO	0.0	0.0	0.163	0.116	0.178	0.028	0.009	0.024	0.177	0.053	0.011	0.066	0.124	0.132	0.368	0.159	0.034
Total	94.739	95.370	93.578	95.438	93.220	94.287	96.085	92.886	94.231	95.560	94.405	96.033	93.753	94.200	93.870	94.407	98.931
Atoms per 8 oxygens																	
Si	2.994	2.967	2.993	2.996	2.921	2.986	2.992	3.003	3.000	3.004	3.004	2.981	2.994	2.995	2.986	2.989	2.999
Ti	0.0	0.007	0.001	0.0	0.0	0.0	0.0	0.0	0.0	0.0	0.002	0.002	0.0	0.0	0.0	0.0	0.0
Al	0.994	1.000	0.995	0.991	1.053	0.997	0.996	0.987	0.991	0.977	0.989	0.990	0.984	0.997	0.996	0.983	0.984
Fe	0.004	0.008	0.008	0.0	0.005	0.004	0.004	0.008	0.003	0.012	0.005	0.007	0.0	0.004	0.002	0.012	0.010
Mn	0.004	0.003	0.0	0.0	0.002	0.003	0.0	0.0	0.0	0.0	0.006	0.002	0.003	0.0	0.0	0.0	0.0
Mg	0.013	0.024	0.0	0.009	0.008	0.014	0.012	0.009	0.003	0.009	0.002	0.016	0.012	0.005	0.013	0.013	0.002
Ca	0.013	0.024	0.003	0.004	0.035	0.008	0.011	0.004	0.003	0.004	0.004	0.008	0.006	0.003	0.006	0.007	0.007
Na	0.407	0.409	0.184	0.150	0.445	0.313	0.110	0.634	0.332	0.356	0.452	0.320	0.259	0.444	0.496	0.166	0.167
K	0.568	0.576	0.825	0.858	0.606	0.695	0.880	0.350	0.670	0.645	0.523	0.710	0.762	0.555	0.513	0.861	0.846
Ba	0.0	0.0	0.003	0.002	0.003	0.0	0.0	0.0	0.003	0.0	0.0	0.001	0.002	0.002	0.007	0.003	0.0
Rock Type	CGS	CGS	USS	USS	USS	USS	USS	USS	USS	MMS	MMS	MMS	MMS	MMS	MMS	MMS	MMS
Crystal	1.	1.	4.	4.	4.	8.	8.	8.	8.	4.	4.	4.	5.	5.	1.	1.	1.
Position	1.	7.	1.	4.	7.	7.	1.	7.	1.	1.	4.	7.	1.	1.	8.	8.	8.
Molecular percent																	
Ab	39.8	39.1	17.3	14.1	39.6	29.6	10.4	62.8	31.7	34.1	44.7	29.6	24.1	42.9	47.4	15.3	15.6
Or	58.9	58.4	82.4	85.5	57.1	69.6	88.5	36.8	67.9	65.5	54.9	69.6	75.3	56.8	52.0	84.0	83.7
An	1.3	2.4	0.3	0.4	3.3	0.8	1.1	0.4	0.3	0.4	0.4	0.8	0.6	0.3	0.6	0.7	0.7

FELDSPAR ANALYSES

	64.23	64.24	64.25	64.26	44.24	44.24	44.25	44.26	44.27	44.28	197.18	197.19	197.20	197.21	197.22	197.23	64.22
Weight % oxide																	
SiO2	65.613	63.640	63.390	64.088	63.995	62.501	62.306	64.069	62.868	64.214	63.320	62.349	63.342	61.533	63.456	64.316	62.731
TiO2	0.0	0.0	0.063	0.086	0.0	0.003	0.170	0.095	0.140	0.072	0.0	0.061	0.133	0.044	0.0	0.0	0.200
Al2O3	18.416	17.787	17.561	17.787	17.876	17.473	17.235	17.708	17.357	17.759	17.935	17.733	18.076	17.497	17.979	17.593	17.424
FeO	0.210	0.283	0.443	0.198	0.199	0.415	0.441	0.298	0.077	0.139	0.055	0.126	0.142	0.011	0.039	0.553	0.271
MnO	0.080	0.048	0.0	0.100	0.109	0.066	0.025	0.002	0.0	0.0	0.0	0.0	0.0	0.090	0.0	0.0	0.0
MgO	0.066	0.120	0.191	0.011	0.003	0.114	0.039	0.166	0.115	0.154	0.022	0.121	0.258	0.065	0.144	0.212	0.0
CaO	0.0	0.130	0.104	0.142	0.044	0.199	0.037	0.022	0.002	0.117	0.0	0.133	0.0	0.036	0.069	0.121	0.044
Na2O	4.948	2.855	0.700	1.674	2.507	1.647	1.809	10.318	2.771	3.410	4.305	2.307	4.311	2.864	6.606	7.566	1.289
K2O	9.514	12.689	16.022	14.110	13.160	14.300	13.660	0.170	12.597	11.698	9.850	12.773	9.307	11.581	5.874	4.851	14.461
BaO	0.307	0.271	0.0	0.176	0.110	0.027	0.0	0.0	0.0	0.025	0.690	0.384	0.149	0.492	0.619	0.002	0.0
Total	99.154	97.823	98.474	98.372	98.003	96.745	95.722	92.848	95.927	97.588	96.177	95.987	95.718	94.213	94.786	95.214	96.420
Atoms per 8 oxygens																	
Si	2.997	2.990	2.990	3.001	2.998	2.987	2.997	3.011	3.001	3.001	2.995	2.985	2.989	2.990	2.996	3.008	2.999
Ti	0.0	0.0	0.002	0.003	0.0	0.0	0.006	0.003	0.005	0.003	0.0	0.002	0.005	0.002	0.0	0.0	0.007
Al	0.992	0.985	0.977	0.982	0.987	0.984	0.977	0.981	0.977	0.978	1.000	1.001	1.006	1.002	1.001	0.970	0.982
Fe	0.008	0.011	0.017	0.008	0.008	0.017	0.018	0.012	0.003	0.005	0.002	0.005	0.006	0.0	0.002	0.022	0.011
Mn	0.003	0.002	0.0	0.004	0.004	0.003	0.001	0.0	0.0	0.0	0.0	0.0	0.0	0.004	0.0	0.0	0.0
Mg	0.004	0.008	0.013	0.0	0.0	0.008	0.003	0.012	0.008	0.011	0.002	0.009	0.018	0.005	0.010	0.015	0.0
Ca	0.0	0.007	0.005	0.007	0.002	0.010	0.002	0.001	0.0	0.006	0.0	0.007	0.0	0.002	0.003	0.006	0.002
Na	0.438	0.260	0.064	0.152	0.228	0.153	0.169	0.940	0.256	0.309	0.395	0.214	0.394	0.270	0.605	0.686	0.119
K	0.554	0.760	0.964	0.843	0.786	0.872	0.838	0.010	0.767	0.697	0.594	0.780	0.560	0.718	0.354	0.289	0.882
Ba	0.005	0.005	0.0	0.003	0.002	0.0	0.0	0.0	0.0	0.0	0.013	0.007	0.003	0.009	0.011	0.0	0.0
Rock Type	MMS	MMS	MMS	MMS	MMS	MMS	MMS	MMS	MMS	MMS	ALGN	ALGN	ALGN	ALGN	ALGN	ALGN	MMS
Crystal	1.	1.	1.	1.	1.	1.	1.	1.	1.	1.	1.	1.	1.	1.	1.	1.	1.
Position	8.	8.	8.	8.	8.	8.	8.	8.	7.	1.	7.	1.	8.	8.	8.	8.	8.
Molecular percent																	
Ab	42.7	24.2	5.9	14.4	21.4	14.1	15.9	98.8	23.9	29.3	38.5	20.4	39.9	26.1	61.5	68.7	11.3
Or	57.3	75.1	93.7	84.9	78.4	85.0	83.9	1.1	76.1	70.1	61.5	78.9	60.1	73.7	38.2	30.7	88.5
An	0.0	0.7	0.5	0.7	0.2	1.0	0.2	0.1	0.0	0.6	0.0	0.7	0.0	0.2	0.3	0.6	0.2

FELDSPAR ANALYSES

	64.23	64.24	64.25	64.26	64.27	41.15	41.16	41.17	41.18	41.19	41.20	41.21	41.22	145.30	145.31	145.32	145.33
Weight % oxide																	
SiO2	62.816	64.873	63.586	63.089	63.241	62.712	65.598	63.598	64.464	63.153	61.876	64.248	62.771	63.683	63.852	64.049	62.881
TiO2	0.188	0.0	0.181	0.0	0.0	0.115	0.0	0.0	0.070	0.136	0.0	0.0	0.0	0.0	0.098	0.0	0.104
Al2O3	17.825	18.041	17.654	17.683	17.814	18.261	18.510	18.159	18.071	17.618	17.031	18.384	17.739	18.210	18.234	18.481	17.978
FeO	0.212	0.259	0.412	0.123	0.068	0.789	0.260	0.437	0.046	0.271	0.811	0.194	0.548	0.119	0.254	0.255	0.187
MnO	0.018	0.0	0.076	0.045	0.0	0.042	0.096	0.044	0.038	0.321	0.0	0.087	0.0	0.0	0.014	0.073	0.013
MgO	0.167	0.061	0.139	0.137	0.151	0.057	0.242	0.074	0.0	0.227	0.109	0.083	0.076	0.090	0.081	0.138	0.084
CaO	0.119	0.158	0.039	0.121	0.092	0.179	0.079	0.128	0.069	0.218	0.292	0.324	0.243	0.099	0.243	0.138	0.242
Na2O	2.035	7.358	3.176	2.824	1.545	3.167	8.407	2.591	7.681	1.875	1.292	4.507	0.667	3.834	4.801	3.534	4.356
K2O	13.672	5.534	11.796	12.016	14.189	11.386	3.946	12.327	4.550	13.763	14.482	9.980	15.519	10.966	9.153	11.599	9.592
BaO	0.0	0.0	0.0	0.065	0.169	0.0	0.037	0.035	0.0	0.0	0.122	0.021	0.143	0.245	0.0	0.211	0.0
Total	97.052	96.284	97.059	96.103	97.269	96.708	97.175	97.393	94.989	97.582	96.015	97.828	97.706	97.246	96.730	98.478	95.437
Atoms per 8 oxygens																	
Si	2.979	3.004	2.994	2.998	2.994	2.965	2.993	2.987	3.007	2.984	2.990	2.980	2.983	2.984	2.984	2.974	2.984
Ti	0.007	0.0	0.006	0.0	0.0	0.004	0.0	0.0	0.002	0.005	0.0	0.0	0.0	0.0	0.003	0.0	0.004
Al	0.997	0.985	0.980	0.991	0.994	1.018	0.996	1.005	0.994	0.981	0.970	1.005	0.994	1.006	1.005	1.012	1.006
Fe	0.008	0.010	0.016	0.005	0.003	0.031	0.010	0.017	0.002	0.011	0.033	0.008	0.022	0.005	0.010	0.010	0.007
Mn	0.0	0.0	0.003	0.002	0.0	0.002	0.004	0.002	0.002	0.013	0.0	0.003	0.0	0.0	0.0	0.003	0.0
Mg	0.012	0.004	0.010	0.010	0.011	0.004	0.016	0.005	0.0	0.016	0.008	0.006	0.005	0.006	0.006	0.010	0.006
Ca	0.006	0.008	0.002	0.006	0.005	0.009	0.004	0.006	0.003	0.011	0.015	0.016	0.012	0.005	0.012	0.007	0.012
Na	0.187	0.661	0.290	0.260	0.142	0.290	0.744	0.236	0.695	0.172	0.121	0.405	0.061	0.348	0.435	0.318	0.401
K	0.827	0.327	0.709	0.728	0.857	0.687	0.230	0.739	0.271	0.830	0.893	0.591	0.941	0.656	0.546	0.687	0.581
Ba	0.0	0.0	0.0	0.001	0.003	0.0	0.0	0.0	0.0	0.0	0.002	0.0	0.003	0.004	0.0	0.004	0.0
Rock Type	MMS	MMS	MMS	MMS	MMS	XPS	XPS	XPS	XPS	XPS	XPS	XPS	XPS	XPS	XPS	XPS	XPS
Crystal	1.	1.	1.	1.	1.	4.	4.	5.	5.	9.	9.	6.	1.	4.	4.	4.	1.
Position	8.	8.	8.	8.	8.	7.	1.	7.	1.	9.	9.	1.	8.	1.	4.	7.	8.
Molecular percent																	
Ab	17.5	65.0	27.8	25.0	13.4	28.2	75.0	23.0	70.5	16.2	11.2	38.6	5.7	33.2	42.4	30.2	38.9
Or	81.9	34.1	72.0	74.4	86.1	70.9	24.6	76.4	29.2	82.7	87.4	59.8	93.1	66.3	56.4	69.1	59.8
An	0.6	0.8	0.2	0.6	0.5	0.9	0.4	0.6	0.3	1.1	1.5	1.6	1.2	0.5	1.2	0.7	1.2

FELDSPAR ANALYSES

	145.34	145.35	169.42	169.43	42.44	169.45	169.46	169.47	169.48	172.25	172.26	172.27	172.28	172.29	172.30	172.31	172.32
Weight % oxide																	
SiO2	65.604	64.117	62.663	61.648	62.237	64.449	64.781	64.143	65.077	63.606	64.960	64.642	62.403	59.368	64.612	63.280	61.112
TiO2	0.0	0.0	0.0	0.0	0.0	0.100	0.076	0.014	0.022	0.095	0.062	0.030	0.0	0.002	0.0	0.0	0.116
Al2O3	18.797	18.425	17.451	17.079	17.668	18.260	18.292	18.192	18.486	17.861	18.736	18.100	17.497	16.859	18.119	17.916	16.635
FeO	0.183	0.250	0.0	0.305	0.003	0.0	0.155	0.110	0.085	0.0	0.281	0.134	0.112	0.141	0.036	0.196	0.033
MnO	0.014	0.0	0.052	0.0	0.051	0.0	0.0	0.007	0.055	0.006	0.0	0.073	0.070	0.030	0.079	0.0	0.0
MgO	0.208	0.140	0.099	0.001	0.090	0.162	0.103	0.209	0.115	0.262	0.295	0.0	0.260	0.152	0.166	0.135	0.115
CaO	0.043	0.155	0.214	0.109	0.026	0.0	0.001	0.0	0.076	0.110	0.095	0.046	0.105	0.0	0.057	0.156	0.197
Na2O	10.812	4.955	2.234	2.840	5.514	9.631	9.083	8.563	10.277	4.391	10.545	8.229	4.038	1.272	9.760	8.250	3.226
K2O	0.049	9.012	13.040	12.080	7.956	1.412	2.671	2.977	0.400	9.808	0.057	3.584	10.033	14.042	0.832	3.494	10.421
BaO	0.052	0.172	0.165	0.350	0.145	0.0	0.222	0.0	0.013	0.0	0.004	0.180	0.008	0.159	0.016	0.152	0.057
Total	95.762	97.226	95.918	94.412	93.690	94.014	95.384	94.215	94.606	96.139	95.035	95.018	94.526	92.025	93.677	93.579	91.912
Atoms per 8 oxygens																	
Si	2.990	2.982	2.999	2.999	2.992	3.001	2.997	2.999	3.001	2.994	2.984	3.008	2.994	2.984	3.011	2.994	3.017
Ti	0.0	0.0	0.0	0.0	0.0	0.004	0.003	0.0	0.0	0.003	0.002	0.001	0.0	0.0	0.0	0.0	0.004
Al	1.010	1.010	0.985	0.979	1.001	1.002	0.998	1.003	1.005	0.991	1.014	0.993	0.990	0.999	0.995	0.999	0.968
Fe	0.007	0.010	0.0	0.012	0.0	0.0	0.006	0.004	0.003	0.0	0.011	0.005	0.004	0.006	0.001	0.008	0.001
Mn	0.0	0.0	0.002	0.0	0.002	0.0	0.0	0.0	0.002	0.0	0.0	0.003	0.003	0.001	0.003	0.0	0.0
Mg	0.014	0.010	0.007	0.0	0.006	0.011	0.007	0.015	0.008	0.018	0.020	0.0	0.019	0.011	0.012	0.010	0.008
Ca	0.002	0.008	0.011	0.006	0.001	0.0	0.0	0.0	0.004	0.006	0.005	0.002	0.005	0.0	0.003	0.008	0.010
Na	0.956	0.447	0.207	0.268	0.514	0.869	0.815	0.776	0.919	0.401	0.939	0.743	0.376	0.124	0.882	0.757	0.309
K	0.003	0.535	0.796	0.750	0.488	0.084	0.158	0.178	0.024	0.589	0.003	0.213	0.614	0.900	0.049	0.211	0.656
Ba	0.0	0.003	0.003	0.007	0.003	0.0	0.004	0.0	0.0	0.0	0.0	0.003	0.0	0.003	0.0	0.003	0.001
Rock Type	XPS	XPS	GS-A	GS-A	GS-A	GS-A	GS-A	GS-A	GS-A	GS-A	GS-A	GS-A	GS-A	GS-A	GS-A	GS-A	GS-A
Crystal	1.	1.	4.	4.	5.	5.	1.	1.	1.	4.	4.	1.	1.	1.	1.	5.	5.
Position	8.	8.	6.	1.	1.	7.	8.	8.	8.	7.	1.	8.	7.	1.	1.	7.	8.
Molecular percent																	
Ab	99.4	43.7	19.5	25.1	49.8	90.7	82.9	80.4	96.9	38.9	99.1	76.5	36.4	11.5	94.1	76.5	30.4
Or	0.3	55.5	79.4	74.4	50.1	9.3	17.1	19.6	2.7	60.5	0.3	23.3	63.1	88.5	5.5	22.6	68.5
An	0.2	0.8	1.1	0.6	0.1	0.0	0.0	0.0	0.4	0.6	0.6	0.2	0.5	0.0	0.3	0.9	1.0

FELDSPAR ANALYSES

	168.19	68.20	168.21	168.22	168.23	168.24	84.21	84.22	84.23	84.24	84.25	84.26	186.18	186.19	186.20	186.21	186.23
Weight % oxide																	
SiO2	63.857	61.614	62.456	61.902	62.274	63.557	63.651	64.284	65.093	65.434	64.020	64.072	61.906	62.302	62.176	63.455	64.532
TiO2	0.0	0.0	0.077	0.116	0.0	0.157	0.155	0.077	0.037	0.0	0.0	0.016	0.0	0.0	0.0	0.0	0.0
Al2O3	17.966	17.389	17.765	17.877	17.758	18.362	18.192	18.312	18.466	18.844	18.668	18.244	17.768	17.667	18.336	17.961	18.167
FeO	0.044	0.011	0.207	0.082	0.0	0.662	0.377	0.168	0.0	0.084	0.0	0.135	0.312	0.027	0.0	0.109	0.187
MnO	0.0	0.123	0.0	0.0	0.065	0.064	0.010	0.070	0.111	0.0	0.013	0.0	0.0	0.084	0.0	0.0	0.015
MgO	0.147	0.181	0.141	0.327	0.103	0.477	0.314	0.108	0.200	0.220	0.219	0.200	0.150	0.185	0.332	0.193	0.228
CaO	0.098	0.235	0.240	0.204	0.160	0.152	0.197	0.242	0.118	0.174	0.295	0.226	0.320	0.265	0.160	0.113	0.203
Na2O	7.216	0.945	3.386	2.032	3.112	6.032	3.843	5.028	7.052	6.461	7.653	3.796	1.139	1.593	6.075	5.227	7.298
K2O	5.535	15.223	11.436	13.746	11.718	7.891	10.923	9.382	5.742	6.909	5.277	11.300	14.779	14.188	7.585	8.615	5.141
BaO	0.0	0.068	0.044	0.0	0.0	0.193	0.0	0.0	0.0	0.048	0.090	0.049	0.0	0.253	0.114	0.0	0.048
Total	94.863	95.789	95.752	96.286	95.190	97.547	97.662	97.671	96.819	98.174	96.235	98.038	96.374	96.564	94.778	95.673	95.819
Atoms per 8 oxygens																	
Si	2.998	2.983	2.980	2.964	2.986	2.952	2.971	2.980	2.994	2.983	2.969	2.980	2.973	2.981	2.957	2.991	2.996
Ti	0.0	0.0	0.003	0.004	0.0	0.005	0.005	0.003	0.001	0.0	0.0	0.0	0.0	0.0	0.0	0.0	0.0
Al	0.995	0.992	0.999	1.009	1.004	1.005	1.001	1.001	1.001	1.013	1.021	1.000	1.006	0.997	1.028	0.998	0.994
Fe	0.002	0.0	0.008	0.003	0.0	0.026	0.015	0.007	0.0	0.003	0.0	0.005	0.013	0.001	0.0	0.004	0.007
Mn	0.0	0.005	0.0	0.0	0.003	0.003	0.0	0.003	0.004	0.0	0.0	0.0	0.0	0.003	0.0	0.0	0.0
Mg	0.010	0.013	0.010	0.023	0.007	0.033	0.022	0.007	0.014	0.015	0.015	0.014	0.011	0.013	0.024	0.014	0.016
Ca	0.005	0.012	0.012	0.010	0.008	0.008	0.010	0.012	0.006	0.009	0.015	0.011	0.016	0.014	0.008	0.006	0.010
Na	0.657	0.089	0.313	0.189	0.289	0.543	0.348	0.452	0.629	0.571	0.688	0.342	0.106	0.148	0.560	0.478	0.657
K	0.332	0.940	0.696	0.840	0.717	0.468	0.650	0.555	0.337	0.402	0.312	0.671	0.905	0.866	0.460	0.518	0.305
Ba	0.0	0.001	0.0	0.0	0.0	0.004	0.0	0.0	0.0	0.0	0.002	0.0	0.0	0.005	0.002	0.0	0.0
Rock Type	GS-B	GS-B	GS-B	GS-B	GS-B	GS-B	GS-B	GS-B	GS-B	GS-B	GS-B	GS-B	PMS	PMS	PMS	PMS	PMS
Crystal	1.	4.	4.	5.	1.	1.	14.	14.	1.	14.	14.	14.	4.	4.	5.	5.	6.
Position	8.	1.	7.	7.	8.	8.	-1.	-1.	8.	-1.	-1.	-1.	7.	1.	7.	1.	7.
Molecular percent																	
Ab	64.8	8.1	29.4	17.3	27.3	51.8	33.2	42.9	63.4	56.7	66.5	32.1	9.8	13.7	53.0	46.2	66.3
Or	34.7	90.7	69.4	81.7	71.9	47.4	65.8	55.9	36.0	42.3	32.0	66.8	88.6	84.9	46.2	53.1	32.6
An	0.5	1.2	1.2	1.0	0.8	0.8	1.0	1.2	0.6	0.9	1.5	1.1	1.6	1.4	0.8	0.6	1.1

FELDSPAR ANALYSES

	186.24	178.21	178.22	178.26	178.27	178.28	178.29	178.30	239.17	239.18	239.19	239.20	239.21	146.17	146.18	146.19	146.20
Weight % oxide																	
SiO2	62.093	62.026	62.545	62.690	61.546	59.659	63.028	63.120	65.911	65.119	64.021	59.805	64.779	66.701	65.297	66.486	66.544
TiO2	0.0	0.091	0.010	0.0	0.0	0.137	0.105	0.105	0.0	0.018	0.108	0.094	0.047	0.098	0.0	0.0	0.105
Al2O3	17.667	18.292	17.972	17.769	19.136	19.769	18.146	17.813	20.141	19.625	18.284	22.349	20.050	19.036	18.630	19.111	18.781
FeO	0.254	0.157	0.225	0.187	0.275	0.204	0.175	0.335	0.050	0.130	0.325	0.105	0.0	0.666	1.044	0.0	0.232
MnO	0.0	0.067	0.037	0.0	0.049	0.0	0.0	0.0	0.0	0.042	0.0	0.001	0.115	0.020	0.062	0.018	0.0
MgO	0.238	0.325	0.208	0.331	0.353	0.321	0.347	0.260	0.463	0.133	0.308	0.349	0.234	0.352	0.281	0.280	0.324
CaO	0.187	0.254	0.233	0.286	0.234	0.270	0.393	0.337	1.306	1.142	0.317	4.187	1.202	0.0	0.0	0.0	0.0
Na2O	3.368	3.776	3.688	1.574	2.443	3.923	2.003	1.468	10.132	9.876	4.752	8.326	10.001	11.021	10.756	10.758	10.620
K2O	11.214	10.530	10.973	14.071	13.867	12.057	13.615	14.094	0.127	0.164	9.817	1.123	0.199	0.147	0.115	0.088	0.155
BaO	0.097	0.164	0.215	0.012	0.156	0.235	0.0	0.0	0.159	0.292	0.0	0.317	0.0	0.0	0.0	0.0	0.0
Total	95.118	95.682	96.106	96.920	98.059	96.575	97.812	97.532	98.289	96.541	97.932	96.656	96.627	98.041	96.185	96.741	96.761
Atoms per 8 oxygens																	
Si	2.981	2.955	2.973	2.981	2.909	2.858	2.966	2.982	2.937	2.954	2.969	2.761	2.934	2.980	2.978	2.993	2.999
Ti	0.0	0.003	0.0	0.0	0.0	0.005	0.004	0.004	0.0	0.0	0.004	0.003	0.002	0.003	0.0	0.0	0.004
Al	1.000	1.027	1.007	0.996	1.066	1.116	1.007	0.992	1.058	1.050	1.000	1.216	1.071	1.002	1.002	1.014	0.998
Fe	0.010	0.006	0.009	0.007	0.011	0.008	0.007	0.013	0.002	0.005	0.013	0.004	0.0	0.025	0.040	0.0	0.009
Mn	0.0	0.003	0.001	0.0	0.002	0.0	0.0	0.0	0.0	0.002	0.0	0.0	0.004	0.0	0.002	0.0	0.0
Mg	0.017	0.023	0.015	0.023	0.025	0.023	0.024	0.018	0.031	0.009	0.021	0.024	0.016	0.023	0.019	0.019	0.022
Ca	0.010	0.013	0.012	0.015	0.012	0.014	0.020	0.017	0.062	0.056	0.016	0.207	0.058	0.0	0.0	0.0	0.0
Na	0.313	0.349	0.340	0.145	0.224	0.364	0.183	0.134	0.875	0.869	0.427	0.745	0.878	0.955	0.951	0.939	0.928
K	0.687	0.640	0.665	0.853	0.836	0.737	0.817	0.849	0.007	0.009	0.581	0.066	0.011	0.008	0.007	0.005	0.009
Ba	0.002	0.003	0.004	0.0	0.003	0.004	0.0	0.0	0.003	0.005	0.0	0.006	0.0	0.0	0.0	0.0	0.0
Rock Type	PMS	PMS	PMS	PMS	PMS	PMS	PMS	PMS	ALGN	ALGN	ALGN	ALGN	ALGN	ALGN	ALGN	ALGN	ALGN
Crystal	6.	4.	4.	5.	5.	1.	1.	1.	1.	1.	1.	1.	1.	1.	1.	1.	1.
Position	1.	7.	1.	1.	7.	8.	8.	8.	8.	8.	8.	8.	8.	7.	1.	7.	1.
Molecular percent																	
Ab	29.7	33.5	32.1	13.6	19.9	31.4	17.1	12.7	92.3	92.7	40.3	72.0	92.3	99.1	99.2	99.4	99.0
Or	69.2	65.2	66.7	84.9	78.9	67.4	80.9	85.6	0.8	1.0	58.1	6.8	1.2	0.9	0.8	0.6	1.0
An	1.0	1.3	1.2	1.5	1.1	1.3	2.0	1.7	6.9	6.3	1.6	21.2	6.5	0.0	0.0	0.0	0.0

FELDSPAR ANALYSES

	146.21	74.13	74.14	74.15	74.16	272.14	272.15	272.16	272.17	272.18	272.18	52.16	52.18	52.19	52.20	52.21	52.22
Weight % oxide																	
SiO2	67.344	64.509	64.583	64.996	64.845	65.400	65.242	61.023	60.396	62.909	60.849	63.293	66.289	62.175	66.442	62.455	62.429
TiO2	0.0	0.127	0.0	0.0	0.025	0.0	0.0	0.006	0.0	0.019	0.0	0.071	0.0	0.0	0.0	0.013	0.0
Al2O3	19.105	18.160	18.234	17.747	18.023	18.245	18.251	17.149	16.708	17.380	17.072	17.770	18.683	17.481	18.676	17.418	17.579
FeO	0.156	0.191	0.078	0.0	0.0	0.126	0.033	0.125	0.233	0.764	0.080	0.042	0.220	0.0	0.046	0.124	0.062
MnO	0.0	0.004	0.0	0.111	0.0	0.110	0.0	0.0	0.057	0.064	0.053	0.0	0.141	0.033	0.115	0.012	0.0
MgO	0.317	0.215	0.254	0.044	0.105	0.166	0.057	0.063	0.0	0.150	0.151	0.147	0.336	0.181	0.250	0.101	0.093
CaO	0.027	0.052	0.035	0.280	0.055	0.0	0.040	0.0	0.008	0.167	0.0	0.202	0.187	0.455	0.276	0.267	0.187
Na2O	11.014	10.297	10.416	10.474	10.417	10.805	10.212	0.332	0.371	5.591	5.598	5.409	10.984	0.268	10.666	1.554	0.224
K2O	0.095	0.043	0.072	0.085	0.016	0.097	0.074	15.512	15.842	7.896	7.262	7.800	0.124	16.239	0.039	14.413	16.168
BaO	0.046	0.0	0.022	0.0	0.0	0.154	0.229	0.306	0.135	0.082	0.0	0.022	0.0	0.415	0.031	0.251	0.182
Total	98.104	93.598	93.694	93.737	93.486	95.103	94.138	94.516	93.750	95.022	91.065	94.756	96.964	97.247	96.541	96.608	96.924
Atoms per 8 oxygens																	
Si	2.995	3.003	3.003	3.022	3.017	3.005	3.018	2.997	2.999	2.993	3.000	2.999	2.990	2.981	3.001	2.990	2.992
Ti	0.0	0.004	0.0	0.0	0.0	0.0	0.0	0.0	0.0	0.0	0.0	0.003	0.0	0.0	0.0	0.0	0.0
Al	1.002	0.997	1.000	0.973	0.989	0.988	0.995	0.993	0.978	0.975	0.992	0.993	0.994	0.988	0.995	0.983	0.993
Fe	0.006	0.007	0.003	0.0	0.0	0.005	0.001	0.005	0.010	0.030	0.003	0.002	0.008	0.0	0.002	0.005	0.002
Mn	0.0	0.0	0.0	0.004	0.0	0.004	0.0	0.0	0.002	0.003	0.002	0.0	0.005	0.001	0.004	0.0	0.0
Mg	0.021	0.015	0.018	0.003	0.007	0.011	0.004	0.005	0.0	0.011	0.011	0.010	0.023	0.013	0.017	0.007	0.007
Ca	0.001	0.003	0.002	0.014	0.003	0.0	0.002	0.0	0.0	0.009	0.0	0.010	0.009	0.023	0.013	0.014	0.010
Na	0.950	0.929	0.939	0.944	0.940	0.963	0.916	0.032	0.036	0.516	0.535	0.497	0.961	0.025	0.934	0.144	0.021
K	0.005	0.003	0.004	0.005	0.0	0.006	0.004	0.972	1.004	0.479	0.457	0.472	0.007	0.993	0.002	0.880	0.988
Ba	0.0	0.0	0.0	0.0	0.0	0.003	0.004	0.006	0.003	0.002	0.0	0.0	0.0	0.008	0.0	0.005	0.003
Rock Type	ALGN	CBT	CBT	CBT	CBT	ALSY	ALSY	ALSY	ALSY	ALSY	ALSY	CBT	CBT	CBT	CBT	CBT	CBT
Crystal	1.	1.	1.	1.	1.	4.	4.	1.	1.	5.	5.	1.	1.	1.	1.	1.	1.
Position	7.	8.	8.	8.	8.	7.	1.	8.	8.	7.	1.	8.	8.	8.	7.	1.	7.
Molecular percent																	
Ab	99.3	99.3	99.3	97.9	99.7	99.3	99.3	3.0	3.3	49.9	52.5	49.3	98.3	2.3	98.3	13.2	1.9
Or	0.6	0.3	0.4	0.6	0.0	0.7	0.5	97.0	96.7	49.2	47.5	49.7	0.8	95.5	0.2	85.5	97.1
An	0.1	0.3	0.2	1.5	0.3	0.0	0.2	0.0	0.0	0.9	0.0	1.1	1.0	2.2	1.5	1.4	1.0

FELDSPAR ANALYSES

	103.14	103.15	103.16	103.17	103.18	107.15	107.16	107.17
Weight % oxide								
SiO2	66.028	62.161	65.855	65.321	62.084	67.298	66.593	66.139
TiO2	0.0	0.0	0.141	0.0	0.017	0.149	0.074	0.0
Al2O3	18.395	17.264	18.687	18.605	17.457	18.759	18.365	18.421
FeO	0.0	0.017	0.0	0.864	0.0	0.147	0.024	0.195
MnO	0.112	0.030	0.081	0.171	0.002	0.0	0.021	0.0
MgO	0.086	0.124	0.072	0.293	0.062	0.215	0.126	0.176
CaO	0.151	0.375	0.283	0.151	0.306	0.006	0.121	0.080
Na2O	10.380	0.373	10.726	10.568	0.441	10.885	11.020	10.588
K2O	0.025	15.932	0.050	0.104	15.515	0.0	0.077	0.0
BaO	0.081	0.481	0.0	0.063	0.099	0.0	0.0	0.095
Total	95.258	96.757	95.895	96.140	95.983	97.459	96.421	95.694
Atoms per 8 oxygens								
Si	3.017	2.992	2.995	2.980	2.995	3.008	3.012	3.012
Ti	0.0	0.0	0.005	0.0	0.0	0.005	0.003	0.0
Al	0.991	0.980	1.002	1.001	0.993	0.988	0.979	0.989
Fe	0.0	0.0	0.0	0.033	0.0	0.005	0.0	0.007
Mn	0.004	0.001	0.003	0.007	0.0	0.0	0.0	0.0
Mg	0.006	0.009	0.005	0.020	0.004	0.014	0.008	0.012
Ca	0.007	0.019	0.014	0.007	0.016	0.0	0.006	0.004
Na	0.920	0.035	0.946	0.935	0.041	0.943	0.967	0.935
K	0.001	0.978	0.003	0.006	0.955	0.0	0.004	0.0
Ba	0.001	0.009	0.0	0.001	0.002	0.0	0.0	0.002
Rock Type	CBT	CBT	CBT	CBT	CBT	CBT	CBT	CBT
Crystal	1.	1.	1.	1.	1.	1.	1.	1.
Position	8.	8.	8.	8.	8.	8.	8.	8.
Molecular percent								
Ab	99.1	3.2	98.1	98.5	3.8	100.0	98.9	99.5
Or	0.1	95.0	0.3	0.7	94.6	0.0	0.4	0.0
An	0.8	1.8	1.5	0.8	1.6	0.0	0.7	0.5

ZIRCON ANALYSES - Total Fe as FeO

	168.06	180.04	180.05	180.06	183.14	202.13
Weight % oxide						
SiO2	32.232	32.230	31.868	31.108	31.600	32.047
TiO2	0.092	0.0	0.067	0.134	0.177	0.018
Al2O3	0.0	0.061	0.0	0.0	0.0	0.0
FeO	0.104	0.016	0.361	0.227	0.481	0.0
MnO	0.057	0.083	0.0	0.078	0.017	0.0
MgO	0.054	0.114	0.140	0.162	0.093	0.0
CaO	0.0	0.0	0.013	0.099	0.0	0.010
Na2O	0.214	0.175	0.764	0.042	0.197	0.098
K2O	0.023	0.044	0.028	0.0	0.0	0.017
BaO	0.0	0.0	0.0	0.0	0.0	0.0
ZrO2	67.405	67.005	65.338	65.790	66.573	67.755
Total	100.181	99.728	98.579	97.640	99.138	99.945
Atoms per 4 oxygens						
Si	0.986	0.989	0.989	0.978	0.979	0.984
Ti	0.002	0.0	0.002	0.003	0.004	0.0
Al	0.0	0.002	0.0	0.0	0.0	0.0
Fe	0.003	0.0	0.009	0.006	0.012	0.0
Mn	0.001	0.002	0.0	0.002	0.0	0.0
Mg	0.002	0.005	0.006	0.008	0.004	0.0
Ca	0.0	0.0	0.0	0.003	0.0	0.0
Na	0.013	0.010	0.046	0.003	0.012	0.006
K	0.0	0.002	0.001	0.0	0.0	0.0
Ba	0.0	0.0	0.0	0.0	0.0	0.0
Zr	1.005	1.003	0.989	1.009	1.006	1.014
Rock Type	XPS	ALSY	ALSY	ALSY	PEG	PMS
Crystal	1.	1.	1.	1.	14.	1.
Position	8.	8.	8.	8.	-1.	8.

APATITE ANALYSES

	* 27193.17	* 27193.18	* 27193.20	* 138048.13	* 138048.14	* 138048.15	* 27259.22	* 27259.23	* 27259.24	* 138001.20	* 138001.21
Weight % oxide											
SiO2	0.440	0.831	1.165	0.478	0.871	1.130	0.700	0.682	0.701	0.059	0.209
FeO	0.055	0.185	0.150	0.110	0.300	0.256	0.042	0.066	0.222	0.035	0.042
MnO	0.015	0.0	0.018	0.041	0.054	0.023	0.012	0.043	0.037	0.053	0.071
MgO	0.005	0.0	0.008	0.0	0.006	0.0	0.0	0.0	0.009	0.0	0.002
CaO	54.122	53.074	52.003	54.378	53.523	52.664	53.109	53.076	53.664	54.330	54.240
Na2O	0.0	0.0	0.0	0.0	0.0	0.0	0.0	0.0	0.0	0.0	0.0
K2O	0.0	0.0	0.0	0.0	0.0	0.0	0.0	0.0	0.0	0.0	0.0
BaO	0.0	0.0	0.0	0.0	0.0	0.0	0.0	0.0	0.0	0.0	0.0
Cl	0.0	0.0	0.0	0.008	0.0	0.017	0.0	0.0	0.0	0.0	0.012
P2O5	40.887	39.405	39.236	40.750	39.509	38.669	39.946	40.037	39.746	40.807	39.039
O equiv Cl	0.0	0.0	0.0	-0.002	0.0	-0.004	0.0	0.0	0.0	0.0	-0.003
Total	95.524	93.495	92.580	95.763	94.263	92.755	93.809	93.904	94.379	95.284	93.612
Atoms per 12 oxygens, anhydrous											
Si	0.037	0.071	0.100	0.040	0.073	0.096	0.060	0.058	0.059	0.005	0.018
Fe	0.004	0.013	0.011	0.008	0.021	0.018	0.003	0.005	0.016	0.003	0.003
Mn	0.001	0.0	0.001	0.003	0.004	0.002	0.0	0.003	0.003	0.004	0.005
Mg	0.0	0.0	0.001	0.0	0.0	0.0	0.0	0.0	0.001	0.0	0.0
Ca	4.920	4.845	4.787	4.909	4.828	4.788	4.876	4.875	4.862	4.984	4.956
Na	0.0	0.0	0.0	0.0	0.0	0.0	0.0	0.0	0.0	0.0	0.0
K	0.0	0.0	0.0	0.0	0.0	0.0	0.0	0.0	0.0	0.0	0.0
Ba	0.0	0.0	0.0	0.0	0.0	0.0	0.0	0.0	0.0	0.0	0.0
Cl	0.0	0.0	0.0	0.001	0.0	0.002	0.0	0.0	0.0	0.0	0.002
P	0.587	0.568	0.571	0.581	0.563	0.556	0.580	0.581	0.569	0.592	0.564
Rock Type	MUS	MUS	MUS	LSS	LSS	LSS	MUS	MUS	MUS	CGBS	CGBS
Crystal	1.	1.	1.	10.	10.	10.	1.	1.	10.	1.	1.
Position	-1.	-1.	-1.	-1.	-1.	-1.	6.	1.	-1.	7.	1.

APATITE REE ANALYSES (All using WDS)

Sample	27259.	27259.	27259.	27259.	27259.	27259.	27259.	27259.	27259.	31854.	31854.	31854.	31854.	31854.	31854.
Rock type	MUS	MUS	MUS	MUS	MUS	MUS	MUS	MUS	MUS	XPS	XPS	XPS	XPS	XPS	XPS
REE (wt %)															
La2O3	0.56	0.61	0.59	0.57	0.57	0.56	0.61	0.52	0.71	0.14	0.17	0.18	0.17	0.14	0.17
Ce2O3	1.45	1.47	1.44	1.41	1.55	1.42	1.52	1.33	1.78	0.46	0.46	0.49	0.51	0.38	0.53
Pr2O3	0.23	0.21	0.16	0.23	0.17	0.25	0.14	0.21	0.25	0.14	0.12	0.12	0.11	0.0	0.15
Nd2O3	0.70	0.72	0.71	0.73	0.79	0.69	0.72	0.72	0.85	0.28	0.26	0.28	0.31	0.26	0.30
Sm2O3	0.14	0.13	0.18	0.17	0.18	0.14	0.18	0.15	0.20	0.02	0.06	0.07	0.04	0.06	0.08

Sample	138048.	138048.	138048.	138048.	138048.	138048.	138048.	138048.	138048.	138011.	138011.	138011.	138011.	138011.	138011.
Rock type	LSS	LSS	LSS	LSS	LSS	LSS	LSS	LSS	LSS	CGBS	CGBS	CGBS	CGBS	CGBS	CGBS
REE (wt %)															
La2O3	0.43	0.59	0.72	0.44	0.36	0.79	0.39	0.36	0.23	0.23	0.25	0.26	0.30	0.28	
Ce2O3	1.68	1.13	1.66	1.76	1.19	0.85	1.94	1.13	1.04	0.60	0.64	0.69	0.75	0.79	0.79
Pr2O3	0.20	0.21	0.29	0.25	0.13	0.22	0.24	0.18	0.14	0.11	0.13	0.10	0.15	0.12	0.10
Nd2O3	0.91	0.64	0.95	0.95	0.72	0.50	0.98	0.62	0.61	0.34	0.34	0.40	0.46	0.40	0.47
Sm2O3	0.19	0.13	0.13	0.16	0.08	0.10	0.17	0.14	0.13	0.03	0.08	0.09	0.12	0.11	0.09

Sample	138011.	138011.	138011.	138011.	138011.	138011.	138011.	138011.	138011.	138011.	138011.	138011.	138011.
Rock type	CGBS	CGBS	CGBS	CGBS	CGBS	CGBS	CGBS	CGBS	CGBS	CGBS	CGBS	CGBS	CGBS
REE (wt %)													
La2O3	0.25	0.27	0.30	0.25	0.25	0.19	0.21	0.22	0.22	0.27	0.26	0.19	0.24
Ce2O3	0.73	0.76	0.72	0.70	0.67	0.57	0.58	0.62	0.65	0.65	0.59	0.63	0.59
Pr2O3	0.08	0.15	0.16	0.19	0.08	0.10	0.07	0.11	0.12	0.16	0.16	0.12	0.12
Nd2O3	0.42	0.48	0.38	0.41	0.39	0.40	0.34	0.37	0.41	0.39	0.35	0.36	0.36
Sm2O3	0.11	0.11	0.08	0.08	0.09	0.10	0.07	0.11	0.08	0.07	0.08	0.08	0.10

CANCRINITE ANALYSES

	27113.26	138044.13	138044.14	138048.24	138048.25	138046.15	138046.16	138001.17	138001.18	138001.19	138025.23	138025.24	138055.17	138055.18	168.07	168.08	168.09
Weight % oxide																	
SiO2	42.773	53.729	43.618	41.175	39.806	41.557	41.322	45.662	46.125	46.232	40.585	40.200	44.315	44.928	37.570	37.253	37.484
Al2O3	30.891	24.625	36.976	30.732	30.804	30.352	31.154	33.486	33.123	33.102	30.952	30.731	32.195	31.030	27.663	28.126	27.624
FeO	0.031	0.379	1.566	0.042	0.009	0.139	0.081	0.057	0.034	0.018	0.072	0.092	0.0	0.0	0.191	0.084	0.103
MnO	0.0	0.031	0.194	0.010	0.005	0.009	0.017	0.089	0.061	0.063	0.012	0.012	0.0	0.0	0.103	0.030	0.019
MgO	0.009	0.020	0.362	0.010	0.007	0.0	0.008	0.012	0.0	0.0	0.007	0.0	0.0	0.0	0.380	0.488	0.045
CaO	6.940	0.279	0.037	6.897	7.176	7.046	7.091	3.582	3.468	3.650	6.649	6.705	2.879	2.481	3.234	3.295	3.300
Na2O	7.300	13.138	0.195	10.769	10.321	8.734	8.136	9.252	9.379	8.562	9.261	8.920	4.143	5.489	17.394	17.507	16.689
K2O	0.019	0.288	10.819	0.020	0.023	0.0	0.006	0.005	0.023	0.017	0.016	0.014	0.214	0.0	0.0	0.0	0.020
BaO	0.026	0.310	0.012	0.003	0.013	0.021	0.043	0.054	0.014	0.020	0.0	0.0	0.0	0.0	0.0	0.0	0.0
S	0.0	0.0	0.0	0.0	0.0	0.0	0.0	0.0	0.023	0.001	0.028	0.0	0.0	0.0	0.006	0.026	0.0
Total	87.989	92.799	93.779	89.658	88.164	87.858	87.858	92.199	92.250	91.665	87.582	86.674	83.746	83.928	86.541	86.809	85.284
Atoms per 24 oxygens, anhydrous																	
Si	6.632	7.828	6.469	6.392	6.292	6.521	6.468	6.702	6.761	6.793	6.404	6.403	6.960	7.061	6.210	6.142	6.256
Al	5.647	4.230	6.465	5.624	5.740	5.615	5.749	5.794	5.724	5.734	5.758	5.771	5.962	5.749	5.391	5.467	5.435
Fe	0.004	0.046	0.194	0.005	0.001	0.018	0.011	0.007	0.004	0.002	0.010	0.012	0.0	0.0	0.026	0.012	0.014
Mn	0.0	0.004	0.024	0.001	0.0	0.001	0.002	0.011	0.008	0.008	0.002	0.002	0.0	0.0	0.014	0.004	0.003
Mg	0.002	0.004	0.080	0.002	0.002	0.0	0.002	0.003	0.0	0.0	0.002	0.0	0.0	0.0	0.094	0.120	0.011
Ca	1.153	0.044	0.006	1.147	1.215	1.185	1.189	0.563	0.545	0.575	1.124	1.144	0.485	0.418	0.573	0.582	0.590
Na	2.195	3.712	0.056	3.242	3.163	2.658	2.469	2.633	2.666	2.439	2.833	2.755	1.262	1.673	5.575	5.597	5.400
K	0.004	0.054	2.047	0.004	0.005	0.0	0.001	0.0	0.004	0.003	0.003	0.003	0.043	0.0	0.0	0.0	0.004
Ba	0.002	0.018	0.0	0.0	0.0	0.001	0.003	0.003	0.0	0.001	0.0	0.0	0.0	0.0	0.0	0.0	0.0
S	0.0	0.0	0.0	0.0	0.0	0.0	0.0	0.0	0.006	0.0	0.008	0.0	0.0	0.0	0.002	0.008	0.0
Rock Type	LSS	LSS	LSS	LSS	LSS	LSS	LSS	CGBS	CGBS	CGBS	LSS	LSS	PEG	PEG	XPS	XPS	XPS
Crystal	8.	8.	8.	8.	8.	8.	8.	8.	8.	8.	8.	8.	8.	8.	8.	8.	8.
Position	-1.	-1.	-1.	-1.	-1.	-1.	-1.	-1.	-1.	-1.	-1.	-1.	-1.	-1.	-1.	-1.	-1.

CANCRINITE ANALYSES

	168.10	168.13	168.14
Weight % oxide			
SiO2	37.311	37.174	33.739
Al2O3	27.259	27.720	29.710
FeO	0.0	0.0	0.075
MnO	0.023	0.0	0.0
MgO	0.304	0.223	0.391
CaO	3.362	3.323	3.436
Na2O	18.611	17.979	16.745
K2O	0.0	0.0	0.033
BaO	0.0	0.0	0.0
S	0.103	0.061	0.153
Total	86.973	86.480	84.282
Atoms per 24 oxygens, anhydrous			
Si	6.178	6.166	5.756
Al	5.321	5.421	5.975
Fe	0.0	0.0	0.011
Mn	0.003	0.0	0.0
Mg	0.075	0.055	0.099
Ca	0.596	0.591	0.628
Na	5.975	5.782	5.539
K	0.0	0.0	0.007
Ba	0.0	0.0	0.0
S	0.032	0.019	0.049
Rock Type	XPS	XPS	XPS
Crystal	8.	8.	8.
Position	-1.	-1.	-1.

ANALCITE ANALYSES

	43.18	43.19	172.15	172.16	172.18	118.12	118.13	136.06	136.07	136.08	136.10
Weight % oxide											
SiO2	51.909	52.133	54.205	53.751	51.452	54.653	55.095	52.267	52.976	52.797	53.485
Al2O3	24.750	24.755	22.901	22.744	23.236	23.176	23.044	22.250	22.498	22.643	23.033
FeO	0.0	0.0	0.032	0.0	0.0	0.083	0.249	0.346	0.076	0.004	0.262
MnO	0.0	0.0	0.0	0.087	0.0	0.112	0.0	0.0	0.073	0.023	0.0
MgO	0.0	0.0	0.285	0.245	0.280	0.167	0.261	0.123	0.271	0.274	0.446
CaO	0.0	0.0	0.033	0.066	0.747	0.003	0.0	0.163	0.016	0.027	0.277
Na2O	20.660	22.583	13.346	13.317	13.566	13.229	13.236	12.542	12.846	12.660	12.867
K2O	0.158	0.226	0.157	0.091	0.114	0.090	0.148	0.221	0.298	0.185	0.094
BaO	0.0	0.0	0.0	0.0	0.0	0.0	0.0	0.014	0.146	0.106	0.104
Total	97.477	99.697	90.959	90.301	89.395	91.513	92.033	87.926	89.200	88.719	90.568
Atoms per 8 oxygens											
Si	2.476	2.452	2.670	2.668	2.598	2.672	2.679	2.666	2.665	2.662	2.649
Al	1.392	1.373	1.330	1.331	1.383	1.336	1.321	1.338	1.334	1.346	1.345
Fe	0.0	0.0	0.001	0.0	0.0	0.003	0.010	0.015	0.003	0.0	0.011
Mn	0.0	0.0	0.0	0.004	0.0	0.005	0.0	0.0	0.003	0.0	0.0
Mg	0.0	0.0	0.021	0.018	0.021	0.012	0.019	0.009	0.020	0.021	0.033
Ca	0.0	0.0	0.002	0.004	0.040	0.0	0.0	0.009	0.0	0.001	0.015
Na	1.911	2.060	1.274	1.281	1.328	1.254	1.248	1.240	1.253	1.238	1.236
K	0.010	0.014	0.010	0.006	0.007	0.006	0.009	0.014	0.019	0.012	0.006
Ba	0.0	0.0	0.0	0.0	0.0	0.0	0.0	0.0	0.003	0.002	0.002
Rock Type	USS	USS	GS-A	GS-A	GS-A	USS	USS	ALSY	ALSY	ALSY	ALSY
Crystal	1.	1.	14.	14.	14.	16.	16.	1.	1.	1.	1.
Position	7.	1.	-1.	-1.	-1.	-1.	-1.	8.	8.	8.	8.

SODALITE ANALYSES

	180.11	180.12	180.13	180.14	135.12	135.13	135.14
Weight % oxide							
SiO2	36.870	46.736	38.040	37.349	37.844	38.127	38.092
Al2O3	30.822	26.523	29.978	30.769	30.547	30.680	30.836
FeO	0.040	0.0	0.082	0.144	0.263	0.035	0.357
MnO	0.0	0.007	0.0	0.0	0.026	0.199	0.0
MgO	0.308	0.418	0.195	0.429	0.275	0.009	0.013
CaO	0.0	0.007	0.016	0.0	1.522	0.042	0.0
Na2O	23.879	17.363	23.019	23.822	22.994	24.147	24.077
K2O	0.094	0.100	0.028	0.059	0.063	0.112	0.080
Cl	8.636	3.511	8.233	8.676	6.504	8.043	8.062
S	0.0	0.014	0.028	0.0	0.213	0.242	0.237
O equiv Cl	-1.949	-0.792	-1.858	-1.958	-1.468	-1.815	-1.819
Total	98.700	93.887	97.761	99.290	98.783	99.821	99.935
Atoms per 21 oxygens							
Si	5.086	6.215	5.256	5.126	5.148	5.189	5.175
Al	5.012	4.158	4.884	4.978	4.899	4.923	4.938
Fe	0.005	0.0	0.009	0.017	0.030	0.004	0.041
Mn	0.0	0.0	0.0	0.0	0.003	0.023	0.0
Mg	0.063	0.083	0.040	0.088	0.056	0.002	0.003
Ca	0.0	0.0	0.002	0.0	0.222	0.006	0.0
Na	6.387	4.477	6.167	6.339	6.065	6.372	6.342
K	0.017	0.017	0.005	0.010	0.011	0.019	0.014
Cl	2.019	0.791	1.928	2.018	1.499	1.855	1.856
S	0.0	0.003	0.007	0.0	0.054	0.062	0.060
Rock Type	ALSY	ALSY	ALSY	ALSY	USS	USS	USS
Crystal	1.	1.	1.	1.	1.	1.	1.
Position	8.	8.	8.	8.	8.	8.	8.

CARBONATE ANALYSES - Total Fe as FeO

	26.18	272.07	156.10	156.12	136.14	136.15	136.16	46.03	46.04	46.05	46.05	46.07	52.06	52.07	52.08	52.09	52.10
Weight % oxide																	
SiO2	0.199	0.200	0.105	0.189	0.222	0.219	0.183	0.012	0.119	0.115	0.025	0.100	0.181	0.185	0.129	0.101	0.148
TiO2	0.0	0.0	0.0	0.0	0.0	0.0	0.0	0.075	0.100	0.030	0.177	0.0	0.0	0.039	0.0	0.0	0.004
Al2O3	0.065	0.108	0.0	0.157	0.159	0.137	0.122	0.141	0.189	0.111	0.127	0.036	0.028	0.079	0.125	0.027	0.029
FeO	1.087	0.792	0.449	0.298	0.023	0.159	0.349	1.914	1.741	1.748	1.723	1.802	51.996	52.957	51.624	53.654	52.844
MnO	1.885	0.711	0.507	0.840	0.636	1.184	1.584	1.032	1.223	1.200	1.164	0.928	4.872	1.797	2.005	1.826	1.741
MgO	0.028	0.102	0.079	0.132	0.0	0.063	0.163	0.136	0.183	0.137	0.190	0.205	3.446	4.731	4.102	4.297	4.529
CaO	50.075	51.076	50.333	51.271	52.532	51.537	50.287	50.394	50.819	50.147	49.579	49.990	0.819	1.184	2.383	1.268	1.219
Na2O	0.114	0.086	0.149	0.013	0.137	0.0	0.043	0.071	0.026	0.0	0.070	0.139	0.320	0.123	0.133	0.258	0.124
K2O	0.0	0.040	0.0	0.050	0.0	0.032	0.0	0.0	0.0	0.032	0.0	0.0	0.001	0.079	0.0	0.024	0.057
BaO	0.0	0.0	0.0	0.0	0.252	0.127	0.135	0.0	0.007	0.053	0.0	0.084	0.285	0.0	0.226	0.066	0.0
ZrO2	0.0	0.0	0.0	0.0	0.0	0.0	0.0	0.0	0.0	0.0	0.0	0.0	0.0	0.085	0.137	0.002	0.0
Total	53.453	53.115	51.622	52.950	53.961	53.458	52.866	53.775	54.407	53.573	53.055	53.284	61.948	61.174	60.727	61.521	60.695
Atoms per 3 oxygens																	
Si	0.004	0.004	0.002	0.003	0.004	0.004	0.003	0.0	0.002	0.002	0.0	0.002	0.003	0.003	0.002	0.002	0.003
Ti	0.0	0.0	0.0	0.0	0.0	0.0	0.0	0.0	0.001	0.0	0.002	0.0	0.0	0.0	0.0	0.0	0.0
Al	0.001	0.002	0.0	0.003	0.003	0.003	0.003	0.003	0.004	0.002	0.003	0.0	0.0	0.002	0.003	0.0	0.0
Fe	0.016	0.012	0.007	0.004	0.0	0.002	0.005	0.028	0.025	0.026	0.026	0.027	0.798	0.806	0.794	0.820	0.815
Mn	0.028	0.011	0.008	0.013	0.009	0.018	0.024	0.015	0.018	0.018	0.017	0.014	0.076	0.028	0.031	0.028	0.027
Mg	0.0	0.003	0.002	0.003	0.0	0.002	0.004	0.004	0.005	0.004	0.005	0.005	0.094	0.128	0.112	0.117	0.124
Ca	0.944	0.963	0.977	0.967	0.974	0.965	0.955	0.945	0.939	0.944	0.941	0.946	0.016	0.023	0.047	0.025	0.024
Na	0.004	0.003	0.005	0.0	0.005	0.0	0.001	0.002	0.0	0.0	0.002	0.005	0.011	0.004	0.005	0.009	0.004
K	0.0	0.0	0.0	0.001	0.0	0.0	0.0	0.0	0.0	0.0	0.0	0.0	0.0	0.002	0.0	0.0	0.001
Ba	0.0	0.0	0.0	0.0	0.002	0.0	0.0	0.0	0.0	0.0	0.0	0.0	0.002	0.0	0.002	0.0	0.0
Rock Type	ALGN	ALSY	MUS	MUS	ALSY	ALSY	ALSY	CBT	CBT	CBT	CBT	CBT	CBT	CBT	CBT	CBT	CBT
Crystal	1.	1.	14.	14.	14.	14.	14.	1.	1.	1.	1.	1.	1.	1.	1.	1.	1.
Position	8.	8.	-1.	-1.	-1.	-1.	-1.	8.	8.	8.	8.	8.	7.	1.	7.	1.	7.

CARBONATE ANALYSES - Total Fe as FeO

	52.11	52.12	52.13	52.14	52.15	74.07	74.08	74.09	74.10	74.11	74.12	103.09	103.10	103.11	103.12	103.13	107.11
Weight % oxide																	
SiO2	0.147	0.215	0.170	0.159	0.007	0.242	0.281	0.201	0.170	0.229	0.144	0.030	0.0	0.065	0.131	0.084	0.188
TiO2	0.0	0.0	0.0	0.0	0.011	0.0	0.0	0.0	0.0	0.0	0.025	0.0	0.0	0.039	0.0	0.0	0.0
Al2O3	0.0	0.023	0.0	0.005	0.064	0.083	0.041	0.046	0.031	0.0	0.0	0.0	0.057	0.133	0.113	0.145	0.097
FeO	53.849	1.435	0.952	1.161	0.968	1.166	1.400	1.358	1.063	0.947	1.142	1.263	1.194	0.965	1.263	1.224	0.634
MnO	2.104	1.649	1.157	1.548	0.436	0.521	0.443	0.489	0.655	0.648	0.473	0.668	0.575	0.837	0.790	1.112	2.265
MgO	4.012	0.091	0.0	0.038	0.101	0.192	0.179	0.131	0.171	0.134	0.224	0.029	0.133	0.166	0.210	0.068	0.108
CaO	0.628	50.464	51.878	51.032	51.916	51.583	51.287	51.044	51.376	52.095	52.072	51.658	51.697	51.643	51.150	51.009	50.113
Na2O	0.193	0.097	0.066	0.077	0.043	0.008	0.0	0.003	0.039	0.117	0.169	0.144	0.107	0.092	0.138	0.153	0.058
K2O	0.003	0.024	0.041	0.0	0.0	0.0	0.006	0.035	0.0	0.031	0.0	0.0	0.0	0.0	0.0	0.0	0.0
BaO	0.044	0.158	0.0	0.073	0.0	0.126	0.0	0.105	0.087	0.151	0.003	0.054	0.019	0.050	0.0	0.151	0.242
Total	60.980	54.156	54.264	54.093	53.546	53.921	53.637	53.412	53.592	54.352	54.252	53.846	53.782	53.990	53.795	53.946	53.705
Atoms per 3 oxygens																	
Si	0.003	0.004	0.003	0.003	0.0	0.004	0.005	0.004	0.003	0.004	0.002	0.0	0.0	0.001	0.002	0.001	0.003
Ti	0.0	0.0	0.0	0.0	0.0	0.0	0.0	0.0	0.0	0.0	0.0	0.0	0.0	0.0	0.0	0.0	0.0
Al	0.0	0.0	0.0	0.0	0.001	0.002	0.0	0.0	0.0	0.0	0.0	0.0	0.001	0.003	0.002	0.003	0.002
Fe	0.834	0.021	0.014	0.017	0.014	0.017	0.020	0.020	0.016	0.014	0.016	0.018	0.017	0.014	0.018	0.018	0.009
Mn	0.033	0.024	0.017	0.023	0.006	0.008	0.007	0.007	0.010	0.009	0.007	0.010	0.009	0.012	0.012	0.016	0.034
Mg	0.111	0.002	0.0	0.0	0.003	0.005	0.005	0.003	0.004	0.003	0.006	0.0	0.003	0.004	0.005	0.002	0.003
Ca	0.012	0.941	0.962	0.952	0.973	0.959	0.957	0.960	0.962	0.962	0.962	0.967	0.967	0.960	0.954	0.953	0.942
Na	0.007	0.003	0.002	0.003	0.001	0.0	0.0	0.0	0.001	0.004	0.006	0.005	0.004	0.003	0.005	0.005	0.002
K	0.0	0.0	0.0	0.0	0.0	0.0	0.0	0.0	0.0	0.0	0.0	0.0	0.0	0.0	0.0	0.0	0.0
Ba	0.0	0.001	0.0	0.0	0.0	0.0	0.0	0.0	0.0	0.001	0.0	0.0	0.0	0.0	0.0	0.001	0.002
Rock Type	CBT	CBT	CBT	CBT	CBT	CBT	CBT	CBT	CBT	CBT	CBT	CBT	CBT	CBT	CBT	CBT	CBT
Crystal	1.	1.	1.	1.	1.	1.	1.	1.	1.	1.	1.	1.	1.	1.	1.	1.	1.
Position	1.	7.	1.	7.	1.	7.	1.	7.	1.	8.	8.	8.	7.	1.	7.	1.	7.

CARBONATE ANALYSES - Total Fe as FeO

	107.12	107.13	107.14	265.06	265.07	265.09	265.10	265.11	265.12	47.03	47.04	47.05	47.06	47.08	47.09	47.10	265.13
Weight % oxide																	
SiO2	0.126	0.184	0.091	0.147	0.118	0.102	0.131	0.130	0.112	0.078	0.068	0.153	0.031	0.040	0.078	0.049	0.094
TiO2	0.0	0.0	0.038	0.083	0.011	0.107	0.0	0.139	0.0	0.0	0.0	0.022	0.0	0.0	0.0	0.0	0.0
Al2O3	0.088	0.057	0.0	0.193	0.103	0.085	0.028	0.113	0.071	0.101	0.0	0.044	0.039	0.121	0.116	0.062	0.018
FeO	0.074	1.041	0.111	1.837	1.416	1.191	0.857	1.292	0.893	0.926	1.124	10.189	1.133	1.096	0.901	0.698	0.986
MnO	2.170	0.939	1.996	0.994	1.877	2.317	2.475	2.165	1.850	1.449	1.767	2.446	1.418	1.354	1.429	1.592	2.140
MgO	0.006	0.117	0.0	0.097	0.089	0.092	0.101	0.087	0.026	0.223	0.235	0.432	0.270	0.305	0.506	0.267	0.110
CaO	51.401	50.898	50.934	49.864	49.842	49.262	49.780	49.637	49.859	50.920	50.816	41.523	49.458	51.018	50.229	50.081	49.984
Na2O	0.043	0.160	0.015	0.084	0.0	0.100	0.029	0.110	0.220	0.051	0.076	0.185	0.034	0.215	0.096	0.083	0.096
K2O	0.0	0.0	0.0	0.006	0.010	0.050	0.021	0.0	0.045	0.060	0.037	0.0	0.046	0.075	0.0	0.0	0.068
BaO	0.300	0.162	0.0	0.004	0.017	0.065	0.261	0.0	0.046	0.314	0.0	0.0	0.0	0.524	0.244	0.113	0.0
Total	54.208	53.558	53.185	53.309	53.483	53.371	53.683	53.673	53.122	54.122	54.123	54.994	52.429	54.748	53.599	52.945	53.496
Atoms per 3 oxygens																	
Si	0.002	0.003	0.002	0.003	0.002	0.002	0.002	0.002	0.002	0.001	0.001	0.003	0.0	0.0	0.001	0.0	0.002
Ti	0.0	0.0	0.0	0.001	0.0	0.001	0.0	0.002	0.0	0.0	0.0	0.0	0.0	0.0	0.0	0.0	0.0
Al	0.002	0.001	0.0	0.004	0.002	0.002	0.0	0.002	0.001	0.002	0.0	0.0	0.0	0.002	0.002	0.001	0.0
Fe	0.001	0.015	0.002	0.027	0.021	0.018	0.013	0.019	0.013	0.013	0.016	0.151	0.017	0.016	0.013	0.010	0.015
Mn	0.032	0.014	0.030	0.015	0.028	0.035	0.037	0.032	0.028	0.021	0.026	0.037	0.022	0.020	0.021	0.024	0.032
Mg	0.0	0.003	0.0	0.003	0.002	0.002	0.003	0.002	0.0	0.006	0.006	0.011	0.007	0.008	0.013	0.007	0.003
Ca	0.957	0.956	0.964	0.941	0.941	0.933	0.940	0.933	0.947	0.950	0.947	0.790	0.951	0.943	0.943	0.953	0.944
Na	0.001	0.005	0.0	0.003	0.0	0.003	0.0	0.004	0.008	0.002	0.003	0.006	0.001	0.007	0.003	0.003	0.003
K	0.0	0.0	0.0	0.0	0.0	0.001	0.0	0.0	0.001	0.001	0.0	0.0	0.001	0.002	0.0	0.0	0.002
Ba	0.002	0.001	0.0	0.0	0.0	0.0	0.002	0.0	0.0	0.002	0.0	0.0	0.0	0.004	0.002	0.0	0.0
Rock Type	CBT	CBT	CBT	CBT	CBT	CBT	CBT	CBT	CBT	CBT	CBT	CBT	CBT	CBT	CBT	CBT	CBT
Crystal	1.	1.	1.	1.	1.	1.	1.	1.	1.	1.	1.	14.	1.	14.	14.	14.	1.
Position	1.	7.	1.	7.	1.	7.	1.	7.	1.	7.	1.	-1.	7.	-1.	-1.	-1.	8.

CARBONATE ANALYSES - Total Fe as FeO

	265.14	265.15	265.16	265.19	265.20	265.21	47.11	47.12	265.21	107.14	107.15	107.16	107.17	107.18	46.08	46.09	46.10
Weight % oxide																	
SiO2	0.244	0.102	0.080	0.246	0.189	0.133	0.074	0.072	0.073	0.118	0.162	0.253	0.180	0.140	0.221	0.105	0.129
TiO2	0.007	0.042	0.0	0.092	0.042	0.0	0.0	0.0	0.0	0.054	0.030	0.017	0.091	0.0	0.015	0.0	0.009
Al2O3	0.028	0.021	0.0	0.180	0.138	0.080	0.019	0.0	0.004	0.0	0.046	0.0	0.034	0.0	0.0	0.0	0.025
FeO	1.131	1.026	47.407	54.223	54.352	51.756	0.487	0.663	1.173	0.632	0.757	0.0	1.178	0.334	1.740	1.226	1.792
MnO	2.096	2.190	3.161	3.515	2.801	3.721	1.370	1.383	1.467	1.598	1.600	1.945	1.247	1.991	0.966	0.939	0.977
MgO	0.106	0.094	2.186	2.704	2.297	3.338	0.140	0.127	0.206	0.309	0.033	0.061	0.131	0.129	0.121	0.075	0.122
CaO	49.577	50.287	6.289	0.482	0.481	0.609	50.532	49.415	50.246	49.225	50.307	49.177	50.493	50.725	49.943	50.514	49.920
Na2O	0.113	0.102	0.139	0.284	0.050	0.226	0.092	0.129	0.150	0.0	0.0	0.060	0.032	0.142	0.099	0.137	0.079
K2O	0.030	0.0	0.035	0.054	0.008	0.0	0.0	0.045	0.024	0.0	0.0	0.0	0.0	0.0	0.003	0.038	0.002
BaO	0.0	0.0	0.0	0.0	0.0	0.0	0.0	0.0	0.0	0.0	0.0	0.0	0.0	0.0	0.0	0.0	0.0
Total	53.332	53.864	59.297	61.780	60.358	59.863	52.714	51.834	53.343	51.936	52.935	51.513	53.386	53.461	53.108	53.034	53.055
Atoms per 3 oxygens																	
Si	0.004	0.002	0.002	0.005	0.004	0.003	0.001	0.001	0.001	0.002	0.003	0.005	0.003	0.002	0.004	0.002	0.002
Ti	0.0	0.0	0.0	0.001	0.0	0.0	0.0	0.0	0.0	0.0	0.0	0.0	0.001	0.0	0.0	0.0	0.0
Al	0.0	0.0	0.0	0.004	0.003	0.002	0.0	0.0	0.0	0.0	0.0	0.0	0.0	0.0	0.0	0.0	0.0
Fe	0.017	0.015	0.752	0.838	0.866	0.819	0.007	0.010	0.017	0.010	0.011	0.0	0.017	0.005	0.026	0.018	0.027
Mn	0.031	0.032	0.051	0.055	0.045	0.060	0.021	0.021	0.022	0.024	0.024	0.030	0.019	0.030	0.014	0.014	0.015
Mg	0.003	0.002	0.062	0.074	0.065	0.094	0.004	0.003	0.005	0.008	0.0	0.002	0.003	0.003	0.003	0.002	0.003
Ca	0.937	0.943	0.128	0.010	0.010	0.012	0.964	0.960	0.950	0.952	0.956	0.958	0.950	0.955	0.947	0.959	0.949
Na	0.004	0.003	0.005	0.010	0.002	0.008	0.003	0.005	0.005	0.0	0.0	0.002	0.001	0.005	0.003	0.005	0.003
K	0.0	0.0	0.0	0.001	0.0	0.0	0.0	0.001	0.0	0.0	0.0	0.0	0.0	0.0	0.0	0.0	0.0
Ba	0.0	0.0	0.0	0.0	0.0	0.0	0.0	0.0	0.0	0.0	0.0	0.0	0.0	0.0	0.0	0.0	0.0
Rock Type	CBT	CBT	CBT	CBT	CBT	CBT	CBT	CBT	CBT	CBT	CBT	CBT	CBT	CBT	CBT	CBT	CBT
Crystal	1.	1.	1.	1.	1.	1.	14.	1.	1.	1.	1.	1.	1.	1.	1.	1.	1.
Position	8.	8.	8.	8.	8.	8.	-1.	7.	1.	8.	7.	1.	7.	1.	7.	1.	7.

CARBONATE ANALYSES - Total Fe as FeO

	46.11	146.14	146.15	146.16
Weight % oxide				
SiO2	0.175	0.197	0.233	0.183
TiO2	0.120	0.0	0.0	0.032
Al2O3	0.0	0.0	0.104	0.082
FeO	1.305	0.888	1.356	1.326
MnO	0.836	0.048	0.147	0.0
MgO	0.0	0.004	0.053	0.150
CaO	49.556	52.332	51.665	51.808
Na2O	0.0	0.123	0.105	0.098
K2O	0.043	0.031	0.0	0.0
BaO	0.0	0.046	0.033	0.055
Total	52.035	53.669	53.696	53.734
Atoms per 3 oxygens				
Si	0.003	0.003	0.004	0.003
Ti	0.002	0.0	0.0	0.0
Al	0.0	0.0	0.002	0.002
Fe	0.020	0.013	0.020	0.019
Mn	0.013	0.0	0.002	0.0
Mg	0.0	0.0	0.001	0.004
Ca	0.957	0.977	0.963	0.965
Na	0.0	0.004	0.004	0.003
K	0.0	0.0	0.0	0.0
Ba	0.0	0.0	0.0	0.0
Rock Type	CBT	ALGN	ALGN	ALGN
Crystal	1.	1.	14.	14.
Position	1.	8.	-1.	-1.
Crystal	1.	1.	1.	14.
Position	7.	1.	8.	-1.

APPENDIX III

XRF Analysis

III.1: Sample preparation

For whole-rock geochemical analysis, it was decided to use only samples for which the precise field relationships were known, ie. those collected during the 1987 field season. Most samples collected were analysed (see table I.1), the main exceptions being samples of xenolithic or heterogeneous rock.

Weathered surfaces were removed using a hydraulic rock splitter, and the remaining fresh portion broken into centimetre-sized fragments. The fresh material was passed through a 'Sturtevant' jaw crusher, and the resulting millimetre-sized gravel hand picked to remove any remaining weathered material. Around 150g of gravel chips were then ground to a fine powder in a tungsten-carbide 'Tema' swing-mill for several minutes. The resulting powder should produce a fine slurry when added to a small quantity of water, with no trace of 'grittiness' remaining. Grinding was continued if the powder failed this test. Two batches of gravel were ground for very coarse samples (eg. G45, a Coarse-Grained Syenite), and the apparatus meticulously cleaned by scrubbing between each sample. The syenites and carbonatites were crushed and powdered on separate occasions to reduce the possibility of cross-contamination.

Trace elements were analysed using pressed pellets, prepared from ≈5g of powder mixed with a few drops of a 2% solution of PVA ('Moviol'), pressed at around 7 tons p.s.i., and dried for two hours at 110°C. Major element analysis was carried out on fused glass discs (Norrish and Hutton 1969). Precisely 0.45g of rock powder, which had been dried overnight at 110°C was mixed with 2.25g of La_2O_3-doped flux (Johnson-Mattey Spectroflux 105) and fused for two hours in Pt-Au crucibles at 1050°C. The fused sample was cast into graphite moulds and allowed to anneal on a hot-plate at 220°C. Care was taken not to remove the discs

from the hot-plate too soon or to allow them to cool too quickly on removal, as fracturing of the disc would inevitably occur. The discs were stored in a desiccator in individual sealed polythene bags prior to XRF analysis.

III.2: Analyses

All whole-rock major and trace element analyses of the syenites and carbonatites were carried out using a Phillips PW1400 X-ray spectrometer, incorporating a PW1500/10 sample changer, and using a Rh X-ray tube. Operating conditions are set out in table III.2. Mass absorbtion coefficients (MAC's) were taken from Heinrich (1967) and initial standard compositions from Govindaraju (1984), the compositions of which are given in the pocket at the rear of this thesis.

Major elements

All major elements, apart from Na (described below), were analysed in the form of fused glass discs, prepared as described in the previous section. These have the advantage over pressed pellets of better homogeneity, and overcomes the problem of phyllosilicates which may have been forced parallel to the surface of the pellet during compression, resulting in anomalously high values of some elements (eg. K). In addition, the lower concentration of elements in the fused disc, together with the presence of La_2O_3 as a heavy absorber, results in a reduction in errors due to inter-element and MAC effects.

Calibration of the results was achieved using a wide range of international standards, and the data processed using the program `XRF.CBI` (modified by Dave Stephenson), which was based on an earlier program, `XRF.QD`, written by Colin Watson. Both programs use an iterative process, recalculating element compositions and MAC's until a convergence has been achieved. The difference between the programs is that `XRF.CBI` fits a cubic calibration to the results, rather than a linear or quadratic fit, as used by `XRF.QD`.

As mentioned above, problems were encountered in analysing for Na by the fused disc method. The hygroscopic nature of the La_2O_3 in the flux appeared

to have resulted in Na being absorbed in moisture from the fingers, so that even handling the discs at the back and sides resulted in the analytical surface being contaminated (Ron Hardy, pers. comm.). The quality of the standards used for calibration thus deteriorated over a period of time. In addition, absorbtion of Na from the fireproof lining of the same furnace as used for loss-on-ignition determinations may have resulted in contamination of the unknowns. In view of the non-systematic nature of these errors, it was decided to analyse Na from pressed pellets, and recalculate the fusion data, which had already been normalised taking into account the Na values from fused discs.

Traces

Trace elements were analysed from pressed powder pellets, the preparation of which was described in section III.1. The method of analysis follows that employed by GGU, as described by Bailey (1976), and uses the general formula:

$$\text{ppm(element)} = \text{counts per second } (cs^{-1}) \times \text{MAC} \times K$$

where:

cs^{-1} = (peak - background) - blank.

MAC = calculated using the coefficients of Heinrich (1967).

K = Constant.

For a standard of known major and trace element composition, K can be calculated, and an average value of K used to determine the composition of the unknowns. The calculations were carried out using the program KFACTOR, which is based on several programs originally written by N.J.G. Pearce, and are fully described in Pearce (1988).

III.3: Detection limits

Theoretical detection limits can be calculated using the following formula (from Bailey 1976), and are shown in table III.1.

$$LLD = \frac{6}{m}\sqrt{\frac{C_b}{T}}$$

LLD = Lower limit of detection.

m = Counts per second per ppm.

C_b = Background counts per second.

T = Count time for peak plus backgrounds.

Table III.1

Element	LLD	Element	LLD	Element	LLD
Ba	15.27	Zn	4.47	V	7.93
Nb	0.045	Cu	4.53	Cr	7.75
Zr	3.17	Ni	7.48	Nd	11.94
Y	2.52	Pb	7.81	Ga	4.31
Sr	2.21	U	6.29	La	16.21
Rb	1.82	Th	6.83	Ce	28.11

Increasing the count rates enables smaller abundances to be detected. The relatively short count-time of 40s was used for the trace element peaks in order to complete a run successfully, though the relatively high concentrations of most trace elements in these rocks means that the accuracy should not be significantly affected.

III.4: Carbonatites

The method of XRF analysis of the carbonatites of Grønnedal-Íka follows that of Pearce (1988), and is based on that used at Leicester University (after Hodgson 1985). As for the syenites, trace elements were analysed using pressed pellets, prepared as described in section III.1. Major elements were analysed from fused discs, prepared from carbonatite samples which had been ashed for two hours at 1050°C. The crushed residue was then fused with Johnson-Mattey Spectroflux 105, as outlined in section III.1.

Seven carbonatite samples from the Igaliko dyke swarm were used as calibration standards, analysed for majors and traces by Pearce (1988), using the methods just described. These samples had major and trace element totals of 100±0.3%, as shown in table III.3. Fused discs and pressed pellets were prepared from powders of these samples following precisely the same method as for the unknowns. As some elements are particularly scarce in these samples (eg. Zr, Ti, K), the unknowns were also run using international standards.

Because of the overlap of the SrK and ZrK peaks (a potential problem in such Sr-rich samples), Zr abundances for the carbonatites were calculated separately. The extent of interference in Zr-poor international standards was determined, for which the Zr values were known, and the unknown Zr abundances in the carbonatites recalculated accordingly.

III.5: Norms

Normative abundances for the syenites were calculated using `NORM.PL1`, a program based on `NORMCAL`, originally written by Gill (1972a). The Fe^{2+}/Fe^{3+} ratio is required to run the program; these values for the different units were taken from Gill (*op. cit.*), which were determined using wet-chemical methods. Major element abundances in the metasomatised rocks have been recalculated to a 100 oxygen cell, following the method of McKie (1966) to illustrate the chemical variations in this type of rock.

The following tables thus consist of:

1. Major element (in weight % oxide) and trace element (in ppm by weight of element) data, given in sample number order, for all samples analysed by XRF methods (cf. table I.1).

2. Normative data for the syenites, and major elements recalculated to 100(O) for the metasomatised gneisses and syenites.

Table III.2

XRF operating conditions

Element	Line	Crystal	Angle($2\theta°$)	+bkg	-bkg	Time(pk)	Time(bkg)
Trace elements							
Ba	K_α	1	15.61	1.38	0.78	40	20
Nb	K_α	1	30.495	0.60	0.60	40	20
Zr	K_α	1	32.155	0.90	–	40	20
Y	K_α	1	33.96	1.00	0.90	40	20
Sr	K_α	1	35.925	0.90	–	40	20
Rb	K_α	1	38.045	0.70	1.00	40	20
Zn	K_α	1	60.665	1.00	–	40	20
Cu	K_α	1	65.645	1.10	–	40	20
Ni	K_α	1	71.355	2.00	–	40	20
Pb	K_α	1	40.46	1.20	1.60	40	20
U	L_α	1	37.38	1.40	–	40	20
Th	L_α	1	39.31	1.60	0.76	40	20
V	K_α	1	13.335	–	2.00	40	20
Cr	K_α	1	107.305	2.00	–	40	20
Nd	L_α	1	112.82	1.40	–	40	20
Ga	K_α	1	56.27	0.90	0.40	40	20
La	L_α	1	139.075	2.00	–	40	20
Ce	L_β	1	111.84	2.60	1.50	40	20
Major elements							
Si	K_α	3	109.235	3.80	–	20	10
Al	K_α	3	145.19	1.80	–	20	10
Fe	K_α	2	57.635	2.30	–	20	10
Mg	K_α	6	23.28	3.20	–	80	20
Ca	K_α	2	113.285	4.30	–	20	10
Na	K_α	6	28.075	2.92	–	100	20
K	K_α	2	136.885	3.00	–	20	10
Ti	K_α	2	86.28	5.00	–	20	10
Mn	K_α	1	95.415	4.60	–	20	10
P	K_α	5	141.025	4.00	–	40	10

1 - LIF220; 2 - LIF200; 3 - PE; 5 - GE; 6 - PX1. (Crystal 4, THAP, not used).

'–' indicates background not used in calculation of peak height.

Count times for peak and backgrounds in seconds.

Table III.3

Carbonatite Standards (after Pearce 1988)

	41982	325908	326263	326323	326329	326336	326343
Majors, wt %							
SiO_2	10.16	1.71	9.79	8.42	1.47	9.33	3.33
Al_2O_3	1.97	0.01	1.50	1.41	0.05	0.08	0.15
Fe_2O_3	6.73	7.37	18.12	6.67	8.42	11.20	10.07
MgO	0.87	0.54	1.53	0.45	0.45	1.38	0.98
CaO	40.36	44.01	31.64	43.07	35.95	38.19	37.23
Na_2O	0.83	0.05	0.53	0.01	0.05	0.30	0.12
K_2O	0.76	0.01	0.64	0.79	0.01	0.01	0.22
TiO_2	0.14	0.03	0.34	0.15	0.06	0.13	0.05
MnO	3.04	2.19	3.09	3.12	1.67	2.44	1.78
P_2O_5	0.33	1.11	0.05	0.35	2.62	3.53	3.11
Traces, ppm							
Ba	276	4779	1146	485	3859	5299	5394
Nb	47	512	275	95	481	221	286
Zr	35	0	0	0	0	0	0
Y	1365	602	488	1797	651	786	812
Sr	5970	42064	38631	6130	45885	45946	41605
Rb	107	0	17	123	0	0	0
Zn	545	805	3553	611	892	1065	836
Cu	−1	−1	−1	−1	−1	−1	−1
Ni	22	19	26	25	22	27	25
Pb	−1	−1	−1	−1	−1	−1	−1
U	6	46	31	6	45	47	45
Th	133	161	646	235	285	233	271
V	0	4	28	0	19	27	37
Cr	0	0	1	1	0	0	0
Nd	1463	2032	1707	1482	1558	1870	1759
Ga	13	3	8	11	4	4	0
La	2099	2182	1998	2171	1686	2325	2126
Ce	4104	4790	4086	4180	3702	4610	4268

NEPHELINE SYENITE ANALYSES

	G1	G2	G3	G4	G5	G6	G7	G8	G10	G11	G12	G13	G15	G16	G17	G19	G20
Rock type	LSS	LSS	LSS	LSS	LSS	LSS	LSS	MISC	CGBS	LSS	GS-B	LSS	LSS	USS	USS	USS	USS
Major elements, weight %																	
SiO2	55.03	56.38	56.49	55.77	59.81	52.05	54.02	45.17	50.19	52.59	47.81	57.26	56.84	55.57	57.11	57.96	54.08
Al2O3	19.32	22.34	21.16	21.54	21.69	17.38	21.03	11.21	20.17	16.47	20.00	20.00	19.61	20.01	21.14	22.24	19.96
Fe2O3	5.77	3.00	4.42	4.81	4.28	9.98	6.52	17.58	10.95	11.36	9.98	4.74	7.11	7.87	4.44	6.92	8.80
MgO	0.26	0.0	0.04	0.05	0.09	0.52	0.14	1.68	0.42	0.46	0.72	0.15	0.26	0.52	0.10	0.29	0.71
CaO	2.52	0.13	0.12	0.08	0.25	4.54	0.95	10.86	1.91	4.23	4.06	0.08	0.11	0.31	0.33	0.08	2.06
Na2O	5.54	8.92	8.26	8.52	3.85	8.52	7.45	8.46	7.93	7.72	10.08	7.51	6.01	7.76	9.60	4.53	5.53
K2O	7.32	7.40	7.67	7.56	7.97	4.76	6.30	1.62	5.47	4.59	4.00	7.96	7.93	5.79	5.95	5.32	5.59
TiO2	0.11	0.08	0.17	0.17	0.09	0.09	0.17	0.12	0.28	0.16	0.17	0.19	0.29	0.33	0.20	0.24	0.29
MnO	0.17	0.03	0.05	0.07	0.12	0.31	0.14	0.97	0.28	0.34	0.29	0.09	0.12	0.15	0.09	0.11	0.24
P2O5	0.05	0.02	0.0	0.0	0.0	0.06	0.0	0.11	0.01	0.05	0.13	0.0	0.0	0.02	0.03	0.03	0.03
LOI	4.05	1.93	1.81	1.62	1.91	1.98	3.49	2.49	2.55	2.17	3.07	2.20	1.84	1.81	1.23	2.29	2.81
Total	100.14	100.23	100.19	100.19	100.06	100.19	100.21	100.27	100.16	100.14	100.31	100.18	100.12	100.14	100.22	100.01	100.10
Trace elements ppm																	
Ba	263.	199.	190.	172.	401.	162.	207.	146.	143.	153.	113.	159.	212.	290.	242.	352.	370.
Nb	61.	44.	52.	72.	94.	52.	94.	110.	143.	86.	94.	73.	81.	146.	96.	148.	179.
Zr	463.	471.	269.	231.	234.	787.	405.	737.	742.	1005.	552.	129.	215.	208.	419.	549.	749.
Y	14.	0.	2.	1.	2.	17.	13.	50.	17.	28.	20.	3.	2.	8.	12.	7.	22.
Sr	918.	390.	275.	251.	177.	215.	281.	683.	318.	334.	191.	265.	330.	271.	246.	147.	753.
Rb	153.	163.	195.	199.	182.	155.	178.	95.	248.	156.	129.	243.	217.	197.	167.	171.	171.
Zn	80.	39.	52.	65.	134.	121.	101.	448.	168.	144.	143.	75.	97.	145.	92.	163.	134.
Cu	18.	17.	17.	17.	17.	20.	18.	20.	19.	18.	18.	17.	17.	17.	17.	18.	18.
Ni	8.	8.	9.	8.	9.	10.	8.	11.	11.	9.	9.	9.	9.	9.	8.	9.	9.
Pb	11.	10.	11.	10.	17.	11.	12.	12.	11.	11.	11.	10.	10.	11.	11.	12.	13.
U	3.	2.	2.	1.	2.	2.	2.	3.	2.	2.	2.	2.	2.	2.	2.	2.	2.
Th	8.	8.	8.	9.	9.	8.	8.	10.	7.	8.	9.	8.	8.	9.	9.	10.	10.
V	2.	0.	10.	7.	5.	7.	3.	0.	4.	4.	3.	3.	9.	12.	2.	7.	3.
Cr	8.	6.	6.	5.	7.	6.	6.	7.	8.	5.	6.	7.	6.	6.	6.	5.	5.
Nd	31.	13.	10.	16.	21.	58.	36.	148.	46.	69.	68.	8.	10.	28.	21.	37.	58.
Ga	37.	43.	39.	42.	42.	38.	43.	25.	49.	39.	36.	37.	38.	45.	47.	52.	40.
La	23.	8.	18.	6.	31.	46.	43.	155.	29.	65.	56.	17.	18.	31.	34.	50.	51.
Ce	41.	15.	23.	25.	34.	88.	56.	257.	54.	107.	100.	15.	22.	32.	56.	48.	100.

SUMMARY NORM TABLE

	G1	G2	G3	G4	G5	G6	G7	G8	G10	G11	G12	G13	G15	G16	G17	G19	G20
Rock type	LSS	LSS	LSS	LSS	LSS	LSS	LSS	MISC	CGBS	LSS	GS-B	LSS	LSS	USS	USS	USS	USS
Quartz	0.0	0.0	0.0	0.0	6.50	0.0	0.0	0.0	0.0	0.0	0.0	0.0	0.0	0.0	0.0	10.70	0.0
Corundum	0.0	0.0	0.0	0.0	6.60	0.0	0.90	0.0	0.0	0.0	0.0	0.0	1.10	0.80	0.0	9.00	1.70
Zircon	0.30	0.30	0.20	0.10	0.10	0.50	0.20	0.0	0.40	0.60	0.30	0.10	0.10	0.10	0.30	0.30	0.50
Orthoclase	43.20	43.60	45.30	44.60	47.10	28.10	37.20	0.0	32.30	27.10	23.70	47.00	46.90	34.20	35.10	31.50	33.00
Albite	28.60	22.30	22.00	20.60	32.60	19.20	30.70	0.0	23.40	28.10	14.70	23.90	31.90	38.70	30.50	38.40	38.30
Anorthite	6.20	0.0	0.0	0.0	0.50	0.0	2.80	0.0	3.30	0.0	0.0	0.0	0.0	0.50	0.0	0.0	8.50
Nepheline	9.90	27.70	23.90	26.00	0.0	23.60	17.50	0.0	23.60	16.80	35.70	18.80	10.30	14.60	24.30	0.0	4.50
Acmite	0.0	1.50	3.30	3.00	0.0	8.10	0.0	0.0	0.0	5.40	4.10	4.40	0.0	0.0	4.90	0.0	0.0
Na Metasil	0.0	0.0	0.0	0.0	0.0	0.0	0.0	0.0	0.0	0.0	0.0	0.0	0.0	0.0	0.0	0.0	0.0
Diopside	0.40	0.0	0.20	0.0	0.0	7.20	0.0	0.0	0.0	6.00	0.0	0.0	0.0	0.0	0.50	0.0	0.0
Wollaston.	0.0	0.0	0.0	0.0	0.0	4.90	0.0	0.0	0.60	4.80	5.50	0.0	0.0	0.0	0.10	0.0	0.0
Hypersthen	0.0	0.0	0.0	0.0	0.20	0.0	0.0	0.0	0.0	0.0	0.0	0.0	0.0	0.0	0.0	0.70	0.0
Olivine	0.30	0.0	0.0	0.10	0.0	0.0	0.20	0.0	0.0	0.0	0.0	0.30	0.50	0.90	0.0	0.0	1.20
Magnetite	0.0	0.0	1.20	2.30	0.50	3.70	0.0	0.0	7.50	6.20	5.40	0.60	5.10	3.60	1.50	1.00	1.50
Chromite	0.0	0.0	0.0	0.0	0.0	0.0	0.0	0.0	0.0	0.0	0.0	0.0	0.0	0.0	0.0	0.0	0.0
Hematite	3.10	1.10	0.40	0.0	2.00	0.0	3.50	0.0	0.90	0.0	0.0	0.60	0.30	2.70	0.20	3.90	4.80
Ilmenite	5.30	2.80	3.40	3.10	3.60	3.80	6.10	0.0	4.80	4.10	5.80	4.20	3.50	3.40	2.30	4.40	5.30
Titanite	0.0	0.0	0.0	0.0	0.0	0.0	0.0	0.0	0.0	0.0	0.0	0.0	0.0	0.0	0.0	0.0	0.0
Perovskite	2.20	0.30	0.0	0.0	0.0	0.0	0.50	0.0	0.0	0.0	0.0	0.0	0.0	0.0	0.0	0.0	0.0
Rutile	0.0	0.30	0.0	0.0	0.0	0.0	0.0	0.0	0.0	0.0	0.0	0.0	0.0	0.0	0.0	0.0	0.0
Apatite	0.40	0.10	0.10	0.20	0.30	0.70	0.30	0.0	0.70	0.80	0.70	0.20	0.30	0.40	0.20	0.30	0.60
Fluorite	0.10	0.0	0.0	0.0	0.0	0.10	0.0	0.0	0.40	0.10	0.0	0.0	0.0	0.0	0.10	0.10	0.0
Calcite	0.0	-0.10	0.0	-0.0	0.0	0.0	0.0	0.0	0.0	0.0	0.0	-0.10	-0.10	0.0	0.0	-0.20	0.0
Water	0.10	0.10	0.20	0.20	0.10	0.10	0.20	0.0	0.30	0.20	0.20	0.20	0.30	0.30	0.20	0.20	0.30
Na/(Na+K)	0.53	0.0	0.62	0.0	0.42	0.73	0.64	0.0	0.69	0.72	0.79	0.0	0.0	0.67	0.71	0.0	0.60
(Na+K)/Al	0.88	1.02	1.03	1.03	0.69	1.10	0.91	0.0	0.94	1.07	1.05	1.05	0.94	0.95	1.05	0.59	0.76
F3/(F2+F3)	0.54	0.54	0.54	0.54	0.54	0.54	0.54	0.0	0.56	0.54	0.52	0.54	0.54	0.66	0.66	0.66	0.66
Diff Index	81.70	95.10	94.50	94.20	86.20	79.00	85.40	0.0	79.30	77.40	78.20	94.10	89.10	87.50	94.80	80.60	75.80
Qz residua	38.87	31.03	32.50	31.46	48.46	29.52	35.28	33.33	31.11	34.14	22.90	34.83	39.13	37.14	32.40	51.98	41.95
Ks residua	30.05	26.47	28.23	27.79	31.05	22.52	24.75	33.33	23.15	21.39	18.18	29.78	29.91	22.21	22.19	22.21	24.74
Ne residua	31.08	42.50	39.27	40.74	20.49	47.96	39.97	33.33	45.74	44.47	58.92	35.39	30.95	40.64	45.41	25.81	33.31

NEPHELINE SYENITE ANALYSES

	G49	G59	G60	G61	G62	G63	G64	G64A	G67D	G68A	G70	G71	G72	G77	G78	G79	G80
Rock type	USS	USS	GS-B	GS-B	CGBS	MMS	MMS	MMS	XPS	XPS	CGS	CGS	USS	PMS	XPS	XPS	XPS
Major elements, weight %																	
SiO2	57.14	54.59	53.07	52.02	54.56	54.17	52.77	53.19	52.36	52.52	56.58	55.08	48.98	54.43	51.20	52.08	55.41
Al2O3	22.60	20.01	21.64	22.51	25.07	20.54	21.41	20.81	18.79	17.54	23.70	24.84	23.08	20.44	17.92	18.82	21.30
Fe2O3	5.65	6.90	7.52	6.55	6.26	7.48	6.83	7.09	8.10	8.63	4.97	4.54	3.89	7.87	8.63	7.73	5.96
MgO	0.16	0.39	0.34	0.29	0.25	0.39	0.43	0.55	0.34	0.41	0.39	0.31	0.26	0.32	0.30	0.32	0.42
CaO	0.80	2.77	1.87	1.49	0.89	1.34	1.64	2.02	3.94	3.88	0.77	0.29	3.89	1.33	3.43	2.93	1.57
Na2O	4.46	8.56	5.99	9.47	3.01	8.22	7.63	7.51	6.34	6.74	5.94	5.45	6.38	6.57	9.27	8.98	9.02
K2O	6.31	4.78	5.90	5.88	6.39	6.06	6.79	7.12	4.57	4.91	3.90	5.90	5.99	6.73	4.86	4.96	2.31
TiO2	0.19	0.07	0.20	0.18	0.19	0.16	0.33	0.34	0.19	0.21	0.33	0.30	0.15	0.27	0.20	0.18	0.25
MnO	0.14	0.19	0.20	0.20	0.12	0.19	0.17	0.17	0.25	0.27	0.12	0.12	0.14	0.17	0.25	0.19	0.14
P2O5	0.07	0.25	0.17	0.14	0.21	0.22	0.21	0.25	0.29	0.40	0.11	0.10	0.78	0.11	0.26	0.24	0.21
LOI	2.55	1.67	3.26	1.45	3.07	1.39	1.97	1.07	5.01	4.66	3.24	3.17	6.73	1.89	3.98	3.84	3.62
Total	100.07	100.18	100.16	100.18	100.02	100.16	100.18	100.12	100.18	100.17	100.05	100.10	100.27	100.13	100.30	100.27	100.21
Trace elements ppm																	
Ba	325.	187.	189.	206.	281.	161.	256.	238.	591.	439.	813.	702.	795.	165.	442.	431.	353.
Nb	86.	54.	117.	144.	145.	97.	94.	60.	243.	294.	149.	95.	118.	62.	223.	182.	187.
Zr	472.	748.	597.	626.	443.	376.	216.	181.	1361.	1417.	315.	328.	312.	229.	1300.	1126.	1443.
Y	31.	23.	24.	31.	19.	8.	14.	17.	49.	41.	17.	17.	62.	1.	38.	34.	43.
Sr	133.	262.	806.	347.	238.	219.	523.	706.	1218.	1132.	933.	1013.	2778.	334.	711.	671.	908.
Rb	198.	141.	173.	162.	178.	184.	152.	126.	127.	135.	91.	146.	120.	193.	146.	153.	67.
Zn	122.	94.	130.	119.	199.	120.	118.	85.	131.	129.	158.	122.	121.	98.	136.	141.	106.
Cu	18.	16.	19.	19.	18.	19.	20.	20.	19.	19.	19.	20.	22.	21.	18.	19.	18.
Ni	9.	10.	10.	9.	8.	8.	8.	9.	8.	10.	7.	7.	11.	7.	10.	10.	9.
Pb	12.	12.	12.	12.	13.	10.	11.	11.	14.	14.	13.	12.	14.	10.	13.	12.	12.
U	2.	1.	3.	2.	3.	1.	2.	3.	4.	4.	3.	3.	5.	2.	3.	3.	4.
Th	10.	9.	10.	10.	11.	8.	9.	9.	10.	10.	9.	10.	11.	9.	10.	9.	10.
V	5.	1.	5.	3.	8.	4.	8.	7.	4.	10.	8.	6.	4.	4.	9.	9.	11.
Cr	6.	6.	6.	6.	6.	5.	5.	5.	5.	5.	7.	6.	4.	6.	5.	6.	6.
Nd	53.	77.	47.	68.	46.	41.	55.	75.	99.	110.	47.	43.	99.	37.	98.	92.	72.
Ga	45.	42.	35.	35.	45.	35.	28.	27.	33.	35.	32.	38.	32.	34.	34.	36.	32.
La	73.	80.	55.	69.	43.	23.	53.	78.	125.	107.	65.	61.	95.	21.	100.	90.	88.
Ce	120.	121.	88.	98.	95.	56.	75.	104.	214.	172.	95.	86.	169.	35.	178.	154.	128.

SUMMARY NORM TABLE

	G49	G59	G60	G61	G62	G63	G64	G64A	G67D	G68A	G70	G71	G72	G77	G78	G79	G80
Rock type	USS	USS	GS-B	GS-B	CGBS	MMS	MMS	MMS	XPS	XPS	CGS	CGS	USS	PMS	XPS	XPS	XPS
Quartz	5.90	0.0	0.0	0.0	11.10	0.0	0.0	0.0	0.0	0.0	5.80	0.0	0.0	0.0	0.0	0.0	0.0
Corundum	8.00	0.0	2.50	0.0	12.40	0.0	0.0	0.0	1.30	0.0	9.70	9.50	6.10	0.50	0.0	0.0	3.90
Zircon	0.30	0.40	0.40	0.40	0.30	0.20	0.10	0.10	0.80	0.80	0.20	0.20	0.20	0.10	0.80	0.70	0.90
Orthoclase	37.30	28.20	34.90	34.70	37.80	35.80	40.10	42.10	26.90	28.90	23.10	34.90	35.50	39.80	28.50	29.10	13.60
Albite	37.70	35.00	32.90	19.20	25.50	28.80	20.20	18.00	42.50	38.50	50.30	46.20	29.40	29.50	20.10	26.80	61.90
Anorthite	1.30	2.10	8.00	1.60	2.20	1.30	4.10	2.00	5.60	3.10	0.0	0.0	0.0	5.00	0.0	0.0	0.0
Nepheline	0.0	20.20	9.70	33.00	0.0	22.10	24.00	24.70	5.90	9.90	0.0	0.0	13.40	14.20	24.10	22.80	7.60
Acmite	0.0	0.0	0.0	0.0	0.0	0.0	0.0	0.0	0.0	0.0	0.0	0.0	0.0	0.0	11.70	5.90	0.0
Na Metasil	0.0	0.0	0.0	0.0	0.0	0.0	0.0	0.0	0.0	0.0	0.0	0.0	0.0	0.0	0.0	0.0	0.0
Diopside	0.0	2.10	2.20	4.30	0.0	2.10	1.40	3.70	0.0	2.20	0.0	0.0	0.0	0.0	1.60	1.70	0.0
Wollaston.	0.0	2.70	0.0	0.80	0.0	0.10	0.0	0.40	0.0	0.20	0.0	0.0	0.0	0.0	2.20	1.20	0.0
Hypersthen	0.40	0.0	0.0	0.0	0.60	0.0	0.0	0.0	0.0	0.0	1.00	0.80	0.0	0.0	0.0	0.0	0.0
Olivine	0.0	0.0	0.60	0.0	0.0	0.0	0.30	0.0	0.60	0.0	0.0	0.0	0.50	0.60	0.0	0.0	0.70
Magnetite	0.0	2.20	1.70	4.90	0.0	5.60	3.70	6.00	0.0	0.0	0.0	0.0	0.0	5.00	0.0	0.0	0.0
Chromite	0.0	0.0	0.0	0.0	0.0	0.0	0.0	0.0	0.0	0.0	0.0	0.0	0.0	0.0	0.0	0.0	0.0
Hematite	3.70	3.00	2.70	0.0	3.50	0.50	1.40	0.0	6.40	6.80	3.00	2.80	2.60	1.10	2.70	4.00	4.70
Ilmenite	4.00	3.20	6.20	2.80	5.60	2.60	3.70	2.00	3.60	3.90	4.40	4.00	2.80	3.60	3.80	3.40	2.90
Titanite	1.00	0.0	0.0	0.0	0.20	0.0	0.0	0.0	0.0	0.0	2.30	0.90	0.0	0.0	0.0.	0.0	0.0
Perovskite	0.0	0.0	0.0	0.0	0.0	0.0	0.0	0.0	5.20	4.40	0.0	0.10	8.90	0.0	3.30	3.40	3.50
Rutile	0.0	0.0	0.0	0.0	0.0	0.0	0.0	0.0	0.0	0.0	0.0	0.60	0.0	0.0	0.0	0.0	0.0
Apatite	0.30	0.40	0.50	0.50	0.30	0.40	0.40	0.40	0.60	0.60	0.30	0.30	0.30	0.40	0.60	0.40	0.30
Fluorite	0.10	0.50	0.0	0.0	0.0	0.40	0.40	0.50	0.60	0.80	0.20	0.20	1.60	0.20	0.50	0.50	0.40
Calcite	0.0	0.0	0.0	0.0	0.0	0.0	0.0	0.0	0.0	0.0	-0.30	-0.50	-1.40	0.0	0.0	0.0	-0.50
Water	0.20	0.10	0.20	0.20	0.20	0.20	0.30	0.30	0.20	0.20	0.30	0.30	0.10	0.30	0.20	0.20	0.30
Na/(Na+K)	0.52	0.73	0.61	0.71	0.42	0.67	0.63	0.62	0.68	0.68	0.0	0.0	0.0	0.60	0.74	0.73	0.0
(Na+K)/Al	0.63	0.96	0.75	0.97	0.47	0.98	0.93	0.96	0.82	0.94	0.59	0.62	0.74	0.89	1.14	1.07	0.81
F3/(F2+F3)	0.66	0.66	0.52	0.52	0.56	0.58	0.58	0.58	0.79	0.79	0.61	0.61	0.66	0.58	0.79	0.79	0.79
Diff Index	80.90	83.40	77.50	86.90	74.40	86.70	84.30	84.80	75.30	77.30	79.20	81.10	78.30	83.50	84.40	84.60	83.10
Oz residua	48.55	33.83	38.90	27.36	52.56	33.05	31.52	31.16	41.29	38.97	49.02	44.69	36.78	36.77	29.59	31.57	41.20
Ks residua	26.20	19.22	25.59	22.69	28.87	23.47	27.03	28.21	20.30	21.25	16.58	24.46	25.77	27.09	22.28	21.01	9.30
Ne residua	25.24	46.95	35.51	49.94	18.57	43.48	41.45	40.63	38.41	39.79	34.40	30.86	37.45	36.14	48.13	47.42	49.50

NEPHELINE SYENITE ANALYSES

	G81	G82	G84	G85	G87	G88	G89	G91	G92	G93	G109	G110	G111	G112	G113	G114	G115
Rock type	GS-B	CGBS	GS-B	CGBS	GS-B	XPS	XPS	USS	XPS	XPS	USS	MMS	USS	USS	Gneiss	Gneiss	USS
Major elements, weight %																	
SiO2	50.23	56.66	45.37	58.58	49.12	52.54	53.22	51.92	56.83	52.76	57.45	55.40	54.16	54.69	66.01	64.67	55.42
Al2O3	19.57	24.99	20.88	23.66	17.94	17.43	18.27	16.41	18.96	18.72	20.48	17.77	19.28	20.58	15.22	15.07	20.68
Fe2O3	9.61	4.97	10.60	3.84	10.83	10.02	7.73	8.97	6.91	8.41	4.89	11.21	8.39	7.56	4.05	4.41	4.12
MgO	0.61	0.12	0.62	0.0	0.84	0.54	0.15	0.18	0.20	0.45	0.24	0.50	0.33	0.29	1.28	1.42	0.17
CaO	4.17	0.21	4.89	0.36	5.11	3.55	3.07	6.83	2.06	2.81	1.89	1.02	1.45	1.39	3.04	2.99	1.15
Na2O	9.30	4.04	9.78	4.80	8.94	7.95	9.16	6.61	6.21	7.16	3.21	5.67	9.30	6.55	4.69	4.95	7.89
K2O	4.01	6.49	3.68	6.13	3.61	4.27	4.17	1.85	4.98	4.91	8.89	6.01	5.28	5.43	3.69	3.89	6.70
TiO2	0.15	0.14	0.14	0.07	0.15	0.20	0.17	0.04	0.18	0.26	0.12	0.23	0.27	0.33	0.79	0.72	0.14
MnO	0.23	0.10	0.27	0.10	0.34	0.35	0.26	0.39	0.15	0.20	0.16	0.28	0.22	0.21	0.05	0.07	0.09
P2O5	0.33	0.0	1.58	0.15	0.10	0.31	0.08	0.09	0.20	0.32	0.05	0.0	0.0	0.03	0.24	0.22	0.03
LOI	2.02	2.32	2.43	2.37	3.28	3.02	4.01	6.88	3.44	4.22	2.68	2.00	1.53	3.11	1.02	1.70	3.81
Total	100.23	100.04	100.24	100.06	100.26	100.18	100.29	100.17	100.12	100.22	100.06	100.09	100.21	100.17	100.08	100.11	100.20
Trace elements ppm																	
Ba	146.	259.	111.	276.	128.	461.	309.	1017.	573.	474.	613.	221.	201.	280.	1471.	1288.	386.
Nb	90.	145.	213.	64.	121.	301.	596.	118.	256.	261.	134.	101.	85.	110.	23.	44.	136.
Zr	598.	558.	964.	405.	826.	1671.	1765.	194.	1312.	1111.	996.	523.	885.	770.	360.	385.	458.
Y	20.	23.	65.	10.	17.	29.	36.	40.	16.	34.	24.	1.	18.	20.	16.	31.	24.
Sr	178.	189.	215.	221.	193.	1167.	986.	2485.	897.	1149.	719.	366.	145.	306.	670.	611.	647.
Rb	121.	174.	124.	154.	105.	133.	131.	90.	127.	152.	196.	243.	201.	181.	105.	109.	197.
Zn	117.	129.	161.	76.	135.	156.	141.	241.	141.	152.	153.	183.	131.	123.	68.	84.	107.
Cu	18.	17.	18.	17.	18.	20.	19.	22.	17.	20.	19.	21.	17.	17.	20.	23.	17.
Ni	9.	10.	12.	9.	8.	9.	8.	10.	7.	8.	9.	10.	11.	9.	11.	12.	10.
Pb	11.	14.	12.	12.	11.	11.	13.	12.	12.	12.	13.	12.	11.	11.	15.	15.	12.
U	2.	2.	2.	2.	2.	4.	5.	4.	4.	4.	2.	2.	2.	2.	2.	3.	3.
Th	8.	11.	9.	9.	9.	9.	10.	15.	8.	11.	10.	9.	9.	9.	13.	12.	10.
V	3.	0.	1.	3.	8.	4.	2.	6.	8.	7.	1.	0.	4.	10.	70.	57.	6.
Cr	6.	6.	6.	5.	8.	5.	7.	4.	5.	5.	6.	7.	5.	6.	14.	15.	7.
Nd	87.	49.	219.	45.	57.	129.	126.	311.	65.	68.	73.	24.	45.	45.	69.	84.	50.
Ga	39.	39.	41.	33.	36.	38.	28.	38.	39.	32.	34.	44.	41.	44.	19.	23.	34.
La	58.	70.	167.	45.	49.	90.	133.	233.	59.	70.	130.	23.	57.	52.	121.	142.	52.
Ce	113.	70.	325.	72.	87.	178.	223.	412.	112.	124.	172.	31.	73.	89.	173.	206.	83.

SUMMARY NORM TABLE

	G81	G82	G84	G85	G87	G88	G89	G91	G92	G93	G109	G110	G111	G112	G113	G114	G115
Rock type	GS-B	CGBS	GS-B	CGBS	GS-B	XPS	XPS	USS	XPS	XPS	USS	MMS	USS	USS	Gneiss	Gneiss	USS
Quartz	0.0	7.90	0.0	6.70	0.0	0.0	0.0	0.0	0.0	0.0	1.40	0.0	0.0	0.0	0.0	0.0	0.0
Corundum	0.0	11.20	0.0	9.10	0.0	0.0	0.0	0.0	2.60	0.40	3.70	0.80	0.0	2.20	0.0	0.0	0.40
Zircon	0.40	0.30	0.60	0.20	0.50	1.00	1.10	0.10	0.80	0.70	0.60	0.30	0.50	0.50	0.0	0.0	0.30
Orthoclase	23.80	38.30	22.10	36.30	21.30	25.10	24.40	10.90	29.30	28.90	52.40	35.60	31.10	32.00	0.0	0.0	39.50
Albite	24.80	34.20	12.90	40.70	23.50	36.60	35.00	56.00	52.30	39.10	27.10	42.70	25.70	40.80	0.0	0.0	31.10
Anorthite	0.0	0.40	2.20	0.0	0.0	0.0	0.0	9.60	2.00	3.50	5.00	3.20	0.0	4.80	0.0	0.0	0.0
Nepheline	29.10	0.0	38.50	0.0	26.40	15.60	19.00	0.0	0.0	11.50	0.0	2.90	23.80	7.80	0.0	0.0	19.30
Acmite	0.30	0.0	0.0	0.0	3.00	1.20	5.90	0.0	0.0	0.0	0.0	0.0	7.80	0.0	0.0	0.0	0.0
Na Metasil	0.0	0.0	0.0	0.0	0.0	0.0	0.0	0.0	0.0	0.0	0.0	0.0	0.0	0.0	0.0	0.0	0.0
Diopside	3.60	0.0	4.50	0.0	0.10	2.90	0.80	1.00	0.0	0.0	0.0	0.0	2.40	0.0	0.0	0.0	0.0
Wollaston.	5.80	0.0	6.70	0.0	7.20	3.20	1.90	2.90	0.0	0.0	0.0	0.0	1.10	0.0	0.0	0.0	0.0
Hypersthen	0.0	0.30	0.0	0.0	0.0	0.0	0.0	0.0	0.50	0.0	0.60	0.0	0.0	0.0	0.0	0.0	0.0
Olivine	0.0	0.0	0.0	0.0	0.0	0.0	0.0	0.0	0.0	0.80	0.0	0.90	0.0	0.50	0.0	0.0	0.30
Magnetite	7.10	0.10	8.10	0.0	6.10	0.0	0.0	0.0	0.0	0.0	0.0	8.60	4.10	0.0	0.0	0.0	0.0
Chromite	0.0	0.0	0.0	0.0	0.0	0.0	0.0	0.0	0.0	0.0	0.0	0.0	0.0	0.0	0.0	0.0	0.0
Hematite	0.0	2.70	0.0	2.20	0.40	7.40	4.00	5.90	5.40	6.60	3.20	0.50	0.0	5.00	0.0	0.0	2.70
Ilmenite	3.80	4.40	4.70	3.40	6.20	4.40	3.40	5.90	3.10	3.90	3.40	3.80	2.90	5.60	0.0	0.0	3.00
Titanite	0.0	0.0	0.0	1.30	0.0	0.0	0.0	0.50	0.70	0.0	2.20	0.0	0.0	0.0	0.0	0.0	0.0
Perovskite	0.0	0.0	0.0	0.0	0.0	1.20	3.70	6.10	2.50	3.70	0.0	0.0	0.0	0.30	0.0	0.0	2.80
Rutile	0.0	0.0	0.0	0.10	0.0	0.0	0.0	0.0	0.0	0.0	0.0	0.0	0.0	0.0	0.0	0.0	0.60
Apatite	0.50	0.20	0.60	0.20	0.80	0.80	0.60	0.90	0.40	0.50	0.40	0.70	0.50	0.50	0.0	0.0	0.20
Fluorite	0.0	0.30	0.0	0.30	0.0	0.60	0.10	0.10	0.40	0.60	0.10	0.0	0.0	0.0	0.0	0.0	0.10
Calcite	0.0	0.0	0.0	-0.50	0.0	0.0	0.0	0.0	0.0	0.0	0.0	0.0	0.0	0.0	0.0	0.0	-0.30
Water	0.10	0.10	0.10	0.10	0.10	0.20	0.20	0.0	0.20	0.30	0.10	0.20	0.30	0.30	0.0	0.0	0.10
Na/(Na+K)	0.78	0.49	0.80	0.0	0.79	0.74	0.77	0.84	0.65	0.69	0.35	0.59	0.73	0.65	0.0	0.0	0.0
(Na+K)/Al	1.00	0.55	0.96	0.61	1.04	1.02	1.07	0.78	0.82	0.91	0.73	0.89	1.09	0.81	0.0	0.0	0.98
F3/(F2+F3)	0.52	0.56	0.52	0.56	0.52	0.79	0.79	0.66	0.79	0.79	0.66	0.58	0.66	0.66	0.0	0.0	0.66
Diff Index	78.00	80.40	73.50	83.70	74.20	78.50	84.30	66.90	81.60	79.50	80.90	81.20	88.40	80.60	0.0	0.0	89.90
Qz residua	27.85	49.89	21.02	49.01	28.04	35.72	33.90	45.40	44.87	38.23	45.04	43.03	31.27	40.34	33.33	33.33	34.82
Ks residua	17.41	27.07	17.09	24.65	17.00	18.45	17.69	9.26	20.41	20.66	36.81	24.92	21.93	22.56	33.33	33.33	24.97
Ne residua	54.74	23.04	61.89	26.34	54.96	45.83	48.42	45.34	34.72	41.11	18.15	32.06	46.80	37.10	33.33	33.33	40.21

NEPHELINE SYENITE ANALYSES

	G116	G117	G118A	G118B	G119	G120	G122	G123	G124	G125	G127	G128	G129	G130	G131	G132	G134
Rock type	USS	LSS	USS	USS	USS	USS	PMS	PMS	PMS	PMS	USS	USS	USS	USS	USS	USS	XPS
Major elements, weight %																	
SiO2	59.67	59.26	56.66	39.32	53.55	53.24	58.37	53.53	53.52	54.02	57.59	60.48	55.45	57.66	56.84	50.97	53.49
Al203	20.71	19.49	19.23	7.34	19.06	20.71	19.27	20.94	20.71	21.19	18.49	20.67	17.15	23.13	23.64	18.92	18.63
Fe203	6.50	5.63	6.63	34.19	10.01	7.23	7.73	7.42	7.31	6.56	10.95	1.84	10.75	4.83	4.20	6.41	8.50
MgO	0.43	0.09	0.28	1.46	0.39	0.37	0.0	0.52	0.46	0.18	0.79	0.04	0.89	0.38	0.60	0.70	0.27
CaO	0.98	0.20	1.51	7.89	1.24	1.54	0.27	1.62	1.06	0.98	0.43	1.87	2.09	0.38	0.98	4.85	3.76
Na20	4.33	5.91	10.12	5.49	7.92	8.23	7.48	8.10	8.48	9.67	8.32	6.58	6.09	4.82	3.53	1.24	3.57
K20	6.78	8.04	3.65	1.96	4.99	6.03	5.78	5.84	6.09	5.87	1.23	5.37	5.33	6.15	6.80	10.61	6.83
TiO2	0.24	0.22	0.15	0.71	0.31	0.24	0.15	0.23	0.25	0.16	0.34	0.07	0.43	0.23	0.22	0.31	0.16
MnO	0.18	0.11	0.22	0.64	0.16	0.15	0.05	0.16	0.17	0.16	0.25	0.17	0.25	0.10	0.09	0.31	0.28
P205	0.19	0.0	0.08	0.09	0.04	0.33	0.0	0.15	0.20	0.0	0.0	0.08	0.02	0.02	0.08	0.35	0.26
LOI	0.0	1.13	1.73	1.00	2.54	2.12	1.05	1.66	1.94	1.43	1.78	2.97	1.66	2.37	3.06	5.39	4.34
Total	100.01	100.08	100.26	100.09	100.21	100.19	100.15	100.17	100.19	100.22	100.17	100.14	100.11	100.07	100.04	100.06	100.09
Trace elements ppm																	
Ba	0.	623.	569.	143.	232.	167.	154.	143.	155.	220.	271.	551.	211.	426.	557.	1349.	754.
Nb	0.	146.	58.	124.	93.	63.	48.	96.	141.	106.	328.	110.	189.	133.	97.	316.	112.
Zr	0.	739.	153.	1851.	325.	184.	297.	316.	570.	834.	1381.	693.	906.	427.	172.	192.	1781.
Y	0.	45.	20.	21.	9.	15.	0.	8.	15.	5.	10.	50.	17.	13.	8.	68.	37.
Sr	0.	426.	907.	257.	545.	284.	637.	323.	252.	332.	291.	765.	139.	282.	460.	2062.	1233.
Rb	0.	179.	121.	126.	152.	169.	121.	168.	193.	169.	47.	126.	175.	176.	180.	297.	208.
Zn	0.	127.	108.	294.	128.	85.	60.	122.	150.	104.	244.	126.	190.	137.	104.	176.	190.
Cu	0.	19.	18.	20.	19.	19.	17.	19.	19.	19.	25.	18.	19.	16.	18.	24.	22.
Ni	0.	13.	7.	7.	6.	10.	6.	8.	10.	8.	7.	9.	10.	9.	9.	14.	11.
Pb	0.	13.	11.	10.	10.	11.	11.	11.	12.	12.	13.	17.	12.	14.	14.	15.	14.
U	0.	2.	3.	3.	2.	2.	2.	2.	2.	2.	3.	3.	3.	2.	2.	4.	3.
Th	0.	10.	8.	6.	9.	9.	8.	8.	8.	9.	11.	11.	9.	9.	10.	11.	12.
V	0.	9.	3.	31.	8.	7.	4.	9.	5.	5.	14.	1.	16.	8.	12.	13.	6.
Cr	0.	6.	5.	7.	5.	6.	7.	6.	6.	6.	6.	5.	5.	4.	6.	6.	8.
Nd	0.	92.	77.	89.	45.	42.	12.	47.	43.	28.	32.	145.	35.	38.	25.	220.	62.
Ga	0.	37.	31.	29.	40.	33.	40.	33.	36.	42.	43.	36.	38.	50.	34.	25.	49.
La	0.	121.	82.	84.	38.	32.	10.	30.	44.	13.	35.	219.	28.	54.	23.	231.	63.
Ce	0.	181.	128.	145.	74.	60.	6.	57.	73.	42.	82.	308.	70.	67.	35.	378.	127.

SUMMARY NORM TABLE

	G116	G117	G118A	G118D	G119	G120	G122	G123	G124	G125	G127	G128	G129	G130	G131	G132	G134
Rock type	USS	LSS	USS	USS	USS	USS	PMS	PMS	PMS	PMS	USS	USS	USS	USS	USS	USS	XPS
Quartz	6.50	0.0	0.0	0.0	0.0	0.0	0.0	0.0	0.0	0.0	2.80	0.0	0.0	5.10	8.30	0.0	0.90
Corundum	5.30	1.00	0.0	0.0	0.0	0.0	0.30	0.0	0.0	0.0	3.30	4.00	0.0	8.50	10.50	1.60	2.70
Zircon	0.0	0.40	0.10	1.10	0.20	0.10	0.20	0.20	0.30	0.50	0.80	0.40	0.50	0.30	0.10	0.10	1.10
Orthoclase	40.20	47.40	21.50	11.60	29.50	35.60	34.20	34.50	35.90	34.60	7.20	31.60	31.50	36.30	40.30	62.70	40.10
Albite	36.70	36.20	43.10	9.50	37.10	26.50	46.30	27.50	26.70	21.60	70.10	55.50	41.80	40.80	29.90	6.40	30.00
Anorthite	2.70	0.30	0.0	0.0	1.70	1.80	1.00	3.50	0.50	0.0	0.50	0.0	3.70	0.0	0.0	10.30	7.20
Nepheline	0.0	7.40	19.20	9.50	16.20	23.30	9.20	22.20	24.40	29.50	0.0	0.0	5.20	0.0	0.0	2.20	0.0
Acmite	0.0	0.0	6.20	17.30	0.0	0.0	0.0	0.0	0.0	4.80	0.0	0.0	0.0	0.0	0.0	0.0	0.0
Na Metasil	0.0	0.0	0.0	0.0	0.0	0.0	0.0	0.0	0.0	0.0	0.0	0.0	0.0	0.0	0.0	0.0	0.0
Diopside	0.0	0.0	1.50	17.60	2.10	2.00	0.0	2.10	2.10	2.30	0.0	0.0	3.90	0.0	0.0	0.0	0.0
Wollaston.	0.0	0.0	1.60	5.80	0.20	0.30	0.0	0.0	0.0	0.40	0.0	0.0	0.0	0.0	0.0	0.0	0.0
Hypersthen	1.60	0.0	0.0	0.0	0.0	0.0	0.0	0.0	0.0	0.0	2.00	0.10	0.0	0.90	1.50	0.0	0.70
Olivine	0.0	0.40	0.0	0.0	0.0	0.0	0.20	0.20	0.10	0.0	0.0	0.0	0.30	0.0	0.0	1.20	0.0
Magnetite	6.20	4.40	2.00	24.10	3.50	1.80	6.50	5.00	4.10	3.10	6.70	0.0	7.20	0.0	0.0	0.0	0.0
Chromite	0.0	0.0	0.0	0.0	0.0	0.0	0.0	0.0	0.0	0.0	0.0	0.0	0.0	0.0	0.0	0.0	0.0
Hematite	0.0	0.0	0.90	0.0	4.20	3.60	0.0	0.90	1.40	0.0	2.60	1.20	2.10	3.20	2.80	4.20	6.70
Ilmenite	0.0	2.10	3.30	1.90	4.80	4.00	2.00	3.20	3.70	2.70	3.40	1.30	3.10	3.60	3.20	4.80	3.70
Titanite	0.0	0.0	0.0	0.0	0.0	0.0	0.0	0.0	0.0	0.0	0.0	4.70	0.0	1.20	3.40	0.0	5.80
Perovskite	0.0	0.0	0.0	0.0	0.0	0.0	0.0	0.0	0.0	0.0	0.0	0.60	0.0	0.0	0.0	4.90	0.0
Rutile	0.0	0.0	0.0	0.0	0.0	0.0	0.0	0.0	0.0	0.0	0.0	0.0	0.0	0.0	0.0	0.0	0.0
Apatite	0.40	0.30	0.50	1.50	0.40	0.40	0.10	0.40	0.40	0.40	0.60	0.40	0.60	0.20	0.20	0.70	0.70
Fluorite	0.40	0.0	0.10	0.10	0.10	0.70	0.0	0.30	0.40	0.0	0.0	0.10	0.0	0.0	0.20	0.70	0.50
Calcite	0.0	0.0	0.0	0.0	0.0	0.0	0.0	0.0	0.0	0.0	0.0	-0.0	0.0	-0.20	-0.30	0.0	0.0
Water	0.20	0.20	0.10	0.70	0.30	0.20	0.10	0.20	0.30	0.20	0.30	0.10	0.40	0.20	0.20	0.30	0.20
Na/(Na+K)	0.49	0.53	0.81	0.81	0.71	0.67	0.66	0.68	0.68	0.71	0.91	0.0	0.63	0.0	0.0	0.15	0.44
(Na+K)/Al	0.70	0.95	1.07	1.52	0.97	0.97	0.96	0.94	0.99	1.05	0.81	0.80	0.92	0.63	0.56	0.71	0.71
F3/(F2+F3)	0.66	0.54	0.66	0.66	0.66	0.66	0.58	0.58	0.58	0.58	0.66	0.66	0.66	0.66	0.66	0.66	0.79
Diff Index	83.40	91.00	90.00	47.90	82.80	85.40	89.70	84.20	87.00	90.50	80.10	87.10	78.50	82.20	78.50	71.30	71.00
Oz residua	48.77	40.72	34.65	30.59	35.92	32.22	40.12	32.66	31.88	28.98	47.48	44.86	41.73	48.02	50.19	42.08	45.01
Ks residua	27.39	29.60	14.58	21.54	20.25	23.69	21.67	23.29	23.45	22.94	5.11	20.62	22.80	25.10	29.18	49.98	32.10
Ne residua	23.84	29.68	50.77	47.86	43.84	44.09	38.22	44.06	44.67	48.08	47.41	34.52	35.47	26.89	20.63	7.95	22.89

NEPHELINE SYENITE ANALYSES

	G135	G137	G138	G140	G141	G142	G143	G144	G145	G148	G149	G150	G151	G152B	G153	G155	G156
Rock type	USS	XPS	XPS	XPS	XPS	USS	PMS	XPS	XPS	MUS	USS	MUS	USS	PMS	USS	USS	USS
Major elements, weight %																	
SiO2	53.72	59.66	57.39	58.04	56.68	57.15	53.36	55.07	54.00	48.46	56.16	48.12	54.05	55.57	50.92	53.71	56.05
Al2O3	20.38	17.41	18.53	20.67	20.63	20.62	21.50	24.43	18.69	19.16	19.46	12.90	21.98	21.67	20.61	22.96	20.39
Fe2O3	6.98	3.67	7.00	4.85	7.04	4.85	6.56	5.62	8.07	13.76	6.13	15.83	6.33	5.77	4.83	4.62	4.09
MgO	0.31	0.10	0.18	0.21	0.11	0.06	0.52	0.38	0.40	0.81	0.24	1.90	0.50	0.36	0.25	0.59	0.33
CaO	2.87	3.35	2.19	1.80	1.17	1.09	1.57	1.50	2.42	2.87	1.93	9.15	0.77	1.28	1.12	2.29	1.37
Na2O	9.40	5.19	5.99	4.46	4.37	7.15	8.58	4.79	7.12	7.03	7.91	6.03	6.18	7.40	9.81	3.08	6.17
K2O	4.70	6.82	4.70	6.35	6.38	6.95	6.77	4.20	4.84	5.18	6.15	3.29	6.47	6.74	6.86	8.61	7.45
TiO2	0.07	0.02	0.17	0.46	0.15	0.17	0.31	0.25	0.22	0.46	0.12	0.49	0.28	0.23	0.30	0.22	0.30
MnO	0.21	0.20	0.34	0.14	0.23	0.11	0.12	0.13	0.27	0.24	0.16	0.43	0.13	0.16	0.24	0.13	0.15
P2O5	0.22	0.08	0.13	0.10	0.27	0.01	0.19	0.13	0.35	0.09	0.13	1.36	0.20	0.09	0.01	0.10	0.04
LOI	1.31	3.63	3.49	3.00	3.06	2.00	0.65	3.56	3.77	2.08	1.72	0.61	3.26	0.81	5.32	3.77	3.86
Total	100.17	100.13	100.11	100.08	100.09	100.16	100.13	100.06	100.15	100.14	100.11	100.11	100.15	100.08	100.27	100.08	100.20
Trace elements ppm																	
Ba	163.	450.	381.	487.	723.	198.	179.	334.	689.	169.	153.	188.	278.	149.	319.	1179.	437.
Nb	54.	75.	469.	172.	270.	64.	48.	143.	223.	94.	60.	65.	75.	47.	109.	69.	78.
Zr	837.	947.	1338.	444.	1142.	221.	121.	981.	1262.	289.	307.	631.	170.	167.	328.	228.	93.
Y	21.	113.	63.	13.	42.	10.	1.	28.	19.	11.	16.	78.	10.	7.	4.	19.	44.
Sr	186.	410.	345.	462.	437.	374.	315.	658.	1253.	203.	273.	429.	527.	488.	913.	971.	580.
Rb	144.	163.	154.	157.	232.	183.	143.	146.	133.	186.	144.	96.	187.	164.	155.	205.	146.
Zn	97.	144.	158.	165.	134.	67.	59.	123.	201.	128.	69.	136.	78.	61.	53.	156.	91.
Cu	18.	19.	19.	22.	19.	19.	20.	20.	19.	20.	20.	22.	19.	20.	22.	20.	16.
Ni	9.	15.	11.	10.	10.	9.	5.	11.	7.	8.	9.	11.	8.	8.	8.	9.	11.
Pb	12.	13.	13.	13.	15.	12.	11.	15.	13.	11.	12.	10.	11.	11.	13.	13.	14.
U	2.	2.	4.	3.	3.	2.	2.	2.	3.	2.	2.	2.	2.	2.	3.	3.	3.
Th	9.	14.	11.	10.	10.	9.	8.	12.	9.	9.	9.	9.	9.	7.	11.	10.	10.
V	2.	0.	5.	11.	8.	8.	5.	13.	3.	16.	2.	19.	9.	5.	8.	7.	10.
Cr	6.	4.	6.	6.	7.	5.	7.	6.	7.	7.	6.	7.	6.	6.	6.	4.	6.
Nd	64.	250.	140.	46.	72.	28.	39.	54.	59.	56.	52.	311.	50.	32.	32.	50.	156.
Ga	44.	49.	36.	25.	38.	38.	29.	42.	40.	38.	37.	23.	37.	30.	27.	34.	34.
La	59.	239.	171.	73.	71.	29.	22.	78.	54.	47.	56.	226.	50.	42.	31.	55.	174.
Ce	121.	397.	245.	99.	112.	45.	50.	113.	108.	62.	78.	438.	65.	70.	56.	89.	293.

SUMMARY NORM TABLE

	G135	G137	G138	G140	G141	G142	G143	G144	G145	G148	G149	G150	G151	G152B	G153	G154	G156
Rock type	USS	XPS	XPS	XPS	XPS	USS	PMS	XPS	XPS	MUS	USS	MUS	USS	PMS	USS	USS	USS
Quartz	0.0	0.0	1.90	5.20	5.40	0.0	0.0	8.80	0.0	0.0	0.0	0.0	0.0	0.0	0.0	0.0	0.0
Corundum	0.0	0.0	3.00	5.60	6.50	0.0	0.0	12.00	1.00	0.0	0.0	0.0	4.80	0.40	0.0	7.40	2.20
Zircon	0.50	0.60	0.80	0.30	0.70	0.10	0.10	0.60	0.80	0.20	0.20	0.40	0.10	0.10	0.20	0.10	0.10
Orthoclase	27.70	40.10	27.60	37.50	37.70	41.00	40.00	24.80	28.50	30.70	36.30	19.50	38.30	39.90	40.50	50.90	44.10
Albite	30.80	43.70	50.40	37.70	36.90	32.40	18.00	40.50	43.90	20.10	32.50	20.70	36.90	28.30	7.70	26.10	33.40
Anorthite	0.0	4.10	1.70	2.40	0.0	3.60	0.20	0.0	2.10	5.50	0.0	0.0	0.0	4.90	0.0	3.20	0.0
Nepheline	25.80	0.0	0.0	0.0	0.0	15.20	29.60	0.0	8.70	21.50	18.00	14.90	8.40	18.60	32.60	0.0	10.20
Acmite	0.80	0.0	0.0	0.0	0.0	0.0	0.0	0.0	0.0	0.0	0.90	2.60	0.0	0.0	9.20	0.0	0.0
Na Metasil	0.0	0.0	0.0	0.0	0.0	0.0	0.0	0.0	0.0	0.0	0.0	0.0	0.0	0.0	1.10	0.0	0.0
Diopside	1.70	0.50	0.0	0.0	0.0	0.30	4.50	0.0	0.0	5.70	1.30	23.00	0.0	0.0	0.0	0.0	0.0
Wollaston.	4.00	0.10	0.0	0.0	0.0	0.0	0.10	0.0	0.0	0.0	2.60	3.40	0.0	0.0	0.0	0.0	0.0
Hypersthen	0.0	0.0	0.40	0.50	0.30	0.0	0.0	0.90	0.0	0.0	0.0	0.0	0.0	0.0	0.0	1.50	0.0
Olivine	0.0	0.0	0.0	0.0	0.0	0.0	0.0	0.0	0.70	1.40	0.0	0.0	0.90	0.90	0.40	0.0	0.60
Magnetite	3.30	0.0	0.0	0.0	0.0	0.0	5.50	0.0	0.0	10.20	1.40	10.40	0.0	4.80	0.0	0.0	0.0
Chromite	0.0	0.0	0.0	0.0	0.0	0.0	0.0	0.0	0.0	0.0	0.0	0.0	0.0	0.0	0.0	0.0	0.0
Hematite	2.10	2.90	5.50	3.80	5.60	3.20	0.0	4.40	6.30	0.0	2.70	0.0	4.20	0.0	0.0	3.00	2.70
Ilmenite	2.50	1.50	3.10	2.90	3.10	3.50	1.20	2.80	3.70	4.00	3.30	1.20	4.70	1.50	3.80	3.50	3.30
Titanite	0.0	3.40	4.50	3.60	3.50	0.0	0.0	5.10	0.0	0.0	0.0	0.0	0.0	0.0	0.0	1.70	0.0
Perovskite	0.0	2.40	0.0	0.0	0.0	0.30	0.0	0.0	3.10	0.0	0.0	0.0	1.40	0.0	2.70	2.10	3.30
Rutile	0.0	0.0	0.0	0.0	0.0	0.0	0.0	0.0	0.0	0.0	0.0	0.0	0.0	0.0	1.70	0.0	0.20
Apatite	0.50	0.50	0.80	0.30	0.50	0.30	0.30	0.30	0.60	0.60	0.40	1.00	0.30	0.40	0.60	0.30	0.40
Fluorite	0.40	0.10	0.20	0.20	0.50	0.0	0.40	0.30	0.70	0.20	0.30	2.80	0.40	0.20	0.0	0.20	0.10
Calcite	0.0	0.0	0.0	0.0	-0.70	0.0	0.0	-0.50	0.0	0.0	0.0	0.0	-0.30	0.0	-0.60	0.0	-0.40
Water	0.10	0.0	0.20	0.50	0.10	0.20	0.30	0.30	0.20	0.50	0.10	0.50	0.30	0.20	0.30	0.20	0.30
Na/(Na+K)	0.75	0.54	0.66	0.52	0.0	0.61	0.66	0.0	0.69	0.67	0.66	0.74	0.0	0.63	0.0	0.35	0.0
(Na+K)/Al	1.01	0.91	0.81	0.69	0.68	0.94	1.00	0.51	0.91	0.90	1.01	1.05	0.78	0.90	1.14	0.63	0.89
F3/(F2+F3)	0.66	0.79	0.79	0.79	0.79	0.66	0.58	0.79	0.79	0.51	0.66	0.51	0.66	0.58	0.66	0.66	0.66
Diff Index	85.10	83.80	79.90	80.40	80.00	88.60	87.60	74.10	81.10	72.30	87.70	57.70	83.60	86.80	91.10	77.00	87.70
Qz residua	30.93	44.56	46.20	48.09	48.23	36.74	29.13	51.37	39.98	31.07	35.21	32.50	40.01	34.79	26.01	44.07	39.16
Ks residua	18.67	27.19	19.63	26.51	26.78	26.30	25.95	19.02	19.97	24.13	23.77	20.11	26.04	26.12	28.49	37.57	28.58
Ne residua	50.40	28.25	34.17	25.40	24.99	36.97	44.92	29.61	40.05	44.80	41.02	47.39	33.96	39.09	45.51	18.36	32.26

NEPHELINE SYENITE ANALYSES

	G157	G158	G159	G160	G161	G162	G163	G164	G165	G166	G167	G168	G169	G170	G171	G172	G174
Rock type	PMS	USS	PMS	USS	CGBS	GS-B	GS-B	GS-B	GS-B	GS-B	PMS	GS-A	GS-A	GS-B	GS-B	GS-A	GS-B
Major elements, weight %																	
SiO2	54.59	52.99	41.31	52.11	53.01	52.62	66.21	61.03	65.65	53.85	69.68	53.27	57.75	55.66	56.26	55.12	52.64
Al2O3	19.90	18.65	15.31	21.50	23.51	22.96	17.92	14.57	18.06	22.35	13.97	22.63	17.83	19.06	22.15	17.17	21.93
Fe2O3	6.08	4.72	14.02	5.92	7.52	6.22	0.69	8.41	1.82	7.36	4.24	4.08	7.53	6.88	6.80	8.68	7.32
MgO	0.39	0.46	1.88	0.42	0.39	0.28	0.0	0.09	0.0	0.20	0.0	0.09	0.26	0.40	0.25	0.78	0.24
CaO	1.85	3.83	9.54	2.41	1.39	1.37	1.34	3.20	0.99	0.40	0.65	0.55	1.71	1.78	0.60	2.46	0.54
Na2O	4.68	7.90	9.88	6.81	2.15	8.82	8.55	8.51	8.86	4.78	6.24	10.91	7.66	7.95	8.01	7.82	8.06
K2O	6.62	7.00	1.92	7.53	8.06	5.90	3.72	2.84	3.40	5.92	4.37	5.70	5.10	5.05	5.37	4.50	6.18
TiO2	0.27	0.11	0.38	0.25	0.20	0.15	0.01	0.05	0.01	0.21	0.27	0.14	0.44	0.41	0.18	0.48	0.27
MnO	0.22	0.25	0.61	0.14	0.20	0.16	0.08	0.33	0.13	0.25	0.11	0.11	0.19	0.16	0.21	0.20	0.15
P2O5	0.27	0.14	0.08	0.25	0.15	0.14	0.07	0.45	0.02	0.10	0.0	0.03	0.09	0.13	0.18	0.20	0.03
LOI	5.26	4.13	5.39	2.80	3.46	1.48	1.47	0.59	1.18	4.72	0.55	2.71	1.57	2.73	2.27	2.70	2.79
Total	100.13	100.18	100.32	100.14	100.04	100.10	100.06	100.07	100.12	100.14	100.08	100.22	100.13	100.21	102.28	100.11	100.15
Trace elements ppm																	
Ba	560.	835.	688.	632.	820.	193.	126.	257.	166.	273.	85.	182.	366.	319.	187.	379.	211.
Nb	208.	140.	143.	74.	121.	52.	173.	176.	165.	192.	347.	109.	203.	249.	158.	279.	155.
Zr	888.	391.	406.	337.	612.	311.	2014.	1410.	1753.	957.	1628.	570.	960.	1041.	501.	1142.	405.
Y	36.	32.	45.	12.	22.	9.	28.	55.	27.	19.	193.	11.	71.	76.	15.	48.	18.
Sr	1658.	1418.	2099.	1335.	399.	339.	268.	414.	238.	276.	25.	374.	342.	603.	321.	944.	292.
Rb	149.	153.	94.	132.	262.	165.	83.	71.	77.	177.	211.	155.	166.	189.	193.	190.	193.
Zn	159.	107.	307.	84.	144.	89.	24.	131.	51.	214.	180.	95.	150.	151.	169.	172.	149.
Cu	19.	18.	24.	20.	19.	18.	14.	19.	15.	21.	14.	23.	20.	19.	21.	21.	19.
Ni	9.	9.	10.	8.	10.	8.	8.	9.	8.	7.	17.	8.	12.	13.	8.	11.	9.
Pb	12.	13.	13.	11.	12.	11.	12.	14.	13.	13.	24.	13.	14.	14.	12.	14.	11.
U	4.	7.	4.	3.	2.	2.	4.	4.	3.	2.	3.	2.	3.	4.	2.	4.	1.
Th	10.	11.	10.	9.	9.	8.	12.	11.	9.	10.	20.	9.	10.	10.	9.	11.	8.
V	4.	4.	29.	10.	7.	2.	0.	0.	2.	10.	9.	5.	15.	14.	2.	21.	5.
Cr	8.	5.	13.	6.	7.	6.	6.	5.	6.	7.	5.	6.	7.	6.	6.	7.	5.
Nd	99.	104.	182.	47.	69.	54.	87.	109.	63.	41.	214.	27.	81.	86.	44.	98.	48.
Ga	30.	25.	37.	24.	40.	38.	52.	27.	45.	47.	36.	41.	36.	35.	39.	31.	40.
La	101.	122.	262.	50.	59.	44.	97.	92.	81.	22.	321.	25.	70.	85.	28.	101.	41.
Ce	152.	184.	370.	74.	81.	81.	154.	175.	131.	50.	446.	53.	131.	128.	59.	190.	81.

SUMMARY NORM TABLE

	G157	G158	G159	G160	G161	G162	G163	G164	G165	G166	G167	G168	G169	G170	G171	G172	G174
Rock type	PMS	USS	PMS	USS	CGBS	GS-B	GS-B	GS-B	GS-B	GS-B	PMS	GS-A	GS-A	GS-B	GS-B	GS-A	GS-B
Quartz	0.0	0.0	0.0	0.0	6.90	0.0	0.70	0.0	0.10	2.50	16.10	0.0	0.0	0.0	0.0	0.0	0.0
Corundum	5.00	0.0	0.0	0.0	9.50	0.0	0.0	0.0	0.0	8.10	0.0	0.0	0.0	0.0	2.50	0.0	1.40
Zircon	0.50	0.20	0.20	0.20	0.40	0.20	1.20	0.90	1.00	0.60	1.00	0.30	0.60	0.60	0.30	0.70	0.20
Orthoclase	39.10	41.30	7.00	44.50	47.60	34.90	21.80	16.80	19.90	35.00	25.70	33.60	30.00	29.80	31.10	26.50	36.50
Albite	39.60	13.20	0.0	14.10	18.20	22.20	70.90	54.40	73.40	40.50	47.30	18.20	45.60	39.50	41.10	40.60	27.00
Anorthite	0.0	0.0	0.0	5.90	4.90	5.60	0.0	0.0	0.0	0.0	0.0	0.0	0.0	1.40	1.60	0.0	1.70
Nepheline	0.0	23.70	36.90	23.50	0.0	28.50	0.0	2.70	0.0	0.0	0.0	35.90	9.50	15.00	13.70	12.20	22.30
Acmite	0.0	8.70	13.70	0.0	0.0	0.0	0.80	11.40	0.90	0.0	4.60	6.70	1.30	0.0	0.0	2.50	0.0
Na Metasil	0.0	0.0	0.0	0.0	0.0	0.0	0.0	0.0	0.0	0.0	0.0	0.0	0.0	0.0	0.0	0.0	0.0
Diopside	0.0	2.50	10.10	1.70	0.0	0.0	10.70	0.0	0.0	2.10	2.20	0.0	1.40	0.0	0.0	4.20	0.0
Wollaston.	0.0	2.10	12.60	0.0	0.0	0.0	0.90	0.70	1.30	0.0	0.0	0.0	2.10	1.50	0.0	1.60	0.0
Hypersthen	1.00	0.0	0.0	0.0	1.00	0.0	0.0	0.0	0.0	0.50	0.60	0.0	0.0	0.0	0.0	0.0	0.0
Olivine	0.0	0.0	0.0	0.20	0.0	0.50	0.0	0.0	0.0	0.0	0.0	0.20	0.0	0.0	0.40	0.0	0.40
Magnetite	0.0	0.0	2.70	0.0	0.20	4.70	0.0	0.60	0.0	0.0	1.20	0.0	1.90	3.00	3.40	0.0	3.00
Chromite	0.0	0.0	0.0	0.0	0.0	0.0	0.0	0.0	0.0	0.0	0.0	0.0	0.0	0.0	0.0	0.0	0.0
Hematite	3.50	0.10	1.50	3.90	4.00	0.0	0.10	0.0	0.60	3.80	0.0	0.80	4.00	1.50	1.10	5.80	1.70
Ilmenite	5.40	3.30	10.20	4.30	6.60	2.80	0.60	1.10	1.70	7.20	1.00	2.10	3.00	5.20	4.20	4.80	5.30
Titanite	4.20	0.0	0.0	0.0	0.0	0.0	2.70	0.0	0.70	1.40	0.0	0.0	0.0	0.0	0.0	0.0	0.0
Perovskite	1.20	4.10	0.0	0.90	0.0	0.0	0.0	0.0	0.0	0.0	0.0	1.30	0.0	0.0	0.0	0.30	0.0
Rutile	0.0	0.0	0.0	0.0	0.0	0.0	0.0	0.0	0.0	0.40	0.0	0.80	0.0	0.0	0.0	0.0	0.0
Apatite	0.50	0.60	1.40	0.30	0.50	0.40	0.20	0.80	0.30	0.60	0.30	0.30	0.40	0.40	0.50	0.50	0.40
Fluorite	0.50	0.30	0.10	0.50	0.20	0.0	0.0	0.0	0.0	0.0	0.0	0.10	0.20	0.0	0.0	0.40	0.0
Calcite	-0.70	0.0	0.0	0.0	0.0	0.0	0.0	0.0	0.0	-0.60	0.30	-0.30	0.0	0.0	0.0	0.0	0.0
Water	0.30	0.10	0.40	0.30	0.20	0.10	0.0	0.0	0.0	0.20	89.00	0.10	0.40	0.40	0.20	0.50	0.30
Na/(Na+K)	0.0	0.63	0.89	0.58	0.29	0.69	0.78	0.82	0.80	0.0	1.07	0.0	0.70	0.71	0.69	0.73	0.66
(Na+K)/Al	0.75	1.10	1.20	0.90	0.52	0.91	1.01	1.17	1.01	0.64	0.58	1.07	1.02	0.97	0.86	1.03	0.91
F3/(F2+F3)	0.58	0.66	0.58	0.66	0.56	0.52	0.52	0.52	0.52	0.52	0.0	0.77	0.77	0.52	0.52	0.77	0.52
Diff Index	78.70	86.90	57.60	82.10	72.70	85.60	94.20	85.30	94.30	78.00	93.70	94.40	86.40	84.30	85.90	81.80	85.80
Qz residua	44.51	30.54	6.88	31.27	49.23	29.49	45.62	43.55	45.32	46.37	54.85	26.05	39.78	36.73	37.56	37.89	32.79
Ks residua	28.23	30.01	9.06	30.80	37.21	23.17	13.26	12.92	12.11	25.50	16.39	21.77	20.03	20.09	20.58	18.99	24.18
Ne residua	27.26	39.45	84.05	37.93	13.56	47.34	41.12	43.53	42.57	28.13	28.76	52.18	40.19	43.18	41.87	43.12	43.04

NEPHELINE SYENITE ANALYSES

	G175	G176	G177	G178	G181	G184	G185	G186	G187	G188	G189	G191	G192	G193	G194	G195
Rock type	LSS	LSS	LSS	PMS	LSS	PMS	USS	USS	MUS	MUS	MUS	USS	USS	LSS	LSS	LSS
Major elements, weight %																
SiO2	52.20	51.60	53.70	53.41	57.60	55.84	56.10	53.45	51.53	51.61	50.40	54.62	56.34	51.44	55.94	58.00
Al2O3	19.90	20.82	22.09	21.72	19.45	21.06	20.00	20.75	17.58	20.12	18.92	21.88	20.90	24.79	22.13	20.03
Fe2O3	7.72	9.00	4.99	7.40	9.81	6.26	7.01	7.46	11.61	8.17	9.48	5.29	5.34	4.51	6.22	7.11
MgO	0.24	0.39	0.25	0.29	0.24	0.24	0.14	0.26	1.15	0.81	0.95	0.15	0.18	0.07	0.10	0.33
CaO	1.37	2.26	2.39	1.26	0.18	1.25	1.42	2.09	3.74	4.37	5.48	1.17	1.25	0.37	0.44	0.26
Na2O	9.79	8.07	4.03	8.62	5.33	7.04	7.89	8.62	4.48	4.88	7.32	8.43	7.67	11.26	5.91	4.46
K2O	6.22	4.68	7.03	6.03	5.86	6.32	5.94	5.54	6.14	5.66	4.63	6.39	6.88	5.37	6.18	7.55
TiO2	0.23	0.13	0.15	0.22	0.16	0.19	0.17	0.21	0.64	0.21	0.30	0.14	0.16	0.12	0.12	0.30
MnO	0.23	0.26	0.16	0.21	0.14	0.15	0.17	0.21	0.30	0.26	0.31	0.19	0.17	0.09	0.09	0.14
P2O5	0.0	0.15	0.0	0.13	0.04	0.15	0.07	0.20	0.64	0.60	0.86	0.02	0.01	0.0	0.01	0.01
LOI	2.40	2.59	5.28	0.75	1.25	1.59	1.21	1.31	2.30	3.43	1.49	1.87	1.20	2.15	2.99	1.88
Total	100.30	99.95	100.07	100.04	100.06	100.09	100.12	100.10	100.11	100.12	100.14	100.15	100.10	100.17	100.13	100.07
Trace elements ppm																
Ba	154.	195.	635.	277.	229.	150.	163.	251.	294.	279.	242.	180.	207.	153.	219.	225.
Nb	169.	137.	142.	64.	185.	94.	136.	62.	102.	65.	47.	56.	51.	138.	113.	172.
Zr	1337.	552.	791.	553.	957.	355.	936.	598.	469.	630.	594.	303.	239.	684.	658.	1223.
Y	34.	20.	54.	7.	25.	6.	4.	8.	36.	38.	46.	8.	4.	18.	13.	12.
Sr	176.	288.	644.	626.	168.	492.	264.	382.	817.	968.	458.	267.	293.	238.	476.	226.
Rb	172.	212.	224.	168.	184.	191.	188.	137.	188.	147.	122.	176.	179.	165.	171.	233.
Zn	172.	163.	92.	141.	167.	112.	112.	88.	166.	112.	115.	81.	81.	90.	90.	149.
Cu	18.	17.	19.	20.	19.	19.	19.	19.	22.	20.	18.	17.	17.	18.	17.	17.
Ni	8.	10.	10.	9.	11.	7.	8.	5.	9.	10.	10.	8.	9.	9.	9.	10.
Pb	12.	12.	13.	11.	13.	11.	11.	11.	11.	11.	11.	11.	11.	12.	11.	11.
U	2.	2.	3.	2.	2.	3.	3.	2.	2.	3.	3.	1.	2.	2.	3.	3.
Th	9.	8.	10.	8.	11.	8.	8.	8.	9.	9.	9.	9.	8.	9.	9.	8.
V	3.	4.	5.	4.	5.	4.	3.	0.	21.	6.	12.	1.	1.	6.	1.	1.
Cr	7.	7.	6.	5.	6.	7.	6.	7.	7.	7.	8.	7.	7.	6.	7.	8.
Nd	70.	40.	39.	55.	64.	35.	21.	79.	157.	125.	207.	26.	20.	40.	26.	23.
Ga	45.	40.	54.	37.	43.	40.	44.	32.	34.	36.	32.	41.	36.	45.	47.	40.
La	48.	35.	35.	42.	81.	23.	17.	61.	128.	88.	149.	35.	21.	30.	31.	22.
Ce	85.	79.	52.	81.	118.	41.	31.	104.	202.	165.	291.	53.	36.	55.	48.	41.

SUMMARY NORM TABLE

	G175	G176	G177	G178	G181	G184	G185	G186	G187	G188	G189	G191	G192	G193	G194	G195
Rock type	LSS	LSS	LSS	PMS	LSS	PMS	USS	USS	MUS	MUS	MUS	USS	USS	LSS	LSS	LSS
Quartz	0.0	0.0	0.30	0.0	3.00	0.0	0.0	0.0	0.0	0.0	0.0	0.0	0.0	0.0	0.0	2.30
Corundum	0.0	0.0	7.50	0.0	4.30	1.00	0.0	0.0	0.0	0.0	0.0	0.0	0.0	0.0	5.10	4.40
Zircon	0.80	0.30	0.50	0.30	0.60	0.20	0.60	0.40	0.30	0.40	0.40	0.20	0.10	0.40	0.40	0.70
Orthoclase	36.60	27.70	41.50	35.60	34.60	37.40	35.00	32.70	36.40	33.50	27.40	37.70	40.60	31.70	36.50	44.50
Albite	8.10	30.80	34.00	25.00	45.10	34.50	35.10	28.30	27.60	27.30	23.10	26.00	28.90	18.10	43.50	37.60
Anorthite	0.0	6.80	1.00	2.80	0.0	4.50	1.60	1.60	9.80	16.30	5.10	3.00	2.30	1.20	1.60	0.40
Nepheline	32.10	20.40	0.0	26.00	0.0	13.60	17.10	24.20	5.70	7.60	21.10	24.50	19.50	41.70	3.50	0.0
Acmite	12.00	0.0	0.0	0.0	0.0	0.0	0.0	0.0	0.0	0.0	0.0	0.0	0.0	0.0	0.0	0.0
Na Metasil	0.30	0.0	0.0	0.0	0.0	0.0	0.0	0.0	0.0	0.0	0.0	0.0	0.0	0.0	0.0	0.0
Diopside	4.50	1.60	0.0	1.20	0.0	0.0	0.70	1.40	2.90	0.50	8.40	0.80	1.00	0.0	0.0	0.0
Wollaston.	0.0	0.0	0.0	0.0	0.0	0.0	1.30	1.90	0.0	0.0	2.20	0.20	0.60	0.0	0.0	0.0
Hypersthen	0.0	0.0	0.60	0.0	1.90	0.0	0.0	0.0	0.0	0.0	0.0	0.0	0.0	0.0	0.0	0.80
Olivine	0.40	0.20	0.0	0.70	0.0	0.40	0.0	0.0	2.40	1.30	0.0	0.0	0.0	0.10	0.20	0.0
Magnetite	0.0	5.00	0.0	6.20	7.70	3.60	3.90	4.20	8.60	2.30	7.00	0.20	2.30	0.20	0.0	5.00
Chromite	0.0	0.0	0.0	0.0	0.0	0.0	0.0	0.0	0.0	0.0	0.0	0.0	0.0	0.0	0.0	0.0
Hematite	0.0	1.40	2.70	0.0	0.0	1.10	1.90	2.00	0.0	2.60	0.0	3.30	1.90	2.30	3.30	0.40
Ilmenite	4.50	4.90	4.70	1.40	2.40	3.00	2.30	2.50	4.40	6.50	2.80	3.50	2.30	4.10	5.70	3.60
Titanite	0.0	0.0	6.90	0.0	0.0	0.0	0.0	0.0	0.0	0.0	0.0	0.0	0.0	0.0	0.0	0.0
Perovskite	0.0	0.0	0.0	0.0	0.0	0.0	0.0	0.0	0.0	0.0	0.0	0.0	0.0	0.0	0.0	0.0
Rutile	0.0	0.0	0.0	0.0	0.0	0.0	0.0	0.0	0.0	0.0	0.0	0.0	0.0	0.0	0.0	0.0
Apatite	0.50	0.60	0.40	0.50	0.30	0.40	0.40	0.50	0.70	0.60	0.70	0.40	0.40	0.20	0.20	0.30
Fluorite	0.0	0.30	0.0	0.20	0.10	0.30	0.10	0.40	1.30	1.20	1.70	0.0	0.0	0.0	0.0	0.0
Calcite	0.0	0.0	0.0	0.20	-0.10	0.20	0.0	0.0	0.0	0.0	0.0	0.0	0.0	0.0	0.0	0.0
Water	0.20	0.10	0.10	86.60	0.20	85.40	0.20	0.20	0.60	0.20	0.30	0.10	0.20	0.10	0.10	0.30
Na/(Na+K)	0.71	0.72	0.47	0.95	0.0	0.87	0.67	0.70	0.53	0.57	0.71	0.67	0.63	0.76	0.59	0.47
(Na+K)/Al	1.15	0.88	0.64	0.58	0.78	0.58	0.97	0.97	0.80	0.70	0.90	0.95	0.96	0.98	0.74	0.77
F3/(F2+F3)	0.54	0.54	0.54	0.0	0.54	0.0	0.66	0.66	0.51	0.51	0.51	0.66	0.66	0.54	0.54	0.54
Diff Index	89.10	78.90	75.80	86.60	82.70	85.50	87.20	85.20	69.70	68.40	71.60	88.20	89.00	91.50	83.50	84.40
Qz residua	25.41	33.05	44.59	30.98	46.68	37.38	35.78	31.79	40.69	39.44	31.31	31.96	34.58	24.02	42.75	45.90
Ks residua	27.08	19.95	31.11	23.36	23.78	24.86	22.81	21.81	29.68	27.83	21.75	24.29	25.92	19.69	24.84	29.96
Ne residua	47.51	47.00	24.30	45.66	29.54	37.76	41.41	46.40	29.63	32.73	46.95	43.75	39.50	56.29	32.41	24.13

NEPHELINE SYENITE ANALYSES

	G196	G199	G201	G202A	G202B	G203	G204	G206	G207	G208	G209	G210	G211	G212	G213	G214	G215
Rock type	LSS	PMS	LSS	PMS	PMS	LSS	USS	USS	MUS	USS	MUS	MUS	GS-B	GS-B	CGBS	GS-B	CGBS
Major elements, weight %																	
SiO2	57.15	63.63	55.39	54.50	54.90	54.87	58.05	55.39	49.40	52.51	48.63	53.79	48.51	51.45	52.95	51.97	56.30
Al2O3	19.95	20.39	20.64	21.89	20.18	20.76	17.93	20.87	14.57	21.43	16.25	20.63	16.74	26.21	28.58	21.46	25.42
Fe2O3	6.72	2.23	8.69	6.46	7.49	6.97	9.15	7.08	13.81	7.70	13.32	8.25	13.31	2.77	1.86	7.69	3.90
MgO	0.09	0.02	0.59	0.57	0.53	0.21	0.48	0.23	1.50	0.33	1.39	0.67	0.65	0.09	0.0	0.30	0.0
CaO	0.15	0.13	0.14	1.31	2.16	1.76	0.77	1.12	7.75	1.94	8.26	2.13	5.21	0.36	0.70	1.70	0.18
Na2O	6.72	5.97	4.40	7.34	7.57	8.23	5.72	8.50	6.83	7.84	4.30	2.87	8.91	11.60	6.00	7.82	4.33
K2O	7.19	6.38	7.71	5.17	5.14	5.68	6.32	5.24	3.72	6.10	3.80	7.26	3.06	4.32	5.02	5.80	6.82
TiO2	0.26	0.11	0.41	0.19	0.21	0.18	0.30	0.21	0.45	0.32	0.30	0.35	0.16	0.08	0.07	0.24	0.14
MnO	0.08	0.04	0.19	0.16	0.19	0.16	0.19	0.16	0.44	0.20	0.37	0.19	0.40	0.06	0.05	0.22	0.08
P2O5	0.0	0.0	0.0	0.18	0.17	0.04	0.0	0.01	1.11	0.24	1.21	0.22	0.14	0.03	0.08	0.18	0.11
LOI	1.82	1.15	1.93	2.35	1.61	1.26	1.20	1.31	0.53	1.49	2.27	3.68	3.10	3.22	4.78	2.79	2.79
Total	100.13	100.05	100.09	100.12	100.15	100.12	100.11	100.12	100.11	100.10	100.10	100.04	100.19	100.19	100.09	100.17	100.07
Trace elements ppm																	
Ba	166.	353.	195.	335.	266.	162.	174.	179.	184.	278.	343.	540.	126.	132.	181.	201.	143.
Nb	121.	104.	164.	105.	87.	45.	139.	112.	63.	107.	54.	92.	161.	79.	57.	116.	125.
Zr	236.	690.	56.	385.	558.	342.	365.	484.	975.	393.	739.	351.	1482.	392.	165.	569.	214.
Y	3.	14.	9.	9.	11.	11.	14.	12.	78.	20.	65.	23.	44.	6.	14.	22.	9.
Sr	263.	215.	359.	572.	320.	259.	252.	258.	366.	394.	1123.	506.	208.	214.	890.	399.	136.
Rb	245.	166.	327.	197.	194.	166.	220.	130.	132.	169.	131.	169.	140.	113.	124.	177.	173.
Zn	108.	50.	173.	114.	119.	82.	174.	95.	165.	130.	126.	154.	196.	63.	50.	138.	94.
Cu	18.	18.	18.	17.	18.	18.	17.	17.	20.	21.	22.	22.	19.	16.	17.	20.	16.
Ni	8.	8.	13.	9.	8.	10.	9.	7.	11.	8.	10.	9.	10.	8.	7.	9.	9.
Pb	11.	12.	13.	12.	11.	12.	12.	12.	11.	11.	10.	12.	12.	11.	13.	12.	12.
U	2.	2.	2.	2.	2.	2.	2.	2.	3.	2.	3.	2.	2.	2.	2.	2.	2.
Th	9.	10.	9.	8.	9.	8.	9.	9.	8.	9.	9.	9.	10.	8.	9.	8.	10.
V	10.	4.	8.	4.	8.	4.	14.	3.	17.	11.	7.	11.	4.	3.	2.	6.	1.
Cr	6.	6.	5.	6.	7.	5.	6.	6.	7.	7.	8.	6.	5.	5.	6.	6.	6.
Nd	6.	32.	25.	38.	40.	41.	41.	45.	315.	66.	252.	76.	100.	31.	28.	71.	39.
Ga	39.	42.	44.	37.	34.	37.	40.	38.	28.	33.	28.	37.	39.	48.	43.	32.	42.
La	11.	46.	30.	17.	35.	38.	24.	41.	278.	53.	210.	76.	65.	20.	49.	56.	44.
Ce	33.	42.	37.	37.	56.	60.	46.	71.	481.	98.	380.	115.	157.	50.	56.	102.	60.

SUMMARY NORM TABLE

	G196	G199	G201	G202A	G202B	G203	G204	G206	G207	G208	G209	G210	G211	G212	G213	G214	G215
Rock type	LSS	PMS	LSS	PMS	PMS	LSS	USS	USS	MUS	USS	MUS	MUS	GS-B	GS-B	CGBS	GS-B	CGBS
Quartz	0.0	4.20	0.0	0.0	0.0	0.0	0.0	0.0	0.0	0.0	0.0	4.70	0.0	0.0	0.0	0.0	4.80
Corundum	1.00	3.60	5.10	2.60	0.0	0.0	0.70	0.0	0.0	0.0	0.0	5.00	0.0	2.40	13.30	0.0	10.90
Zircon	0.10	0.40	0.0	0.20	0.30	0.20	0.20	0.30	0.60	0.20	0.40	0.20	0.90	0.20	0.10	0.30	0.10
Orthoclase	42.50	37.60	45.70	30.50	30.40	33.60	37.40	30.90	22.00	36.00	22.50	43.00	18.10	25.50	29.70	34.30	40.40
Albite	35.80	50.40	36.80	39.30	36.20	31.30	45.70	36.60	20.60	23.50	27.70	24.30	24.10	26.80	48.20	24.70	36.70
Anorthite	0.20	0.10	0.0	4.50	5.90	2.90	2.60	3.30	0.0	5.30	13.90	8.20	0.0	0.0	0.0	6.30	0.0
Nepheline	11.40	0.0	0.30	12.30	15.10	20.80	1.50	19.10	18.30	23.20	4.70	0.0	24.30	38.60	1.40	22.50	0.0
Acmite	0.0	0.0	0.0	0.0	0.0	0.0	0.0	0.0	3.10	0.0	0.0	0.0	5.60	0.0	0.0	0.0	0.0
Na Metasil	0.0	0.0	0.0	0.0	0.0	0.0	0.0	0.0	0.0	0.0	0.0	0.0	0.0	0.0	0.0	0.0	0.0
Diopside	0.0	0.0	0.0	0.0	2.10	2.00	0.0	0.90	19.70	1.40	11.20	0.0	6.60	0.0	0.0	0.50	0.0
Wollaston.	0.0	0.0	0.0	0.0	0.0	0.90	0.0	0.0	2.70	0.0	2.00	0.0	6.40	0.0	0.0	0.0	0.0
Hypersthen	0.0	0.0	0.0	0.0	0.0	0.0	0.0	0.0	0.0	0.0	0.0	1.70	0.0	0.0	0.0	0.0	0.0
Olivine	0.20	0.0	1.30	1.00	0.20	0.0	2.00	0.10	0.0	0.10	0.0	0.0	0.0	0.20	0.0	0.40	0.0
Magnetite	4.60	0.0	6.80	1.70	5.10	5.50	7.20	3.90	8.70	4.30	9.90	2.20	7.20	0.0	0.0	3.40	0.0
Chromite	0.0	0.0	0.0	0.0	0.0	0.0	0.0	0.0	0.0	0.0	0.0	0.0	0.0	0.0	0.0	0.0	0.0
Hematite	0.50	1.30	0.0	2.60	0.80	0.0	0.0	2.00	0.0	2.10	0.0	2.70	0.0	1.40	1.00	1.60	2.20
Ilmenite	3.50	2.00	3.70	4.50	3.10	2.40	2.30	2.50	1.00	2.80	4.30	7.00	5.90	2.70	1.70	5.30	3.60
Titanite	0.0	0.20	0.0	0.0	0.0	0.0	0.0	0.0	0.0	0.0	0.0	0.0	0.0	0.0	0.0	0.0	0.60
Perovskite	0.0	0.0	0.0	0.0	0.0	0.0	0.0	0.0	0.0	0.0	0.0	0.0	0.0	0.90	1.70	0.0	0.0
Rutile	0.0	0.0	0.0	0.0	0.0	0.0	0.0	0.0	0.0	0.0	0.0	0.0	0.0	1.30	2.90	0.0	0.70
Apatite	0.20	0.10	0.50	0.40	0.40	0.40	0.50	0.40	1.00	0.50	0.90	0.50	0.90	0.10	0.10	0.50	0.20
Fluorite	0.0	0.0	0.0	0.40	0.30	0.10	0.0	0.0	2.20	0.50	2.50	0.40	0.0	0.0	0.20	0.0	0.10
Calcite	0.0	0.10	-0.20	0.20	0.20	0.0	0.0	0.0	0.0	0.0	0.0	0.0	0.0	-0.10	-0.30	0.0	-0.40
Water	0.30	92.20	0.40	82.20	81.60	0.20	0.30	0.20	0.40	0.30	0.30	0.30	0.20	0.10	0.10	0.20	0.10
Na/(Na+K)	0.59	0.82	0.0	0.81	0.89	0.69	0.58	0.71	0.74	0.66	0.63	0.38	0.82	0.0	0.0	0.67	0.0
(Na+K)/Al	0.94	0.58	0.76	0.58	0.58	0.95	0.91	0.94	1.05	0.91	0.69	0.61	1.07	0.91	0.54	0.89	0.57
F3/(F2+F3)	0.54	0.0	0.54	0.0	0.0	0.54	0.54	0.66	0.51	0.66	0.51	0.51	0.52	0.52	0.56	0.52	0.56
Diff Index	89.70	92.20	82.80	82.10	81.70	85.70	84.60	86.60	64.00	82.70	54.90	72.00	72.10	90.90	79.30	81.50	81.90
Qz residua	38.75	47.21	44.20	37.98	36.37	33.66	43.84	34.77	31.10	31.82	40.82	47.78	28.36	25.62	44.02	32.06	47.69
Ks residua	26.93	23.18	31.37	21.11	21.15	22.28	25.12	20.28	20.53	24.74	23.29	33.94	15.47	15.94	21.28	23.92	28.03
Ne residua	34.33	29.61	24.44	40.91	42.48	44.06	31.04	44.95	48.37	43.45	35.89	18.28	56.17	58.44	34.69	44.02	24.27

NEPHELINE SYENITE ANALYSES

	G216	G217	G218	G219	G220	G221	G222	G223	G224	G225	G226	G227	G228	G229	G230	G231	G232
Rock type	CGBS	CGBS	LSS	LSS	LSS	LSS	LSS	PMS	PMS	LSS	GS-B	GS-B	LSS	LSS	LSS	LSS	LSS
Major elements, weight %																	
SiO2	52.03	53.80	56.16	49.98	54.30	57.24	63.36	51.53	53.77	55.06	54.70	55.05	54.09	53.43	54.12	52.10	52.20
Al2O3	20.91	24.45	19.13	21.92	21.92	21.65	19.69	19.54	21.67	21.54	20.63	19.99	19.11	19.93	21.22	20.69	17.42
Fe2O3	6.00	5.55	6.11	7.45	4.72	5.34	2.26	10.70	7.70	8.10	5.35	8.01	7.98	7.96	6.37	7.60	11.59
MgO	0.21	0.26	0.34	0.36	0.10	0.06	0.0	0.36	0.42	0.27	0.24	0.17	0.39	0.47	0.15	0.29	0.56
CaO	1.21	0.82	2.91	3.17	1.66	0.15	0.14	3.17	1.49	1.06	1.91	0.99	2.39	2.80	1.73	3.17	4.92
Na2O	4.07	4.02	6.30	10.76	9.48	6.92	5.44	10.67	7.03	4.86	9.08	6.62	7.34	7.31	8.83	9.72	6.86
K2O	8.75	6.29	6.22	4.53	6.13	6.50	7.91	3.61	5.91	5.87	5.59	6.67	6.14	5.55	5.43	4.97	4.42
TiO2	0.18	0.19	0.09	0.12	0.08	0.12	0.10	0.13	0.24	0.28	0.15	0.21	0.15	0.16	0.13	0.08	0.13
MnO	0.44	0.11	0.20	0.23	0.15	0.11	0.03	0.24	0.20	0.18	0.18	0.23	0.25	0.23	0.18	0.26	0.37
P2O5	0.08	0.16	0.03	0.20	0.0	0.0	0.0	0.0	0.20	0.06	0.13	0.08	0.03	0.01	0.0	0.02	0.01
LOI	6.29	4.43	2.67	1.45	1.61	2.05	1.15	0.23	1.49	2.81	2.16	2.12	2.28	2.25	1.99	1.24	1.67
Total	100.17	100.08	100.16	100.17	100.15	100.14	100.08	100.18	100.12	100.09	100.12	100.14	100.15	100.10	100.15	100.14	100.15
Trace elements ppm																	
Ba	706.	239.	206.	151.	183.	168.	173.	177.	332.	403.	303.	144.	168.	176.	179.	164.	157.
Nb	111.	127.	87.	54.	77.	131.	46.	28.	74.	93.	118.	149.	132.	63.	81.	82.	61.
Zr	43.	504.	928.	497.	545.	309.	217.	1652.	266.	350.	541.	421.	698.	506.	454.	876.	1079.
Y	56.	19.	14.	17.	13.	0.	0.	3.	7.	15.	29.	24.	25.	13.	6.	19.	15.
Sr	359.	280.	881.	196.	267.	249.	302.	147.	568.	558.	534.	344.	265.	410.	254.	206.	598.
Rb	187.	164.	149.	132.	157.	192.	207.	122.	170.	135.	150.	188.	169.	158.	159.	143.	140.
Zn	125.	115.	97.	107.	75.	113.	41.	84.	122.	109.	111.	182.	145.	115.	108.	108.	135.
Cu	20.	20.	18.	18.	17.	17.	16.	19.	21.	19.	18.	21.	17.	17.	17.	18.	19.
Ni	11.	7.	8.	8.	10.	9.	9.	7.	8.	8.	9.	9.	10.	9.	7.	9.	8.
Pb	14.	12.	12.	10.	11.	11.	11.	10.	11.	13.	12.	11.	11.	11.	11.	12.	12.
U	2.	2.	3.	1.	2.	2.	1.	1.	2.	2.	3.	2.	2.	2.	3.	2.	2.
Th	13.	10.	9.	9.	9.	8.	9.	7.	7.	9.	10.	10.	9.	8.	9.	9.	8.
V	5.	8.	0.	5.	4.	2.	1.	3.	6.	9.	6.	6.	7.	3.	0.	2.	7.
Cr	5.	7.	5.	6.	5.	7.	6.	7.	5.	5.	7.	6.	6.	5.	7.	5.	6.
Nd	207.	53.	33.	64.	42.	8.	13.	27.	50.	48.	73.	49.	64.	55.	31.	43.	54.
Ga	25.	41.	32.	45.	42.	40.	40.	45.	32.	44.	28.	34.	34.	35.	40.	38.	40.
La	218.	33.	29.	60.	40.	9.	6.	9.	26.	51.	67.	42.	47.	38.	20.	29.	34.
Ce	355.	79.	45.	108.	67.	18.	14.	50.	57.	99.	108.	70.	91.	88.	29.	64.	71.

SUMMARY NORM TABLE

	G216	G217	G218	G219	G220	G221	G222	G223	G224	G225	G226	G227	G228	G229	G230	G231	G232
Rock type	CGBS	CGBS	LSS	LSS	LSS	LSS	LSS	PMS	PMS	LSS	GS-B	GS-B	LSS	LSS	LSS	LSS	LSS
Quartz	0.0	5.00	0.0	0.0	0.0	0.0	1.20	0.0	0.0	2.20	0.0	0.0	0.0	0.0	0.0	0.0	0.0
Corundum	4.80	11.10	0.0	0.0	0.0	3.20	2.00	0.0	1.80	5.80	0.0	0.60	0.0	0.0	0.0	0.0	0.0
Zircon	0.0	0.30	0.60	0.30	0.30	0.20	0.10	1.00	0.20	0.20	0.30	0.30	0.40	0.30	0.30	0.50	0.60
Orthoclase	52.00	37.20	36.70	26.80	36.20	38.40	46.70	21.20	35.00	34.70	33.00	39.50	36.30	32.80	32.10	29.30	26.10
Albite	23.00	34.10	33.60	15.30	22.40	41.10	46.00	18.90	32.70	41.20	28.40	32.80	28.80	29.30	30.10	20.00	32.40
Anorthite	0.0	0.0	5.50	0.0	0.0	0.0	0.50	0.0	5.10	3.80	0.0	3.40	1.10	5.20	2.20	0.0	3.70
Nepheline	6.30	0.0	10.60	39.10	30.40	9.50	0.0	33.10	14.60	0.0	25.20	12.60	18.00	17.70	24.10	31.80	13.90
Acmite	0.0	0.0	0.0	3.10	1.40	0.0	0.0	8.70	0.0	0.0	1.60	0.0	0.0	0.0	0.0	3.10	0.0
Na Metasil	0.0	0.0	0.0	0.0	0.0	0.0	0.0	0.0	0.0	0.0	0.0	0.0	0.0	0.0	0.0	0.0	0.0
Diopside	0.0	0.0	1.80	3.90	0.50	0.0	0.0	10.60	0.0	0.0	1.30	0.0	2.10	2.50	0.80	4.10	5.20
Wollaston.	0.0	0.0	2.10	3.60	2.70	0.0	0.0	0.80	0.0	0.0	2.80	0.0	2.70	1.70	1.70	3.80	5.00
Hypersthen	0.0	0.60	0.0	0.0	0.0	0.0	0.0	0.0	0.0	0.70	0.0	0.0	0.0	0.0	0.0	0.0	0.0
Olivine	0.40	0.0	0.0	0.0	0.0	0.10	0.0	0.0	0.70	0.0	0.0	0.30	0.0	0.0	0.0	0.0	0.0
Magnetite	0.0	0.0	0.70	4.30	1.90	1.60	0.0	4.60	5.90	3.60	1.70	5.70	4.50	4.60	3.20	4.40	9.10
Chromite	0.0	0.0	0.0	0.0	0.0	0.0	0.0	0.0	0.0	0.0	0.0	0.0	0.0	0.0	0.0	0.0	0.0
Hematite	3.40	3.10	2.80	0.0	0.70	1.80	1.20	0.0	0.40	1.90	1.10	0.20	1.20	1.10	1.30	0.0	0.0
Ilmenite	5.40	5.10	5.10	2.80	3.10	3.90	2.20	0.40	2.80	5.30	4.10	4.00	4.30	4.30	3.80	2.40	3.20
Titanite	0.0	2.90	0.0	0.0	0.0	0.0	0.0	0.0	0.0	0.0	0.0	0.0	0.0	0.0	0.0	0.0	0.0
Perovskite	3.00	0.0	0.0	0.0	0.0	0.0	0.0	0.0	0.0	0.0	0.0	0.0	0.0	0.0	0.0	0.0	0.0
Rutile	1.70	0.60	0.0	0.0	0.0	0.0	0.0	0.0	0.0	0.0	0.0	0.0	0.0	0.0	0.0	0.0	0.0
Apatite	1.00	0.30	0.50	0.50	0.40	0.30	0.10	0.60	0.50	0.40	0.40	0.50	0.60	0.50	0.40	0.60	0.90
Fluorite	0.30	0.0	0.0	0.40	0.0	0.0	0.0	0.0	0.40	0.10	0.0	0.0	0.0	0.0	0.0	0.0	0.0
Calcite	-1.20	-0.60	0.0	0.0	0.0	0.0	0.0	0.10	0.20	0.0	0.0	0.0	0.0	0.0	0.0	0.0	0.0
Water	0.20	0.20	0.10	0.10	0.10	0.10	0.10	73.30	82.20	0.30	0.10	0.20	0.10	0.20	0.10	0.10	0.10
Na/(Na+K)	0.0	0.0	0.61	0.78	0.70	0.62	0.51	1.10	0.83	0.56	0.71	0.60	0.64	0.67	0.71	0.75	0.70
(Na+K)/Al	0.77	0.55	0.89	1.03	1.01	0.85	0.89	0.58	0.58	0.67	1.02	0.91	0.98	0.90	0.96	1.03	0.92
F3/(F2+F3)	0.56	0.56	0.54	0.54	0.54	0.54	0.54	0.0	0.0	0.54	0.52	0.52	0.54	0.54	0.54	0.54	0.54
Diff Index	81.30	76.30	80.90	84.30	90.40	89.00	93.90	81.90	82.30	78.10	88.20	84.90	83.10	79.80	86.30	84.20	72.40
Oz residua	40.58	48.08	38.62	22.88	29.09	39.79	45.20	24.34	36.57	46.17	31.48	37.79	34.74	34.57	32.04	26.90	36.07
Ks residua	36.35	27.71	25.78	18.76	23.12	24.52	28.26	16.46	24.17	25.25	21.66	26.44	24.82	23.36	21.14	20.53	20.49
Ne residua	23.07	24.21	35.60	58.36	47.79	35.69	26.54	59.21	39.26	28.58	46.86	35.77	40.43	42.07	46.82	52.57	43.44

NEPHELINE SYENITE ANALYSES

	G233	G234B	G235	G236A	G236B	G238	G240	G244	G245	G246	G247	G248	G249	G250	G251	G252	G253A
Rock type	LSS	PMS	USS	CGBS	CGBS	USS	MUS	XPS	XPS	USS	MUS	MUS	USS	XPS	USS	USS	PMS
Major elements, weight %																	
SiO2	56.89	53.95	54.40	53.69	53.33	51.00	50.33	44.59	54.37	53.59	50.78	52.54	53.59	55.93	53.37	54.83	50.36
Al2O3	18.55	23.18	23.57	24.65	24.97	27.73	19.99	15.87	18.96	22.84	16.56	15.93	20.12	19.85	20.76	21.73	18.15
Fe2O3	8.78	5.10	3.72	4.92	5.15	4.24	7.62	12.43	9.70	4.61	10.68	11.12	7.00	7.30	8.54	5.50	10.97
MgO	0.30	0.24	0.11	0.50	0.50	0.19	0.82	1.64	0.37	0.13	0.87	0.81	0.23	0.45	0.62	0.19	3.11
CaO	0.93	1.15	1.01	1.81	1.74	1.23	4.66	9.41	1.07	1.60	4.95	4.41	1.73	2.60	2.35	0.51	5.16
Na2O	4.74	8.59	5.62	4.47	4.03	4.97	5.24	8.99	8.06	10.32	8.26	7.72	7.91	5.38	4.90	9.27	6.62
K2O	7.83	6.44	7.44	5.14	5.32	5.48	4.81	1.80	4.99	5.98	4.54	4.66	5.91	4.40	5.89	5.68	2.40
TiO2	0.30	0.18	0.17	0.25	0.28	0.18	0.32	0.11	0.25	0.10	0.29	0.23	0.19	0.27	0.30	0.22	1.54
MnO	0.19	0.09	0.09	0.18	0.20	0.10	0.24	0.66	0.14	0.14	0.37	0.37	0.25	0.21	0.21	0.10	0.18
P2O5	0.0	0.12	0.03	0.0	0.01	0.18	0.80	0.04	0.01	0.10	0.76	0.66	0.06	0.10	0.22	0.03	0.24
LOI	1.57	1.09	4.01	4.51	4.57	4.77	5.29	4.75	2.25	0.73	2.09	1.65	3.18	3.58	2.94	2.08	1.37
Total	100.08	100.13	100.17	100.12	100.10	100.07	100.12	100.29	100.17	100.14	100.15	100.10	100.17	100.07	100.10	100.14	100.10
Trace elements ppm																	
Ba	158.	157.	618.	522.	503.	368.	473.	592.	329.	168.	194.	205.	201.	448.	199.	252.	333.
Nb	113.	37.	44.	87.	93.	75.	109.	53.	334.	50.	233.	173.	157.	386.	88.	62.	80.
Zr	328.	129.	218.	173.	69.	387.	407.	1351.	1706.	529.	1361.	1605.	899.	1723.	755.	173.	383.
Y	17.	3.	11.	0.	0.	19.	57.	38.	16.	11.	143.	59.	20.	62.	16.	4.	38.
Sr	344.	294.	1892.	319.	315.	1296.	1092.	2190.	659.	256.	414.	370.	432.	400.	844.	260.	529.
Rb	269.	175.	106.	160.	164.	159.	134.	88.	212.	147.	131.	141.	173.	139.	201.	171.	115.
Zn	134.	54.	56.	168.	168.	70.	136.	250.	194.	84.	186.	215.	175.	214.	128.	93.	110.
Cu	17.	17.	21.	19.	19.	21.	18.	22.	18.	15.	19.	18.	17.	19.	18.	18.	24.
Ni	10.	8.	7.	8.	7.	8.	10.	9.	11.	7.	17.	10.	9.	12.	10.	6.	18.
Pb	13.	12.	13.	15.	15.	11.	12.	12.	12.	12.	13.	13.	12.	13.	11.	11.	12.
U	2.	1.	4.	2.	2.	4.	3.	4.	3.	1.	4.	3.	2.	4.	2.	2.	2.
Th	9.	8.	10.	10.	10.	9.	11.	9.	8.	7.	12.	11.	10.	11.	9.	9.	9.
V	9.	2.	6.	8.	6.	5.	10.	3.	12.	2.	7.	2.	3.	5.	11.	2.	140.
Cr	6.	7.	5.	7.	6.	6.	5.	6.	7.	4.	5.	5.	6.	7.	4.	5.	14.
Nd	44.	28.	34.	40.	49.	46.	128.	118.	30.	52.	340.	185.	43.	121.	47.	26.	56.
Ga	38.	35.	32.	28.	28.	37.	26.	35.	48.	38.	33.	32.	40.	41.	40.	41.	27.
La	43.	25.	61.	55.	96.	40.	103.	175.	40.	55.	287.	175.	34.	127.	36.	29.	46.
Ce	56.	25.	83.	83.	117.	74.	189.	252.	56.	67.	505.	301.	67.	222.	63.	31.	89.

SUMMARY NORM TABLE

	G233	G234B	G235	G236A	G236B	G238	G240	G244	G245	G246	G247	G248	G249	G250	G251	G252	G253A
Rock type	LSS	PMS	USS	CGBS	CGBS	USS	MUS	XPS	XPS	USS	MUS	MUS	USS	XPS	USS	USS	PMS
Quartz	0.0	0.0	0.0	5.40	7.10	0.0	0.0	0.0	0.0	0.0	0.0	0.0	0.0	3.30	0.0	0.0	0.0
Corundum	1.00	0.40	6.30	11.50	12.40	13.60	1.30	0.0	0.0	0.0	0.0	0.0	0.0	4.40	3.00	0.0	0.0
Zircon	0.20	0.10	0.10	0.10	0.0	0.20	0.20	0.80	1.00	0.30	0.80	1.00	0.50	1.00	0.50	0.10	0.20
Orthoclase	46.40	38.10	44.00	30.40	31.50	32.40	28.40	10.60	29.30	35.30	26.80	27.50	34.80	25.80	34.80	33.60	14.20
Albite	34.60	22.90	32.50	37.80	34.10	42.10	33.50	19.30	38.20	18.00	17.20	23.10	29.80	45.20	36.50	31.10	35.80
Anorthite	3.40	4.50	0.0	0.60	0.40	0.0	13.30	0.0	0.80	0.0	0.0	0.0	1.90	5.00	9.20	0.90	12.70
Nepheline	3.00	27.00	8.10	0.0	0.0	0.0	5.90	28.10	16.00	35.80	23.10	17.70	20.00	0.0	2.70	25.60	11.00
Acmite	0.0	0.0	0.0	0.0	0.0	0.0	0.0	3.90	0.0	2.80	8.80	8.20	0.0	0.0	0.0	0.0	0.0
Na Metasil	0.0	0.0	0.0	0.0	0.0	0.0	0.0	0.0	0.0	0.0	0.0	0.0	0.0	0.0	0.0	0.0	0.0
Diopside	0.0	0.0	0.0	0.0	0.0	0.0	0.0	8.80	2.00	0.70	11.70	12.50	1.20	0.0	0.0	0.60	8.40
Wollaston.	0.0	0.0	0.0	0.0	0.0	0.0	0.0	10.00	0.40	2.30	1.80	0.60	0.50	0.0	0.0	0.0	0.0
Hypersthen	0.0	0.0	0.0	1.20	1.20	0.50	0.0	0.0	0.0	0.0	0.0	0.0	0.0	1.10	0.0	0.0	0.0
Olivine	1.10	0.40	0.20	0.0	0.0	0.0	1.40	0.0	0.0	0.0	0.0	0.0	0.0	0.0	1.10	0.10	4.80
Magnetite	6.90	3.60	0.0	0.0	0.0	0.0	0.0	0.0	0.20	2.70	3.50	4.10	0.0	0.0	0.90	0.10	9.20
Chromite	0.0	0.0	0.0	0.0	0.0	0.0	0.0	0.0	0.0	0.0	0.0	0.0	0.0	0.0	0.0	0.0	0.0
Hematite	0.0	0.40	2.50	2.80	2.90	2.80	3.90	8.40	7.50	0.20	0.0	0.0	4.60	5.70	5.00	3.60	0.0
Ilmenite	3.00	2.10	2.80	4.70	4.90	3.10	7.80	5.20	4.20	1.40	4.00	3.10	4.90	3.50	5.60	3.90	2.60
Titanite	0.0	0.0	0.0	5.10	4.90	2.50	0.0	0.0	0.0	0.0	0.0	0.0	0.0	4.30	0.0	0.0	0.0
Perovskite	0.0	0.0	2.40	0.0	0.0	1.30	2.00	3.40	0.0	0.0	0.0	0.0	1.00	0.0	0.0	0.0	0.0
Rutile	0.0	0.0	1.10	0.0	0.0	1.40	0.0	0.0	0.0	0.0	0.0	0.0	0.0	0.0	0.0	0.0	0.0
Apatite	0.50	0.20	0.20	0.40	0.50	0.20	0.60	1.60	0.30	0.30	0.90	0.90	0.60	0.50	0.50	0.20	0.40
Fluorite	0.0	0.20	0.10	0.0	0.30	0.40	1.60	0.0	0.0	0.20	1.50	1.30	0.10	0.20	0.40	0.10	0.50
Calcite	0.0	0.20	-0.30	0.0	0.0	-0.60	0.0	0.0	0.0	0.0	0.0	0.0	0.0	0.0	0.0	0.0	1.50
Water	0.30	87.90	0.20	0.30	0.30	0.20	0.30	0.10	0.30	0.10	0.30	0.20	0.20	0.30	0.30	0.20	61.00
Na/(Na+K)	0.48	0.91	0.0	0.57	0.54	0.0	0.62	0.88	0.71	0.72	0.73	0.72	0.67	0.65	0.56	0.71	0.74
(Na+K)/Al	0.88	0.58	0.73	0.52	0.50	0.51	0.69	1.05	0.98	1.03	1.12	1.11	0.96	0.69	0.70	0.98	0.58
F3/(F2+F3)	0.54	0.0	0.66	0.56	0.56	0.66	0.51	0.79	0.79	0.66	0.51	0.51	0.66	0.79	0.66	0.66	0.0
Diff Index	84.00	88.00	84.60	73.60	72.70	74.50	67.80	61.90	83.50	91.90	75.90	76.50	84.60	74.30	74.00	90.30	61.00
Qz residua	42.72	30.62	40.06	48.71	49.97	44.67	40.73	23.14	36.11	26.36	28.99	32.88	33.90	47.31	42.91	31.85	36.95
Ks residua	31.39	24.60	29.56	23.47	24.62	24.72	23.80	10.39	19.94	22.52	22.70	22.88	23.38	19.73	26.73	21.15	13.23
Ne residua	25.88	44.78	30.38	27.82	25.41	30.61	35.47	66.47	43.94	51.12	48.31	44.24	42.72	32.95	30.37	47.01	49.82

NEPHELINE SYENITE ANALYSES

	G254	G255	G256	G257	G259	G260	G261	G262	G263	G264	G267	G269	G274	G275
Rock type	GS-B	GS-B	CGBS	GS-B	LSS	LSS	LSS	LSS	LSS	MISC	USS	USS	PMS	CGS
Major elements, weight %														
SiO2	50.10	54.08	52.52	50.06	60.72	55.64	60.92	59.14	58.95	58.31	55.81	61.27	50.71	53.15
Al2O3	23.95	22.09	22.86	21.76	21.97	22.43	21.23	24.02	21.23	13.92	22.04	18.26	19.65	21.48
Fe2O3	4.53	7.70	8.07	8.49	3.75	3.74	4.08	3.20	6.20	8.81	3.20	2.73	6.38	6.60
MgO	0.14	0.45	0.39	0.25	0.06	0.48	0.06	0.14	0.22	4.48	0.0	0.0	0.37	0.29
CaO	2.63	2.12	1.71	2.48	0.07	2.82	0.08	0.07	0.10	1.32	0.34	2.97	2.71	1.21
Na2O	10.33	3.87	3.07	9.60	4.77	3.61	3.92	3.85	4.16	8.05	10.53	7.43	10.03	9.30
K2O	4.79	6.01	7.64	4.71	7.03	7.25	8.06	7.65	7.22	1.51	5.69	4.09	5.94	5.05
TiO2	0.12	0.21	0.29	0.19	0.08	0.11	0.14	0.09	0.23	1.87	0.14	0.10	0.47	0.32
MnO	0.12	0.25	0.19	0.24	0.06	0.09	0.06	0.05	0.07	0.10	0.08	0.15	0.17	0.15
P2O5	1.48	0.18	0.17	0.57	0.0	0.02	0.01	0.0	0.0	0.14	0.02	0.09	0.21	0.13
LOI	1.97	3.11	3.16	1.79	1.57	3.88	1.51	1.84	1.68	1.59	2.30	3.05	3.54	2.47
Total	100.16	100.07	100.07	100.14	100.08	100.07	100.07	100.05	100.06	100.10	100.15	100.14	100.18	100.15
Trace elements ppm														
Ba	112.	2217.	388.	127.	215.	288.	243.	334.	255.	1277.	233.	209.	464.	820.
Nb	120.	177.	141.	115.	117.	105.	60.	69.	115.	28.	102.	9706.	217.	106.
Zr	485.	791.	290.	666.	1371.	327.	70.	261.	892.	209.	536.	1841.	631.	542.
Y	91.	28.	23.	44.	30.	21.	16.	9.	10.	0.	21.	52.	85.	22.
Sr	293.	692.	467.	192.	100.	329.	124.	100.	139.	404.	196.	503.	1990.	682.
Rb	165.	165.	223.	153.	185.	199.	184.	204.	202.	75.	172.	108.	141.	163.
Zn	103.	274.	160.	159.	49.	76.	73.	147.	84.	98.	84.	74.	133.	144.
Cu	19.	24.	22.	20.	18.	18.	17.	15.	17.	24.	17.	21.	20.	18.
Ni	12.	10.	11.	10.	9.	10.	10.	8.	9.	6.	9.	10.	11.	9.
Pb	11.	22.	13.	11.	11.	11.	12.	12.	11.	10.	12.	36.	15.	11.
U	3.	3.	3.	2.	2.	2.	2.	1.	2.	2.	2.	50.	4.	3.
Th	9.	10.	9.	10.	10.	10.	9.	8.	9.	10.	9.	15.	13.	8.
V	3.	10.	10.	1.	2.	4.	3.	1.	12.	272.	2.	1.	14.	11.
Cr	5.	5.	8.	7.	6.	5.	5.	6.	7.	8.	7.	5.	7.	7.
Nd	289.	51.	61.	136.	48.	45.	42.	19.	29.	50.	44.	186.	133.	54.
Ga	43.	36.	34.	42.	43.	50.	42.	46.	47.	21.	45.	0.	26.	32.
La	220.	53.	58.	87.	49.	41.	67.	29.	41.	72.	49.	232.	132.	60.
Ce	407.	87.	100.	184.	88.	67.	83.	30.	43.	136.	73.	379.	237.	99.

SUMMARY NORM TABLE

	G254	G255	G256	G257	G259	G260	G261	G262	G263	G264	G267	G269	G274	G275
Rock type	GS-B	GS-B	CGBS	GS-B	LSS	LSS	LSS	LSS	LSS	MISC	USS	USS	PMS	CGS
Quartz	0.0	3.90	2.00	0.0	5.70	1.90	7.20	7.10	6.60	0.0	0.0	0.0	0.0	0.0
Corundum	0.0	6.00	7.20	0.0	6.50	6.40	6.10	9.40	6.50	0.0	0.0	0.0	0.0	0.0
Zircon	0.30	0.50	0.20	0.40	0.80	0.20	0.0	0.20	0.50	0.0	0.30	1.10	0.40	0.30
Orthoclase	28.70	35.60	45.20	28.00	41.40	42.80	47.70	45.20	42.60	0.0	33.60	24.00	35.00	29.80
Albite	17.10	32.80	26.00	21.60	40.20	30.50	33.20	32.60	35.10	0.0	26.10	61.80	7.50	30.30
Anorthite	4.90	8.90	6.40	2.40	0.0	6.20	0.0	0.0	0.0	0.0	0.0	4.40	0.0	2.00
Nepheline	38.70	0.0	0.0	32.50	0.0	0.0	0.0	0.0	0.0	0.0	30.00	0.30	32.70	26.20
Acmite	0.0	0.0	0.0	0.0	0.0	0.0	0.0	0.0	0.0	0.0	6.10	0.0	10.70	0.0
Na Metasil	0.0	0.0	0.0	0.0	0.0	0.0	0.0	0.0	0.0	0.0	0.10	0.0	1.10	0.0
Diopside	0.80	0.0	0.0	2.30	0.0	0.0	0.0	0.0	0.0	0.0	0.0	0.0	2.00	1.60
Wollaston.	2.70	0.0	0.0	2.30	0.0	0.0	0.0	0.0	0.0	0.0	0.0	0.80	3.20	0.20
Hypersthen	0.0	1.10	1.00	0.0	0.10	1.20	0.10	0.30	0.50	0.0	0.0	0.0	0.0	0.0
Olivine	0.0	0.0	0.0	0.0	0.0	0.0	0.0	0.0	0.0	0.0	0.0	0.0	0.0	0.0
Magnetite	1.00	2.40	2.10	6.40	0.70	0.0	1.50	0.0	4.20	0.0	0.0	0.0	0.0	1.40
Chromite	0.0	0.0	0.0	0.0	0.0	0.0	0.0	0.0	0.0	0.0	0.0	0.0	0.0	0.0
Hematite	1.70	2.30	3.10	0.0	1.50	2.00	1.10	1.70	0.50	0.0	0.0	1.80	0.0	3.10
Ilmenite	3.80	5.90	6.00	3.40	3.00	3.50	2.90	3.00	3.20	0.0	2.40	2.00	6.10	4.70
Titanite	0.0	0.0	0.0	0.0	0.0	5.00	0.0	0.20	0.0	0.0	0.0	0.0	0.0	0.0
Perovskite	0.0	0.0	0.0	0.0	0.0	0.0	0.0	0.0	0.0	0.0	0.80	3.40	0.60	0.0
Rutile	0.0	0.0	0.0	0.0	0.0	0.0	0.0	0.20	0.0	0.0	0.60	0.0	0.0	0.0
Apatite	0.30	0.60	0.50	0.60	0.10	0.20	0.10	0.10	0.20	0.0	0.20	0.40	0.40	0.40
Fluorite	0.0	0.0	0.0	0.0	0.0	0.0	0.0	0.0	0.0	0.0	0.0	0.20	0.40	0.30
Calcite	0.0	0.0	0.0	0.0	-0.0	0.0	-0.0	-0.10	0.0	0.0	-0.20	0.0	0.50	0.0
Water	0.10	0.20	0.30	0.20	0.10	0.10	0.10	0.10	0.20	0.0	0.10	0.10	75.20	0.30
Na/(Na+K)	0.77	0.49	0.38	0.76	0.0	0.43	0.0	0.0	0.47	0.0	0.0	0.73	1.17	0.74
(Na+K)/Al	0.93	0.58	0.58	0.96	0.70	0.61	0.71	0.61	0.69	0.0	1.07	0.91	0.58	0.97
F3/(F2+F3)	0.52	0.52	0.56	0.52	0.54	0.54	0.54	0.54	0.54	0.0	0.66	0.66	0.0	0.61
Diff Index	84.50	72.30	73.20	82.10	87.30	75.20	88.10	84.90	84.30	0.0	95.90	86.10	87.00	86.30
Qz residua	42.72	30.62	40.06	48.71	49.97	44.67	40.73	23.14	36.11	26.36	28.99	32.88	33.90	47.31
Ks residua	31.39	24.60	29.56	23.47	24.62	24.72	23.80	10.39	19.94	22.52	22.70	22.88	23.38	19.73
Ne residua	25.88	44.78	30.38	27.82	25.41	30.61	35.47	66.47	43.94	51.12	48.31	44.24	42.72	32.95

CARBONATITE ANALYSES

	G28	G29	G30	G31	G46	G47	G52	G53	G55	G56	G66	G73	G74	G95	G96	G97	G101
Rock type	CBT	CBT	CBT	CBT	CBT	CBT	CBT	CBT	CBT	CBT	CBT	CBT	CBT	CBT	CBT	CBT	CBT
Major elements, weight %																	
SiO2	1.64	19.07	1.54	0.0	0.63	0.0	5.81	2.00	0.97	9.63	0.58	0.05	1.19	0.30	1.55	1.02	0.78
Al2O3	0.28	5.35	0.05	0.0	0.0	0.0	1.16	0.60	0.39	2.50	0.03	0.08	0.28	0.0	0.48	0.46	0.47
Fe2O3	1.17	12.90	9.03	13.85	1.70	13.39	4.96	2.47	16.01	10.11	3.29	1.83	0.84	6.27	10.04	23.09	5.59
MgO	0.22	10.83	0.57	0.48	0.11	0.58	0.36	0.17	0.75	0.38	0.17	0.11	0.14	0.47	0.84	1.26	0.29
CaO	52.42	17.07	45.49	44.85	52.71	44.72	45.65	51.03	40.32	40.32	51.38	53.08	53.27	48.85	47.36	37.95	48.41
Na2O	0.18	0.21	0.18	0.20	0.17	0.21	0.22	0.17	0.19	0.26	0.18	0.19	0.18	0.18	0.21	0.21	0.18
K2O	0.29	4.02	0.0	0.0	0.08	0.0	0.54	0.0	0.22	1.02	0.02	0.06	0.0	0.0	0.25	0.09	0.22
TiO2	0.03	2.52	0.02	0.02	0.03	0.0	0.03	0.02	0.05	0.05	0.04	0.01	0.06	0.03	0.06	0.02	0.08
MnO	0.94	0.42	1.78	1.28	1.04	2.93	1.25	1.22	1.54	1.13	1.02	0.87	0.43	1.19	1.16	1.79	1.46
P2O5	0.0	0.41	0.13	3.24	0.02	0.04	0.06	0.30	1.99	0.06	2.47	0.93	2.81	2.08	1.64	3.64	0.99
LOI	41.97	26.62	40.34	33.04	42.56	36.56	38.47	40.59	35.39	32.69	39.19	41.54	39.62	39.80	34.08	27.81	38.57
Total	99.15	99.43	99.14	96.96	99.06	98.44	98.50	98.57	97.83	98.16	98.37	98.74	98.82	99.16	97.67	97.35	97.04
Trace elements ppm																	
Ba	617.	765.	166.	2861.	291.	123.	360.	180.	778.	1266.	225.	460.	210.	272.	1601.	4987.	19778.
Nb	37.	178.	161.	461.	13.	23.	49.	204.	41.	132.	293.	49.	111.	189.	60.	894.	29.
Zr	0.	210.	0.	0.	4.	0.	10.	16.	0.	0.	12.	0.	2.	0.	0.	0.	0.
Y	157.	57.	374.	316.	189.	372.	229.	276.	393.	250.	508.	166.	171.	408.	483.	350.	235.
Sr	7174.	3624.	6114.	31730.	12276.	15277.	16325.	15530.	21680.	17396.	18263.	16048.	13830.	6500.	24623.	20940.	16727.
Rb	46.	160.	41.	18.	33.	34.	40.	28.	32.	56.	28.	30.	29.	36.	27.	38.	34.
Zn	326.	287.	143.	85.	42.	69.	62.	81.	899.	240.	85.	41.	23.	266.	146.	191.	101.
Cu	0.	33.	0.	0.	0.	0.	0.	0.	0.	0.	0.	0.	0.	0.	0.	0.	0.
Ni	12.	54.	21.	16.	13.	21.	13.	16.	20.	14.	22.	11.	9.	20.	24.	18.	12.
Pb	2.	2.	2.	3.	2.	2.	2.	2.	2.	2.	2.	2.	2.	2.	2.	3.	3.
U	11.	7.	9.	37.	15.	16.	16.	19.	20.	16.	20.	18.	16.	12.	24.	41.	17.
Th	66.	44.	61.	57.	50.	45.	44.	53.	205.	108.	50.	51.	50.	70.	62.	158.	270.
V	0.	257.	0.	7.	0.	0.	0.	0.	0.	0.	0.	0.	0.	6.	0.	0.	15.
Cr	1.	155.	5.	4.	3.	4.	2.	5.	5.	3.	3.	7.	4.	1.	1.	0.	0.
Nd	1126.	130.	1539.	942.	331.	1827.	1096.	1264.	1371.	1071.	1014.	364.	427.	1069.	846.	1120.	1305.
Ga	0.	30.	2.	0.	2.	0.	6.	0.	1.	0.	0.	0.	0.	0.	1.	0.	0.
La	950.	114.	1194.	591.	294.	954.	781.	853.	977.	918.	640.	332.	685.	1052.	700.	819.	1152.
Ce	1850.	228.	2366.	1273.	569.	2108.	1583.	1822.	1945.	1731.	1408.	657.	934.	1839.	1288.	1598.	2176.

CARBONATITE ANALYSES

	G102	G103	G104	G107	G133	G265	G268	G271
Rock type	CBT	CBT	CBT	CBT	CBT	CBT	CBT	CBT
Major elements, weight %								
SiO2	0.0	4.29	0.12	15.16	0.24	12.16	2.39	0.0
Al2O3	0.17	0.97	0.0	1.35	0.0	4.91	0.42	0.16
Fe2O3	0.89	3.94	1.20	6.45	7.59	13.03	2.65	1.52
MgO	0.0	0.12	0.07	0.73	0.20	0.76	0.08	0.03
CaO	54.29	48.47	52.76	37.93	48.81	30.92	50.45	53.61
Na2O	0.16	0.18	0.16	1.15	0.18	0.41	0.18	0.16
K2O	0.0	0.63	0.04	0.04	0.0	0.13	0.41	0.02
TiO2	0.02	0.05	0.04	0.09	0.03	0.10	0.03	0.05
MnO	0.10	1.00	1.39	1.44	1.91	2.12	1.23	0.24
P2O5	0.0	0.19	0.01	3.28	0.92	2.72	2.96	0.06
LOI	43.02	38.86	42.22	29.34	38.01	30.33	37.69	42.72
Total	98.66	98.71	98.02	96.97	97.90	97.59	98.48	98.59
Trace elements ppm								
Ba	2435.	580.	226.	1279.	884.	1370.	330.	388.
Nb	23.	88.	17.	359.	263.	860.	80.	16.
Zr	0.	0.	0.	12.	0.	40.	0.	0.
Y	240.	366.	178.	280.	402.	311.	485.	300.
Sr	13861.	14245.	24812.	24751.	21889.	18663.	15973.	17370.
Rb	28.	41.	22.	14.	23.	40.	36.	27.
Zn	2029.	95.	94.	1147.	149.	973.	165.	30.
Cu	0.	0.	0.	0.	0.	0.	0.	0.
Ni	13.	20.	11.	16.	18.	18.	23.	14.
Pb	2.	2.	2.	3.	3.	2.	2.	2.
U	15.	16.	26.	24.	22.	20.	17.	20.
Th	65.	50.	44.	93.	36.	72.	56.	94.
V	0.	0.	0.	0.	0.	0.	3.	0.
Cr	6.	6.	4.	0.	0.	0.	4.	4.
Nd	434.	798.	1044.	1921.	1535.	1258.	1097.	822.
Ga	0.	3.	0.	0.	0.	0.	3.	0.
La	231.	485.	856.	2288.	1082.	2460.	762.	572.
Ce	495.	1048.	1694.	4016.	2395.	3061.	1552.	1157.

ATOMS PER 100 OXYGENS

	G146B	G155	G180	G197	G198	G237	G239	G242	G266	G272	G273A	G276
Rock type	ALGN	ALGN	ALSY	ALGN	ALGN	ALGN	ALGN	ALGN	ALSY	ALSY	ALSY	ALSY
Si	32.92	33.73	33.19	37.04	37.95	28.29	34.61	32.96	35.14	34.13	33.60	28.80
Al	9.30	10.49	14.56	10.00	9.60	12.08	9.35	12.95	13.52	14.93	15.25	7.40
Fe	8.90	3.24	1.95	1.52	1.38	5.89	3.87	4.82	1.77	2.17	2.07	5.04
Mg	0.04	2.16	0.12	1.07	0.98	5.53	2.09	0.13	0.12	0.03	0.0	13.62
Ca	1.04	3.28	0.53	1.50	1.20	4.96	2.88	1.50	0.79	0.55	1.41	7.03
Na	8.78	5.96	11.38	7.40	6.41	3.71	7.98	6.86	3.63	5.61	5.50	1.29
K	1.80	2.21	4.72	2.70	2.93	1.68	1.98	3.58	7.55	4.58	4.32	0.46
Ti	0.13	0.71	0.04	0.33	0.26	1.20	0.32	0.17	0.03	0.13	0.11	0.79
Mn	0.11	0.06	0.07	0.03	0.03	0.07	0.12	0.09	0.16	0.09	0.11	0.09
P	0.04	0.38	0.0	0.13	0.09	0.32	0.08	0.06	0.03	0.02	0.07	0.23

METASOMATISED ROCKS

	G146B	G155	G180	G197	G198	G237	G239	G242	G266	G272	G273A	G276
Rock type	ALGN	ALGN	ALSY	ALGN	ALGN	ALGN	ALGN	ALGN	ALSY	ALSY	ALSY	ALSY
Major elements, weight %												
SiO2	53.56	57.81	55.49	65.57	67.49	45.86	58.67	53.62	58.44	58.36	56.59	39.89
Al2O3	12.83	15.26	20.65	15.02	14.49	16.62	13.45	17.88	19.08	21.65	21.79	8.69
Fe2O3	19.24	7.38	4.34	3.57	3.26	12.70	8.73	10.42	3.91	4.94	4.64	9.27
MgO	0.04	2.49	0.13	1.27	1.17	6.02	2.38	0.14	0.13	0.04	0.0	12.66
CaO	1.58	5.24	0.83	2.48	2.00	7.51	4.56	2.28	1.23	0.87	2.21	9.09
Na2O	7.37	5.27	9.81	6.76	5.88	3.10	6.98	5.76	3.11	4.95	4.78	0.92
K2O	2.30	2.97	6.19	3.75	4.09	2.13	2.63	4.57	9.84	6.14	5.71	0.50
TiO2	0.29	1.61	0.10	0.77	0.62	2.58	0.73	0.37	0.07	0.30	0.24	1.45
MnO	0.22	0.12	0.13	0.07	0.06	0.14	0.25	0.17	0.31	0.18	0.22	0.14
P2O5	0.08	0.77	0.0	0.28	0.19	0.61	0.17	0.11	0.05	0.04	0.13	0.37
LOI	2.60	1.19	2.49	0.55	0.86	2.77	1.57	4.83	3.92	2.60	3.77	17.07
Total	100.11	100.11	100.16	100.09	100.11	100.04	100.12	100.15	100.09	100.07	100.08	100.05
Trace elements ppm												
Ba	286.	1341.	157.	1040.	1303.	797.	534.	328.	3008.	587.	692.	917.
Nb	490.	50.	175.	49.	37.	46.	94.	532.	191.	179.	138.	32.
Zr	3624.	566.	606.	414.	364.	249.	491.	1936.	102.	808.	158.	396.
Y	42.	66.	18.	119.	27.	15.	69.	30.	35.	28.	39.	13.
Sr	260.	924.	258.	518.	704.	1035.	662.	469.	773.	306.	451.	4280.
Rb	88.	105.	202.	162.	145.	82.	84.	193.	223.	206.	196.	59.
Zn	198.	113.	124.	102.	76.	118.	182.	322.	127.	114.	101.	102.
Cu	20.	25.	19.	22.	20.	26.	23.	21.	18.	17.	18.	44.
Ni	9.	17.	9.	17.	14.	23.	18.	10.	11.	10.	11.	105.
Pb	18.	14.	11.	16.	16.	11.	13.	13.	12.	13.	14.	13.
U	5.	3.	3.	2.	3.	3.	3.	3.	4.	2.	2.	5.
Th	12.	13.	9.	16.	16.	10.	10.	9.	11.	11.	10.	11.
V	17.	130.	2.	54.	42.	206.	85.	10.	4.	11.	7.	203.
Cr	6.	20.	6.	12.	20.	20.	24.	8.	6.	6.	6.	330.
Nd	108.	157.	36.	107.	79.	50.	87.	104.	97.	92.	134.	42.
Ga	51.	22.	44.	25.	23.	24.	16.	26.	31.	42.	34.	18.
La	94.	223.	38.	199.	178.	24.	99.	89.	112.	115.	162.	25.
Ce	159.	346.	72.	299.	254.	49.	154.	167.	179.	165.	234.	33.

ATOMS PER 100 OXYGENS

	G14	G26	G27	G42	G51	G54	G57	G75	G83	G86	G90	G94	G105	G106	G136	G146A
Rock type	ALGN	ALGN	ALSY	ALGN	ALGN	ALGN	ALGN	ALSY	ALSY	ALSY	ALSY	ALSY	ALGN	ALGN	ALSY	ALGN
Si	38.61	22.98	31.51	32.42	34.24	32.81	35.63	5.75	32.78	31.59	33.47	19.97	33.89	32.96	28.43	32.45
Al	8.74	8.12	11.67	15.53	11.36	13.95	9.79	3.79	16.83	20.18	13.26	6.91	11.80	12.90	14.12	9.24
Fe	1.77	20.41	5.42	2.58	5.27	3.45	3.45	6.98	2.67	1.23	3.23	12.51	3.80	4.44	4.94	9.81
Mg	0.12	2.90	0.43	0.24	0.06	0.38	0.36	2.64	0.13	0.12	0.37	6.00	1.38	1.54	1.08	0.0
Ca	1.34	4.08	4.68	0.88	0.68	2.58	1.99	40.81	0.24	0.06	2.37	13.00	1.28	1.08	6.36	0.95
Na	8.98	1.69	6.81	7.93	1.62	4.90	9.51	0.0	6.07	5.37	5.35	1.48	8.96	7.68	9.34	8.93
K	1.52	5.02	2.83	4.77	9.37	4.62	2.48	0.03	2.52	3.52	4.82	4.05	1.79	1.69	2.58	1.33
Ti	0.06	0.10	0.04	0.08	0.09	0.06	0.11	0.14	0.08	0.03	0.06	2.50	0.24	0.30	0.12	0.15
Mn	0.05	0.26	0.19	0.09	0.15	0.10	0.19	0.31	0.05	0.02	0.11	0.72	0.20	0.12	0.20	0.12
P	0.06	0.18	0.45	0.12	0.01	0.14	0.05	11.32	0.12	0.0	0.10	1.38	0.04	0.02	0.28	0.02

METASOMATISED ROCKS

	G14	G26	G27	G42	G51	G54	G57	G75	G83	G86	G90	G94	G105	G106	G136	G146A
Rock type	ALGN	ALGN	ALSY	ALGN	ALGN	ALGN	ALGN	ALSY	ALSY	ALSY	ALSY	ALSY	ALGN	ALGN	ALSY	ALGN
Major elements. weight %																
SiO2	68.12	31.61	48.28	53.96	55.06	53.18	60.21	5.68	56.60	54.89	54.35	22.72	55.36	54.51	41.96	52.71
Al2O3	13.08	9.47	15.17	21.93	15.50	19.19	14.04	3.17	24.66	29.75	18.27	6.67	16.35	18.10	17.68	12.73
Fe2O3	4.16	37.31	11.03	5.70	11.26	7.44	7.76	9.16	6.13	2.84	6.97	18.91	8.26	9.77	9.68	21.17
MgO	0.14	2.68	0.44	0.27	0.07	0.41	0.41	1.75	0.15	0.14	0.40	4.58	1.51	1.71	1.07	0.0
CaO	2.20	5.24	6.70	1.37	1.02	3.90	3.14	37.60	0.39	0.09	3.59	13.81	1.95	1.67	8.76	1.44
Na2O	8.17	1.20	5.38	6.81	1.34	4.10	8.29	0.0	5.41	4.81	4.48	0.87	7.55	6.55	7.11	7.48
K2O	2.10	5.41	3.40	6.22	11.81	5.87	3.29	0.02	3.41	4.79	6.14	3.61	2.29	2.19	2.99	1.69
TiO2	0.13	0.19	0.09	0.17	0.20	0.13	0.24	0.18	0.19	0.08	0.14	3.79	0.53	0.66	0.24	0.32
MnO	0.10	0.42	0.35	0.17	0.29	0.20	0.37	0.36	0.11	0.04	0.22	0.97	0.39	0.24	0.34	0.23
P2O5	0.12	0.29	0.82	0.23	0.01	0.26	0.10	13.27	0.25	0.0	0.20	1.85	0.08	0.03	0.49	0.03
LOI	1.88	5.78	8.51	3.33	3.48	5.32	2.29	21.47	2.74	2.61	5.34	22.17	5.92	4.69	10.02	2.25
Total	100.20	99.60	100.17	100.16	100.04	100.00	100.14	92.66	100.04	100.04	100.10	99.94	100.19	100.12	100.34	100.05
Trace elements ppm																
Ba	181.	327.	438.	249.	595.	251.	241.	0.	246.	310.	416.	396.	1069.	728.	649.	292.
Nb	55.	979.	399.	155.	789.	539.	91.	173.	177.	69.	874.	781.	42.	40.	228.	1055.
Zr	139.	499.	3427.	526.	2403.	1507.	599.	257.	345.	355.	2109.	124.	246.	332.	1324.	3347.
Y	18.	97.	124.	11.	56.	53.	40.	905.	20.	3.	66.	8.	6.	28.	102.	36.
Sr	204.	2420.	3402.	435.	158.	738.	509.	8957.	185.	246.	1846.	2085.	555.	478.	4686.	245.
Rb	52.	368.	127.	194.	233.	309.	112.	29.	119.	125.	208.	84.	75.	105.	102.	73.
Zn	45.	675.	170.	121.	358.	179.	168.	77.	134.	65.	175.	879.	74.	117.	196.	196.
Cu	17.	17.	25.	17.	21.	18.	18.	35.	20.	17.	18.	27.	20.	36.	26.	20.
Ni	7.	13.	16.	7.	15.	14.	10.	43.	8.	6.	13.	36.	18.	25.	13.	9.
Pb	12.	1.	13.	12.	13.	13.	14.	2.	13.	12.	12.	3.	16.	14.	14.	24.
U	2.	5.	6.	2.	5.	3.	2.	16.	2.	2.	5.	5.	2.	2.	6.	13.
Th	10.	40.	11.	9.	8.	9.	13.	80.	10.	10.	8.	40.	12.	11.	11.	13.
V	4.	11.	0.	4.	11.	3.	21.	11.	7.	0.	2.	180.	33.	93.	11.	13.
Cr	5.	6.	5.	5.	6.	5.	6.	0.	6.	5.	6.	75.	25.	60.	5.	8.
Nd	36.	196.	264.	40.	166.	116.	169.	3755.	53.	13.	191.	24.	129.	60.	221.	96.
Ga	19.	49.	41.	37.	4.	41.	34.	3.	46.	58.	26.	11.	16.	27.	20.	27.
La	34.	182.	221.	27.	111.	91.	213.	4274.	58.	30.	164.	0.	207.	71.	220.	95.
Ce	59.	311.	422.	54.	232.	175.	315.	7174.	86.	29.	309.	35.	292.	97.	349.	157.

APPENDIX IV

Neutron activation analysis

Instrumental neutron activation analysis (INAA) was carried out on sixteen syenites, six carbonatites, and four metasomatised samples (two gneisses and two syenites), as shown in Appendix I. This was done principally to determine REE abundances, although Ta and Hf proved very useful in helping to develop a petrogenetic model for the origin of the carbonatite. The other elements which were analysed by this method were U, Th, W, Cr, Sc, and Cs. The high cost of this method (around £11 per sample at 1989 prices) meant that samples had to be carefully chosen. The choice was based on their XRF analyses for La, Ce, and Nd, those selected representing 'average' compositions from the different units.

Powdered samples are used, and thus avoids the problem of phases which are difficult to dissolve (eg. baddeleyite, ZrO_2), often encountered with analytical methods using solutions.

Chips of the selected samples were ground to a fine powder using an agate swing-mill. Around 0.2g of this powder were weighed into plastic capsules, and irradiated for five days in batches of nine samples at the University of London reactor centre at Silwood Park. Three calibration standards were irradiated along with each batch of unknowns, which were positioned at the top, middle, and bottom of each irradiation tube to achieve satisfactory corrections for flux variations. Standards were in the form of filter papers onto which multi-element chemical solutions had been dried. In addition, a sample of Ailsa Craig granite was irradiated and analysed along with the Grønnedal samples, as a 'monitor' sample (table IV.1).

Irradiated samples were loaded onto a horizontal wheel autochanger, which gave a consistent sample-detector distance of 1.5–2.0cm. Gamma rays were collected by an EG&G ORTEC planar high purity Ge, low energy photon detector.

tor. Resolution was around 550eV full-width-half-maximum at 122keV. Separate counts of 5400s per sample were made at 5 days and 18 days after irradiation, following procedures similar to those of Henderson and Williams (1981), Potts *et al.* (1981), and Potts (1987). Gamma rays were collected in the range 50–900keV, and processed as 4096 channel spectra. The efficiency of the detector is good up to 300–400keV, but in the range 400–920keV, efficiency declines dramatically (eg. Henderson and Williams 1981). Nevertheless, good results for REE's and other trace elements have been determined using the following peaks with energies >300keV: La (328.8 and 487.1keV); Th (311.8keV); Sc (889.4keV). (After Leat *et al.* 1989, in press).

Some REE's were not analysed for a variety of reasons:

Dy, Er – Half-lives too short, with ^{165}Dy having $t_{1/2}$=2.334 hours, and ^{171}Er having $t_{1/2}$=7.52 hours.

Pr – All isotopes of this element produced by neutron bombardment emit γ-rays only weakly, or not at all.

In addition, Gd and Ho were analysed, but found to give consistently anomalous results when normalised to chondritic abundances, and compared to normalised values of the other REE's. These elements can sometimes be measured using epithermal neutron activation methods (Henderson and Pankhurst 1984).

The results of the Ailsa Craig granite analyses are compared with those of Leat *et al.* (1989, in press), and recommended values for the newly proposed Ailsa Craig international standard, AC-E (table IV.1). Most elements agree reasonably well, although both Ce and Nd are rather high as determined in this work possibly as a result of interference. If this is a systematic error for all the samples, it may account for the apparent positive Ce and Nd anomalies observed in many of the analyses, particularly the carbonatites.

Compared to XRF analyses for La, Ce, and Nd, the INAA results are consistently higher (fig. IV.1), a feature also apparent in the basaltic rocks of the western USA (Leat, pers. comm.). No satisfactory explanation could be given for this, although it serves as a useful reminder not to compare analyses for different elements obtained using different methods.

Table IV.1

Comparison of Ailsa Craig microgranite analysis with published results

Element	This work	A	B
La	62.5	62	59
Ce	185.6	165	154
Nd	110.7	99	92
Sm	26.7	24.9	24.2
Eu	1.72	1.91	2
Gd	24.3	28.2	26
Tb	4.86	5.15	4.8
Ho	8.74	7.2	6.5
Yb	18.24	17.7	17.4
Lu	2.51	2.44	2.45
Ta	7.02	6.49	6.4
Hf	28.1	28.3	27.9
Th	19.9	18.9	18.5
U	4.23	4.2	4.6
Cs	3.69	3.5	3

A – Leat *et al.* (1989. in press).

B – Working values for international standard AC-E.

Analyses in ppm of element.

Fig. IV.1

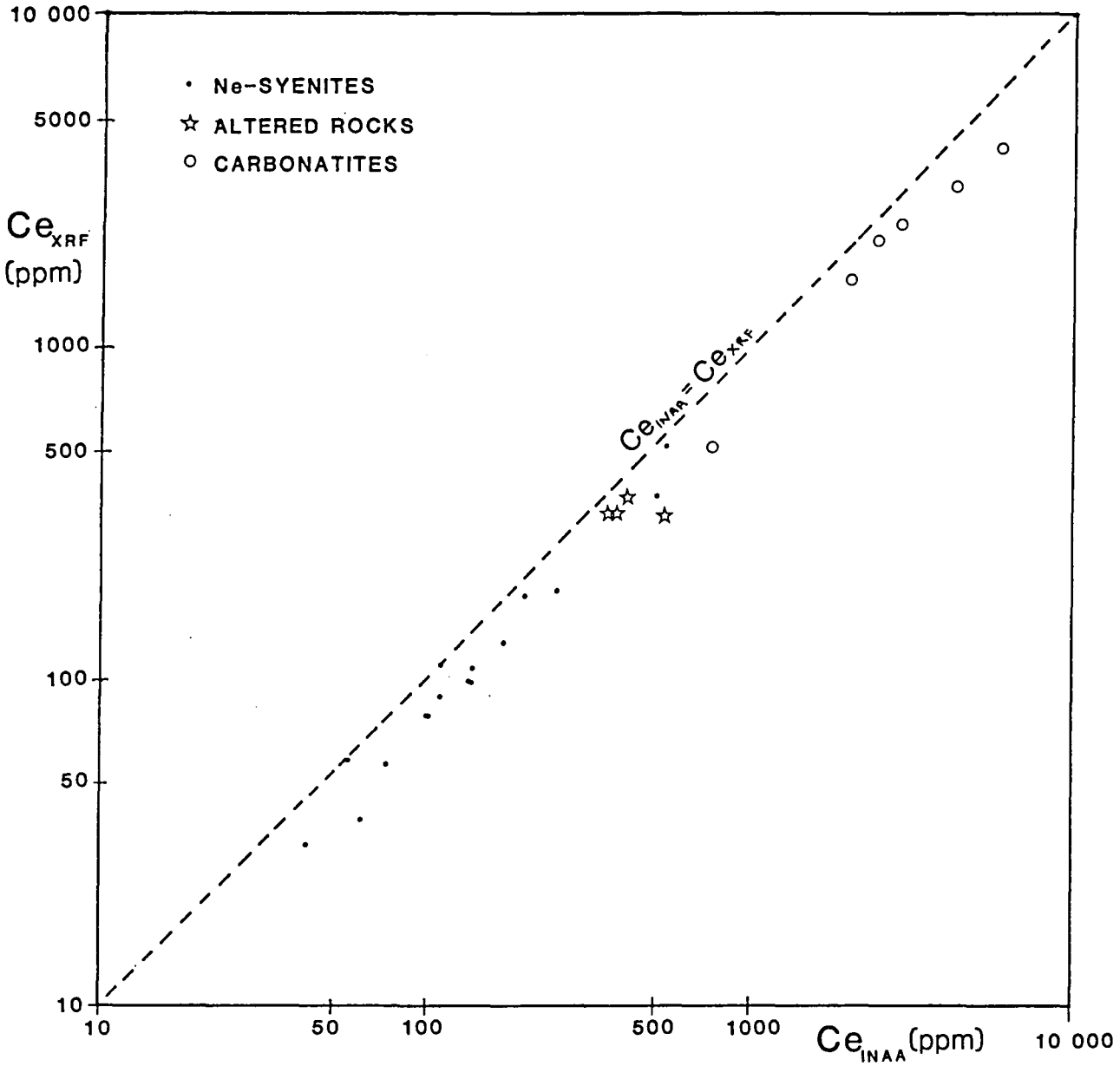

Fig. IV.1. Comparison between Ce data obtained using XRF and INAA methods. The $XRF_{Ce}/INAA_{Ce}$ ratio remains very similar over the entire range of analyses.

Table IV.2

Peak energies and half-lives of isotopes counted

Isotope	Half-life (×1000s)	Energies(keV)
^{140}La	144.97	328.8
		487.1
^{141}Ce	2797.6	145.50
^{147}Nd	955.58	91.10
^{153}Sm	168.31	103.20
		69.67
^{152}Eu	400510	121.80
		344.30
^{153}Gd	20909	97.50
^{160}Tb	6229.4	86.80
		298.60
^{166}Ho	96.509	80.57
^{175}Yb	362.02	396.30
		113.80
^{177}Yb	2652.5	177.18
		130.50
		63.12
^{177}Lu	579.74	208.40
^{182}Ta	9936.0	152.40
		100.11
		67.80
^{181}Hf	3853.4	482.20
		133.10
U(^{238}Np)	203.47	106.10
Th(^{233}Pa)	2367.4	311.80
		98.60
		94.66
^{187}W	86.400	72.30
^{51}Cr	2401.9	320.00
^{46}Sc	7257.6	889.40
^{134}Cs	66226	795.80
	65280	604.70

I N A A : RESULTS (ppm element)

Sample:	G26	G30	G43	G47	G52	G57	G64	G78	G90
Rock-type:	ALGN	CBT	USS	CBT	CBT	ALGN	MMS	XPS	ALSY
La	199.00	882.00	43.40	680.00	631.10	162.00	37.10	90.10	155.00
Ce	527.00	2852.00	99.90	2425.00	2016.00	358.00	98.50	201.00	380.00
Nd	304.00	2129.00	42.80	2290.00	1681.00	162.00	51.50	95.50	203.00
Sm	49.20	248.70	7.04	270.10	209.70	22.00	8.80	15.90	28.70
Eu	12.30	66.80	1.39	57.70	47.60	5.20	2.10	4.09	8.04
Gd	2.96	40.80	5.09	23.40	23.10	15.50	0.88	12.90	2.15
Tb	5.69	27.60	0.62	21.30	16.00	2.05	0.65	1.40	2.51
Ho	30.00	103.90	1.27	198.50	92.00	9.55	0.60	6.42	20.40
Yb	8.63	10.30	3.02	17.60	6.55	4.11	1.02	3.28	2.43
Lu	1.27	0.84	0.55	2.15	0.59	0.72	0.22	0.67	0.40
Ta	19.00	6.17	9.17	2.53	2.91	13.00	3.40	20.80	60.70
Hf	1.99	4.60	12.90	1.66	2.20	20.20	5.04	27.30	38.90
U	1.59	4.66	1.93	38.30	20.20	2.71	0.28	5.50	11.20
Th	8.36	12.90	5.50	7.98	10.80	18.80	1.39	10.89	7.07
W	9.60	152.00	7.81	24.00	172.00	29.50	2.52	25.80	32.90
Cr	19.40	84.50	5.50	58.70	46.70	11.90	5.50	7.20	6.80
Sc	0.39	1.13	0.91	0.76	0.52	5.13	0.65	0.40	0.24
Cs	9.76	3.95	1.74	3.74	3.04	1.85	1.05	1.54	1.90

Sample:	G102	G107	G136	G145	G169	G185	G193	G202A	G208
Rock-type:	CBT	CBT	ALSY	XPS	GSA	USS	LSS	PMS	MUS
La	214.00	2118.00	173.00	41.90	68.00	17.50	29.90	23.20	51.40
Ce	753.00	5812.00	412.00	109.00	170.00	43.30	74.00	61.70	133.00
Nd	836.00	2638.00	214.00	55.00	87.00	23.00	30.40	35.80	64.90
Sm	117.40	244.40	40.60	9.56	12.50	3.58	4.80	5.40	9.46
Eu	35.00	49.30	9.21	2.52	3.10	0.67	1.13	1.30	2.16
Gd	12.70	20.00	3.32	3.77	1.98	0.62	5.37	0.72	1.24
Tb	18.70	18.30	3.77	0.92	1.72	0.41	0.65	0.50	1.24
Ho	36.70	92.40	13.40	1.71	5.40	1.03	0.68	0.43	0.88
Yb	6.11	17.40	4.19	2.61	5.70	2.53	1.27	0.90	1.07
Lu	0.50	1.60	0.72	0.53	0.82	0.41	0.15	0.20	0.30
Ta	8.60	0.47	7.37	18.50	12.20	12.00	7.90	4.40	4.70
Hf	0.34	6.00	14.90	26.00	22.10	25.50	17.20	11.10	17.30
U	1.28	0.69	0.91	4.37	4.70	4.54	6.56	0.44	0.40
Th	11.00	72.80	9.46	4.41	8.53	1.92	5.52	1.81	4.28
W	37.00	167.00	34.20	5.90	11.80	7.96	5.91	5.41	7.99
Cr	16.70	10.30	9.04	7.20	0.0	5.70	5.00	13.80	6.00
Sc	0.72	0.80	2.71	0.38	1.74	0.57	0.17	1.61	1.30
Cs	2.36	4.02	9.79	2.98	2.33	1.33	1.49	2.90	1.30

I N A A : RESULTS (ppm element)

Sample:	G216	G219	G245	G247	G257	G259	G265	G275
Rock-type:	CGBS	LSS	XPS	MUS	GSB	CGBS	CBT	CGS
La	186.00	48.00	27.20	202.00	85.60	43.10	1877.00	59.60
Ce	509.00	135.00	57.30	538.00	245.00	109.00	4161.00	136.00
Nd	254.00	69.70	30.30	289.00	152.00	45.70	1770.00	57.30
Sm	31.90	10.60	5.66	40.50	20.80	6.26	157.00	8.47
Eu	7.60	1.86	3.50	6.85	3.19	1.53	42.60	2.26
Gd	6.70	1.76	4.05	5.52	10.10	7.64	41.30	12.00
Tb	3.98	1.14	0.55	4.08	2.30	0.91	16.30	0.87
Ho	11.40	1.46	1.43	19.30	7.15	1.24	71.20	0.80
Yb	1.33	2.29	2.19	5.91	3.37	2.39	15.40	2.00
Lu	0.17	0.40	0.42	1.04	0.41	0.37	1.50	0.33
Ta	6.10	1.94	26.30	19.00	5.46	7.30	2.80	6.20
Hf	0.57	14.00	44.70	36.90	18.89	26.90	1.33	11.40
U	2.42	0.43	4.32	4.10	0.83	1.96	1.89	1.23
Th	21.00	1.50	5.06	17.10	8.70	8.34	39.60	10.50
W	16.50	8.59	5.24	37.40	19.20	1.99	94.50	12.40
Cr	16.50	18.10	7.69	8.72	17.60	5.20	57.10	6.00
Sc	0.39	0.87	0.49	2.47	0.81	0.14	1.13	1.25
Cs	8.40	1.36	4.20	1.80	1.20	1.00	4.92	1.50

REFERENCES

ANDERSON, T. 1988. Evolution of peralkaline calcite carbonatite magma in the Fen complex, south-east Norway. Lithos, **22**, 99-112.

ANDERSEN, T. 1989. Carbonatite-related contact metasomatism in the Fen complex, Norway: effects and petrogenetic implications. Mineralogical Magazine, **53**, 395-414.

AOKI, K. 1964. Pyroxenes from the alkaline rocks of Japan. American Mineralogist, **49**, 1199-1223.

BAILEY, D.K. 1966. Carbonatite volcanoes and shallow intrusions in Zambia. In Tuttle, O.F., and Gittins, J. (eds.) *Carbonatites*, 127-154. Wiley and Sons.

BAILEY, J. 1976. Trace element techniques in the Insitute for Petrology, University of Copenhagen. In Bailey, J., and Sørensen, I., *X-ray fluorescence analysis.* Internal report, University of Copenhagen.

BAILEY, S.W. 1984. Classification and structure of the micas. In Bailey, S.W. (ed.) *Reviews in mineralogy, volume 13: micas.* Mineralogical Society of America.

BEDSON, P. 1983. The origin of the carbonatites and their relation to other rocks by liquid immiscibility. Unpublished PhD thesis, University of Manchester.

BEDSON, P. 1984. Rare-earth element distribution between immiscible silicate and carbonate liquids. In *Progress in Experimental Petrology*, Volume 6. Natural Environment Research Council, Publications Series D, no. 25.

BLAXLAND, A.B., VAN BREEMAN, O., EMELEUS, C.H., and ANDERSEN, J.G. 1978. Age and origin of the major syenite centres in the Gardar Province of South Greenland: Rb-Sr studies. Geological Society of America Bulletin, **89**, 231-244.

BØGVAD, R. 1951. Det Grønlandske Åsskrift Magnetjernstenen: Grønnedal ved Ivigtut.

BOWEN, N.L. 1937. Recent high temperature research on silicates and its significance in igneous geology. American Mineralogist, **33**, 1-21.

BOYNTON, W.V. 1984. Geochemistry of the rare-earth elements: meteorite studies. In Henderson, P. (ed.) *Rare-earth element geochemistry*, 63-114. Elsevier.

BRADSHAW, C. 1985. The alkaline rocks of the Motzfeldt centre; progress report on the 1984 field season. Rapport Grønlands Geologiske Undersøgelse no.125, 62-64.

BRØGGER, W.C. 1921. Die Eruptivgesteine des Kristianiagebietes, IV, das Fengebiet in Telemark. Vidensk.–Skr. Kristiania **9**.

BROOKS, C.R., and GILL, R.C.O. 1982 Compositional variations in the pyroxenes and amphiboles of the Kangerdlugssuaq intrusion, East Greenland: further evidence for the crustal contamination of syenite magma. Mineralogical Magazine, **45**, 1-9.

BROUCE, R. and RANCON, J.P. 1984. Crystallisation trends of pyroxenes from agpaitic phonolites (Cantal, France). Mineralogical Magazine, **48**, 39-45.

BUDDINGTON, A.F., and LINDSLEY, D.H. 1964. Iron-titanium oxide minerals and synthetic equivalents. Journal of Petrology, **5**, 310-357.

CALLISEN, K. 1943. Igneous rocks of the Ivigtût region, Greenland. Part I: The nepheline-syenites of the Grønne Dal – Íka area. Meddelelser om Grønland, **131**, no.8.

CARMICHAEL, I.S.E. 1967. The iron-titanium oxides of salic volcanic rocks and their associated ferromagnesian silicates. Contributions to Mineralogy and Petrology, **14**, 36-64.

CARMICHAEL, I.S.E, and NICHOLLS, J. 1967. Iron-titanium oxides and oxygen fugacities in volcanic rocks. Journal of Geophysical Research, **72**, 4655-87.

CAWTHORN, R.G. 1976. Some chemical controls on igneous amphibole compositions. Geochimica et Cosmochimica acta, **40**, 1319-1328.

CAWTHORN, R.G, and COLLERSON, K.D. 1974. The recalculation of pyroxene end-member parameters, and estimation of ferrous and ferric iron contents from electron-probe analysis. American Mineralogist, **59**, 1203-8.

CHAMBERS, A.D. 1976. The petrology and geochemistry of the North Qôroq Centre, Igaliko Complex, South Greenland. Unpublished PhD thesis, University of Durham.

CHARLES, R.W. 1975. The phase equilibria of richterite and ferrorichterite. American Mineralogist, **60**, 367-374.

CULLERS, R.L, and GRAF, J.L. 1984. Rare-earth elements in igneous rocks of the continental crust: predominantly basic and ultrabasic rocks. In Henderson, P. (ed.) *Rare-earth element geochemistry*, 237-274. Elsevier.

CULLERS, R.L., and MEDARIS, G. 1977. Rare-earth elements in carbonatites and cogenetic alkaline rocks: examples from Seabrook Lake and Callander Bay, Ontario. Contributions to Mineralogy and Petrology, **65**, 143-153.

DAWSON, J.B, and HAWTHORN, J.B. 1973. Magmatic sedimentation and differentiation in the kimberlite sills at Benfontein, South Africa. Journal of the Geological Society of London, **129**, 61-85.

DEER, W.A, HOWIE, R.A., and ZUSSMAN, J. 1966. *An Introduction to the Rock Forming Minerals.* Longman, London.

DEER, W.A., HOWIE, R.A., and ZUSSMAN, J. 1978. *Rock Forming Minerals, volume 2: Chain Silicates.* Longman.

DUNCUMB, P., and JONES, E.M. 1969. Tube Investments Company Report, No. 260.

DUNCUMB, P., and REED, S.J.B. 1968. Quantitative electron probe microanalysis. National Bureau of Science Special Publication, **298**, 133-154.

EBY, G.N. 1975. Abundance and distribution of the rare-earth elements and Y in the rocks and minerals of the Oka carbonatite complex, Quebec. Geochimica et Cosmochimica acta, **39**, 597-620.

EMELEUS, C.H. 1964. The Grønnedal-Íka alkaline complex, South Greenland. Meddelelser om Grønland, Bd 172. no. 3. (also Grønlands Geologiske Undersøgelse Bulletin, **85**).

DEER, W. A., HOWIE, R. A., ZUSSMAN, J. 1982. "An introduction to the rock-forming minerals." Longman, London.

EMELEUS, C.H., and HARRY, W.T. 1970. The Igaliko nepheline syenite complex. Meddelelser om Grønland, Bd 186. no. 3. (also Grønlands Geologiske Undersøgelse Bulletin, **85**).

EMELEUS, C.H, and UPTON, B.G.J. 1976. The Gardar Period in Southern Greenland. In Escher, A., and Watt, W.S. (eds.) *The Geology of Greenland*, 153-181. Grønlands Geologiske Undersøgelse, København.

ERNST, W.G. 1962. Synthesis, stability, and occurrence of the riebeckite-arfvedsonite solid-solution series. Journal of Geology, **70**, 689-736.

FERGUSON, J. 1964. Geology of the Ilímaussaq alkaline intrusion, South Greenland. Grønlands Geologiske Undersøgelse Bulletin, **39**. Also Meddelelser om Grønland, Bd. 172, nr. 4.

FREESTONE, I.C., and HAMILTON, D.L. 1980. The role of liquid immiscibility in the genesis of carbonatites – an experimental study. Contributions to Mineralogy and Petrology, **73**, 105-117.

GARSON, M.S. 1962. Geological Survey Dep. Malawi Memoir, **2**, 1-248.

GASPAR, J.G, and WYLLIE, P.J. 1983. Magnetite in carbonatites from the Jacupiranga Complex, Brazil. American Mineralogist, **68**, 195-213.

GILL, R.C.O. 1972a. The geochemistry of the Grønnedal-Íka alkaline complex, South Greenland. Unpublished PhD thesis, University of Durham.

GILL, R.C.O.1972b. Chemistry of peralkaline phonolite dykes from the Grønnedal-Íka area, South Greenland. Contributions to Mineralogy and Petrology, **34**, 87-100.

GITTINS, J. 1989. Reply to Kjarsgaard, B.A, and Hamilton, D.L. *Carbonatite origin and diversity* (Nature **338**). Nature, **338**, p548.

GOLD, D.P. 1963. Average composition of carbonatites. Economic Geology, **58**, 988-991.

GOLDSCHMIDT, J.V. 1954. *Geochemistry.* Clarendon Press, Oxford.

GOVINDARAJU, K. 1984. Composition of working values and sample description for 170 international reference standards of mainly silicate rocks and minerals. Geostandards Newsletter Volume III, Special Issue.

GRAPES, R., YAGI, K., and OKUMURA, K. 1979. Aenigmatite, sodic pyroxene, arfvedsonite, and associated minerals from Morutu, Sakhalin. Contributions to Mineralogy and Petrology, **69**, 97-103.

HAMILTON, D.L. 1961. Nephelines as crystallisation temperature indicators. Journal of geology, **69**, 321-329.

HAMILTON, D.L, BEDSON, P., and ESSON, J. 1989. The behaviuor of trace elements in the evolution of carbonatites. In Bell, K (ed.) *Carbonatites: genesis and evolution*, 405-427. Unwin and Hyman, London.

HAMILTON, D.L., and MACKENZIE, W.S. 1960. Nepheline solid-solution in the system $NaAlSiO_4$-$KAlSiO_4$-SiO_2. Journal of Petrology, **1**, p56.

HAMILTON, D.L., and MACKENZIE, W.S. 1965. Phase equilibrium studies in the system $NaAlSiO_4$(nepheline)-$KAlSiO_4$(kalsilite)-SiO_2-H_2O. Mineralogical Magazine, **34**, 214-231.

HEINRICH, E.W. 1966. *The Geology of Carbonatites.* Rand-McNally, Chicago.

HEINRICH, K.F.J. 1967. 2nd national conference on electron-probe microanalysis, Boston, USA. Paper no. 7.

HELZ, R.T. 1973. Phase relationships of basalts in their melting range at p_{H_2O}=5kb as a function of oxygen fugacity. Part I: mafic phases. Journal of Petrology, **14**, 249-302.

HENDERSON, C.M.B., and GIBB, F.G.F. 1977. Formation of analcime in the Dippin Sill of Arran. Mineralogical Magazine, **41**, 534-537.

HENDERSON, C.M.B., PENDLEBURY, K., and FOLAND, K.A. 1989. Mineralogy and petrology of the Red Hill alkaline igneous complex, New Hampshire, USA. Journal of Petrology, **30**, 627-666.

HENDERSON, P. 1982. *Inorganic Geochemistry.* Pergamon Press, Oxford.

HENDERSON, P., and PANKHURST, R.J. 1984. Analytical chemistry. In Henderson, P. (ed.), *Rare-earth element geochemistry*, 467-499. Elsevier.

HENDERSON, P., and WILLIAMS, C.T. 1981. Application of intrinsic Ge detectors to the instrumental neutron activation analysis for rare-earth elements in rocks and minerals. Journal of Radioanalytical Chemistry, **67**, 445-452.

HENRIKSEN, N. 1960. Structural analysis of a fault in south-west Greenland. Meddelelser om Grønland. Bd 162, no. 9. (Also Grønlands Geologiske Undersøgelse Bulletin, **26**).

HENRIKSEN, N. 1969. Boundary relations between Precambrian fold belts in the Ivigtût area, south-west Greenland. Geological Society of Canada Special Paper, **5**, 143-154.

HODGSON, N.A. 1985. Carbonatites and associated rocks from the Cape Verde Islands. Unpublished PhD thesis, University of Leicester.

HOLST, N.O. 1886. Berättelse om en år 1880 i geologisk syfte företagen resa till Grönland. Sveriges Geol. Undersökn., Ser. C, **81**.

IRVING, A.J. 1978. A review of experimental studies of crystal/liquid trace-element partitioning. Geochimica et Cosmochimica acta, **42**, 743-770.

JONES, A.P. 1980. The petrology and structure of the Motzfeldt Centre, Igaliko, South Greenland. Unpublished PhD thesis, University of Durham.

JONES, A.P. 1984. Mafic silicates from nepheline syenites of the Motzfeldt Centre, South Greenland. Mineralogical Magazine, **48**, 1-12.

JONES, A.P., and PECKETT, A. 1980. Zirconium-bearing aegirines from from Motzfeldt, South Greenland. Mineralogical Magazine, **75**, 251-255.

KEMPE, D.R.C., and DEER, W.A. 1970. The mineralogy of the Kangerdlugssuaq alkaline intrusion, East Greenland. Meddelelser om Grønland, **190(3)**.

KIM, K.T., and BURLEY, B.J. 1971. Phase equilibria in the system $NaAlSi_3O_8$-$NaAlSiO_4$-H_2O, with special emphasis on the stability of analcite. Canadian Journal of Earth Scienes, **8**, 311-337.

KJARSGAARD, B.A., and HAMILTON, D.L. 1988. Liquid immiscibilty and the origin of alkali-poor carbonatites. Mineralogical Magazine, **52**, 43-55.

KJARSGAARD, B.A., and HAMILTON, D.L. 1989. The genesis of carbonatites by liquid immiscibility. In Bell, K. (ed.) *Carbonatites: Genesis and Evolution*, 388-404. Unwin and Hyman, London.

KOGARKO, L.N. 1974. Role of volatiles. In Sørensen, H. (ed.) *The Alkaline Rocks*, 474-487. Wiley and Sons: London and New York.

KOSTER VAN GROOS, A.F. 1975. The distribution of Sr between co-existing silicate and carbonate liquids at elevated pressures and temperatures. Geochimica et Cosmochimica acta, **39**, 27-34.

KOSTER VAN GROOS, A.F., and WYLLIE, P.J. 1966. Liquid immiscibility in the system Na_2O-Al_2O_3-SiO_2-CO_2 at pressures to 1kb. American Mineralogist, **264**, 234-255.

KOSTER VAN GROOS, A.F., and WYLLIE, P.J. 1968. Liquid immiscibility in the join $NaAlSi_3O_8$-Na_2CO_3-H_2O and its bearing on the genesis of carbonatites.

LARSEN, J.G. 1977. Petrology of the late lavas of the Eriksfjord Formation, Gardar Province, South Greenland. Grønlands Geologiske Undersøgelse Bulletin, **125**.

LARSEN, L.M. 1976. Clinopyroxenes and co-existing mafic minerals from the alkaline Ilímaussaq intrusion, South Greenland. Journal of Petrology, **17**, 258-290.

LARSEN, L.M. 1977. Aenigmatite from the Ilímaussaq intrusion, South Greenland: chemistry and petrological implications. Lithos, **10**, 257-270.

LE BAS, M.J. 1977. *Carbonatite-Nephelinite Volcanism.* John Wiley and Son, New York.

LE BAS, M.J. 1981. Carbonatite magmas. Mineralogical Magazine, 44, 133-140.

LE BAS, M.J. 1987. Nephelinites and carbonatites. In Fitton, J.G., and Upton, B.G.J. (eds.) *Alkaline Igneous Rocks*, Geological Society Special Publication **30**, 53-83.

LEAKE, B.E. 1978. Nomenclature of the amphiboles. Mineralogical Magazine, **42**, 533-563.

LEAT, P.T., THOMPSON, R.N., MORRISON, M.A., HENDRY, G.L., and DICKEN, A.P. 1989. Geochemistry of mafic lavas in the early Rio Grande Rift, Yarmony Mountains, Colorado. Chemical Geology (in press).

LEVINSON, A.A., and BORUP, R.A. 1959. High hafnium zircon from Norway. Bulletin of the Geological Society of America, **70**, 1638.

LINDSLEY, D.H. 1976. The crystal chemistry and structure of the oxide minerals as exemplified by the iron-titanium oxides. In Ribbe, P.H. *Reviews in mineralogy* **3***: oxide minerals.* Mineralogical Society of America.

MACDONALD, R. The petrology of alkaline dykes from the Tugtutôq region, South Greenland. Bulletin of the Geological Society of Denmark, **19**, 257-282.

MACKENZIE, W.S., and SMITH, J.V. 1961. Experimental and geological evidence for the stability of alkali feldspars. Instituto Lucas Mallada C.S.I.C. Cursillos Conference, Madrid, **8**, 53-64.

MARTIN, R.F., WHITLEY, J.E., and WOOLEY, A.R. 1978. An investigation of rare-earth mobility: fenitized quartzites, Borralan complex, NW Scotland. Contributions to Mineralogy and Petrology, **66**, 69-73.

MARAVIC, H., and MORTEANI, G. 1980. Petrology and geochemistry of the carbonatite and syenite complex of Lueshe, NE Zaire. Lithos, **13**, 159-170.

MCKENZIE, D.P. 1984. The generation and compaction of partially molten rock. Journal of Petrology, **25**, 713-765.

MCKENZIE, D.P. 1985. The extraction of magma from the crust and mantle. Earth and Planetary Science Letters, **74**, 81-91.

MCKIE, D. 1966. Fenitization. In Tuttle, O.F., and Gittins, J. (eds.) *Carbonatites*, 261-294. Wiley and Sons.

MIAN, I., and LE BAS, M.J. 1986. Sodic amphiboles in fenites from the Loe Shilman carbonatite complex, NW Pakistan. Mineralogical Magazine, **50**, 187-197.

MIAN, I., and LE BAS, M.J. 1987. The biotite-phlogopite series in fenites from the Loe Shilman carbonatite complex, NW Pakistan. Mineralogical Magazine, **51**, 397-408.

MIDDLEMOST, E.A.K. 1985. *Magmas and Magmatic Rocks. An introduction to igneous petrology.* Longman, London and New York.

MITCHELL, R.H., and PLATT, R.G. 1978. Mafic mineralogy of ferro-augite syenite from the Coldwell alkaline complex, Ontario, Canada. Journal of Petrology, **19**, 627-651.

MÖLLER, P., MORTEANI, G., and SCHLEY, F. 1980. Discussion of rare-earth element distribution patterns of carbonatites and alkalic rocks. Lithos, **13**, 171-179.

MORTEANI, G., MÖLLER, P., ACKERMAND, D., DULSKI, P., KRONIMUS, B., and SPIEGEL, W. 1986. *Developmnt of petrological and geochemical indicators for the discovery of Nb and P-rich carbonatites.* Lehrstuhl für Angewandte Mineralogie und Geochimie: Technische Universität München.

MORSE, S.A. 1969. *Syenites.* Annual Report of the Director of the Geophysical Laboratory, Washington. **67**, 112-120.

MYSEN, B.O. 1976. The role of volatiles in silicate melts: solubility of CO_2 and water in feldspar, pyroxene, and feldspathoid melts to 30kb and 1625°C. American Journal of Science, **276**, 969-996.

NASH, W.P., and WILKINSON, J.F.G. 1970. Shonkin Sag laccolith, Montana. I. Mafic minerals and temperature estimates of temperature, pressure, oxygen fugacity, and silica activity. Contributions to Mineralogy and Petrology, **25**, 241-269.

NIELSEN, T.F.D. 1979. The occurrence and formation of Ti-aegirines in peralkaline syenites. Contributions to Mineralogy and Petrology, **69**, 235-244.

NORRISH, K., and HUTTON, J.T. 1969. An accurate X-ray spectrographic method for the analysis of a wide range of geological samples. Geochimica et Cosmochimica acta, **33**, 431-453.

PARSONS, I. 1978. Feldspar and fluids in cooling plutons. Mineralogical Magazine, **42**, 1-18.

PARSONS, I. 1979. The Klokken gabbro-syenite complex, South Greenland: cryptic variation and the origin of inversely graded layering. Journal of Petrology, **20**, 653-694.

PASTER, T.P, SCHAUWECKER, D.S., and HASKIN, L.A. 1974. The behaviour of some trace elements during solidification of the Skaergaard layered series. Geochimica et Cosmochimica acta, **38**, 1549-1577.

PEARCE, N.J.G. 1988. The petrology and geochemistry of the Igaliko dyke swarm, South Greenland. Unpublished PhD thesis, University of Durham.

PEARCE, N.J.G. 1989. Zirconium-bearing amphiboles from the Igaliko dyke swarm, South Greenland. Mineralogical Magazine, **53**, 107-110.

PECORA, W.T. 1956. *Carbonatites: a review.* Bulletin of the Geological Society of America, **67**, 1537-1566.

PHILIBERT, J. 1963. X-ray optics and X-ray microanalysis: 3rd International Symposium. Academic Press, 379-392.

PHILLIPS, R. 1965. Amphibole compositional space. Mineralogical Magazine, **35**, 945-952.

PIPER, J.D.A. 1982. The Precambrian palaeomagnetic record. The case for the Proterozoic Supercontinent. Earth and Planetary Science Letters, **59**, 61-81.

PLATT, R.G., and WOOLLEY, A.R. 1986. The mafic mineralogy of the peralkaline syenites and granites of the Mulanje complex, Malawi. Mineralogical Magazine, **50**, 85-99.

POINTER, C.M., ASHWORTH, J.R., and IXER, R.A. 1988. The zircon – thorite mineral group metasomatized granite, Ririwai, Nigeria. 2: Zoning, alteration, and exsolution in zircon. Mineralogy and Petrology, **39(1)**, 21-37.

POLDERVAART, A. 1956. Zircon in rocks: 2. Igneous rocks. American Journal of Science, **254**, 521.

POLDERVAART, A., and HESS, H.H. 1951. Pyroxenes in the crystallisation of basic magma. Journal of Geology, **59**, 472-489.

POTTS, P.J. 1987. *A Handbook of Silicate Rock Analysis.* Bell and Bain, Glasgow.

POTTS, P.J., WILLIAMS-THORPE, O., and WATSON, J.S. 1981. Determination of the rare-earth element abundances in 29 international rock standards by instrumental neutron activation analysis: a critical appraisal of calibration errors. Chemical Geology, **34**, 331-352.

POWELL, M. 1978. The crystallisation history of the Igdlerfigssalik nepheline-syenite intrusion, SW Greenland. Lithos, **11**, 99-120.

POWELL, R., and POWELL, M. 1977. Geothermometry and oxygen barometry using co-existing iron-titanium oxides: a reappraisal. Mineralogical Magazine, **41**, 257-263.

RAE, D.A., and CHAMBERS, A.D. 1988. Metasomatism in the North Qôroq centre, South Greenland: cathodoluminescence and mineral chemistry of alkali feldspars. Transactions of the Royal Society of Edinburgh: Earth Sciences, **79**, 1-12.

REED, S.J.B. 1965. Characteristic fluorescence corrections in electronprobe microanalysis. British Journal of Applied Physics, **16**, 913-926.

ROEDDER, E. 1984. (Ed.). Fluid inclusions. *Reviews in mineralogy,* **12**. Mineralogical Society of America.

ROUX, J., and HAMILTON, D.L. 1976. Primary igneous analcite – an experimental study. Journal of Petrology, **17**, 244-257.

ROWBOTHAM, G. 1973. Hydrothermal synthesis and mineralogy of the alkali amphiboles. Unpublished PhD thesis, University of Durham.

RUBIE, D.C. 1982. Mass transfer and volume change during alkali metasomatism at Kisingiri, western Kenya. Lithos, **15**, 99-109.

RUBIE, D.C., and GUNTER, W.D. 1983. The role of speciation in alkaline igneous fluids during fenite metasomatism. Contributions to Mineralogy and Petrology, **82**, 165-175.

RUSTAMOV, M.I., VOLFENZON, E.F., and BABAEV, B.S. 1988. Zircons from granitic rocks of volcano-plutonic and plutonic associations in the Araks zone (Lesser Caucasus). Zapiski Vsesoyuznogo Mineralogicheskogo Obshchestva, **117(3)**, 360-369.

SAETHER, E. 1957. The alkaline rock province of the Fen area in southern Norway. Det. Kgl. Norske Vidensk. Selskabs Skrifter, **1**.

SECHER, K., and LARSEN, L.M. 1980. Geology and mineralogy of the Sarfartôq carbonatite complex, southern West Greenland. Lithos, **13**, 199-212.

SHIRLEY, D.N. 1987. Differentiation and compaction in the Palisades Sill, New Jersey. Journal of Petrology, **28(5)**, 835-866.

SMITH, J.V. 1974. *Feldspar minerals 2: chemical and textural properties.* Springer–Verlag.

SOBOLEV, V.S., BAZAROVA, T.Y., and KOSTYUK, V.P. 1974. Inclusions in the minerals of some types of alkaline rocks. In Sørensen, H. (ed.) *The Alkaline Rocks*, 389-401. Wiley and Sons, New York.

SØRENSEN, H., and PETERSEN, O.V., 1981. The mineralogy of the Ilímaussaq intrusion. Rapport Grønlands Geologiske Undersøgelse, **103**, 19-24.

SPEER, J.A., and RIBBE, P.H. 1982. Miscellaneous orthosilicates. In Ribbe, P.H. (ed.), *Reviews in mineralogy, volume 5: orthosilicates.* Mineralogical Society of America.

SPENCER, K.J, and LINDSLEY, D.H. 1981. A solution model for co-existing iron-titanium oxides. American Mineralogist, **66**, 1189-1201.

SPERA, F.J., and BERGMAN, S.C. 1980. CO_2 in igneous petrogenesis: I. Aspects of the dissolution of CO_2 in silicate liquids.

STEPHENSON, D. 1973. The petrology and mineralogy of the South Qôroq centre, Igaliko Complex, South Greenland. Unpublished PhD thesis, University of Durham.

STEPHENSON, D. 1976. The South Qôroq centre nepheline-syenites, South Greenland – petrology, felsic mineralogy, and petrogenesis. Grønlands Geologiske Undersøgelse Bulletin, **118**.

STEPHENSON, D. 1976b. A simple-shear model for the ductile deformation of high-level intrusions in South Greenland. Journal of the Geological Society, **132**, 307-318.

STEPHENSON, D., and UPTON, B.G.J. 1982. Ferromagnesian silicates in a differentiated alkaline complex: Kûngnât Fjeld, South Greenland. Mineralogical Magazine, **46**, 283-300.

STEWART, J.W. 1970. Precambrian alkaline-ultramafic/carbonatite volcanism at Qagssiarssuk, South Greenland. Grønlands Geologiske Undersøgelse Bulletin, **84**, and Meddelelser om Grønland, **186**, no. 4.

STORMER, J.S. Jr. 1983. The effects of recalculation on estimates of temperature and oxygen fugacity from analyses of multicomponent iron-titanium oxides. American Mineralogist, **68**, 586-592.

STRECKEISEN, A.L. 1980. Classification and nomenclature of volcanic rocks, lamprophyres, carbonatites, and melilitic rocks: I.U.G.S. subcommission on the systematics of igneous rocks. Geol. Rundsch., **69**, 194-207.

SUTHERLAND, D.S. 1969. Sodic amphiboles and pyroxenes from fenites in East Africa. Contributions to Mineralogy and Petrology, **24**, 114-135.

THOMPSON, R.N. 1982. Magmatism of the British Tertiary Volcanic Province. Scottish Journal of Geology, **18**, 49-107.

THORNTON, C.P., and TUTTLE, O.F. 1960. Chemistry of igneous rocks I: differentiation index. American Journal of Science, **258**, 664-684.

TILLEY, C.E. 1954. Nepheline – alkali feldspar paragenesis. American Journal of Science, **252**, 65-75.

TUKIAINEN, T. 1984. Geological mapping and exploration in the Motzfeldt Centre of the Igaliko nepheline-syenite complex, South Greenland. Rapport Grønlands Geologiske Undersøgelse, **125**, 56-61.

TUKIAINEN, T., BRADSHAW, C., and EMELEUS, C.H. 1983. Geological and radiometric mapping of the Motzfeldt centre of the Igaliko complex, South Greenland. Rapport Grønlands Geologiske Undersøgelse, **120**, 78-83.

TWYMAN, J.D., and GITTINS, J. 1987. Alkalic carbonatite magmas: parental or derivative? In Fitton, J.G., and Upton, B.G.J. (eds.) *Alkaline igneous rocks.* Geological Society Special Publication, **30**, 85-94.

TYLER, R.C., and KING, B.C. 1967. The pyroxenes of the alkaline igneous complexes of eastern Uganda. Mineralogical Magazine, **36**, 5-22.

UPTON, B.G.J. 1964. The geology of Tugtutôq and neighbouring islands, South Greenland. Part IV, the nepheline-syenites of the Hviddal composite dyke. Grønlands Geologiske Undersøgelse Bulletin, **48**, 49-80.

UPTON, B.G.J. 1974. The alkaline province of south-west Greenland. In Sørensen, H. (ed.), *The Alkaline Rocks*, 221-238. John Wiley and Sons: London.

UPTON, B.G.J., and EMELEUS, C.H. 1987. Mid-Proterozoic alkaline magmatism in South Greenland: the Gardar Province. In Fitton, J.G., and Upton, B.G.J. (eds.), *Alkaline igneous rocks.* Geological Society Special Publication, **30**, 449-471.

UPTON, B.G.J., STEPHENSON, D., and MARTIN, A.R. The Tugtutôq Older Giant Dyke complex: mineralogy and geochemistry of an alkali-gabbro – augite-syenite – foyaite association in the Gardar Province of South Greenland. Mineralogical Magazine, **49**, 623-642.

VON ECKERMANN, H. 1948. The alkaline district of Alnö Island. Stockholm AB Kartografuka Institutet Sveriges Geologiska Undersökning, **36**.

WAGER, L.R., and BROWN, G.M. 1968. *Layered Igneous Rocks.* Edinburgh and London: Oliver and Boyd.

WALLACE, M.E., and GREEN, D.H. 1989. An experimental determination of primary carbonatite magma compositions. Nature, **335**, 343-346.

WATSON, E.B. 1979. Zircon saturation in felsic liquids: experimental results and applications to trace element geochemistry. Contributions to Mineralogy and Petrology, **70**, 407-419.

WEGMANN, C.E. 1938. Geological investigations in South Greenland. Part I. On the structural divisions of south Greenland. Meddelelser om Grønland, **158**, no. 4.

WELLMAN, T.R. 1970. The stability of sodalite in a synthetic syenite plus aqueous chloride fluid system. Journal of Petrology, **11**, 49-71.

WENDLANDT, R.F., and HARRISON, W.J. 1979. Rare-earth partitioning between immiscible carbonate and silicate liquids and CO_2 vapor: results and implications for the formation of light rare-earth enriched rocks. Contributions to Mineralogy and Petrology, **69**, 409-419.

WILSON, M. 1989. *Igneous petrogenesis – a global tectonic approach.* Unwin and Hyman.

WONES, D.R. and EUGSTER, H.P. 1965. Stability of biotite: experiment, theory, and application. American Mineralogist, **50**, 1228-1272.

WOOLLEY, A.R. 1982. A discussion of carbonatite evolution and nomenclature, and the generation of sodic and potassic fenites. Mineralogical Magazine, **46**, 13-17.

WOOLLEY, A.R., SYMES, R.F., and ELLIOTT, C.J. 1972. Metasomatized (fenitized) quartzites from the Borralan complex, Scotland. Mineralogical Magazine, **38**, 819-836.

YAGI, K. 1966. The system acmite–diopside and its bearing on the stability of natural pyroxenes of the acmite–hedenbergite–diopside series. American Mineralogist, **51**, 976-1000.

YAKOWITZ, H., MYKLEBUST, R.L., and HEINRICH, K.J.F. 1973. FRAME: An on-line correction procedure for quantitative electronprobe microanalysis. National Bureau of Science Technical Note, **796**.

YODER, H.S. Jr. STEWART, D.B., and SMITH, J.R. 1957. Ternary feldspars. Yearbook of the Carnegie Institute of Washington, **56**, 206-214.

THE GRONNEDAL-IKA COMPLEX

1987 Field season sample localities*

Geology after Emeleus (1964) and the author (1989)

Scale 1:15 000

0 0.5 1km

Minor Intrusions (Post-complex)

- Porphyritic basalts
- Olivine dolerite, etc

NB. Alkaline dykes omitted

Pre-Gardar

- Metasediments
- Gneiss

Nepheline syenites

- Xenolithic porphyritic syenite
- Porphyritic microsyenite

Lower Series

- Granular syenite
- Foyaite
- Coarse-grained brown syenite

Upper Series

- Coarse-grained syenite
- Foyaite and pulaskite
- Mafic (pyroxene-rich) syenite

Carbonate rocks

- Carbonatite
- Carbonated rocks

- Superficial deposits
- Geological boundaries
- Faults and crush zones
- • 219 Sample locality (G series)
- △585 Spot heights (metres)
- ① ▲ Camp 1 (30/6/87-29/7/87)
- ② ▲ Camp 2 (30/7/87-5/8/87)
- Road and hut

* Pre-1987 sample localities probed X 138011
Pre-1987 " " not probed, but mentioned in text ⊗ 27136

GRØNLANDS GEOLOGISKE UNDERSØGELSE
THE GEOLOGICAL SURVEY OF GREENLAND

MEDD. OM GRØNL. BD. 172, NR. 3. (C. H. EMELEUS)

MAP 1

GEOLOGICAL MAP OF THE GRØNNEDAL - ÍKA COMPLEX, SOUTH GREENLAND

Scale 1 : 15 000

0,1 0 0,5 1km

Minor intrusions (post Igneous Complex)

- Trachyte, phonolite, etc.
- Porphyritic basalts
- Olivine dolerite etc.

(N.B. Many impersistent dykes are not shown)

Pre-Gardar

- Metasediments
- Gneiss

Members of the Igneous Complex

- Carbonatite and breccia.
- Carbonate-impregnated rocks

Nepheline Syenites:

- Xenolithic porphyritic syenite
- Porphyritic microsyenite

Upper Series

- Coarse-grained syenite
- Foyaite and pulaskite
- Pyroxene-rich syenite

Lower Series

- Granular syenite
- Foyaite
- Coarse-grained brown syenite

- Superficial deposits
- Faults and crush zones
- Geological boundaries, established
- ,, , inferred
- ,, , arbitrary
- 70 Strike and dip of igneous lamination
- Strike of vertical igneous lamination
- 30 Strike and dip of mineral layering
- Heights in metres
- Contour interval 100m
- Road and Hut

Topography based on preliminary 1:20,000 maps prepared photogrammetrically from vertical aerial photographs by the Geodetic Institute, Copenhagen.

	AN-G	BE-N	MA-N	T-1	NIM-D	NIM-G	NIM-L	NIM-N	NIM-P	NIM-S
Major elements (wt. %)										
SiO2	46.30	38.20	66.60	62.70	38.96	75.70	52.40	52.64	51.10	63.63
Al2O3	29.80	10.07	17.62	16.69	0.30	12.08	13.64	16.50	4.18	17.34
Fe2O3	0.87	5.34	0.13	2.71	0.71	0.58	8.74	0.80	1.02	1.07
FeO	2.24	6.74	0.31	2.88	14.63	1.30	1.13	7.30	10.59	0.3
MnO	0.04	0.20	0.04	0.10	0.22	0.02	0.77	0.18	0.22	0.01
MgO	1.80	13.15	0.04	1.89	43.51	0.06	0.28	7.50	25.33	0.46
CaO	15.90	13.87	0.59	5.08	0.28	0.78	3.22	11.50	2.66	0.68
Na2O	1.63	3.18	5.84	4.39	0.04	3.36	8.37	2.46	0.37	0.43
K2O	0.13	1.39	3.18	1.24	0.01	4.99	5.51	0.25	0.09	15.35
TiO2	0.22	2.61	0.01	0.58	0.02	0.09	0.48	0.20	0.20	0.04
P2O5	0.01	1.05	1.39	0.14	0.01	0.01	0.06	0.03	0.02	0.12
H2O+	0.61	2.24	1.08	1.52	0.30	0.49	2.31	0.33	0.26	0.22
H2O-	0.11	0.50	0.21	-	-	-	-	-	-	-
CO2	0.13	0.74	0.13	0.07	0.40	0.10	0.17	0.10	0.08	0.09
Fe2O3T	3.36	12.84	0.47	5.90	16.96	2.02	9.96	8.91	12.76	1.40
Trace elements (ppm)										
Ba	34	1025	42	660	10	120	450	100	46	2400
Nb	2	100	173	-	-	53	960	2	-	4
Zr	15	265	27	150	20	300	1.1%	23	30	33
Y	8	30	1	-	-	143	22	7	5	20
Sr	76	1370	84	390	3	10	4600	260	32	62
Rb	1	47	3600	32	-	320	190	6	5	530
Zn	20	120	220	180	90	50	400	68	100	10
Cu	19	72	140	48	10	12	13	14	18	19
Ni	35	267	3	10	2050	8	11	120	560	7
Pb	2	4	29	37	7	40	43	7	6	5
U	-	2.4	12	-	-	15	14	0.6	0.4	0.6
Th	-	11	1	-	0.8	51	66	0.6	1	1.0
V	70	235	4.6	96	40	2	81	220	230	10
Cr	50	360	3	20	2900	12	10	30	2.4%	12
Nd	2	70		-	-	72	48	3	-	6
Ga	18	17	59	20	-	27	54	16	8	11
La	2	82	1	-	0.2	109	250	3	2	5
Ce	4.7	152	10	-	-	195	240	6	-	11.9

STANDARD COMPOSITIONS USED (After Govindaraju 1984)

('-' indicates data unavailable for a particular element)

	G-1	AGV-1	BCR-1	DTS-1	G-2	GSP-1	PCC-1	SY-2	SY-3
Major elements (wt. %)									
SiO2	72.46	59.25	54.53	40.47	69.22	67.37	41.88	60.10	59.68
Al2O3	14.23	17.15	13.72	0.32	15.40	15.16	0.74	12.12	11.80
Fe2O3	0.87	4.47	3.48	1.01	1.07	1.75	2.72	2.28	2.44
FeO	0.98	2.06	8.96	6.95	1.44	2.31	5.06	3.62	3.58
MnO	0.03	0.10	0.18	0.12	0.03	0.04	0.12	0.32	0.32
MgO	0.39	1.53	3.48	49.65	0.75	0.99	43.23	2.70	2.67
CaO	1.38	4.94	6.97	0.14	1.96	2.04	0.52	7.98	8.26
Na2O	3.33	4.25	3.30	0.02	4.06	2.80	0.03	4.34	4.15
K2O	5.48	2.90	1.70	0.00	4.46	5.51	0.01	4.48	4.20
TiO2	0.25	1.06	2.26	-	0.48	0.66	0.01	0.14	0.15
P2O5	0.09	0.48	0.36	0.00	0.13	0.28	0.00	0.43	0.54
H2O+	0.34	0.80	0.67	0.43	0.50	0.53	4.71	0.43	0.42
H2O-	0.05	1.02	-	0.06	0.10	0.08	0.42	-	-
CO2	0.07	-	0.02	-	0.08	0.11	0.15	0.46	0.38
Fe2O3T	1.96	6.76	13.41	8.73	2.69	4.32	8.34	6.28	6.42
Trace elements (ppm)									
Ba	1080	1220	680	2.35	1900	1310	1.2	460	430
Nb	20	15	19	-	13	26	1	23	130
Zr	201	225	185	10	300	530	8	80	320
Y	13	21	40	0.05	11	29	-	130	740
Sr	249	660	330	0.33	480	234	0.4	275	306
Rb	215	67	47	0.00	170	254	0.07	220	208
Zn	45	88	125	48	84	103	42	250	240
Cu	12	60	16	7	10	34	10	5	16
Ni	3.4	17	10	2350	3.5	10	2400	10	11
Pb	46	36	14	12	30	54	11	80	130
U	3.5	1.89	1.7	3.6	2.1	2.2	0.00	290	650
Th	50	6.5	6.1	0.01	25	105	0.00	380	990
V	18	123	420	12	36	53	30	52	51
Cr	20	12	15	4000	8	13	2730	12	10
Nd	57	34	26	0.03	58	190	0.00	71	800
Ga	19.5	20	22	0.15	23	22	0.7	28	26
La	104	37	27	0.03	92	185	0.09	88	1350
Ce	173	66	53	0.07	160	400	0.1	210	2200

	MRG-1	GR	GA	GH	BR	DR-N	UB-N	BIR-1	GS-N
Major elements (wt. %)									
SiO2	39.32	65.90	69.90	75.80	38.20	52.85	39.43	47.96	65.80
Al2O3	8.50	14.75	14.50	12.50	10.20	17.52	2.90	15.53	14.67
Fe2O3	8.26	1.65	1.36	0.41	5.58	3.70	5.36	2.06	1.92
FeO	8.63	2.16	1.32	0.84	6.57	6.73	5.40	8.34	1.65
MnO	0.17	0.06	0.09	0.05	0.20	0.22	0.12	0.18	0.06
MgO	13.49	2.40	0.95	0.03	13.28	4.40	35.21	9.70	2.30
CaO	14.77	2.50	2.45	0.69	13.80	7.05	1.20	13.32	2.50
Na2O	0.71	3.80	3.55	3.85	3.05	2.99	0.10	1.82	3.77
K2O	0.18	4.50	4.03	4.76	1.40	1.70	0.02	0.03	4.63
TiO2	3.69	0.65	0.38	0.08	2.60	1.09	0.11	0.96	0.68
P2O5	0.06	0.28	0.12	0.01	1.04	0.25	0.04	0.02	0.28
H2O+	0.98	0.70	0.87	0.46	2.30	2.22	10.84	0.09	1.07
H2O-	-	0.10	0.09	0.14	0.50	0.25	1.26	0.08	0.28
CO2	1.00	0.26	0.11	0.30	0.86	0.10	0.39	-	0.18
Fe2O3T	17.82	4.05	2.83	1.34	12.88	9.70	8.34	11.33	3.75
Trace elements (ppm)									
Ba	50	1050	850	22	1050	385	30	6	1400
Nb	20	-	10	85	100	6	-	2.3	23
Zr	105	180	150	150	250	125	8	18	235
Y	16	19	21	70	30	30	11	16	19
Sr	260	550	310	10	1320	400	10	107	570
Rb	8	75	75	390	47	70	6	-	185
Zn	190	60	80	85	150	45	92	70	48
Cu	135	345	16	14	72	50	28	125	20
Ni	195	55	7	3	260	16	2000	166	34
Pb	10	32	30	45	8	55	18	-	53
U	0.3	-	4	18	3	1.5	-	-	8
Th	1	-	17	90	12	5	-	-	44
V	520	65	38	5	235	225	75	312	65
Cr	450	110	12	6	380	42	2300	373	55
Nd	19	-	25	25	60	22	-	-	50
Ga	18	20	16	23	20	22	5	15	22
La	10	75	38	25	80	21	-	0.63	75
Ce	25	-	70	50	140	46	-	1.6	140

MEDD. OM GRØNL. BD. 172. NR. 3 (C. H. EMELEUS)

GRØNLANDS GEOLOGISKE UNDERSØGELSE
THE GEOLOGICAL SURVEY OF GREENLAND

MAP 2

A RECONSTRUCTION OF THE GRØNNEDAL - ÍKA COMPLEX

Scale 1 : 22000

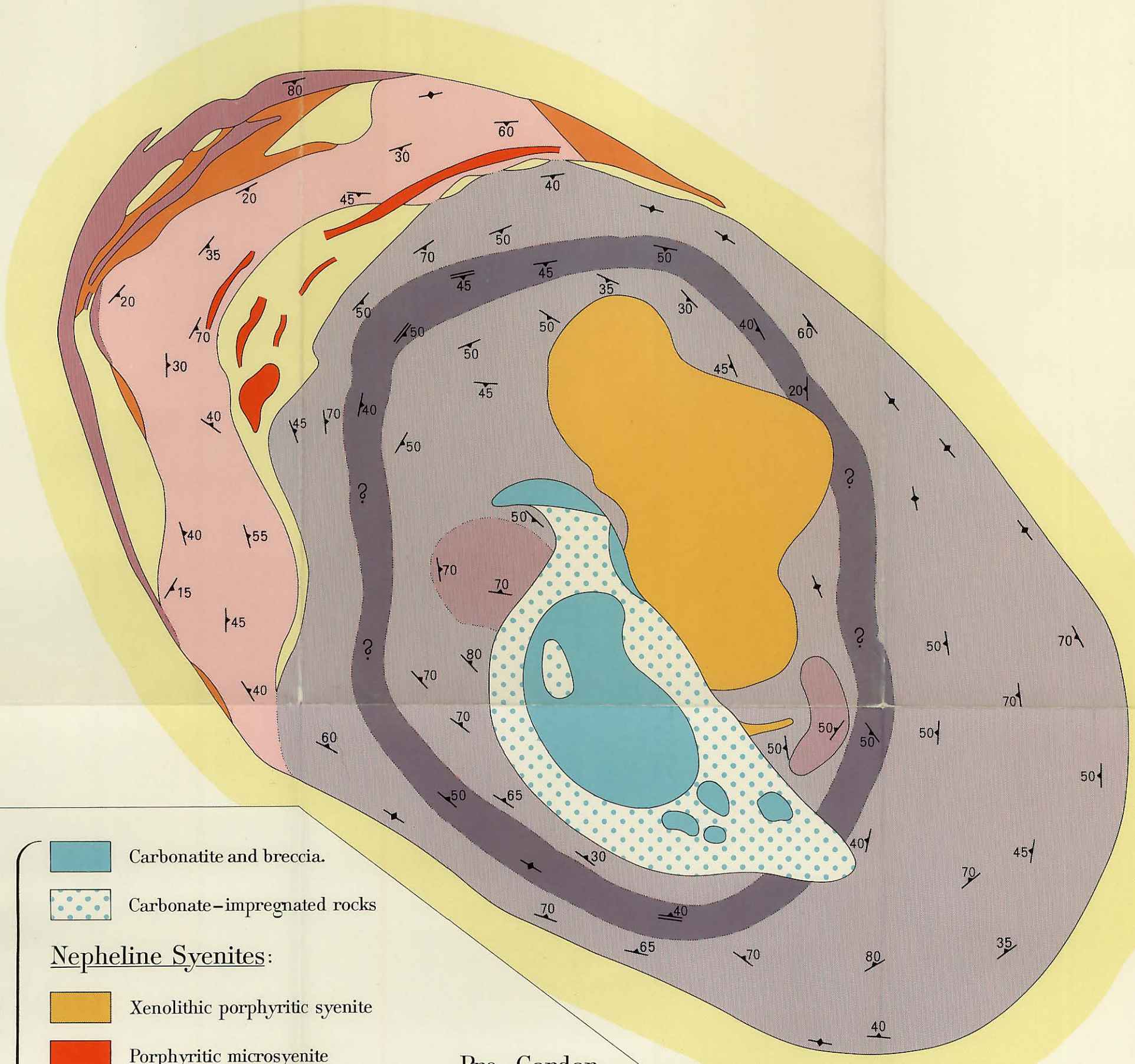

Members of the Igneous Complex

Carbonatite and breccia.

Carbonate–impregnated rocks

Nepheline Syenites:

Xenolithic porphyritic syenite

Porphyritic microsyenite

Upper Series

Coarse–grained syenite

Foyaite and pulaskite

Pyroxene–rich syenite

Lower Series

Granular syenite

Foyaite

Coarse–grained brown syenite

Pre–Gardar

Metasediments and gneisses

Geological boundaries

" , arbitrary

70 Strike and dip of igneous lamination

Strike of vertical igneous lamination

30 Strike and dip of mineral layering

THE GRONNEDAL-IKA COMPLEX

Microprobe sample localities

Geology after Emeleus (1964) and the author (1989)

Scale 1:15 000

0 0.5 1km

Minor Intrusions (Post-complex)

- Porphyritic basalts
- Olivine dolerite, etc.

NB. Alkaline dykes omitted

Pre-Gardar

- Metasediments
- Gneiss

Nepheline syenites

- Xenolithic porphyritic syenite
- Porphyritic microsyenite

Lower Series

- Granular syenite
- Foyaite
- Coarse-grained brown syenite

Upper Series

- Coarse-grained syenite
- Foyaite and pulaskite
- Mafic (pyroxene-rich) syenite

Carbonate rocks

- Carbonatite
- Carbonated rocks

- Superficial deposits
- Geological boundaries
- Faults and crush zones
- △585 Spot heights (metres)
- ①▲ Camp 1 (30/6/87-29/7/87)
- ②▲ Camp 2 (30/7/87-5/8/87)
- Road and hut